Comparison of Performances of Structural Fibers and Development of a Specification for Using Them in Thin Concrete Overlays

Manik Barman, Principal Investigator
University of Minnesota Duluth
Department of Civil Engineering

August 2018

LRRB
LOCAL
ROAD RESEARCH
BOARD

To request this document in an alternative format, such as braille or large print, call 651-366-4718 or 1-800-657-3774 (Greater Minnesota) or email your request to ADArequest.dot@state.mn.us. Please request at least one week in advance.

1. Report No. MN/RC 2018-29	2.	3. Recipients Accession No.
4. Title and Subtitle Comparison of Performances of Structural Fibers and Development of a Specification for Using Them in Thin Concrete Overlays		5. Report Date August 2018
		6.
7. Author(s) Manik Barman, Ph. D. Bryce Hansen		8. Performing Organization Report No.
9. Performing Organization Name and Address University of Minnesota Duluth Department of Civil Engineering 221 SCvi University Drive Duluth, Minnesota, 55812		10. Project/Task/Work Unit No. CTS#2017010
		11. Contract (C) or Grant (G) No. (C) 99008 (WO) 238
12. Sponsoring Organization Name and Address Local Road Research Board Minnesota Department of Transportation Research Services & Library 395 John Ireland Boulevard, MS 330 St. Paul, Minnesota 55155-1899		13. Type of Report and Period Covered Final Report
		14. Sponsoring Agency Code

15. Supplementary Notes

http:// mndot.gov/research/reports/2018/201829.pdf

16. Abstract (Limit: 250 words)

Structural fibers improve the long-term performance of concrete pavements and overlays and potentially are useful to reduce the slab thickness. These fibers are available in different parent material compositions, stiffness, shapes, and aspect ratios. The main objective of this study was to characterize the post-crack flexural and joint performance of fiber reinforced concrete to develop a specification for the selection of structural fibers for concrete overlays and/or pavements. The study included a literature review, an online survey, and a large-scale laboratory testing. It was found that the majority (almost 94%) of the FRC overlays in this country were constructed with structural synthetic fibers, which provided equal or better performance than projects using the steel fibers. In the laboratory study, a total of 43 different mixes were prepared with 11 different types of fibers. Fiber dosage, stiffness, and geometry significantly influenced the residual strength ratio (RSR) and residual strength (RS). In general, embossed, twisted, and crimped fibers performed better on average than straight-flat synthetic fibers when the comparison was made in terms of RSR or RS. From the joint performance testing, it was found that fibers can greatly improve the performance of the pavement with respect to load transfer efficiency (LTE), differential displacement, and differential joint energy dissipation. The findings from this were used to recommend the target ranges post-crack flexural performance, and joint performance parameters.

17. Document Analysis/Descriptors Fiber reinforced concrete, Pavements, Overlays (Pavements), Cracking of concrete pavements, Pavement joints	18. Availability Statement No restrictions. Document available from: National Technical Information Services, Alexandria, Virginia 22312
19. Security Class (this report) Unclassified	20. Security Class (this page) Unclassified	21. No. of Pages 275	22. Price

Comparison of Performances of Structural Fibers and Development of a Specification for Using Them in Thin Concrete Overlays

FINAL REPORT

Prepared by:

Manik Barman, Ph.D.
Bryce Hansen
University of Minnesota Duluth
Department of Civil Engineering

August 2018

ACKNOWLEDGMENTS

TABLE OF CONTENTS

LIST OF FIGURES

LIST OF TABLES

EXECUTIVE SUMMARY

Structural fibers improve the long-term performance of concrete pavements and overlays and are potentially useful in reducing the slab thickness. These fibers improve the post-crack performance of concrete by keeping cracks tight, which helps reduce the severity of cracking. Fibers have shown to increase the load transfer between concrete slabs as well, which decreases joint deterioration and subsequently joint faulting. Structural fibers are commercially available in different parent material compositions, stiffnesses, shapes, and aspect ratios (ratio of length to effective diameter). Among the various types of structural fibers, structural synthetic fibers have become predominant in the last few decades due to their ease of handling, better dispersion characteristics, and resistance to corrosion. The difficulties involved in dealing with the heavyweight steel fibers during mixing is likely the reason for the less frequent use of steel fibers as opposed to the synthetic fibers. The Minnesota Department of Transportation (MnDOT), and many other transportation agencies, have used structural synthetic fibers in concrete overlays for decades. The performance review of many of these concrete overlays provides evidence of the qualitative benefit of using structural fibers; however, it does not provide a comprehensive quantification of the benefits. Incidentally, no significant research studies have been conducted to recognize the optimum dosage of fibers, and no fiber selection criterion have been established. Because of this, paving agencies face challenges in deciding the most appropriate fiber type and its optimum dosage for prevailing conditions.

The main objective of this research was to characterize the post-crack flexural performance and joint performance of fiber reinforced concrete (FRC) to develop a specification for the selection of structural fibers for use in thin concrete overlays and/or pavements. The study was completed through four tasks: Task 1- literature review and online survey, Task 2- fabricating test setups to conduct post- crack flexural performance (ASTM C1609) and joint performance tests, Task 3- conducting post-crack performance tests along with several other fresh and hardened concrete tests, and Task 4- conducting joint performance testing.

The literature search and the online survey were conducted to understand the usage of structural fibers in concrete pavements and overlays. It was found that the majority (almost 94%) of the FRC overlays in this country were constructed with structural synthetic fibers, which provided equal or better performance than projects using the steel fibers. Fibers with aspect ratio between 50 and 100 and below 1% volume fraction were found to be suitable for avoiding fiber balling in the concrete mixture. It was found that fibers less than 0.25% volume fraction do not provide notable improvement in the post-crack flexural and joint performance of fiber reinforced concrete.

In the laboratory testing, ten different fibers were included and varied in length, geometry, and stiffness to study the influence of these fiber properties on the post-crack performance of the resulting concrete. All ten of the fibers were tested at three dosages of 0.25%, 0.5%, and 0.75% volume fractions. In joint performance testing, five fibers were included, including the one used in 2017 MnROAD cells, which was not considered among the ten fibers in the post-crack flexural performance testing. In total, 43 different concrete mixes were prepared with 11 different types of fibers: 30 FRC mixes (10 fibers x 3 dosages), one plain concrete mix for post-crack performance tests, and 12 additional FRC mixes for joint performance testing.

For the lab mixing used in this study, longer and stiffer fibers showed a greater tendency to ball and form matts; however, the improvised mixing method adopted in this study was able to reduce these issues. Achieving proper workability for concretes with smaller effective diameter fibers (coincidentally

having a higher aspect ratio) was difficult, especially at higher dosages, and a higher admixture dosage was required.

Synthetic fibers showed very little effect on the compressive strength and modulus of elasticity of concrete, as well as little to moderate influence on the modulus of rupture. Steel fibers showed higher performance in terms of the above-mentioned three properties. Fiber dosage, stiffness, and geometry significantly influenced the residual strength ratio (RSR) and residual strength (RS). The RSR and fiber volume fraction have an excellent correlation with an R^2 equal to 0.86. Embossed, twisted, and crimped fibers performed better on average than straight-flat synthetic fibers when comparison was made in terms of RSR or RS. Results also suggested that longer, large effective diameter fibers perform better than shorter, smaller effective diameter fibers.

From the joint performance testing, it was found that the load transfer efficiency (LTE), differential displacement, and differential joint energy dissipation were less influenced by the individual fiber's cross-section area and geometry. However, when low-stiffness-straight fibers were used, the peak displacement under the dynamic load was 20% to 35% greater than what other synthetic structural fibers provided. It was found that synthetic fibers did not deteriorate or fatigue with 500,000 load cycles in the test regime followed in this study. The joint performance considerably varied with fiber dosage and crack width. For example, LTE corresponding to a 50-mil crack width could be increased by 20% and 30% with the addition of 0.25% and 0.50% fiber volume fractions, respectively. At wider crack widths, fibers contributed even more because there is less contribution of aggregate interlock. The LTE could be increased by 25% and 40% with the addition of 0.25% and 0.50% fiber volume fractions, respectively, when the crack width is 100-mil. At very low crack width, such as 20 mils, LTE for plain concrete and FRC specimens were similar. The load transfer contribution of fibers was influenced by the crack width expanding and contracting as well. During the winter, when crack widths remained expanded, it appeared that fibers most likely elongate beyond their plastic limit, or slightly pullout of the concrete under the combined influence of longitudinal tensile stress and dynamic load. Then, come summer, after the crack width contracts, fibers may become lose and their participation in load transfer goes down.

It is suggested that in addition to conducting ASTM C1609 tests for post-crack flexural performance, the joint performance contribution of the fibers be considered in the fiber selection process during the trial batching, if possible.. Along with LTE, criteria on the differential displacement and loaded side peak displacement may be considered. The nomograms created correlating with the fiber properties, post-crack flexural performance and joint performance parameters can be used to aid in the selection of fiber type and dosage. Recommendation on the target range RSR, RS, and joint performance parameters are provided in this report.

CHAPTER 1: INTRODUCTION

Thin concrete overlays are an economic rehabilitation alternative for moderately distressed concrete and asphalt pavements. These are constructed as bonded or unbonded overlays. Thin concrete pavements-at-grade are constructed on low-volume roads and parking lots; these are mostly constructed directly on top of an unstabilized aggregate base layer. The thickness of these types of overlays or pavements varies from 3 to 6 inches; when the thickness is less than or equal to 4 inches, they are referred to as the ultra-thin overlays or pavements-at-grade. In general, the bonded concrete overlays are relatively thinner than the unbonded overlays. Fick and Harrington (2014) recognized six different concrete overlay types. These overlay types include a combination of design principles and materials including interface bonding and the use of concrete or asphalt as a substrate material. Figure 1-1 shows schematics of six different types of overlays (Fick and Harrington, 2014).

Bonded Concrete Resurfacing of Asphalt Pavements
–previously called ultra-thin whitetopping–

Unbonded Concrete Resurfacing of Asphalt Pavements
–previously called conventional whitetopping–

Bonded Concrete Resurfacing of Composite Pavements
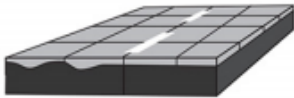
Unbonded Concrete Resurfacing of Composite Pavements
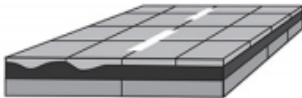
Bonded Concrete Resurfacing of Concrete Pavements
–previously called bonded overlays–

Unbonded Concrete Resurfacing of Concrete Pavements
–previously called unbonded overlays–
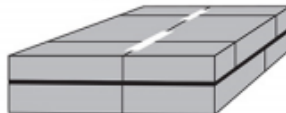
Figure 1-1. Types of concrete overlays (Fick and Harrington, 2014)

Due to the inherent tendency for thin concrete layers to warp and curl because of environmental effects, thin concrete pavements and overlays are often designed with small-sized panels. In addition, because of their thickness limitations and paving industry's desire to reduce costs, thin concrete overlays are often constructed without dowel bars spanning the transverse joints (Harrington and Fick, 2014). Many agencies use structural fibers instead of dowel bars. The results of a survey reported in the National Cooperative Highway Research Program (NCHRP) synthesis study 238 (NCHRP -238) indicated that 65% of the respondents in that survey used structural fiber reinforced concrete (FRC) in bonded concrete overlays on asphalt (Rasmussen and Rozycki, 2004).

FRC may increase the long-term performance of overlays, sometimes allowing for a reduced design thickness. Structural fibers improve the post-crack performance of concrete (Rollings, 1986; Roesler et al. 2003; Kevern et al., 2016) by keeping cracks tight, which helps reduce the severity of panel fatigue

cracking (e.g., longitudinal, corner, and transverse cracks). Fibers were also found to increase the load transfer between concrete slabs (Barman 2014), which eventually decreases joint deterioration and subsequently joint faulting.

Structural fibers are currently available in different material compositions, stiffnesses, shapes, and aspect ratios (ratio of length to effective diameter). Among the various types of structural fibers, structural synthetic fibers have become predominant in the last few decades due to their ease of handling, better dispersion characteristics, and resistance to corrosion. The difficulties involved in dealing with the heavy-weight steel fibers during mixing is likely the reason for the less frequent use of steel fibers as opposed to synthetic fibers. The Minnesota Department of Transportation (MnDOT) and many other transportation agencies had used structural synthetic fibers in concrete overlays for decades. Many combinations of fiber types, lengths, and dosages were used in overlays. The performance review of many of these concrete overlays provided evidence of the qualitative benefit of using structural fibers, however, it does not provide a comprehensive quantification of the benefits. Incidentally, no significant research studies were conducted to recognize the optimum dosage of fibers and no fiber selection criterion have yet been established. Because of this, many paving agencies often wonder about the most appropriate fibers and their optimum dosage. The main objective of this research was to characterize the post-crack performance and joint performance of fiber reinforced concrete to develop a specification for the selection of structural fibers for thin concrete overlays or pavements.

The study was completed through four tasks: Task 1- literature review and online survey, Task 2- fabricating test setups to conduct post-crack flexural performance (ASTM C1609) and joint performance tests, Task 3- characterizing post-crack performance of FRC, and Task 4- characterizing joint performance testing. The literature search and online survey were conducted to understand the use of structural fibers in concrete. In the laboratory tests, as many as eleven structural fibers varying with geometry, cross section, parent material, length, and aspect ratio were considered. Based on the findings of this study, conclusions and recommendations were made for the selection of structural fibers for use in thin concrete overlays and pavements.

CHAPTER 2: BACKGROUND

This chapter provides a discussion on the different properties of fibers and fiber reinforced concretes. A large variety of fibers, with varying mechanical properties, such as tensile strength, modulus of elasticity, and strain at failure, are available in the market. In addition to the mechanical properties, fibers also vary in longitudinal geometry, effective diameter, cross-section shape, and aspect ratio. The properties of fibers can influence the behavior of the resulting fiber reinforced concrete mixture.

2.1 FIBER TYPES

Fibers, as a whole, can be classified into two categories: (i) structural or macro fibers, and (ii) non-structural or micro fibers. According to Barborak (2011), structural fibers carry load and can be used to replace traditional reinforcement in certain non-structural applications, as well as minimize and/or eliminate both early and late age cracking. Typical length for macro-fibers is greater than or equal to 1.5 inches. Non-structural fibers, which are laterally less stiff than structural fibers, are generally utilized to minimize early age cracking. According ACI 544.3R (2008), the diameter or equivalent diameter of micro-synthetic fibers is less than 0.012 inch (0.3 mm); and macro-synthetic fibers have a diameter or equivalent diameter greater than 0.012 inch (0.3 mm). Per ASTM C1116 (2015), fibers are grouped into four categories that describe the parent material of the fiber: Type I-steel; Type II- glass; Type III-synthetic, and Type IV-natural fibers.

2.1.1 Steel Fibers

Steel fibers are typically produced from carbon steel. Because carbon steels are subject to corrosion, fibers may be produced from stainless steel if deemed necessary (ACI 544.1R, 2009). The ASTM A820 (2016) has identified five types of steel fibers and categorized them based on the parent material source and production process and designated them as Type I through Type V: Type I- cold drawn wire, Type II- cut sheet, Type III- melt extracted, Type IV- mill cut, and Type V- modified cold drawn wire. Figure 2-1 shows different categories of steel fibers. Figure 2-2 through Figure 2-4 show photographs of some commonly available commercial steel fibers.

Straight sheet or wire

Deformed slit sheet or wire

Hooked end wire

Flattened-end slit sheet or wire

Machined chip

Melt extract
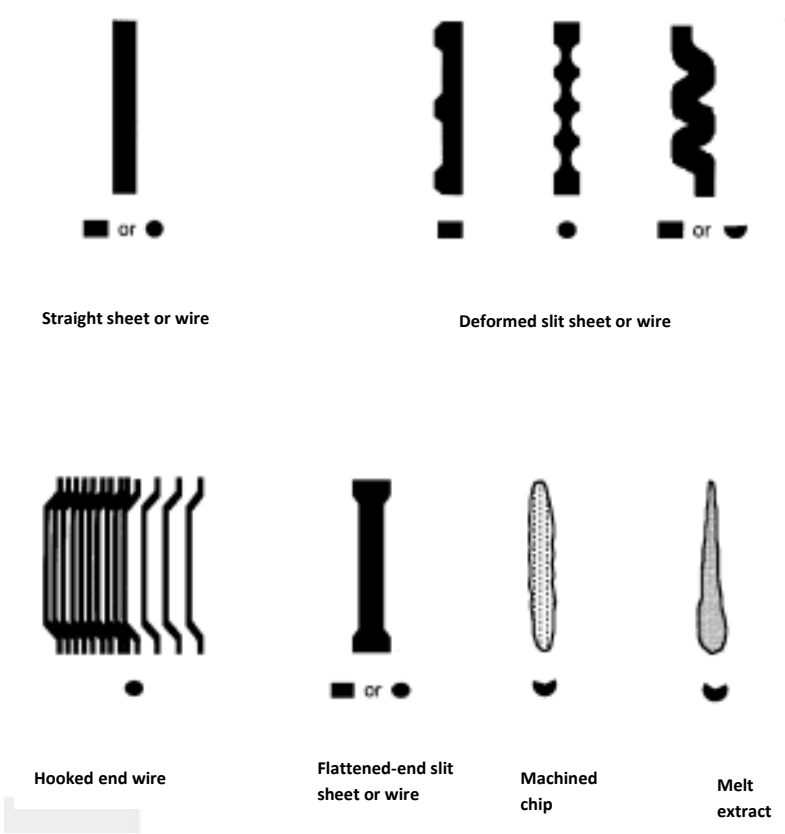
Figure 2-1. Various steel fiber geometries (after ACI 544.1R, 2009).
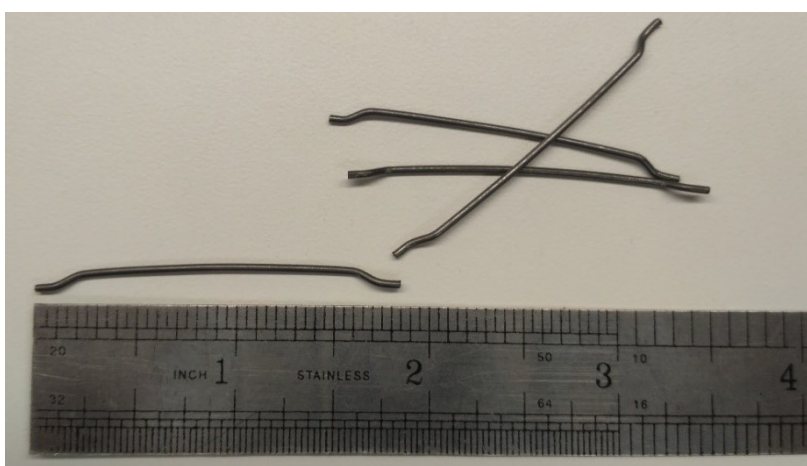
Figure 2-2. Steel fibers with hooked-end geometry.

4
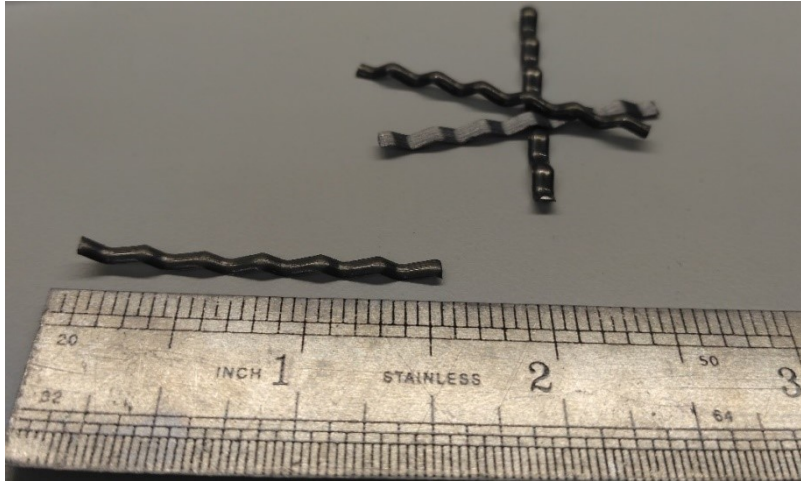
Figure 2-3. Steel fibers with whole length crimped geometry.
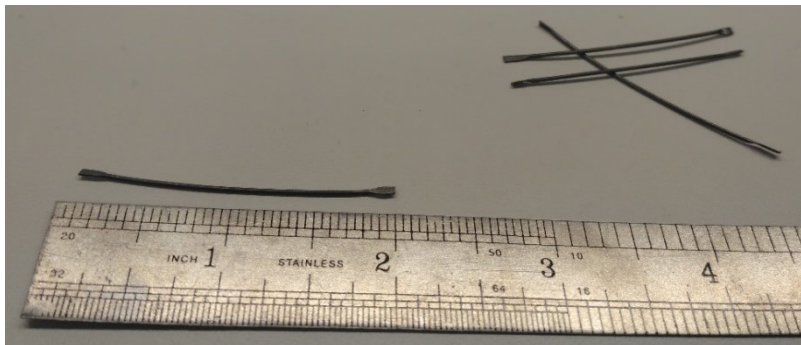
Figure 2-4. Steel fibers with flattened end.

ASTM A820 (2016) also specified the mechanical properties of steel fibers. This specification requires that all steel fibers shall have a minimum average tensile strength of 50 ksi and shall be capable of being bent around a 0.125-inch diameter pin to an angle of 90° at a temperature not greater than 60°F without breaking. The bending test provision in ASTM A820 (2016) is an indication of ductility to ensure that the fibers will not break during handling.

2.1.2 Synthetic Fibers

Structural synthetic fibers are the most commonly used fibers in concrete pavements or overlays over the last few decades. Synthetic fibers are produced from a wide range of materials, such as acrylic, aramid, carbon, nylon, polyester, basalt, polyolefin, polyethylene, and polypropylene (PCA, 2015). Among all of these, the polypropylene is the most popular one. These fibers can be monofilament, micro-fibrillated, or macro-monofilament. Micro-monofilaments are typically small, thin single fibers, as shown in Figure 2-5. Fibrillated fibers are long, interconnected bundles that unfurl when mixed into the concrete, see Figure 2-6 for an example. Macro or structural fibers are like monofilaments, but are typically much stiffer (laterally) and larger than monofilaments as shown in Figure 2-7. Synthetic fibers may also have embossed, crimped or textured surfaces to enhance the mechanical bondage.

The most popular synthetic fiber material, polypropylene, is chemically inert, hydrophobic, and light-weight. The polypropylene fibers can be produced as slender fibers with a rectangular cross section or as continuous cylindrical monofilaments and cut to a specified length. They can be of straight and flat, crimped, twisted, or embossed geometry along the length. Figure 2-8 shows photographs of two structural polypropylene fibers. Their wide use can be attributed to their chemical properties, resistance to fatigue and corrosion, and relatively low cost.

Figure 2-5. Monofilament synthetic fibers.
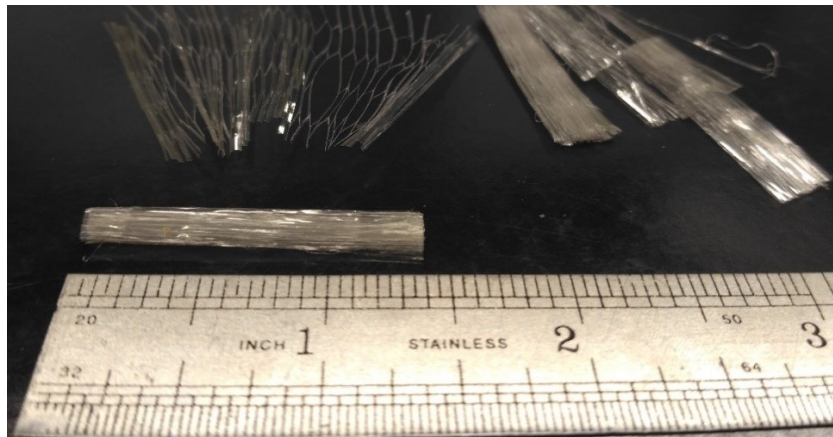
Figure 2-6. Fibrillated synthetic fibers.
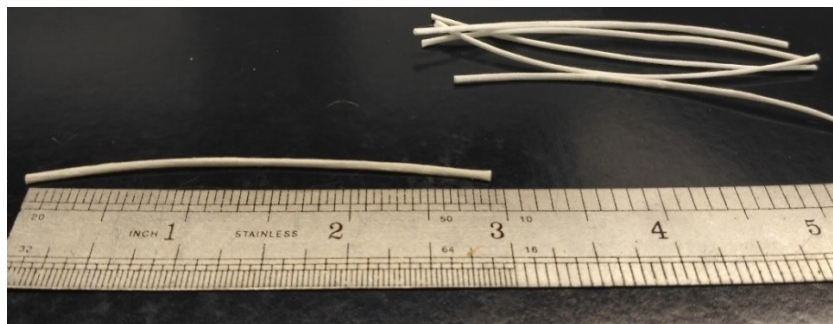
Figure 2-7. Macro synthetic fibers.
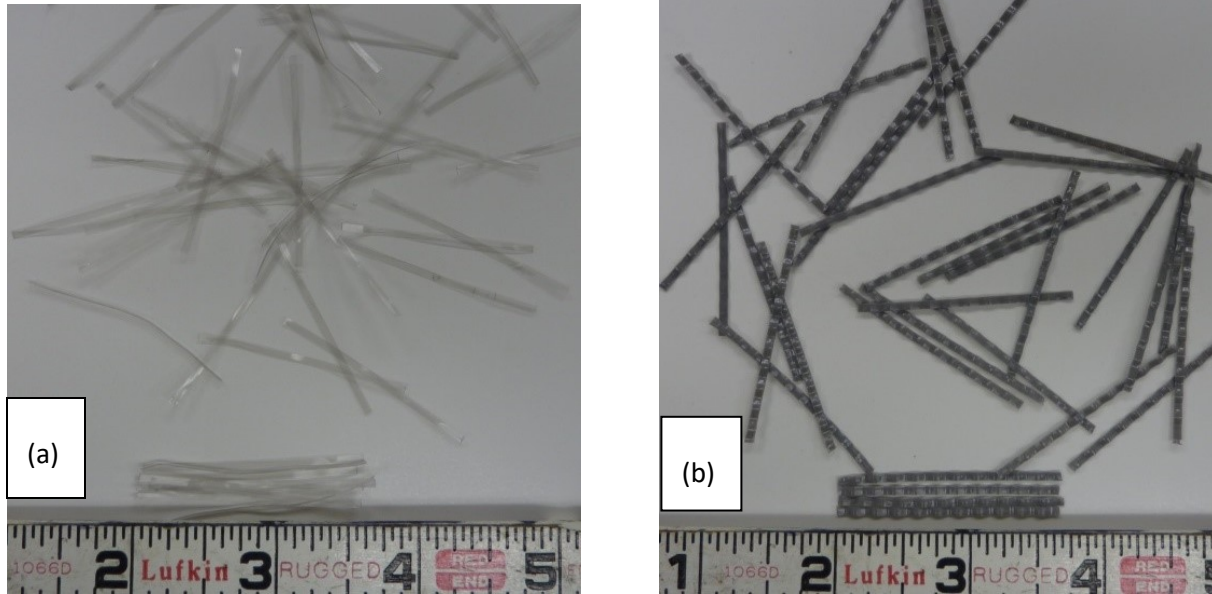
Figure 2-8. Photographs of the structural polypropylene fibers (a) straight geometry, (b) crimped geometry.

2.1.3 Other Fiber Types

A number of other fiber types are available for use in FRC. Those types include glass and natural fibers (ASTM C1116, 2015). These fibers have limited applications in concrete overlays because of some concerns. Natural fibers were found to absorb moisture and have poor durability. Glass fibers are subject to embrittlement due to alkali attack, even when alkali resistant glass is used; the long-term durability is a concern (ACI 544.1R, 2009) as well. Glass fibers also have a low strain capacity and are not conducive to compatibility in concrete joints that experience large crack widths and expansion and contraction of cracks. .

2.2 FIBER REINFORCED CONCRETE (FRC)

Fiber reinforced concrete is known for its enhanced durability, reduced plastic shrinkage, reduced spalling, and high impact strength. In general, fibers do not significantly increase the compressive strength and modulus of elasticity of concrete, especially when non-steel fibers are used, and tend to decrease the workability of concrete (Issa, 2017; Barman, 2014; Roesler et al., 2008). As depicted in Figure 2-9, structural fibers improve the post-crack performance of concrete by bridging cracks and increasing the toughness, residual strength (RS) and residual strength ratio (RSR) (ACI 544.1R, 2009; Roesler et al., 2008), load transfer efficiency (LTE) (Barman, 2014), and fatigue resistance (Rollings, 1986) of concrete. Based on full-scale slab studies, Beckett (1990) and Falkner et al. (1995) showed that structural fibers (steel or polymeric) increased the flexural and ultimate load carrying capacity of concrete slabs; the magnitude of the increase was related to the fiber volume and aspect ratio. Roesler (2003) stated that discrete synthetic fibers improved the load-deformation characteristics of concrete slabs. Figure 2-10 shows a representational schematic of load versus deflection curves (4-point bending test) of plain concrete and FRC specimens. This schematic demonstrates the post-peak load or post-crack contribution of fibers. It can be seen that FRC is able to hold some amount of load even after the crack development, which is referred to as the residual load. The residual load can be a function of the

fiber properties such as length, geometry, material composition, aspect ratio, and dosage. This section provides further discussion on the properties of steel and synthetic FRCs due to their popularity in the pavement industry; discussion on other FRCs is omitted because of their limited use in pavements.

Figure 2-9. Fibers bridging a crack and providing post-crack performance (after Gaddam, 2016).
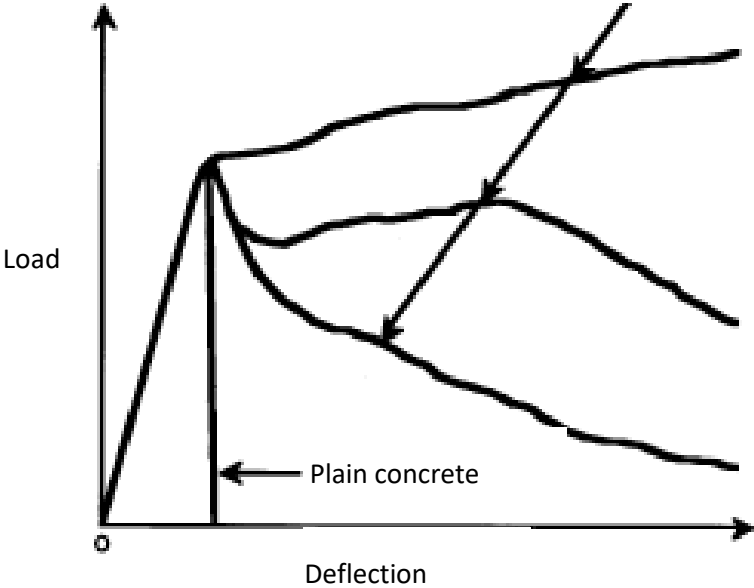
Figure 2-10. Representational schematic of load versus deflection curves for plain and fiber reinforced concrete (after ACI 544.1R, 2009).

2.2.1 Steel Fiber Reinforced Concrete (SFRC)

Even though steel fibers are not as popular as synthetic fibers for paving applications, some concrete overlays in Illinois were constructed with different types of steel fibers. Steel fibers are typically added

to concrete in volume fractions (V_f) of 0.25% to 1.5% and can significantly increase the concrete density (ACI 544.1R, 2009).

2.2.1.1 Fresh Concrete Properties

With typical fiber dosages (0.25% to 1.5% volume fraction), the measured slump may be reduced by 1 to 4 inches compared to plain concrete (ACI 544.1R, 2009). Like other FRCs, the workability of SFRC is also affected by the aspect ratio, geometry, and volume fraction of fibers and fiber-matrix interfacial bond characteristics (Ramakrishanan, 1987). Figure 2-11 shows the decrease in slump as the reinforcement index (RI) of fibers increases. The RI is defined as the volume fraction multiplied by the aspect ratio of the fibers in use.
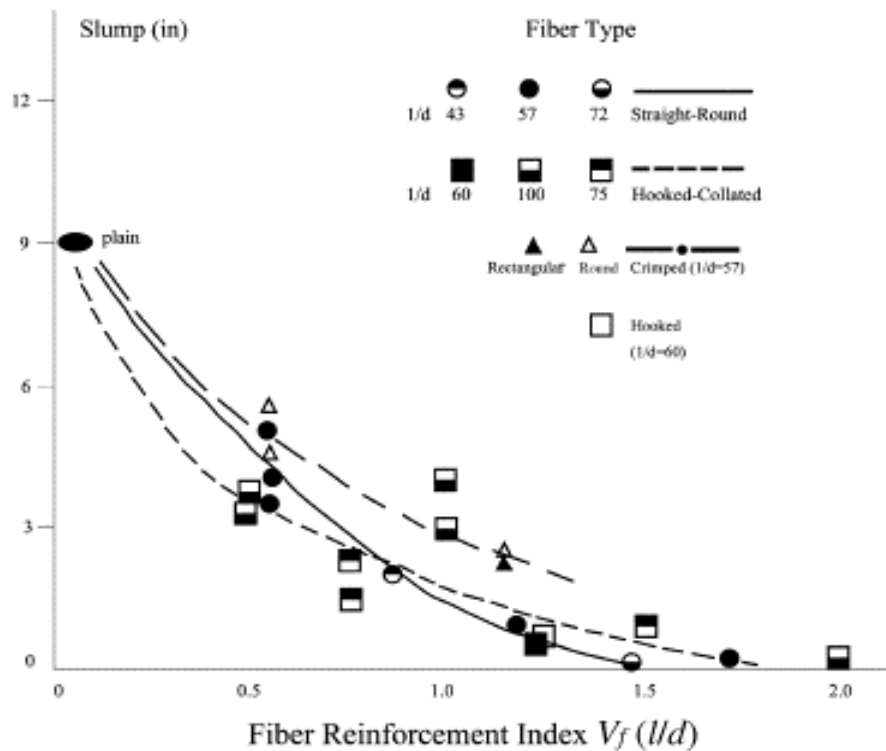
Figure 2-11. Effect of fiber reinforcement index and fiber geometry on the slump (after ACI 544.3R, 2008).

In addition to workability, fiber balling is also an issue in SFRC. Steel fibers with an aspect ratio greater than 100 tend to interlock and either ball or form mats of fibers in the mixture (Hannant, 1978). Fibers with an aspect ratio greater than 60 may require a blower to inhibit balling and matting of fibers (ACI 544.3R, 2008). However, steel fibers with an aspect ratio less than 50 are unable to become interlocked, ball, or form mats within the matrix (Hannant, 1978). Balling and the formation of mats of fibers result in poor dispersion and large variation in the hardened concrete properties. High aspect ratio fibers can positively affect the hardened concrete properties at lower dosages than low aspect ratio fibers, so other considerations must be made to reduce the likelihood of poor fiber dispersion. The American Concrete Institute (ACI, 2002) states that the tendency of SFRC to have poor fiber dispersion is a function of the maximum size and overall aggregate gradation in the matrix (ACI 544.1R, 2002).

Research had shown that fibers do not affect free shrinkage, but delay the fracture of restrained concrete during shrinkage and improve concrete creep characteristics (Altoubat and Lange, 2001). The addition of steel fibers may also increase the number of cracks that form during shrinkage, due to increased internal stresses, but these crack widths are much smaller than that are observed in plain concrete (ACI 544.1R, 2009).

2.2.1.2 Hardened Concrete Properties

The PCA (2015) reported that the addition of steel fibers at 1.5% volume fraction can increase the flexural strength by 150% and the direct tensile strength by up to 40%. In compression, it was found that the addition of steel fibers increases the ultimate strength between 0% and 15% (ACI 544.1R, 2009). Research also showed that the increase in fiber content does not linearly increase the mechanical properties of the concrete. Very high-volume fractions of steel fibers decrease the compressive strength and maximum ultimate flexural strength, as shown in Figure 2-12 and Figure 2-13 (Mahadik and Kamane, 2014). According to ACI 544.1R (2009), the Poisson's ratio and modulus of elasticity of FRC can be approximated to be equal to non-fibrous concrete until the fiber volume fraction exceeds 2%.

SFRC has tensile capacity after the first crack, so it performs superior in toughness and impact strength as compared to plain concrete. Additions of steel fibers of up to 100 lb/yd^3 drastically increase these properties by enhancing the ductility (Balaguru et. al., 1992). SFRC typically fails when the fibers loose mechanical bondage and pullout from the concrete. Fibers with hooked ends give the best toughness results (Balaguru et. al., 1992).
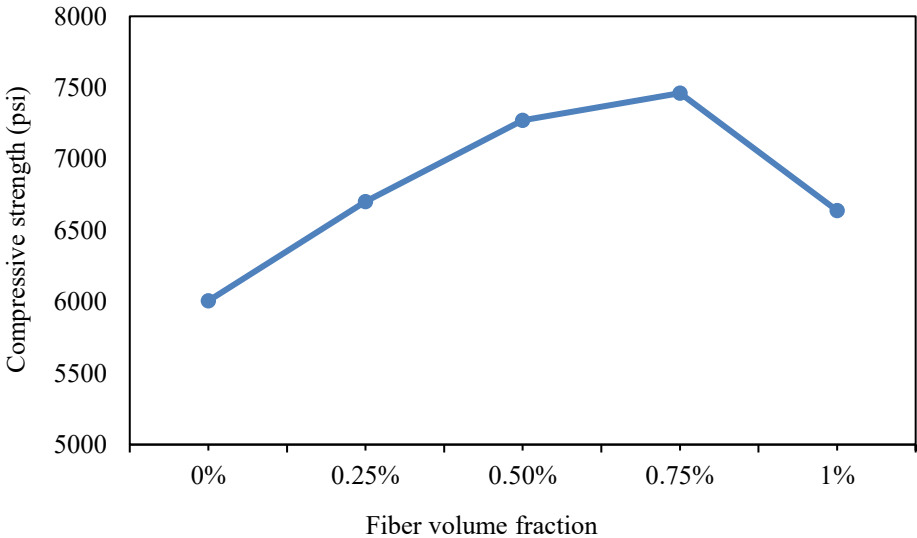
Figure 2-12. Compressive strength versus fiber volume fraction (after Mahadik and Kamane, 2014).
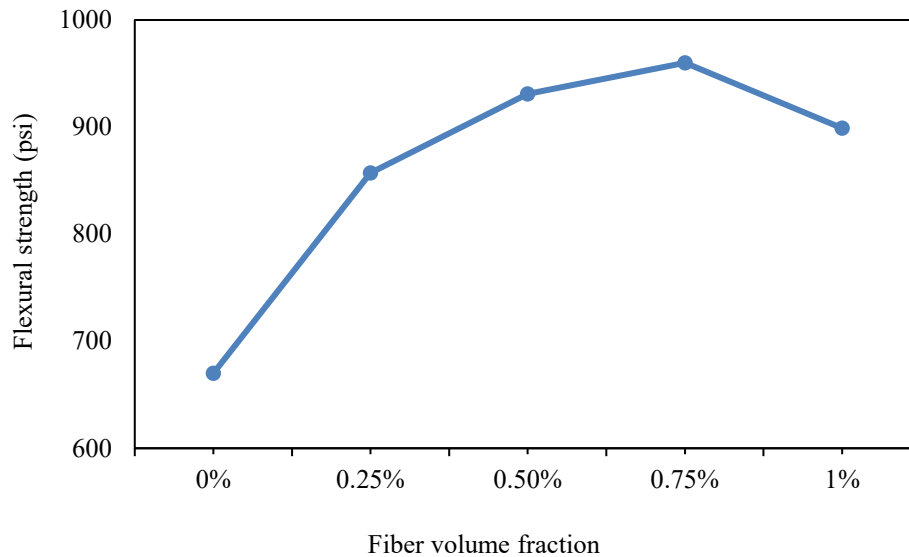
Figure 2-13. Peak flexural strength versus fiber volume fraction (after Mahadik and Kamane, 2014).

Research findings available for freeze-thaw durability of FRC showed that the addition of steel fibers does not significantly affect the end results when compared to plain concrete (Balaguru and Ramakrishnan, 1985). Most of the research available on FRC durability a focused on the corrosion resistance of the fibers (ACI 544.5R, 2010). Currently there are no standards available to evaluate corrosion in SFRC. Like traditional reinforcing bars, high chloride levels primarily cause steel fiber corrosion. ACI recommends limiting chlorine content to less than 0.6 percent by mass; however, research had shown that low carbon content fibers are capable of resisting corrosion when exposed to 2% by mass chloride content in the concrete matrix (Mangat and Gerusamy, 1987). The performance of corroded steel fibers is highly dependent on the value of mass loss in the fibers cross section (Kosa and Naaman, 1990).

2.2.2 Synthetic Fiber Reinforced Concrete (SNFRC)

Structural synthetic fibers are the most commonly used fibers in the paving applications. In a survey conducted in December 2016, as a part of this study, it was found that 94 percent of the FRC concrete overlays in this country were constructed with structural synthetic fibers and only six percent were constructed with steel fibers (mostly in Illinois). An established criterion for selection of synthetic fibers and the corresponding dosages for SNFRC have not yet been developed, but many manufacturers often provide recommendations (ACI 544.1R, 2009) on the dosages. This section provides a discussion on the different properties of synthetic FRC.

2.2.2.1 Fresh Concrete Properties

The addition of fibers generally decreases the workability (e.g., slump value) depending on fiber dosage, aspect ratio, geometry, and a number of other considerations. The reduction in the slump has both advantages and disadvantages in paving application. While the less workability is a problem in achieving the required consolidation, the reduction in workability may increase the cohesiveness of the concrete under the paver, which can improve the slip-form characteristics (Ludirdja and Yougn, 1992). Synthetic

11

fibers placed in concrete at dosages greater than 1.0% V_f tend to form balls, but typically synthetic fibers perform better than steel or glass fibers in these regards (Ludirdja and Yougn, 1992). It was found that the addition of fibers may reduce bleeding, which is believed to be a result of the reduced aggregate settlement and fewer capillary bleed channels. This effect reduces inter-granular pressures and shrinkage cracking (ACI 544.1R, 2009).

2.2.2.2 Hardened Concrete Properties

Structural synthetic fibers have little influence on compressive strength, tensile strength, and modulus of rupture when 0.1% to 0.2% V_f of polypropylene fibers are added in the concrete (Isaa, 2017; Zollo, 1984). In the cracked state, synthetic fiber reinforced concrete had displayed excellent post-crack performance or residual strength and toughness (ACI 544.1R, 2009). The addition of certain synthetic fibers also had a significant effect on the failure mode of specimens in various test procedures. For example, compressive strength specimens with SNFRC tend to fail in a ductile manner and rarely exhibit explosive failure. These specimens can continue to sustain loads well after peak load and endure large deformations (ACI 544.1R, 2009). Research had provided contradictory results for impact strength; where some results showed an increase in impact strength, others showed no increase. On the other hand, improvement in the post-crack performance of SNFRC is one of the biggest arguments for using synthetic fibers in concrete pavements or overlays. Its ability to bond in the concrete greatly affects its post-crack performance. It has been found that twisted collated fibrillated polypropylene fibers or fibers with enlargements at its ends had the best mechanical bond strength (ACI 544.1R, 2009).

Limited research findings are available on the freeze-thaw resistance of SNFRC. Research showed, however, that the addition of synthetic fibers does not completely eliminate concrete degradation due to freeze-thaw damage, deeming it still necessary to air-entrain the concrete in question. To this front, Issa (2017) and Barman (2014) stated that the inclusion of fibers could improve pavement durability against surface scaling.

2.3 RELEVANT RESEARCH STUDIES ON FRC USAGE IN PAVING APPLICATIONS

2.3.1 Illinois

Several synthetic FRC related research studies (Isaa, 2017; Bordelon, 2011; Roesler et al., 2008; Bordelon, 2005) were conducted in Illinois. A number of factors that affect the performance of FRCs were considered, including shape (e.g., straight, crimped and twisted), type, dosage, length, diameter, and aspect ratio of the fibers. Table 2-1 presents the properties of fibers and a few hardened concrete test results for the FRCs prepared with three different synthetic fibers in the Roesler et al. (2008) study. It can be seen that the peak flexural load and modulus of rupture (MOR) slightly varied with the dosage rate, shape, and aspect ratio of the fiber, but a certain trend was not observed. The R^2 for the correlation between the fiber V_f and MOR was 0.14 for the data included in Table 2-1, which indicated that the MOR is not significantly influenced by the properties of structural synthetic fibers. Dosage rates of 4.5 lb/yd^3 in the straight synthetic fiber category and 4.6 lb/yd^3 in the twisted synthetic fiber category seemed to provide the highest peak flexural load and MOR for that study. As shown in Figure 2-14, it appeared that the straight synthetic fibers performed better in terms of MOR than the other two shapes in that particular study. For example, the straight fibers performed better than twisted fibers at 0.30% and 0.50% fiber volume fractions.

Table 2-1. Properties of structural synthetic fibers and FRC in Roesler et al. (2008) study.

Fiber type	Straight synthetic				Twisted synthetic		Crimped synthetic
Cross section	Rectangular				Rectangular		Rectangular
Length (in)	1.57				2.13		2.00
Thickness (in)	0.004				NA		0.03
Width (in)	0.05				NA		0.05
Aspect ratio	90				NA		46
Specific gravity	0.92				0.91		0.91
Volume fraction in the mix (%)	0.19	0.26	0.29	0.58	0.30	0.50	0.40
Dosages used (lb/yd^3)	3.00	4.00	4.50	8.90	4.60	7.70	6.10
Peak flexural load (lb)	6623	5472	9276	8939	8101	6487	8160
Modulus of rupture (psi)	556	456	733	745	675	541	673
Testing age (days)	14	14	14	14	14	14	14

The correlation between fiber V_f and RSR found in a study by Bordelon (2005) is shown in Figure 2-14. The RSR, which is also termed as 'equivalent flexural strength ratio' in ASTM C1609, is determined by a four-point bending test using beam specimens. RSR is expressed using the following equation:

$$RSR = 100 \frac{f_{e,3}}{MOR} \qquad (1)$$

Where, $f_{e,3}$ is the residual strength at mid-span for a deflection up to (span)/150 of a 24-inch (or 22-inch) x 6-inch x 6-inch beam. The span is equal to 18 inches; therefore, the residual strength is measured at a 0.12-inch deflection. It can be seen that the residual load capacity increases with the increase in fiber V_f. Figure 2-15 shows that FRC with 0.58% fiber volume fraction resulted in a greater residual load capacity as compared to the FRCs with 0.26% volume fraction.
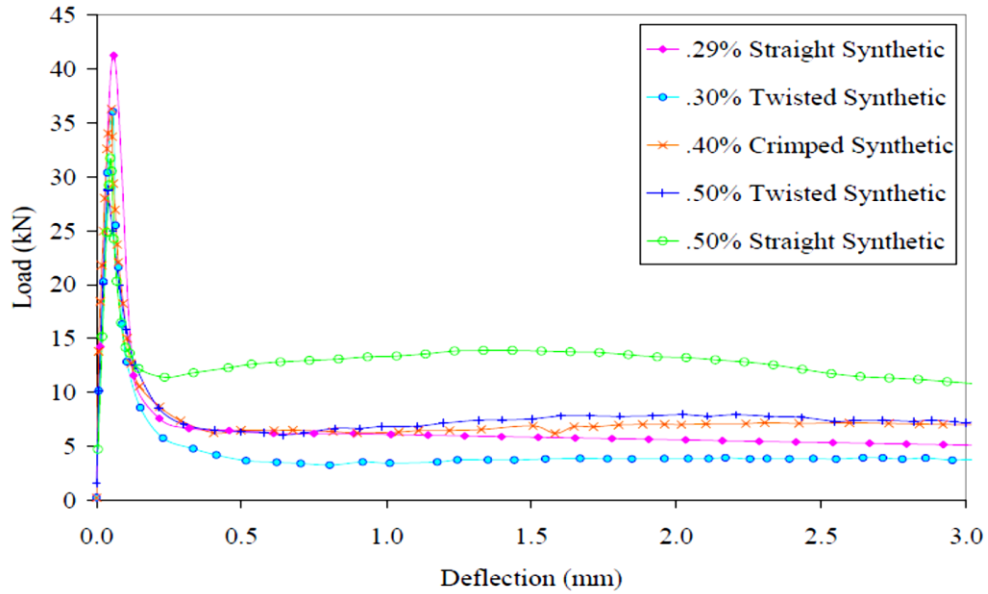
Figure 2-14. Residual load characteristics of different shaped structural synthetic fibers (after Bordelon, 2005)
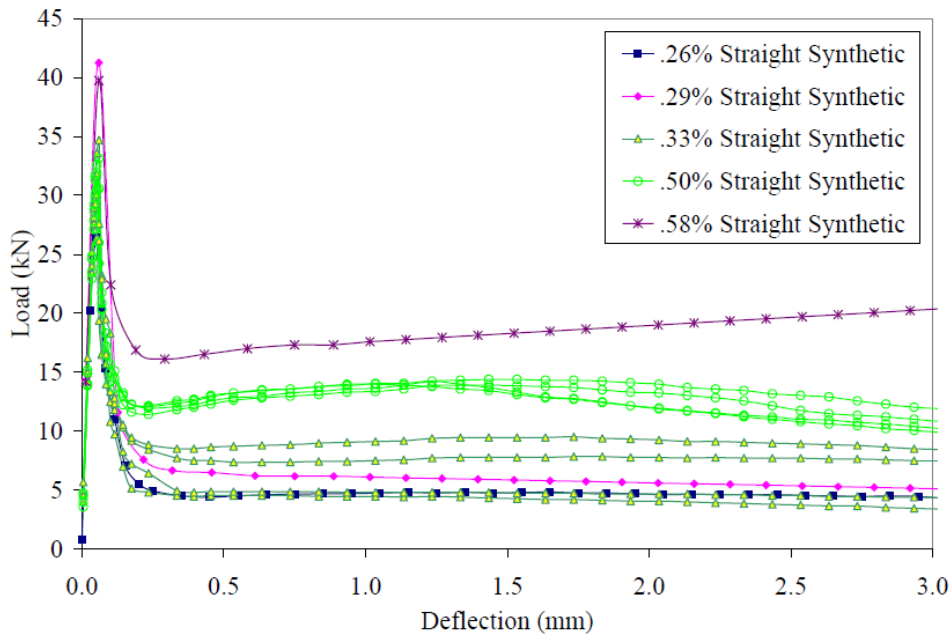
Figure 2-15. Residual load capacities of FRC versus fiber volume fraction for synthetic fibers (after Bordelon, 2005)

Alhassan and Ashur (2012) had conducted a study to identify the potential benefits of synthetic fibers in concrete bridge overlays. These benefits were found to provide a reduction in shrinkage cracking, an increase in toughness, additional post-crack strength, and an increase in crack resistance. Figure 2-16 shows the results of shrinkage versus curing time for various combinations of plain and fiber reinforced concrete mixes. The FRC mixes showed less shrinkage than the plain concrete mix. On an average, the

14

drying shrinkage was found to be 17% lower for FRC mixes than the plain concrete mix. Figure 2-17 shows the flexural test results of FRC mixes prepared with SX fibers mixed at 3 lb/yd^3 fiber dosage for two different curing periods. Table 2-2 shows the results of residual strength for various combinations of FRC mixes. The FRC mix with SX fiber at 3 lb/yd^3 showed higher residual strength than other combinations. This table also presents other hardened concrete properties for the FRC mixes used in the Alhassan and Ashur (2012) study.
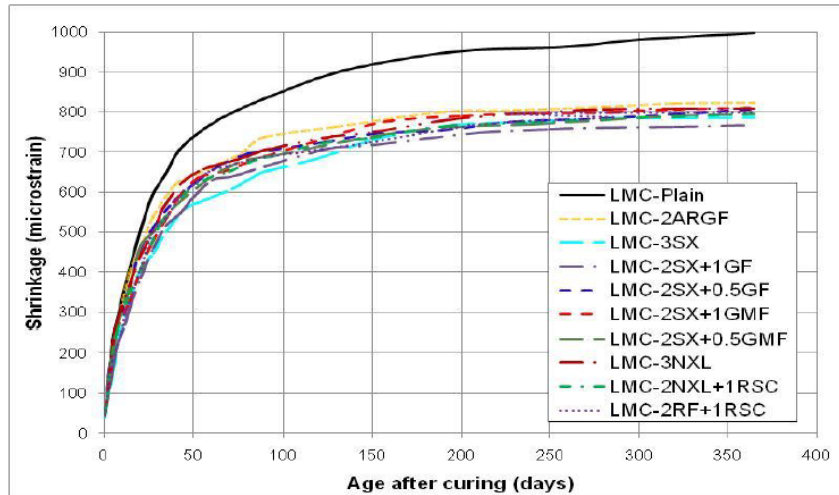
Figure 2-16. Shrinkage versus curing time for plain and FRC mixes in Alhassan and Ashur (2012) study (LMC = latex modified concrete; ARGF = alkali resistant glass fiber; SX= microtype polyolefin fiber; GF = micro type 100% virgin; NXL = macrotype polyolefin fiber; RSC = microtype polyvinyl alcohol fiber; RF = macrotype polyvinyl alcohol fiber).

The study recommended a synthetic fiber content of 3 lb/yd^3 for bridge deck overlays. It was found that higher fiber contents resulted in poor dispersion characteristics with balling and clumping during mixing, placing, and finishing. At a fiber content near to 3 lb/yd^3, drying shrinkage was reduced by up to 15%, and an increase in flexural strength was observed due to internal confinement. It was also recommended that fibers be held between 0.75 inches and 1.75 inches in length.

15
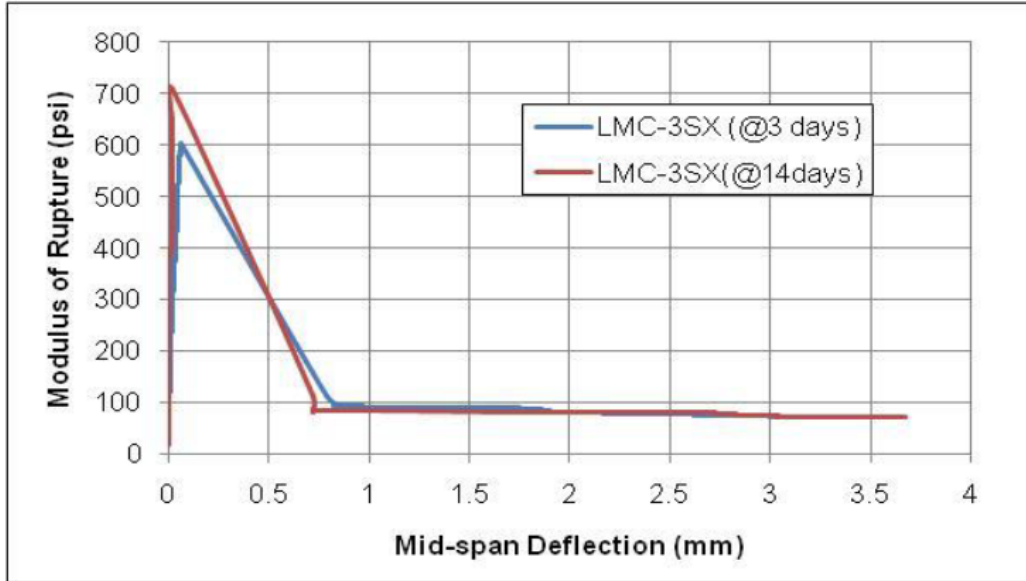
Figure 2-17. Modulus of rupture for fibrous LMC-3SX mix (after Alhassan and Ashur, 2012).

Table 2-2. Hardened concrete properties of the FRC mixes used in Alhassan and Ashur (2012) study.

Mix Design	Compressive strength, psi	Modulus of Rupture, psi	Residual Strength, psi	Residual strength ratio (%)
LMC-3SX	4,420	600	78	13
	6,660	715	78	10.9
LMC-2SX+1GF	4,600	650	52	8
LMC-2RF+1RSC	4,330	600	40	6.7

Isaa (2017) had studied the effect of early-age properties of fiber reinforced concrete on the fatigue damage of concrete pavements. The aim of that study was to minimize the traffic closure times during concrete pavement construction and rehabilitation activities. The study used two types of polypropylene based structural synthetic fibers: straight (Strux 90/40, aspect ratio = 90) – referred to as "F1" and embossed (Master Fiber MAC Matrix, aspect ratio = 67) – referred to as "F2". Two types of mixes were considered in that study: concrete patch mix (PP) and concrete pavement mix (PV). These mixes were prepared with variable fibers dosage such as, 4, 6 and 8 lb/yd^3. Various properties of concrete such as compressive strength, modulus of elasticity, flexure strength and toughness, and load transfer efficiency were studied to investigate the early-age behavior of concrete. Two curing regime temperatures of 45°F and 75°F were utilized, and the samples were tested after 12 hours, 1, 3, 7, and 28 days of curing.

It was found that the synthetic fibers did not have a significant influence on the compressive strength and flexural strength of the PP and PV concrete mixes. The influence of fiber dosages on the flexural toughness was apparent though. Figure 2-18 shows the load versus net deflection relationships for three PV specimens prepared with three dosages of F1 fibers, tested at 14 days. Figure 2-19 shows the toughness versus flexural strength for these specimens. It can be seen that even though the residual load (lbs) at 0.12-inch net deflection look similar, the flexural toughness which depends on the area of the load versus net deflection curves were different and positively influenced by the fiber dosage.
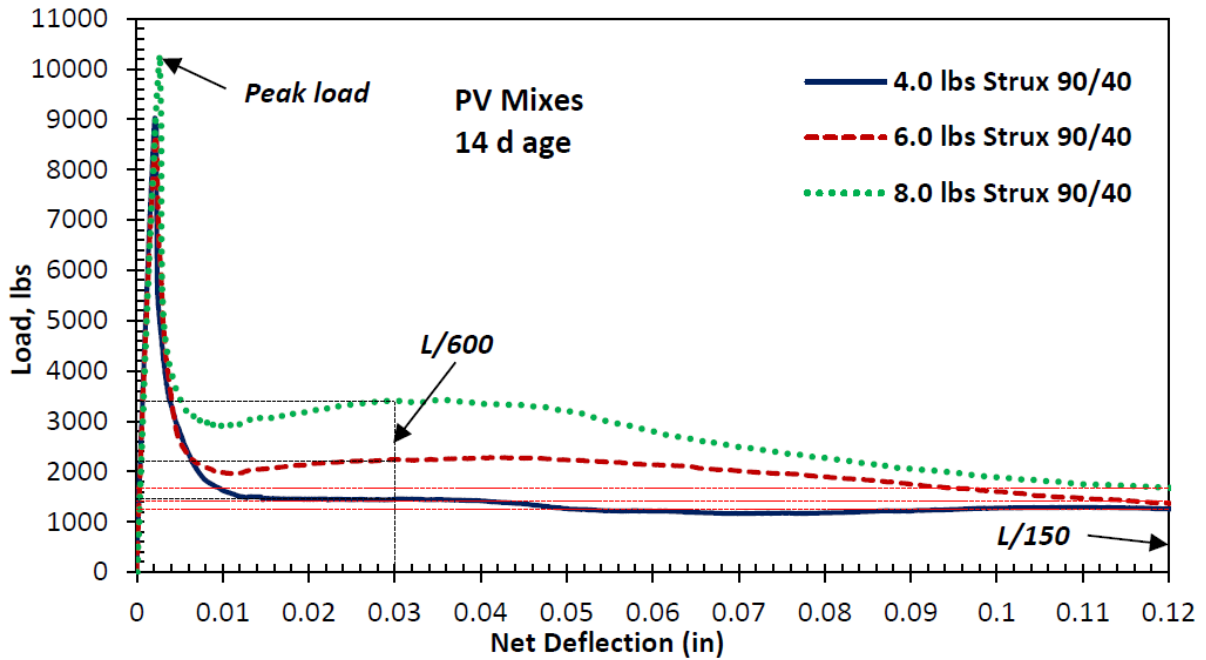
Figure 2-18. Load versus net deflection curves for PVF1 mixes prepared with 4, 6, and 8 lb/yd^3 fiber dosages (after Issa, 2017).
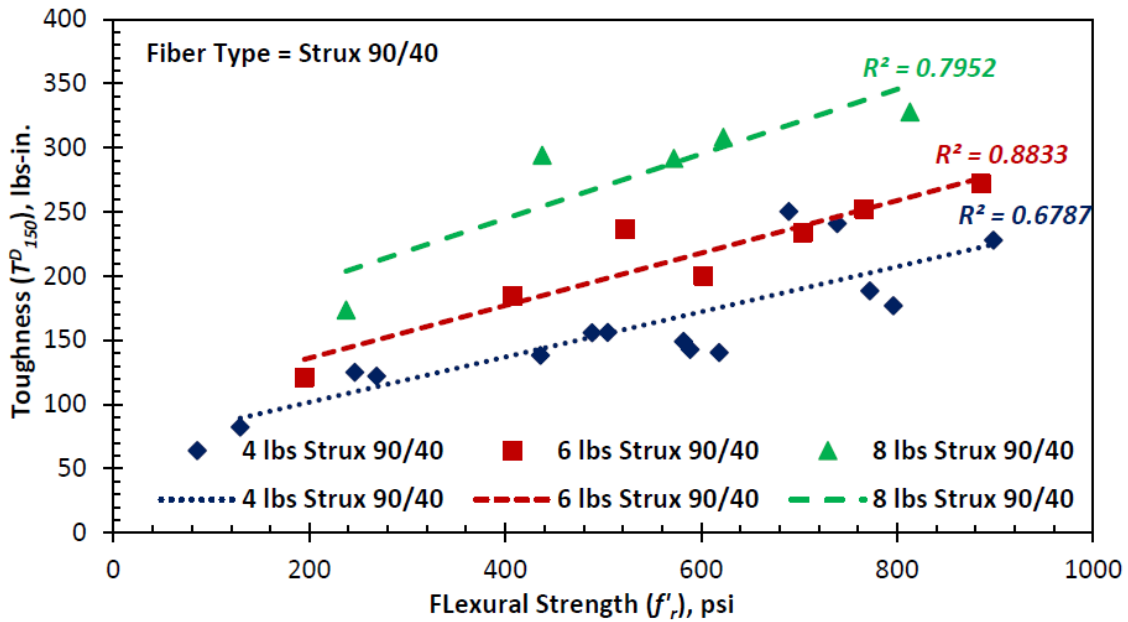
Figure 2-19. Flexural toughness versus flexural strength relationships for PVF1 mixes prepared with 4, 6, and 8 lb/yd^3 fiber dosages (after Issa, 2017).

Figure 2-20 shows toughness versus flexural strength relationships for the PV mixes with F1 and F2 fibers at 4 lb/yd^3 dosage. The mix with F2 fiber showed better flexural toughness than the mix with F1 fiber. The author opined that this could be due to the embossed and deformed texture of F2 (MACMatrix) fiber that had provided better bonding within the concrete mix. Figure 2-21 shows the

results of the relative dynamic modulus (RDM) test performed according to ASTM C666 (rapid freeze-thaw cycles, procedure A) for various specimens among which some were subjected to fatigue loading. These specimens were prepared with 7% entrained air content. All the specimens passed the minimum criteria of 60% RDM irrespective of fiber dosage and fatigue loading. It confirmed the insignificant role of fiber towards the concrete durability against freeze-thaw cycles, and the significance of 7% air content to allow water expansion at freezing temperatures. The mass loss due to freeze-thaw cycles was found to be consistent between the same mixes, irrespective of fatigue loading and ranged from 0.74% to 1.65% for all mixes. It was also found that the mixes with a higher dosage of synthetic fibers showed increased resistance to scaling.
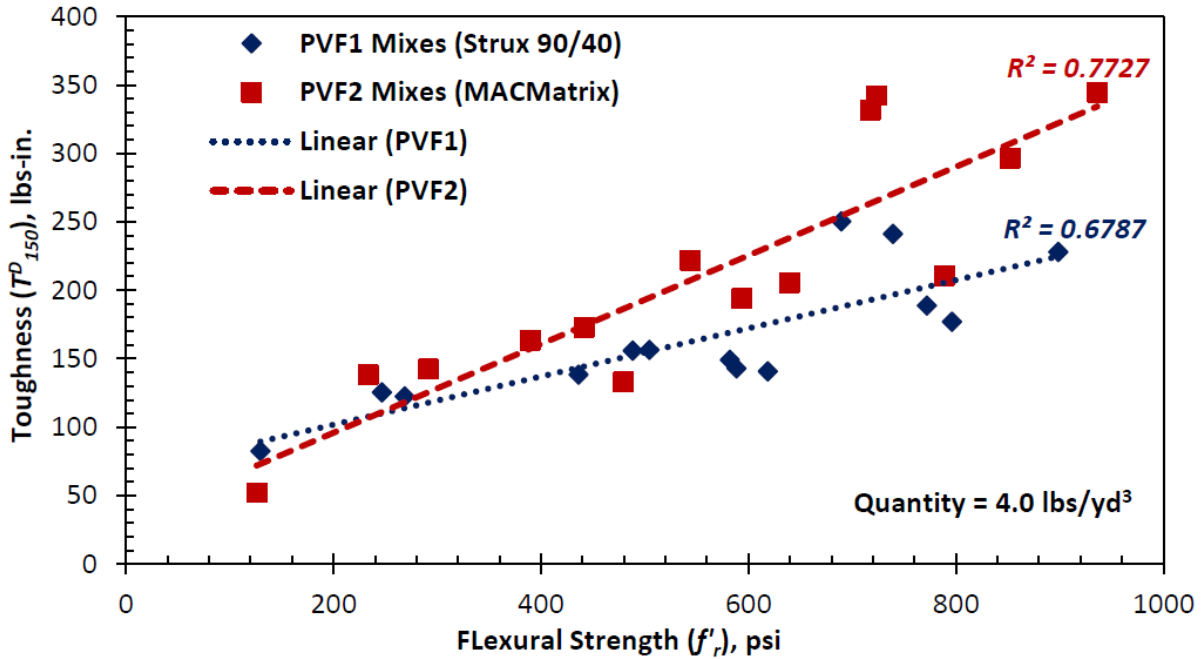
Figure 2-20. Flexural toughness versus flexural strength relationships for PVF1 and PVF2 mixes prepared with 4 lb/yd³ dosage (after Issa, 2017).
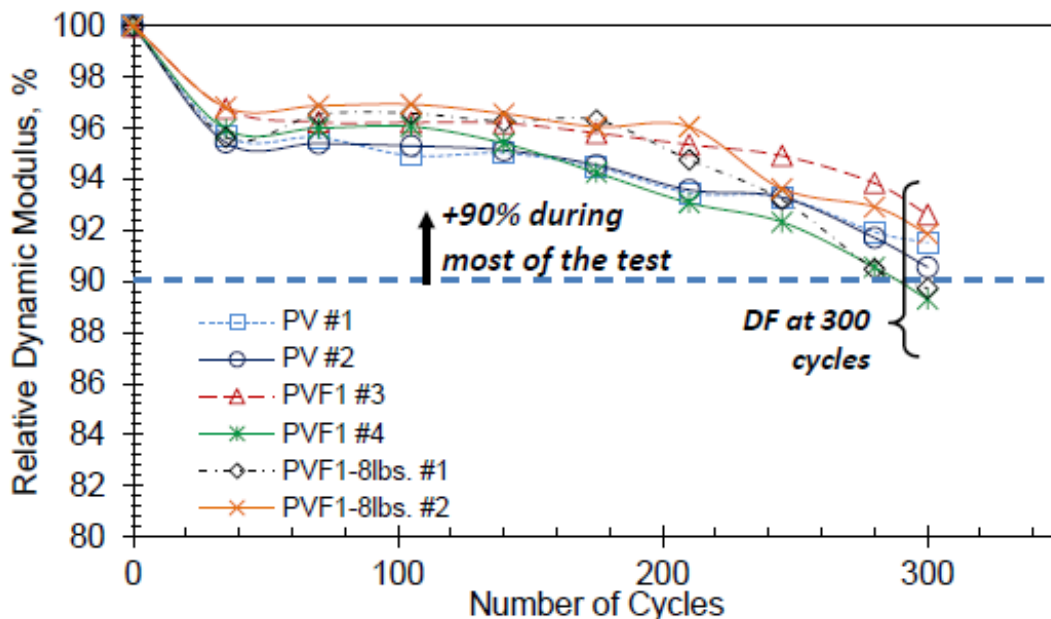
Figure 2-21. Relative dynamic modulus (RDM) versus number of F-T cycles for various PVF1 mixes (after Issa, 2017).

Flexural fatigue testing was conducted on 21-inch x 6-inch x 6-inch beams for all mixes with and without fibers. Cyclic loading at 4 Hz. frequency was applied using a four-point bending configuration. Specimens were tested at 12 hours, and 1, 3, and 7 days. The stress levels considered in fatigue tests were 0.9, 0.8, 0.7, and 0.6 for all the mixes. Based on the fatigue test results, the following conclusions were made:

(i) Concrete at 12 hours can exhibit bond failure in flexural fatigue due to low mortar strength;

(ii) The introduction of higher amounts of fibers (e.g., 8 lb/yd^3) can improve fatigue life for a stress level of 0.6 even at 12 hours;

(iii) Cement paste can gain bond strength at 24 hours to improve the fatigue performance when higher amounts of fibers (e.g., 8 lb/yd^3) are used;

(iv) S-N curves showed that mixes with 8 lb/yd^3 fibers fail at a higher number of load cycles for any given stress level, when compared with the plain-concrete PV mixes;

(v) The two fibers considered in the study did not present any significant difference in fatigue performance when compared to plain-concrete PV mixes;

(vi) A dosage of 4 lb/yd^3 of fiber may not be enough to provide any considerable fatigue resistance at early-age.

2.3.2 Louisiana

The Louisiana Transportation Research Center (LTRC) conducted research investigating the fatigue and toughness characteristics of FRC (Kevern et al., 2016). This study evaluated the use of polypropylene fibrillated, polypropylene macro, carbon, and steel fibers as primary reinforcement in concrete pavements. The properties of the fibers are provided in Table 2-3. Figure 2-22 shows pictures of the different fibers used in that study. In general, it was found that the polypropylene fibers performed better than the steel fibers against fatigue when used in the correct dosages. Regarding the toughness

of the concrete, this study suggested that fibers with high tensile strength result in better residual load carrying capacity and carry a greater load at larger deflections.

Figure 2-22. Fibers used in the Kevern et al. (2016) study: polypropylene fibrillated fiber (left), polypropylene macro fiber (left middle), carbon fiber (right middle) and steel fiber (right).

Table 2-3. Properties of fibers in Kevern et al. (2016) study.

Fiber Type	Specific Gravity	Length (in.)	Tensile Strength (ksi)
Polypropylene Fibrillated	0.91	1.50	83-96
Polypropylene Macro	0.91	2.25	83-96
Carbon	1.70	4.00	600
Steel	7.85	2.00	152

The fatigue property of the concrete was studied by applying a cyclic load on the pre-notched beam specimens as per the RILEM procedure developed by Jenq and Shah (1985). Pre-notched fatigue testing showed that both the tensile strength and length of fibers influenced the fatigue properties of fibers. This study provided the following conclusions: (i) polypropylene fibrillated fibers offer increased fatigue performance in general, but they do not offer any significant post-crack performance, (ii) polypropylene macro fibers used at a dosage between 7.5 lb/yd^3 and 10.5 lb/yd^3 provided the greatest combination of fatigue, toughness and pre-notch fatigue performance, and (iii) the use of fiber reinforcement can result in a reduced pavement thickness.

2.3.3 Pennsylvania

The University of Pittsburgh (Barman et al., 2015; Barman, 2014) conducted a finite element based study for bonded concrete overlay on asphalt (BCOA) to investigate the load transfer shared by the asphalt layer and the concrete overlay. It was found that 68% to 95% of the wheel load is transferred through the asphalt layer and the remaining load is transferred by the concrete slabs. The better the asphalt structure, the better the load transfer contribution of asphalt layer. Even though a significant percentage of the load is transferred by the asphalt layer, it is very important to achieve the load transfer through the concrete slabs, especially to reduce the interlayer debonding. It was found that the debonding can increase the magnitude of the critical stress by a maximum of 40% to 55% (Barman et al., 2017).

In order to understand the contribution of structural fibers in increasing the LTE, a comprehensive laboratory study was conducted by Barman and Vandenbossche (Barman, 2014). A small-scale LTE test procedure was developed with a vision to make the LTE evaluation task very simple and economical so

that the test can be conducted using readily available laboratory resources or with a marginal cost. In the small-scale procedure, the LTE of concrete can be evaluated by using conventional 24-inch x 6-inch x 6-inch beam specimens. The test setup was designed to replicate the abrasive action that occurs on the joints of in-service concrete pavements loaded with an 18-kip single axle load. The loading configuration in the small-scale test procedure was established using a finite element analysis. The small-scale test results were validated by comparing them with the LTE results from a large-scale study in which full-size slabs were used to test the LTE. The LTE of plain and fiber reinforced concretes were compared in the laboratory study. Two types of structural synthetic fibers were used in that study: (i) straight synthetic fibers - Strux 90/40, and (ii) crimped synthetic fibers - Enduro 600. Fiber dosages were selected based on the 20% residual strength ratio criteria as suggested in Roesler et al. (2008) study. The volume fraction and dosages of the two fibers mentioned above are provided in Table 2-4. The LTE test results indicated that the straight synthetic fibers (Strux 90/40, see Figure 2-8*a*) and crimped synthetic (Enduro 600, see Figure 2-8*b*) exhibited somewhat similar LTE versus crack width relationships. Overall, it was found that the structural fibers could increase the LTE of the concrete. FRC prepared with 5.25 to 6.5 lb/yd^3 of structural synthetic fibers were able to provide 20% more load transfer than their plain concrete counterparts. As anticipated, LTE of FRC decreases with the increase in crack width and number of load applications; however, the structural synthetic fibers did not experience significant deterioration even after as much as 10 million load repetitions. The abrasion of the crack faces under the load repetitions were the main reason for the drop in the LTE. Also, the length of the fibers was sufficient enough, as neither of the two fiber types was found to be pulling out of the concrete, even after millions of load applications.

Table 2-4. Volume fraction and dosages of two selected fibers in Barman (2014) study

Straight synthetic, STRUX: 90/40, 1.55-inch long		Crimped synthetic, Enduro 600, 2 inch long	
Volume fraction (percent)	Dosage (lb/yd^3)	Volume fraction (percent)	Dosage (lb/yd^3)
0.36	5.25	0.43	6.20

2.3.4 Utah

The age-dependent flexural properties of fiber reinforced concrete were studied by Kim and Bordelon (2016). This study investigated whether the fiber type, length, aspect ratio, or volume fraction influence the changes in flexural properties of FRC versus age relationship. Two types of steel fibers and two types of synthetic fibers were considered in that study.

Table 2-5 presents the properties and Figure 2-23 shows the photographs of the fibers used in that study. The variations in the residual strength ratio over time were investigated by performing ATSM C1609 test at 3, 7, 14, 28, 56, and 90 days. Two different dosages of fibers, such as 0.5% and 1.0%, were considered for all the four types of fibers. Figure 2-24 shows the trends of the flexural load versus deflection. It can be seen that steel and synthetic fiber reinforced concretes exhibited deflection hardening and deflection softening responses, respectively. In general, the steel fiber reinforced concrete showed larger variation in the post-crack performance compared to the synthetic fiber reinforced concrete.

Table 2-5: Properties of fibers used in Kim and Bordelon (2016) study.

Fiber Type	Short Steel	Long Steel	Long Polymeric	Slender and Long Polymeric
Material	Hooked steel	Hooked steel	Polypropylene	Polypropylene-polyethylene
Cross section	Circular	Circular	Rectangular (bi-tapered)	Rectangular (straight)
Length	35 mm	60 mm	50 mm	40 mm
Diameter	0.55 mm	0.9 mm	-	-
Thickness	-	-	0.4 mm	0.11 mm
Width	-	-	1.2 mm	1.4 mm
Aspect ratio	65	65	75	90
Tensile strength	1345 MPa	1160 MPa	550 MPa	620 MPa
Elastic modulus	210 GPa	210 GPa	7.0 GPa	9.5 GPa
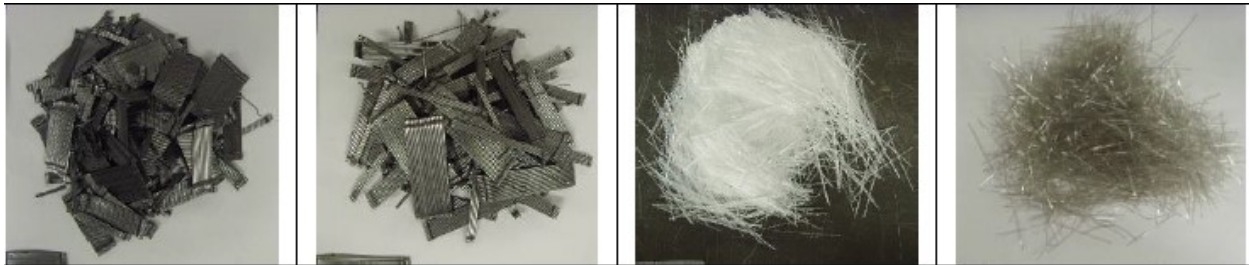
Figure 2-23: Photographs of fibers used in Kim and Bordelon (2016) study.
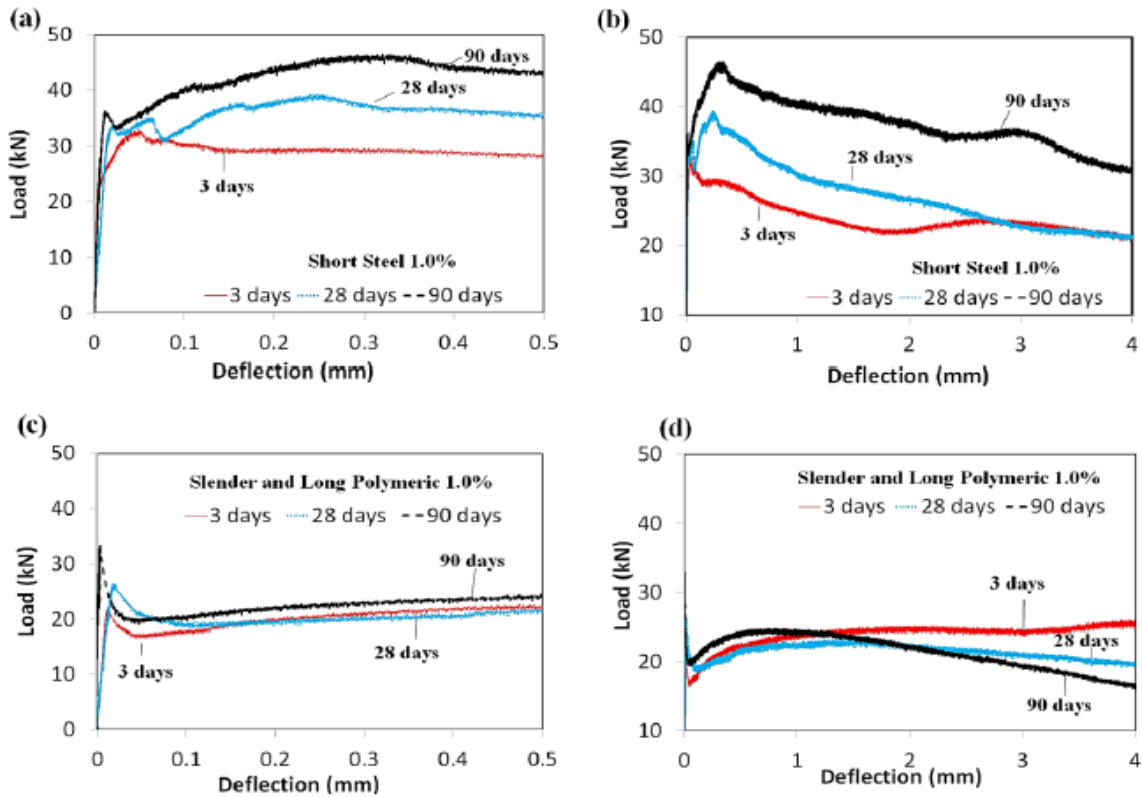
Figure 2-24. Typical flexural load versus deflection of a beam containing either (a) and (b) short steel FRC or (c) and (d) slender and long polymeric FRC; each at 1.0% volume fraction. Plots show both the smaller deflection values (on left) and full deflection test range (on right) (after Kim and Bordelon, 2016).

Figure 2-25 shows the relationship between the residual strength ratio and curing period. It can be seen that the RSR decreased with the curing period. The reason for this may be the fact that the concrete gained more overall flexural strength (such as MOR) than the residual strength with time. This resulted in a decrease in the RSR with the time. This study also suggested that high fiber volume fraction and long fibers increases the post-crack performance and RSR of the concrete, whereas, the aspect ratio can show an opposite trend. Thinner fibers were more likely to fail before complete pull-out resistance is reached. The findings from the study concluded that concrete that cracks at early age may yield more benefits due to the addition of fibers than those cracks at a later stage.

24
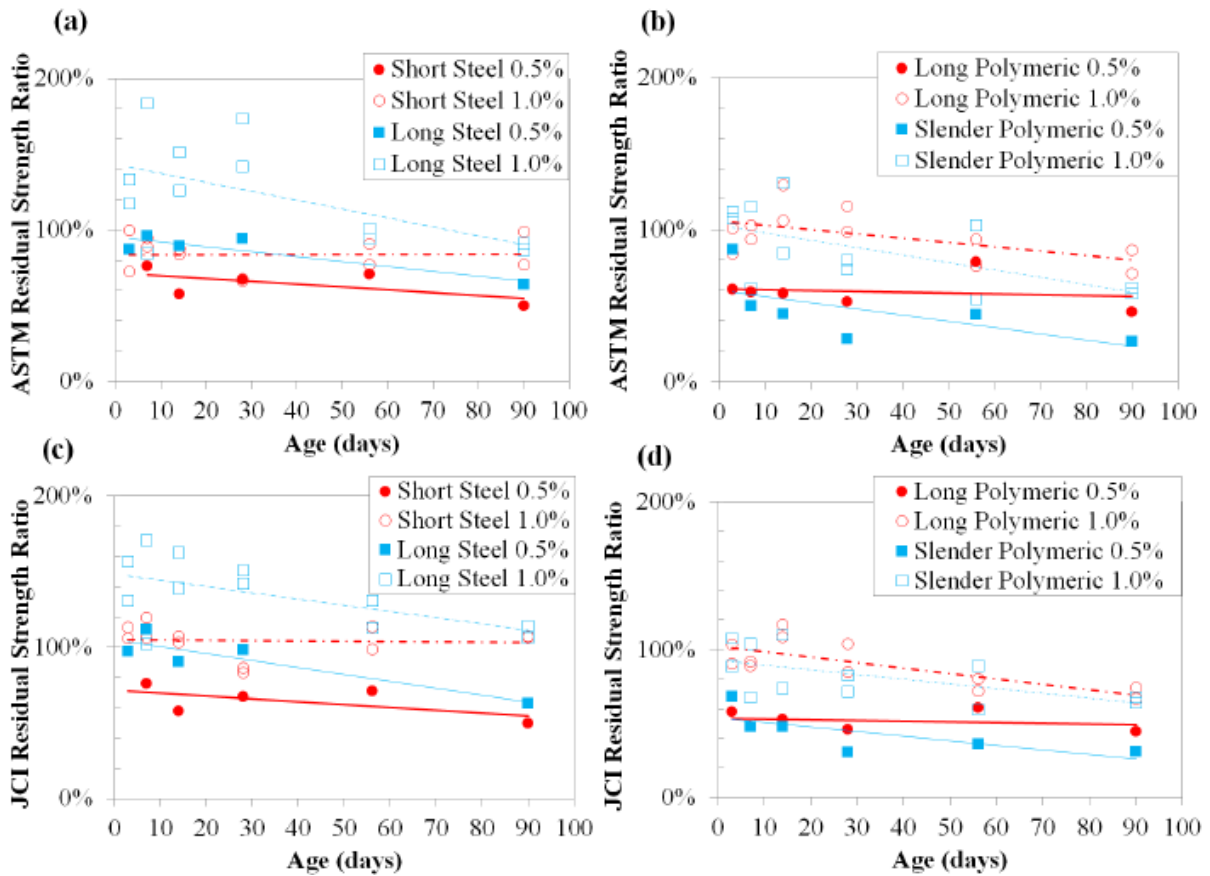
Figure 2-25. Effect of fibers on ASTM or JCI residual strength ratio for steel fiber reinforced concrete (a, c) and synthetic fiber reinforced concrete (b, d) (after Kim & Bordelon, 2016).

CHAPTER 3: FIBERS IN THIN CONCRETE PAVEMENTS AND OVERLAYS

This chapter reviews the performance of various FRC overlays constructed in the United States. Field performance data related to the application of FRC in thin and ultra-thin concrete overlay projects in the United States was collected through an online survey conducted in December, 2016. An example of the survey questionnaire is provided in the Appendix. The survey initially started with the American Concrete Pavement Association's (ACPA's) interactive online database and led to direct communication with local ACPA chapters and state DOTs. The states like Georgia, Illinois, Iowa, Kansas, Virginia, and Oklahoma were included in this this survey. Information on the Minnesota's FRC concrete overlay projetcs was collected from the relevant MnDOT publications. The following subsections summarize the features of various concrete overlay projects and details of the structural fibers associated with those projects.

3.1 GEORGIA

Many ultra-thin overlays were placed in Georgia as early as 1998, and FRC was used in the projects constructed between 2003 and 2010. Table 3-1 presents the location, year of construction, thickness, fiber types, and dosages for these projects. It was found that all of these projects were constructed using polypropylene fibers at a dosage rate of 3 lb/yd^3. No information was available about the fiber geometry or performance of the fibers in these projects; however, the qualified fibers specification of the Georgia DOT was collected and summarized in Table 3-2. Photographs of many of these fibers collected from the websites of the fibers' manufacturers are provided in the Appendix as well.

Table 3-1. Fiber reinforced overlay projects in Georgia (Wouter, 2016).

Project Name	Location	Year Const.	Thickness (inch)	Dosage (lb/yd^3)	Fiber type
US80 / SR26	Chatham	2007	4	3	Polypropylene
SR204	Chatham	2007	4	3	Polypropylene
SR196 / SR119	Liberty	2005	4	3	Polypropylene
US 82 / US 84	Ware	2003	4	3	Polypropylene
SR 99	Glynn	2008	4	3	Polypropylene
SR4 & Woodlawn	Appling	2007	4	3	Polypropylene

Table 3-2. Approved macro-synthetic fibers for concrete reinforcement for Georgia DOT (Wouter, 2016).

Source	Fiber trade name	Length (inch)	Aspect ratio, specific gravity, modulus of elasticity (ksi),tensile strength (ksi)
ABC Polymer Industries	(i)Tuf-Max DOT[TM] (ii) Performance Plus DOT[TM]	1.5 or 2.0	(i) N/A, 0.91, 800, 70 (ii) N/A, 0.91, 800, N/A
BASF Corporation	(i) MasterFiber® MAC 100 (ii) MasterFiber® MAC Matrix	(i) 1.5 (ii) 2.1	(i) 59, 0.91, N/A, N/A (ii) 70, 0.91, N/A, 85
Elasto Plastic Concrete	Bar chip 48 (BC48)[TM]	1.89	N/A, 0.90-0.92, 1450, 93
The Euclid Chemical Corporation	Tuf-Strand SF[TM]	2	74, 0.92, 1380, 87-94
Forta Corporation	FORTA-FERRO®	1.5 or 2.25	N/A, 0.91, N/A, 83-90
Propex Operation Co., LLC	NOVOMESH® 950	1.8-varies	N/A, 0.91, N/A, N/A
W.R. Grace	Strux® 90/40	1.55	90, 0.92, 1378,90

N/A: information not available; all of the above-mentioned are structural synthetic fibers.

3.2 ILLINOIS

Illinois Department of Transportation has used fiber reinforced concrete in approximately 25 ultra-thin and thin concrete overlay projects. Table 3-3 presents various details including overlay thickness, traffic, fiber type, and dosage for some of these projects. It was found that the thickness of these projects varied from 2 to 6 inches with the most common thickness of 4 inches. A majority of the projects used synthetic fibers at a dosage range between 3 lb/yd^3 and 7.5 lb/yd^3, except for few projects with steel fibers at a dosage range between 40 lb/yd^3 and 80 lb/yd^3. Based on the data collected through the survey (Personal communications: Wienrank, 2017 and Riley, 2016) and from a King and Roesler (2014) report, it was found that fibers showed to reduce slab migration and joint separation, faulting, and increased ride quality. Figure 3-1 shows one of such projects (North Lorang Road, Kane County) with a 4.5-inch thick FRC overlay and 4lb/yd^3 synthetic fiber, which is still excellently performing and even exceeded the design life expectations, even though it carries approximately 120 quarry trucks per day. The structural fibers have kept the joints tight and reduced the rate of crack deterioration. This overlay also did not experience any slab migration (Personal communication: Riley, 2016). Based on the King and Roesler (2014) study, a few overlays in which fibers were not used experienced slab migration, as shown in Figure 3-2. It was also found that a loss of bond at the overlay and asphalt interface was the cause for some distresses in the non-fiber reinforced concrete overlays. The poor load transfer at the joints likely resulted in joint deteriorations. As mentioned above, the contribution of the synthetic fibers was well recognized in Illinois. The Illinois DOT has approved several synthetic fibers for use in thin concrete overlays. The list of these fibers is presented in Table 3-4.

Table 3-3. Details of FRC Overlay Projects in Illinois (Riley, 2016; ACPA, 2016; King and Roesler, 2014)

Project Name	Location	Year of Const.	Overlay Thickness (inch)	Average Daily Traffic	Fiber type	Brand	Dosage (lb/yd^3)	Aspect Ratio
Stage Coach Trail Rd.	Stephanson County	1998	3	4500	Synthetic	N/A	3	N/A
N/A	Mendota	1999	4.5	N/A	Steel	N/A	80	N/A
Marion Street	Oak Park	2001	4	3470	Steel	N/A	40	N/A
Jefferson streel Hybrid	Peoria	2002	3	12600	Synthetic	N/A	3	N/A
Cook County Hwy. dept.	Chicago	2003	4	N/A	Synthetic	N/A	N/A	N/A
Il DOT Dist. Parking Lot	Schaumburg	2004	2,3,4,6	N/A	Synthetic	N/A	N/A	N/A
CO HW 6 Xenia Lola Rd	Clay County	2010	5	700	Synthetic	GRT Advantage	4	N/A
Tower Hill	Shelby County	2010	5	1650	Synthetic	GRT Advantage	4	N/A
Western University Dr.	Village of Lombard	2011	5	6700	Synthetic	GRT Advantage	4	N/A
Il Route Old 66	N/A	2012	4	8600	Synthetic	Strux 90/40	4	90
North Ind. Dr.	Village of Lombard	2014	4	3100	Synthetic	Strux 90 /40	4	90
South Michigan Ave. Bus stops	Chicago	2004	4	Bus pads	Synthetic	N/A	4	N/A
Kaneville Quarry entrance	Kane County	2004	4.5	80-120 gravel trucks	Synthetic	N/A	4	N/A
Lake St. Glenview	Cook County	2004	4	27600	Synthetic	N/A	7.5	N/A
Shank Ave	Mundelein	2005	4	11700	Synthetic	N/A	4	N/A
Macomb	Macomb	2009	4	Commercial traffic	Synthetic	N/A	4	N/A
Logan Co Hwy	Logan Co.	2009	5.25	N/A	Synthetic	N/A	4	N/A
Gladstone	Henderson	2010	5	800	Synthetic	N/A	4	N/A
County HW 9	Richland CO.	2010	5.5	550	Synthetic	N/A	4	N/A
Left Ramp	Gilman	2011	4	N/A	Synthetic	N/A	7.5	N/A
Finley Rd.	Village of Lombard	2012	5	N/A	Synthetic	N/A	4	N/A
53 North Bound	Wilmington Center Point	2012	4	1350	Synthetic	N/A	4	N/A

N/A: Information not available; all of the above-mentioned are structural synthetic fibers.

Figure 3-1. Picture of an excellently performing FRC overlay, North Lorang Road, Kane County, IL (King and Roesler, 2014).

Figure 3-2. Slab migration at the outside longitudinal joint of an overlay project (no fiber) in Illinois (Schank Avenue, Mundelein: (King and Roesler, 2014))

Table 3-4. Qualified product list of synthetic fibers for Illinois DOT (September 2, 2016).

Source	Fiber Trade Name	Length (inch)	Aspect ratio, specific gravity, modulus of elasticity (ksi),tensile strength (ksi)
General Resource Technology	Advantage structural fiber	1.5 or 2	N/A, 0.91, N/A, 70
Propex	Fibermesh 650	Graded	96.5, 0.91, N/A, 70
ABC Polymer Industries	Tuf-Max DOT™	1.5 or 2	N/A, 0.91, 800, 70
BASF Corporation	MasterFiber® MAC Matrix	2.1	70, 0.91, N/A, 85
The Eucild Chemical Company	Tuf-Strand SF™	2	74, 0.92, 1380, 87-94
Forta Corporation	FORTA-FERRO®	1.5 or 2.25	N/A, 0.91, N/A, 83-90
GCP Applied Technology	Strux® 90/40	1.55	90, 0.92, 1378,90

N/A: Information Not Available

3.3 IOWA

The Iowa DOT has a significant history of using concrete overlays as a rehabilitation technique, but has limited fiber reinforced overlay projects on record. One known project exists on SH-13 north of Manchester, IA and includes multiple research sections that utilize multiple fiber types (monofilament, fibrillated, and structural at 1, 3 and 3 lb/yd^3, respectively). The overlay was constructed in 2002 and has needed very minimal repairs as of 2014. Later studies showed significant bonding between the asphalt and overlay even though it was designed as an unbonded overlay (Fick and Harrington, 2014).

3.4 KANSAS

Several projects utilizing FRC were identified in Kansas that had mixed success. Several projects showed little distress while others exhibited faulting, spalling, and panel cracking. These projects used polypropylene fibers at a typical dosage rate of 3 lb/yd^3. Table 3-5 presents a list of these projects and the known applicable data. As of 2015, Kansas DOT has approved Tuf-Strand SFTM by Euclid Chemical Co. and Strux 90/40 by W.R. Grace & Company for use in their concrete overlay projects.

3.5 MINNESOTA

The state of Minnesota has a long history of using bonded and unbonded concrete overlays to rehabilitate its roadways. There are, or had been, approximately 11 cells at MnROAD where fiber-reinforced thin and ultra-thin concrete overlays were constructed, observed, and tested until 2016; seven more cells were constructed during June to September of 2017. A test section was also constructed on US-169 near Elk River in 1997 on a very thin asphalt layer, which provided a good

conclusion on the minimum allowable thickness of the existing asphalt layer. See Table 3-6 for a list of known projects in Minnesota constructed with structural synthetic fibers.

3.5.1 MnROAD Cells 93, 94, 95 and 96

In 1997, six bonded concrete overlay cells (Cells 92 to 97) were built on I-94 at the MnROAD pavement test facility that used polypropylene and polyolefin fiber reinforced concrete. Among these cells, Cell 93, 94, and 95 were ultra-thin cells (slab thickness 4 inch and below). The performances of these ultra-thin cells, and the other three thin cells, were found to be directly related to traffic volume, joint spacing, and interface bonding. The importance of keeping the longitudinal joints away from wheel paths was understood from the performance data of these projects (Burham, 2005). To evaluate the contribution of fibers in the performance of the overlays, the load transfer efficiencies of the two cells (Cell 94 and 95) were compared in this section. Cell 94 was constructed with non-structural polypropylene fibers, and Cell 95 was constructed with structural polyolefin fibers. Figure 3-3 shows a picture of the two types of fibers used in Cell 94 and 95. Joint LTE data for these two cells were compared to determine whether the slabs in Cell 95 exhibited higher LTEs than the slabs of Cell 94. It can be seen in Figure 3-4 that the LTEs in Cell 95 were always higher than the LTEs in Cell 94. Another observation was that the contribution of the fibers was greater in the winter when the crack width was larger. The slabs with structural fibers had tighter joints than those with the non-structural fibers. The non-structural fibers could not keep the crack width narrower because of their low stiffness and tensile strength. During the summertime, when thermal expansion forced the joints to be relatively tight, the LTE for the two cells did differ significantly. Therefore, it can be concluded that structural fibers contributed to increasing LTE, but non-structural fibers did not appear to provide any benefit to the slabs.

It shall be noted that Cell 95 was constructed with a fiber content that was much higher than the other projects reported in this study, which may not be cost effective for larger projects. It was also found that Cell 96, which was adjacent to Cell 95 and contained 25 lb/yd^3 polyolefin fibers, developed joint faulting, leading to diamond grinding in the 14th year of service. The exact reason of the joint faulting is not known, but the high fiber content in the concrete mixture might have accelerated the deterioration of the joints (Burnham and Andersen, 2015). However, Cell 96 remains in service with further repair and maintenance works.

Table 3-5. Concrete overlay projects in Kansas (ACPA, 2016).

Project Name	Location	Year Const.	Overlay Thickness (inch)	Average Daily Traffic	Fiber Type	Dosage (lb/yd^3)	Comments
UTW 21st street East Witten berg	Topeka	1997	2, 3	1640	Polypropylene Structural	3	2" section has fair cracking. Bottom 1/3 of 3" is badly cracked
UTW Mission Road 83rd street NB appr.	Prairie Village	1998	3	17500	Polypropylene Structural	3	Overall the UTW is in good condition.
UTW Nieman rd 47th St.	Shawnee	1998	3	6100	Polypropylene Structural	3	Excellent Condition
UTW Quivira rd. and Johnson Drive	Shawnee	1997	3	11720	Polypropylene Structural	3	Good
UTW US 24, Rochester rd. to Kansas ave.	Topeka	1998	3.5	17400	Polypropylene Structural	3	Significant distress near Rochester rd. intersection. Several sections have been replaced
Rehabilitation US504 Lola and La Harpe	Lola	2000	2.8	4750	Structural	N/A	Significant faulting, some greater than ¼ inch. Significant cracking and spalling
UTW central Ave. East 119th	Wichita	1999	3	5700	Polypropylene Structural	3	Excellent. Some patching accomplished
UTW intersection Quivira amd 65th	Shawnee	2000	3	14000	Polypropylene Structural	3	Good. Distress is minimal.

N/A: Information not available

Table 3-6. Fiber reinforced UTW and TWT projects in Minnesota (Vandenbossche and Rettner, 1998; Vandenbossche, 2003)

Project Name	Location	Year Const.	Overlay Thickness (inch)	Average Daily Traffic	Fiber Type	Brand	Dosage (lb/yd³)	Aspect Ratio
Cell 92	MnROAD	1997	6	14000	Polypropylene (non-structural)	Propex Fibermesh	3	N/A
Cell 93	MnROAD	1997	4	14000	Polypropylene (non-structural)	Propex Fibermesh	3	N/A
Cell 94	MnROAD	1997	3	14000	Polypropylene (non-structural)	Propex Fibermesh	3	N/A
Cell 95	MnROAD	1997	3	14000	Polyolefin (structural)	3M	25	50
Cell 96	MnROAD	1997	6	14000	Polyolefin (structural)	3M	25	N/A
Cell 97	MnROAD	1997	6	14000	Polypropylene (non-structural)	Propex Fibermesh	3	50
Cell 160	MnROAD	2013	5	28000	Synthetic (structural)	Propex Fibermesh	6.5	N/A
Cell 161	MnROAD	2013	5	28000	Synthetic (structural)	Propex Fibermesh	6.5	N/A
Cell 162	MnROAD	2013	4	28000	Synthetic (structural)	Propex Fibermesh	6.5	N/A
Cell 163	MnROAD	2013	4	28000	Synthetic (structural)	Propex Fibermesh	6.5	N/A
US - 169	Elk River	2013	3	16000	Varies: Polypropylene / polyolefin (structural & non-structural)	varies	3	50
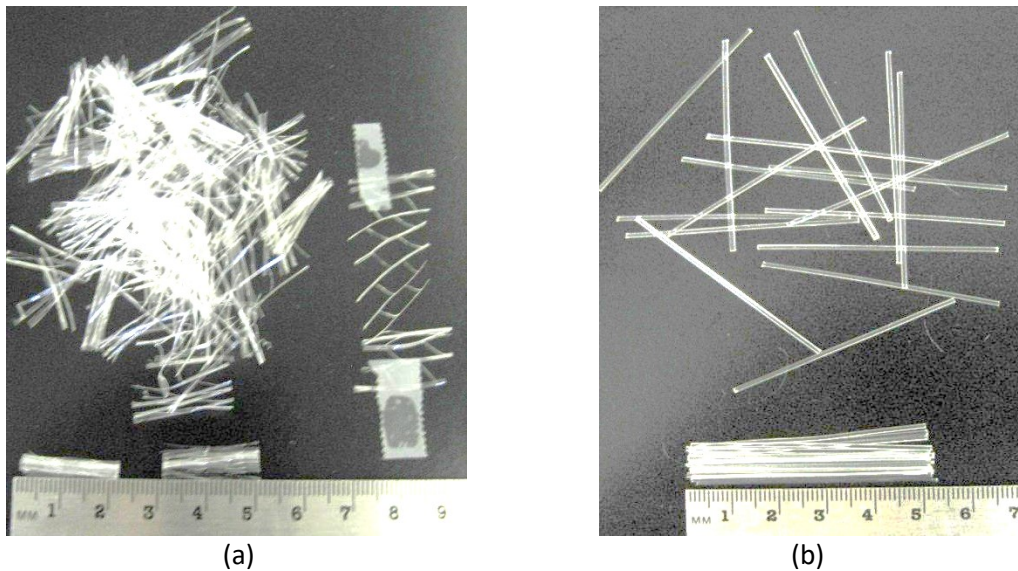
Figure 3-3. Photographs of two types of synthetic fibers used in MnROAD Cells 94 and 95: (a) non-structural polypropylene and (b) structural polyolefin.

3.5.2 MnROAD Cells 140, 160-163

In 2013, several bonded concrete overlay (on asphalt) cells were constructed on the MnROAD mainline using Propex Fibermesh 650, a low stiffness (laterally) straight macro-synthetic fiber. A dosage rate of 6.5 lb/yd^3 was used to achieve 20% RSR for this project. See Table 3-6 for further details on this project. These cells are still young, and some localized distresses were already observed. Burnham and Andersen (2015) noted that the fibers are not contributing well in the failed section, at least in terms of holding the cracks together. Figure 3-5 shows a localized distress observed in Cell 162. While cracking in areas with loss of support could not be mitigated with the fibers used in Cells 160-163, it is believed that the development of joint faulting should have slowed by their presence. Still this observation brings up the question whether a dosage of 6.5 lb/yd^3 of fibers was a sufficient dosage or if the type of the fiber was not suitable.

34
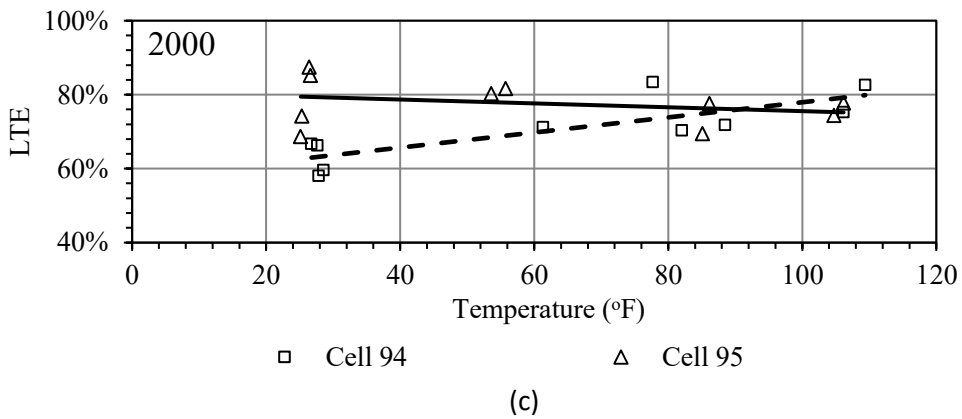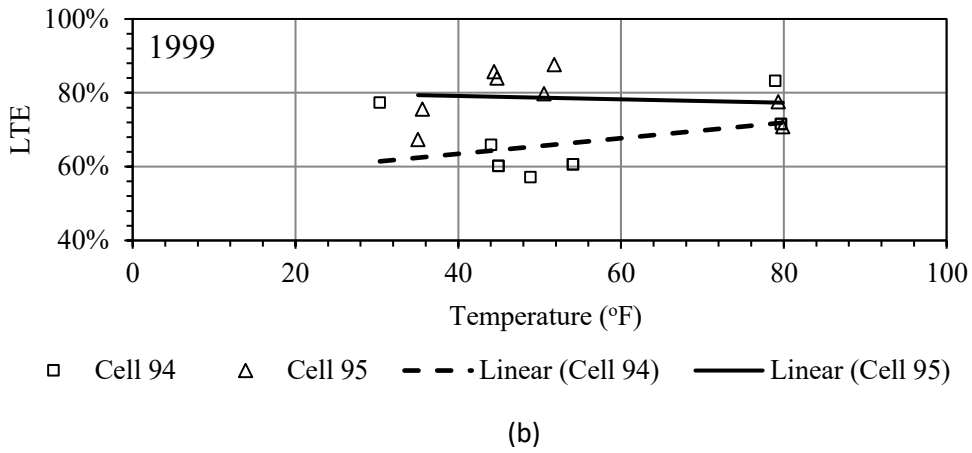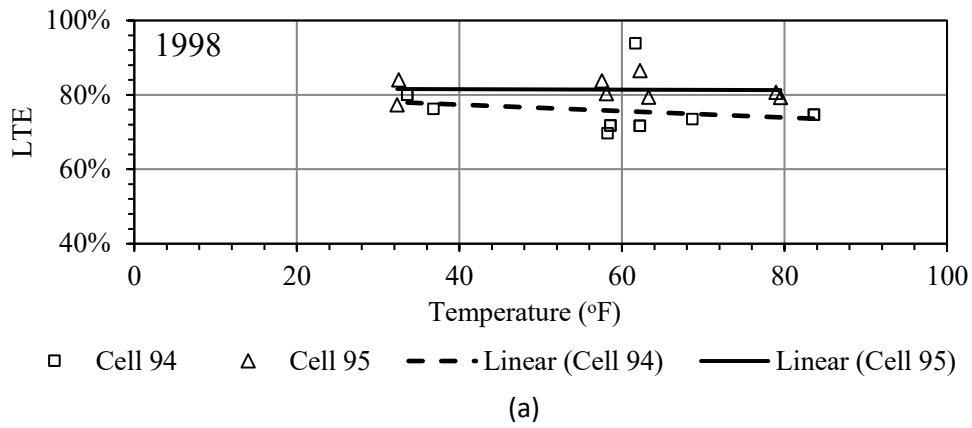
Figure 3-4. Load transfer efficiency of MnROAD Cells 94 and 95 in (a) 1998, (b) 1999, and (c) 2000.

Figure 3-5. (a) Localized distress in Cell 162, (b) fiber visible during removal of distressed concrete (Burnham and Andersen, 2015).

3.5.3 US-169

The Minnesota Department of Transportation constructed three intersections with thin and ultra-thin overlays at US-169. These overlays were in Elk River near Jackson, School, and Main Streets. All of these projects contained either polypropylene or polyolefin fibers (Vandenbossche and Rettner, 1998). The existing asphalt was severely rutted and had locations distressed with raveling. It was found that the weak asphalt layer significantly impacted the performance of the UTW because a quality bond between asphalt and concrete layers could not be achieved. Each test section also developed distinct cracking patterns that included corner breaks, longitudinal cracks, and transverse cracks. These test sections showed that ultra-thin concrete overlay may not be a great rehabilitation technique for distressed asphalt pavement when the asphalt layer is just 3 inches thick and is non- uniform in stiffness and is distressed with raveling. No detailed information was available, however, to understand the contribution of the structural fibers in US-169 project. But it can be concluded that the structural fibers may not be very effective to resist the premature distresses when the underlying supporting layer is too thin or weak.

3.5.4 NRRA MnROAD Sections

In an effort to understand the contribution of fibers with respect to reducing the fatigue cracking, joint faulting, and other distresses, the National Road Research Alliance (NRRA) constructed new FRC cells at MnROAD during June to September, 2017. Table 3-7 presents a summary of the designs and materials used in these fiber-reinforced concrete pavement test cells. Out of the seven FRC cells (plus 1 control section without fibers), Cells 506 through 806 are thin concrete pavement-at-grade containing varying dosages of fibers (0% to 0.75% V_f); Cells 139 and 239 are ultra-thin (3 inches thick) and thin (4 inches thick) concrete pavements-at-grade (city street design), respectively, constructed with an enhanced fiber dosage (See Table 3-7 for the dosage information); and Cells 705 and 805 are thin unbonded concrete overlays constructed with varied panel sizes and a more common fiber dosage (at 20% RSR).

36

These cells are equipped with different types of sensors for measuring: (i) dynamic strain due to wheel load, (ii) strain induced by the environmental forces, (iii) temperature gradient, and (iv) joint movement.

A recently conducted distress (June, 2018) survey revealed that Cell 139, which is a 3-inch thick ultra-thin pavement-at-grade constructed directly on 6-inch thick class 5 aggregate base layer, has experienced significant distresses. Slabs have shattered at multiple locations and rutting was noticed along the wheel path. This short-term failure indicated that a 3-inch thick concrete structure was probably insufficient when slabs were laid directly on the unstabilized aggregate base layers, irrespective of the fiber contents. It may also be noted that the fibers used in this cell were twisted and bundled which disperse well in the concrete mixtures, but the diameter of each fiber strand could be very low when unbundled in the concrete. In such situation, each fiber strand could possess a low lateral stiffness. The observation of rutting or depression along the wheelpath indicated that the support aggregate base layer was weak.

Table 3-7. Summary of the 2017 NRRA MnROAD FRC Cells.

Cell number	Cell Length (ft)	Pavement/ overlay Type	Underlying layer (constr. year)	Type of concrete/ fiber dosage*	Panel size W ft x L ft	Panel thickness (inch)
506	144	Thin pavement on grade	11 in. class 5Q aggregate base (2017)	*Plain concrete*	6 x 6	5
606**	138			*FRC/ standard*		
706				*FRC/ enhanced*		
806				*FRC/ high*		
139	270	Ultra-thin Pavement on grade	6 in. class 5 aggregate base (2017)	FRC/ enhanced	6 x 6	*3*
239	273	Thin Pavement on grade			6 x 6	*4*
705	144	Thin unbonded overlay	Concrete (1993)	FRC/ standard	*Driving: 14 x 12 Passing: 12 x 12*	5
805	124				*Driving: 6 x 12 and 8 x 12 Passing: 6 x 12 and 6 x 12*	5

* Fiber dosages: standard - corresponding to 20% residual strength ratio (ASTM C1609); enhanced - corresponding to 30% residual strength ratio (ASTM C1609); high – corresponding to 0.75 fibers volume fraction.

** Even though the design thickness was 5 inches, the actual measured thickness was found to be 6 inches

3.6 OKLAHOMA

In Oklahoma, multiple FRC overlay projects were identified throughout the state. The Oklahoma ACPA chapter was contacted for information on those projects, but no significant information could be gathered. However, it was found that Oklahoma's projects were typically 5 inches thick and contained

fibrillated polypropylene fibers at a dosage of 3 lb/yd^3 (Burwell, 2016). Per the ACPA data base, these projects are performing well, with little distress (ACPA, 2016).

A field performance investigation was conducted by Rotithor, 2010 on I-69 in areas between Atoka and McAlester. That study indicated that concrete overlay on asphalt was effective even with heavy truck traffic. Some of these sections had thick asphalt layers (10 inches) and that may have significantly contributed to the success of these projects. These projects were distressed primarily at the corners and at the transition of overlay and adjacent pavement (Rotithor, 2010).

3.7 SOUTH CAROLINA

In 1998 and 1999, three 4-inch concrete overlay (on asphalt) projects were constructed in South Carolina. These projects were specified to use chopped and fibrillated polypropylene fibers with a length of 1 to 2 inches, at a dosage of 3 lbs/yd^3 (Johnson, 2016). The rehabilitation of the US-301 intersection at US-21 and the rehabilitation of US-21 at SC-48 were completed in 1999 with a 4-inch slab thickness and 3 ft. joint spacing. It was found that the existing asphalt was only 2 to 3 inches thick and that lead to significant distress soon after construction. The US-21/SC-48 project has a few minor cracks in the panels and several panels at the stop are severely fractured, see Figure 3-6. The US-21 project has remained serviceable due to the fibers (Johnson, 2016).

The overlay project on SC-215 near Columbia, SC was completed in 1998 with 4 ft. panels. South Carolina DOT considered using fibrillated and monofilament fibers for this project and found that the monofilament fibers provided a greater residual flexural strength. At current, 20-30% of the panels are cracked and the serviceability is beginning to fail (Figure 3-7). It was noted that the panels would have come apart much sooner without the fibers (Johnson, 2016).

Figure 3-6. Intersection of US-21 and SC-48 (Johnson, 2016).

Figure 3-7. FRC overlay on SC-215 near Columbia, SC (Google Maps, 2016).

3.8 VIRGINIA

In 1995, the Virginia DOT placed three test sections: I-85 near Petersburg, I-295 near Richmond, and Route 29 South of Charlottesville, all bonded overlays, but on different types of existing layers. The existing pavement on I-85 and I-295 was continuously reinforced concrete pavement (CRCP). These sections were overlaid with concrete to prevent spalling caused by an insufficient concrete cover over the reinforcement. The existing pavement on Route 29 was asphalt and was overlaid to correct rutted asphalt pavement. Overlay thicknesses varied between 2 and 4 inches and included 6 different fiber types. The fiber selection included hooked-end steel fibers, two different brands of monofilament polypropylene, a fibrillated polypropylene, and two different polyolefin fiber lengths (Sprinkel and Ozyildirim, 2000).

Severe corner cracking was observed on Route 29 after the lanes were opened. Cracks in the transverse direction occurred on I-85 and I-295, but no patching was needed after 4 years of service, unlike Route 29, which was patched in 1999. Crack data from Route 29 indicated the highest percentage of cracking occurred in the polypropylene sections because the fibers were unable to hold the sections together. The sections that utilized polyolefin fibers exhibited good resiliency to minimizing cracking and crack width. The hooked-end steel fibers also had a high percentage of cracking. Data from Route 29 showed that the steel fibers were unable to hold sections together. The 5-year evaluation report of these sections concluded that concrete overlays can be successfully placed on both CRCP and asphalt pavement (Sprinkel and Ozyildirim, 2000).

3.9 OTHER STATES

A summary of FRC overlay project in other states and the corresponding information was extracted from Barman (2011) and provided in Table 3-8. It appears that structural synthetic fibers such as polypropylene fibers were used in all those projects listed in Table 3-8. However, information on the contribution of fibers in these projects could not be collected.

Table 3-8. Summary FRC project details in other states (Barman, 2011)

State	Project details	Year of Const.	Traffic (ADT)	Overlay Thickness, Inches	Fiber type and dosage (lb/yd^3)	Distress data
Pennsylvania	Intersection of State Route (SR)-133 and SR-100, Chester County	1988	36,079	4	Polypropylene, 3	N/A
Texas	Intersections on LP-250 at Wadley Road, Holiday Hill Road and Midland Drive, Midland	2005	26,650	3	Polypropylene, 3	A mid slab and corner cracks were observed after one or two years of construction which could be due to the heavy traffic and wheel path adjacent to the longitudinal joint.
Texas	Intersection of LP-250 at Midkiff Road and Garfield Road, Midland	2001	25,000	3	Polypropylene, 3	N/A
New York	Intersection at Waldon Avenue and Central Avenue, near Buffalo	2002	12,250	4	Polypropylene fibers, N/A	Corner cracks along the longitudinal joints were found.
New York	NY-408 and SH-622, Rochester	2002	9,350	4	Polypropylene fibers, N/A	Corner cracks along the longitudinal joints were found.
Michigan	Patterson Avenue, from 44th Street to 36th Street, Kentwood	2006	31,891	4	fibrillated polypropylene, 1.5	The overall performance of the project was good; however, there were a few distresses due to improper alignment of edge of existing asphalt layer and the joint between the overlay and full depth widening.

CHAPTER 4: MATERIALS AND TESTING

A large-scale laboratory testing program was conducted in this research project to characterize the contribution of fibers with respect to post-crack performance and joint load transfer. A total of 11 different types fibers were considered. Testing was conducted in two tasks (Tasks 3 and 4). In Task 3, post-crack performance tests, and in the Task 4, joint performance tests, were conducted. Ten types of fibers were included to investigate the effect of fiber length, geometry and material type on the post-crack performance of FRC; ten fibers were tested at three dosages (0.25%, 0.5%, and 0.75% volume fraction). Five fibers were included in joint performance tests, including four fibers from the Task 3 and a different fiber that was used in MnROAD 2017 cells, and not considered in Task 3. Joint performance tests were conducted at 0.25% and 0.5% volume fractions of fibers. In total, 43 different mixes were prepared and tested: 30 FRC mixes (10 fibers x 3 dosages), one plain concrete mix for post-crack performance tests, and 12 additional mixes for joint performance testing.

4.1 MATERIALS

This section presents the details of the materials used in the laboratory study. Descriptions are provided on the fiber types and their properties, aggregates and their gradations, cement, and admixtures, such as air entrainer and water reducer. Concrete mixture proportions are also presented in this section.

4.1.1 Fibers

The selection of the structural fibers for ultra-thin and thin bonded concrete overlays should be based on the consideration that the flexural strength, joint performance, and post-crack performance of concrete achieves considerable improvement with the addition of the fibers. The literature reviewed in this project revealed that both steel and structural synthetic fibers were used in concrete overlays in this country, and they have contributed to the performance of the overlays. Various combinations of fiber types, lengths and dosages were utilized; however, very little information is available to quantify the contribution of the fibers in terms of the above-mentioned mechanical properties of concrete when used in concrete overlays or in pavements. This section summarizes the main findings of the literature study and surveys conducted in this study to make a decision on the types and dosages of the fibers to use in the laboratory testing.

4.1.1.1 Fiber Type

Table 4-1 presents a statistical summary of the projects reviewed under the scope of this study. It can be seen that as much as 94% of the FRC concrete overlay projects were constructed with structural synthetic fibers and only 6% were constructed with steel fibers, mostly in Illinois. The polypropylene fibers were used in almost all the synthetic FRC projects and polyolefin fibers in a couple of others. The difficulties involved in dealing with the heavy-weight steel fibers during mixing is likely the reason for the less frequent use of steel fibers as opposed to the synthetic fibers. However, for comparison purpose, a steel fiber was also considered in the laboratory study.

4.1.1.2 Fiber Geometry

A clear preference on the geometry of the fibers could not be established from the overlay projects reviewed in this study. It appeared that a larger number of projects contained straight, flat synthetic fibers. However, many researchers found and believed that crimped or embossed geometry fibers (Issa, 2017) provide better bond strength and pullout resistance. Research had also shown that fibers with twisted or fibrillated configurations perform better than straight fibers. It was decided to include straight, crimped, embossed, and fibrillated synthetic fibers in the laboratory study, so that the influence of the many fiber geometries on the mechanical properties of the concrete can be studied.

Table 4-1. Summary and statistics of fiber reinforced concrete overlays reviewed in this Project.

State	Number of Projects	Projects using Steel		Projects using Synthetic			
-	-	%	Dosage lb/yd^3	%	Dosage lb/yd^3	% projects used 3 lb/yd^3 dosage	% projects used other dosages
Georgia	6	0	N/A	100	3	100	0
Illinois	11	18	80,40	82	4, 3, N/A	18	82
Kansas	8	0	N/A	100	3	88	12
Minnesota	11	0	N/A	100	3, 6.5, 25	36	64
South Carolina	3	0	N/A	100	3	100	0
Virginia	3	28	50, 75	72	3, 20, 25, 0.9	17	83
Total	36	6	N/A	94	N/A	53	47

N/A: Information Not Applicable

4.1.1.3 Fiber Aspect Ratio

High aspect ratio fibers generally enhance the properties of the hardened concrete. However, fibers with an aspect ratio greater than 100 tend to interlock and either ball or form mats of fibers in the mixture. Balling and the formation of mats of fibers result in poor dispersion. Fibers with an aspect ratio of less than 50 are less likely to become interlocked, ball, or form mats within the matrix, but do not improve the mechanical strength of concrete significantly. It was therefore suggested that fibers with an aspect ratio between 50 and 100 shall be considered for the laboratory study.

4.1.1.4 Fiber Length

Fibers that are not long enough possess a problem when they are required to resist macro crack propagation and increase joint performance. The concrete overlay projects constructed with structural FRC had 1.5 inch- to 2.25-inch long fibers. It was suggested that fiber lengths should be held to a minimum length of 1.5 inches and a maximum of 2.25 inches. Utilization of fibers longer than 2.25 inches may result in fiber balling, and fibers shorter than 1.5 inches may not provide enough bond strength and pull out resistance.

4.1.1.5 Fiber Dosage

The projects reviewed in this study typically (53%, see Table 4-1) used synthetic fibers at dosages near 3 lb/yd^3, but used dosages as high as 6.5 lb/yd^3 for polypropylene fibers and 25 lb/yd^3 for polyolefin fibers. Few overlay projects had been reported that used steel fibers, but those that did report dosages between 40 lb/yd^3 and 80 lb/yd^3 with mixed success. To function properly, a minimum fiber count at the crack faces is a necessity. It is therefore important to consider the dosages in terms of V_f rather than weight (eg., lb/ yd^3). It was found that fibers above 1% V_f have a higher likelihood of fiber balling, and less than 0.25% does not significantly improve the post-crack and joint performance. It was therefore suggested to use three dosage rates, at 0.25%, 0.50% and 0.75% V_f in this study so that a relevant as well as large range is covered. The 0.25 percent V_f (approximately 3 to 3.5 pounds per cubic yard for synthetic fibers) represents a low, but common dosage implemented in concrete overlays. The 0.75 percent V_f was selected because it is likely the maximum dosage that could be implement without experiencing significant fiber balling or formation of matting, while 0.50 percent V_f represents an intermediate dosage between 0.25 and 0.75 percent V_f.

4.1.1.6 Selected Fibers

Table 4-2 lists the fibers used in this study. Eleven different types of fibers were included for this work based on variables to be considered including fiber type, geometry, length, aspect ratio, and manufacturer. Ten of the fibers selected were synthetic polypropylene, while only one fiber was steel. Of the eleven fibers in this study, four fibers were flat and straight in cross section, three were embossed, two were twisted, one fiber was continuously crimped, and one was end crimped (steel). Photographs of all the fibers used in this study are shown in Figure 4-1, row wise (the top-left and bottom-mid photographs are the Fiber 1 and 11, respectively). See Table 4-2 for other descriptive information related to the fibers selected. The main differences between the four straight synthetic fibers (Fiber 1 through 4) are the manufacturer, length, and aspect ratio; stiffness's of these fibers were similar. Fiber 6 and 11 varied in length and aspect ratio. Fiber 7 and 9 of the three embossed fibers were of same length and manufacturer, except Fiber 7 was chemically enhanced for improved bonding to cementitious matrices.

4.1.2 Aggregate

The fine and coarse aggregates used in this project were collected from a quarry, operated by Duluth Ready Mix near Canyon Minnesota, and can be seen in Figure 4-2. The fine aggregate was washed sand; the gradation can be seen on Figure 4-3 and Table 4-3. The bulk specific gravity of the fine aggregate was 2.68. The coarse aggregate was a rounded to sub rounded gravel with a bulk specific gravity of 2.75. See the gradation in Figure 4-3 and Table 4-3. A Los Angeles Abrasion test was conducted on the coarse aggregate that resulted in a mass loss of 9.2%.

Figure 4-1. Photographs of fibers used in this project.

Table 4-2. Description of fibers investigated in this research

Fiber Serial Number	Geometry / Type	Length (inch)	Aspect Ratio, Specific Gravity, Modulus of Elasticity (ksi), Tensile Strength (ksi)
Fiber 1	Straight / Synthetic	1.5 or 2	*94, 0.91, N/A, 70
Fiber 2	Straight / Synthetic	1.5 or 2	*100, 0.91, N/A, 70
Fiber 3	Straight / Synthetic	1.55	90, 0.92, 1378, 90
† Fiber 4	Straight / Synthetic	*1.625	96.5, 0.91, N/A, 70
† Fiber 5	Twisted Straight / Synthetic	2	74, 0.92, 1380, 87-94
† Fiber 6	Continuously Crimped / Synthetic	2.0	*60, 0.91, N/A, N/A
Fiber 7	Embossed / Synthetic	2.1	70, 0.91, N/A, 85
Fiber 8	Embossed / Synthetic	1.89	*66, 0.90-0.92, 1450, 93
† Fiber 9	Embossed / Synthetic	2.1	70, 0.91, N/A, 85
Fiber 10	End Crimped / Steel	2.4	65, 7.8, 29000, N/A
Fiber 11	Twisted bundle non-fibrillating	*1.5-2.25	*150-200, 0.91, N/A, 90

N/A: Information not available

*Approximate measurement, not by manufacturer

† Phase 2 fibers

Figure 4-2. Coarse aggregate and fine aggregate used in this project.
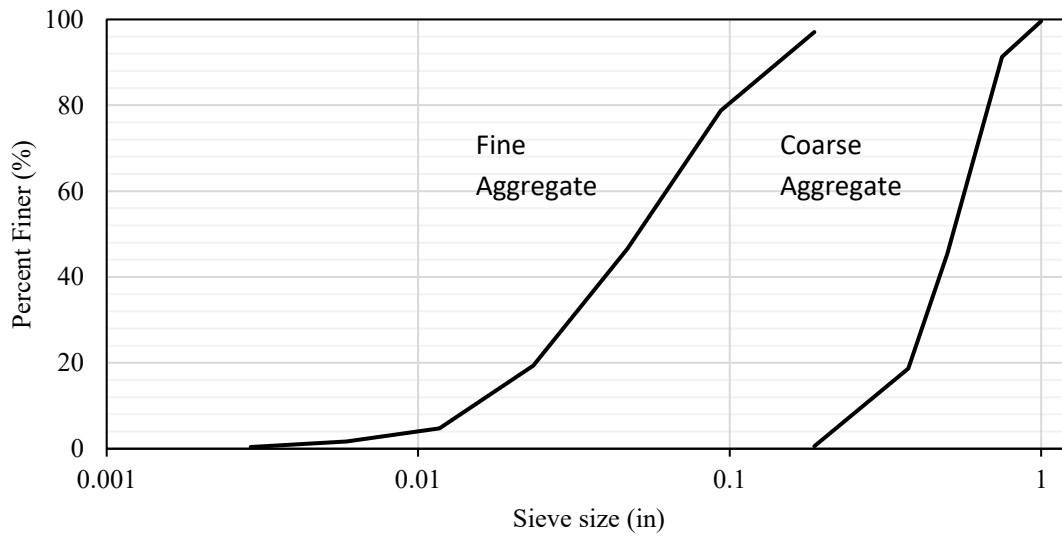
Figure 4-3. Gradations for the coarse and fine aggregates used in this project.

Table 4-3. Percent passing table for fine and coarse aggregate in this study.

Sieve Number	Passing (%)	
	Fine	Coarse
1"	-	99.6
3/4"	-	91.3
1/2"	-	45.4
3/8"	100	18.7
4	97.1	0.7
8	78.7	-
16	46.6	-
30	19.4	-
50	4.8	-
100	1.7	-
200	0.4	-
Pan	0	0.1

4.1.3 Other Ingredients and Mixture Design

The mixture design used in this work was developed after numerous trial batches. Initial trial batching was performed with 580 lb/yd^3 of cement; however, the workability and consolidation issues when using higher fiber dosages encouraged the use of a higher content of cement (615 lb/yd^3). ASTM Type I cement was used. Table 4-4 shows the base concrete design for the mixtures used in this study including both the volume fraction and mass of the ingredients. As the fiber dosage was increased, the sand content was slightly decreased (volume of sand per volume of fibers) to make up the volume difference. No volume change was made in coarse aggregate fraction and cement content as a result of changing the fiber volume fraction. The air entraining admixture (AEA) was increased for an increase in fiber dosage in order to maintain an entrained air content in the range of 5.5 percent to 9 percent by volume. AEA dosage ranged between 0.98 to 1.06 ounces per 100 lb of cement. The mid-range water reducer (WR) was also increased for an increase in fiber dosage (slump was maintained to a range of 0.5 inches to 3 inches) and ranged between 5.93 to 7.25 ounces per 100 lb of cement.

Table 4-4. Base mixture design for concrete mixes for this study.

	Volume (%)	Approx. Mass (lb/yd^3)
Cement (Type I)	11.6	615.0
Coarse Aggregate	42.0	2024.0
Fine Aggregate	25.1	1188.8
Potable Water	13.9	233.7
Fibers	Varied	Varied
BASF MasterAir® 400 (fl. Oz)	-	6.08
MasterPolyheed® 1020 (fl. Oz)	-	36.5

4.1.4 Mixture Designations

To designate each mix design properly and concisely, all the mixes were given designations. The designations describe each mixture according to the fiber's material type, geometry, fiber designation, and fiber dosage (percentage of total volume) used in the respective mix. Table 4-5 describes the nomenclature in the mixture designation. For an example, the mixture designation 'S.S.1.25' represents a mixture that contains synthetic fibers (S) of straight (S) geometry with a serial number of 1 (see Table 4-2 for the length, aspect ratio, density, etc.), and a 0.25% fiber volume fraction.

Table 4-5. Nomenclature for the mixture designation

Fiber Material	Fiber Geometry	Fiber Number	Dosage (V_f %)
Synthetic (S)	Crimped (C)	See Table 4-2	0.25
Steel (L)	End Crimped (EC)		0.5
	Embossed (E)		0.75
	Straight (S)		
	Twisted (T)		

4.2 TESTING

4.2.1 Concrete Mixing Procedure

To produce the required concrete efficiently and consistently for this work, a mixing procedure needed to be developed. Initial trial mixtures were conducted per ASTM C192 - the procedure for making and curing concrete specimens in the laboratory. According to this procedure, all the materials are added to the drum-mixer, the materials are mixed for three minutes, allowed to rest for three minutes, and then finally mixed for an additional two minutes. This procedure was conducted after mixing a butter batch (small batch of concrete to condition the inside of the mixer, and wheel barrow). Figure 4-4 shows an image of the concrete mixer used in this project. The following observations were made:

- Fibers were not properly dispersed.
- It was difficult to consistently obtain the required air entrainment.
- Fibers tended to ball and mat. Figure 4-5 shows an image of fiber balling.

Figure 4-4. Concrete mixer used in this project.

Figure 4-5. Fiber balling in a concrete mixture.

From the above-mentioned observations, an extended procedure was adopted that provided more consistent slump, air entrainment, and fiber distribution. The mixing procedure was conducted after the implementation of a butter batch, and was as follows:

1. All fine aggregate and air entraining admixture (AEA) were added to the drum-mixer with 1/3 of the mixing water and mixed for 2 minutes;
2. The coarse aggregate was added to the stopped drum-mixer;
3. The drum-mixer was turned on and the fibers were placed in it by hand with care to pull apart balls or mats, mixing for a total of 3 minutes;
4. With the drum-mixer still running, the cement, remaining mixing water, and water reducer were added to it and mixed for 3 minutes;
5. The drum-mixer was stopped and the mixture allowed resting for 3 minutes;
6. The mixture was mixed for two final minutes.

4.2.2 Fresh Concrete Testing

In this work, multiple fresh concrete tests were performed including, slump, box, and air content (by pressure method) tests. These tests were conducted as quality control measurements to ensure that the hardened concrete results were comparable. The following subsections briefly describe those tests and the target values for this study.

4.2.2.1 Slump Test

A slump test was conducted in accordance to ASTM C143 after the concrete mixing procedure was completed and again after any additional admixture was added to the mixture (ASTM C143, 2015) to attain the desired workability. The target slump range was 0.5 to 3 inches, which is common for slip form paving. Figure 4-6 shows a photograph of slump test conducted on a low workability fiber reinforced concrete mixture.

Figure 4-6. Slump test on FRC mixture.

4.2.2.2 Air Content and SAM test

Air content was measured by pressure method and was conducted after the mixing procedure was completed and again after any additional admixture was added to the mixture (ASTM C231, 2017). Based on the Ley (2015), the ASTM C231 test was also extended to determine the super air meter number (SAM) number (AASHTO TP 118, 2018), in addition to the air content. The target air content was 6% with an acceptable range of 5.5% to 9%. There was no target range for the SAM number in this study. Figure 4-7 shows an air content test being conducted.

Figure 4-7. The air content by pressure method test in progress.

4.2.2.3 Box Test

The Box test is a procedure that has been recently developed and used in the performance engineered mixtures (PEM) design (Box Test, 2017; AASHTO PP-84, 2018). This test evaluates a concrete mixture's ability to hold an edge and consolidate when used in concrete pavement slip form paver. This is a qualitative test that utilizes a rating system as shown in Figure 4-8. The results of the Box test are highly dependent of the workability of the concrete mixture. Box test results were also not a criterion for accepting or rejecting a mixture in this task. Figure 4-9 shows the box test being conducted.
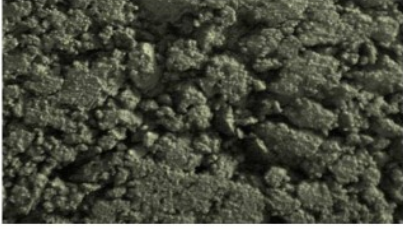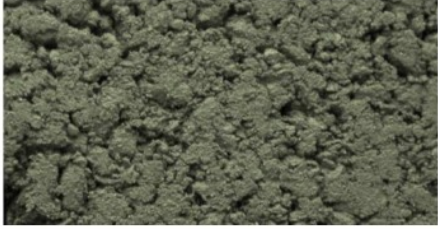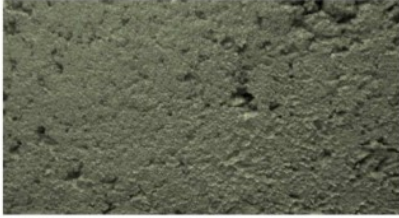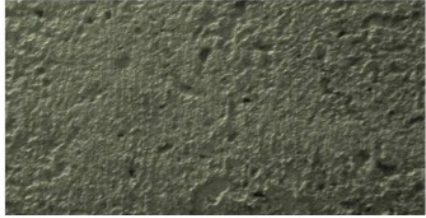
4	3
Over 50% overall surface voids.	30-50% overall surface voids.
2	1
10-30% overall surface voids.	Less than 10% overall surface voids.

Figure 4-8. The box test rating system (After The Box Test, 2017).

Figure 4-9. The Box test in progress.

4.2.3 Hardened Concrete Testing

In this research, multiple hardened concrete tests were conducted: compressive strength, static modulus of elasticity, flexural and post-crack performance, and joint performance tests. The following subsections briefly describe those test procedures.

4.2.3.1 Compressive Strength Testing

Concrete compression testing was conducted on 6-inch diameter by 12-inch height cylindrical specimens to avoid preferential fiber alignment in smaller cylinders. The size of the test cylinders depends on the length of the fibers, where the minimum cylinder diameter should be equal to or greater than three times the maximum fiber length (ACI 544.2R, 1999). A minimum of 4 cylinders were cast for each mixture. The specimens were tested as per ASTM C39 (2017). Figure 4-10 is an example of a compression test taking place at the University of Minnesota Duluth (UMD).
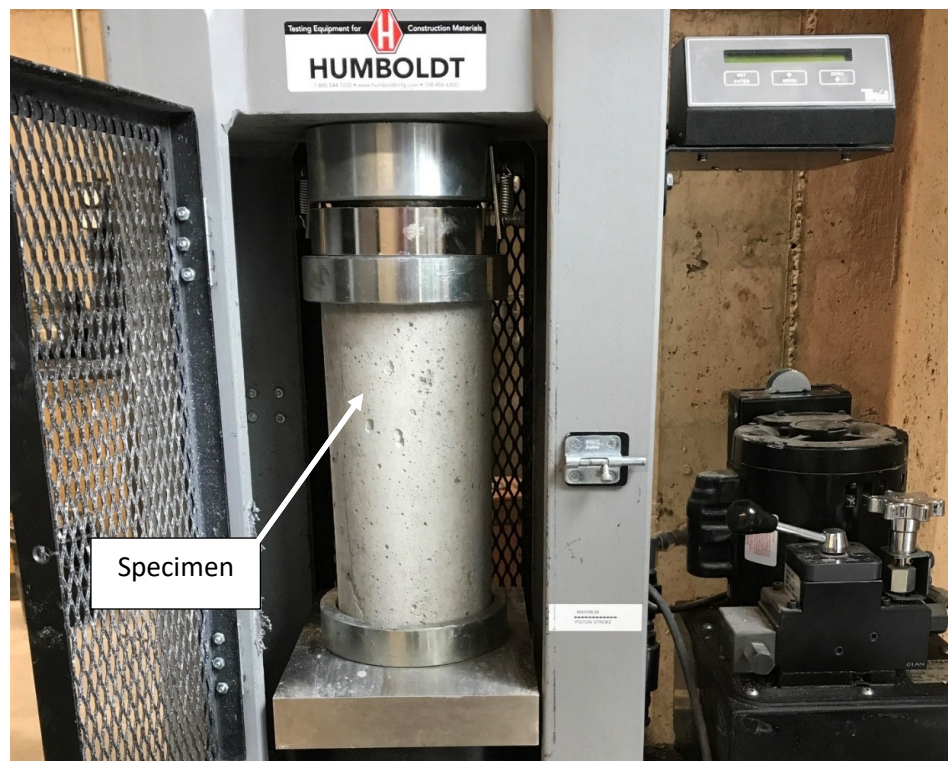
Figure 4-10. An example of a concrete compression test per ASTM C39.

4.2.4 Modulus of Elasticity

The modulus of elasticity test was conducted on 4-inch x 8-inch cylindrical specimens based on the facilities available at UMD. It may be mentioned here that conducting this test with 6-inch x 12-inch specimens would be the most appropriate; however, UMD's civil engineering lab currently does not have the fixture for conducting the test with 6-inch x 12-inch specimens. At least three specimens were tested per mix (ASTM C 469, 2014). After conducting the modulus of elasticity test, specimens were then

broken for ultimate compressive strength per ASTM C39. As 4-inch x 8-inch specimens were used, modulus of elasticity of concrete was also computed based on the compressive strength, obtained using 6-inch x 12-inch specimens; the ACI Equation, shown below, used for this purpose.

$$E_c = 57000 \ (f'c)^{0.5} \quad\quad\quad\quad \text{Equation 2}$$

Where E_c = modulus of elasticity of concrete (psi); f'c = compressive strength of concrete (psi).
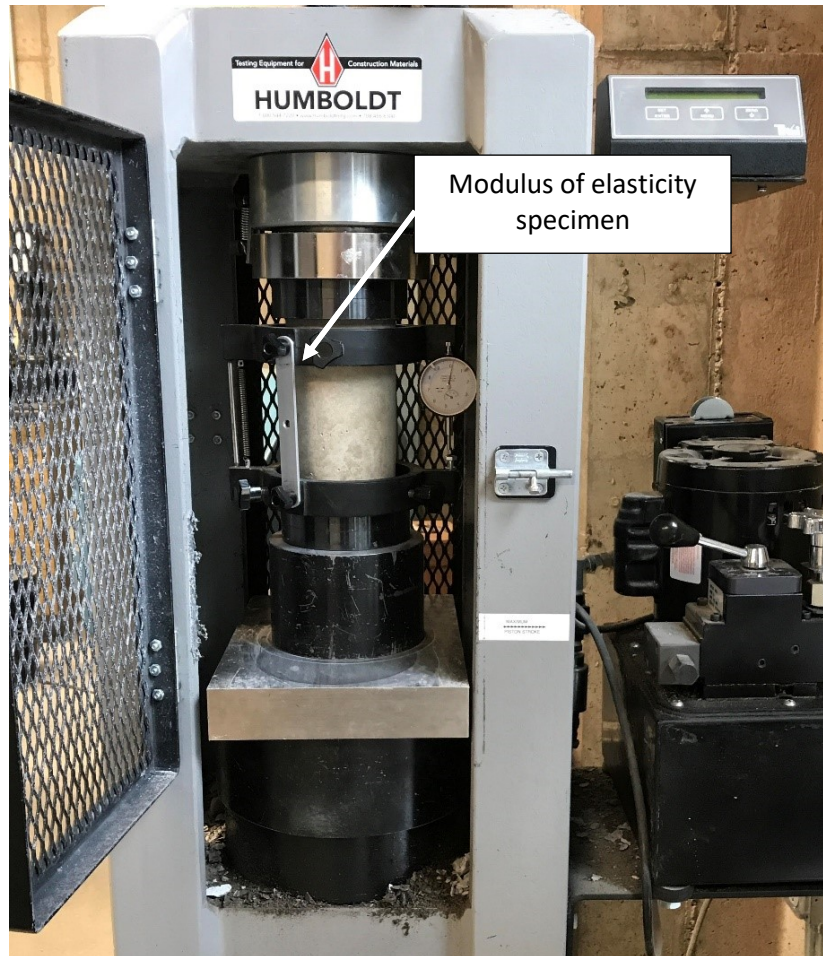
Figure 4-11. An example of a modulus of elasticity test per ASTM C469.

4.2.5 Flexural Testing per ASTM C1609

The flexural performance test was conducted per ASTM C1609 (standard test method for flexural performance of fiber-reinforce concrete). Modulus of rupture, residual strength (RS), residual strength ratio, and toughness can be determined from the flexural performance test. The dimensions of the beam specimens were 21-inch x 6-inch x 6-inch. The length of the span was 18 inches. For each mix, five beam specimens were tested. Figure 4-12 shows a photograph of this test being conducted at UMD and

Figure 4-13 shows fibers restraining a crack during a flexural performance test. For this work, as many as 155 good beams and dozens of trial beams were tested for flexural performance.

In this test, mid-span deflection and applied force are collected to generate the load vs displacement curves as shown in Figure 4-14. These plots can be used to compute the MOR, RS, RSR, and toughness. Figure 4-14 provides examples of load versus displacement curves for synthetic and steel fiber reinforced concrete prepared with a 0.5% V_f fiber dosage. More comparisons are provided in Chapter 5. In the curves for FRC mixes, the applied load does not drop to zero immediately after the peak load, fibers restrain the crack and carry residual load while the displacement increases. In general, the post-peak load drop for synthetic fibers is greater than for steel fibers.

Flexural Specimen

LVDT's (front and back)
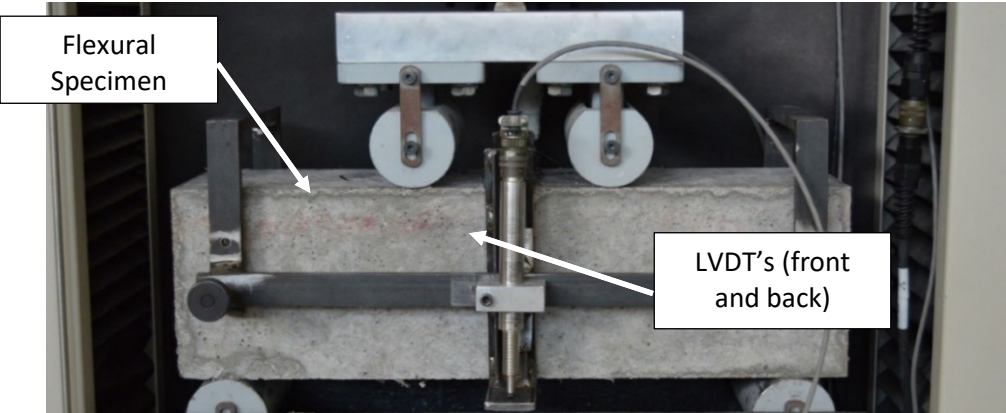
Figure 4-12. An example of a flexural performance test for fiber-reinforced concrete per ASTM C1609.

Figure 4-13. An example of a crack developed after peak load was achieved in a flexural performance test.
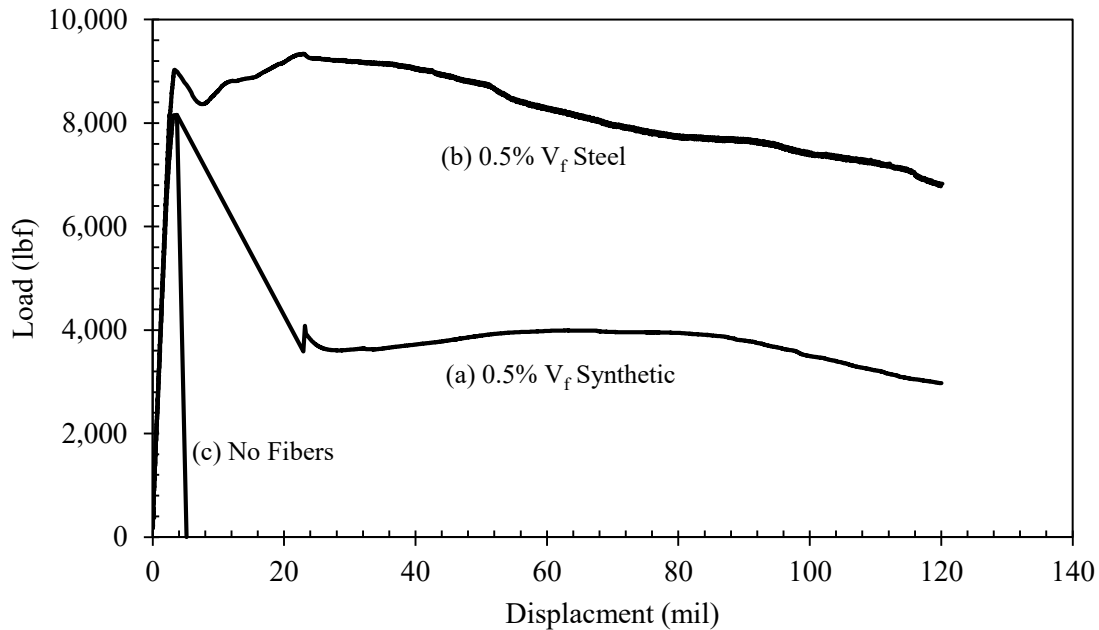
Figure 4-14. Typical displacement versus load plots: (a) synthetic (b) steel fiber, (c) no fibers.

4.2.6 Joint Performance Testing

The joint performance contribution of the structural fibers was studied using a small-scale test setup. In this test setup, 24-inch x 6-inch x 6-inch beams can be tested for determining the joint performance of the concrete. Figure 4-15 shows a picture of the joint performance test setup fabricated at UMD. The working principle of this test setup was similar to the one developed at the University of Pittsburgh by Barman, Vandenbossche and Janssen (Barman, 2014; Barman et al, 2018). This joint performance setup was designed to simulate the abrasive action that occurs in joints and cracks of in-service concrete pavements under a 9-Kip wheel load. The applied load in the joint performance method was 1050 lbs. In order to simulate the in-service pavement condition in the joint performance setup, an actuator was used to apply vertical cyclic loading (both upward and downward) on one side of a pre-cracked concrete beam. The beams were cracked at 18 hours using flexural load at the mid-span and then transferred on a wooden plank. The cracked beam specimens (on the wooden plank) were cured for 28 days in an environmental chamber with 70º degree Fahrenheit temperature and 95% humidity. The beams were tested after 28 days of curing.

Figure 4-16 shows a schematic of the different components of the joint performance test setup. It can be seen that two layers of neoprene pads were provided both above and below the beam specimen. Adjacent to the neoprene pads were either a rigid frame or a rigid testing table. The stiffness of the neoprene pads simulated the stiffness of the layers under an in-service concrete overlay slab. The neoprene pads were compressed under the load both on the loaded side as well as the unloaded side. The magnitudes of the displacements in the loaded side and unloaded side were a function of the crack or joint stiffness. These displacements were measured by LVDTs as shown in Figure 4-16.
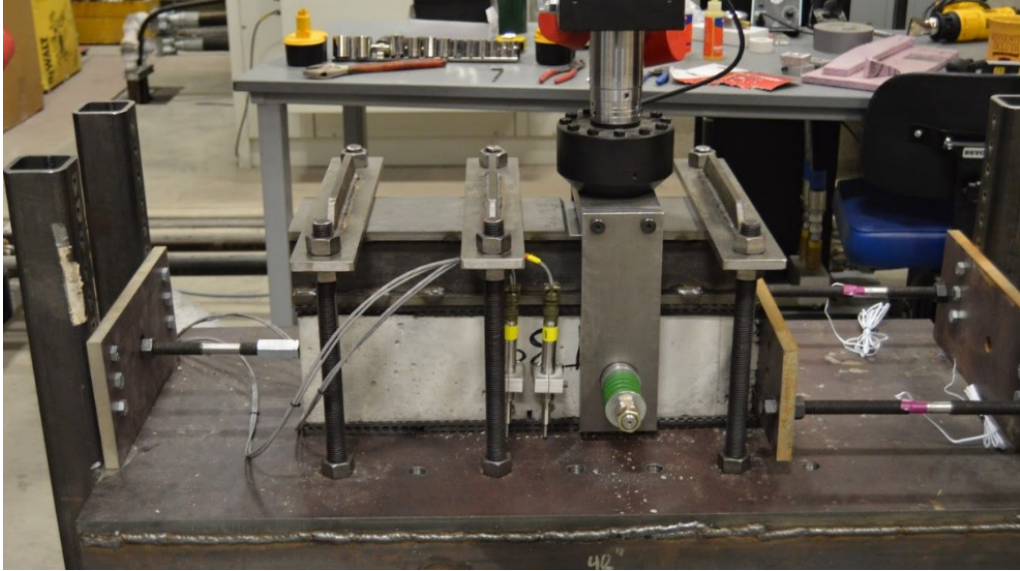
Figure 4-15. Joint performance setup fabricated at UMD.
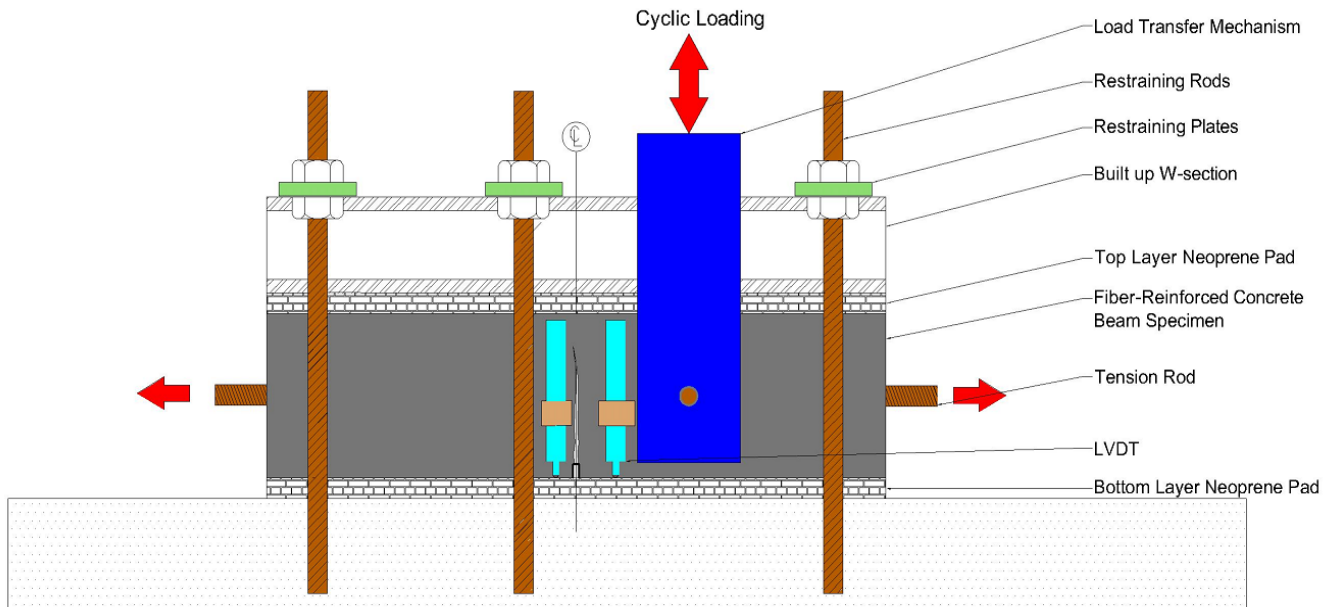
(a)
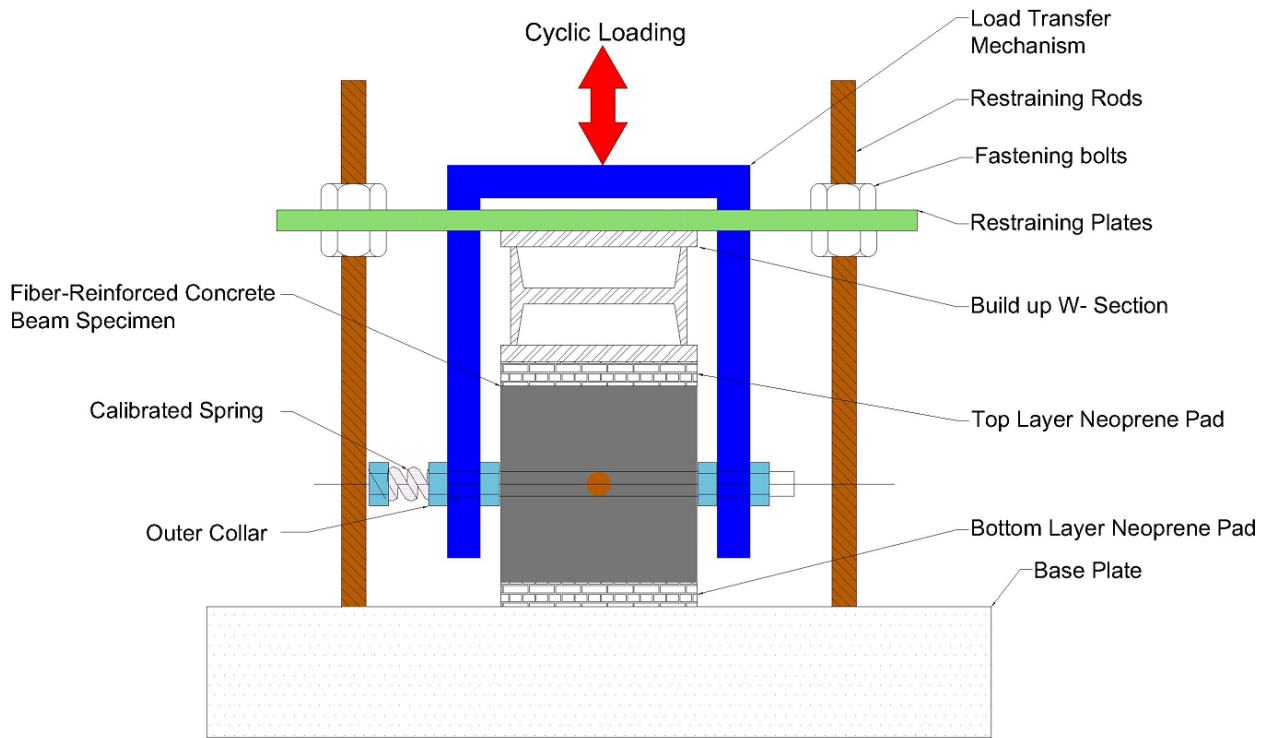
(b)

Figure 4-16: Schematic of joint performance test setup: (a) front view and (b) cross section.

4.2.6.1 Joint Performance using Load Transfer Efficiency (LTE)

An example of primary output from joint performance testing can be seen in Figure 4-17 and includes load, loaded side displacement, and unloaded side displacement. This figure shows load and displacement profiles for one load cycle. The peak values of the loaded side displacement and unloaded side displacement occurred at the same time period, and were used for evaluating the joint performance in terms of LTE, or the other relevant parameters. The LTE was calculated as the ratio of unloaded side peak displacement and loaded side peak displacement, as shown in Equation 2. LTE was calculated separately for the tension load and compression load; the average of the two was reported as the LTE for a given load cycle number and crack width. It shall also be noted that the average of LTEs of five nearby load cycles were considered for calculating the LTE.

$$LTE = \frac{d_u}{d_l} * 100\% \qquad\qquad \text{Equation 3}$$

Where d_l is the loaded slabs peak displacement; d_u is the unloaded slabs peak displacement.

In the University of Pittsburgh Study (Barman, 2014; Barman et al. 2018), it was found that the LTE measured using this setup was comparable with the LTE measured using full-size slabs; see Figure 4-18. In this figure, it can be seen that LTE results of 5 beams and one slab were quite similar.
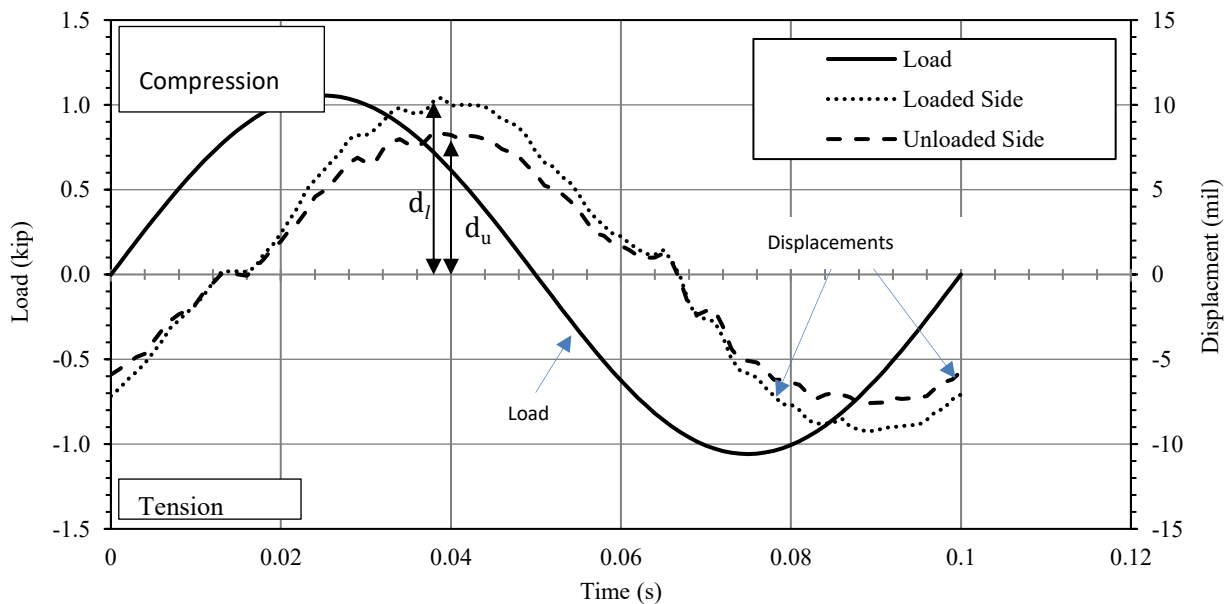
Figure 4-17. Typical examples of load and displacement profiles achieved from a joint performance test.
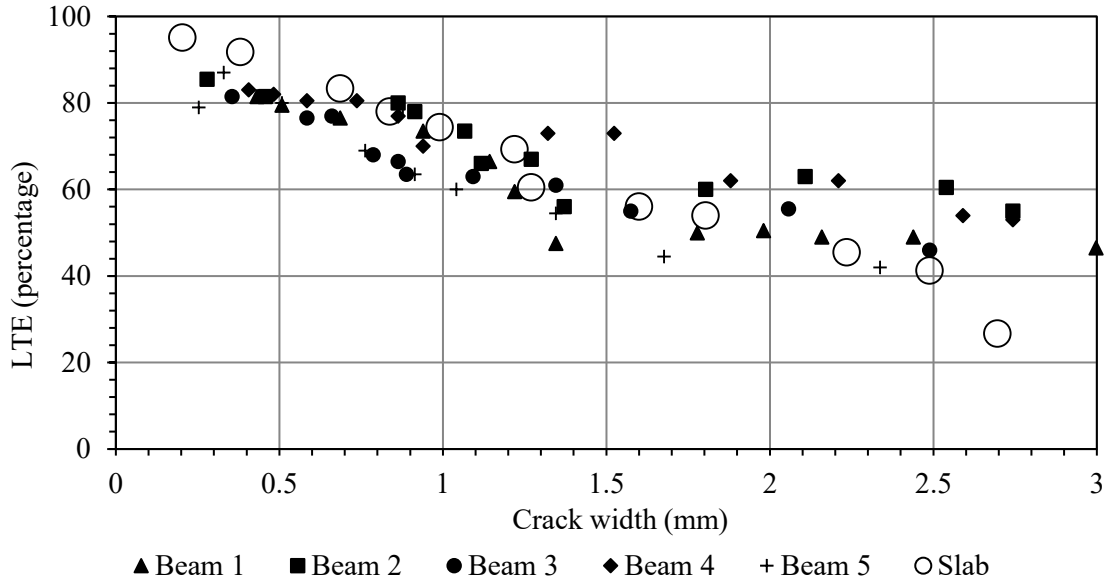
Figure 4-18: Correlation between the beam LTE and slab LTE (Barman, 2014).

4.2.6.2 Joint Performance using Differential Joint Energy Dissipation (DEJD)

Differential Joint Energy Dissipation (DJED) is fundamentally the amount of energy dissipated through the joint during one load cycle. Larger DJED means more joint deterioration; therefore, it is important that the DJED is kept as low as practically possible to mitigate joint related distresses. This property can be represented as the area inside the load versus differential joint displacement hystereses (Figure 4-19). Low DJED values indicate more load is transferred to the adjacent slab through the concrete, or in other words, less energy is dissipated from the joint.
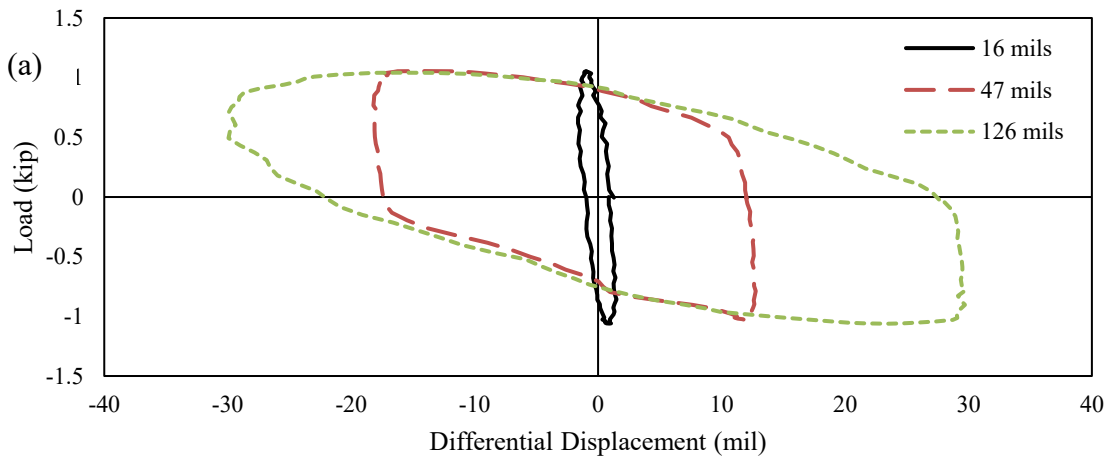
Figure 4-19. Differential joint displacement as a function of load.

CHAPTER 5: POST-CRACK PERFORMANCE TEST RESULTS AND DISCUSSIONS

This chapter provides the results of all the tests conducted in Task 3. The main objective of Task 3 was to characterize the post-crack performance of FRC. All the mixes produced in this stage were tested for fresh concrete properties such as slump, entrained air content, SAM number and box test rating in order to keep consistency between the mixes. In addition to the post-crack performance test (i.e., ASTM C1609 test), all the mixes were tested for other hardened concrete properties as well, such as compressive strength and modulus of elasticity, for comparison purposes.

5.1 FRESH CONCRETE PROPERTIES

To consistently create concrete with an acceptable slump and air entrainment, the admixture contents were altered for each mixture, as required. Since the range of fresh concrete properties was purposefully kept narrow, it would not be appropriate to draw strong quantitative conclusions based on the fresh concrete properties. Qualitatively, some observations can be made regarding air content, super air meter (SAM) number, slump, and the box test results.

5.1.1 Air Content and SAM Number

The average of air contents for all the mixes was 6.9%and ranged from 5.5 to 9%. The average SAM number (Ley, 2015) was 0.28, ranged from 0.04 to 0.61. Figure 5-1 and Figure 5-2 present the plots of the air content and SAM numbers for all the mixes. In these figures, the average air content and SAM number are plotted as a dashed line, while plus and minus one standard deviations are plotted as solid lines. Some qualitative observations are provided below:

- A good correlation between the fiber dosage and SAM number was not apparent from this study. Different geometries of fibers likely interfered in the correlation.
- Mixtures with steel fibers consistently had a higher SAM number.
- An increase in entrained air content directly correlated with a decrease in the SAM number (Figure 5-3). The R^2 for this correlation was 0.55, which could increase with a broad range of fresh concrete properties.
- No proper correlations were observed between the air content and reinforcement index (RI) (V_f x aspect ratio of fibers), or SAM number and RI, at least within the ranges considered in this study.
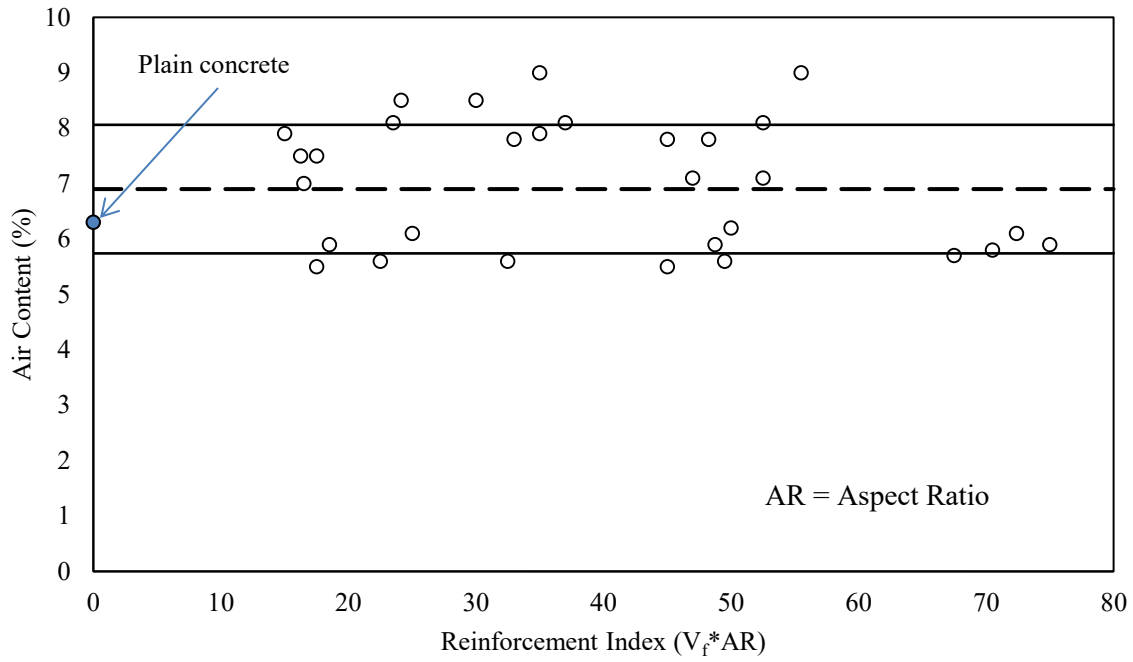
Figure 5-1. Air content as a function of reinforcement index.
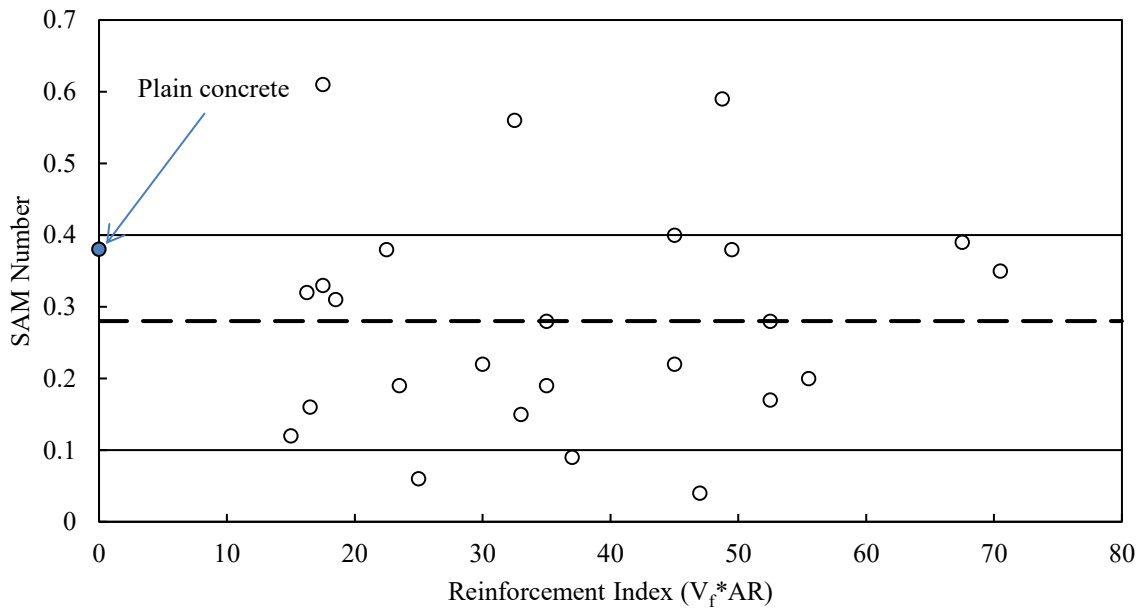
Figure 5-2. The SAM number as a function of reinforcement index.

62
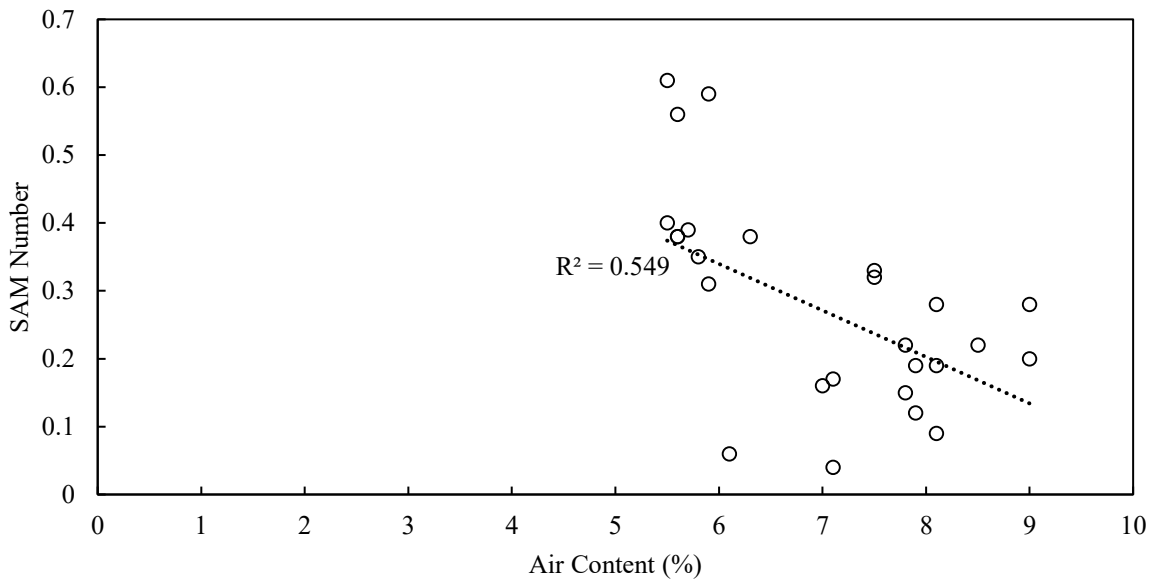
Figure 5-3. The SAM number as a function of air content.

5.1.2 Slump, Box Test and Workability

The average slump in this task was 1.5 inches and ranged from 0.5 to 3 inches. The average Box number rating was 2 (rating system described in Section 4.2.2.3). Figure 5-4 shows the average slump plotted as a dashed line, while plus and minus one standard deviation are plotted as solid lines. Figure 5-5 shows the scatter of box test results as a function of reinforcement index. Some qualitative conclusions are provided below:

- Achieving good workability with smaller effective diameter fibers (coincidentally having a higher aspect ratio) was difficult, especially at higher dosages, meaning more water reducing admixture was required. This observation is similar to what was reported in ACI 544, 2010 where, it stated that the workability decreases with the increase in reinforcement index. Finishing and consolidation were difficult when smaller effective diameter fibers were used.
- An increase in fiber dosage generally led to an increase in the surface void percentage in the box test.
- Trial batches showed that increasing mixing time typically broke up fiber matts and balls.
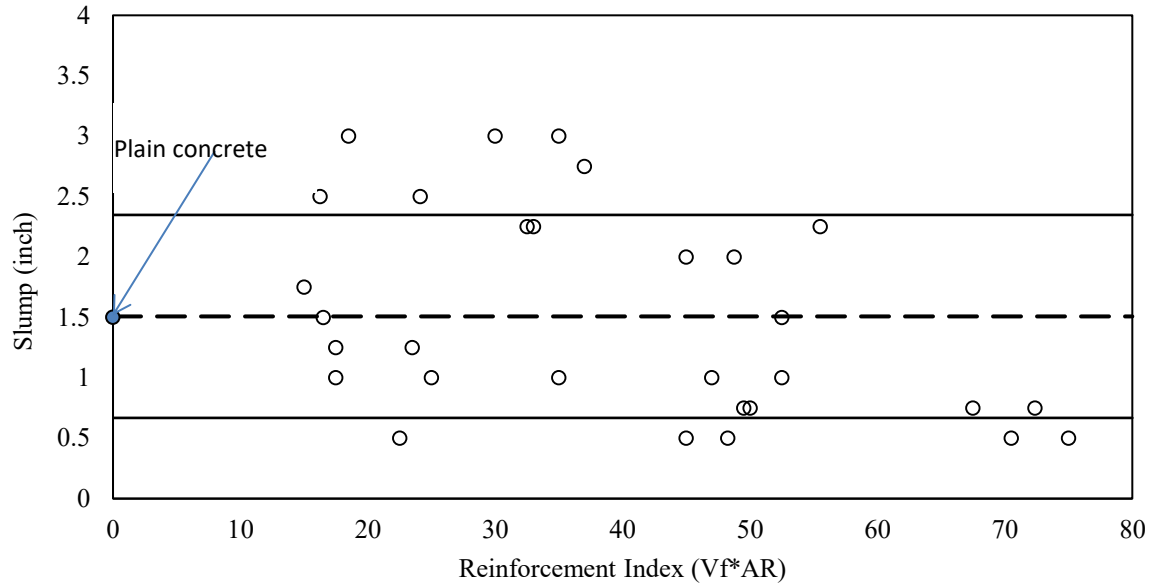
Figure 5-4. Slump as a function of reinforcement index.
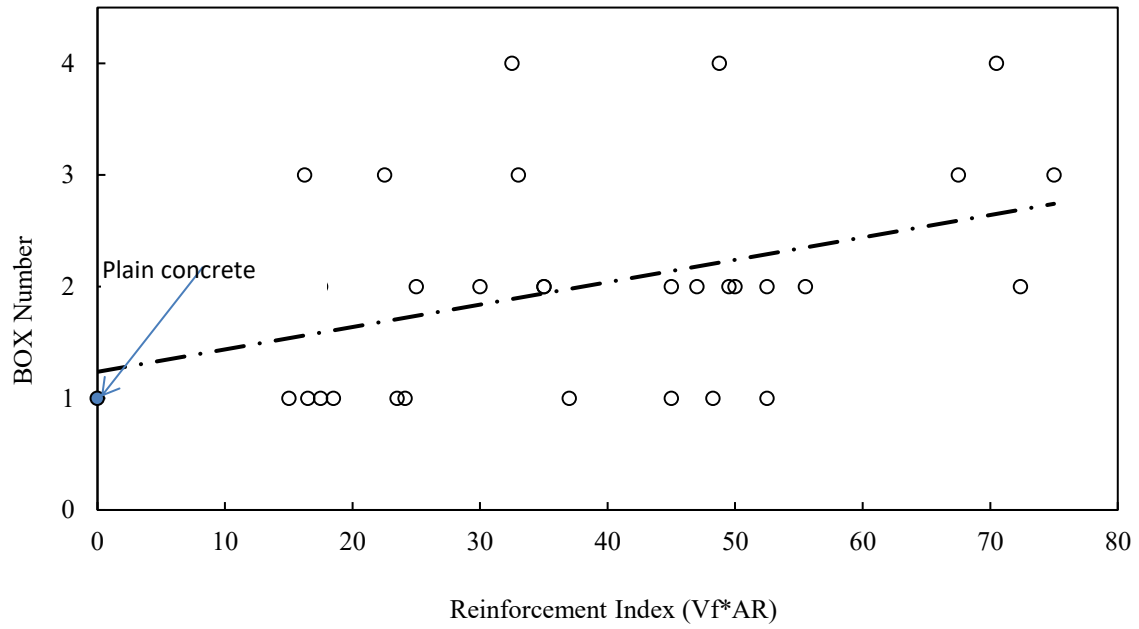
Figure 5-5. Box number as a function of reinforcement index.

5.2 HARDENED CONCRETE RESULTS

The following sections discuss the effects of fiber dosage, type, and geometry on the post-crack performance parameters such as residual strength (RS) and residual strength ratio (RSR) as well as on the other hardened concrete test results, such as compressive strength, modulus of elasticity, and modulus of rupture.

5.2.1 Compressive Strength and Modulus of Elasticity

Figure 5-6 and Figure 5-7 show trends for both steel and synthetic FRC mixtures tested for compressive strength and modulus of elasticity (based on the lab test) as a function of reinforcement index. These figures show that the change in reinforcement index did not significantly influence the compressive strength and modulus of elasticity for synthetic fibers. The average compressive strength for synthetic fiber reinforced concrete was 6,810 psi with a standard deviation and coefficient of variation of 323 psi and 4.74 percent, respectively. The average modulus of elasticity for synthetic FRC was 4,742 ksi with a standard deviation and coefficient of variation of 241 ksi and 5.08 percent, respectively. The compressive strengths of the PCC (6,960 psi) and synthetic FRC were comparable. On the contrary, the one steel FRC tested showed a significant increase in compressive strength and a relatively small increase in modulus of elasticity when the reinforcement index was increased. The compressive strength for the steel FRC increased from 7,330 to 9,320 psi for a change of V_f from 0.25% to 0.75%. This finding is in concordance with the study conducted by Mahadik & Kamane, 2014 where it stated that the compressive strength of steel FRC increases with the increase in fiber content until 0.75 percent V_f, after which it decreases.
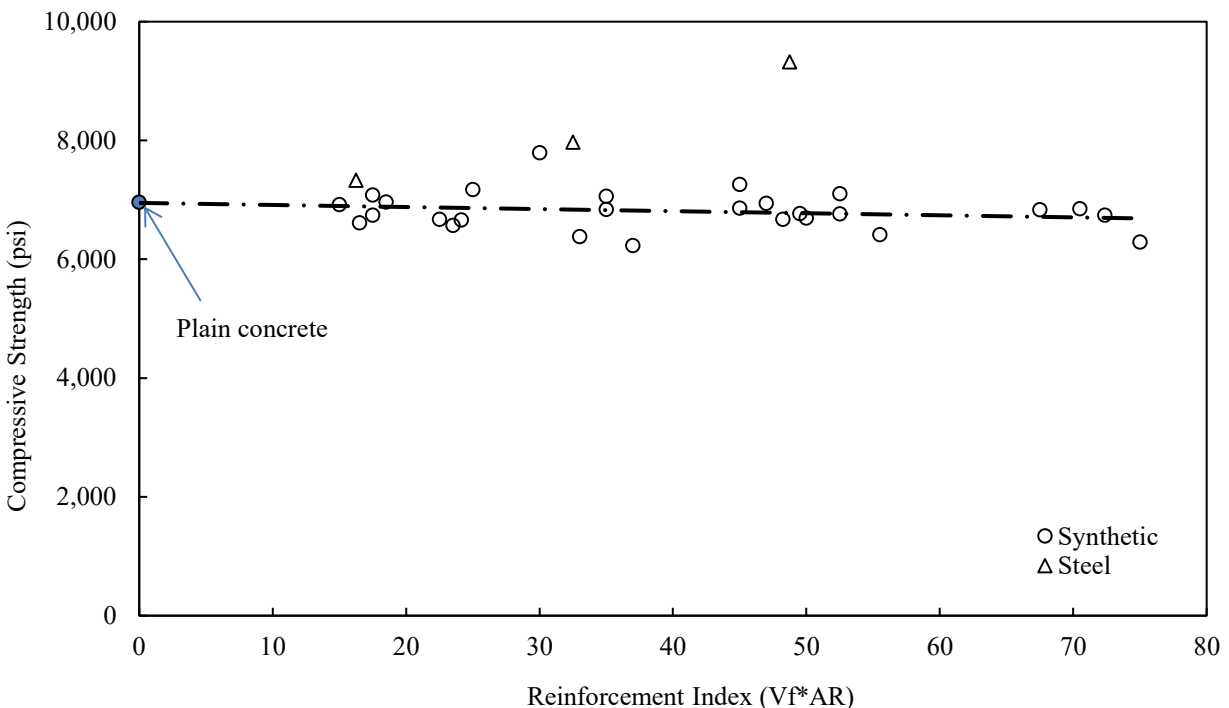
Figure 5-6. Compressive strength as a function of reinforcement index.

65
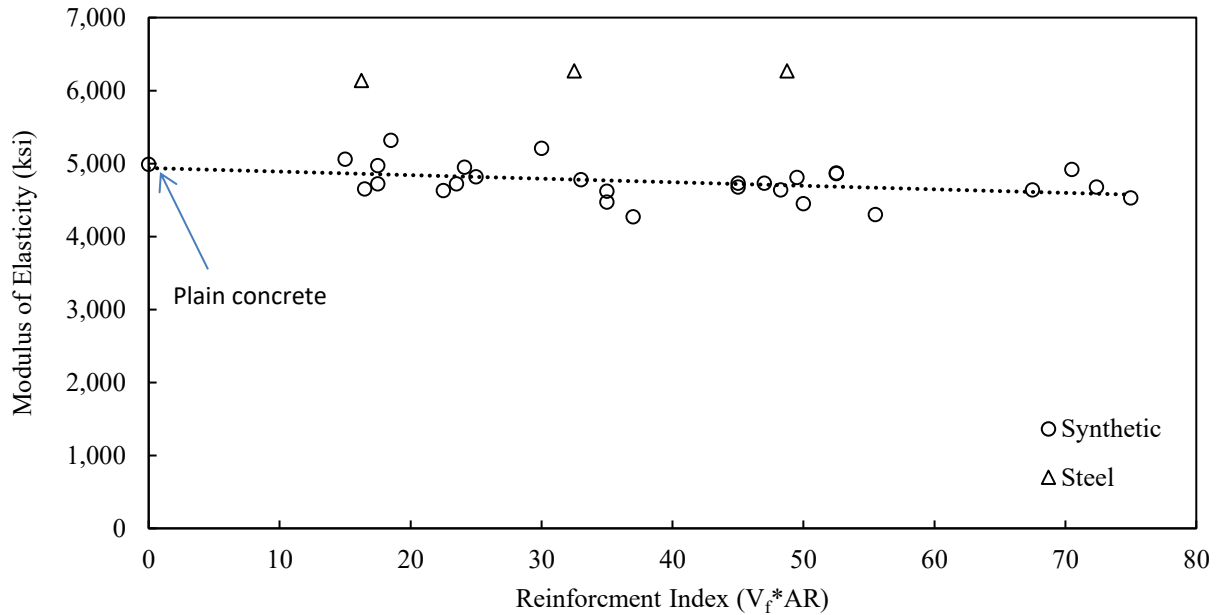
Figure 5-7. The modulus of elasticity as a function of reinforcement index.

5.2.2 Modulus of Rupture (MOR)

The modulus of rupture versus reinforcement index is plotted in Figure 5-8. Similar to the compressive strength, the MOR was also not significantly influenced by the reinforcement index for the synthetic FRCs. The average and standard deviation of the MOR for all the synthetic FRC mixtures was 738 psi and 35 psi, respectively, with a coefficient of variation equal to 4.79 percent. The MOR for the plain concrete was 720 psi which is comparable to MOR of the synthetic FRC mixtures. The MOR for the steel FRC was however found to increase with the increase in reinforcement index, especially when the reinforcement index exceeded 32.5. Figure 5-9 shows the MOR as a function of volume fraction of fibers in the mixture. As anticipated, the MOR also remained minimally influenced by the volume fraction of synthetic fibers. The MOR for the steel FRC increased with the increase in the V_f. It may be stated that the aspect ratio of all fibers considered in this study varied between 65 and 100, which is relatively narrow range, but includes a large variety of commercially available fibers typically used in concrete overlays. Since the volume fraction, aspect ratio, and reinforcement index of the synthetic fibers did not influence the MOR significantly, Figure 5-9 was plotted to investigate the influence of fiber geometry on the MOR. It appeared that the synthetic straight fiber S.S.3 has shown consistently greater MOR for all the three dosages. The MOR for straight synthetic fiber S.S.4 was moderate and was minimally influenced by the V_f. The straight synthetic fiber S.S.1 experienced gain in MOR with the increase in V_f. The MOR of the synthetic continuously crimped S.C.6 fiber had increased with the increase in fiber content. The MOR for this particular FRC was the lowest when the fiber V_f was 0.25% and significantly increased with the increase in V_f. Among the embossed fibers, the MOR of S.E.8 was not significantly influenced by the fiber V_f, and showed the maximum MOR at 0.5%V_f; the MOR of S.E.7 was highest at 0.5% V_f. The MOR of synthetic fiber S.S.2 and twisted fiber S.T.5 were found to be decreasing with the increase in fiber volume fraction. The MOR of the steel FRC, L.E.C.10, was found to be increasing with the increase in fiber volume fraction. Lastly, it can be stated that for all the synthetic FRC mixtures, the

66

MORs approximately lied between 700 psi and 800 psi, meaning a variation of 100 psi, which may not be a significant variation when considering the large variation in fiber dosage.
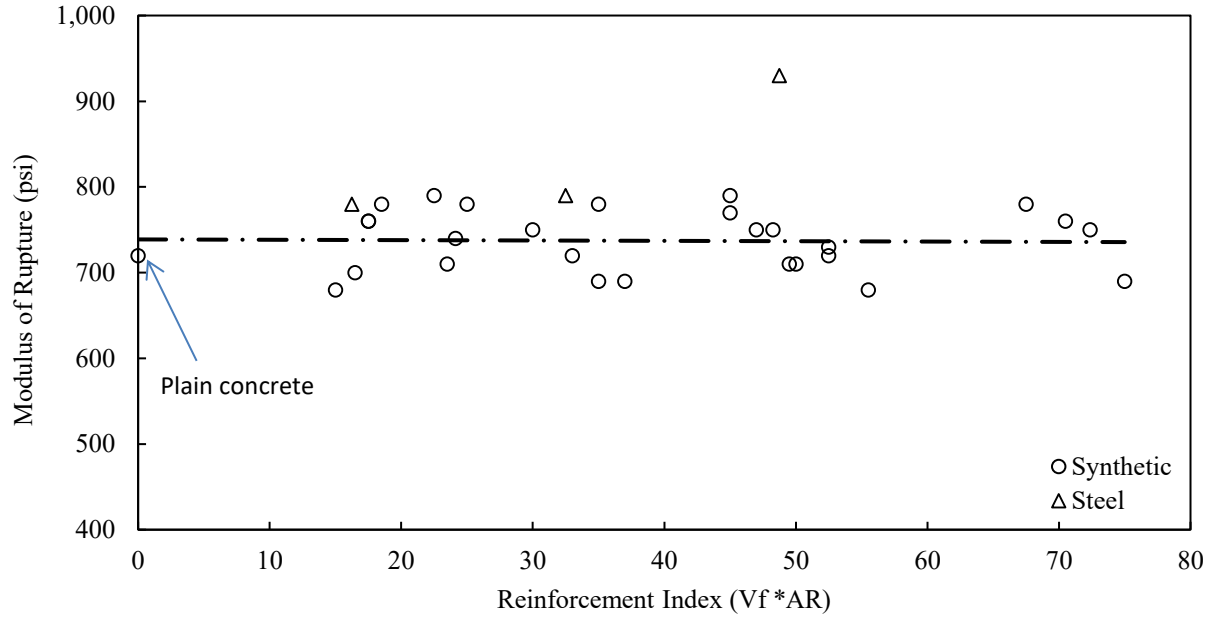
Figure 5-8. Modulus of rupture as a function of volume fraction for FRC mixes together.
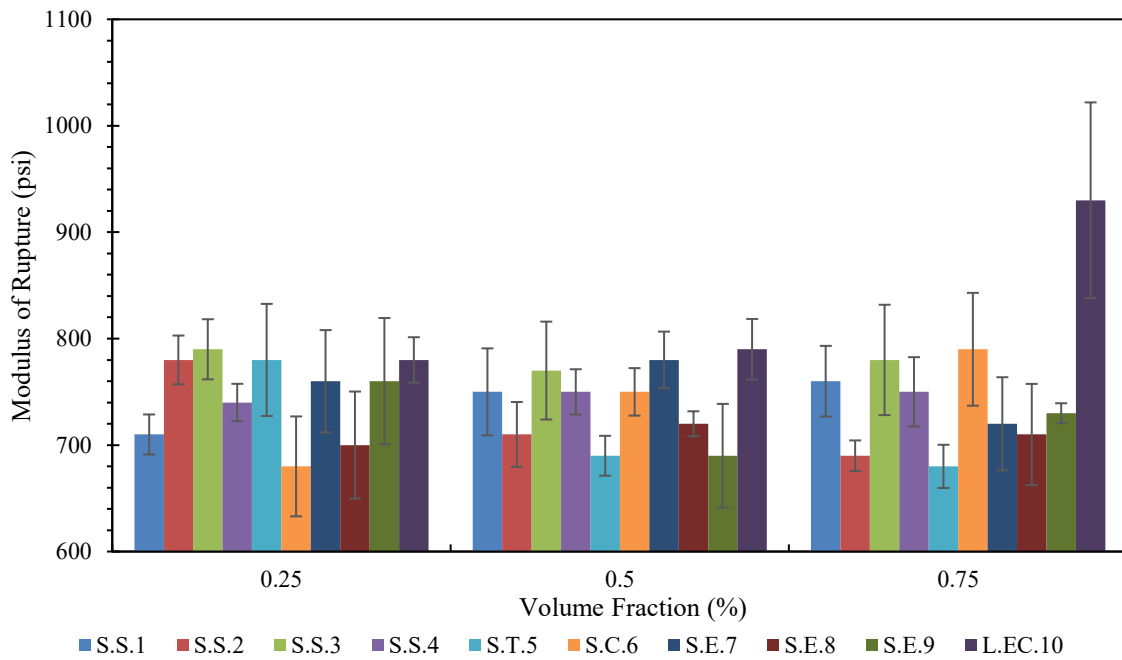
Figure 5-9. The modulus of rupture versus volume fraction for each fiber considered in this task.

5.2.3 Residual Strength Ratio (RSR) and Residual Strength

Residual strength or the post-crack strength of fiber reinforced concrete indicates the ability of fibers in restraining macro-crack propagation. Residual strength in ASTM C1609 test refers to the stress on the beam when the mid-span displacement reaches 0.12 inches. The influence of several factors such as fiber volume fraction, fiber length and aspect ratio, fiber geometry, and reinforcement index on the RSR was studied and discussed below.

5.2.3.1 Influence of V_f on RSR and Residual Strength

Figure 5-10 presents RSR as a function of V_f for each of the fibers evaluated in this study. Unlike other hardened concrete properties such as compressive strength, modulus of elasticity, and MOR, the RSR is highly influenced by the V_f of fibers in the mixture. The RSR has increased with the increase in V_f for all of the synthetic FRCs. The range of the RSR values obtained for all the FRC mixtures was between 3 and 51 percent. However, as anticipated, the rate of increment of RSR with respect to the V_f was not consistent across the fiber types.

It appeared that the synthetic embossed fiber S.E.9 had shown consistently greater RSR for all the three dosages. The other synthetic embossed fiber S.E.7 and synthetic crimped fiber S.C. 6 also resulted in above average RSR values with slightly less incremental increase in RSR beyond 0.5% V_f. The RSR versus V_f trends of S.T.5 and S.S.4 were similar in comparison and performed near the overall average for all synthetic fibers considered. The S.E.8 resulted in good RSR at 0.25% V_f but showed less of an increase at higher dosages; the synthetic straight fiber S.S.2 had shown almost an opposite trend. For fiber S.S.3, the RSR at 0.25% V_f was among the lowest of all the RSR values obtained in this study, but showed moderate RSR at 0.75% V_f. Fiber S.S.1 and S.E.8 have resulted in good RSR values at the 0.25% V_f but were among the lowest RSR values at 0.75% V_f. Overall, the RSR and V_f has an excellent correlation, as can be seen in Figure 5-11; R^2 is equal to 0.86. Steel fibers were not considered in this correlation. The steel fibers resulted in relatively surprising results; the RSR for 0.75% V_f was lower than that observed for 0. 50% V_f.
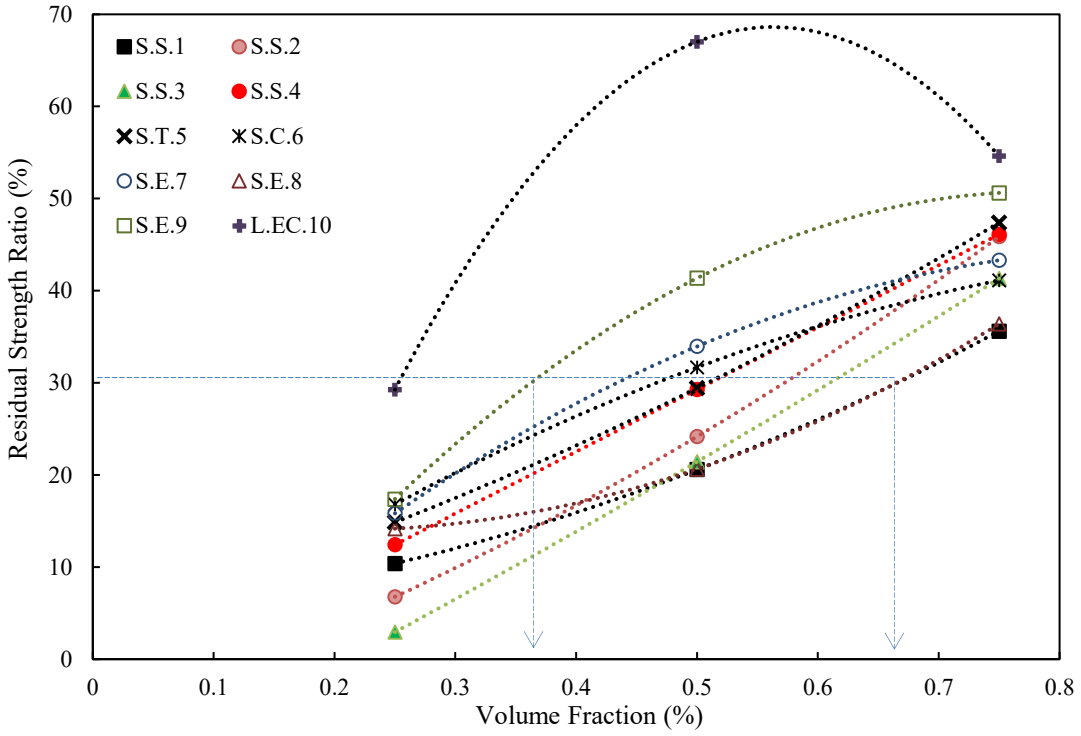
Figure 5-10. The residual strength ratio versus fiber volume fraction for various fibers.
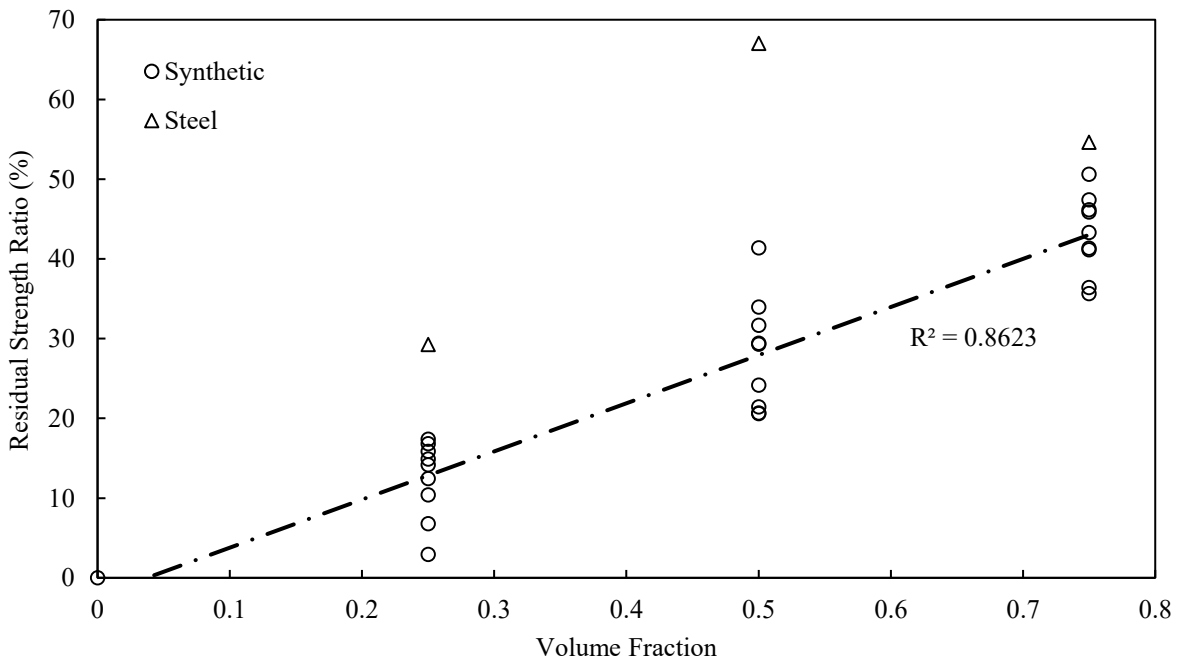
Figure 5-11. Correlation between the RSR and V$_f$.

The residual load (lbf) with respect to the V_f is plotted in Figure 5-12. It can be seen that even though the RSR for the steel fibers was lower at 0.75% V_f as compared to 0. 50% V_f, the residual load was higher at 0.75% V_f. The reason for this surprising result is related to the MOR. As shown in Figure 5-8 and Figure 5-9, the MOR for steel FRC was significantly higher, 9,320 psi at 0.75% V_f as compared to 7,970 psi at 0.50% V_f, which resulted in a downward trend in the RSR versus V_f curve for the steel FRC. Figure 5-13 shows the residual strength (psi) for each fiber considered in this study, in the form of a bar-chart.
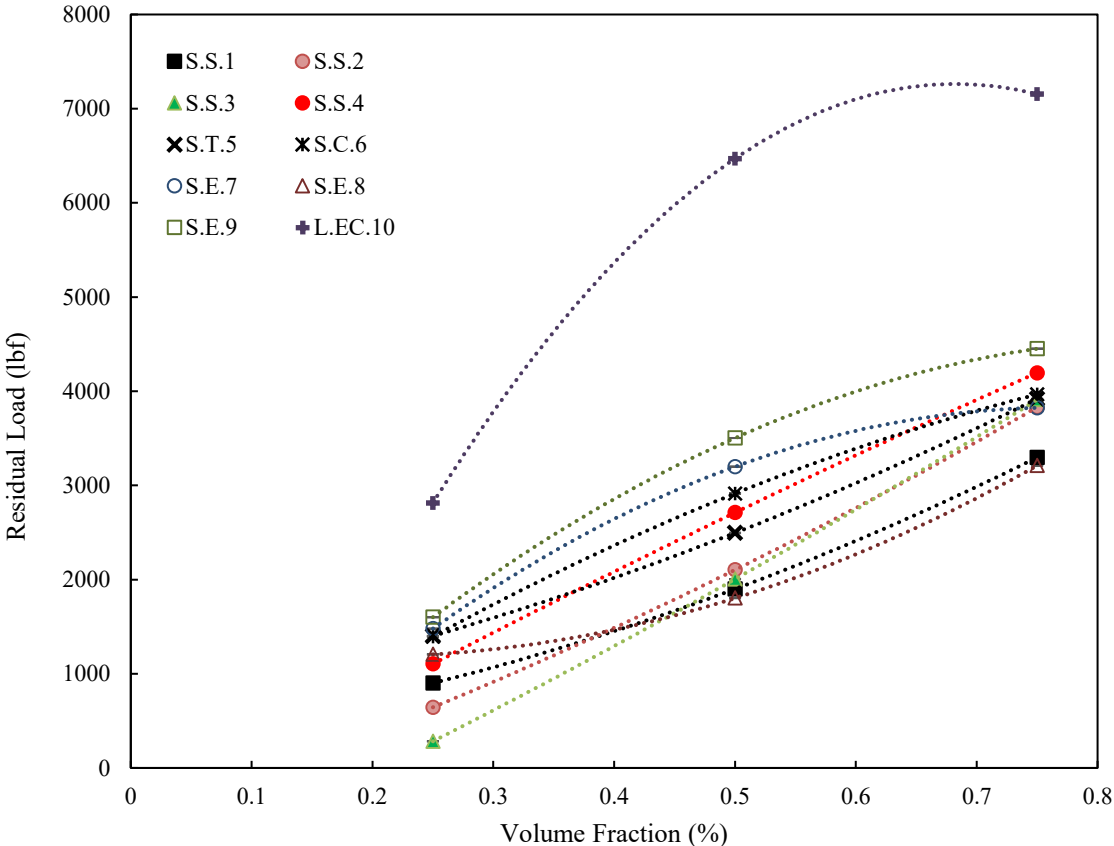
Figure 5-12. The residual load as a function of fiber volume fraction.
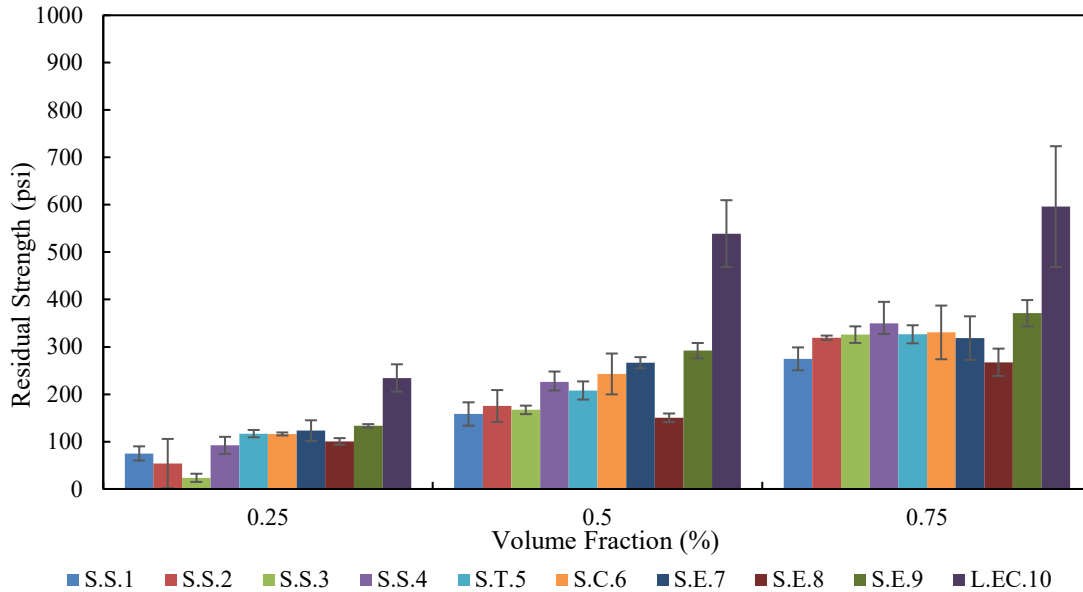
Figure 5-13. The residual strength for each fiber considered in this task.

5.2.3.2 Influence of Fiber Geometry and Materials on RSR and Residual Strength

Figure 5-10 and Figure 5-12 also showed that the geometry and cross section of the fibers affects the RSR and RS. For example, if the required RSR is 30 percent, then that can be achieved using 0.36% V_f (5.25 to 5.75 lb/yd^3) of S.E.9 fibers, whereas 0.66% V_f (9.75 to 10.25 lb/yd^3) of S.E.8 or S.S.1 fibers would be required. In general, these figures suggest that embossed, twisted, and crimped fibers performed better on average than straight synthetic fibers when the comparison was made in terms of RSR or residual strength, as shown in Figure 5-14. This figure shows that continuously crimped and embossed fibers had similar and slightly better RSR than the twisted fibers, up to a 0.65% V_f (Figure 5-14a). The RSR of the straight flat fibers was consistently low. Incidentally, these fibers also had less stiffness than their counterparts. Similar to the RSR trend, the RS for the continuously crimped and embossed fibers were also higher than the other fibers (Figure 5-14b). Therefore, consideration of fiber geometry and stiffness while deciding fibers for concrete overlays or pavements may be an economical choice and can produce more workable concrete mixture with fewer amounts of fibers for a given RSR or RS.

Regarding the influence of the material on the RSR, the steel fibers outperformed the synthetic fibers by a significant margin. Table 5-1 presents a comparison of the RSR values between the synthetic fiber and steel fibers obtained for a range of fibers dosages. Steel fibers at a dosage of 0.25% V_f provided a greater RSR than the synthetic fibers at 0.5% V_f. As was discussed previouly, it is common to specify a residual strength ratio of 20 percent or simply place 3 pounds per cubic yard in a thin overlay. Given the average results of this task, on a conservative estimation, a fiber dosage of 4.6 lb/yd^3 (continuously crimped, embossed and twisted) to 6.8 lb/yd^3 (flat straight) for synthetic fibers and 22 to 28 lb/yd^3 for steel fibers tested in this task can be used to achieve 20 percent RSR. However, as mentioned before, fiber geometry, cross section, and stiffness play a significant role, so these factors shall be considered in selecting the fiber dosage
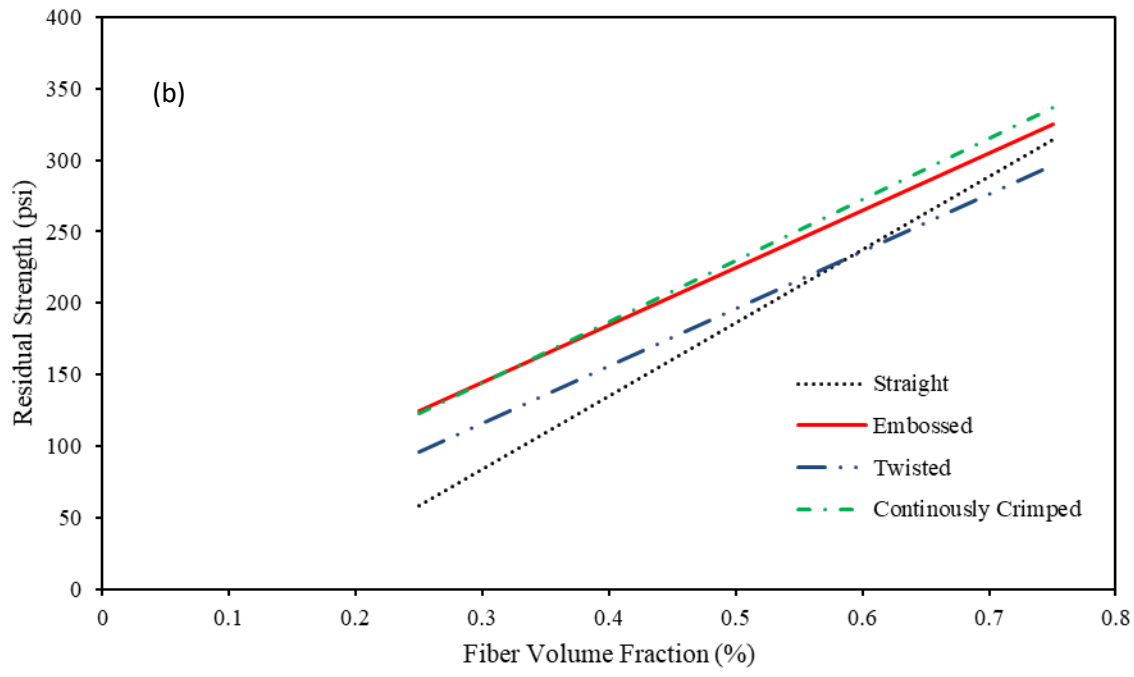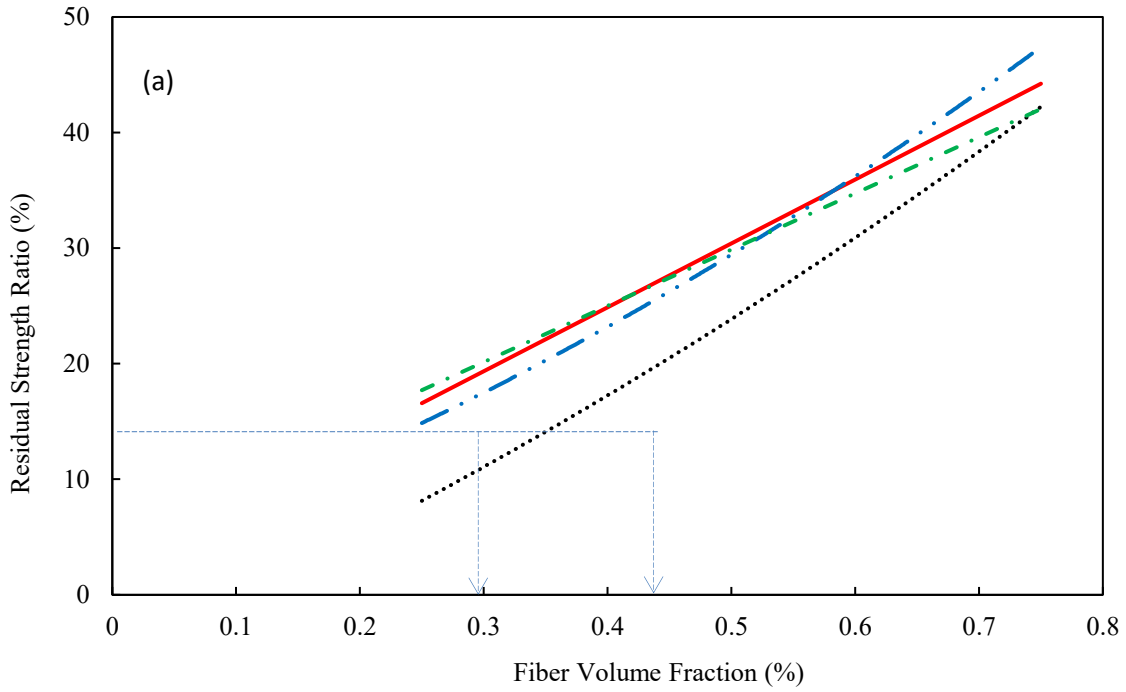
Figure 5-14. The (a) RSR and (b) RS as a function of geometry of fibers.

Dosage V_f, lb/yd³	Synthetic Fiber RSR (%)		Dosage V_f, lb/yd³	Steel Fiber RSR (%)
0.25, 3.8	12.4		0.25, 33	29.3
0.5, 7.6	28.1		0.5, 66	67.0
0.75, 11.8	43.1		0.75, 99	54.6

5.2.3.3 Influence of Fiber Length and Aspect Ratio on RSR

To see the effect of fiber length and aspect ratio on the RSR, the RSR values of FRCs obtained at one fiber dosage have been compared. Figure 5-15 and Figure 5-16 present RSR as a function of fiber length and aspect ratio, respectively, for synthetic fibers with a 0.5% V_f. Data points in these figures were divided in two broad categories. Category 1 included straight, small effective diameter, and low stiffness fibers, and Category 2 included crimped or embossed fibers with large effective diameters and high stiffness. The correlations between the RSR and fiber length, and between the RSR and aspect ratio were not great, possibly because of a narrow range of fiber length (1.5 to 2.4 inch) and aspect ratio (60 to 100) considered in this study. The trend lines in Figure 5-15 and Figure 5-16 indicated that longer fibers with larger effective diameters result in higher residual strength. However, this may also be noted that a majority of the longer, larger diameter fibers were either embossed or crimped, potentially creating a better fiber-concrete bonding condition.
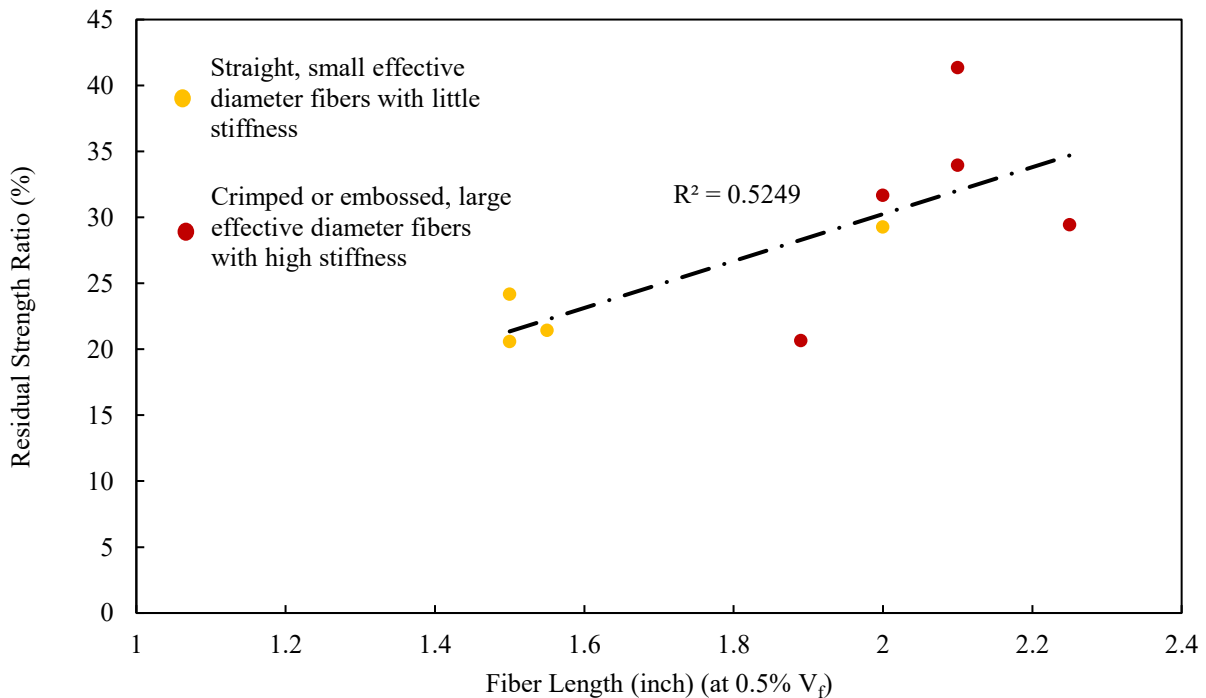
Figure 5-15. Residual strength ratio versus fiber length for synthetic FRCs.

73
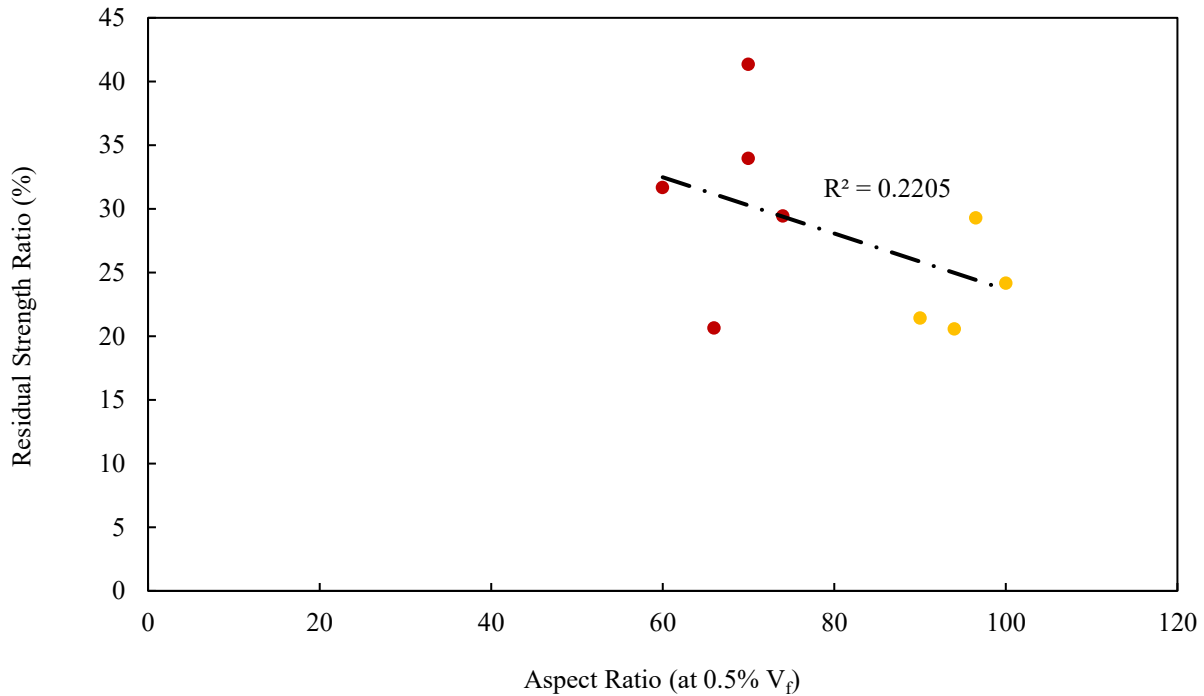
Figure 5-16. Residual strength ratio versus fiber aspect ratio for synthetic FRCs.

5.2.3.4 Influence of Reinforcement Index (RI)on the RSR

The commercially available fibers differ in terms of geometric properties, length, effective diameter, and aspect ratio. As discussed previously, the RSR of FRC largely depends on the V_f, fiber geometry, and somewhat on the fiber length and aspect ratio; therefore, it is logical to correlate the RSR with the reinforcement index of the fibers which allows for flexibility in aspect ratio and volume fraction. Figure 5-17 shows the variation of the residual strength ratio as a function of reinforcement index for all the fibers together. The trends are somewhat like the trends observed in the case of RSR vs V_f, with fibers S.E.9 performing the best and fibers S.S.1 and S.S.2 performing the worst among the synthetic fibers. Figure 5-18 shows the correlation between the RSR and RI. The correlation can be treated as good (R^2 = 0.68) considering the large number of variables involved. Since only one type of steel fiber was used, the steel fiber was not considered in this correlation. This correlation may be useful for selection of fibers for a certain value of RSR when many commercial fibers are available to choose from.
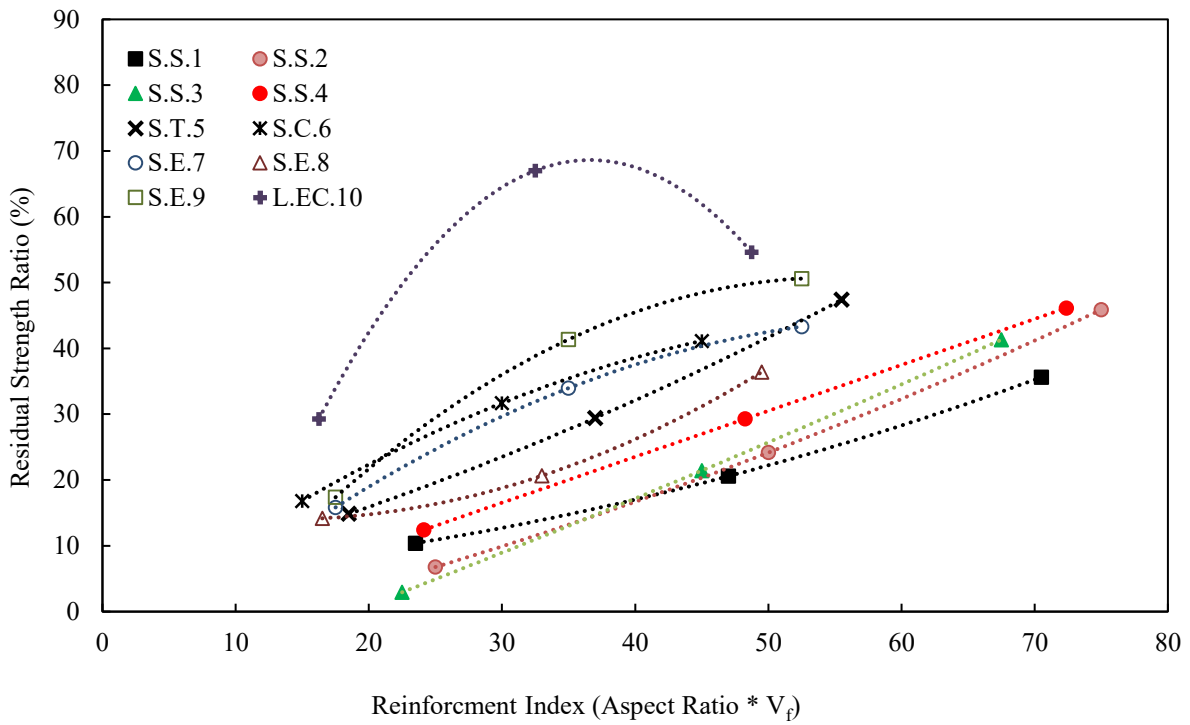
Figure 5-17. Residual strength ratio versus reinforcement index showing all the FRC mixtures separately.
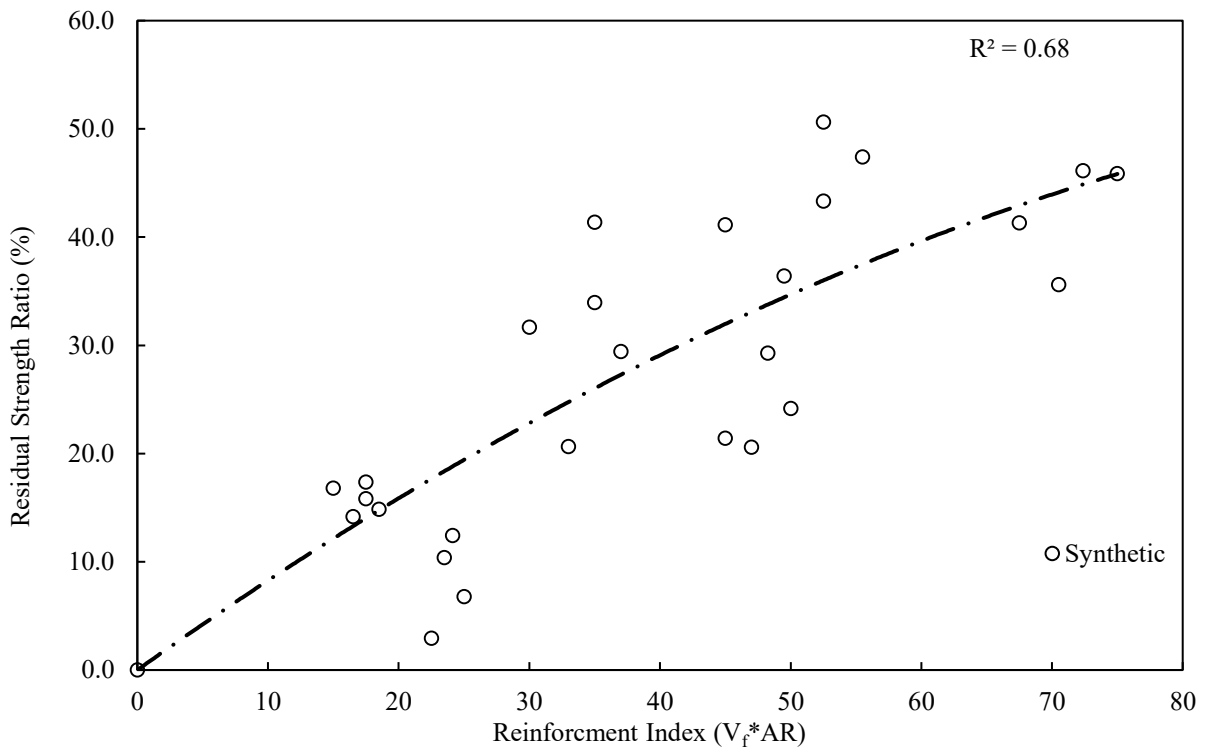
Figure 5-18. Correlation between the residual strength ratio and reinforcement index.

CHAPTER 6: JOINT PERFORMANCE RESULTS AND DISCUSSIONS

This chapter presents the results of the laboratory tests performed in Task 4 for characterizing the joint performance. In this work, mixes were prepared for the following fiber types: S.S.4, S.T.5, S.C.6, S.E.9, S.T. 11 at 0.5% V_f and 0.25% V_f. The concrete mixture design for the mixes prepared in Task 4 were similar to that of the corresponding mixes prepared in the Task 3. In addition to the joint performance tests, concrete mixtures were tested for compressive strength to make sure that the hardened concrete properties of the Task 4 mixes were comparable to the Task 3 mixes for the above mentioned fibers. All the mixtures produced in Task 4 were also tested for slump and air content to ascertain that the target ranges of slump and air content are achieved, as discussed in 5.1

Task 4 tests were completed in four phases, with each phase designed and added based on the results seen in previous phases. The phases are described in the following sections with results and discussion occurring in later sections.

6.1 DESCRIPTION OF WORK

6.1.1 Phase 1 – Joint Performance Versus Fiber Property and Crack Width

Phase 1 investigated the influence of fiber geometry, length, effective diameter, and crack width on the various joint performance characterizing parameters, such as LTE, differential joint energy dissipation, and loaded side peak displacement (D_p). All the FRC mixtures in this phase were prepared using a constant dosage of fibers, i.e., 0.5% V_f, with the intention to conduct more testing at a lower dosage if time was available after the completion of planned work. Along with FRC specimens, a plain concrete (no fibers) mixture was also tested for comparison purposes. All the beam specimens were tested for joint performance at different crack widths; the test started with the lowest possible crack width, very close to the crack width that developed at the time of cracking at 18 hours after casting. The crack width was then gradually increased and tested for joint performance until the measured LTEs was lower than 20% (approximately).

6.1.2 Phase 2 – Joint Performance Versus Load Repetitions

The Phase 2 tests were conducted to evaluate the effect load repetitions have on the joint performance. Specimens tested in this phase were subjected to 500,000 load repetitions (cycles) at a constant crack width of 0.05 inches. This crack width was chosen so that the crack faces are subjected to enough mechanical abrasion under the dynamic load, and at the same time, not too wide to provide only a negligible joint performance. Previous experience with the joint performance study conducted at the University of Pittsburgh (Barman, 2014) led to the conclusion that when FRC concrete is fatigued at or below 0.035-inch crack width, the joint performance is hardly influenced by the load repetitions. During the load repetitions, crack width was periodically measured to make sure it remained at 0.05-inch $\pm$ 0.001-inch. Initially in this phase, three specimens were tested for each mix; however, after recognizing the insignificant influence of the load repetitions (within 500,000 load cycles) on the joint performance, only one specimen was tested for each of the remaining mixes.

6.1.3 Phase 3 – Joint Performance Versus Crack Width Contraction and Expansion

In previous work conducted by Barman and Vandenbossche (Barman, 2014), it was observed that after a crack width had largely expanded (beyond the elastic limit of fibers), the joint performance of the FRC decreased significantly when the crack width was later contracted. The decrease in the joint performance could be attributed to the decrease in stiffness of the fibers, which resulted due to the plastic elongation of fibers under the combined effect of axial tensile stress and vertical dynamic load at an expanded crack width. In Phase 3, the effect of the above-mentioned crack width expansion and contraction on joint performance was studied. Part of the testing in this phase consisted of capturing joint performance, similar to Phase 1, where the crack width was gradually increased. In addition to that, when the crack width reached100 mils, it was contracted to nullify the axial tensile stress in the fibers or to make fibers loose. The beam was tested at this point once for joint performance, then again multiple times with the joint being forced closed (joint face compression). In some cases, the crack width was expanded to approximately 150 mils, and then closed and tested for multiple times. The 100-mil crack width was chosen, reasonably, as the largest crack width that would be observed in field conditions (Barman, 2014; Jensen and Hansen, 200; Hansen, et al., 1998); whereas, the 150-mil crack width was chosen to represent an extreme situation that may occur because of limited number of joint deployments (joint deployment refers to cracking of concrete below the saw cuts).

6.1.4 Phase 4 – Joint Performance Versus Fiber Dosage

In this phase, the influence of fiber dosage on joint performance was studied. Beam specimens were prepared with one more additional fiber dosage, i.e. 0.25% V_f. Due to time constraints, only two fibers, S.S.4 and S.E.9, were tested in this phase: the worst and best performing fibers in Tasks 3. Results from this phase were compared with the results from the Phase 1 to draw conclusions on the influence of fiber dosage on the joint performance.

6.2 PROPERTIES OF CONCRETES USED

The fresh concrete properties and concrete compressive strength for all the mixtures prepared in Task 4 tests are provided in Table 6-1. These results are presented as quality control measures and will not be part of the analysis in this report. The first column of Table 6-1 provides the mixture designation with the phase number [left most digit(s)] at which the test was performed. For example, 1 - S.S.4.5 corresponds to the concrete mixture produced in Phase 1 (of Task 4) for the S.S.4 fibers with 0.5% V_f dosage. Maximum effort was made to keep the fresh concrete properties consistent across the batches and fiber types. It can be seen that the slump value ranged between 1 and 3 inches and the air content ranged between 5.9% and 8.6%. The compressive strength ranged between 6,330 and 7,490 psi.

Table 6-1. Plastic and hardened concrete properties for the mixtures prepared for Task 4 tests.

Designation	Phase	Fiber Volume Fraction % (V_f)	Slump (in)	Air Content (%)	Compressive Strength (psi)
1 - Plain Concrete	1	0	2.5	8.5	6750
1 - S.S.4.5	1	0.5	3	6.6	7190
1 - S.T.5.5	1	0.5	2	6.9	7340
1 - S.C.6.5	1	0.5	1	7.1	7490
1 - S.E.9.5	1	0.5	2.5	8.5	6610
2 - Plain Concrete	2	0	1.5	8.5	6920
2,3 - S.S.4.5	2,3	0.5	1	8.6	6650
2,3 - S.T.5.5	2,3	0.5	3	6.8	7280
2,3 - S.C.6.5	2,3	0.5	1	5.9	7120
2,3 - S.E.9.5	2,3	0.5	1.5	7.5	6550
3,4 - S.E.9.25	3,4	0.25	2	7.8	7470
3,4 - S.S.4.25	3,4	0.25	2	8.5	6330

6.3 TYPICAL JOINT PERFORMANCE TEST RESULTS

This section will discuss typical trends of the joint performance test results. Due to the large volume of test results and plots, the majority of the plots from this task are provided in the Appendix. Photographs of the test specimens are also provided in the Appendix; it should be noted that the crack width shown in those photographs does not represent a specific crack width, as the photographs were taken after the testing; the purpose of providing these photographs is only to document the shape of the crack. Joint performance test results consist of load and displacement profiles for the loaded and unloaded sides of the beam specimen. In order to show differences in the trends of load and displacement profiles with respect to fiber volume fraction and crack width, the data in this section is presented for a plain concrete, 0.25% V_f, and 0.5% V_f beam specimen. A comprehensive analysis and discussion of these results can be found in the following section.

6.3.1 Load and Displacement Profiles in Joint Performance Test

To understand how fiber dosage and crack width affect the load and displacement profiles, Figure 6-1 shows results from three different beams varying with fiber dosages (0% V_f, 0.25% V_f, and 0.50% V_f). It can be seen in Figure 6-1 (i) that an increase in crack width (from 16 mils to 126 mils) led to an increase in the loaded side peak displacement and a decrease in the unloaded side peak displacement, leading to a decrease in the joint performance. Similar observations can also be noticed in Figure 6-1 (ii) and Figure 6-1 (iii). From comparing Figure 6-1 (i), (ii), and (iii), it can be stated that the fibers contribute to keep the difference between the loaded side and unloaded side displacements low for the FRC beams. Figure 6-2 shows how an increase in fiber dosage dramatically affects the LTE, particularly at wider crack widths. In order to see the difference between tension LTE and compression LTE under the dynamic load, both of these LTEs are included in Figure 6-2. The magnitude of tension and compression LTEs are a function of the crack shape (macro texture), and one can be greater than the other depending on the crack shape. In the results of the three beams considered in Figure 6-2, the tension LTE was slightly higher than the compression LTE for the plain concrete beam; however, no trends could be observed for

the FRC beams. Figure 6-2 also compares the trends of static LTEs with dynamic LTEs. Static LTE, opposed to dynamic LTE, is determined by applying a static compression load on the loaded side of the beam specimen and measuring the loaded and unloaded side displacements. In this study, a compression load of 1,050-lbs (equal to the peak load for the dynamic LTEs) was applied on the beam at various crack widths. In each crack width, the load was held for 10 minutes before measuring the displacements on the loaded and unloaded sides. The reason for holding the load for 10 minutes is the visco-elastic behavior of the neoprene pad used at the top and bottom of the beam. Because of this behavior, the neoprene pad continues to be compressed for a certain amount of time; a period of 10 minutes was considered for this study. It can be seen that the static LTEs were slightly higher than the dynamic LTEs for the plain concrete and concrete with 0.25% $V_{f,}$ while similar to dynamic LTEs for the concrete with 0.5% V_f.
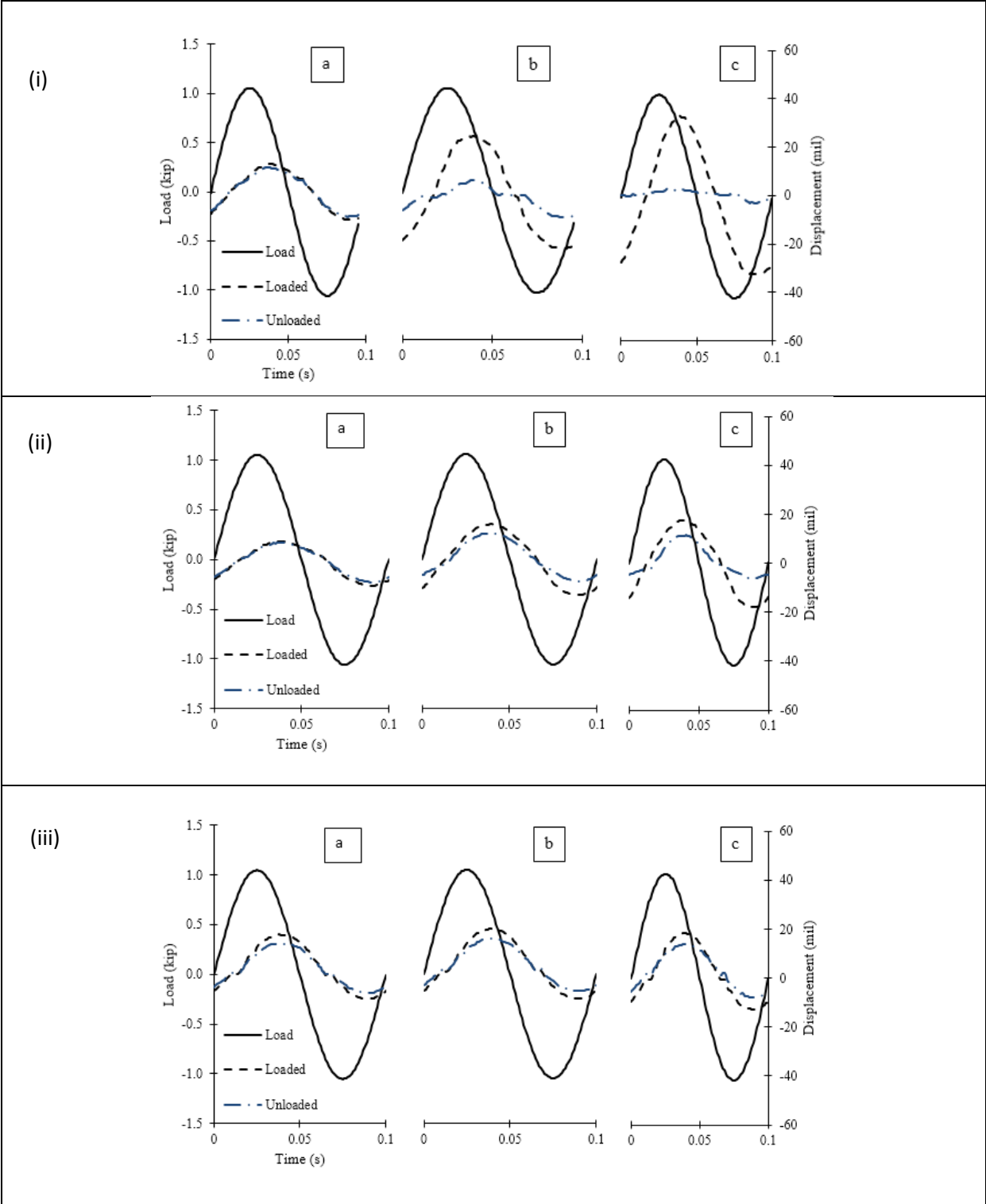
Figure 6-1. Typical load and displacement profiles at increasing crack widths (i) plain concrete (crack widths: a = 16, b = 47, and c = 126 mils); (ii) 0.25% V_f, (crack widths: a = 7.5, b = 57, and c = 81mils); and (iii) 0.50% V_f (a = 6, b = 50, and c = 117mils).

80
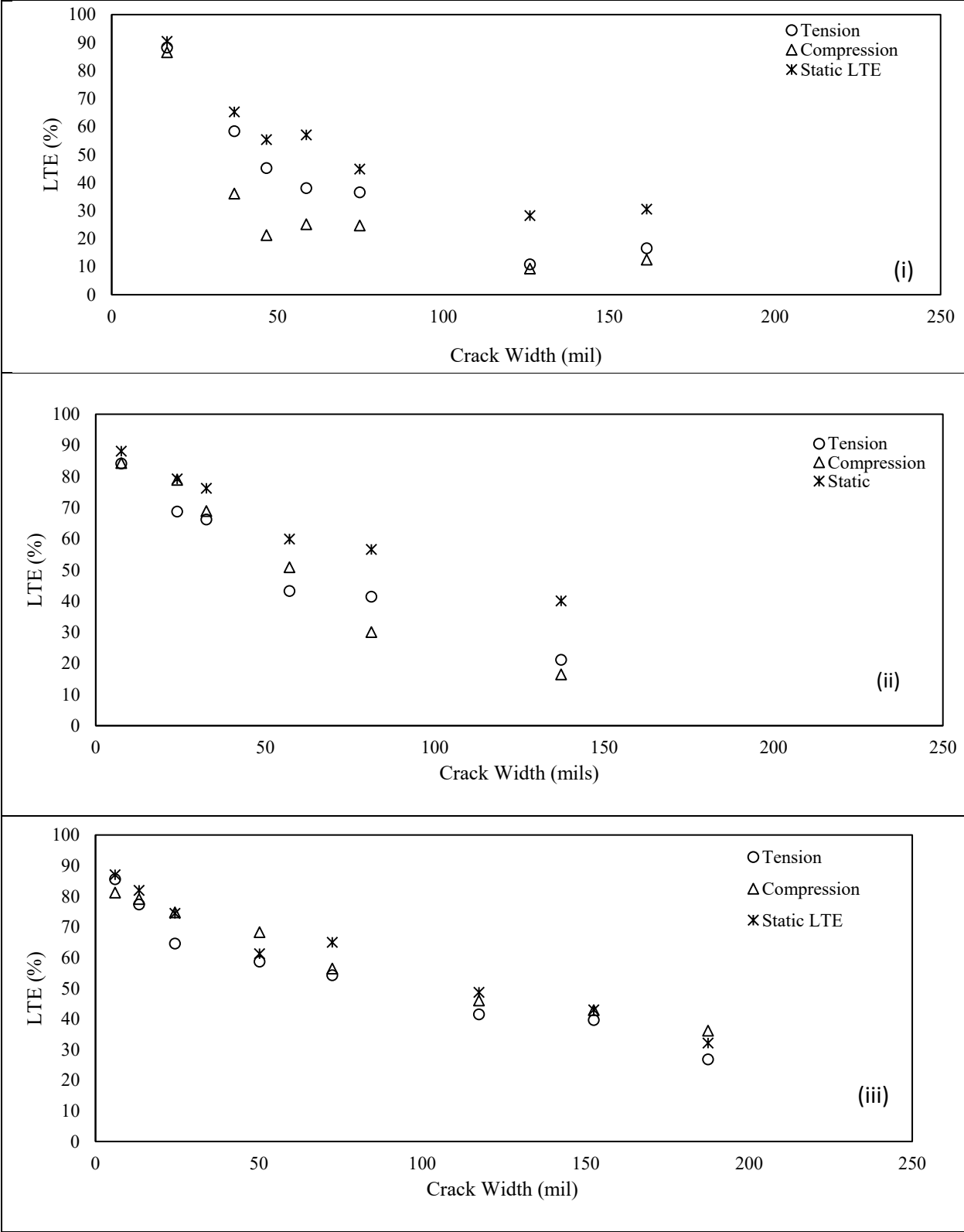
Figure 6-2. LTE as a function of crack width: (i) plain concrete, (ii) 0.25% V_f FRC, and (iii) 0.50% V_f FRC.

6.3.2 Differential Displacement

Differential displacement is described as the difference between the loaded side peak displacement and unloaded side peak displacement. Figure 6-3 shows the differential displacement as crack width increases for plain concrete and FRCs with two fiber dosages. It can be seen, like in Figure 6-1, that an increase in fiber dosage leads to an increase in joint performance (less differential displacement). Comparison between the Figure 6-3 (ii) and Figure 6-1 (iii) shows that beam specimens with 0.5% V_f resulted in less differential displacement compared to the specimens with 0.25% V_f.

6.3.3 Differential Joint Energy Dissipation (DJED)

As the LTE and differential displacement are calculated using only the peak displacement, an effort has also been made to use the entire load and displacement profile to evaluate the joint performance; hysteresis of load - differential displacement is used for this purpose. Figure 6-4 shows examples of differential displacement being plotted against load for various crack widths. Figure 6-4 (i), (ii), and (iii) show the hysteresis for plain and fiber reinforced concrete beams (0.25% V_f, and 0.50% V_f). From these plots, it can be seen that the hysteresis representing plain concrete specimens were significantly wider than those with fibers. This behavior can be expressed by summing the area inside of these plots for each crack width, described as differential joint energy dissipation (DJED).
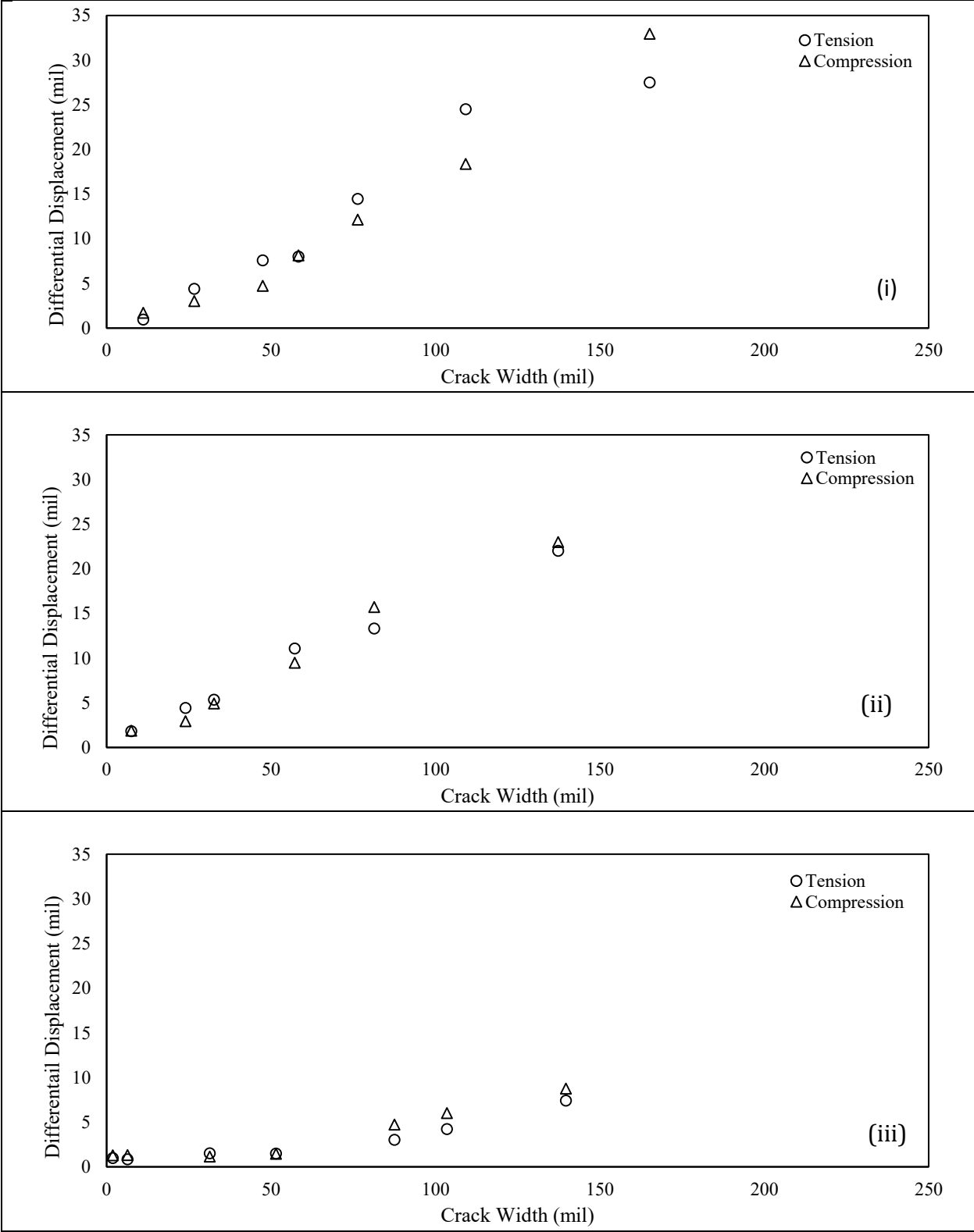
Figure 6-3. Differential displacement versus crack width: (i) plain concrete, (ii) 0.25%, V_f, and (iii) 0.50% V_f.
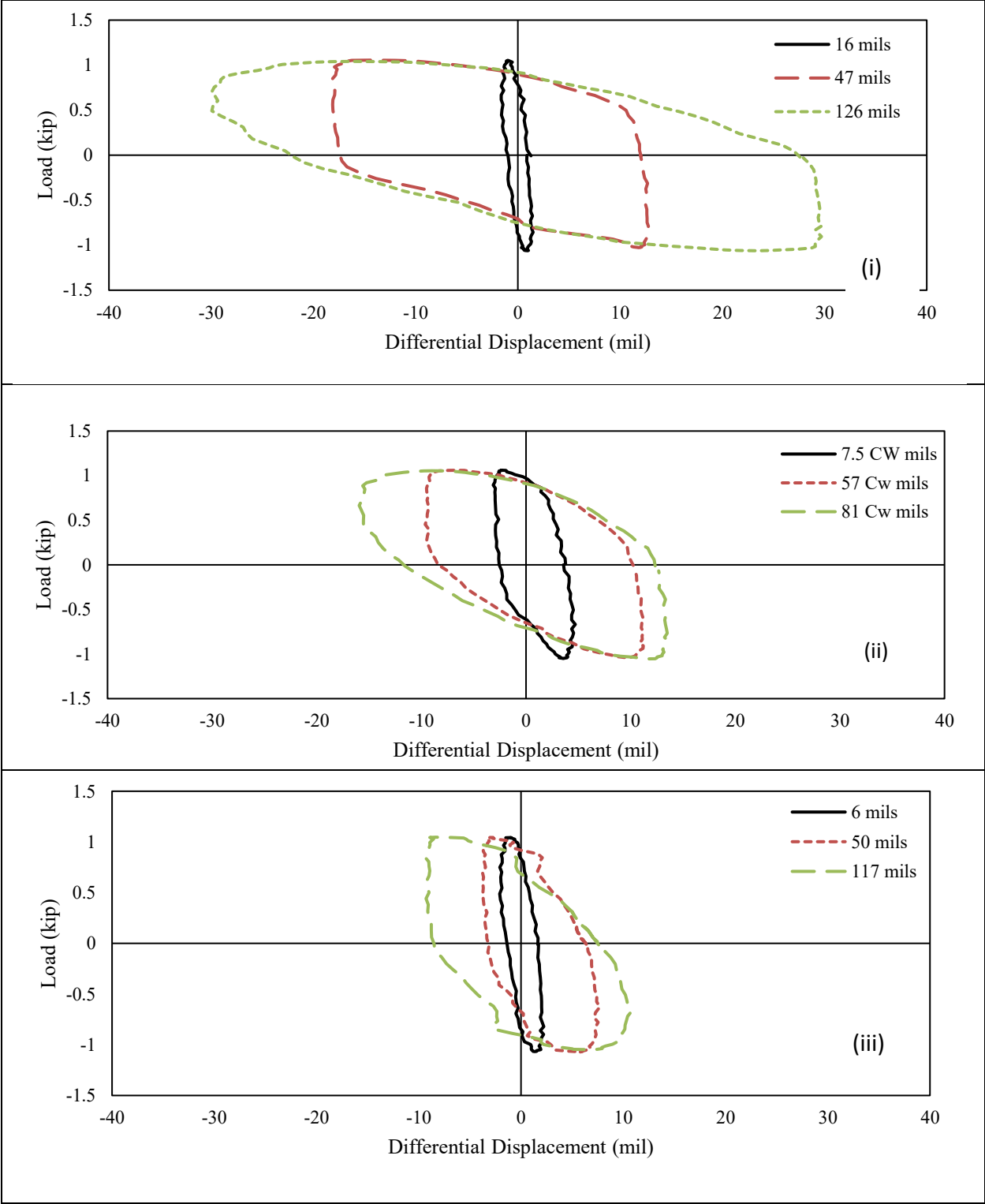
Figure 6-4. Hysteresis as a function of crack width: (i) plain concrete, (ii) 0.25% V$_f$, and (iii) 0.50% V$_f$.

6.3.4 Peak Displacement (D_p)

In addition to the above-mentioned joint performance evaluating parameters, the other important parameter is peak displacement. In weak joints, the displacement at both the loaded and unloaded sides can be similar, but very high. In such cases, LTE can be high and differential displacement and DJED could be low, but the magnitude of the peak displacements could be high and concerning. In order to capture the ability of fibers to minimize the peak displacement, joint performance data was analyzed by comparing the differences in peak loaded side displacement between the fiber and non-fiber reinforced concrete beams. Figure 6-5 displays one such plot, in which it can be seen that a plain concrete beam experienced larger displacement compared to a beam prepared with 0.5% V_f synthetic fibers. The fibers can reduce the peak displacement, which in turn can reduce distresses such as joint faulting, as well as other forms of joint deterioration.
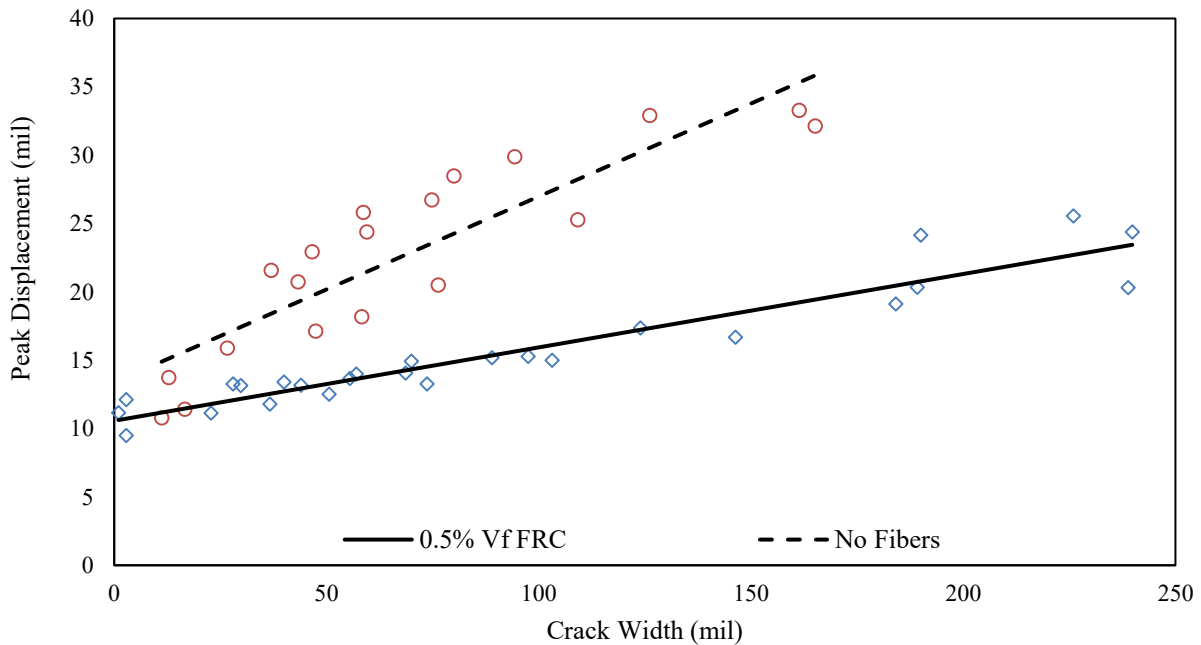
Figure 6-5. Peak displacement as a function of crack width for FRC and plain concrete.

6.4 DISCUSSION OF RESULTS

This section will discuss the effect of fiber properties, fiber dosage, and load repetition on the joint performance. Joint performance will be discussed in terms of LTE, DJED, and D_p, as a function of joint crack width.

6.4.1 Influence of Fiber Properties on Joint Performance

Figure 6-6, Figure 6-7, and Figure 6-8 show the trend lines for LTE, DJED, and D_p with respect to crack width for five different fibers used in Task 4. Each of these trend lines were plotted using the average results of three specimens prepared with 0.5% V_f fiber dosages. In Figure 6-6, it can be seen that the difference in the LTE across the fiber types are not very large, except a bi-linear relationship for the fiber S.T.11. In general, the longer and stiffer fibers such as S.T.5, S.C.6, and S.E.9 performed slightly better than the other two. When joint performance was compared in terms of DJED (Figure 6-7), it was found that the fiber S.T.11, which was used in the MnROAD cells constructed in 2017, resulted in lower joint performance at wider crack widths, especially beyond 110 mils. It may be reminded that Fibers S.S.4, which are laterally less stiff, had shown a lower residual strength ratio compared to other fibers when tested according to ASTM C1609 in Task 3. In general, fibers that have low individual stiffness, less irregularity in its geometry and less effective diameter after dispersion in to the concrete may provide less resistance against pull-out and plastic deformation than their counterparts, and can result in higher displacement or lower DJED during the joint performance test. As shown in Figure 6-8, compared to the other four fiber types, the S.S.4 fiber experienced 20 to 35 percent higher peak displacement when crack width exceeded 40 mils, and the S.T.11 fibers resulted in higher DJED at wider crack widths.
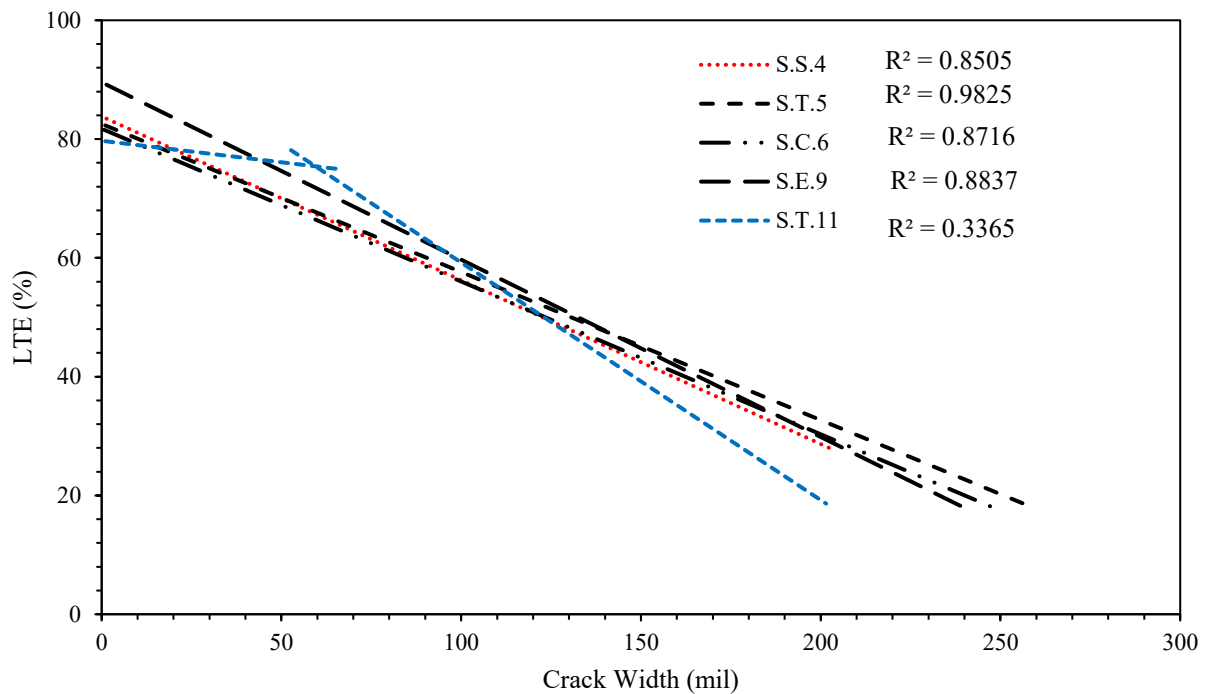
Figure 6-6. LTE as a function of crack width for specimens with 0.5% V_f.

86
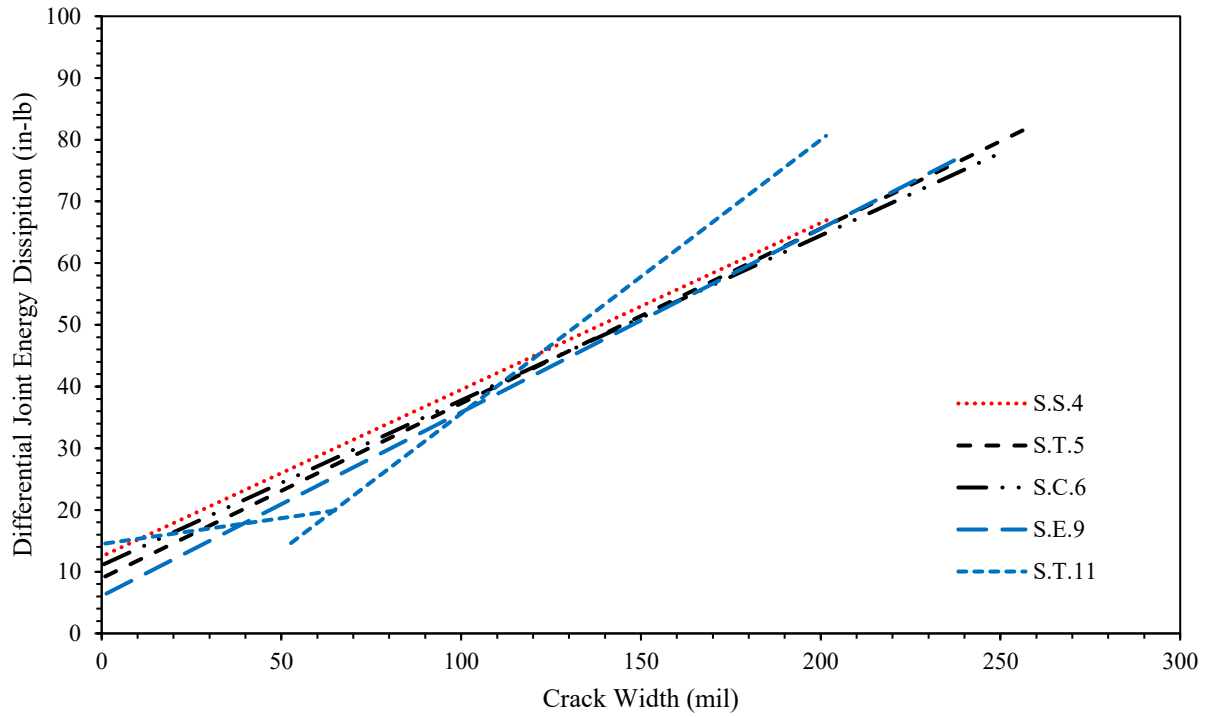
Figure 6-7. DJED as a function of crack width for specimens with 0.5% V_f.
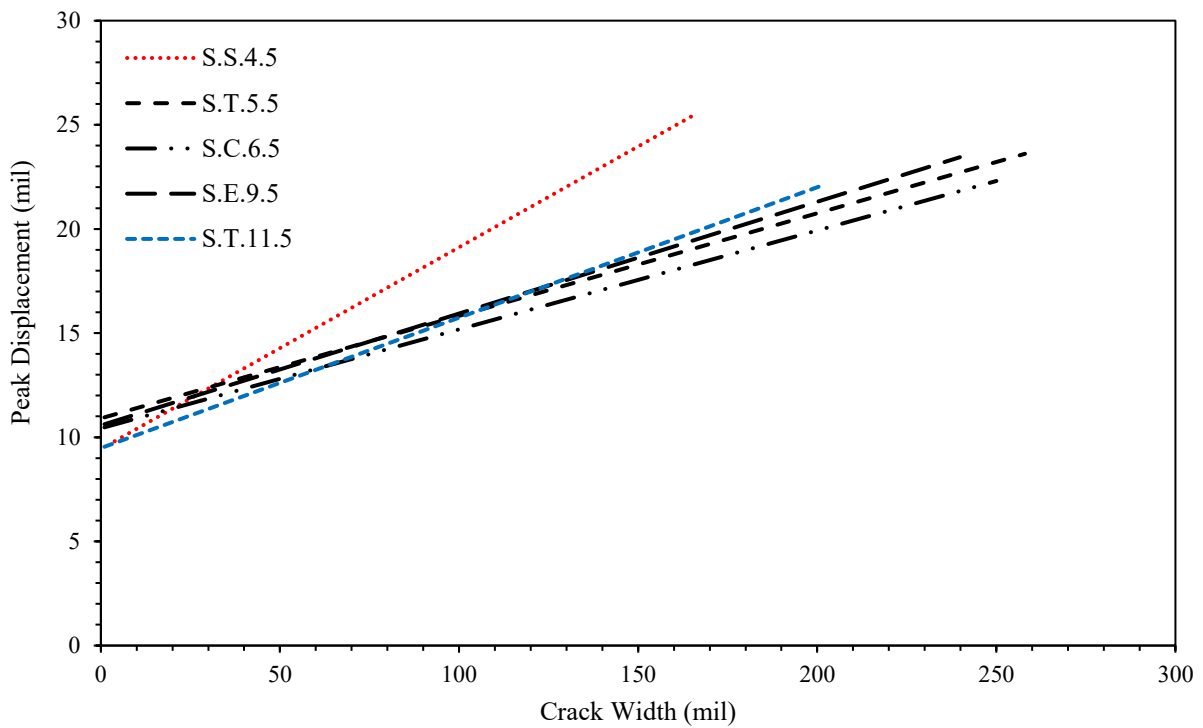
Figure 6-8. Peak displacement versus crack width for specimens with 0.5% V_f.

6.4.2 Influence of Fiber Dosage on Joint Performance

Fiber dosage influences the joint performance of concrete pavements; typically, the greater the dosage, the greater the joint performance. Figure 6-9, Figure 6-10, and Figure 6-11 show average joint performance (LTE, DJED, D_p) results as a function of crack width for plain concrete and FRC mixtures with 0.25% V_f and 0.50% V_f fibers. These plots were drawn using the average results of all mixtures tested in Phases 1 and 4. These figures show that a significant increase in the joint performance is possible with the application of fibers, and that joint performance considerably varies with fiber dosage and crack width. For example, LTE corresponding to 50-mil crack width could be increased by 20% and 30% with the addition of 0.25% V_f and 0.50% V_f fiber dosages, respectively. At wider crack widths, fibers contribute even more. For example, the LTE could be increased by 25% and 40% with the addition of 0.25% V_f and 0.50% V_f fiber dosages, respectively, when the crack width is 100 mil. Similar benefits could also be observed when the joint performance is evaluated using DJED and D_p, as shown in Figure 6-10 and Figure 6-11. It can be seen that the correlation of plain concrete is somewhat bi-linear. The regression models for almost all the plots have strong correlations, and would likely grow stronger with an increase in data points.

To determine the contribution of the fibers at intermediate fiber dosages between 0 and 0.5%V_f, the joint performance data were replotted in Figure 6-12, Figure 6-13, and Figure 6-14. These figures are depicting joint performance as a function of fiber dosage for a range of crack widths. These plots were developed using the regression correlations between LTE and crack width for different fiber dosages (0, 0.25% and 0.5% V_f) obtained in Figure 6-9, Figure 6-10, and Figure 6-11. On the previous point, Figure 6-15 through Figure 6-17 show the increase in joint performance as a function of fiber dosage for a range of crack widths. These plots were also developed using the correlations developed for the data presented in Figure 6-9 and Figure 6-10. The increase was calculated by subtracting the performance of plain concrete from the performance at a given fiber dosage.
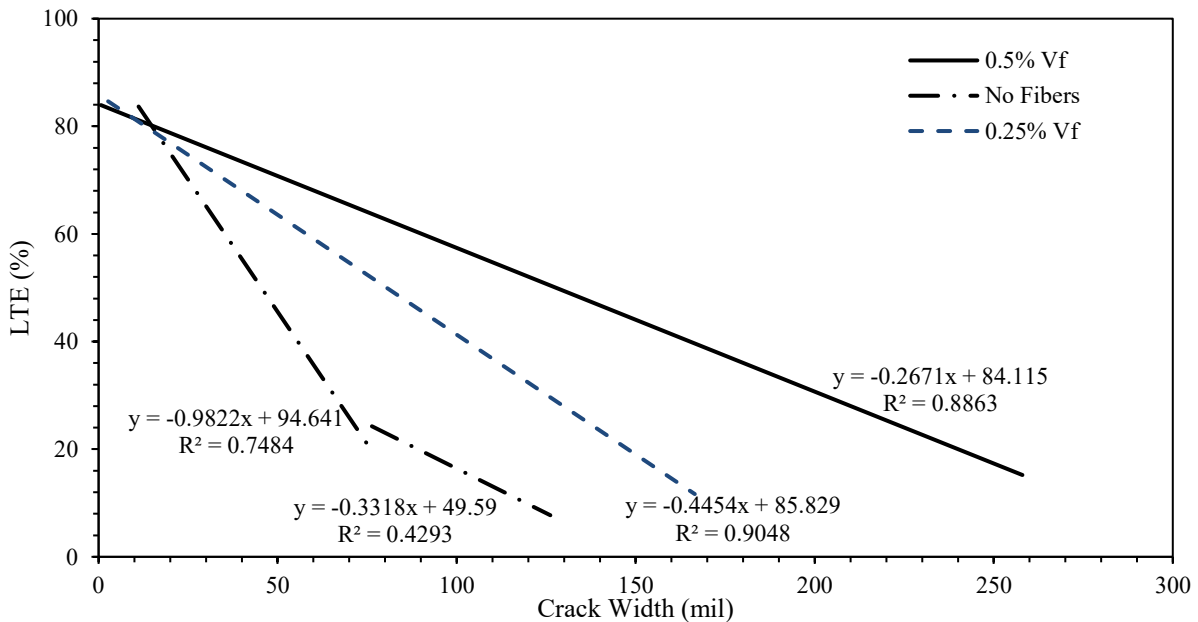
Figure 6-9. LTE as a function of crack width to compare the effect of fiber dosage on joint performance.
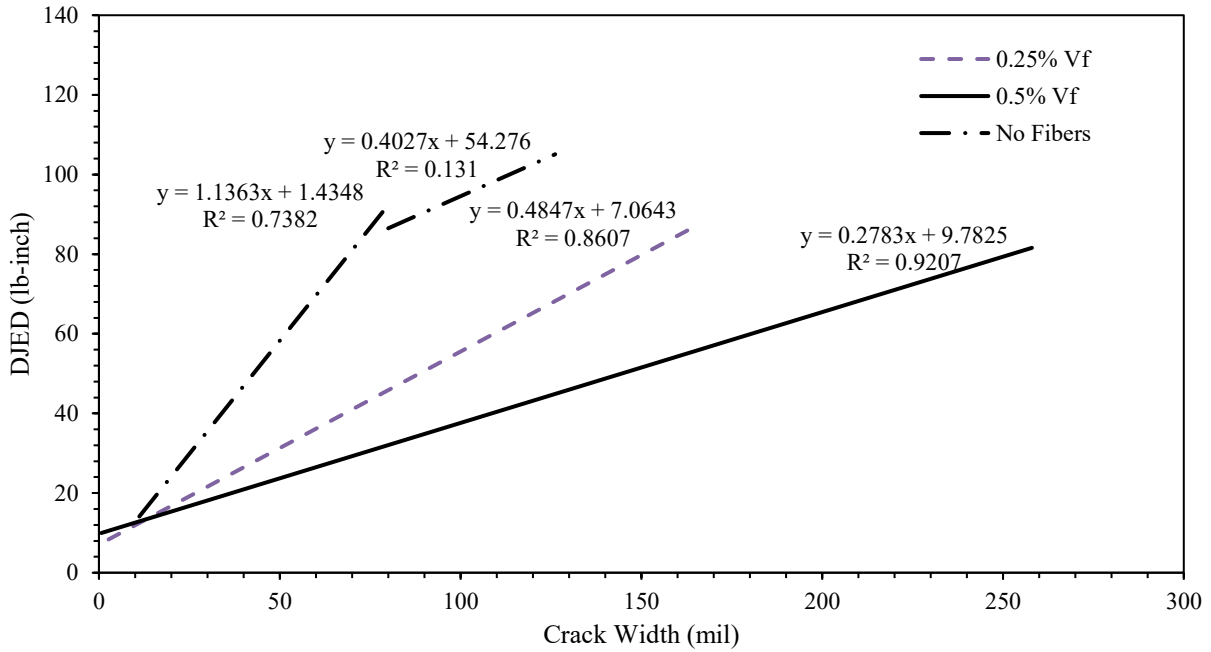
Figure 6-10. DJED as a function of crack width to compare the effect of fiber dosage on joint performance.
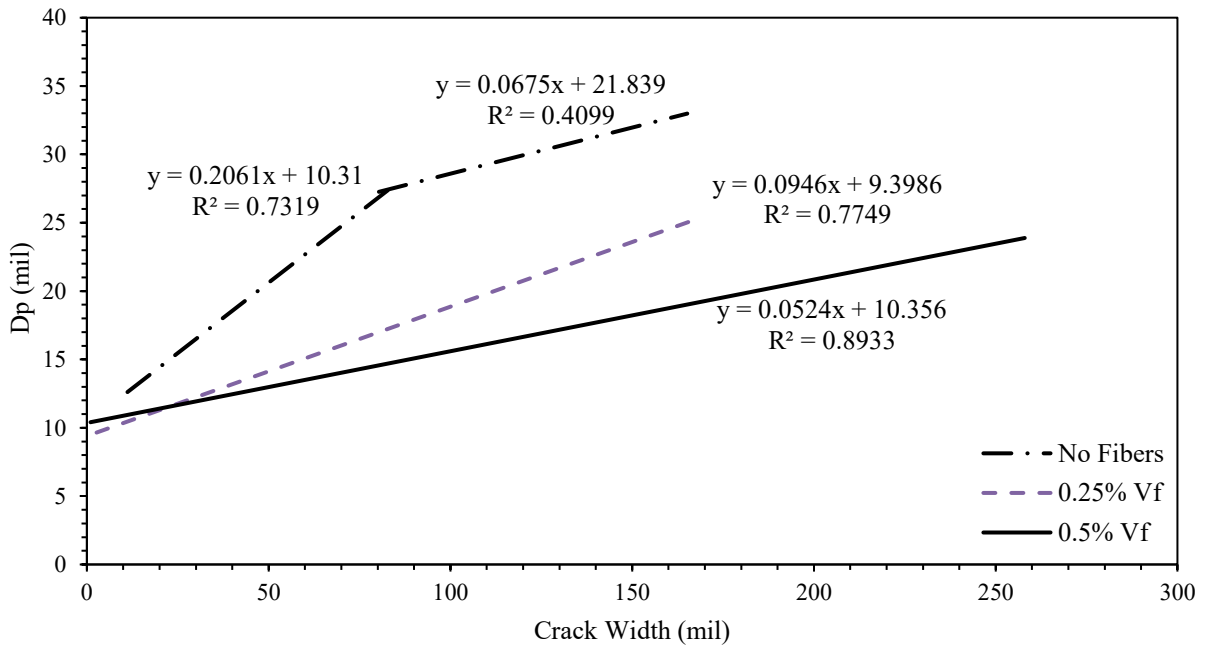
Figure 6-11. Peak displacement as a function of crack width to compare the effect of fiber dosage on joint performance.
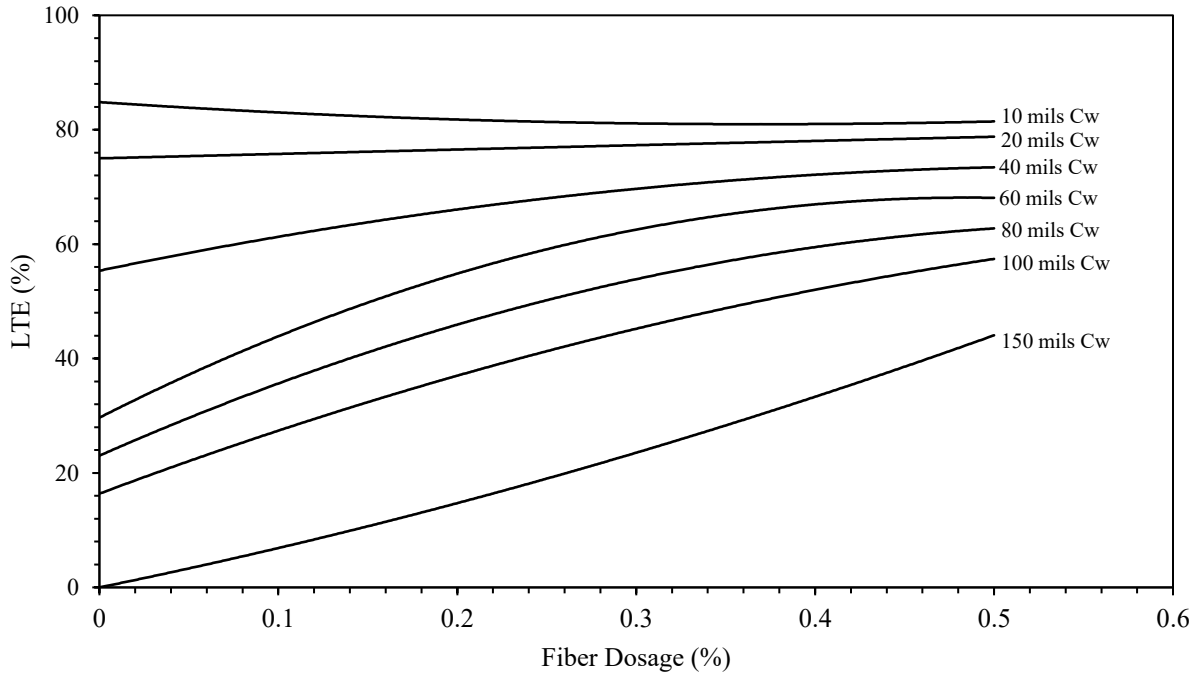
Figure 6-12. LTE as a function of fiber dosage for a range of crack widths.
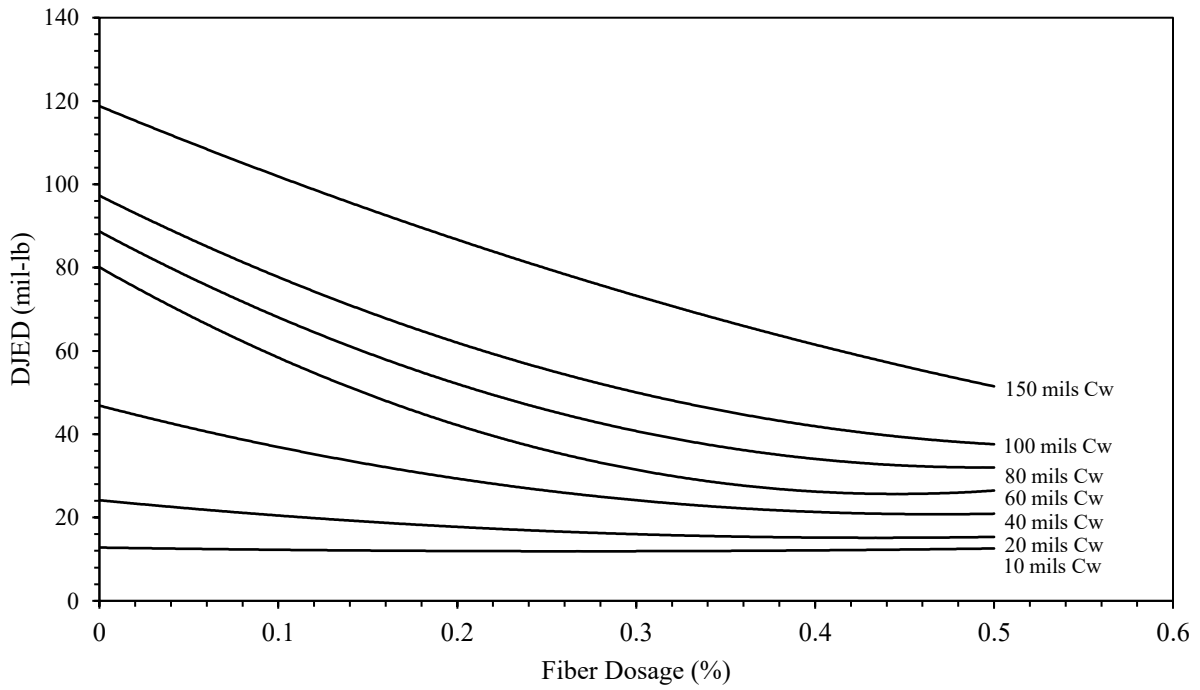
Figure 6-13. DJED as a function of fiber dosage for a range of crack widths.

90
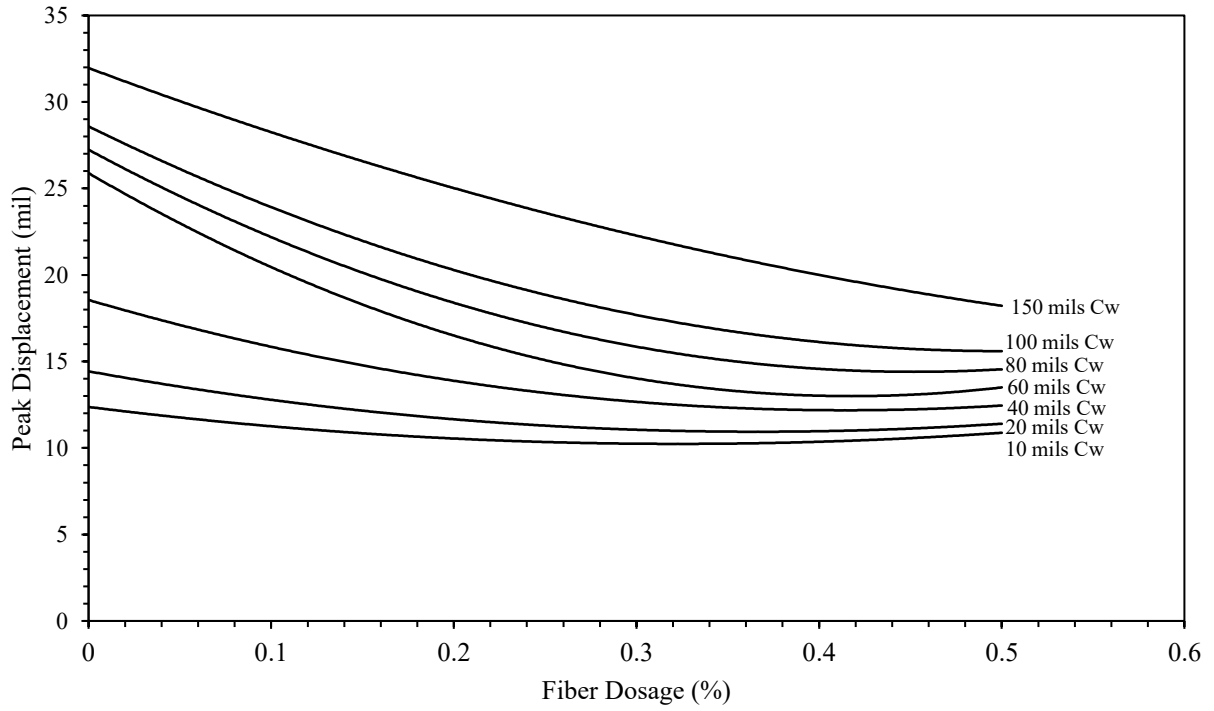
Figure 6-14. Peak displacement as a function of fiber dosage for a range of crack widths.
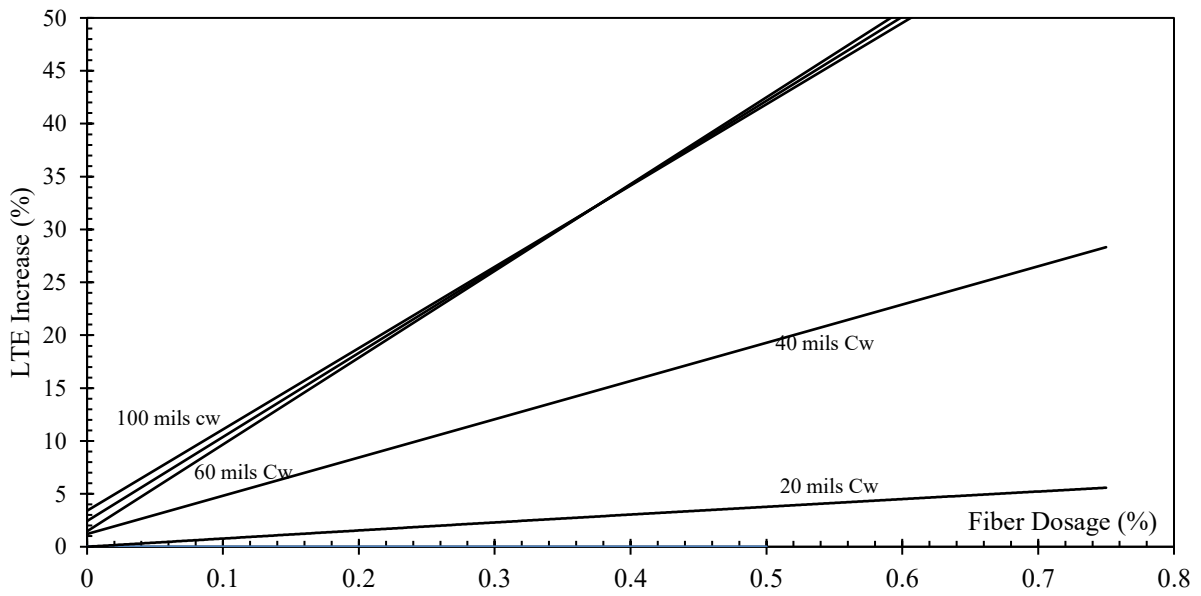
Figure 6-15. Increase in LTE as a function of fiber dosage for a range of crack widths.
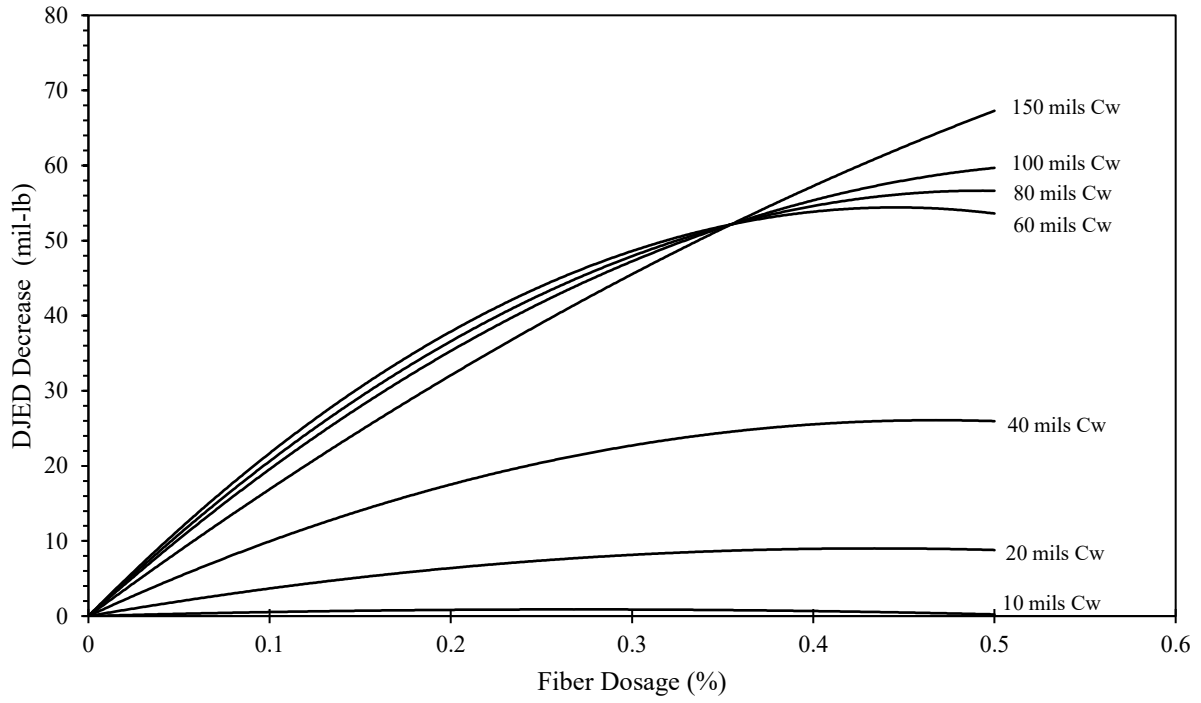
Figure 6-16. Decrease in DJED as a function of fiber dosage for a range of crack widths.
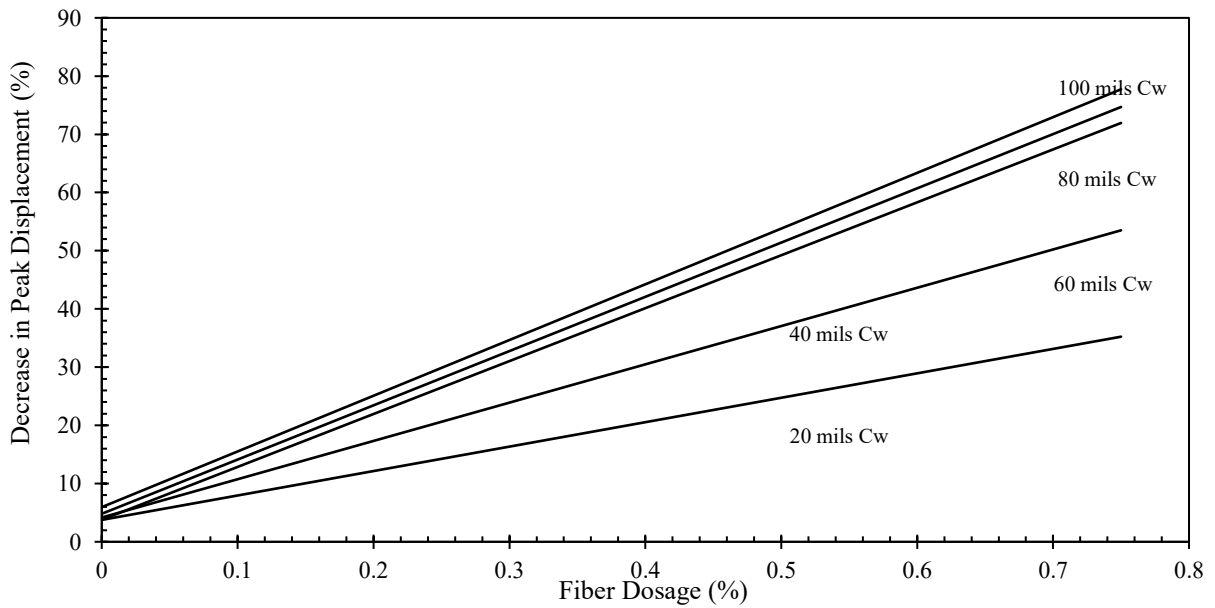
Figure 6-17. Percent decrease in peak displacement for various crack widths as a function of fiber dosage.

92

To investigate the resistance of the fibers against fatiguing, several specimens with and without fibers were loaded to 500,000 cycles of loadings at a single crack width (0.050 inches). Testing of a beam with 500,000 load cycles takes almost three days (including installation of the beam, periodical measurement of crack width, conducting dynamic and static LTE tests, etc.); therefore, the maximum number of load cycles had to be restricted to 500,000 cycles in the interest of time. The testing in this phase started with three beams of plain concrete. For the FRC specimens, two S.S.4, two S.C.6, one S.E.9, and one S.T.11 FRC beams were tested with 500,000 load cycles. Figure 6-18 shows the trend of LTE with respect to number of load cycles. During fatigue testing, a few specimens unintendedly had a significant increase or change in crack width (greater than 4-5 mils.) Results of those specimens are not considered in Figure 6-18; however, those results are provided in the Appendix. It can be seen that the decrease in the LTE with respect to number of load cycles was not large, within 5 to 8% after 500,000 load cycles, and the trend was consistent across test specimens of concretes and fiber types. This particular finding lead to the belief that the fibers themselves did not experience any considerable amount of fatigue related deterioration. Prior to 200,000 cycles, some joint performance was lost but that was probably due to aggregate dislodging at the crack faces; the joint performance became stable (fiber tension, surface texture, etc.) after 200,000 cycles. These results align with those found by Barman, Vandenbossche and Janssen (Barman, 2014; Barman et., 2018), where testing with this same configuration was conducted on specimens from 1 to 10 million load cycles with little decline in the joint performance, reaffirming the fact that polypropylene fibers likely do not deteriorate in this application. Whatever load joint performance is lost is due to the abrasion of the mortar or aggregates, or dislodging of the aggregates at the crack faces.
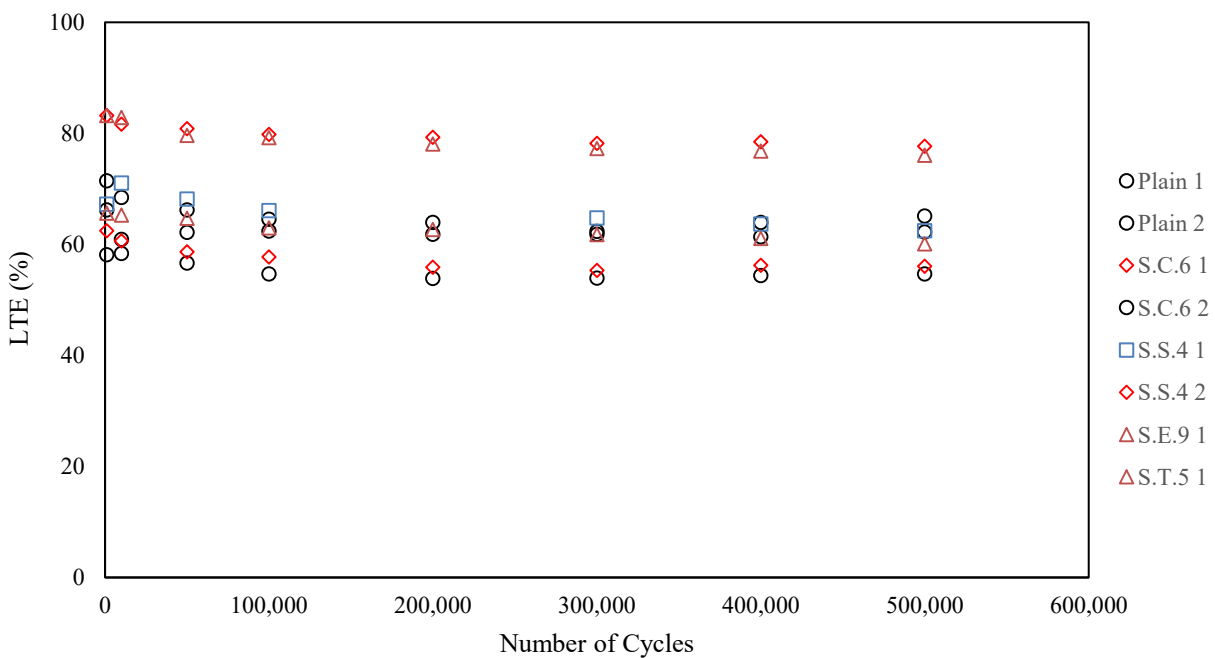
Figure 6-18. LTE versus number of load cycles for the beams subjected to fatigue.

6.4.1 Influence of Crack Width Expansion and Contraction on Joint Performance

A primary concern with the use of fibers, particularly synthetic polypropylene fibers, is how they perform with expanding and contracting crack widths. The Phase 3 of Task 4 addressed this problem by testing joint performance while expanding the crack width to approximately 100 or 150 mils, and then contracting the crack width back to see how the joint LTE of the FRCs changes when the fibers are no longer stretched (no tension in fibers). In order to compare the results of FRC beams with plain concrete beams, similar experiments were also conducted in three plain concrete beams. Figure 6-19 shows the results for two plain concrete beams; results of the third specimen can be found in the Appendix. In each specimen, the crack width was expanded in steps up to approximately 100 mils, with LTE being measured at each step. Then crack width was contracted and LTE was measured at a few more crack widths. As anticipated, LTE was found to increase with the decrease in the crack width; in fact, LTE for a given crack width was typically higher during the crack width contracting exercise than what was measured during the crack width expansion. This is likely due to the fact that the crack faces were under compression during the crack width contracting exercise, also partially due to the presence of dislodged aggregates and mortar (which may not be as significant as this in the field), which could have actually increased the aggregate interlocking.
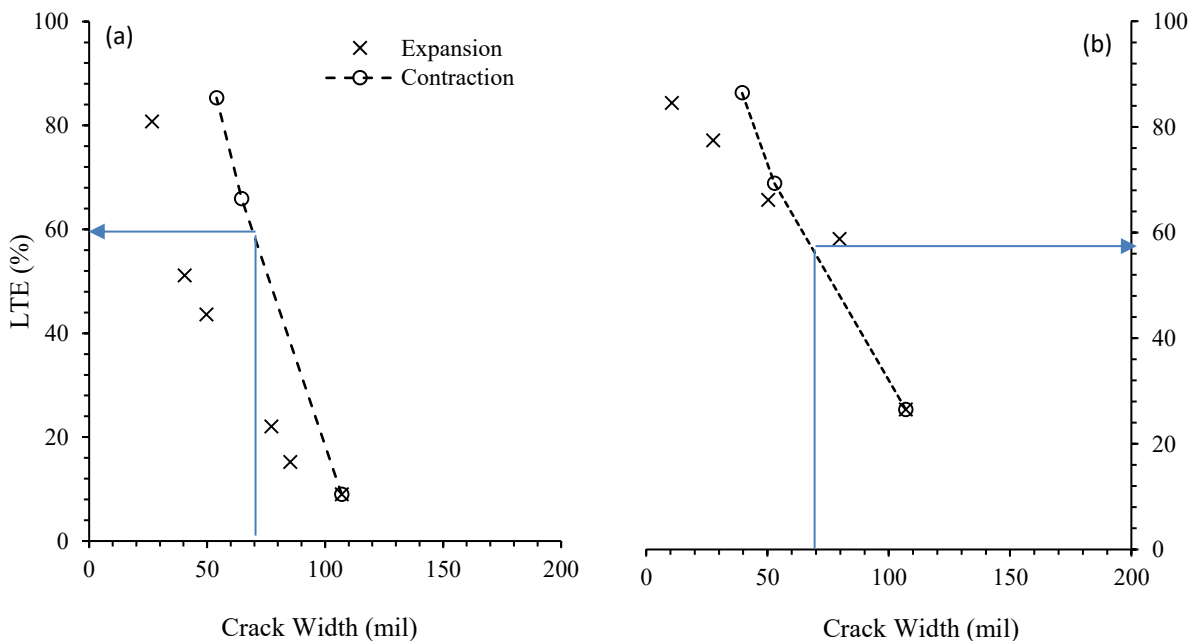
Figure 6-19. The effect of joint expansion and contraction on LTE for plain concrete beams: (a) Specimen 1, and

When the above-mentioned procedure was conducted on FRC specimens, an interesting observation was noticed. Figure 6-20 shows the results for two FRC beams which were prepared using S.C.6 fibers. In contrast to the two plain concrete beams discussed above, in this case, when crack width was contracted, the LTE did not increase at a rate what was observed for the plain concrete beams. As shown in Figure 6-20 (a), for the first specimen, the LTEs measured during the crack width expanding and contracting exercises were similar. For the second specimen, the LTE was even found to be slightly

decreasing when the crack width was decreased from 100 mils to 70 mils, then picking up at other contracted crack widths. The reason for this observation is that fibers likely elongated beyond their plastic limit when the LTE test was conducted at a wider crack width. Then upon contracting the crack width, fibers become lose and their participation in load transfer went down. However, they appeared to be still contributing at a contracted crack width, which can be verified by comparing the slope of LTE vs crack width relationships between plain and fiber concrete beams. For an example, at 70 mils - contracted crack width, the LTEs of the plain beam specimens were 10% to 15% lower than their FRC counterparts.
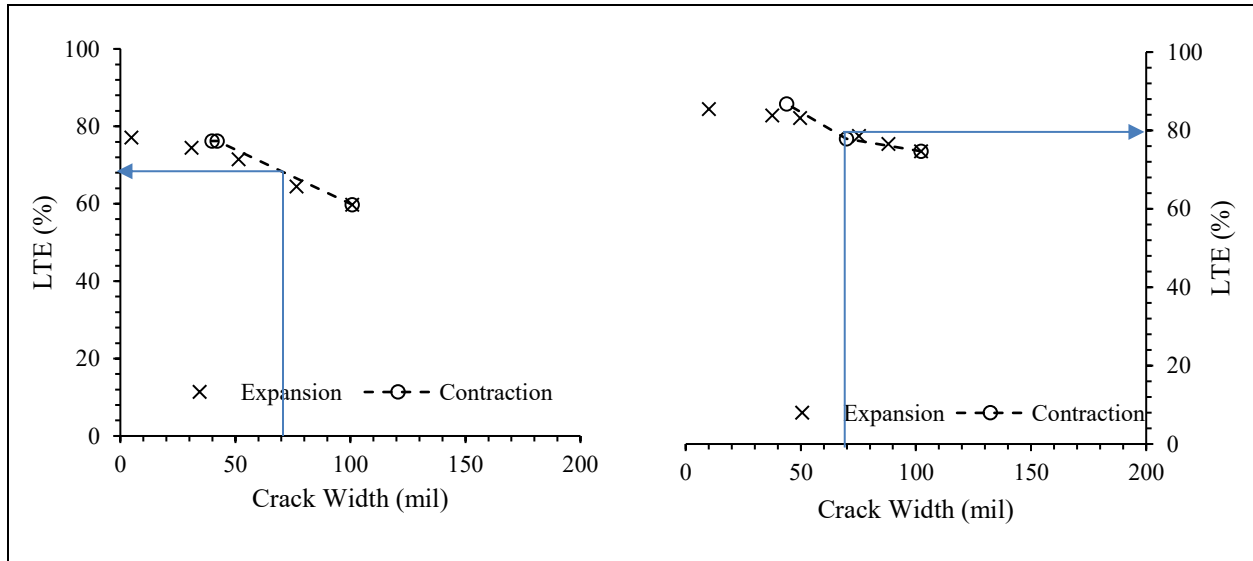
Figure 6-20. The effect of joint expansion and contraction on LTE for S.C.6 FRC beams @ 0.5% V_f: (a) Specimen 1, and (b) Specimen 2.

This influence of the crack width expanding and contracting on the LTE was even more pronounced when the crack width was expanded up to 150 mils. In this exercise, crack width was first expanded up to approximately 100 mils in steps, then contracted to approximately 50 mils in steps, then expanded all the way up to approximately 150 mills, and finally contracted to a final 50-mil crack width in two steps. An LTE measurement was taken in each step of crack width contracting and expanding exercise. FRC beam specimens with S.S.4, S.C.6, S.E.9 fibers, and two different dosages were considered in this exercise. Figure 6-21 and Figure 6-22 show the results for three S.S.4 and three S.C.6 FRC specimens, all prepared with a 0.5% V_f dosage. The evidence of loss of fibers' contribution due to the plastic elongation of fibers is apparent in all six specimens, and the trends are similar. It can also be seen that when crack width was contracted from 150 to 100 mils, LTE basically remained the same or decreased slightly, indicating no or minimal participation of fibers to the load transfer. Figure 6-23 presents similar plots for S.S.4 and S.E.9 fibers, but for a 0.25% V_f dosage; LTE contribution of the fibers also decreased due to the plastic elongation of the fibers. Since the range of LTE is quite low, especially when the crack width was beyond 70 mils, the contribution of fibers may be not large enough to be affecting the overall performance of the joint if the influence of the crack width expanding and contracting is taken in to consideration.
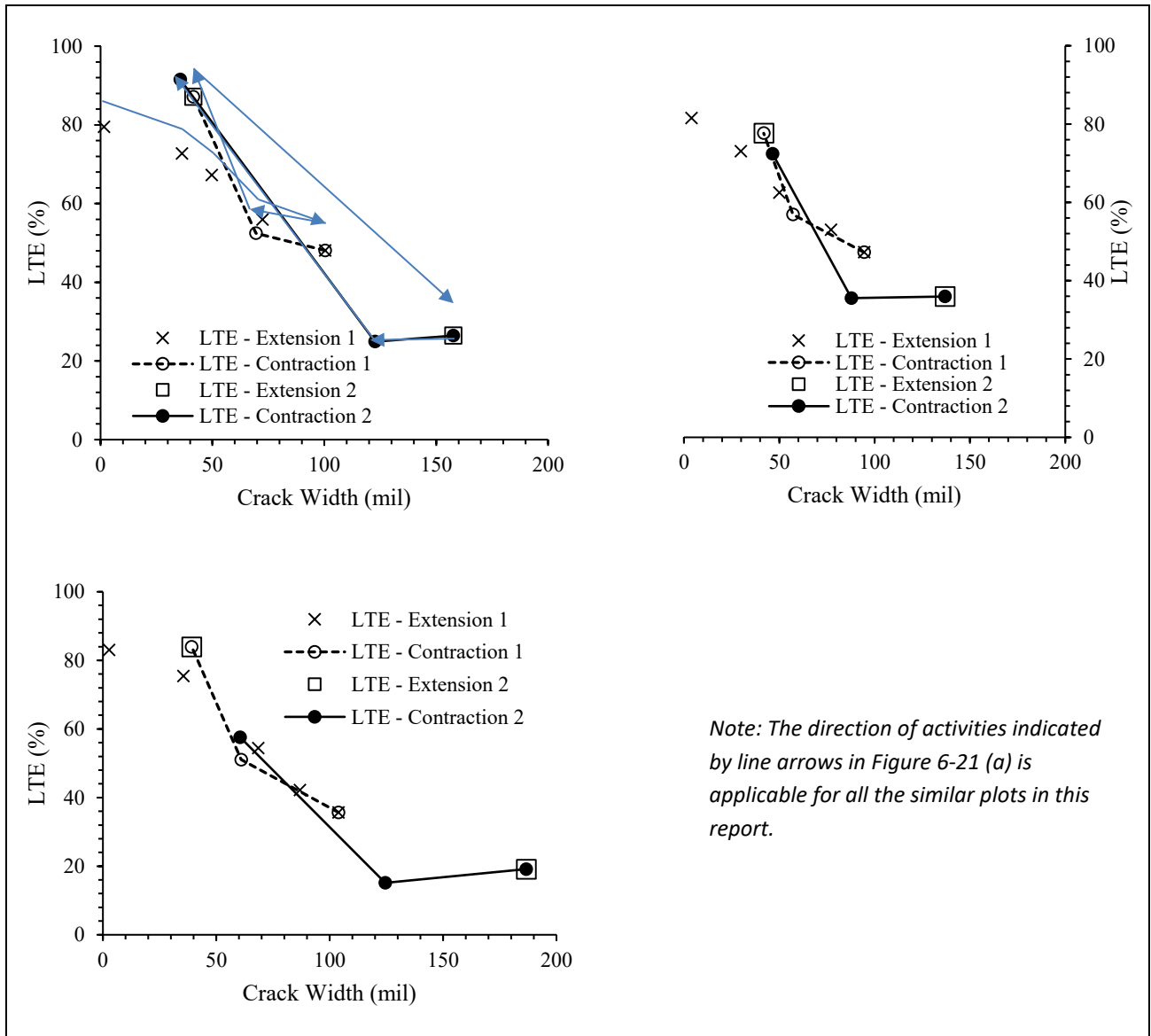
Figure 6-21. The effect of joint expansion and contraction on LTE for S.S.4 FRC beams @ 0.5% V_f: (a) Specimen 1, (b) Specimen 2, and (c) Specimen 3.
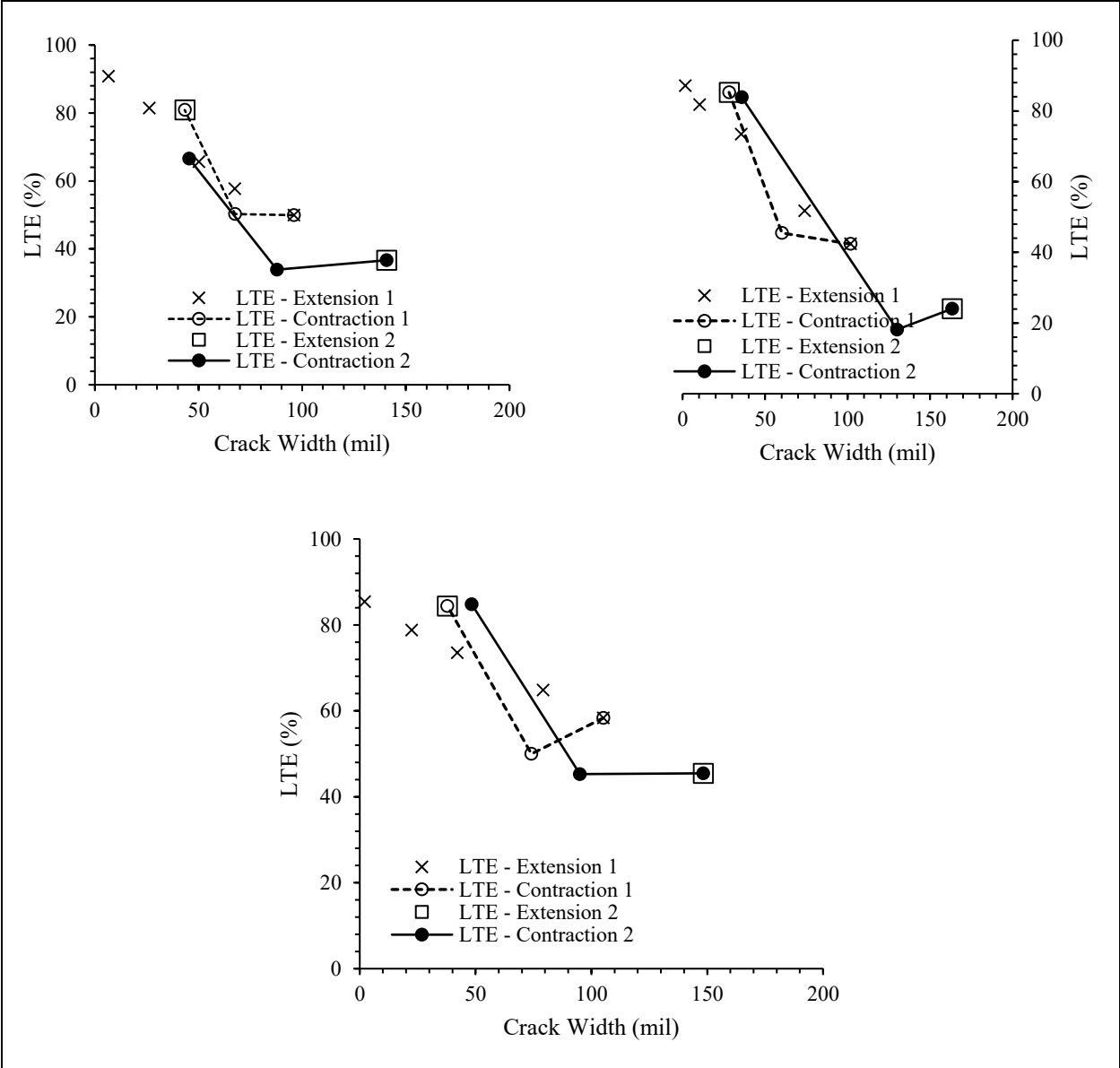
Figure 6-22. The effect of joint expansion and contraction on LTE for S.E.6 FRC beams @ 0.5% V_f: (a) Specimen 1, (b) Specimen 2, and (c) Specimen 3.
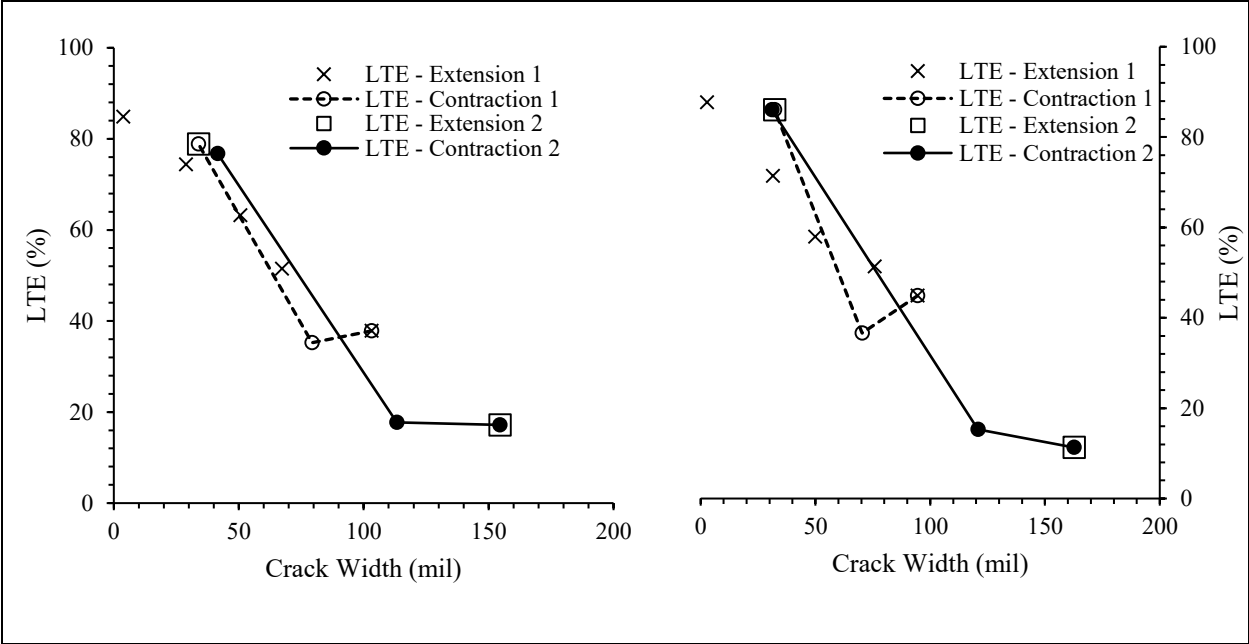
Figure 6-23. The effect of joint expansion and contraction on average LTE for FRC beam @ 0.25% V_f: (a) S.S.4, and (b) S.E.9.

CHAPTER 7: CORRELATIONS AND SPECIFICATION

The current practice for characterizing the behavior of FRCs to use in concrete pavement or overlays mainly relies on the flexural properties of fibers, such as MOR, RS and RSR. Even though there are little field-validated studies establishing relationships between the RSR and fatigue life of the concrete pavement or overlays, the most popular FRC characterizing parameter is still the RSR. However, as the RSR decreases with the increase in MOR for a given value of RS, RSR could be misleading when concrete with higher MOR is used in the pavement; therefore, RS may be a better indicator for characterizing the crack propagation resistance of FRC. On this point, it may be essential to look at the correlation between the RS and LTE, so that both of the performance benefits of FRC can be considered when selecting the fiber type and dosage. In order to establish this correlation, three nomograms were plotted using the relevant laboratory test results from the Task 3 and Task 4, as shown in Figure 7-1 through Figure 7-3. The correlation between the LTE, RS, fiber type, fiber dosage and crack width (CW) is presented in Figure 7-1. This nomogram can be used to determine the required fiber type and dosage for target values of RS and LTE. For example, if an FRC of 150 psi residual strength is needed, then 0.30% V_f of embossed or continuously crimped, or 0.43% V_f of straight synthetic fibers may be required. This dosage however may or may not be sufficient if the specification includes an LTE criterion. For example, if the FRC to be designed is also required to exhibit 70%-beam LTE at 60-mil crack width, then minimum dosage of the fiber would be 0.48% V_f.

Figure 7-2 presents the correlation between the LTE increase, RS, CW, fiber type and fiber dosage. This nomogram can be useful when the specification considers the LTE gain due to the inclusion of fibers, rather than a specific value of LTE. Figure 7-3 shows the nomogram for capturing the benefit of the fibers in terms of the reduction of the peak displacement. As previously mentioned, one of the greatest contributions of the FRCs is the reduction of the peak displacement, which can decrease joint faulting. This nomogram can be helpful if the specification includes a criterion on the fibers' contribution on the peak displacement reduction. For example, if the specification requires that FRC shall yield a 40%-reduction in the peak displacement at 70-mil crack width, then a fiber dosage of 0.4% V_f would be sufficient.
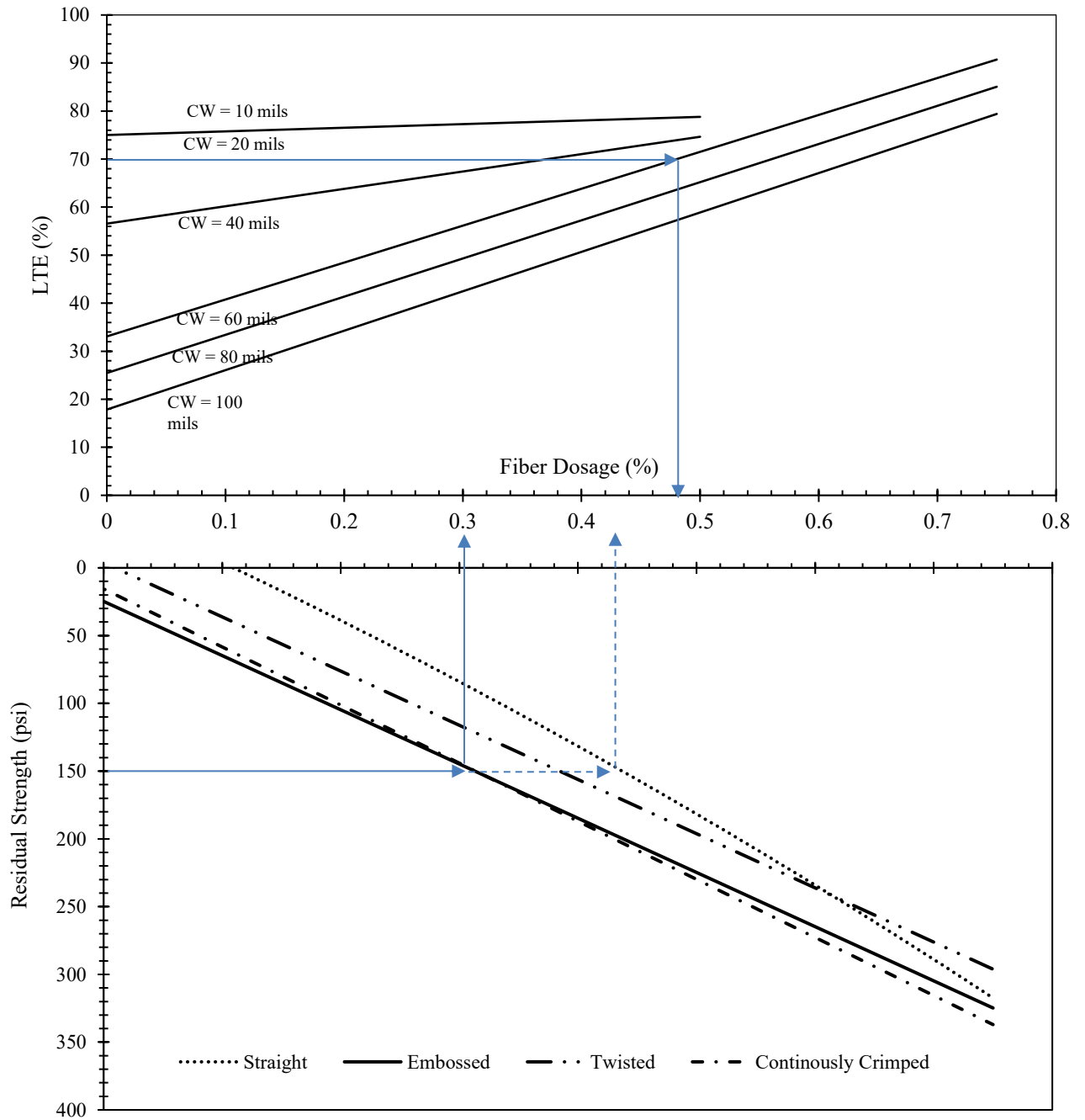
Figure 7-1. Nomogram correlating LTE, RS, fiber type, fiber dosage and crack width (CW).
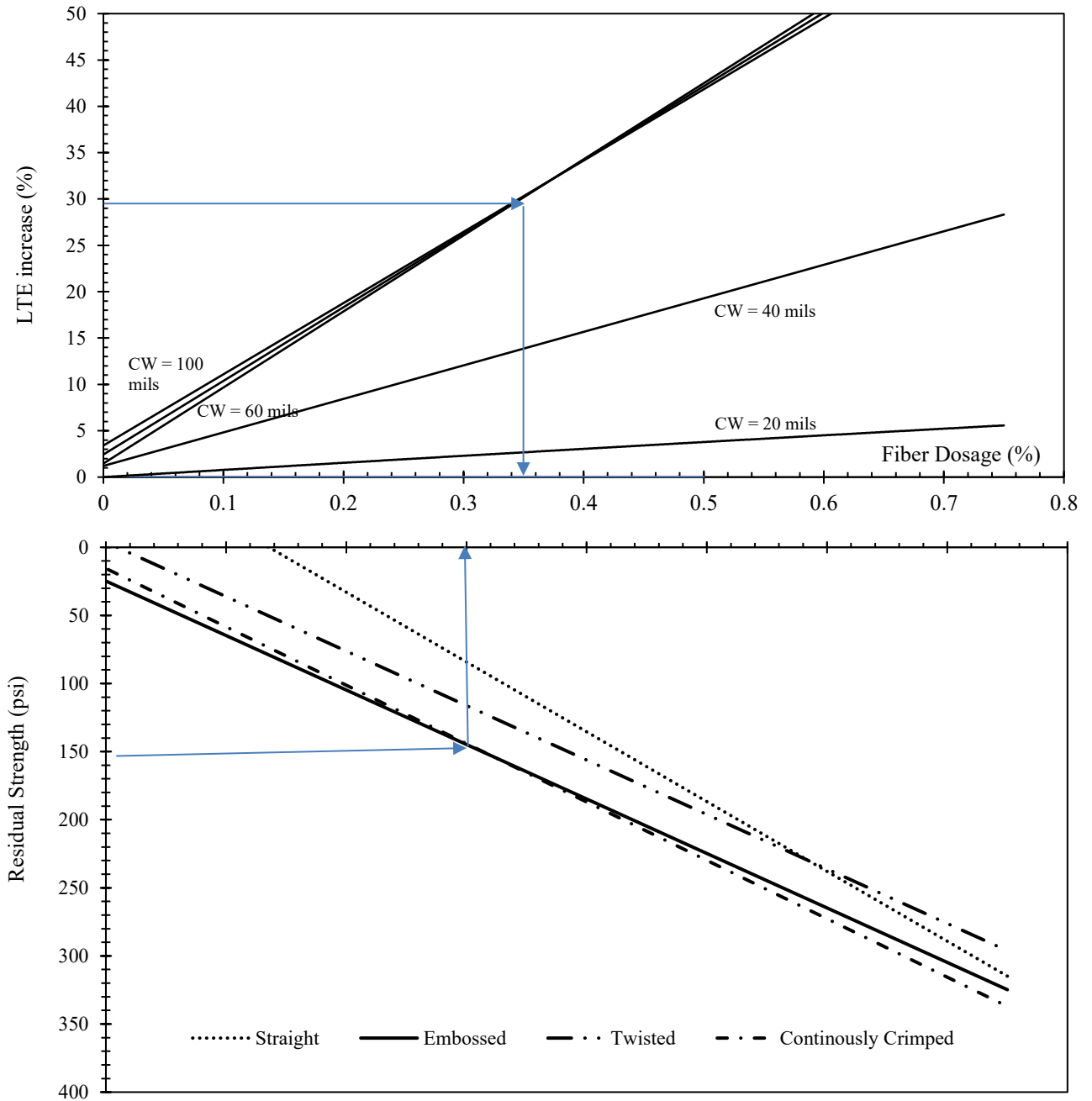
Figure 7-2. Nomogram correlating LTE increase, RS, fiber type, fiber dosage and crack width (CW).

101
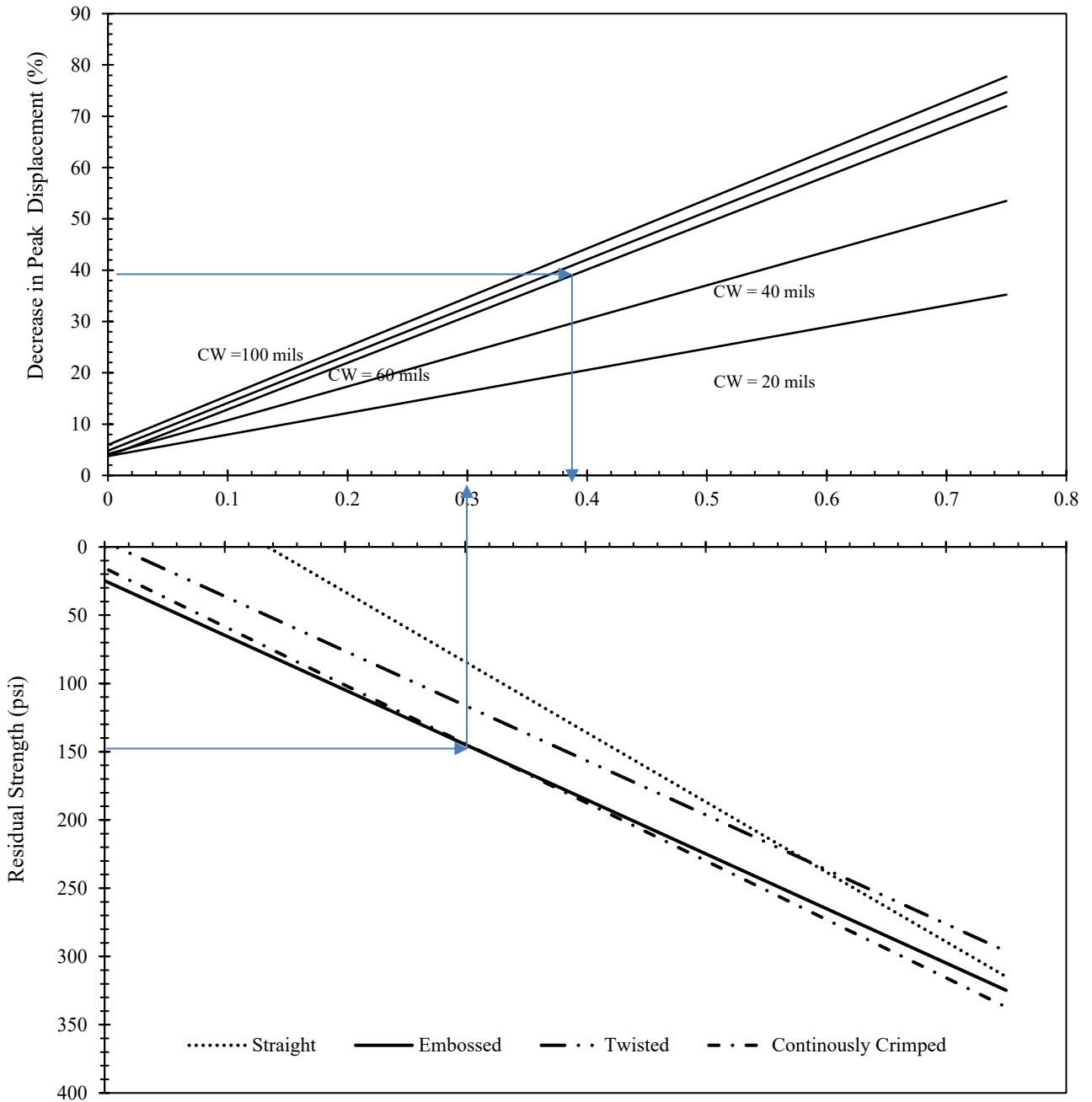
Figure 7-3. Nomogram correlating peak displacement decrease, RS, fiber type, fiber dosage and crack width (CW).

7.1.1 Load Transfer Behavior of Concrete in Field

In thin bonded concrete overlays on asphalt, the overlay is designed to remain bonded with the HMA layer. The HMA layer, which is expected to render a considerable stiffness, is mostly a continuous layer underneath the overlay. Because of interlayer bonding and a considerably stiff HMA layer, a larger portion of the wheel load from one slab to the other slab is transferred through the HMA layer, and the rest through the thin concrete overlay. In the case of thin concrete pavement-at-grade and unbonded

concrete overlay, the majority of the wheel load is transferred through the concrete layer. In either case, the moduli of the layers, including the subgrade, below the concrete influence the combined modulus of subgrade reaction. In the joint performance testing, two layers of neoprene pads were used to achieve a conservative amount of combined modulus of subgrade reaction, i.e., 200 psi/in, which is lower than the typical combined modulus of subgrade reaction for concrete pavements and overlays. Therefore, the LTE results obtained in the laboratory method could be lower than what will be achieved in a concrete overlay or pavement in field. In order to study the load transfer behavior of fiber reinforced concrete in field, the FWD-based LTE results of two former MnROAD cells (Cells 94 and 95) were analyzed. The design features of these two cells are provided in Table 7.1. To evaluate the contribution of fibers towards the performance of the overlays, the LTEs of the two cells were compared, as shown in Figure 7-4. Cell 94 was constructed with non-structural polypropylene fibers, while Cell 95 was constructed with structural polyolefin fibers. It can be seen that the LTEs in Cell 95 were always higher than the LTEs in Cell 94, and the difference was more in the winter (larger crack width). It may be stated that the underlying layers of the pavement remain frozen in Minnesota during the winter, which can also increase the LTE. Assuming the underlying layers of both Cells 94 and 95 were frozen, it can still be seen that Cell 95 yielded greater LTE in the winter. The LTE of the Cell 95 during the winter lies between 67% and 85%. The slabs with structural fibers presumably received LTE contribution from fibers during the winter, when crack width was wider and structural fibers were stretched. The non-structural fibers were seemingly unable to offer the same because of their low lateral stiffness.

Table 7.1. Summary of the design features for Cells 94, 95 and 96 in MnROAD (Barman, Vandenbossche, Mu, & Gatti, 2010; Burnham, 2006; Burnham, 2005; Vandenbossche, 2003).

Cell No.	Age	Thickness of PCC slab (in)	Thickness of HMA layer (in)	Size of the slab (ft × ft)	Sealed joint (Y/N)	Doweled joint (Size/N)	Type of fiber reinforcement
94	Oct 97-Oct 04	3	10	4 × 4	Y	N	Non-structural micro fiber (polypropylene)
95	Oct 97-Oct 04	3	10	5 x 6	Y	N	Structural macro fibers (Polyolefin)
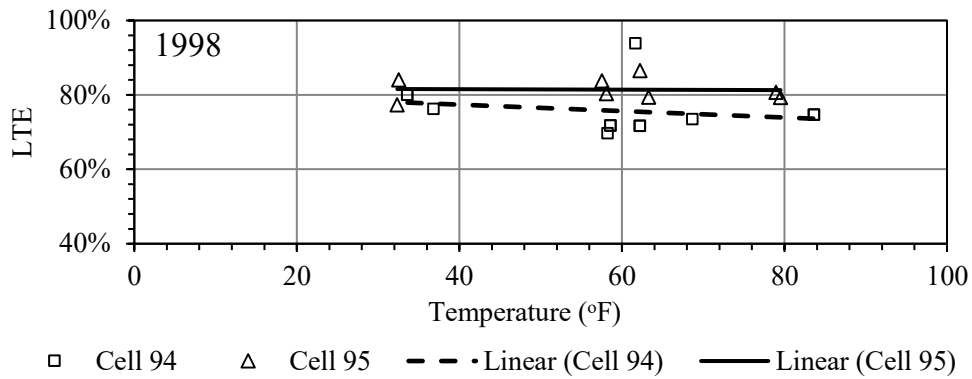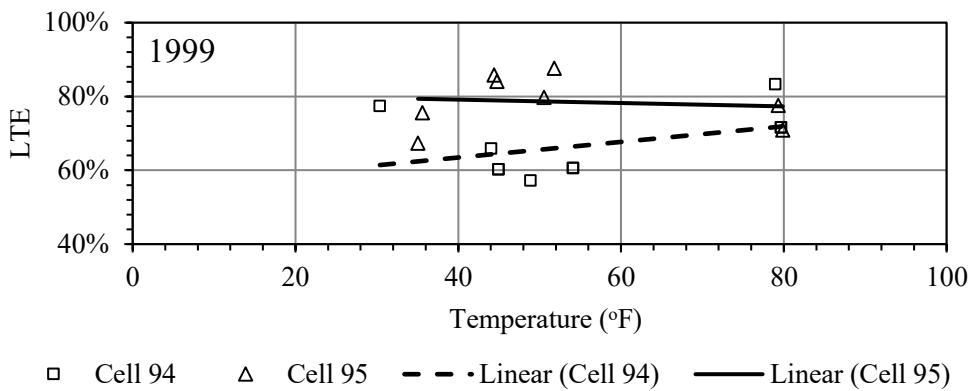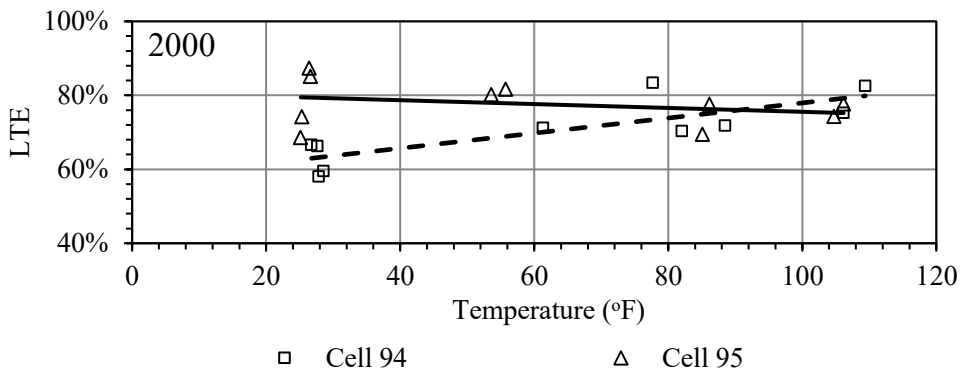
Figure 7-4. Load transfer efficiency of MnROAD Cells 94 and 95 in (a) 1998, (b) 1999, and (c) 2000.

Roesler, et al. (2008) performed a study on the joint performance characteristics of a 3.5-inch x 4-ft x 4-ft ultra-thin FRC concrete overlay constructed over a 2-inch thick HMA layer. This project was constructed in a parking lot at the University of Illinois at Urbana-Champaign (UIUC) campus during August 2006; it was observed that every 5th to 8th joint cracked after approximately 24 hours. FWD and ultrasonic testing were performed to evaluate joint load transfer after construction (August 2006), and again after a couple of months (October 2006). Figure 7-5 and Figure 7-6 present the LTEs measured at

different stations in August 2006 and October 2006, respectively. In Figure 7-5, it can be seen that every 5th to 8th joints resulted in a lower LTE. A considerably low LTE at the joints, compared to the LTE at the center locations, is an indication of the joint deployment. Station numbers 5, 10 and 17 are assumed to have cracked after 24 hours, post construction. In Figure 7-6, it can be seen that almost every other joint cracked two months after construction. The other observation from the two figures is that the joints which cracked 24-hours after construction exhibited a lower LTE than the rest, when tested in October. This makes sense because the initial cracked joints would be wider and have a lower LTE. The next narrower cracked joints would be the next set of joints that cracked (joints 1, 3, 7, & 12). This emphasizes the need of having all the joints deployed at the same time so each joint would have the same cracked width. From this study, it can be concluded that the LTE could go as low as 60% when the concrete overlay or pavement is constructed over a very thin layer.
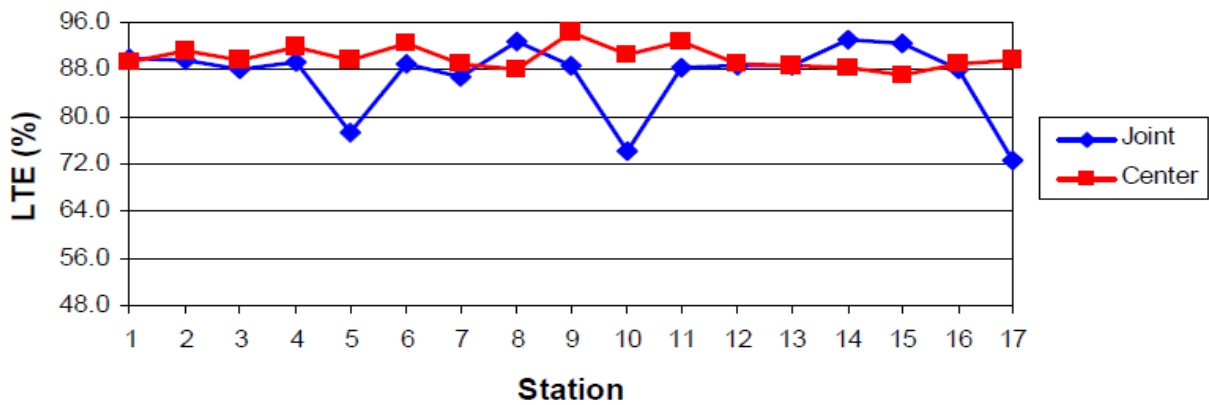
Figure 7-5. Load transfer efficiencies for UIUC E-15 Parking Lot – Parking Bay 1 (August 2006) (Roesler et al., 2008)
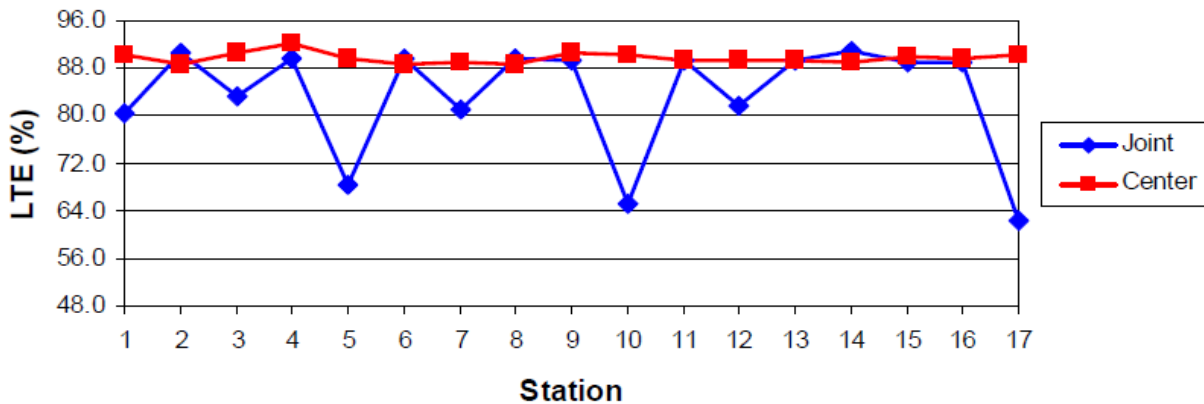
Figure 7-6. Load transfer efficiencies for UIUC E-15 Parking Lot – Parking Bay 1(October 2006) (Roesler et al., 2008)

Roesler and Wang (2009) suggested that since smaller slabs are used in concrete overlays, the joint opening or the crack width typically remains narrow. Crack width data (provided by Dr. Vandenbossche during PI Dr. Barman's Ph.D. study) (Barman, 2014) from MnROAD bonded concrete overlay sections are studied to establish possible crack width range in different seasons, especially in winter. Figure 7-7 and Figure 7-8 present the crack widths for a few successive joints for Cells 94 and 95, respectively, for number of dates. These crack widths were manually measured using gauge studs placed on either sides of the joint. In Figure 7-7 (Cell 94), it can be seen that every other joint exhibited a slightly wider crack width. Joints 2 and 4 had the widest crack width, with the maximum occurring during the winter months (~ 0.042 to 0.070 in). In Figure 7-8 (Cell 95), Joints 2 and 5 exhibited wider crack widths, and again, the widest crack width was observed during the winter months (~ 0.035 to 0.070 in). It can therefore be stated that if the contribution of fibers towards the joint performance is included in the fiber selection criteria, it would be appropriate to consider the benefits of the fibers at wider crack widths, e.g., 40- to 70-mil crack width, to include the somewhat worst-case scenarios. This conservative consideration may also cover for the crack width increase due to drying shrinkage of the slabs for around the first 4 to 5 years of the pavement's service life (Koubaa and Burnham, 2001).
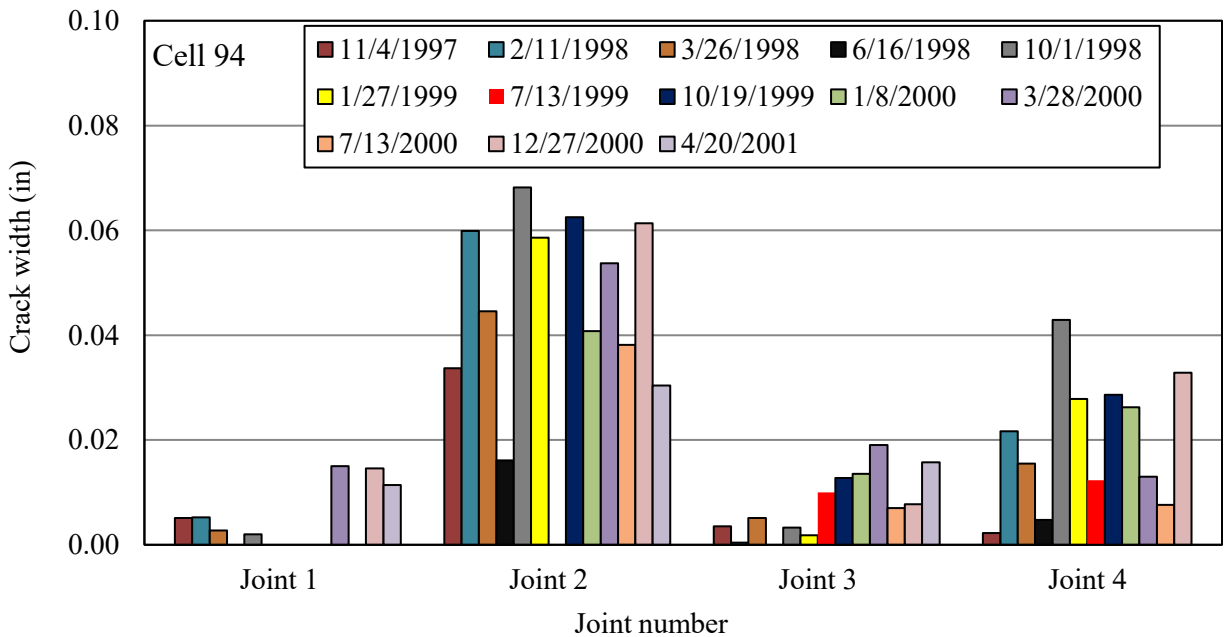
Figure 7-7. Crack width at different joints in MnROAD Cell 94.
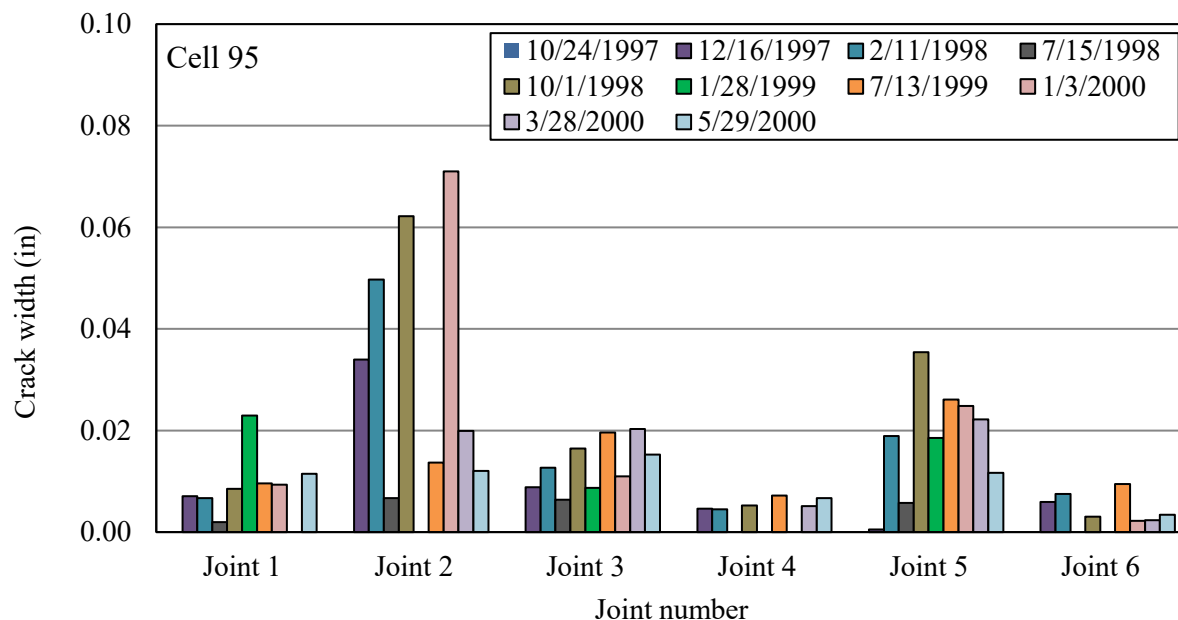
Figure 7-8. Crack width at different joints in MnROAD Cell 95.

7.1.3 Target Post-crack and Joint Performance Parameters for Fiber Usage Specification

This report presented a comprehensive review of the performance of several FRC overlays constructed at different states. From the field performance review and also from many previous laboratory studies included in this report, it was found that fibers have a positive influence on the overall performance of the concrete overlays. However, because of lack of companion field sections or studies comparing the field performances between fiber reinforced and non-fiber reinforced concrete overlays, it is still difficult to pinpoint a certain post-crack performance parameter, such as RS or RSR, and a joint performance parameter, such as LTE, DJED or D_p, which would provide the best performing pavement or overlay with less or no fatigue cracking, joint faulting or other associated distresses. In Chapter 3, it was seen that a vast number (approximately, 53%) of the concrete overlays of this country were constructed with a dosage of 3 lb/yd^3 of structural synthetic fibers. Varieties of fibers with different physical and mechanical properties were used. In Minnesota, various structural synthetic fibers were used with different dosages, up to a maximum of 25 lb/yd^3. It was found that even though fibers did yield a positive influence on the performance of most of the overlays included in this study, the performance varied based on several factors, such as pavement design variables, underlying layer, and most importantly traffic volume.

As the field-validated target values for the RSR, RS, or LTE values to achieve the intended design life are currently not available, the findings from this current study have been used to generate a range post-crack and joint performance parameters that may be considered for writing a formal fiber usage specification for thin and ultra-thin concrete overlays or pavements-at-grade. Table 7.2 presents these ranges. The available information on the use of fibers (e.g., type and dosage, etc.) and their contributions to the performance of concrete overlays and the laboratory test results of similar fibers from the current study were used to generate these ranges. The nomograms developed in this study, by correlating fibers' properties and post-crack and joint performance, were used to decide on the magnitude of RSR, RS and LTE-increase values. The range for these parameters are provided for three

traffic levels: low traffic volume (below 3 million ESALs), moderate traffic volume (between 3 and 10 million ESALs), and high traffic volume (above 10 million ESALs). The allowable ranges of RSR, RS and LTE-increase for the low traffic volume road corresponds to the 20% RSR criterion that was mostly used in this country. The corresponding ranges of RS and LTE-increase for the low traffic volume and the ranges of all the three parameters for the other two traffic volumes were determined by using the nomograms, various correlations developed in this study and traffic volume information of the different overlays considered in this study.

Table 7.2. Suggested ranges of RSR, RS and LTE-increase for fiber usage.

Performance parameters	Design Traffic, ESALS (millions)		
	< 3	3 - 10	> 10
Residual strength Ratio (RSR), min.	20	30	40
Residual strength (RS), min.	150 - 175	175 - 225	> 225
LTE-increase (% of plain concrete LTE), min.	20 - 30	30 - 45	> 45

CHAPTER 8: CONCLUSIONS AND RECOMMENDATIONS

8.1 CONCLUSIONS

Structural fibers are used in thin concrete overlays for improving their long-term performance. These fibers improve the structural integrity of concrete by (i) keeping cracks/joints tight and (ii) transferring the wheel load across the concrete slabs when used in un-dowelled concrete overlays. Structural fibers are currently available in different material compositions, stiffnesses, shapes, and aspect ratios (ratio of length to effective diameter). Among the various types of structural fibers, structural synthetic fibers have become predominant over the last few decades due to their ease of handling, better dispersion characteristics, and resistance to corrosion. The main focus of this study was to investigate the influence of fiber properties such as stiffness, geometry, aspect ratio, length on the post-crack performance and joint performance of the fiber reinforced concrete. The study was accomplished through four different tasks. In Task 1, a literature search and an online survey were conducted to understand the properties of fibers commonly used in concrete pavements and overlays. In Task 2, laboratory testing setups for post-crack performance test (per ASTM C1609) and joint performance test(Barman, 2014; Barman et al., 2018) were fabricated. Task 3 characterized the fresh and hardened concrete properties, including post-crack performance of fiber reinforced concrete as a function of fiber properties. The influence of the crack width, fiber properties and dosage, load repetitions, and crack width contracting and expanding on the joint performance were investigated in Task 4. The conclusions drawn from each of the above-mentioned tasks are provided below.

Task 1:

- Fibers typically contribute to the concrete overlay performance and should be used when slabs are un-dowelled and subjected to heavy and frequent traffic loads.
- The majority (almost 94%) of the FRC overlays in this country were constructed with structural synthetic fibers, which provided equal or better performance than projects using steel fibers.
- A large number of combinations of fiber types, geometries, lengths, and dosages have been utilized in concrete overlays.
- Fibers with aspect ratios between 50 and 100 have been found to be suitable for avoiding fiber balling in the concrete mixture unless other adjustments are made to either alter the fiber delivery method or concrete mixture.
- It was found that fibers above 1% volume fraction may result in fiber balling and fibers below 0.25% do not significantly improve the post-crack and joint performance of FRC.
- Fibers lengths between 1.5 and 2.25 inches are suitable for achieving sufficient post-crack and joint performances.
- Fibers used in 3-inch thick ultra-thin pavement-at-grade in 2017 NRRA cells failed to stop crack initiation and crack propagation. The formation of shattered slabs in the first year of service indicates that fibers may not offer great resistance to crack initiation and propagation when the concrete slab is very thin and placed on a relatively weak supporting layer.

Task 2:

- The results of the UMD beam LTE setup were found to have good correlation with LTE results determined from the slab tests in the study conducted at the University of Pittsburgh (Barman, 2014).

Task 3:

- For the lab mixing used in this study, longer, stiffer fibers showed a greater tendency to ball and form matts; however, the improvised mixing method adopted in this study was able to reduce fiber balling. Balling and matting did not directly correlate with the fiber aspect ratio as previously thought.
- Achieving proper workability for concretes with smaller effective diameter fibers (coincidentally having a higher aspect ratio) was difficult, especially at higher dosages, meaning a higher admixture dosage was required.
- A good correlation between the fiber dosage and super air meter number (SAM) number was not apparent from this study. Different geometries of fibers likely interfered in the correlation.
- Mixtures with steel fibers consistently had a higher SAM number.
- An increase in entrained air content directly correlates to a decrease in the SAM number.
- An increase in fiber dosage generally led to an increase in the surface void percentage in the box test.
- Synthetic fibers have very little effect on the compressive strength and modulus of elasticity of concrete and little to moderate influence on the modulus of rupture. Steel fibers showed higher performance in terms of the above-mentioned three properties.
- Volume fraction of the fiber in the concrete, stiffness, and geometry of the fibers significantly influence the residual strength ratio and residual strength. The RSR and fiber volume fraction have an excellent correlation with an R^2 equal to 0.86.
- Some of the fibers resulted in low modulus of rupture but showed high residual strength(RS), which resulted in higher residual strength ratios (RSRs). Consideration of all three of these parameters in combination may be more appropriate than just having one of them (e.g., RSR) as the selection criteria.
- Embossed, twisted, and crimped fibers performed better on average than straight, flat synthetic fibers when comparison was made in terms of RSR or residual strength.
- RSR or RS results also suggested that longer, large effective diameter fibers perform better than shorter and smaller effective diameter fibers in these applications. However, it may also be noted that a majority of the longer, larger diameter fibers were either embossed or crimped, potentially creating a better fiber-concrete bonding condition.
- Good correlation was achieved between the RSR and reinforcement index. This correlation may be useful for selection of fibers for a certain value of RSR when many commercial fibers are available to choose from.

Task 4

- It was found that the load transfer efficiency, differential displacement, and differential joint energy dissipation is less influenced by the cross section area and geometry of fibers. However, FRCs prepared with low stiffness (lateral) fibers may results in excessive peak displacement under the dynamic load.
- Synthetic fibers do not deteriorate or fatigue with 500,000 load cycles in the test regime followed in this study.
- The joint performance considerably varies with fiber dosage and crack width. For example, LTE corresponding to a 50-mil crack width could be increased by 20% and 30% with the addition of 0.25% V_f and 0.50% V_f dosages, respectively. At wider crack widths, fibers contribute even more. For example, the LTE could be increased by 25% and 40% with the addition of 0.25% V_f and 0.50% V_f dosages, respectively, when the crack width is 100-mil. At

a very low crack width, such as 20 mils, LTE for plain concrete and FRC specimens are similar.

- The load transfer contribution of fibers is influenced by the crack width expanding and contracting. During the winter, when crack width remains expanded, it appears that fibers most likely elongate beyond their plastic limit, or slightly pull out of the concrete, under the combined influence of longitudinal (axial) tensile stress and dynamic load. Then, come summer, after the crack width contracts, fibers may become loose and their participation in load transfer may go down. However, they appear to still contribute, but at a lower rate, if the crack width did not open beyond 100 mils in the previous winter(s).

- This study developed several nomograms correlating fiber properties, post-crack and joint performance parameters to aid in the selection of fiber type and dosage.

8.2 RECOMMENDATIONS

Based on the findings from all the four tasks in this project, the following recommendations are made to include in the specification of the fiber reinforced for using them in thin concrete overlays and pavements:

- As the stiffness and geometry of the fibers play a great role in post-crack performance, it is recommended that fibers that exhibit high lateral stiffness and irregular cross-section shape, such as continuously crimped and embossed, etc., should be used in concrete overlays and pavements-at-grade
- The preferred range of aspect ratio of fibers shall be selected between 50 and 100 for avoiding fiber balling in the concrete mixture.
- Fibers lengths between 1.5 inches and 2.25 inches are suitable for achieving sufficient post-crack and LTE performances. The maximum dosage of the fibers may be capped at 1% volume fraction to avoid fiber balling or formation of matting.
- The optimum dosage of the fibers shall be determined based on the test results of the trial batches. The post-crack performance test, such as ASTM C1609 shall be conducted to determine the residual strength and residual strength ratio.
- It is suggested that the joint performance contribution of the fibers be considered in the fiber selection process as well, if possible. In addition to the LTE-increase, criteria on the differential displacement and peak displacement may be considered.
- Until field-validated results are available, Table 7.2 can be used to determine the target ranges of the RSR, RS and LTE-increase.

8.3 FUTURE STUDIES

The popularity of fiber application is gaining momentum; more agencies and states are coming forward to implement fibers in concrete overlays and pavements. Even though the current study has provided target ranges of the post-crack and joint performance parameters based on the field performance review and laboratory testing, there is a need for field validation of these target ranges from companion field sections. Below are some other value-added future research scopes that may provide additional guidance to the paving industries:

1) Establishing the target values of the fresh concrete properties, such as super air meter (SAM) number and box test rating number for performance engineering mixtures for concrete pavements;
2) Developing correlation between the post-crack and joint performance test parameters with the field performance and distresses through accelerated lab testing;
3) Life-cycle benefits of FRC overlays and pavements-at-grade.

REFERENCES

ACI 544.1R., (2002). *State-of-the-Art Report on Fiber Reinforced Concrete.* Farmington Hills, MI, American Concrete Institute.

ACI 544.1R., (2009). *State-of-the-Art Report on Fiber Reinforced Concrete.* Farmington Hills, MI, American Concrete Institute.

ACI 544.2R, (1999). *Measurement of Properties of Fiber Reinforced Concrete.* Detroit, MI, American Concrete Institute.

ACI 544.3R., (2008). *Guide for Specifying, Proportioning, and Production of Fiber-Reinforced Concrete*. Farmington Hills, MI, American Concrete Institute.

ACI 544.5R., (2010). *Report on the physical properties and durability of fiber reinforced concrete*. Farmington Hills, MI, American Concrete Institute.

ACPA. (2016)., *National Concrete Overlay Explorer*. Retrieved from acpa.org: http://overlays.acpa.org/webapps/overlayexplorer/index.html. (2016.06.20).

Alhassan, M., Ashur, S. A., (2012). *Superiority & Constructability of Fibrous Additives For Bridge Deck Overlays.* Illinois Department of Transportation, Springfield IL.

Altoubat, S., Lange, D., (2001). *Creep, Shrinkage, and Cracking of Restrained Concrete at Early Age*. ACI Materials Journal,Volume 98, Issue 4, pp 323-331.

AASHTO TP118, (2018). *Standard Method of Test for Characterization of the Air-Void System of Freshly Mixed Concrete by the Sequential Pressure Method.* American Association of State Highway and Transportation Officials (AASHTO), Washington, DC.AASHTO PP84, (2018). *Standard Practice for Developing Performance Engineered Concrete Pavement Mixtures.* American Association of State Highway and Transportation Officials (AASHTO), Washington, DC.

ASTM C1116 / C1116M-10a(2015), *Standard Specification for Fiber-Reinforced Concrete*, ASTM International, West Conshohocken, PA, 2015.

ASTM A820, (2016). *Standard Specification for Steel Fibers for Fiber Reinforced Concrete.* ASTM International, West Conshohocken, PA.

ASTM C39, (2017). *Standard Test Method for Compressive Strength of Cylindrical Concrete Specimens.* ASTM International, West Conshohocken, PA.

ASTM C143, (2015). *Standard Test Method for Slump of Hydraulic-Cement Concrete*. ASTM International, West Conshohocken, PA.

ASTM C231, (2017). *Standard Test Method for Air Content of Freshly Mixed Concrete by Pressure Methods.* ASTM International, West Conshohocken, PA.

ASTM C469, (2014). *Standard Test Method for Static Modulus of Elasticity and Poisson's Ratio of Concrete in Compression.* ASTM International, West Conshohocken, PA.

ASTM C1609, (2012). *Standard Test Method for Flexural Performance of Fiber-Reinforced Concrete (Using Beam with Third-Point Loading).* ASTM International, West Conshohocken, PA.

ASTM C1666, (2015). *Standard Specification for Fiber-Reinforced Concrete.* ASTM International, West Conshohocken, PA.

Balaguru, P., Narahari, R., and Patel, M., (1992). *Flexural Toughness of steel fiber reinforced concrete*. ACI Materials Journal, Vol. 89, Issue 6, 541-546.

Balaguru, P., Ramakrishnan, V., (1985). *Freeze-Thaw Durability of Fiber Reinforced Concrete*. ACI Materials Journal, Vol. 83, Issue 3, 374-382

Banthia, N., Sappakittipakorn, M., (2007). *Toughness enhancement in steel fiber reinforced concrete through fiber hybridization.* Cement and Concrete Research, 37(9), 1366-1372.

Barborak, R., (2011). *Fiber Reinforced Concrete (FRC)*. Construction and Materials TIPS. Retrieved from <ftp://ftp.dot.state.tx.us/pub/txdpt-info/cst/tips/frc_4550.pdf>

Barman, M., (2014). *Joint Performance Characterization of Bonded Whitetopping Overlays*. Ph. D Dissertation, University of Pittsburgh, Pittsburgh, PA.

Barman, M., Vandenbossche, J. M. and Li, Z. "Characterization of Load Transfer Behavior for Bonded Concrete Overlays of Asphalt," Transportation Research Record: Journal of the Transportation Research Board, No. 2524, Vol. 2, Transportation Research Board of the National Academies, Washington, DC, 2015, pp. 143-151.

Barman, M., Vandenbossche, J. M. and Janssen, D. "Small-Scale Test Method for Characterizing Joint/Crack Performance for Concrete Pavements," Transportation Research Board 97th Annual Meeting, Washington, DC, 2018.

Barman, M., Vandenbossche, J. M., and Li, Z. I*nfluence of Interface Bond on the Performance of Bonded Concrete Overlays on Asphalt Pavements.* Journal of Journal of Transportation Engineering, Part B: Pavements, ASCE, 143(3): 040170082017, 2017. pp. 1-8.

Beckett, D. (1990). *Comparative Tests on Plain, Fabric Reinforced and Steel Fibre Reinforced Concrete Ground Slabs*, Concrete, 24 (3) 43-45.

Bordelon, A., (2005). *Fracture behavior of concrete materials for rigid pavement systems*. Masters Thesis, the University of Illinois at Urbana Champaign.

Bordelon, A., (2011). *Flowable Fibrous Concrete for Thin Pavement Inlays*. Ph.D. Dissertation, the University of Illinois at Urbana Champaign.

Box Test., (2017). *About Box test*. Retrieved from <http://www.optimizedgraded.com/the-box-test.html>. (March 13th, 2017).

Burnham, T., (2005). *Forensic Investigation Report for Mn/ROAD Ultrathin Whitetopping Test Cells 93, 94, and 95.* Report MN/RC - 2005-45, Minnesota Department of Transportation. Retrieved from http://dotapp7.dot.state.mn.us/research/pdf/200545.pdf.

Burnham, T., Andersen, T. (2015). *Whitetopping Assessment Project - Preliminary Findings Presentation.* Retrieved from <http://www.dot.state.mn.us/mnroad/researchpaysoff/presentations/Research%20Pays%20Off%20-%20%20Whitetopping%20Assessment%20Study%20Update%20-%20Burnham%20-%208-18-15.pdf>

Burwell, B., (2016, September 14). Request for data on whitetopping projects in Oklahoma and Arkansas (Barman, M., Interviewer).

Falkner, H., Huang, Z., and Teutsch, M. (1995). *Comparative Study of Plain and Steel Fibre Reinforced Concrete Ground Slabs*, Concrete International, Vol. 17, No. 1, pp. 45-51.

Fick, G., Harrington, D., (2014). *Technical Brief: Performance History of Concrete Overlays in the United States*. FHWA DTFH61-12-H-00010. Federal Highway Administration, Washington, DC.

Gaddam., (2016). *Fiber reinforced concrete and behavior properties and applications and advantages*. Retrieved from <civiline.blogspot.com> (Sept. 6, 2016).

Google Maps., (2016, September 22). Retrieved from <https://www.google.com/maps/@34.0619158,-81.045126>

Hannant, D., (1978). *Fibre Cements and Fibre Concretes.* John Wiley & Sons Ltd., Chichester, United Kingdon.

Harrington, D., Fick, G., (2014). *Guide to Concrete Overlays, Third Edition.* ACPA Publication TB021.03P. NJ.

Issa, M., A. (2017). *Effect of Early-Age Concrete Elastic Properties on Fatigue Damage in PCC Pavements Containing Fibers.* Publication FHWA-ICT-17-019, Illinois Center for Transportation, IL.

Jenq, Y., Shah, S., (1985). *Two Parameter Model for Concrete*. Journal of Engineering Mechanics*,* 111(10), 1227-1241.

Johnson, A., (2016, September 2016). *Fiber Reinforced Whitetopping projects*. (Hansen, B., Interviewer)

Kim, M ., Bordelon., A. (2016). *Age-Dependent Flexural Properties of Fiber Reinforced Concrete Used in Thin Overlays.* Proc. of 11th International Conference on Concrete Pavements (ICCP), San Antonio, TX.

King, D., Roesler, J. R., (2014). *Structural Performance of Ultra-thin Whitetopping on Illinois Roadways and Parking Lots*. Research Report No. FHWA-ICT-14-018, the University of Illinois at Urbana-Champaign, Illinois Center for Transportation, IL.

Kevern, J., Rupnow T., Mulheron, M., Collier, Z., and Icenogle, P., (2016). *Evaluation of the Fatigue and Toughness of Fiber Reinforced Concrete for use as a New Highway Pavement Design.* Final Report*,* LTRC Project Number: 14-3C. Louisiana Department of Transportation, Baton Rouge, LA.

Kobayashi, K., Cho, R., (1982). *Flexural Characteristics of steel fibre and polyethylene fibre hybrid-reinforced concrete.* Composites, 13 (2), 164-168.

Kosa, K., Naaman, A. E., (1990). *Corrosion of Steel Fiber Reinforced Concrete*. ACI Materials Journal, Vol. 87(1), 27-37.

Koubaa, A ., Burnham., T. (2001). *A New Approach to Estimate the In-situ Thermal Coefficient And Drying Shrinkage for Jointed Concrete Pavement.* Proc. of 7th International Conference on Concrete Pavements (ICCP), Orlando, FL.

Ley, T., (2015). *The Super Air Meter (SAM)*. Pittsburgh Area ACI Chapter News. Retrieved: February 2017.Retrieved from < http://www.superairmeter.com/info.html>

Ludirdja, D., Yougn, J., (1992). *Synthetic Fiber Reinforcement for Concrete.* U.S. Army Construction Engineering Research Laboratories, Champaign, IL.

Mahadik, S., Kamane, A., (2014). *Effect of steel fibers on compressive and flexural strength on concrete*. International Journal of Advanced Structures and Geotechnical Engineering, 3(04), 388-392.

Mangat, P., Gerusamy, K., (1987). *Long Term Properties of Steel Fiber-Reinforce Marine Concrete*. *Materials and Constructions (RILEM)*, 273-282.

MnDOT, (2017). *MnROAD concrete special provision*. (Table 2301-5).

Pilkington, B., (1979). *Design Guide: GlassFibre Reinforced Cement.* Steel House Press. Liverpool, England.

Portland Cement Association (PCA), (2015). *Design and Control of Concrete Mixtures 15th edition.* PCA, Skokie, IL.

Prince, R. (2016)., *Basalt Fiber Properties*. Retrieved from < http://www.build-on-prince.com/basalt-fiber> (Septmber, 2016).

Ramakrishanan, V., (1987)., *Materials and Properties of Fribre Concrete*. Proceedings of the International Symposium on Fibre Reinforced Concrete, Madras, India.

Rollings, R.S. (1986). *Field Performance of Fiber Reinforced Concrete Airfield Pavements.* DOT/FAA/PM-86/26, Federal Aviation Administration, Washington, DC.

Rasmussen, R., Rozycki, D., (2004). *Thin and Ultra-Thin Whitetopping.* NCHRP Synthesis of Highway Practice 338. National Cooperative Highway Research Program, Washington, DC.

Riley, R., (2016, September 09). *Request for data on FRC overlay projects in IL*. (Barman, M., Interviewer)

Roesler, J. R., D. Lange, and G. Ulreich, (2003). *Fracture Behavior of Full-Scale, Fiber-Reinforced Concrete Slabs*. Final Report for W.R. Grace, Inc., University of Illinois, Urbana, IL, 124 pp.

Roesler, J., A. Bordelon, A., Ioannides, M. Beyer, D. Wang., (2008). *Design and Concrete Material Requirements for Ultra-Thin Whitetopping.* Publication FHWA-ICT-08-016. Illinois Center for Transportation, Rantoul, IL.

Rotithor, H., (2010). *Performance of Ultra-Thin Whitetopping (UTW) in Oklahoma.* Masters Thesis, Oklahoma State University, Stillwater, OK.

SAM., (2017). Information-Learn more about SAM. Retrieved from
    <http://www.superairmeter.com/info.html>. (March 13th, 2017).

Sprinkel, M., Ozyildirim, C., (2000). *Evaluation of Hydraulic Cement Concrete Overlays Placed on Three Placements in Virginia.* Virginia Transportation Research Council, Charlottesville, VA.

Tavakoli, M., (1994). *Tensile and Compressive Strengths of Polypropylene Fiber Reinforced Concrete*. Section in *Fiber reinforced concrete: Developments and innovations SP-142.* American Concrete Institute, Detroit, MI.

Vandenbossche, J., (2003). *The construction and Performance of Ultra-Thin Whittetopping Intersections on US-169.* Minnesota Department of Transportation, St. Paul, MN.

Vandenbossche, J., Rettner, D., (1998). *The Construction of US-169 and I-94 Experimental Thin and Ultra-Thin Whitetopping Sections In Minnesota.* Minnesota Department of Transportation, St. Paul, MN.

Vandenbossche, J., Li, Z., (2013). *Redefining the Failure Mode for Thin and Ultra-thin Whitetopping with a 1.8- x 1.8-m (6- x 6-ft) Joint Spacing.* Transportation Research Record, 2368(1), 133-144.

Vasile, C., (2000). *Polyolefin fibers*. Handbook of Polyolefins*.* Marcel Dekker, New York.

Wouter, G., (2016, September 7). *Fiber Reinforced Whitetopping projects*. (Hansen, B., Interviewer)

Zollo, R., (1984). *Collated Fibrillated Polypropylene Fibers in FRC*. In SP-81 Detroit, American Concrete Institute, MI.

APPENDIX A: DATA REQUEST FORM FOR BONDED AND UNBONDED CONCRETE OVERLAYS

Swenson College of Science and Engineering
Department of Civil Engineering

Data Request Form for Bonded and Unbonded Concrete Overlays   **Date:**

Owner:	Contact name:	Contact phone No./email address:
Project Location (Route No., mile point, intersection, section length, etc.):		

General Traffic Data

Average daily traffic:	(%) Trucks:

Overlay Information

Year of overlay construction:
Project size (lane miles or yd^2):
Slab thickness (in):
Joint spacing (ft):
Compressive strength of concrete (psi) (at traffic opening/ 28 days):
Layer type beneath overlay: (thickness, if known):

Fiber Information

Type (polypropylene, steel, etc...):
Brand/ Manufacturer:
Structural/ Non-structural:
Shape (cross section and geometry):
Length(in):
Effective diameter (in):
Aspect ratio:
Dosage (lb/yd^3):

Performance/Distress Data for PCC Overlay

Any distress observed (joint distress, trans. cracks, long. cracks or others)?
Any observed contribution of the fibers (Improve concrete properties, holding cracked slabs, keeping cracks tight, contributing in load transfer)?
Any suggestion on the most suitable fiber type for concrete overlays and dosages?

Figure A-1. Sample project survey form *(shirked to accommodate in one page on this report)*.

APPENDIX B: FIBER PHOTOGRAPHS

Figure B-0-1. Image of Fiber 1.
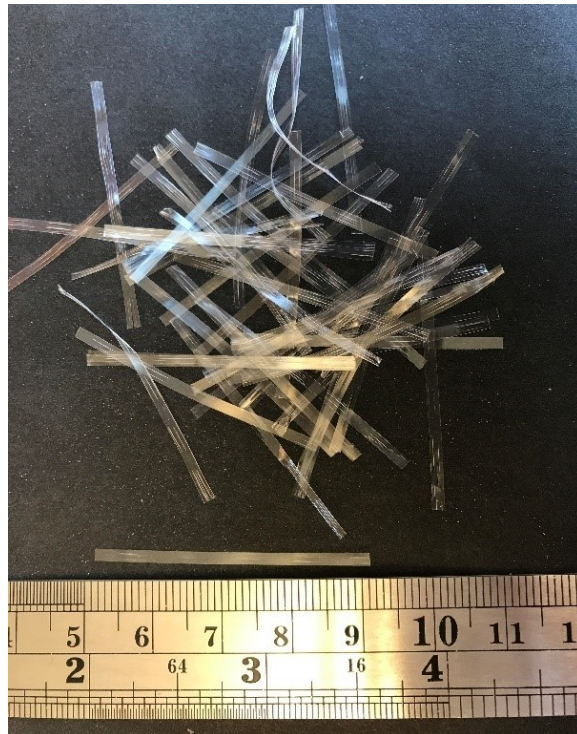
Figure B-0-2. Image of Fiber 2.

Figure B-0-3. Image of Fiber 3.

Figure B-0-4. Image of Fiber 4.

Figure B-0-5. Image of Fiber 5.
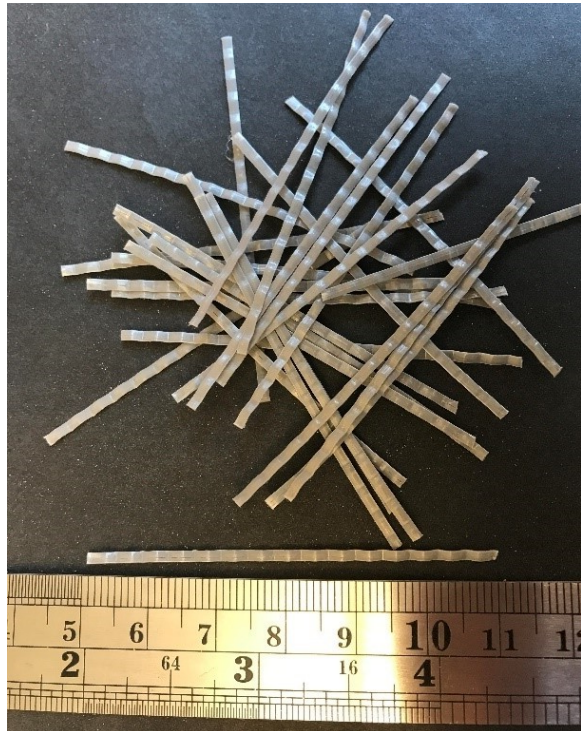
Figure B-0-6. Image of Fiber 6.
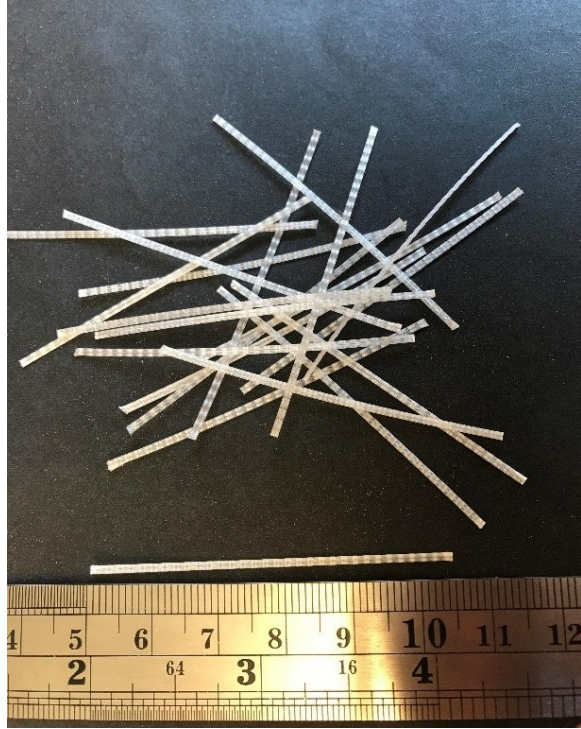
Figure B-0-7. Image of Fiber 7.

Figure B-0-8. Image of Fiber 8.
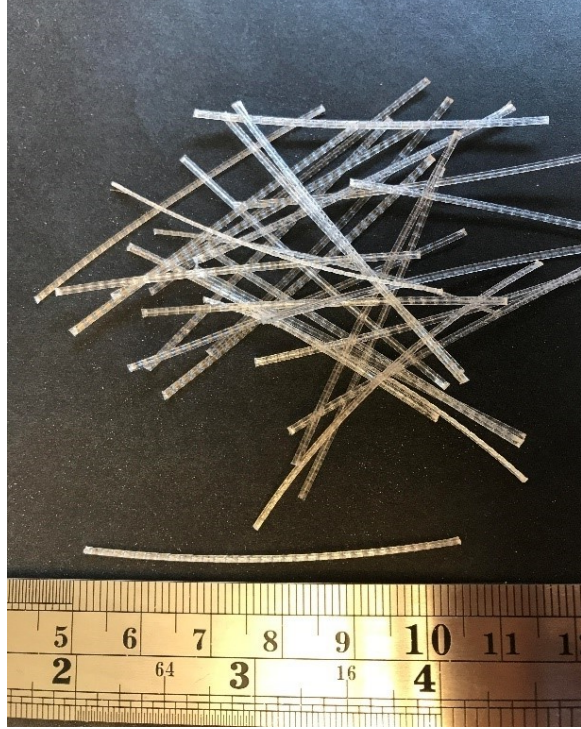
Figure B-0-9. Image of Fiber 9.
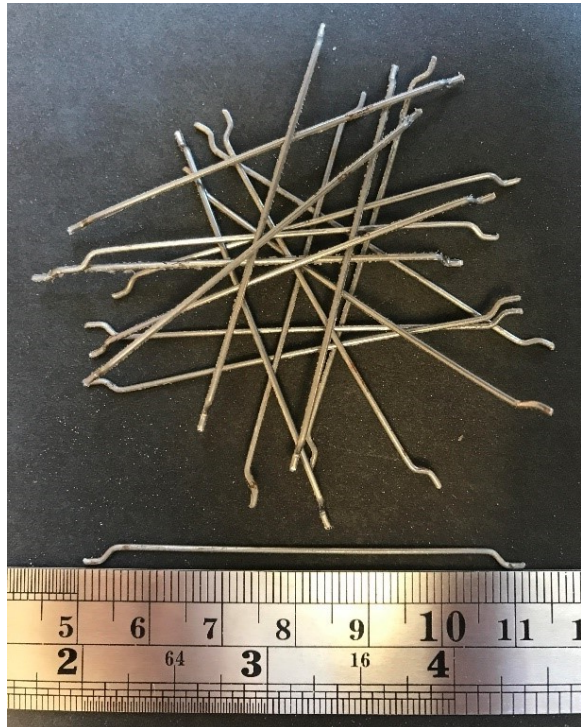
Figure B-0-10. Image of Fiber 10.

APPENDIX C: MIXTURE RESULTS

Table C-1. Fresh concrete properties of the thirty one mixes considered in Task 3.

Designation	Slump (in)	Air (%)	SAM (#)	Box (#*)
S.S.1.25	1.25	8.1	0.19	1
S.S.1.5	1	7.1	0.04	2
S.S.1.75	0.5	5.8	0.35	4
S.S.2.25	0.75	6.5	X	2
S.S.2.5	0.5	5.9	X	2
S.S.2.75	1	6.1	0.06	3
S.S.3.25	0.5	5.6	0.38	3
S.S.3.5	2	7.8	0.22	1
S.S.3.75	0.75	5.7	0.39	3
S.S.4.25	2.5	8.5	X	1
S.S.4.5	0.5	7.8	X	1
S.S.4.75	0.75	6.1	X	3
S.T.5.25	3	5.9	0.31	1
S.T.5.5	2.75	8.1	0.09	1
S.T.5.75	2.25	9	0.2	2
S.C.6.25	1.75	7.9	0.12	1
S.C.6.5	3	8.5	0.22	2
S.C.6.75	0.5	5.5	0.4	3
S.E.7.25	1	5.5	0.61	1
S.E.7.5	1	9	0.28	2
S.E.7.75	1	7.1	0.17	2
S.E.8.25	1.5	7	0.16	1
S.E.8.5	2.25	7.8	0.15	3
S.E.8.75	0.75	5.6	0.38	2
S.E.9.25	1.25	7.5	0.33	1
S.E.9.5	3	7.9	0.19	2
S.E.9.75	1.5	8.1	0.28	3
L.EC.10.25	2.5	7.5	0.32	2
L.EC.10.5	2.25	5.6	0.56	3
L.EC.10.75	2	5.9	0.59	3
Control Mixture	1.5	6.3	0.38	1

X: SAM test apparatus did not function properly; only air content could be collected.

*: Qualitative approximation

Table C-2 Plastic and Hardened concrete properties of the 12 mixtures cast in the joint performance portion of this study.

Designation	Slump (in)	Air Content (%)	Compressive Strength (psi)
J1 - Plain Concrete	2.5	8.5	6750
J1 - S.S.4.5	3	6.6	7190
J1 - S.T.5.5	2	6.9	7340
J1 - S.C.6.5	1	7.1	7490
J1 - S.E.9.5	2.5	8.5	6610
J1 - S.E.9.25	2	7.8	7470
J1 - S.S.4.25	2	8.5	6330
J2 - Plain Concrete	1.5	8.5	6920
J2 - S.S.4.5	1	8.6	6650
J2 - S.T.5.5	3	6.8	7280
J2 - S.C.6.5	1	5.9	7120
J2 - S.E.9.5	1.5	7.5	6550

Table C-3 Hard concrete properties (28 days) of 31 mixes considered in the study.
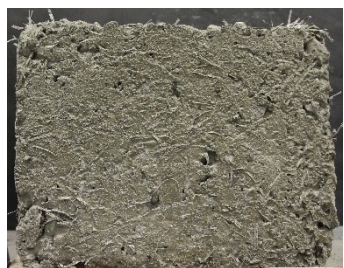
Designation	Compressive Strength (psi)	Modulus of Elasticity (ksi)		MOR (psi)	Residual Strength (lbf)	RSR L/120 (%)
		Lab Test	ACI Equation			
S.S.1.25	6,570	4,720	4,620	710	900	10.4
S.S.1.5	6,940	4,730	4,748	750	1,900	20.6
S.S.1.75	6,850	4,920	4,718	760	3,300	35.6
S.S.2.25	6,690	4,450	4,662	710	640	24.2
S.S.2.5	6,290	4,530	4,521	690	2,100	45.9
S.S.2.75	7,170	4,820	4,827	780	3,830	6.8
S.S.3.25	6,670	4,630	4,655	790	280	2.9
S.S.3.5	6,860	4,730	4,721	770	2,000	21.4
S.S.3.75	6,830	4,640	4,711	780	3,910	41.3
S.S.4.25	6,660	4,950	4,652	740	1,110	12.4
S.S.4.5	6,670	4,640	4,655	750	2,710	29.3
S.S.4.75	6,740	4,680	4,680	750	4,200	46.1
S.T.5.25	6,960	5,320	4,755	780	1,400	14.9
S.T.5.5	6,230	4,270	4,499	690	2,500	29.4
S.T.5.75	6,410	4,300	4,564	680	3,920	47.4
S.C.6.25	6,920	5,060	4,742	680	1,390	16.8
S.C.6.5	7,788	5,210	5,030	750	2,910	31.7
S.C.6.75	7,260	4,680	4,857	790	3,970	41.1
S.E.7.25	6,740	4,970	4,680	720	1,480	15.8
S.E.7.5	7,060	4,470	4,789	780	3,200	34.0
S.E.7.75	6,760	4,860	4,686	760	3,820	43.3
S.E.8.25	6,610	4,650	4,634	700	1,200	14.2
S.E.8.5	6,380	4,780	4,553	720	1,800	20.6
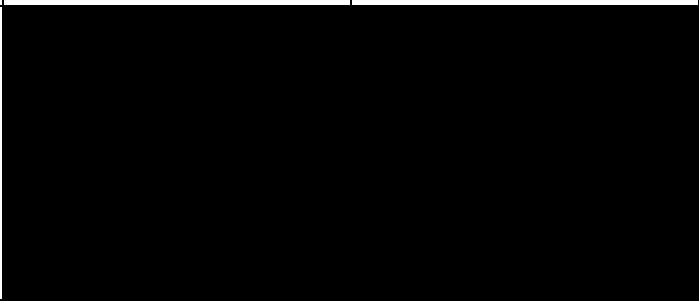
S.E.8.75	6,770	4,810	4,690	710	3,210	36.4
S.E.9.25	7,080	4,720	4,796	760	1,600	17.4
S.E.9.5	6,840	4,620	4,714	690	3,500	41.4
S.E.9.75	7,100	4,870	4,803	730	4,450	50.6
L.EC.10.25	7,330	6,140	4,880	780	2,810	29.3
L.EC.10.5	7,970	6,270	5,089	790	6,470	67.0
L.EC.10.75	9,320	5,940	5,503	930	7,150	54.6
S. Control Mixture	6,960	4,990	4,755	720	-	-

Table C-4. Properties not included in analysis, but collected from ASTM C1609 testing.

Designation	RSR L/800 (%)	Toughness (lb-in)
S.S.1.25	8.8	246
S.S.1.5	30.5	397
S.S.1.75	43.2	519
S.S.2.25	0	266
S.S.2.5	26	376
S.S.2.75	45	520
S.S.3.25	0	364
S.S.3.5	33	399
S.S.3.75	53	626
S.S.4.25	8	256
S.S.4.5	25	391
S.S.4.75	48	570
S.T.5.25	8	308
S.T.5.5	28	391
S.T.5.75	45	521
S.C.6.25	4	282
S.C.6.5	28	473
S.C.6.75	42	594
S.E.7.25	6	334
S.E.7.5	43	548
S.E.7.75	51	553
S.E.8.25	7	297
S.E.8.5	27	396
S.E.8.75	52	546
S.E.9.25	12	343
S.E.9.5	41	502
S.E.9.75	55	615
L.EC.10.25	37	481
L.EC.10.5	89	924
L.EC.10.75	80	955

APPENDIX D: BOX TEST SPECIMENS

Fiber Designation	0.25% V_f	0.50% V_f	0.75% V_f
S.S.1			
S.S.2			
S.S.3			
S.S.4			
S.T.5			

S.C.6			
S.E.7			
S.E.8			
S.E.9			
L.EC.10			
Plain Concrete			

APPENDIX E: ASTM C1609 FLEXURAL TEST CURVES
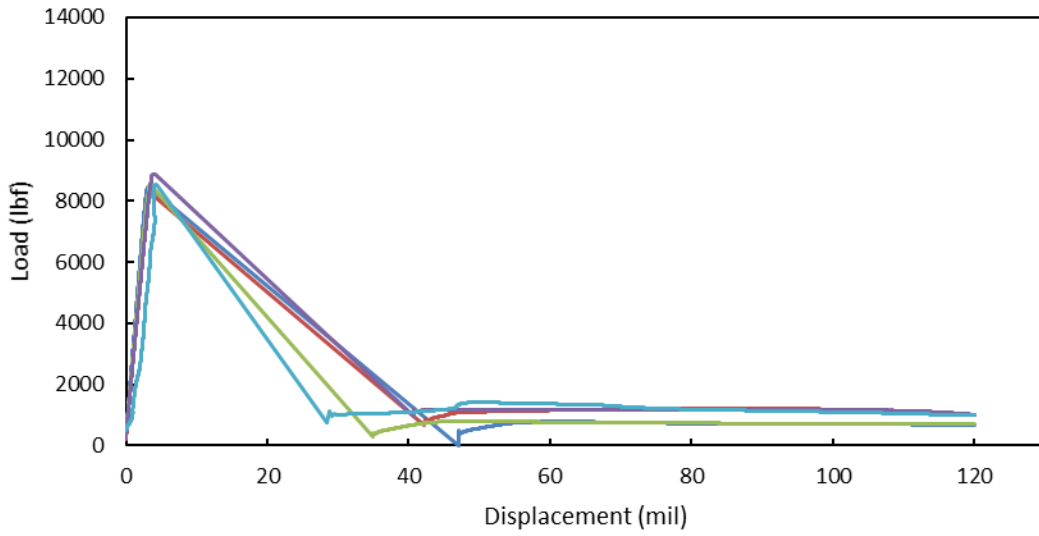
Figure E-1. Load versus displacement curves for S.S.1.25.
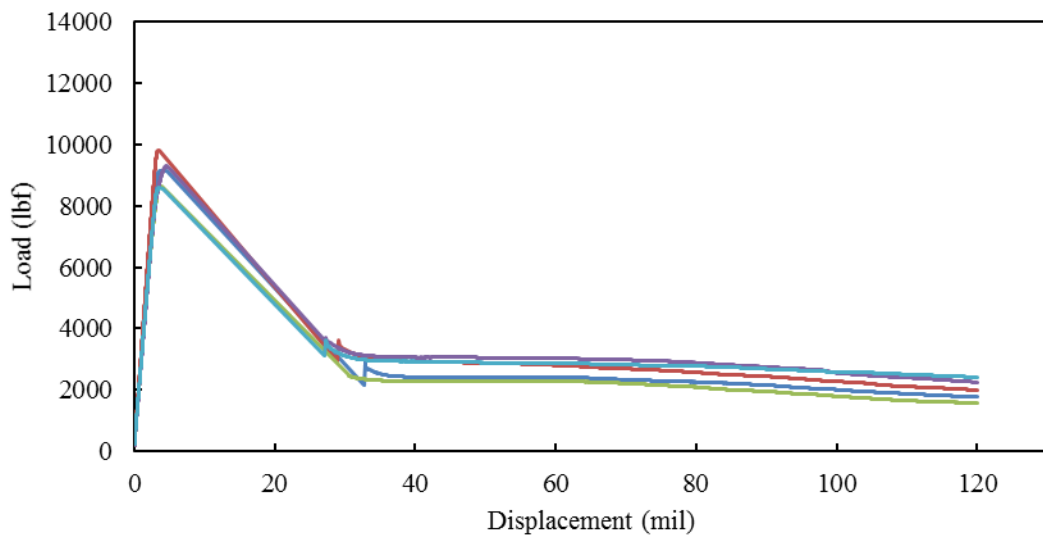
Figure E-2. Load versus displacement curves for S.S.1.5.
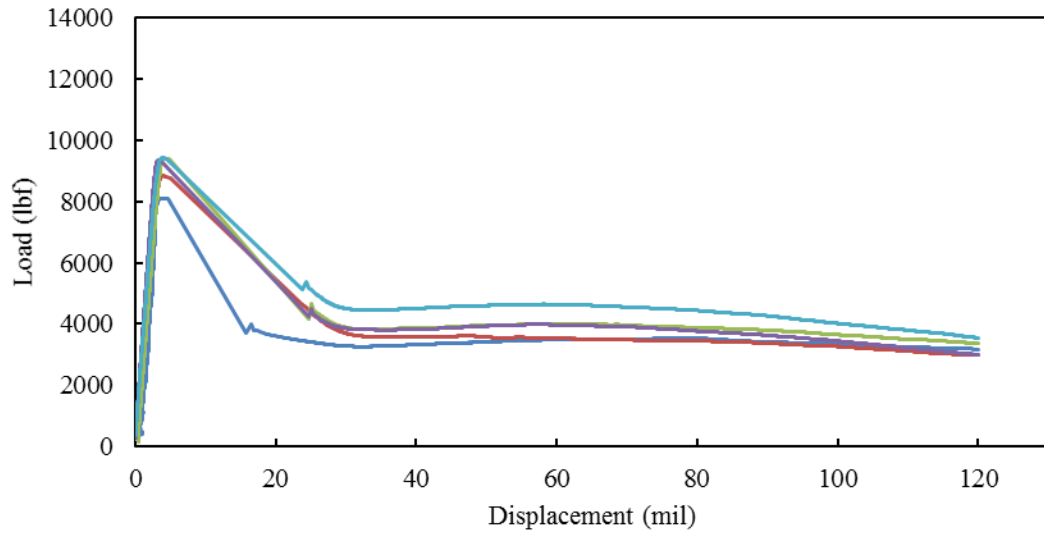
Figure E-3. Load versus displacement curves for S.S.1.75.
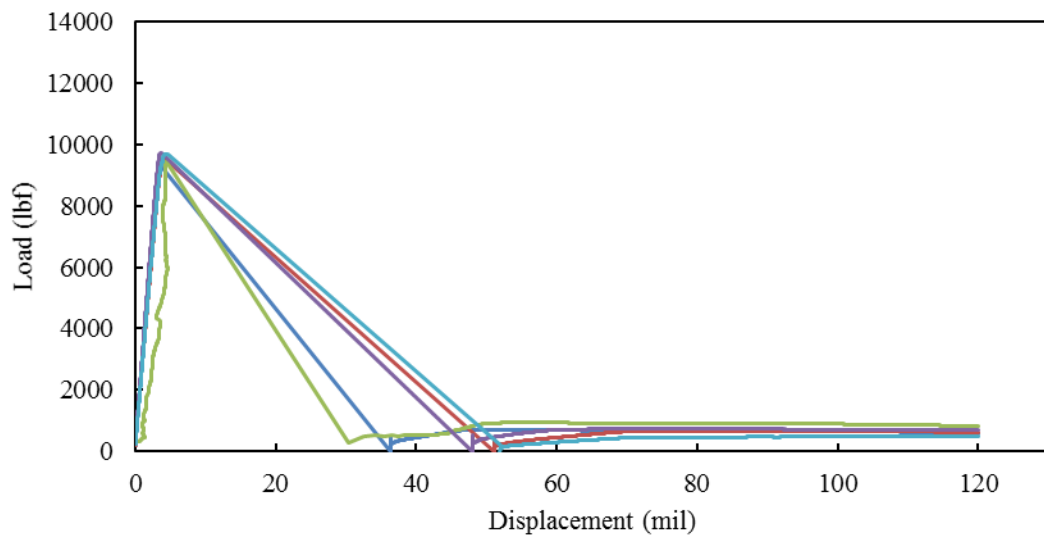
Figure E-4. Load versus displacement curves for S.S.2.25.
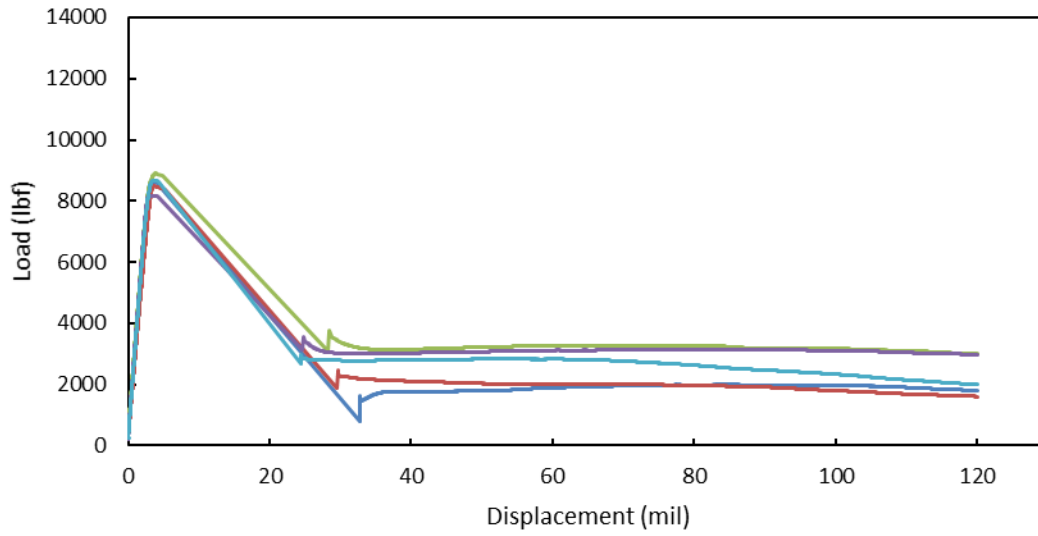
Figure E-5. Load versus displacement curves for S.S.2.5.
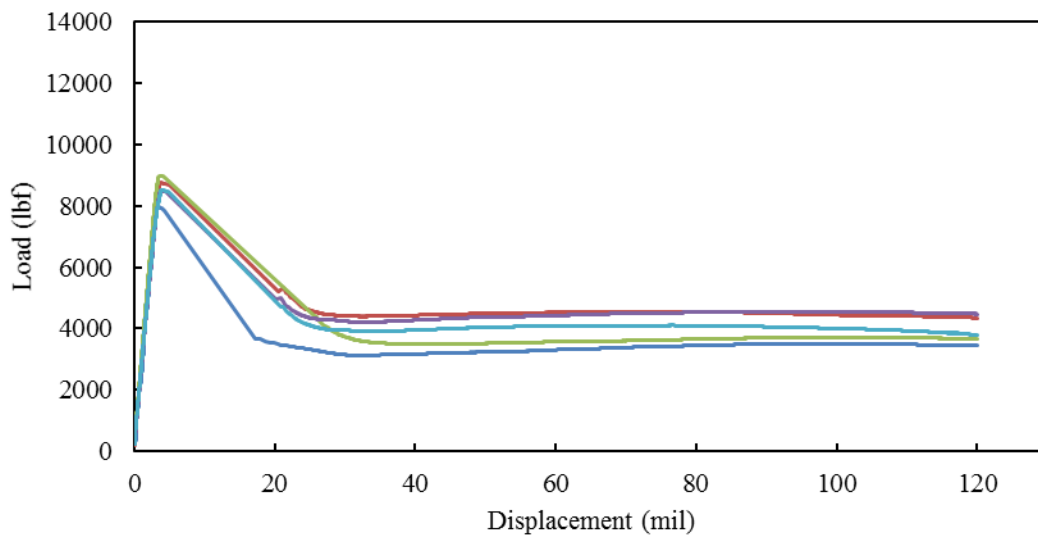
Figure E-6. Load versus displacement curves for S.S.2.75.

E-3
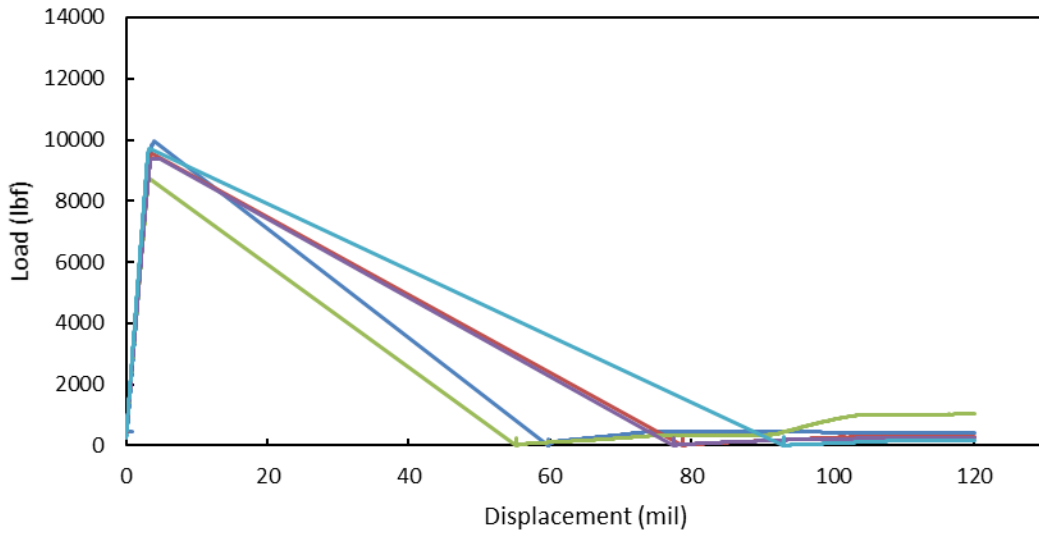
Figure E-7. Load versus displacement curve for S.S.3.25.
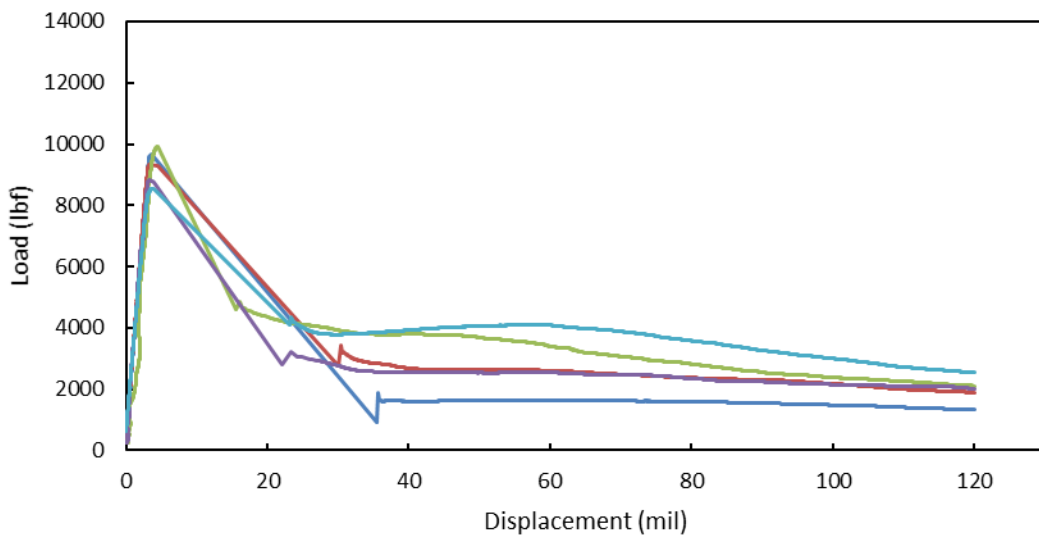
Figure E-8. Load versus displacement curves for S.S.3.5.

E-4
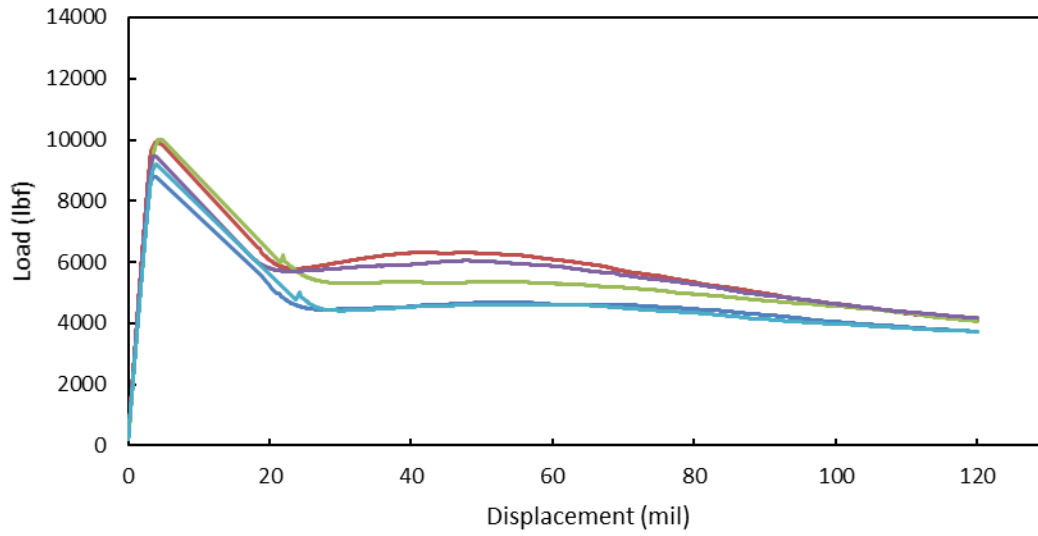
Figure E-9. Load versus displacement curves for S.S.3.75.
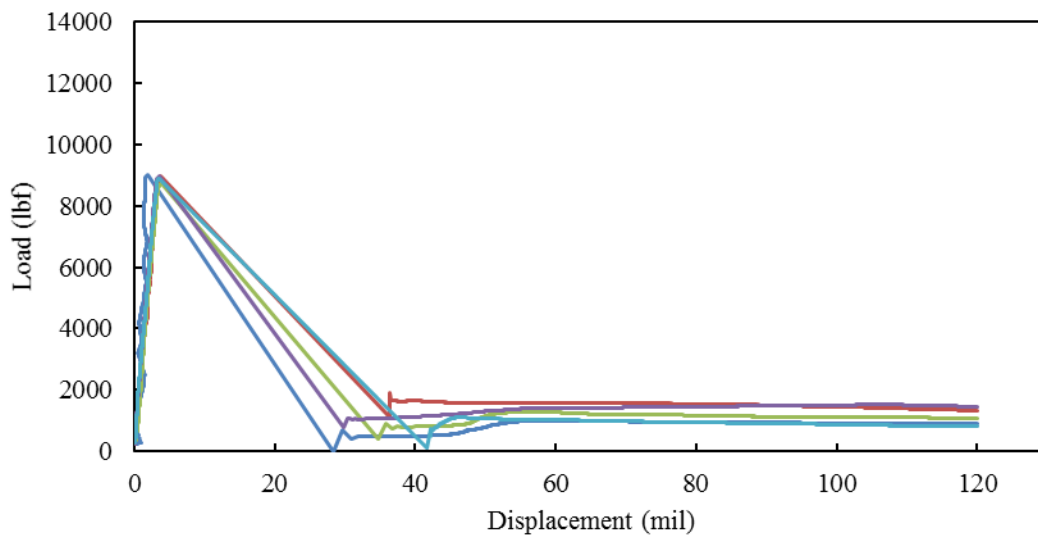
Figure E-10. Load versus displacement curves for S.S.4.25.

E-5
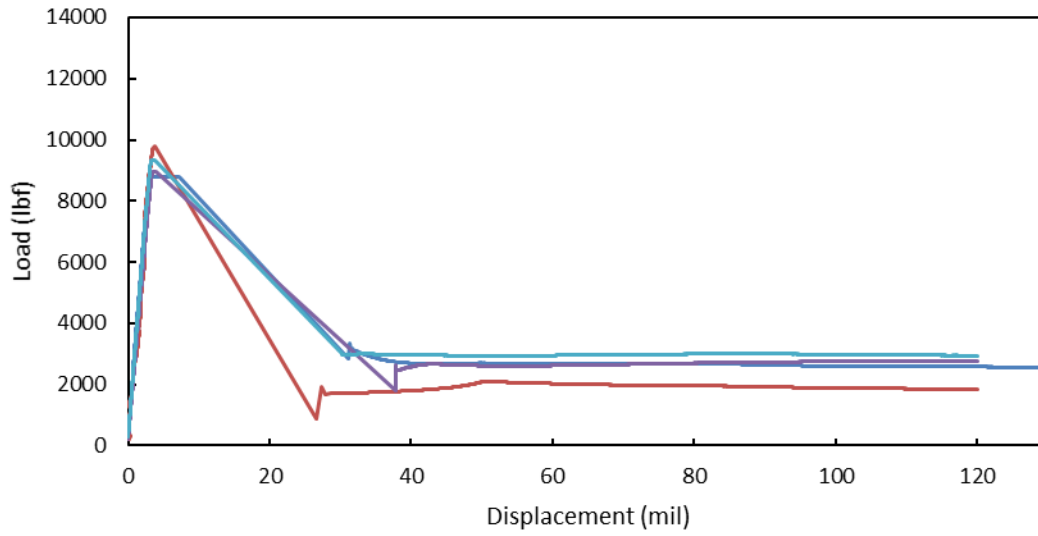
Figure E-11. Load versus displacement curves for S.S.4.5.
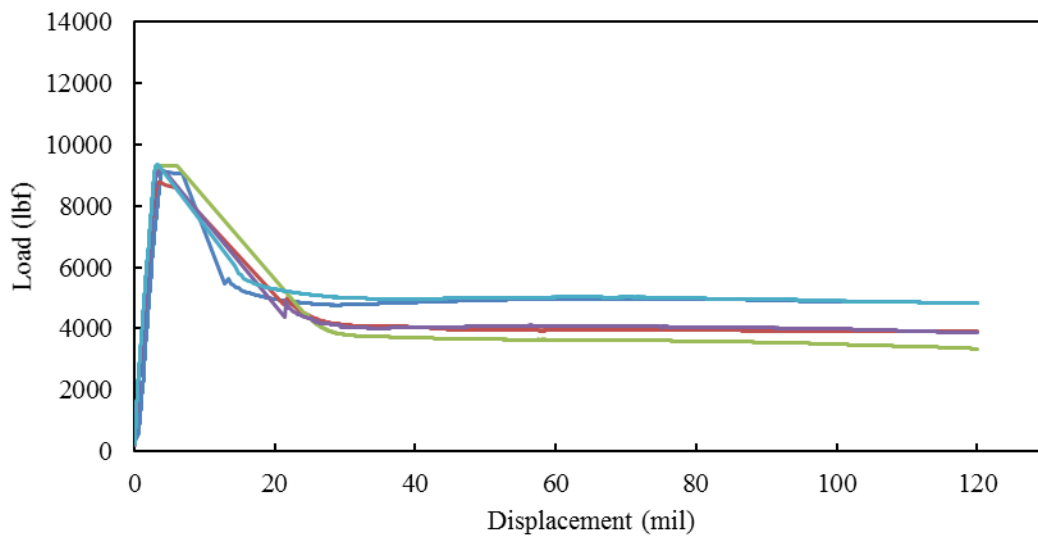
Figure E-12. Load versus displacement curves for S.S.4.75.
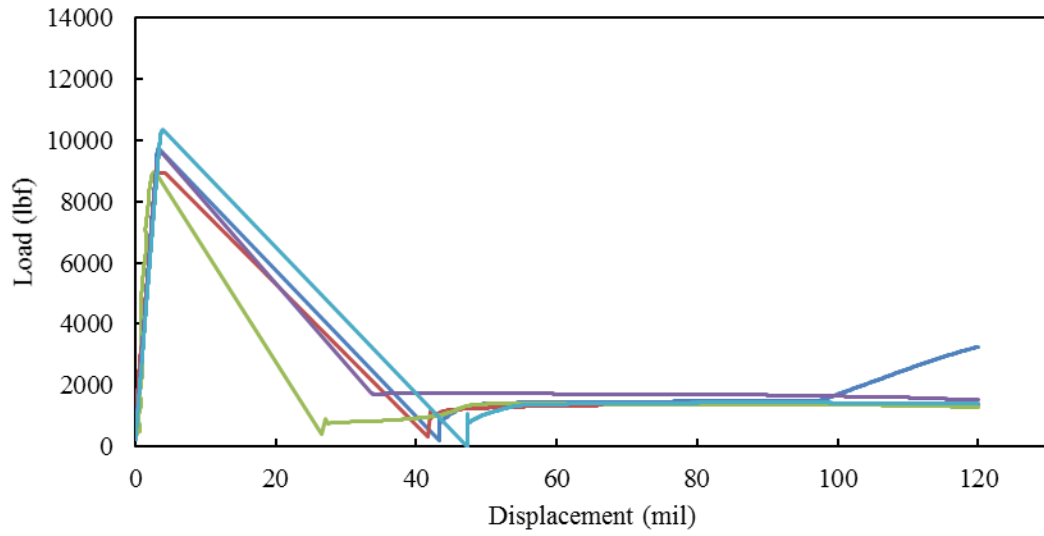
Figure E-13. Load versus displacement curves for S.T.5.25.
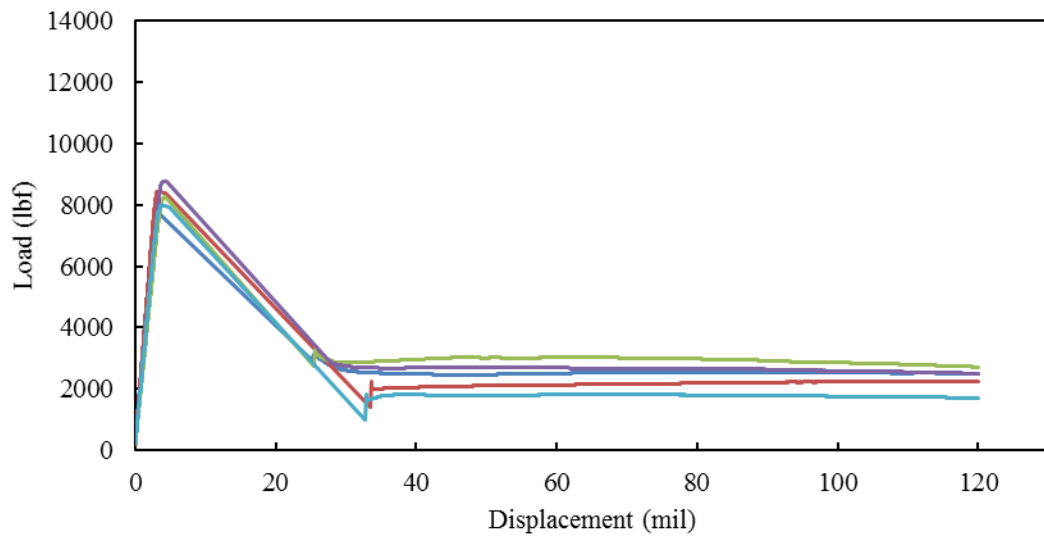
Figure E-14. Load versus displacement curves for S.T.5.5.

E-7
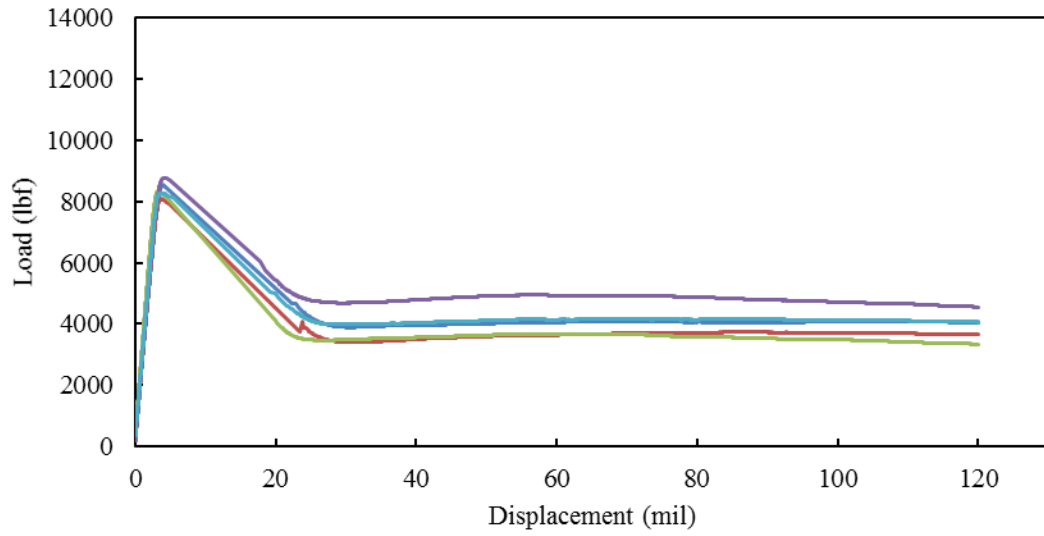
Figure E-15. Load versus displacement curves for S.T.5.75.
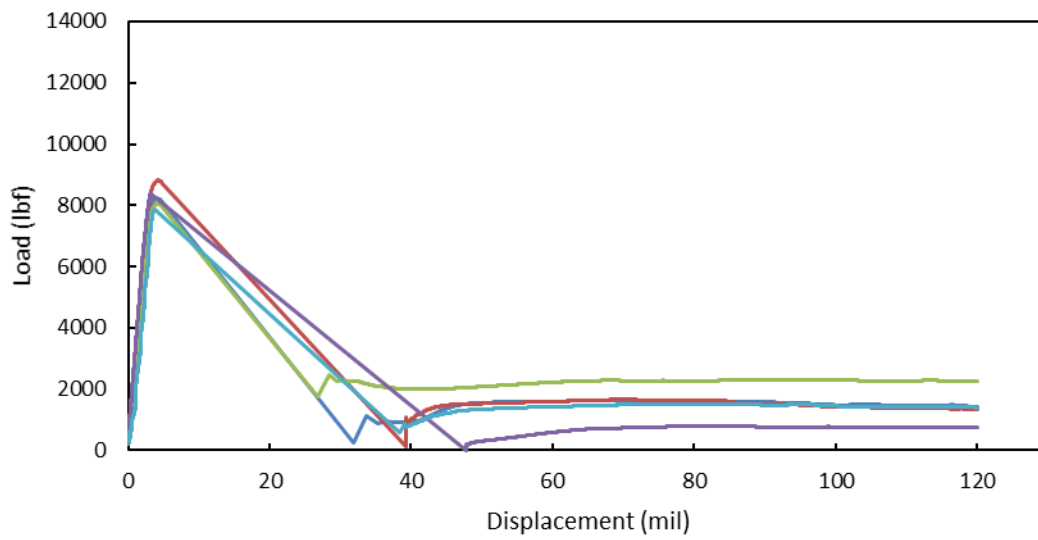
Figure E-16. Load versus displacement curves for S.C.6.25.

E-8
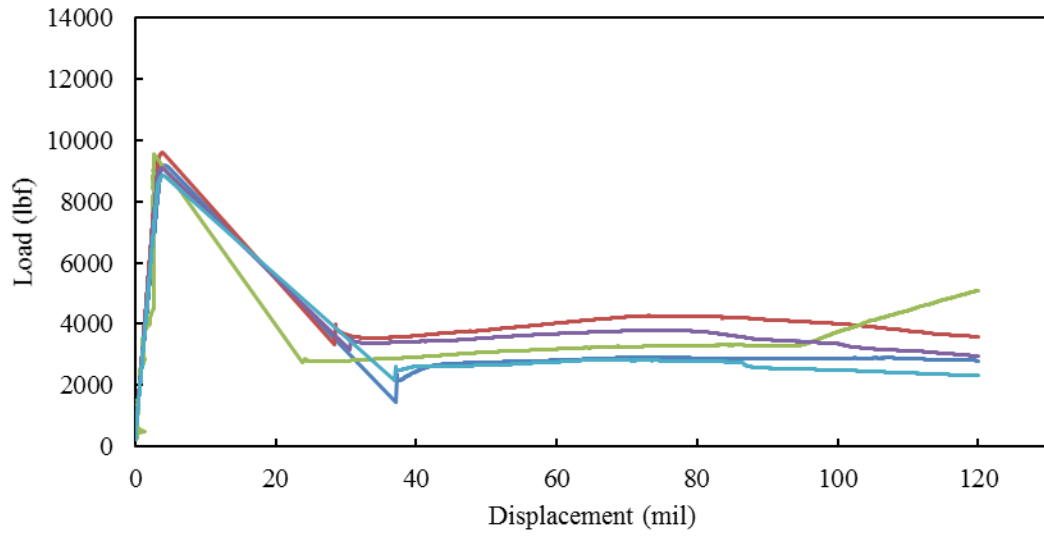
FigureE-17. Load versus displacement curves for S.C.6.5.
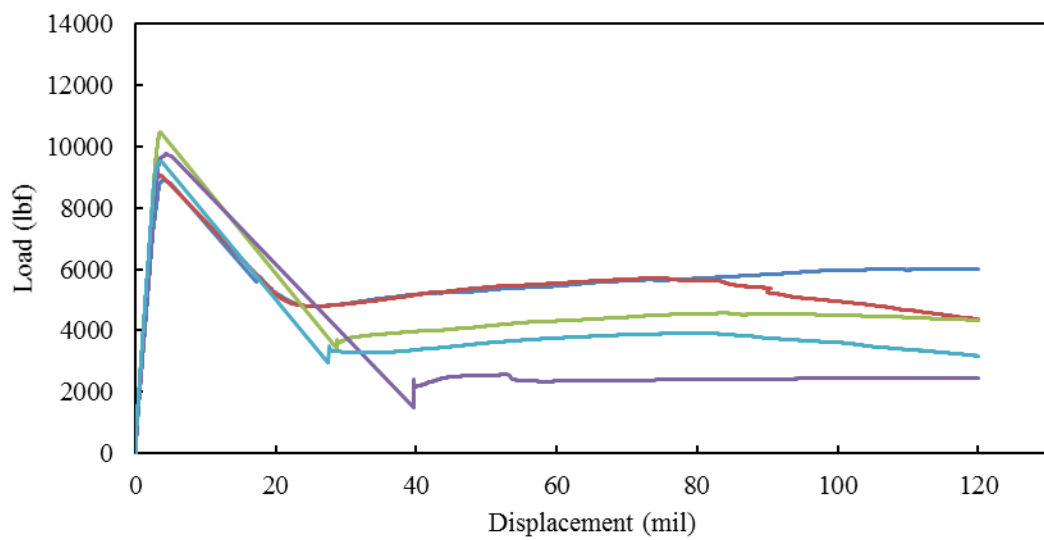
Figure E-18. Load versus displacement curves for S.C.6.75.

E-9
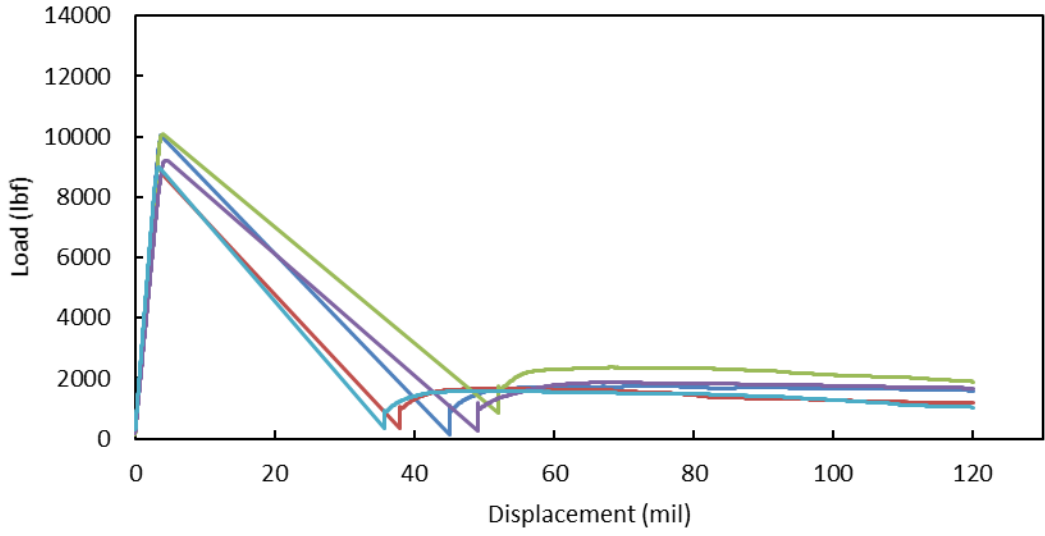
Figure E-19. Load versus displacement curves for S.E.7.25.
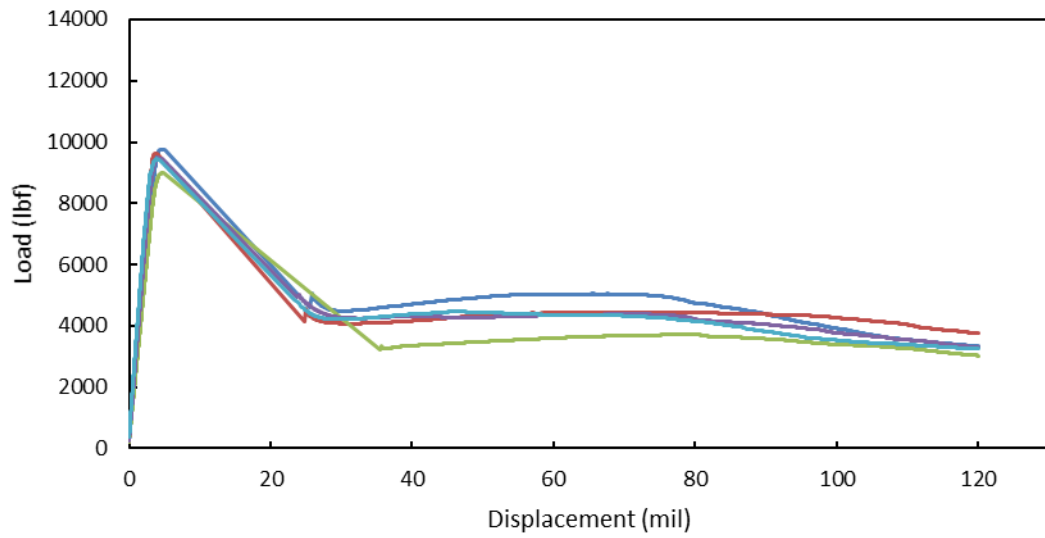
Figure E-20. Load versus displacement curves for S.E.7.5.

E-10
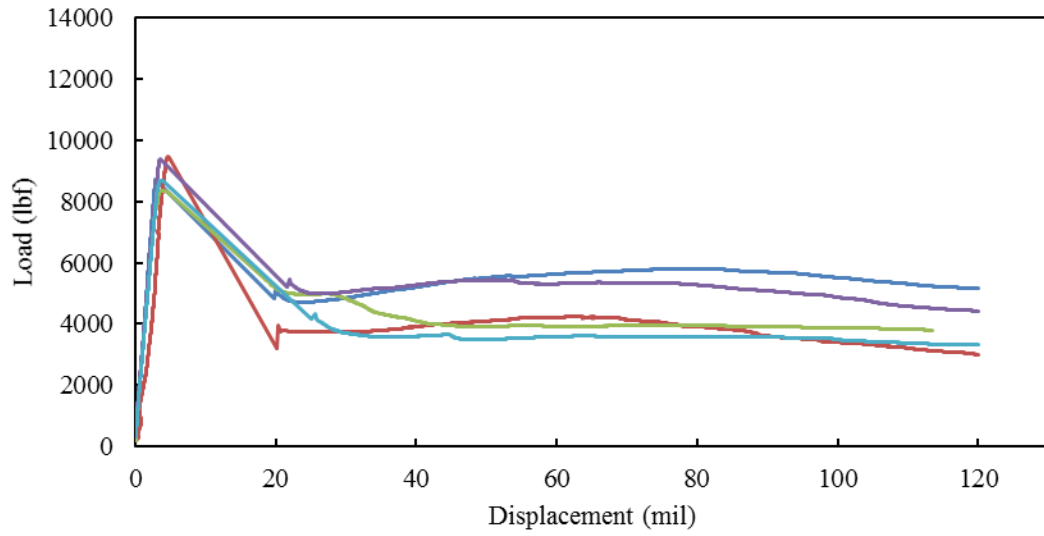
Figure E-21. Load versus displacement curves for S.E.7.75.
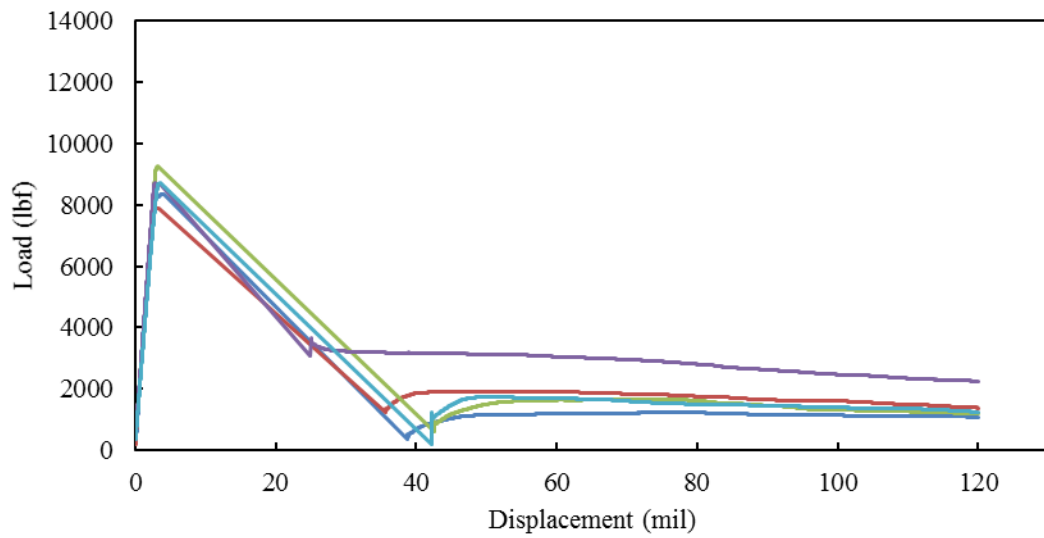
Figure E-22. Load versus displacement curves for S.E.8.25.
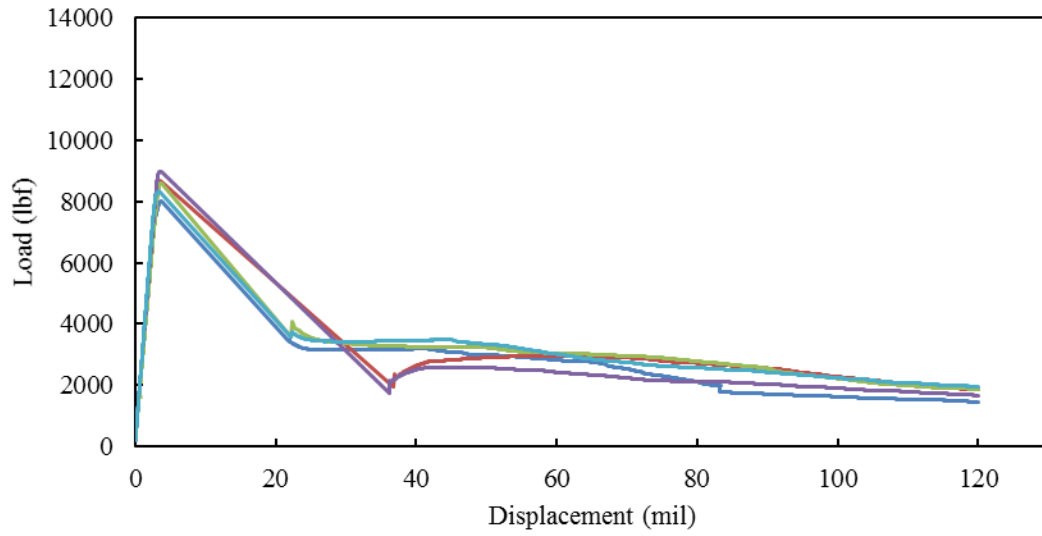
Figure E-23. Load versus displacement curves for S.E.8.5.
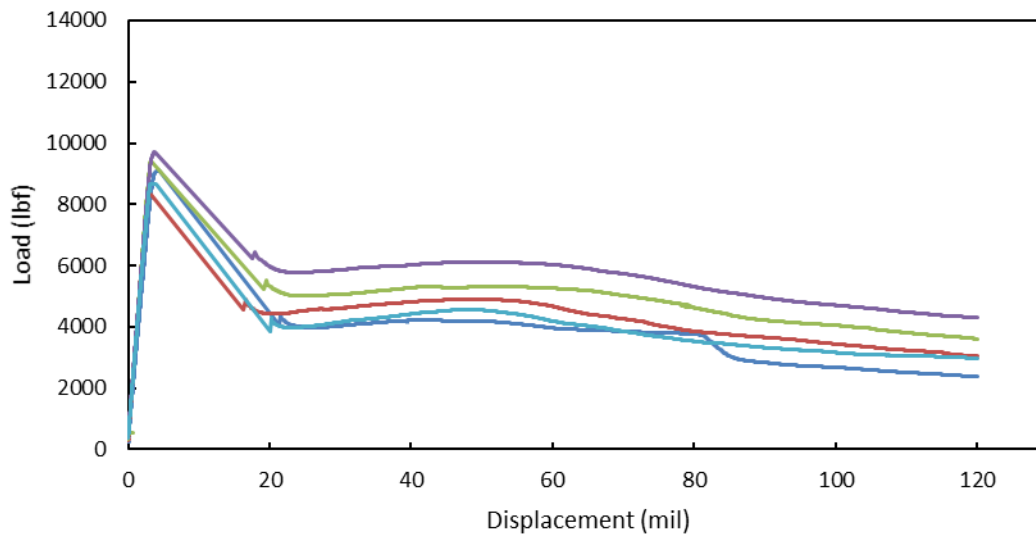
Figure E-24. Load versus displacement curves for S.E.8.75.

E-12
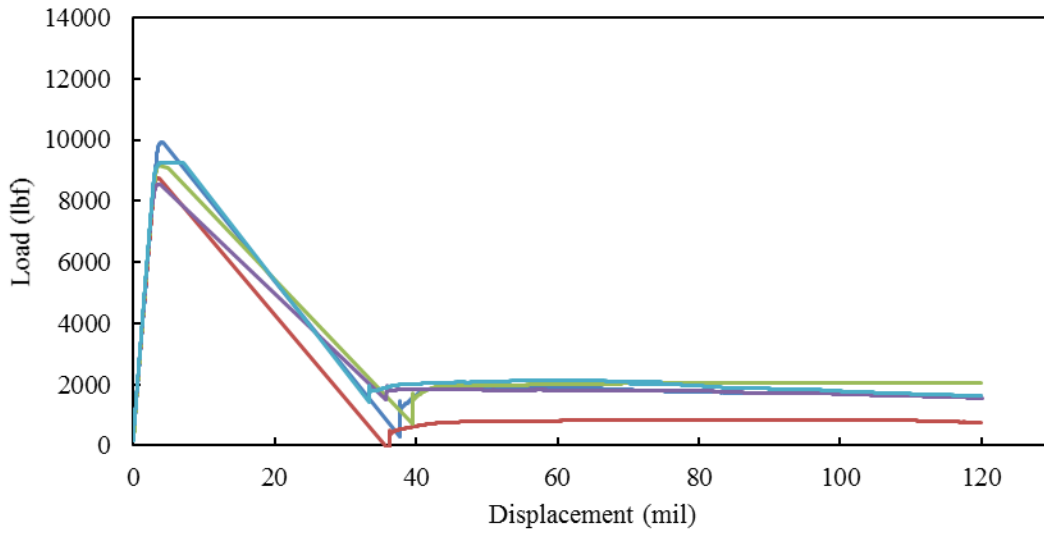
Figure E-25. Load versus displacement curves for S.E.9.25.
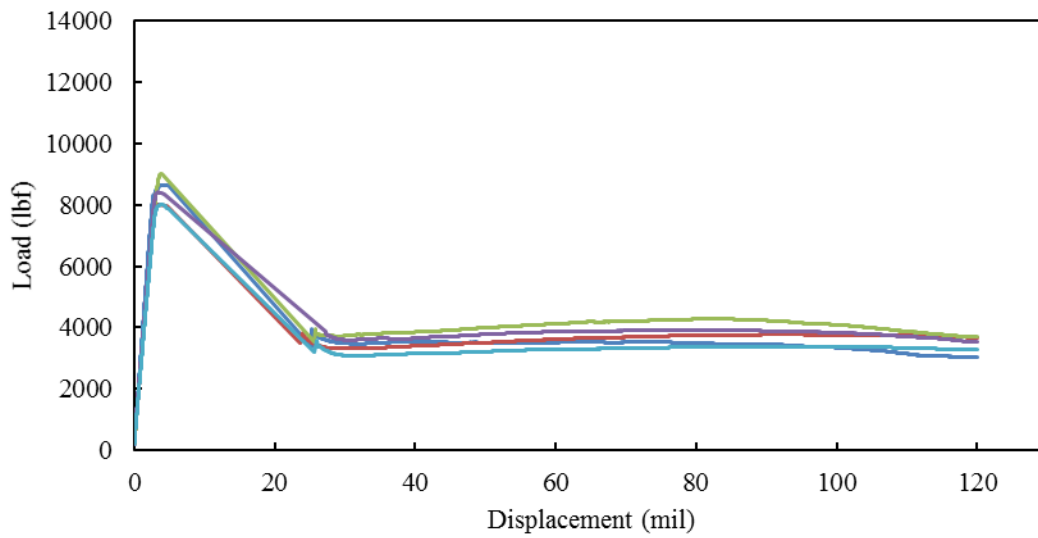
Figure E-26. Load versus displacement curves for S.E.9.5.
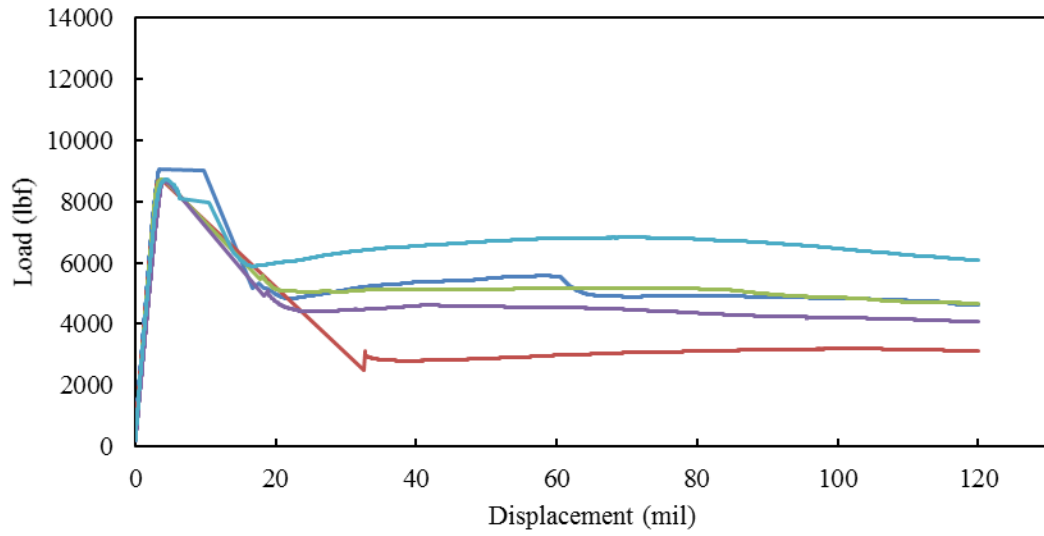
Figure E-27. Load versus displacement curves for S.E.9.75.
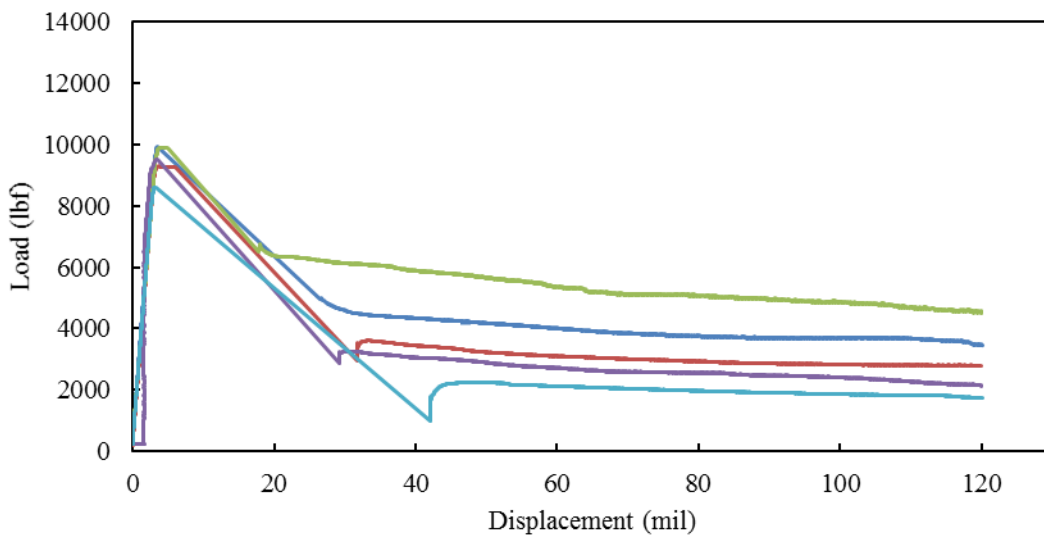
Figure E-28. Load versus displacement curves for L.EC.10.25.

E-14
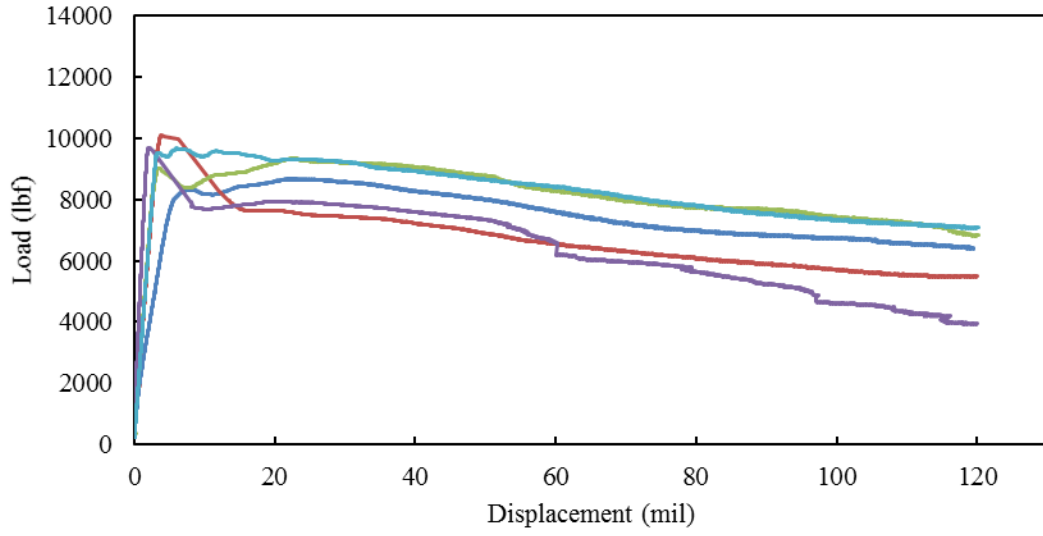
Figure E-29. Load versus displacement curves for L.EC.10.5.
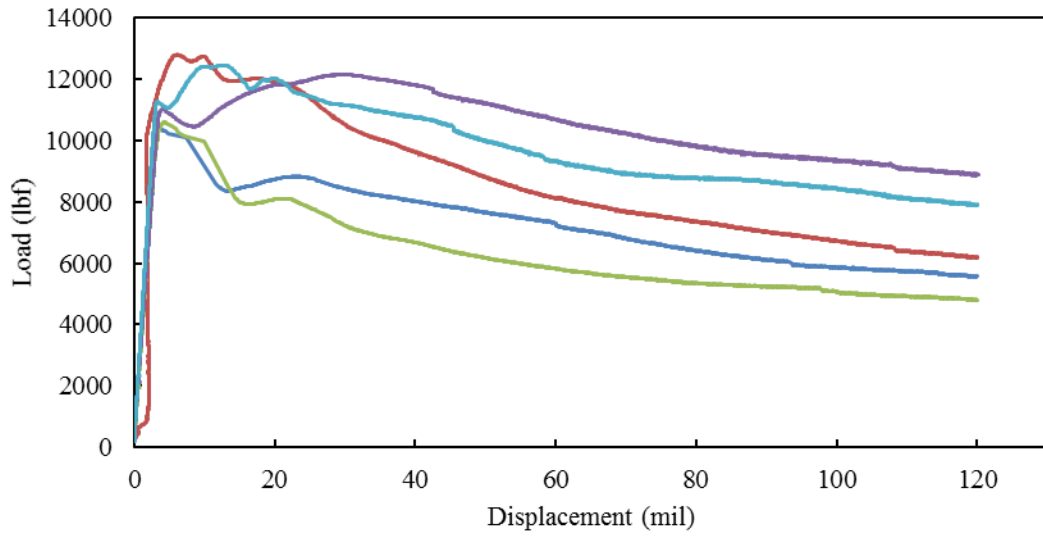
Figure E-31. Load versus displacement curves for L.EC.10.75.

E-15
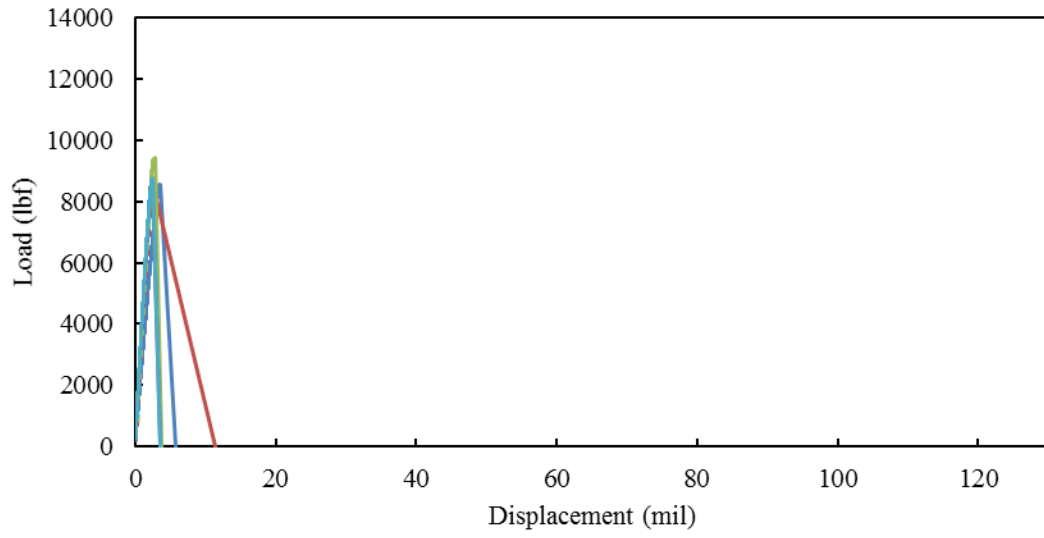
Figure E-31. Load versus displacement curves for a plain concrete mixture.

APPENDIX F: JOINT PERFORMANCE TEST RESULTS

Plain Concrete

Phase 1: Specimen 1
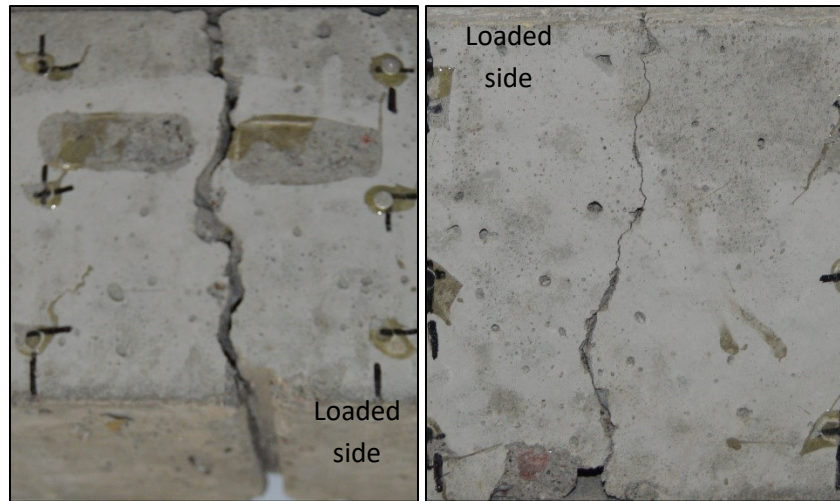
Figure F-1. The front and back of the joint for specimen 1 in phase 1.
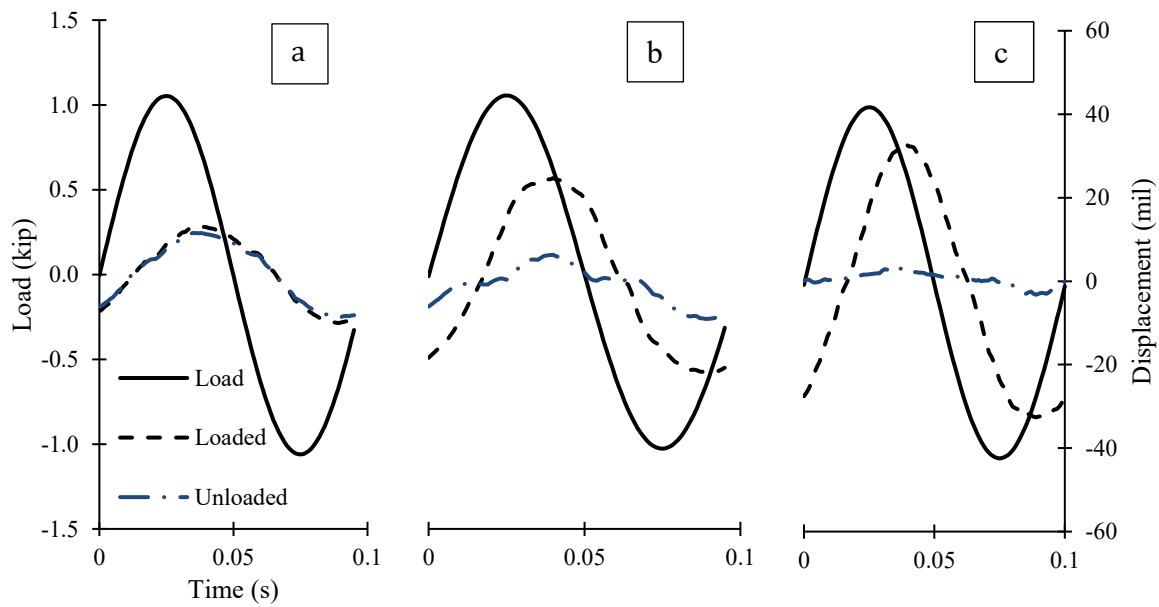
Figure F-2. Cyclical plots at (a) 16 mils, (b) 47 mils, and (c) 126 mils crack widths.
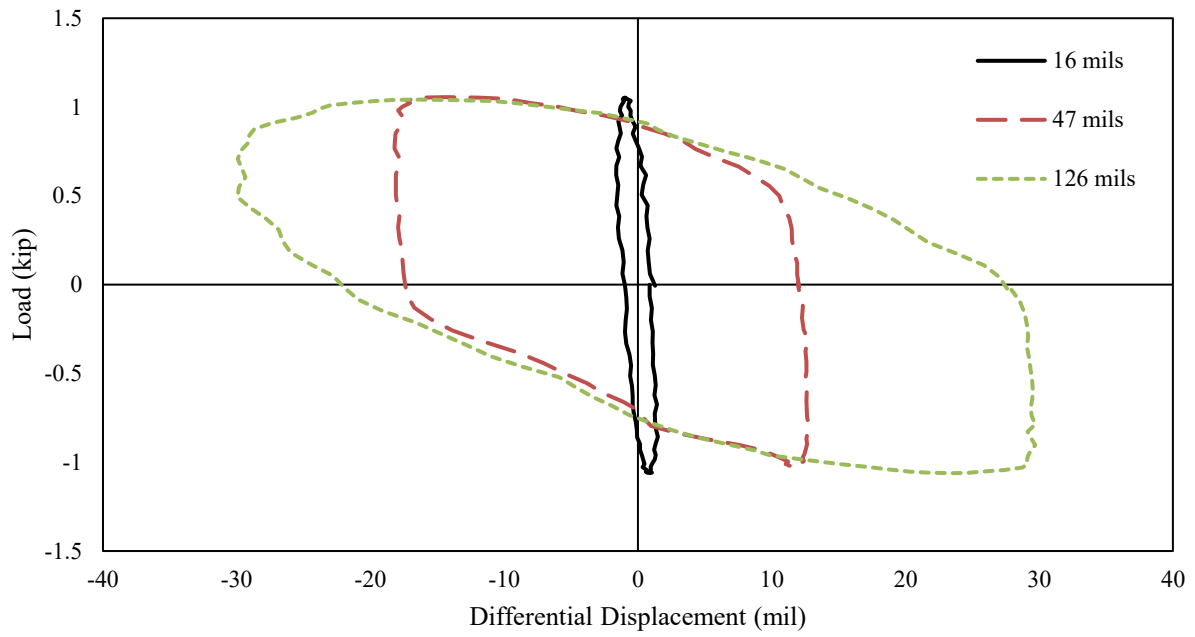
Figure F-3. Hysteresis plot at 16 mils, 47 mils and 126 mils crack widths.
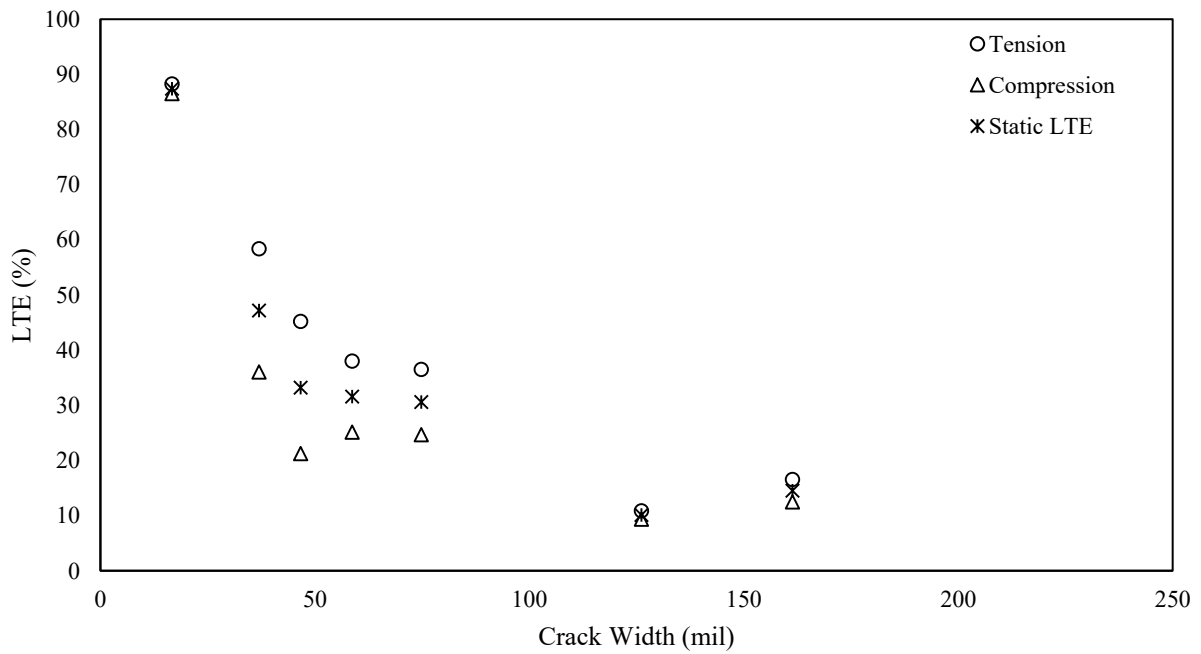
Figure F-4. LTE as a function of crack width.
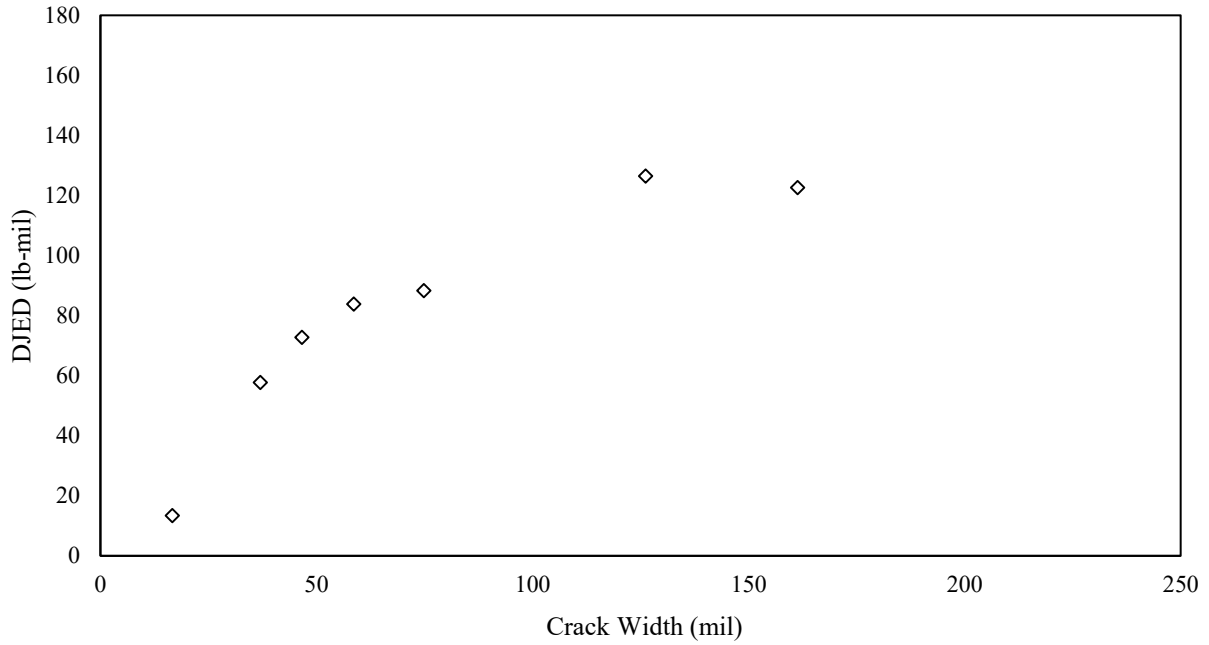
Figure F-5. DJED as a function crack width.
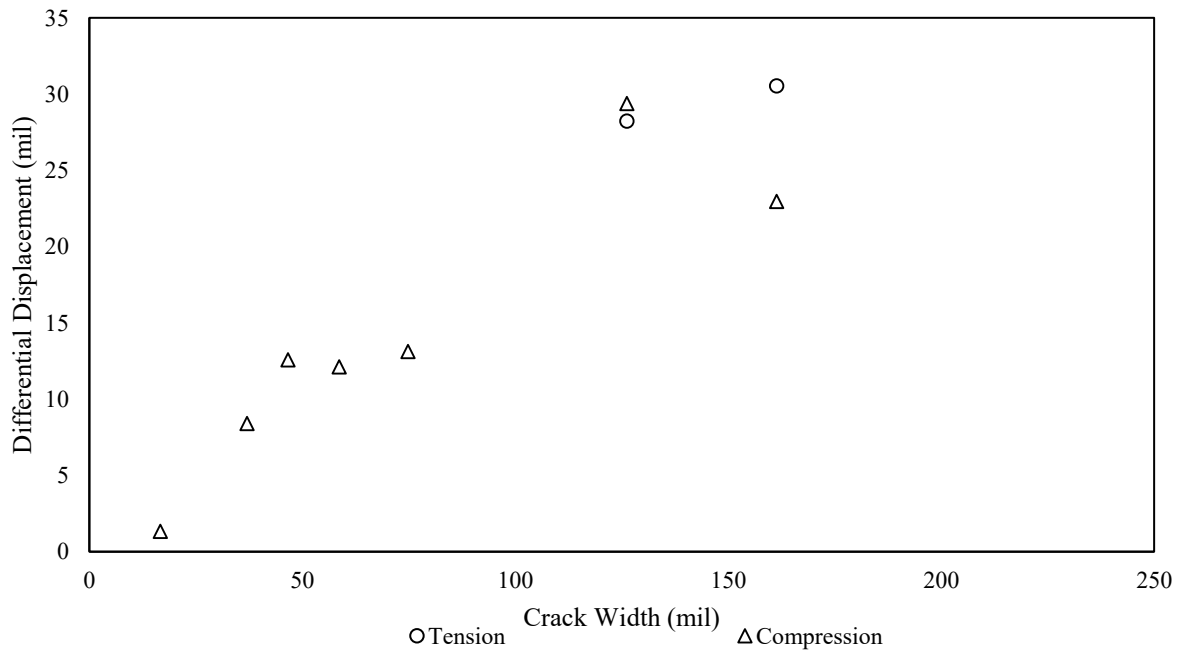
Figure F-6. Differential joint displacement as a function of crack width.
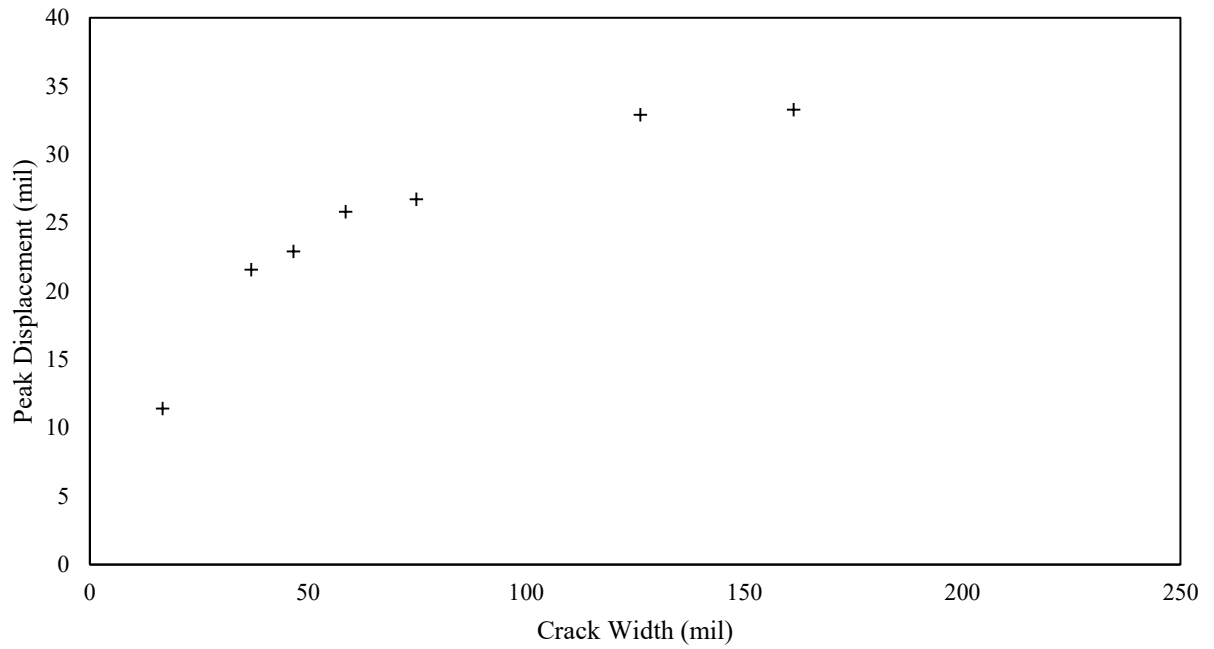
**Figure F-7. Peak displacement as a function of crack width.**
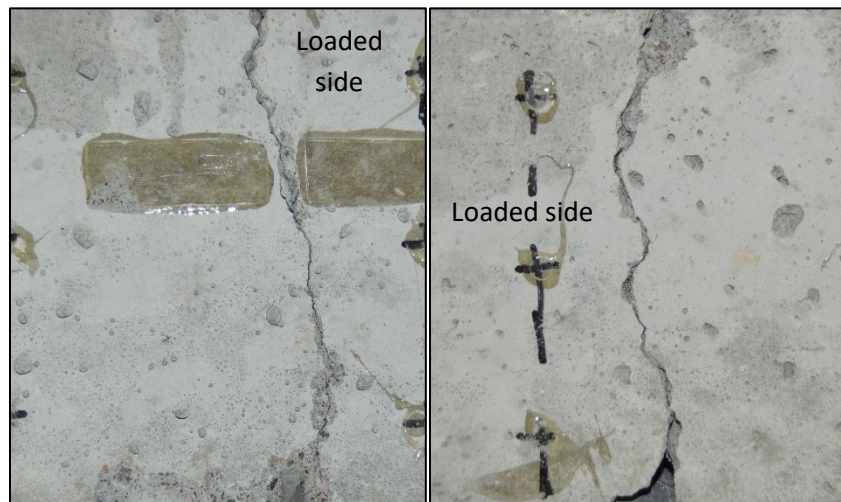
Phase 1: Specimen 2

Figure F-8. The front and back of the joint for specimen 2 in phase 1.
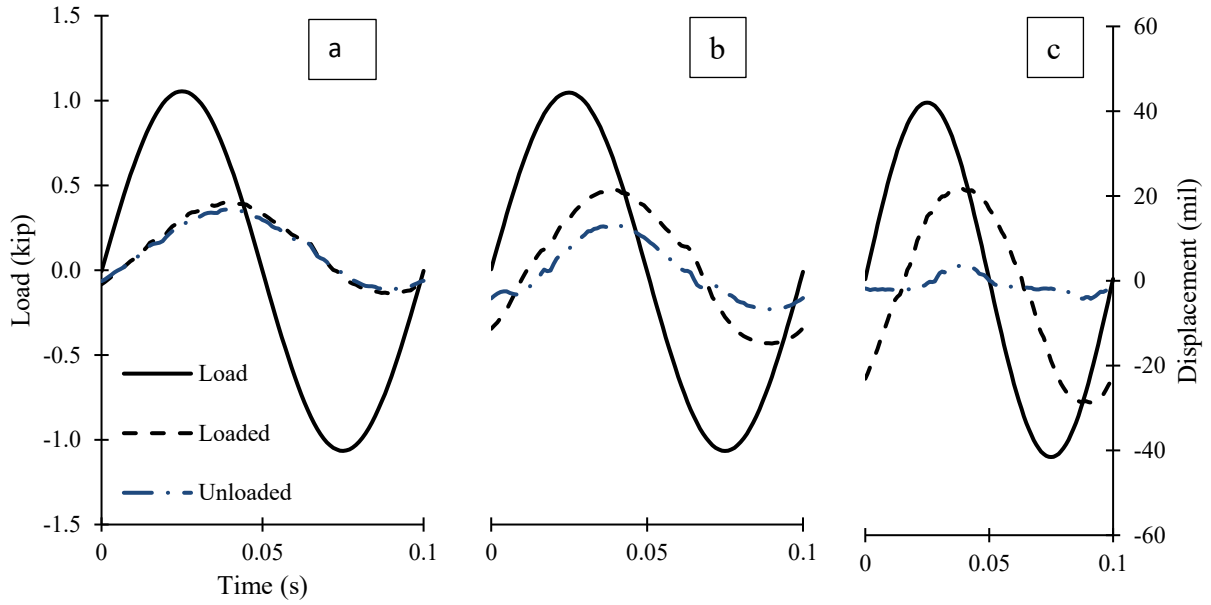
Figure F-9. Cyclical plots at (a) 11 mils, (b) 58 mils, and (c) 109 mils of crack widths.
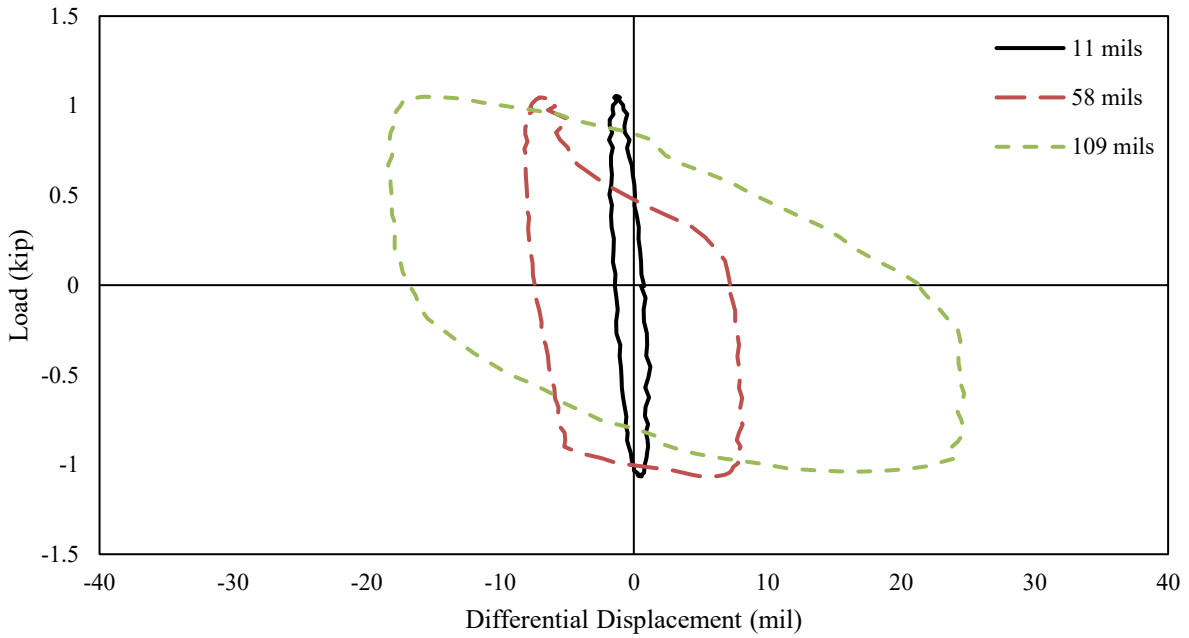
Figure F-10. Hystereses plot 11 mils, 58 mils, 109 mills of crack width.
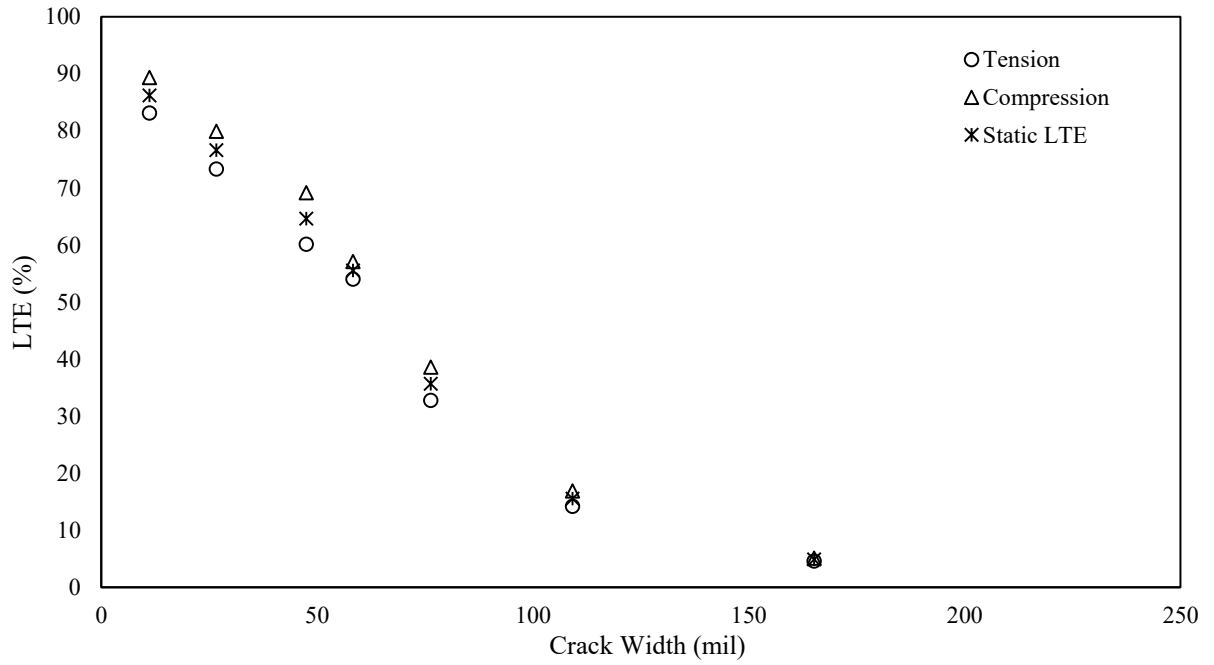
Figure F-11. LTE as a function of crack width.
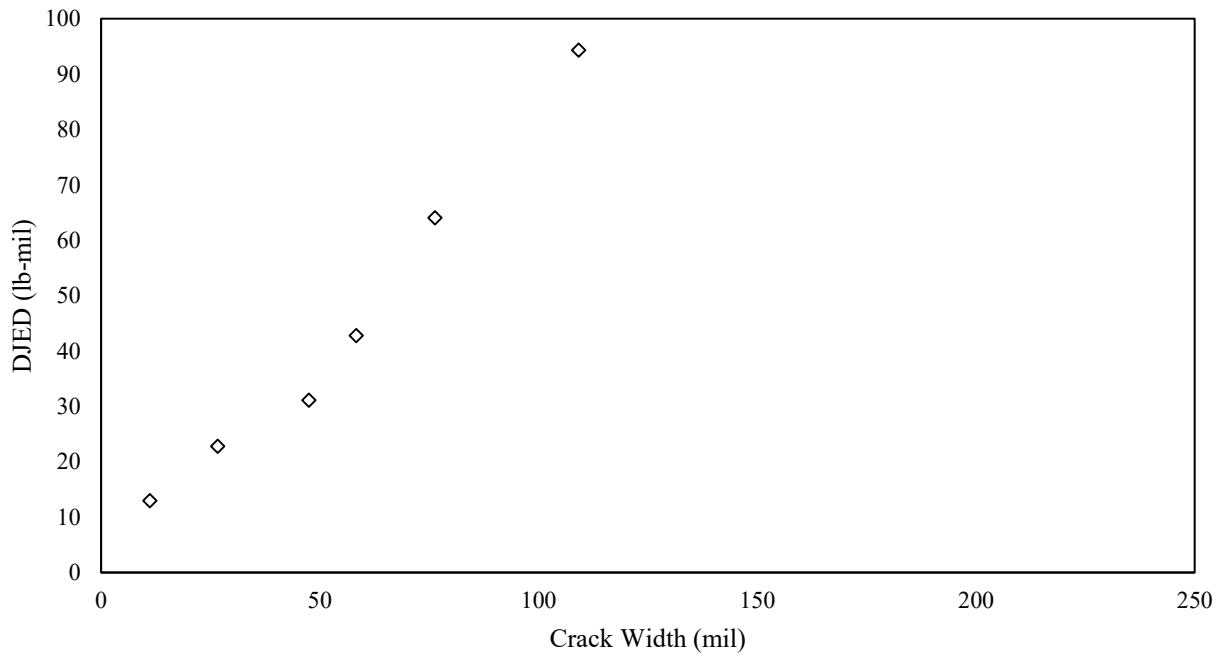
Figure F-12. DJED a function of crack width.
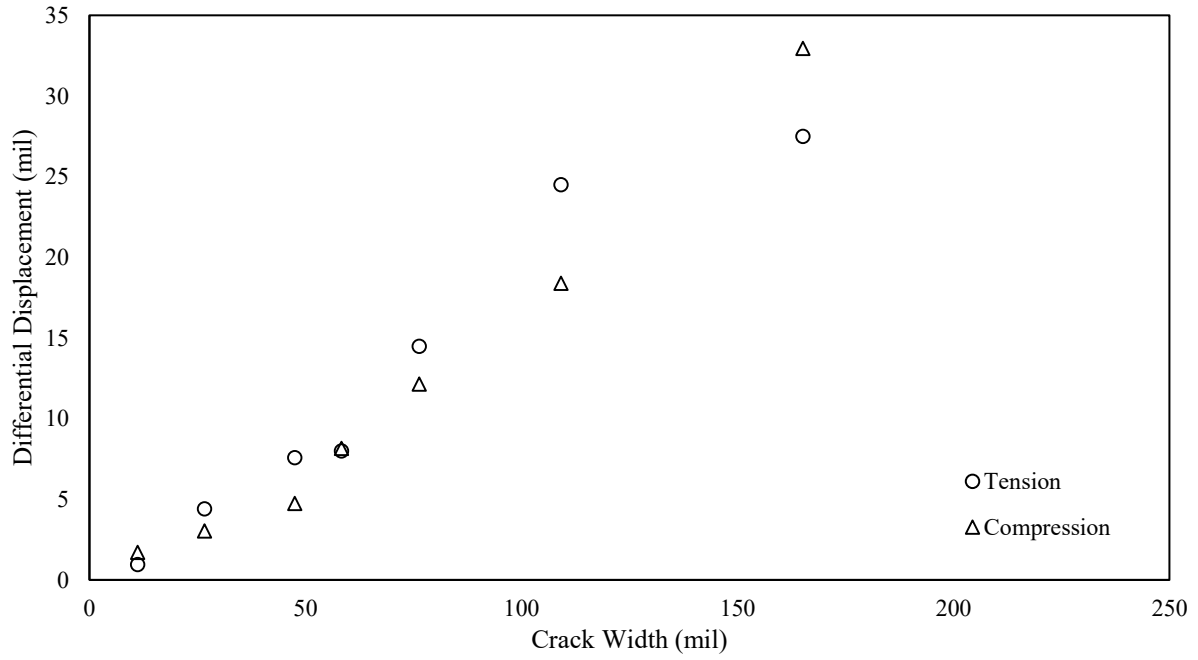
Figure F-13. Differential joint displacement as a function of crack width.
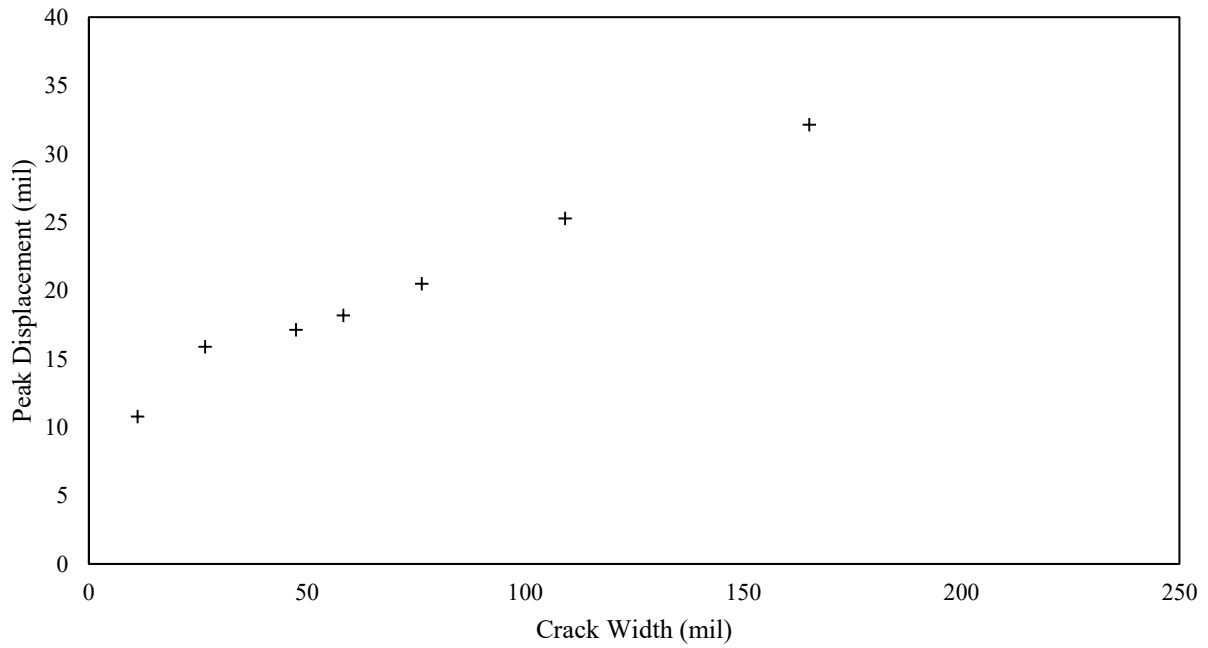
Figure F-14. Peak displacement as a function of crack width.
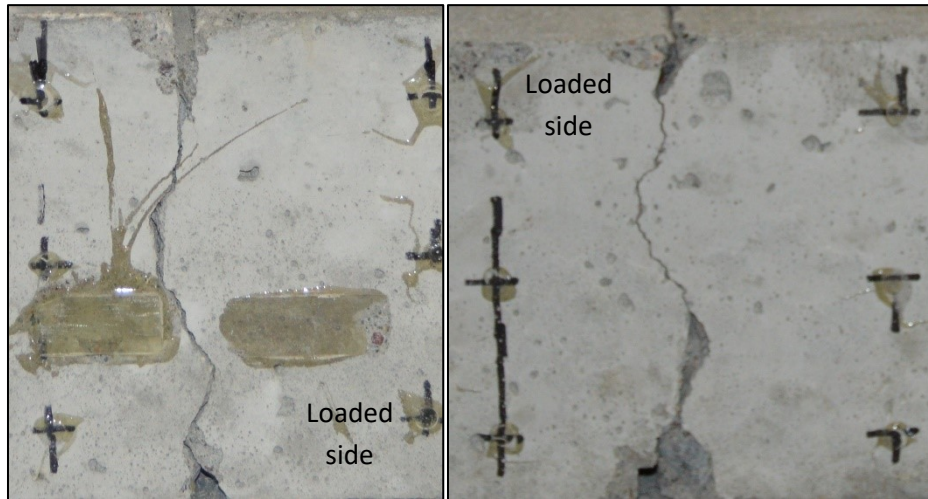
Figure F-15. The front and back of the joint for specimen 3 in phase 1.
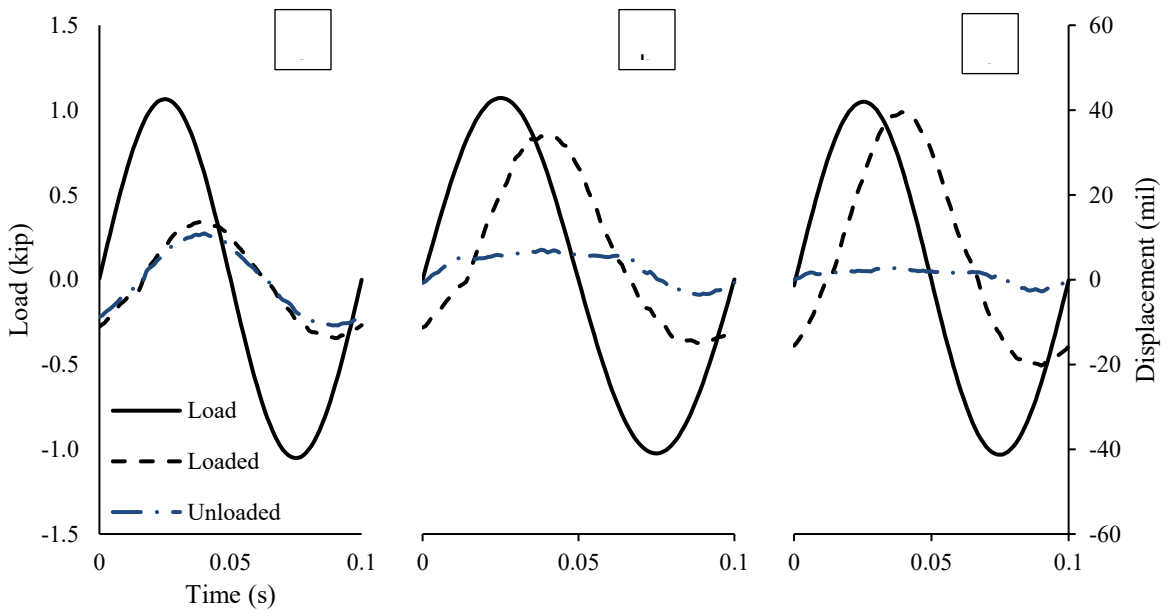
Figure F-16. Cyclical plots for (a) 13 mils, (b) 59 mils, and (c) 94 mils crack widths.
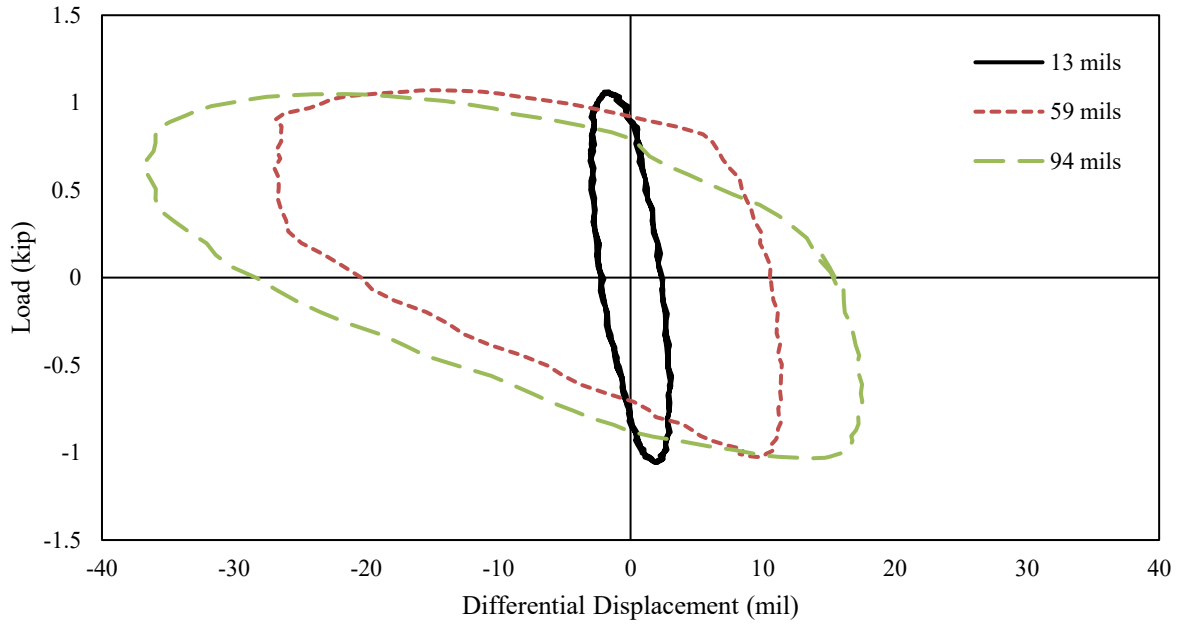
Figure F-17. Hystereses for the 13 mils, 59 mils, and 94 mils crack widths.
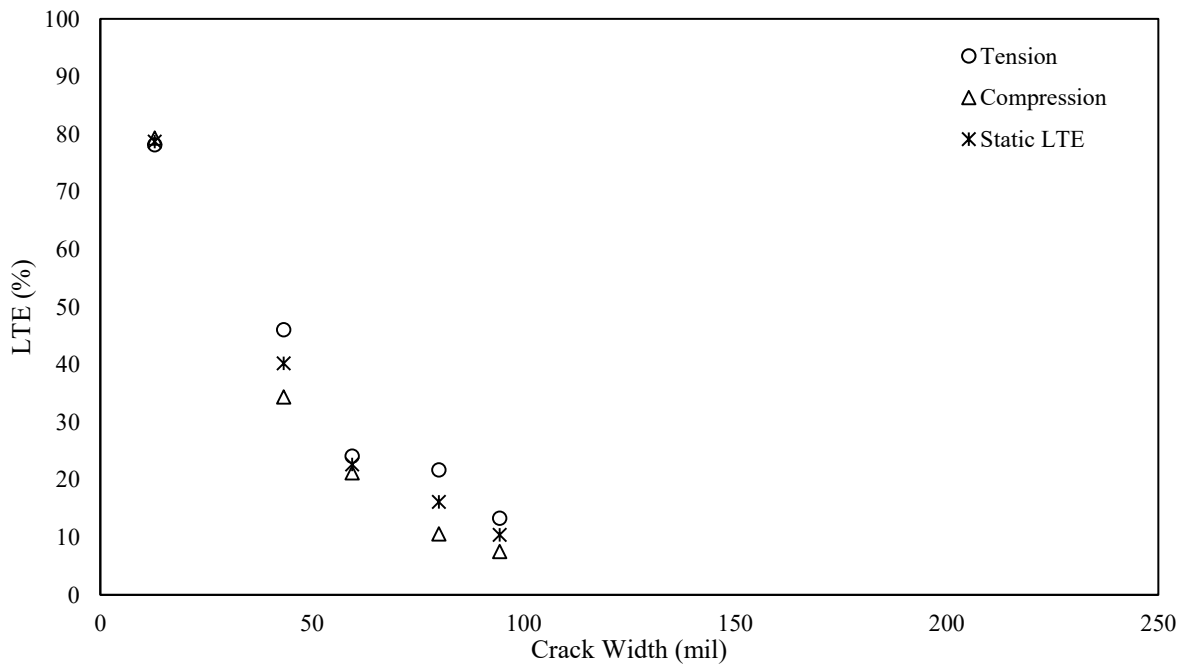
Figure F-18. LTE as a function of crack width.
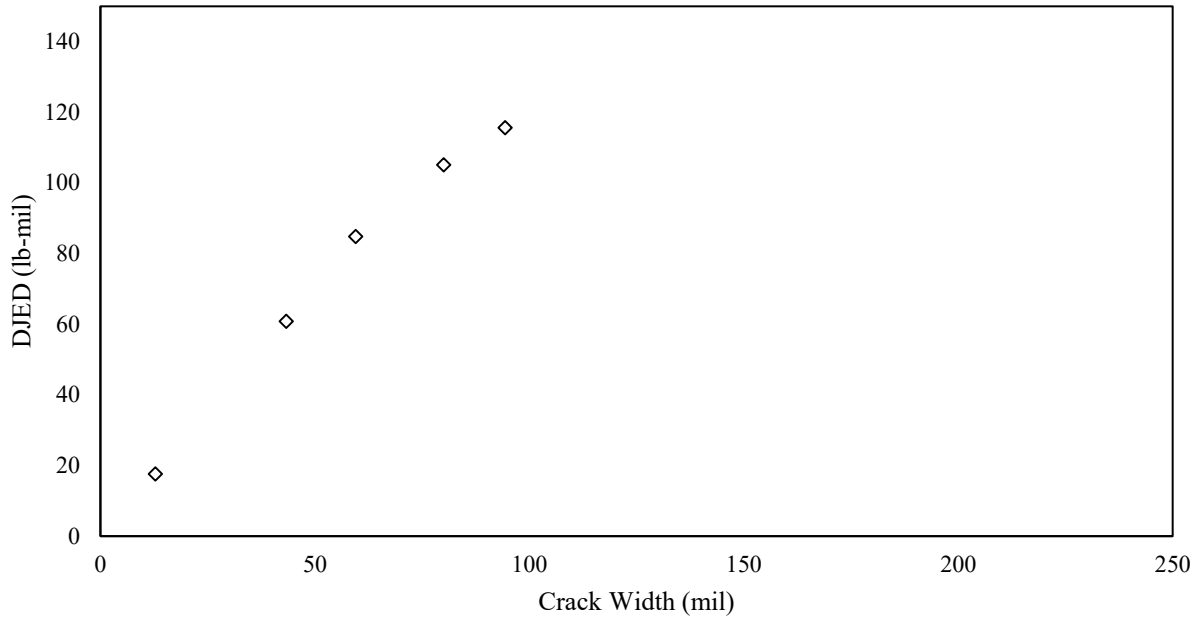
Figure F-19. DJED a function of crack width.
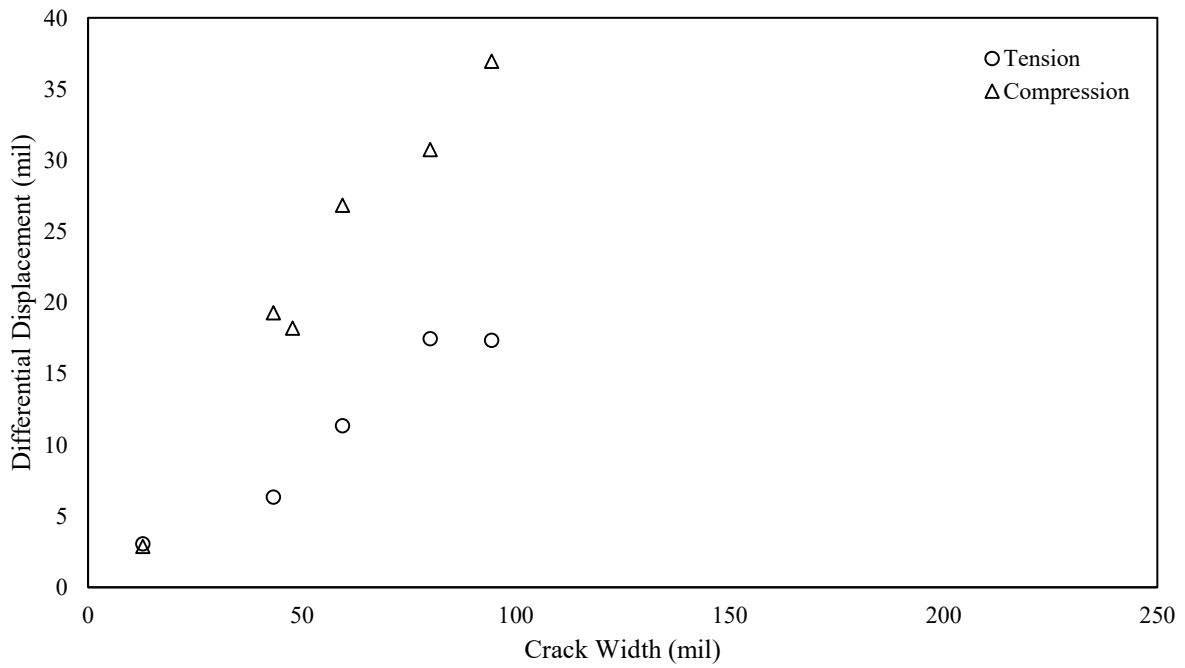
Figure F-20. Differential joint displacement as a function of crack width.
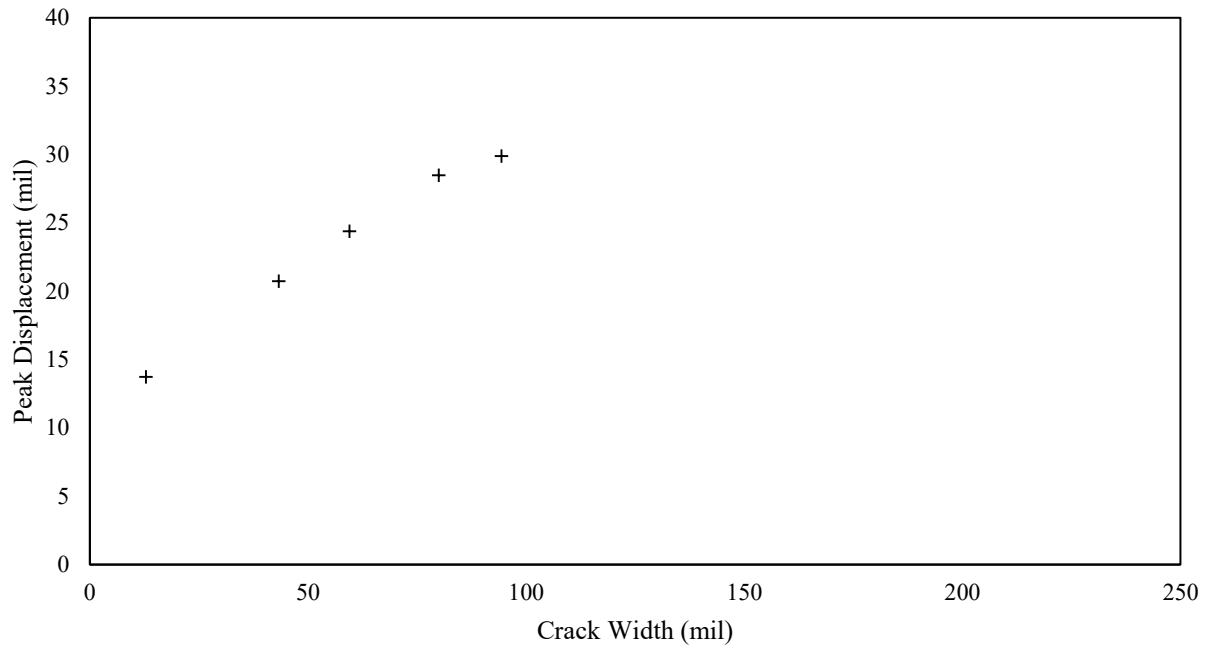
Figure F-21. Peak displacement as a function of crack width.
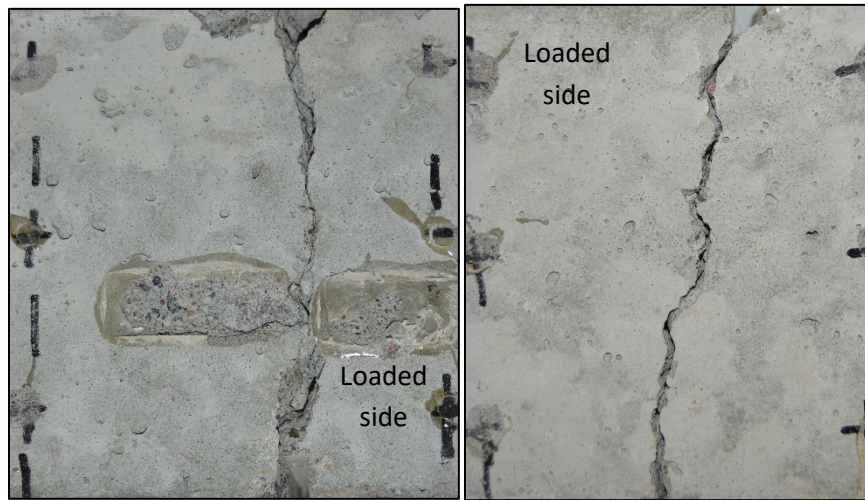
Phase 2: Specimen 1

Figure F-22. The front and back of the joint for specimen 1 in phase 2.
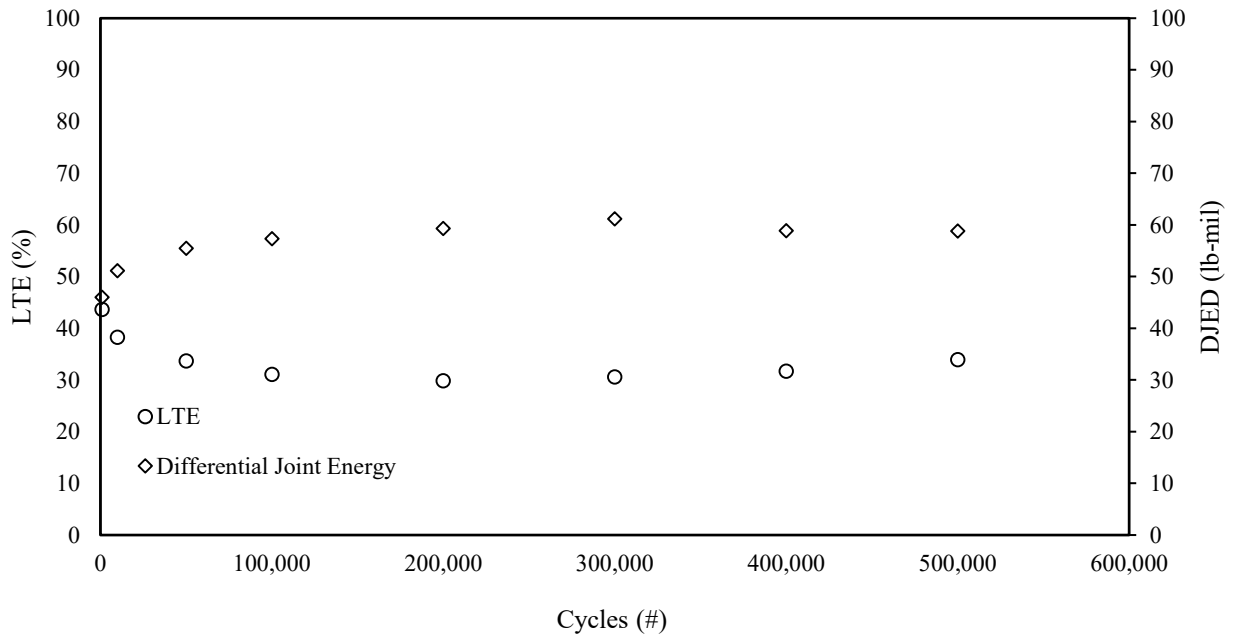
*Crack width ranged from 49 mils to 51 mils

Figure F-23. DJED and Average LTE as a function of cycles (repetitions).
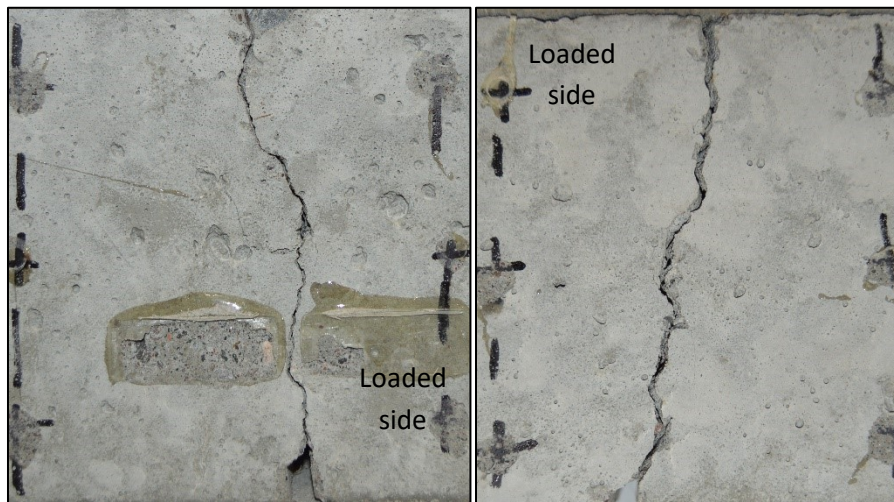
Phase 2: Specimen 2

Figure F-24. The front and back of the joint for specimen 2 in phase 2.
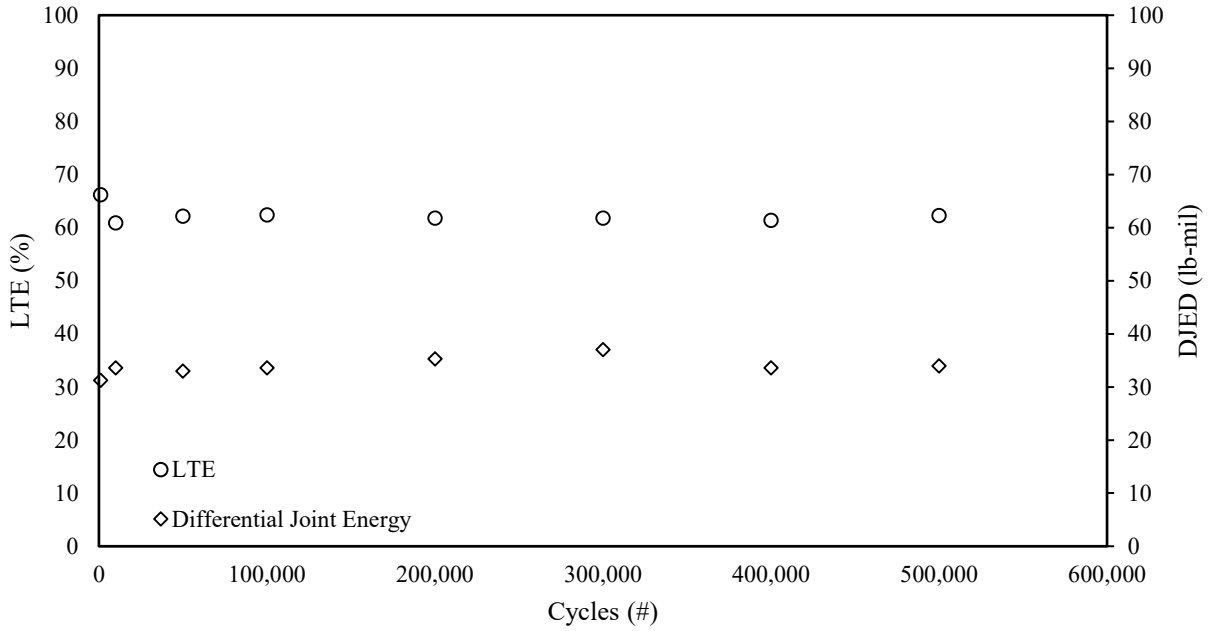
*Crack width ranged from 50 mils

Figure F-25. DJED and Average LTE as a function of cycles (repetitions).
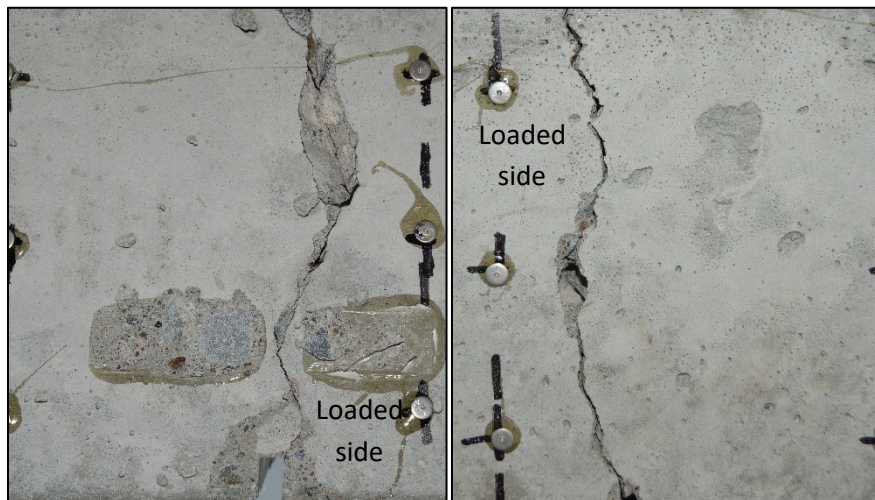
Phase 2: Specimen 3

Figure F-26. The front and back of the joint for specimen 3 in phase 2.
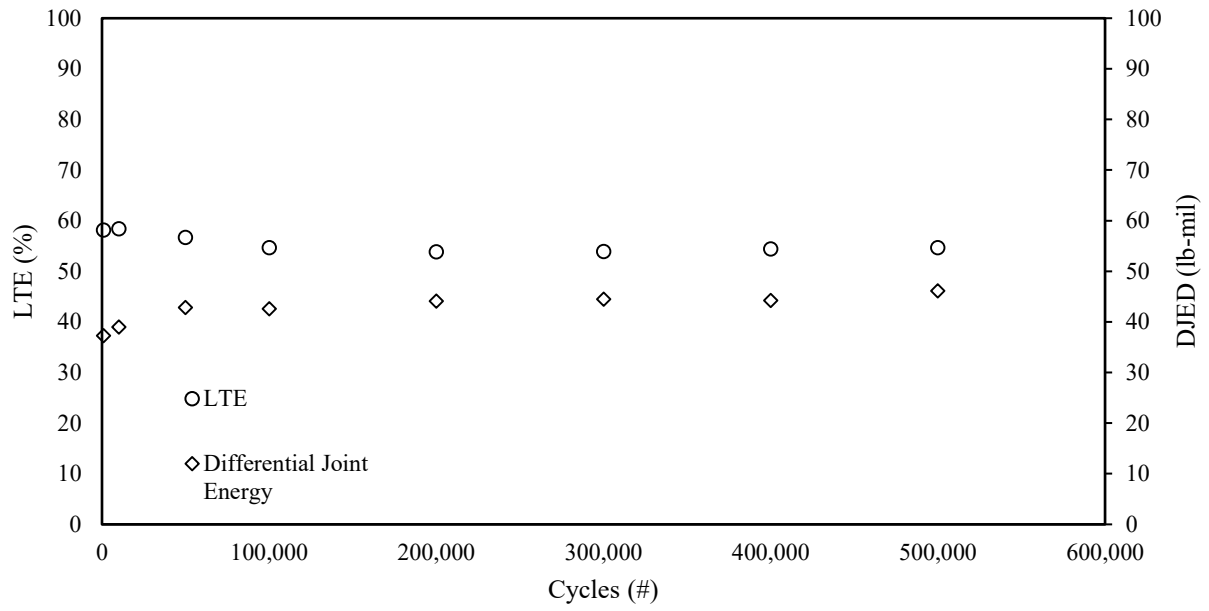
*Crack width ranged from 48 mils to 51 mils

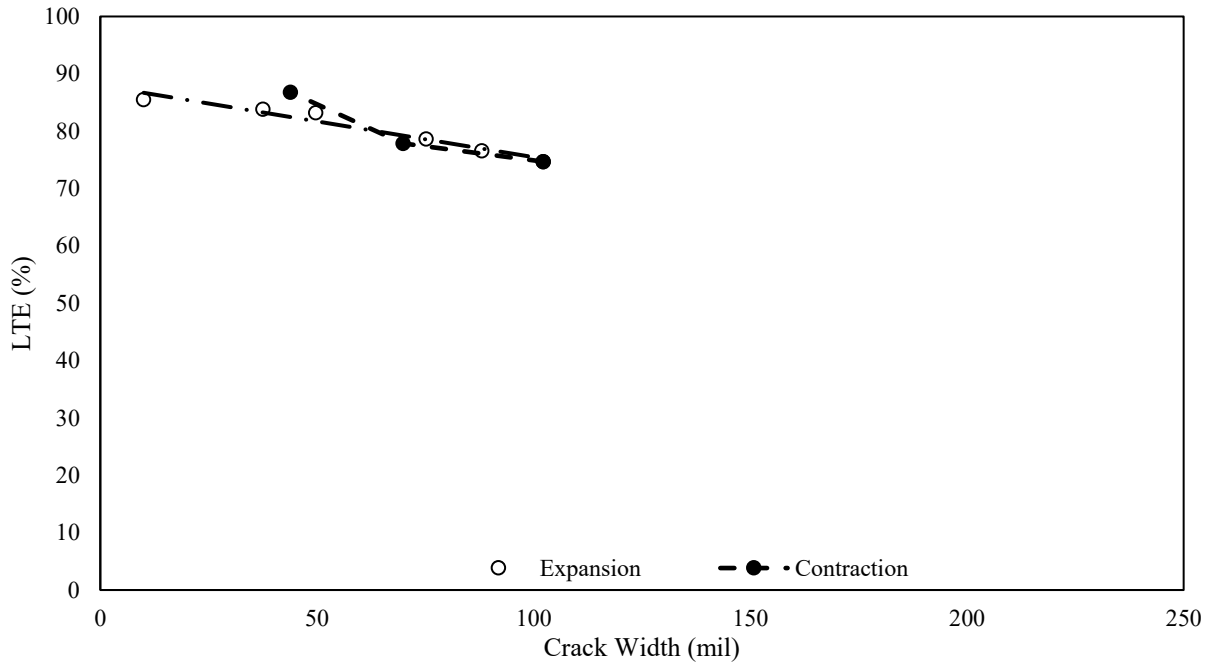**Figure F-27. DJED and Average LTE as a function of cycles (repetitions).**
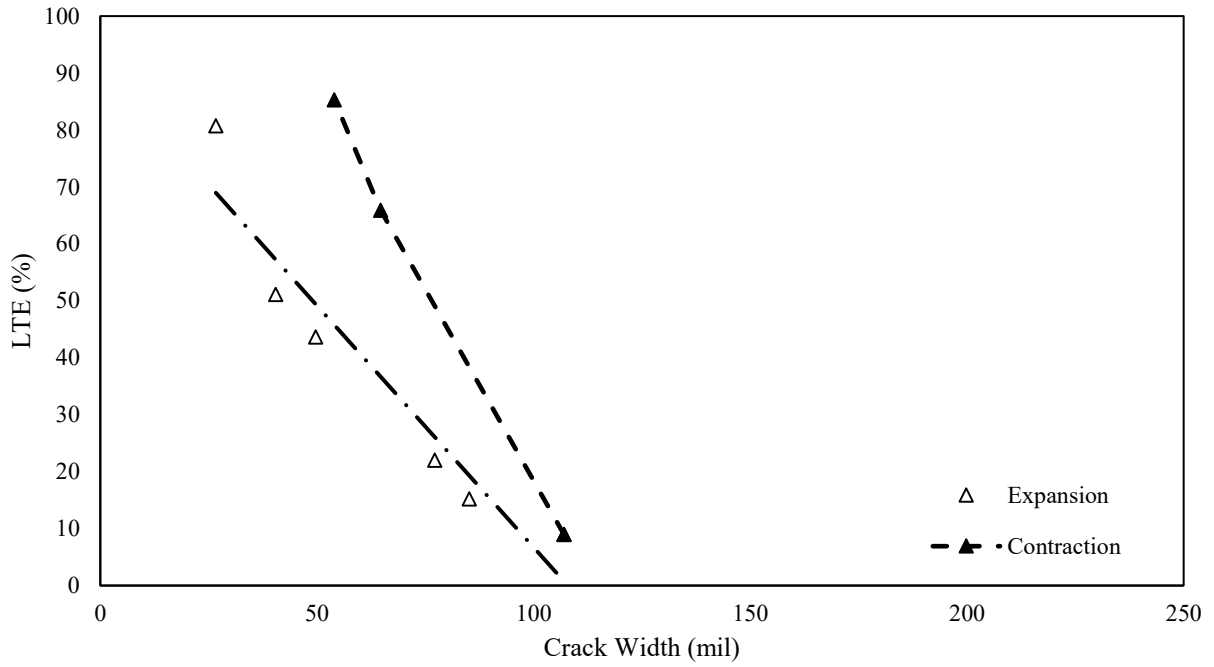
Figure F-28. The effect of joint expansion and contraction on average LTE in terms of crack width (phase 2: specimen 1).
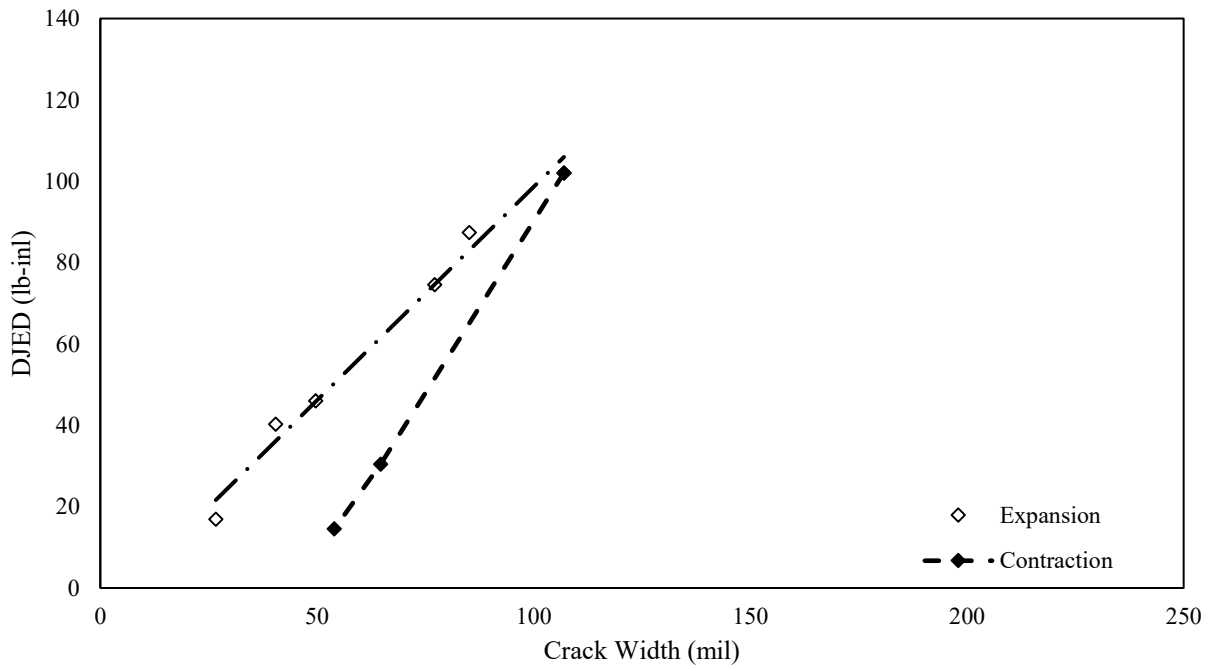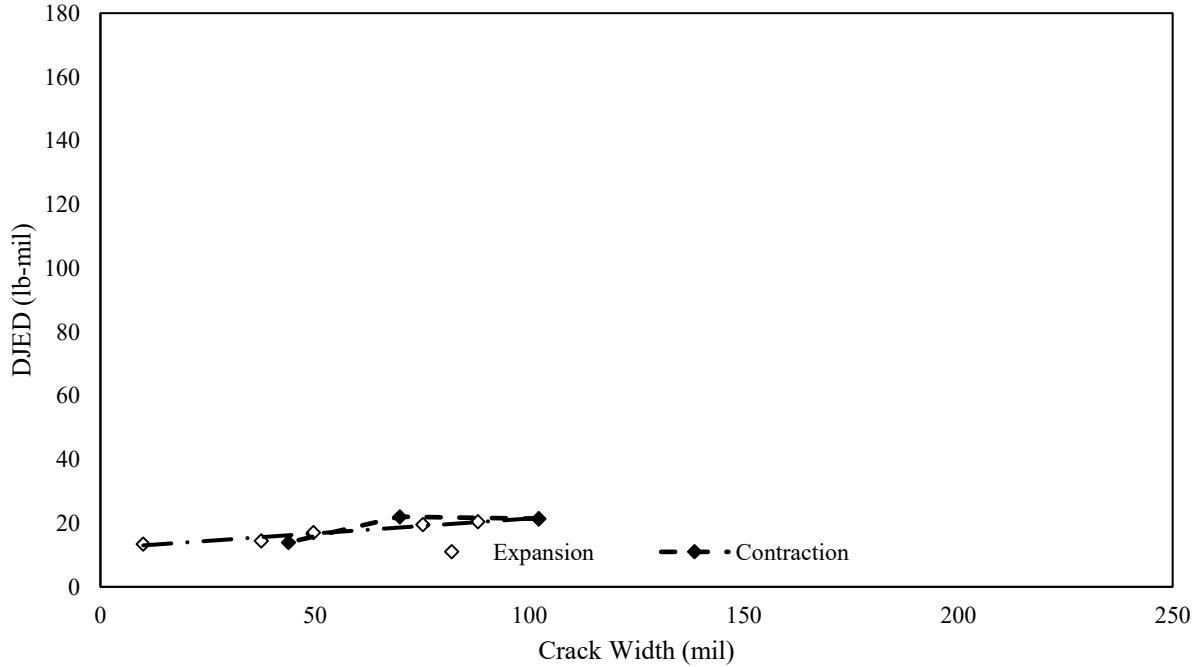

Figure F-29. The effect of joint expansion and contraction on DJED in terms of crack width (phase 2: specimen 1).
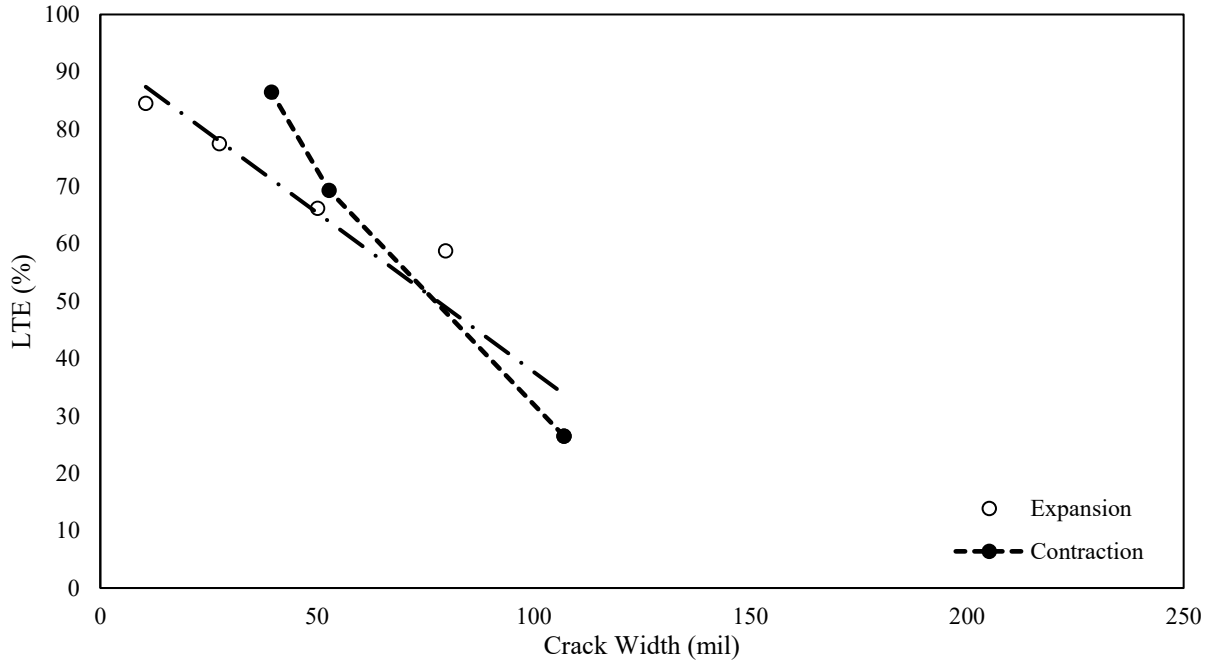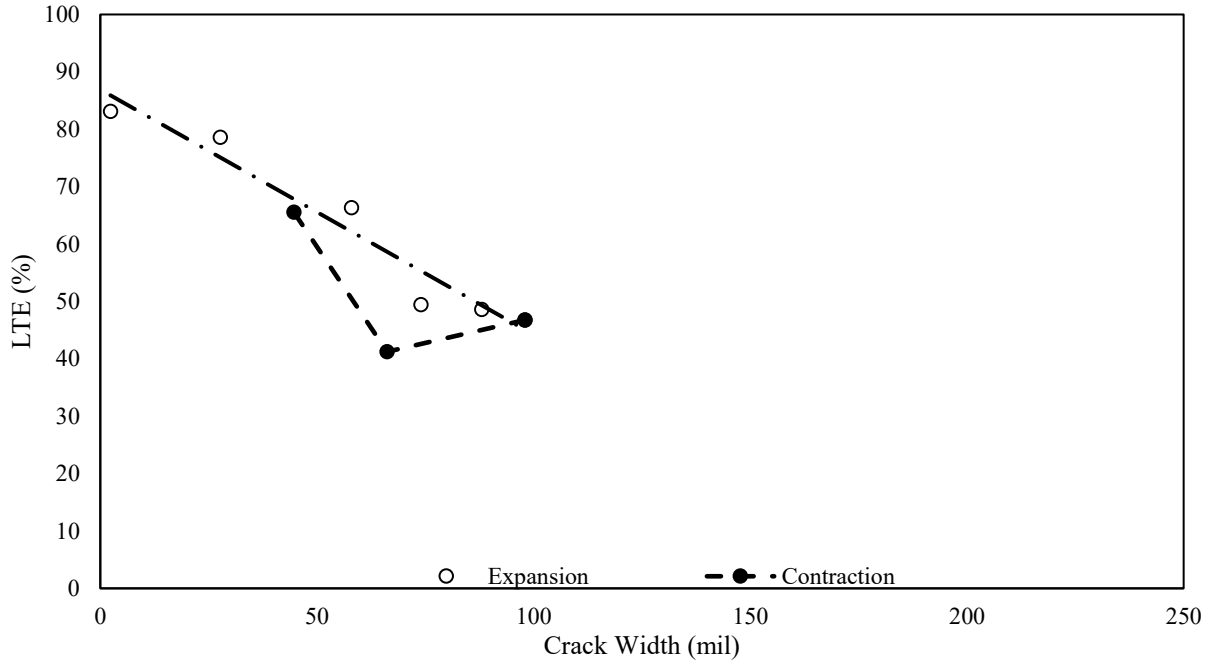
Figure F-30. The effect of joint expansion and contraction on LTE in terms of crack width (phase 2: specimen 2).
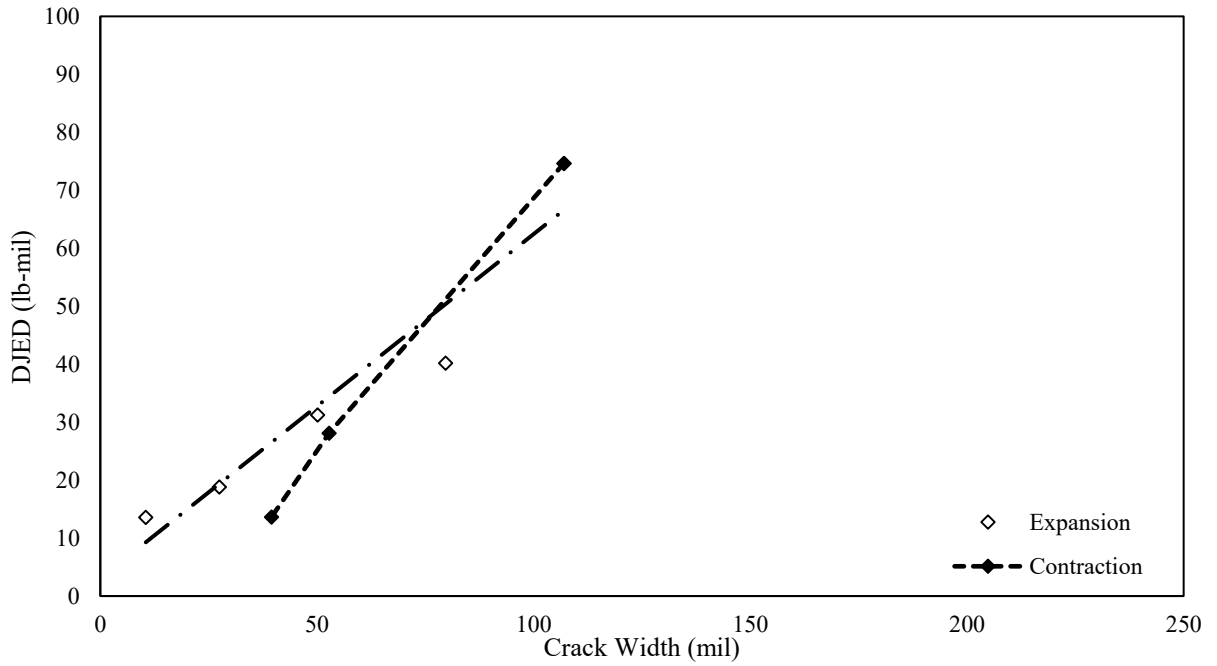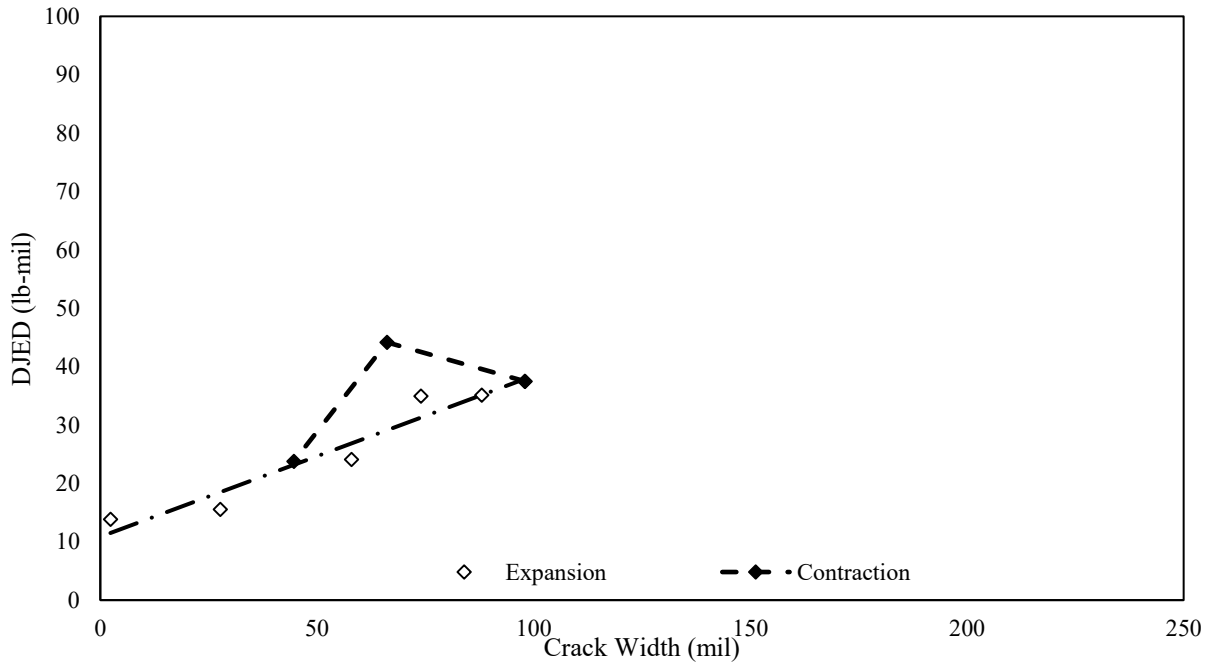

Figure F-31. The effect of joint expansion and contraction on DJED in terms of crack width (phase 2: specimen 2).

Phase 1: Specimen 1
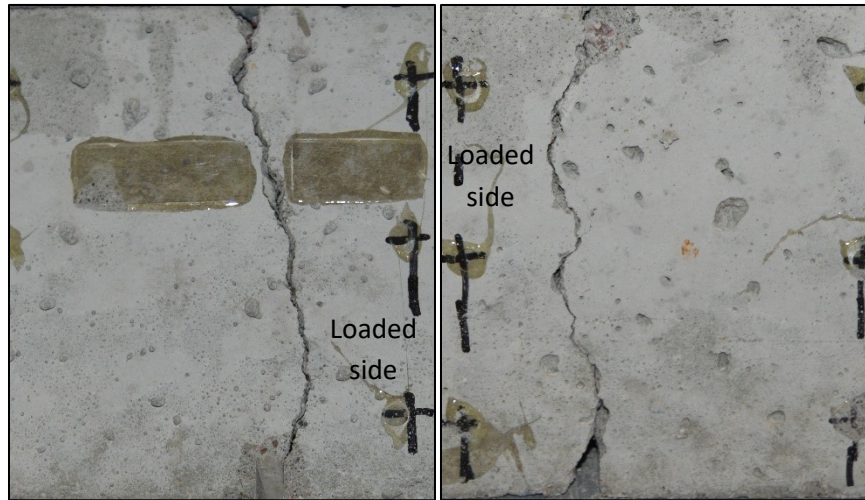
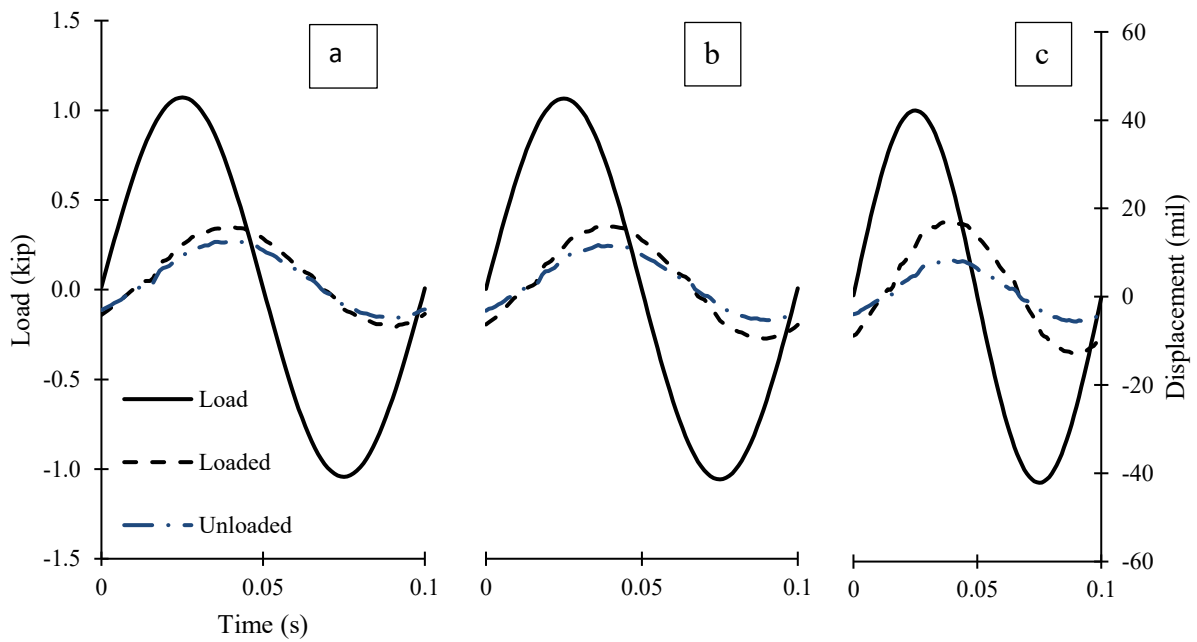**Figure F-32. The front and back of the joint for specimen 1 in phase 1.**
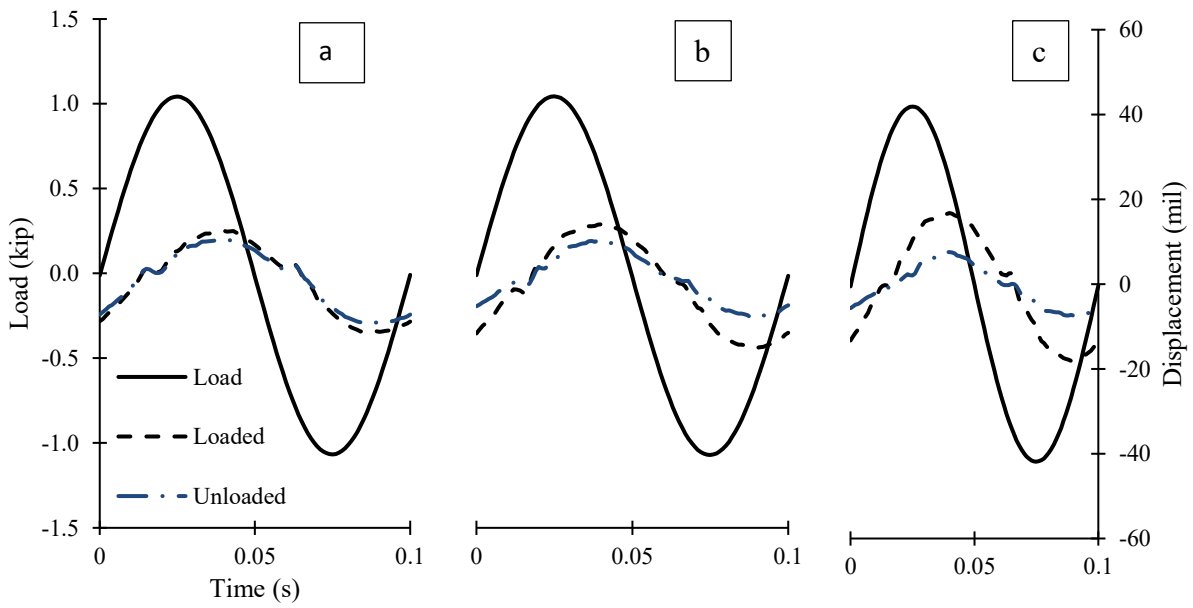
**Figure F-33. Cyclical plots for (a)6 mils, (b) 50 mils, and (c) 117 mils crack widths.**
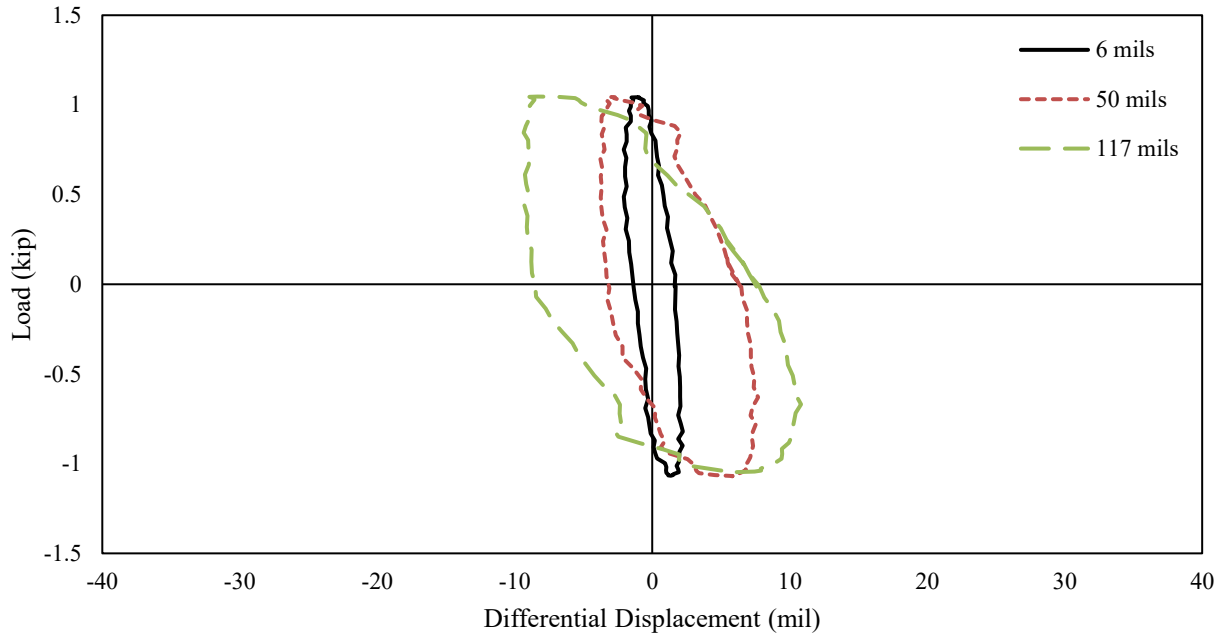
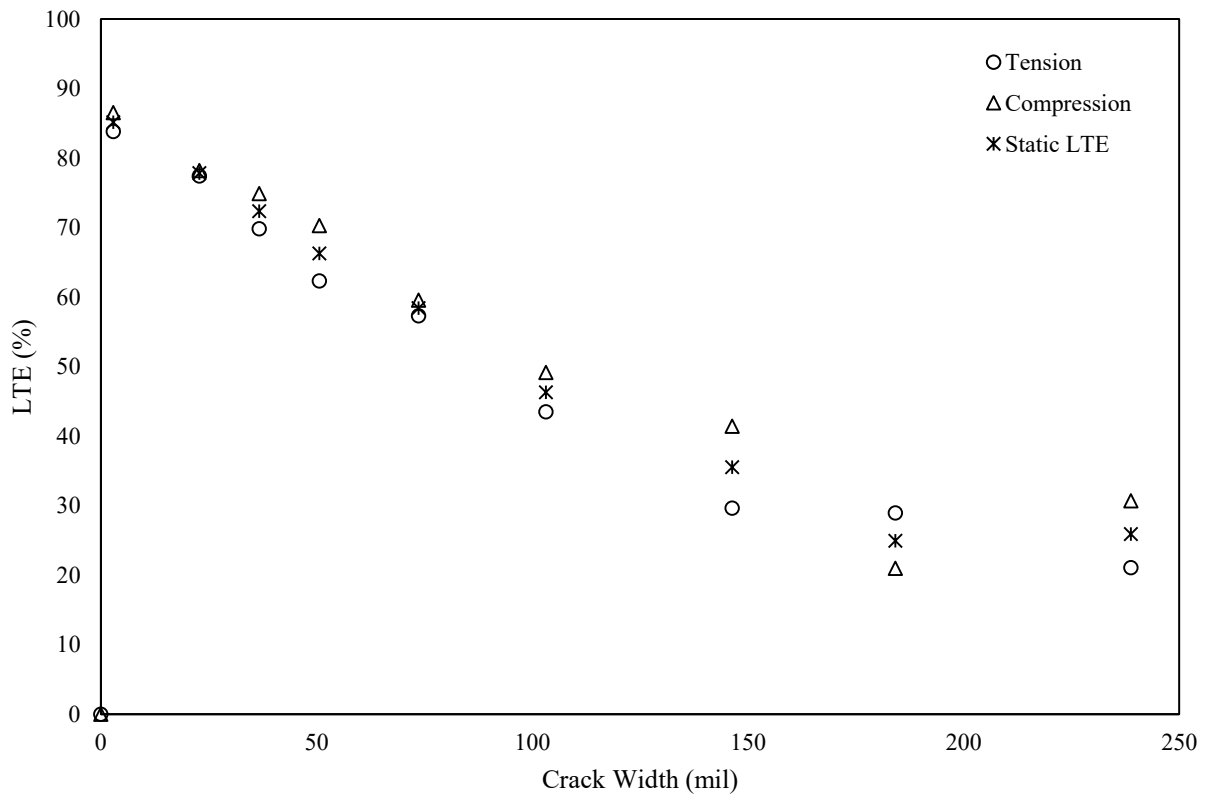**Figure F-34. Hystereses for 6 mils, 50 mils, and 117 mils crack widths.**
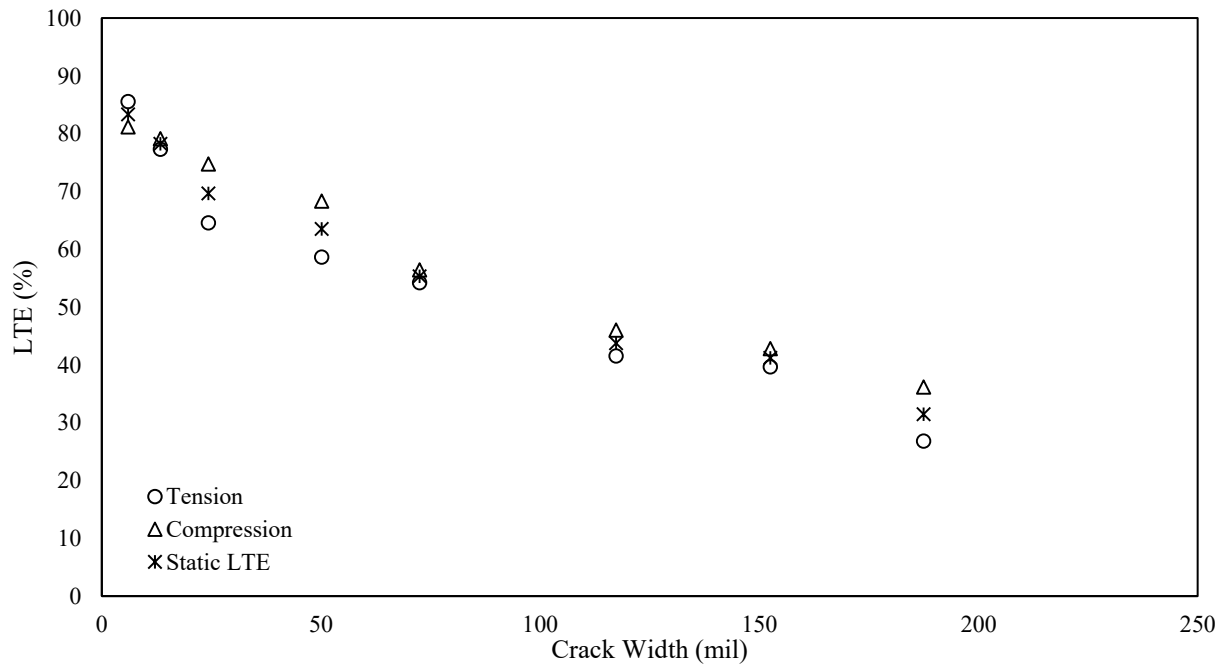
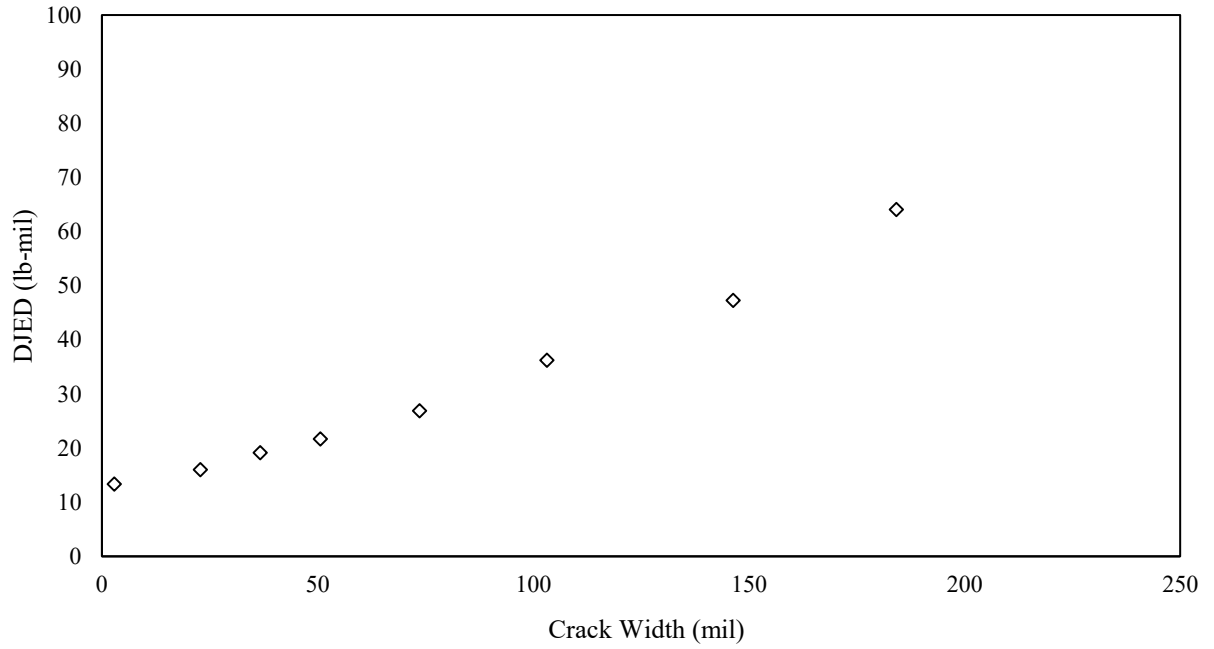**Figure F-35. LTE as a function of crack width.**
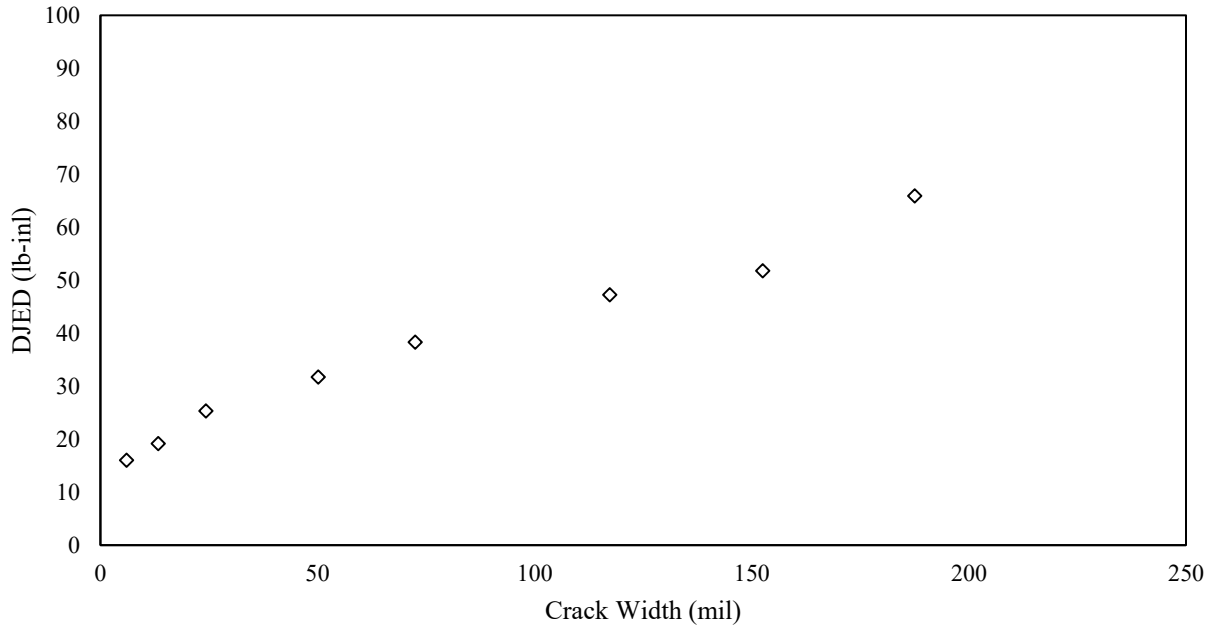
Figure F-36. DJED as a function of crack width.
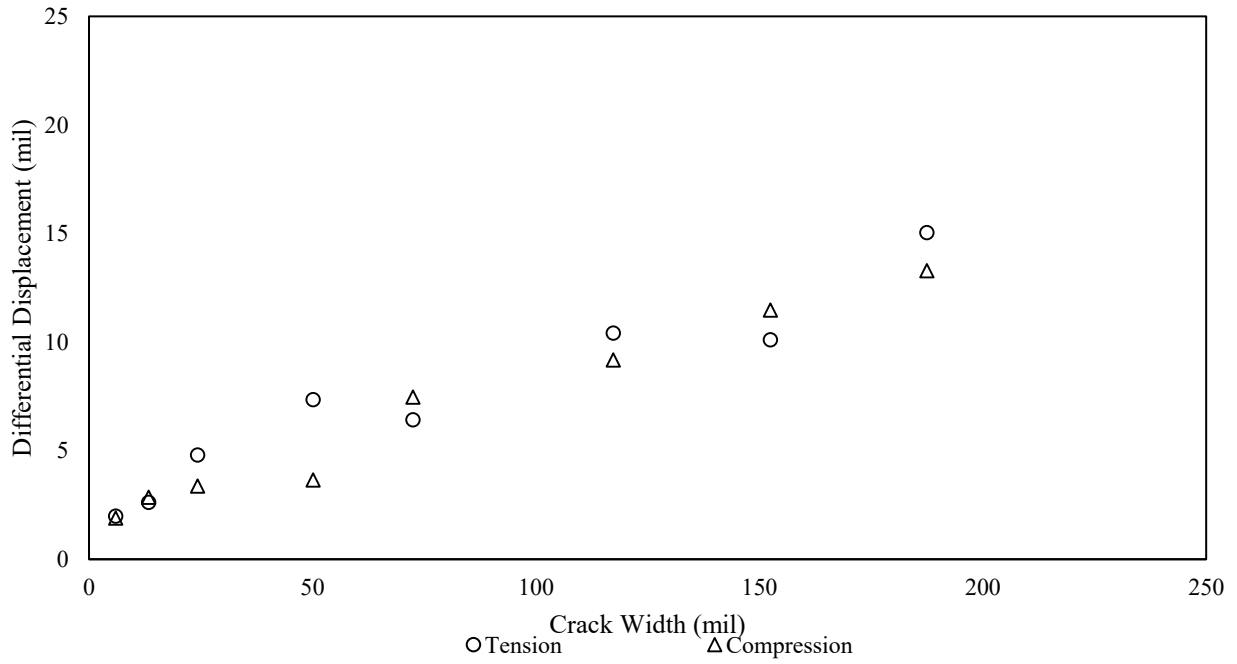
Figure F-37. Differential displacement as a function of crack width.
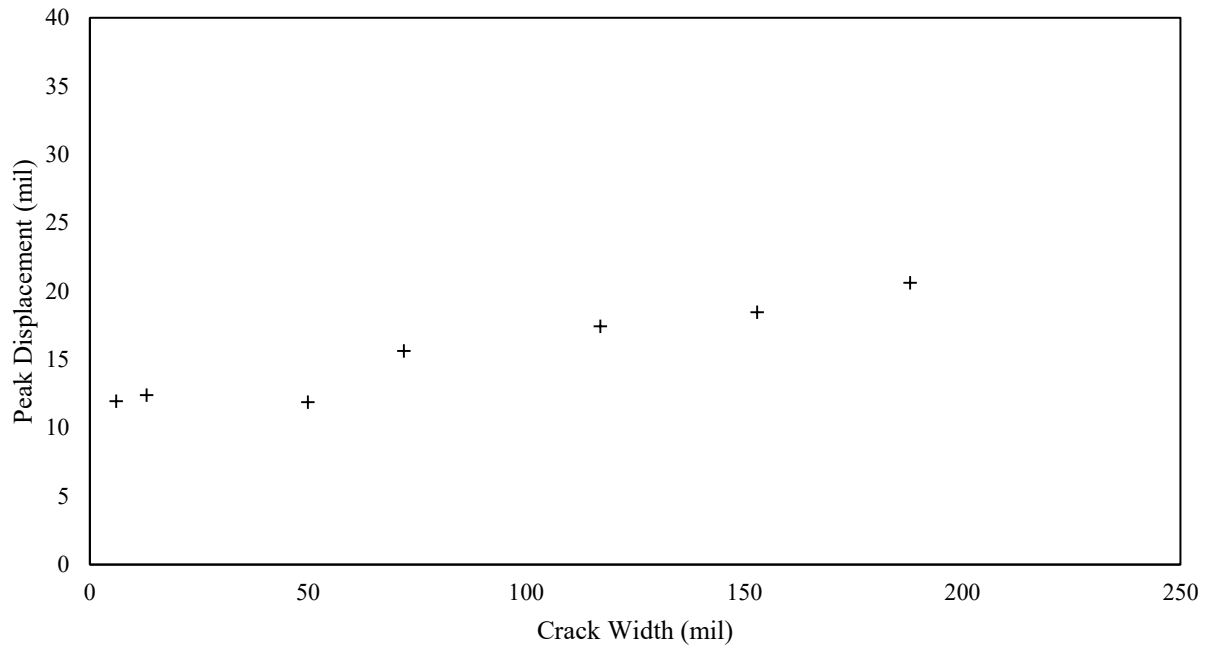
Figure F-38. Peak displacement as a function of crack width.
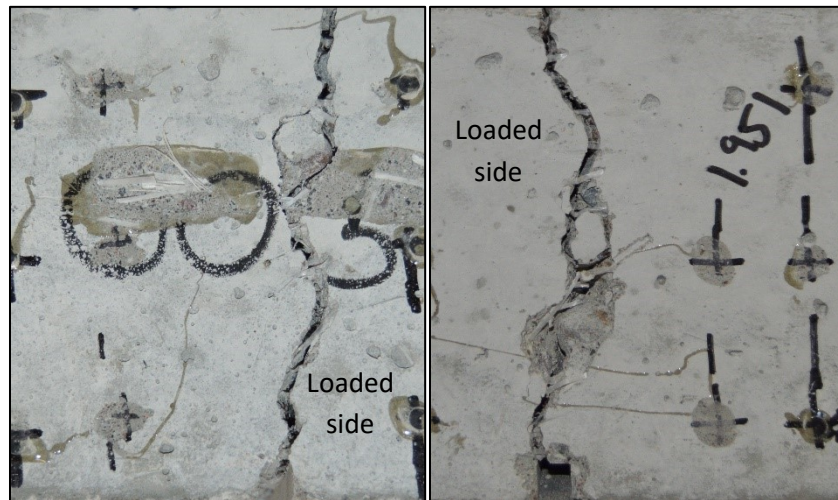
Phase 1: Specimen 2

Figure F-39. The front and back of the joint for specimen 2 in phase 1.
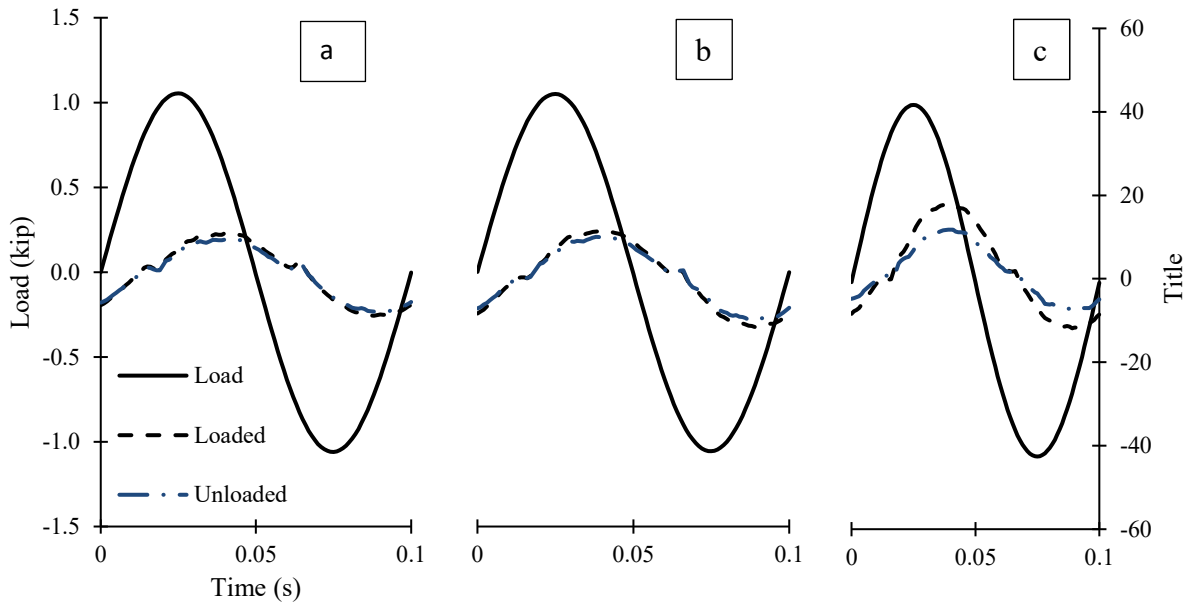
Figure F-40. Cyclical plots for (a) 6 mils, (b) 52 mils, and (c) 104 mils crack widths.
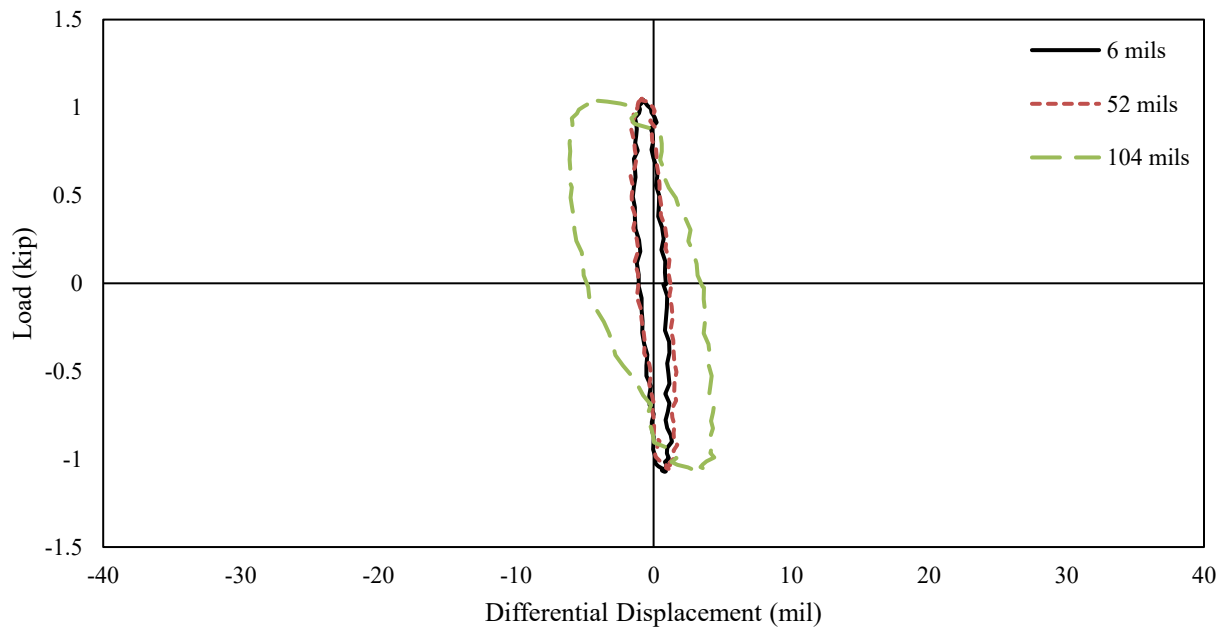
Figure F-41. Hystereses for 6 mils, 52 mils, and 104 mils crack widths.
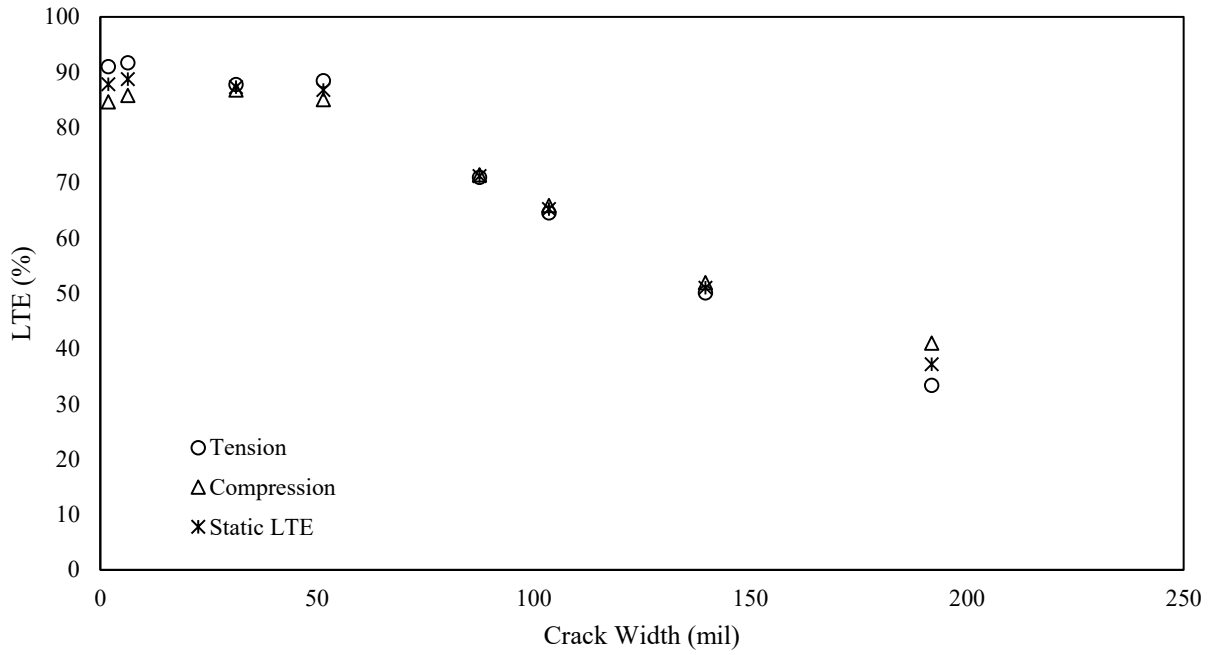
Figure F-42. LTE as a function of crack width.
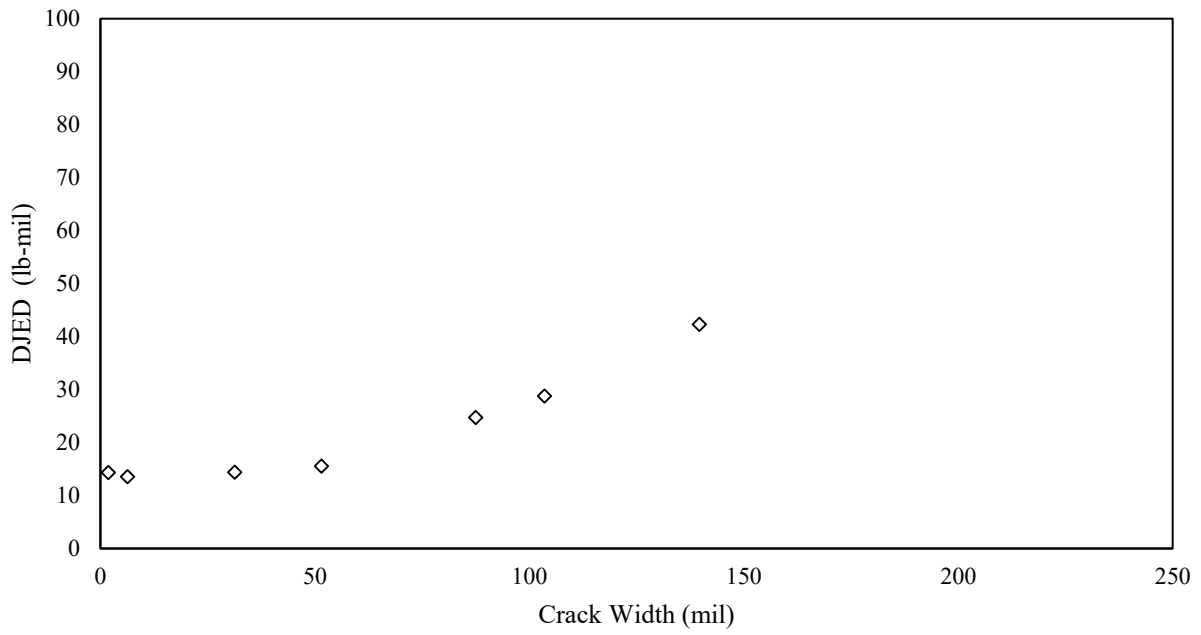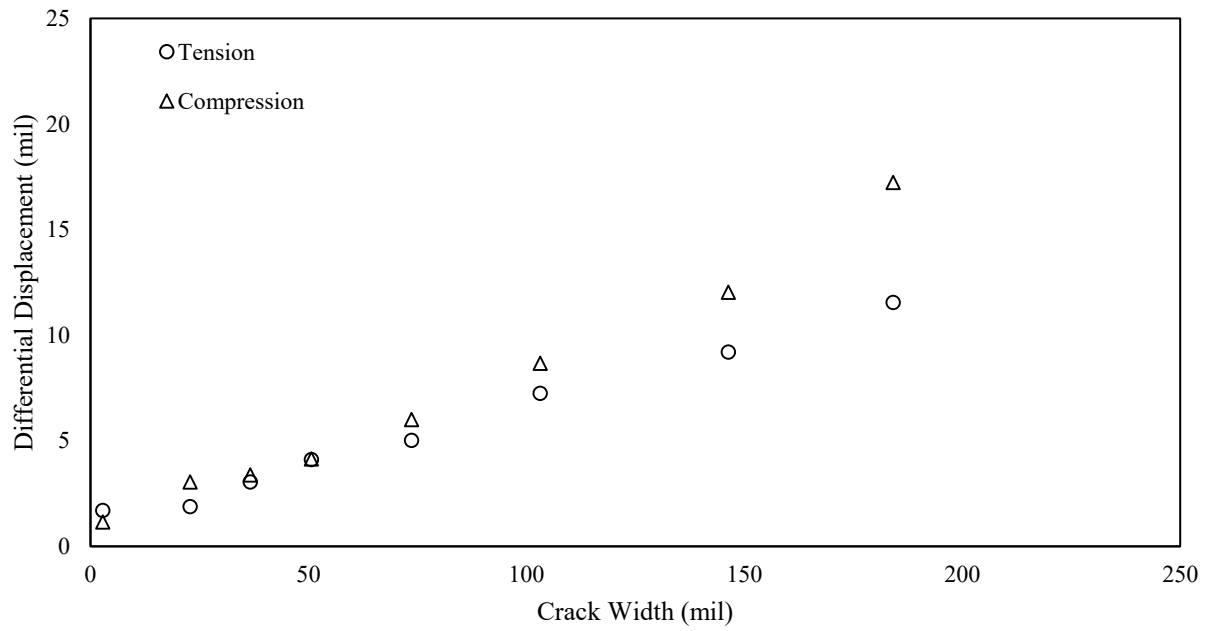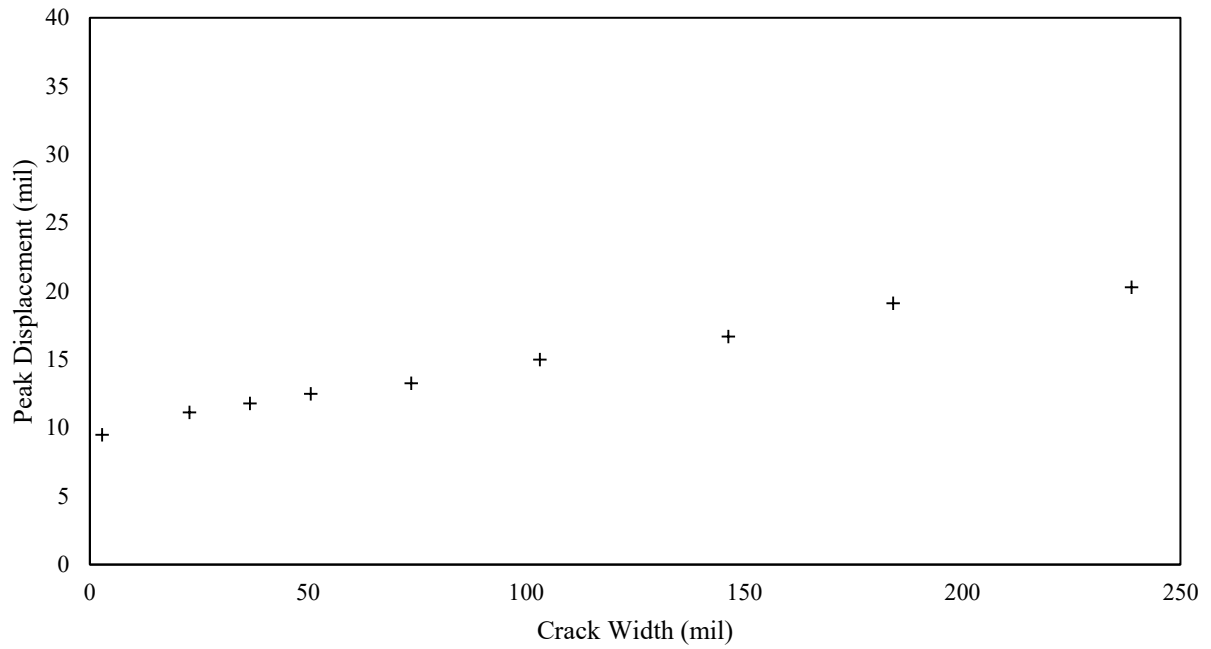

Figure F-43. DJED as a function of crack width.
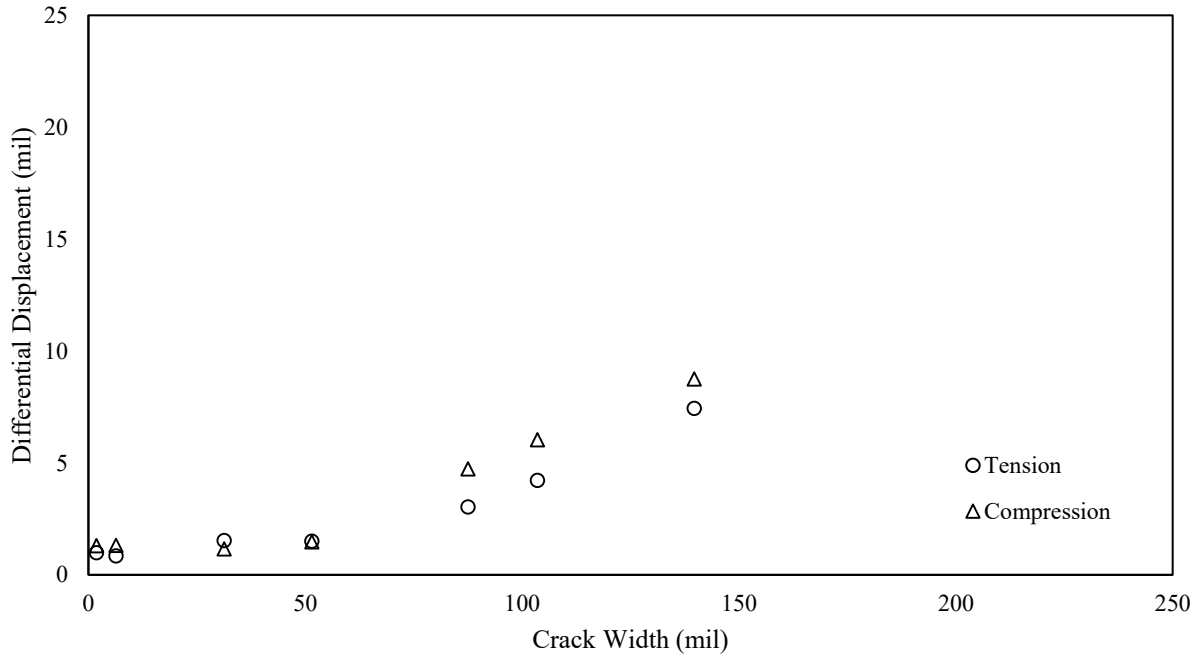
Figure F-44. Differential joint displacement as a function of crack width.
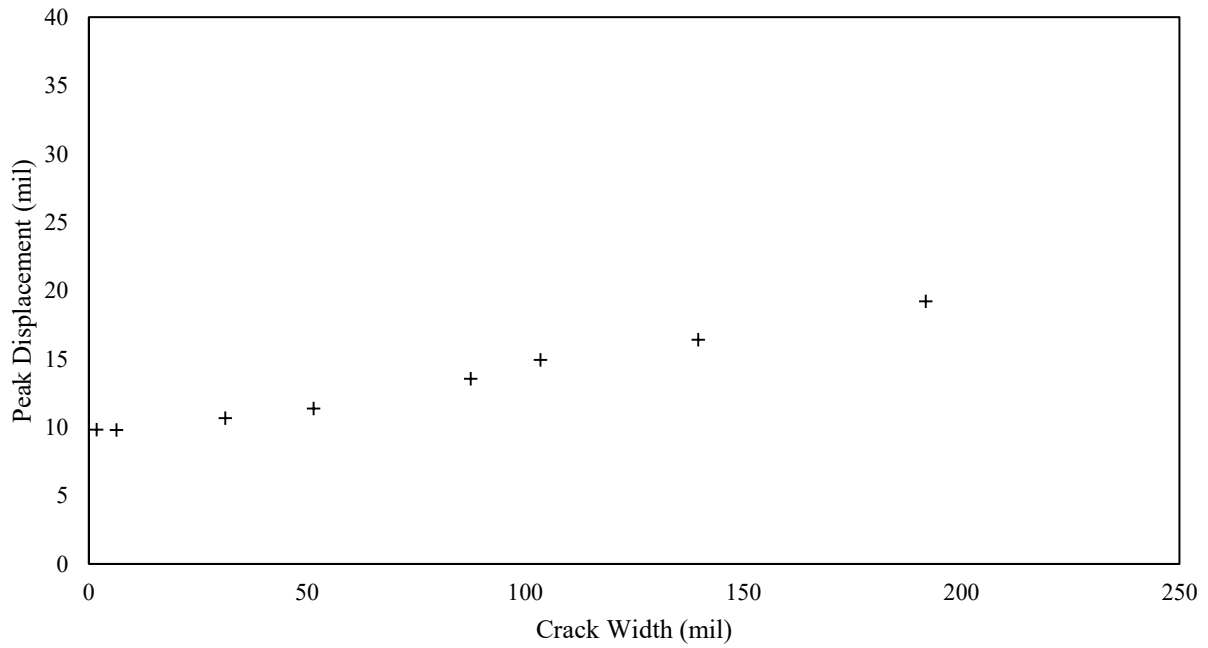
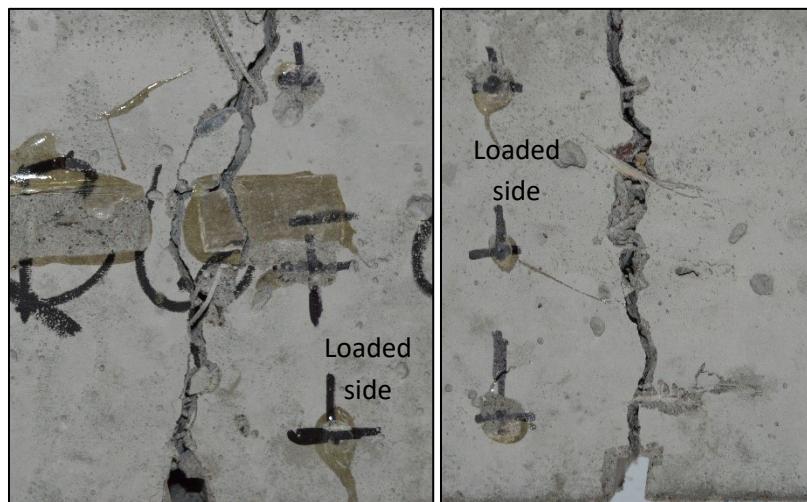**Figure F-45. Peak displacement as a function of crack width.**
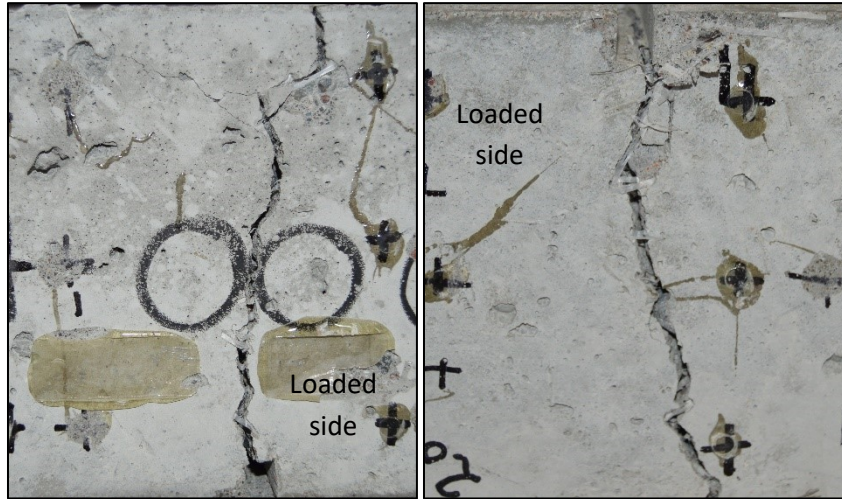
Figure F-46. The front and back of the joint for specimen 3 in phase 1.
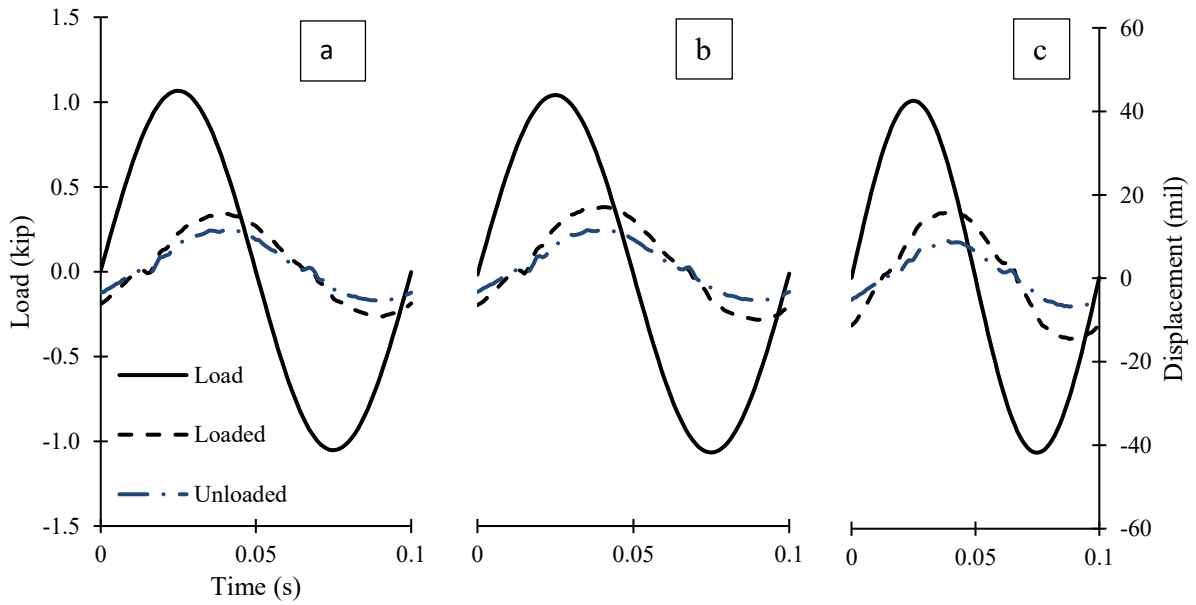
Figure F-47. Cyclical plots for (a)30 mils, (b)47 mils, and (c) 94 mils crack width.
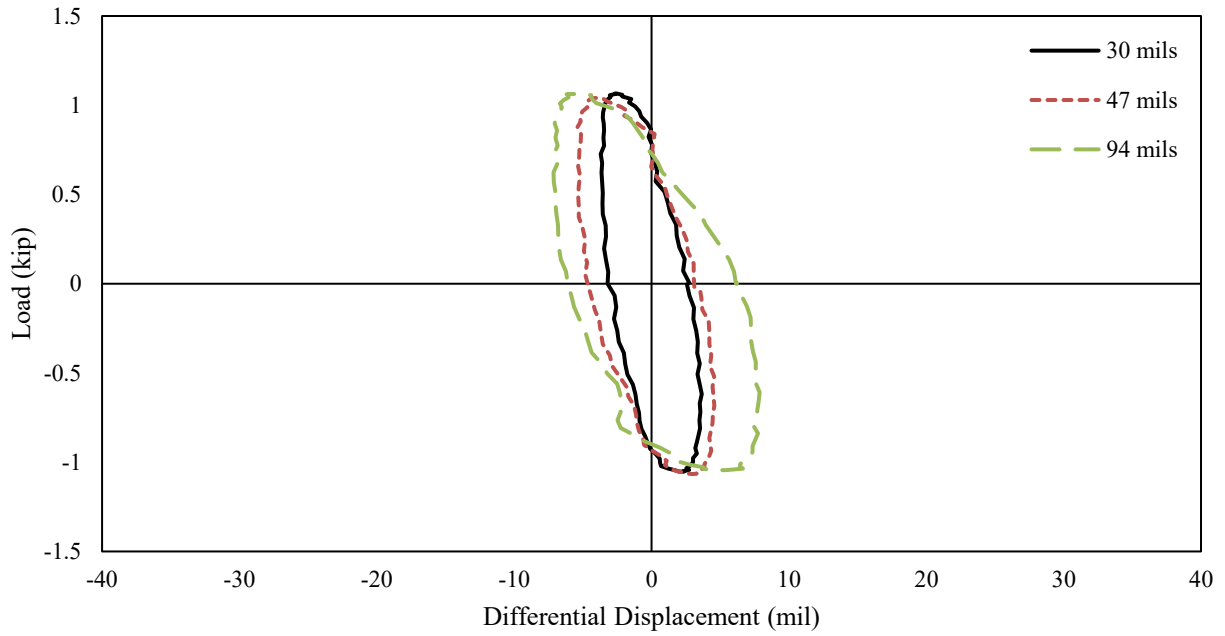
Figure F-48. Hystereses for 30 mil crack width.
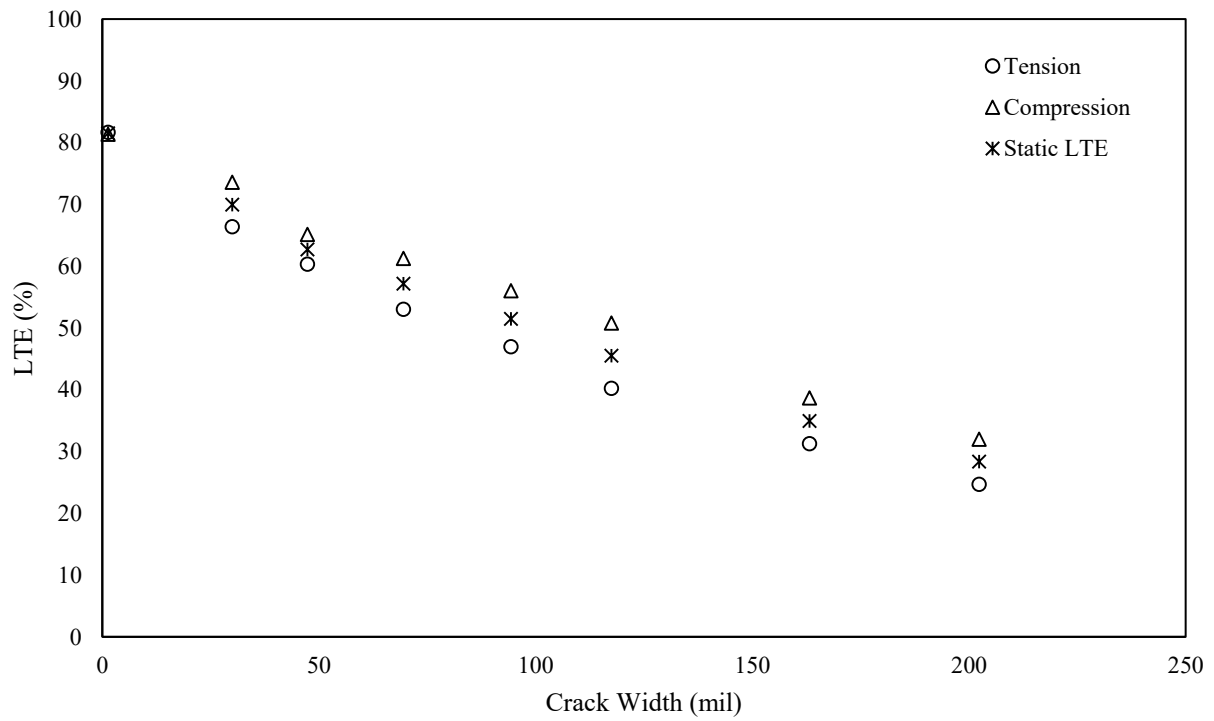
Figure F-49. LTE as a function of crack width.
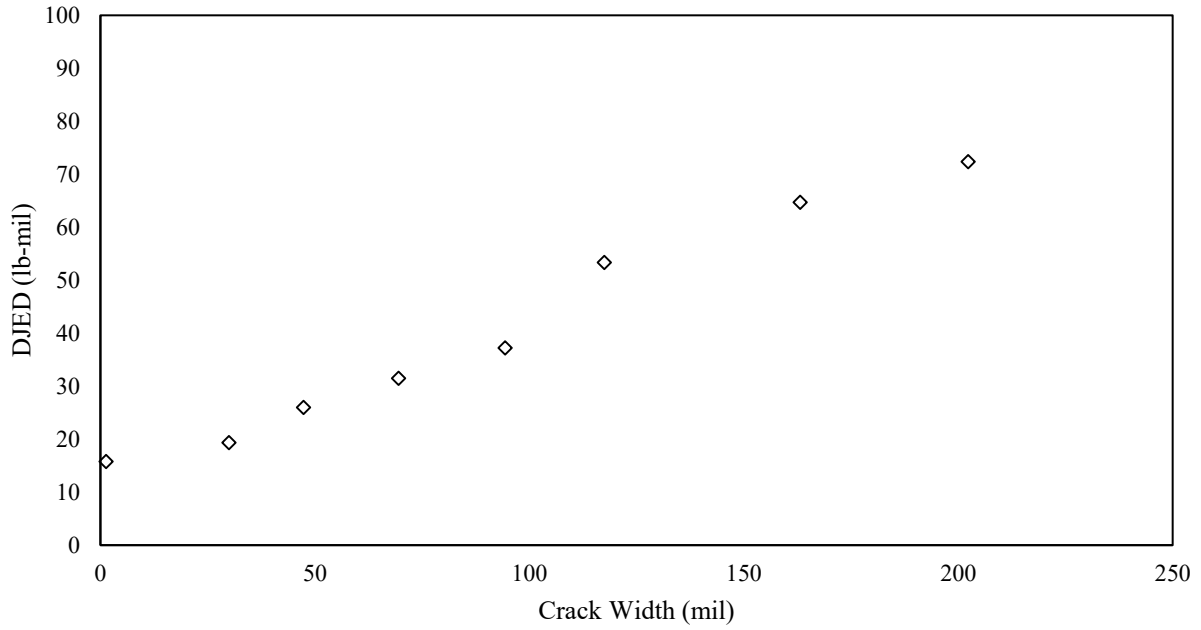
Figure F-50. DJED as a function or crack width.
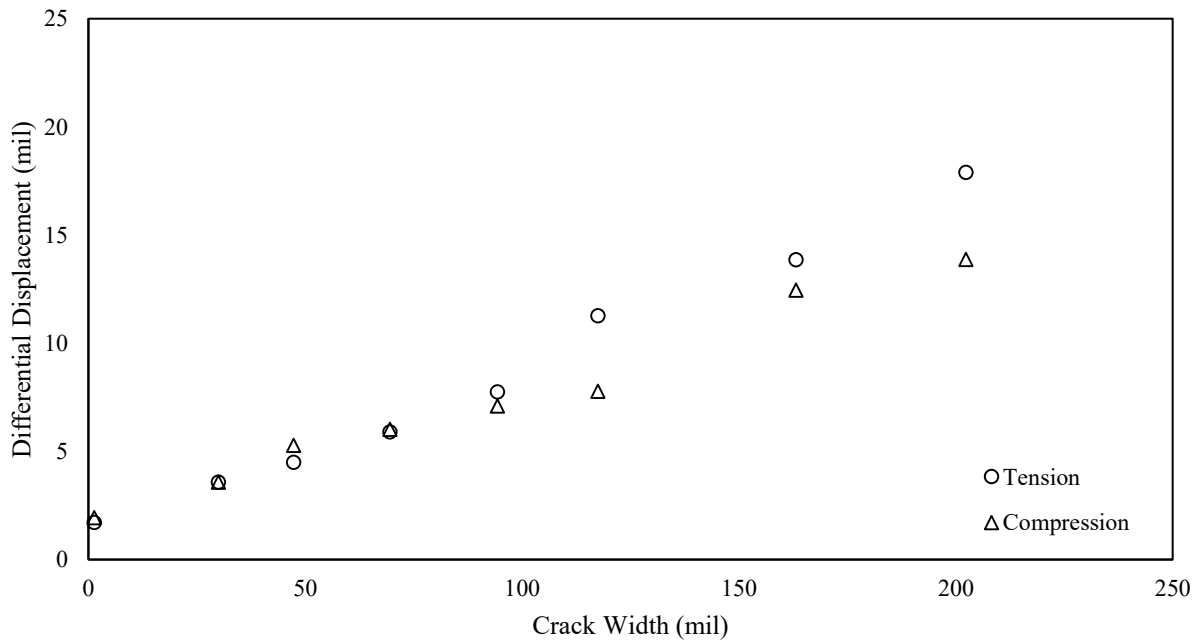
Figure F-51. Differential displacement as a function of crack width.
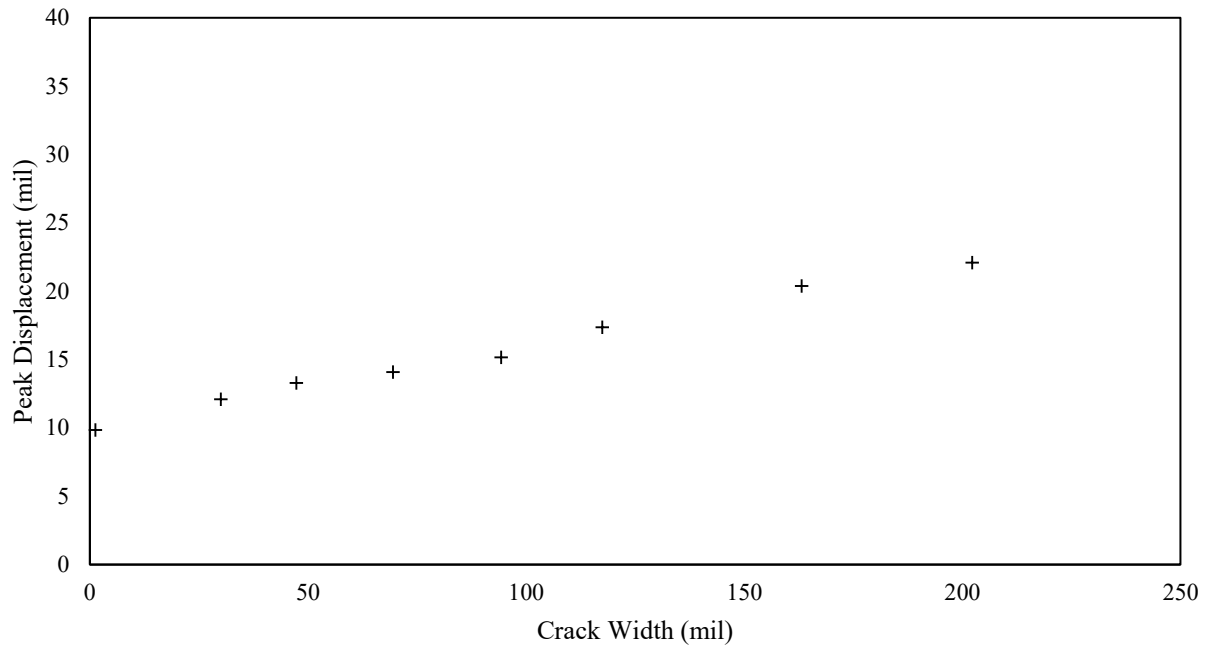
Figure F-52. Peak displacement as a function of crack width.
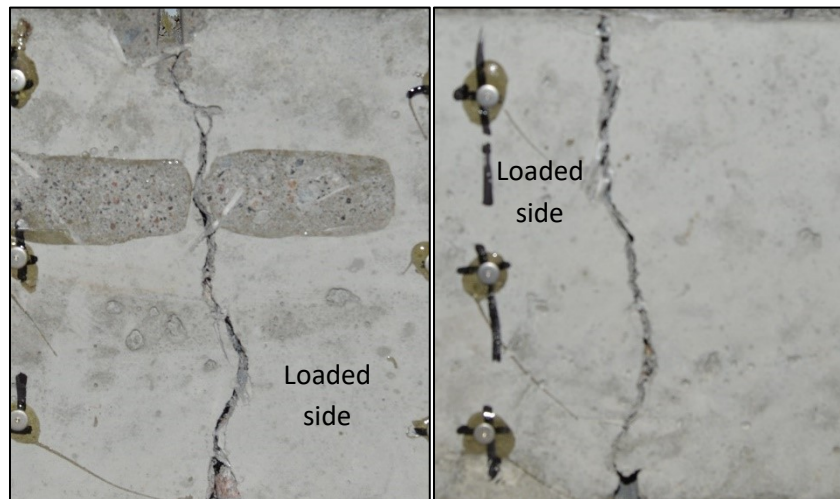
Phase 2: Specimen 1

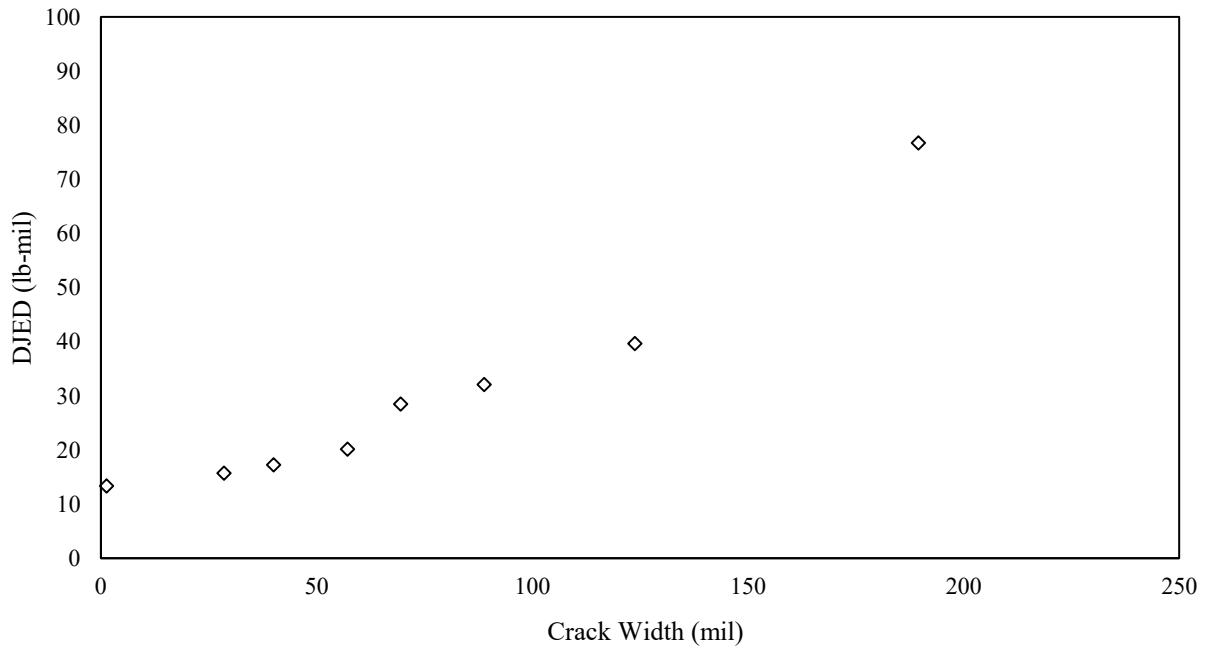**Figure F-53. The front and back of the joint for specimen 1 in phase 2.**
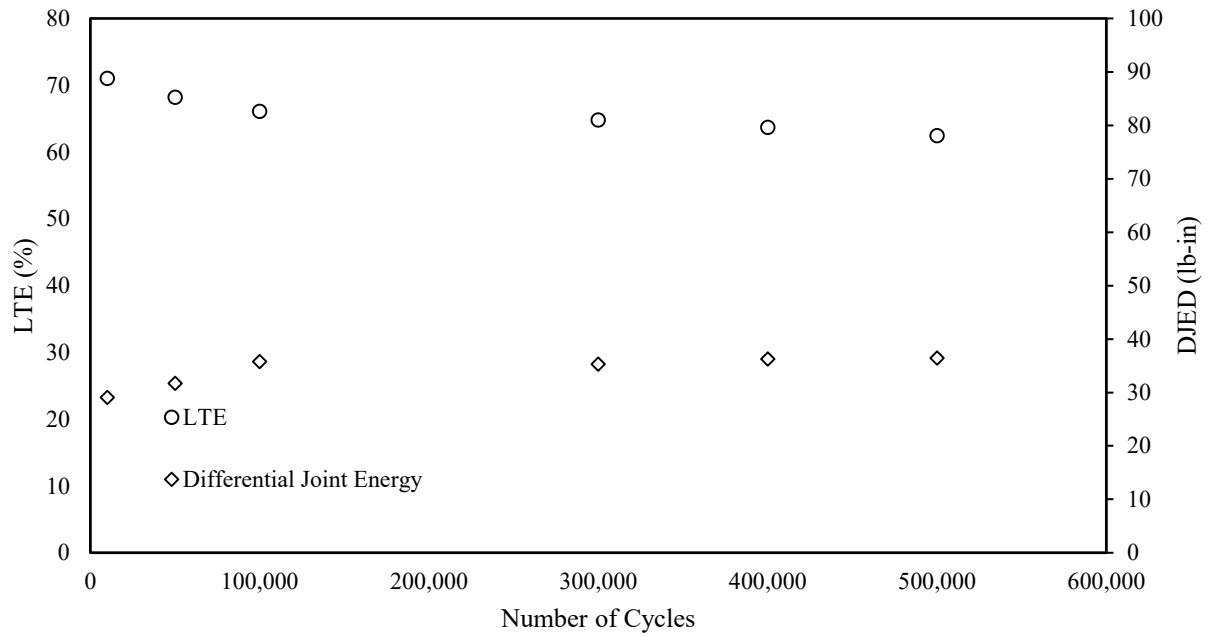
*Crack width ranged from 49 mils to 53 mils

Figure F-54. LTE and DJED as a function of repetitions (cycles).
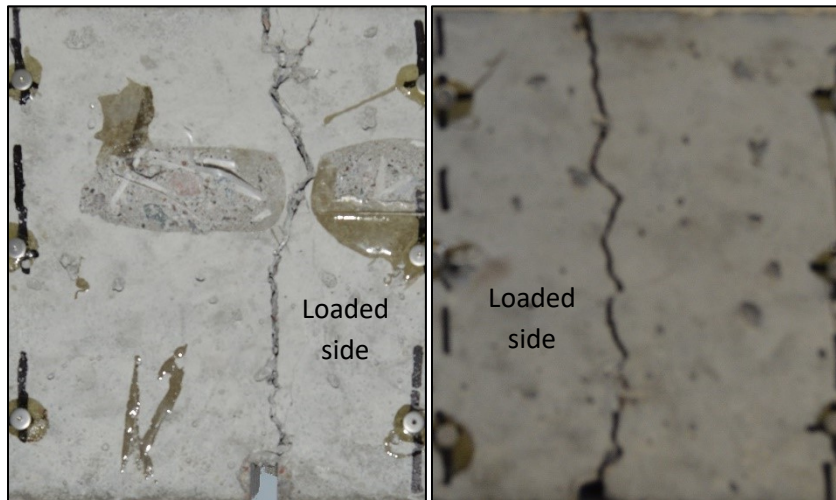
Phase 2: Specimen 2

Figure F-55. The front and back of the joint for specimen 2 in phase 2.
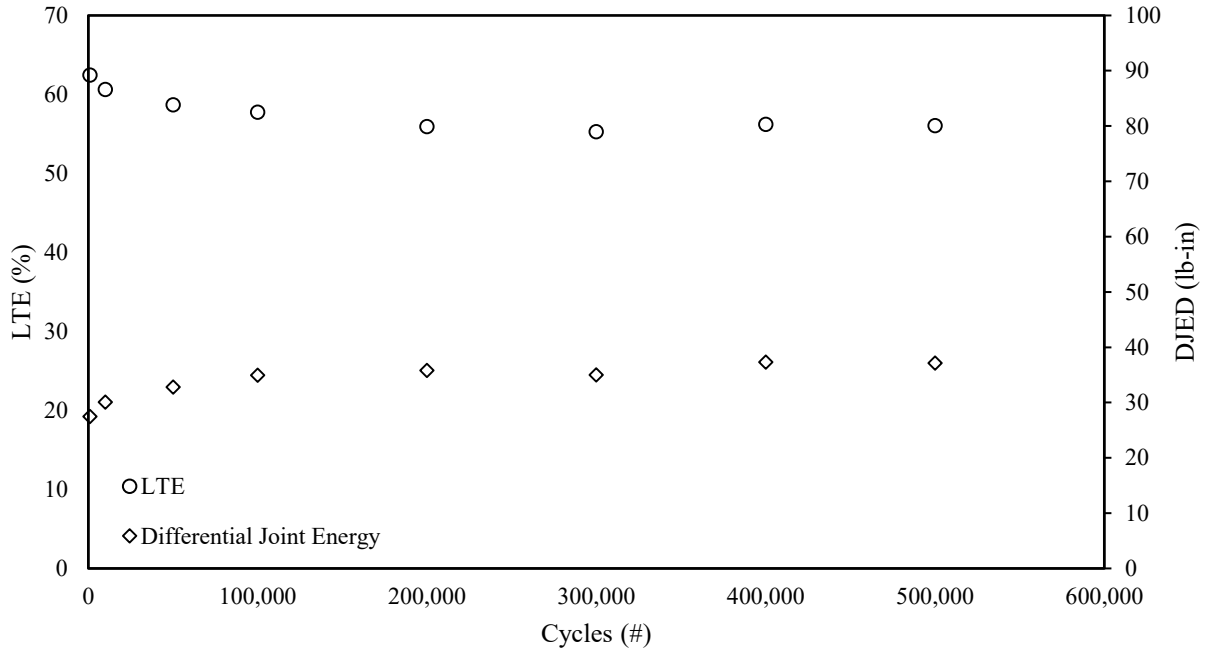
*Crack width ranged from 50 mils to 51 mils

Figure F-56. LTE and DJED as a function of repetitions (cycles).
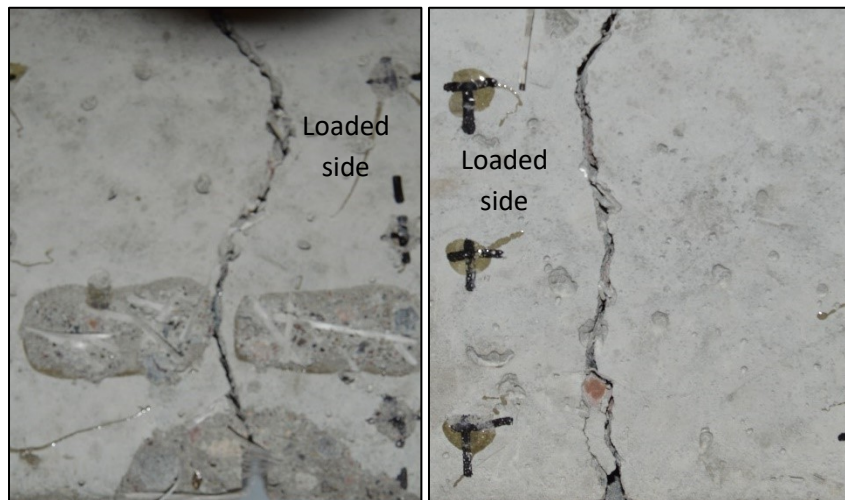
Phase 2: Specimen 3

*NO FATIGUE, ONLY CW VS. PERFORMANCE, SEE PHASE 3
Figure F-57. The front and back of the joint for specimen 3 in phase 2.
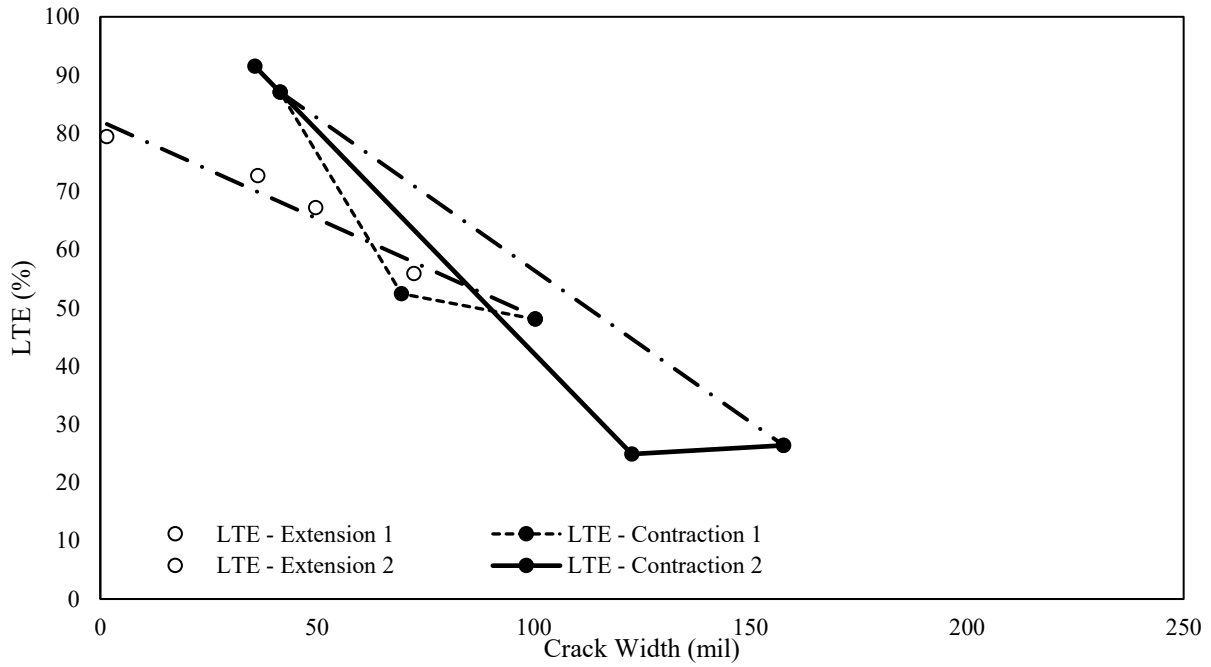
Figure F-58. The effect of joint expansion and contraction on LTE in terms of crack width (phase 2: specimen 1).
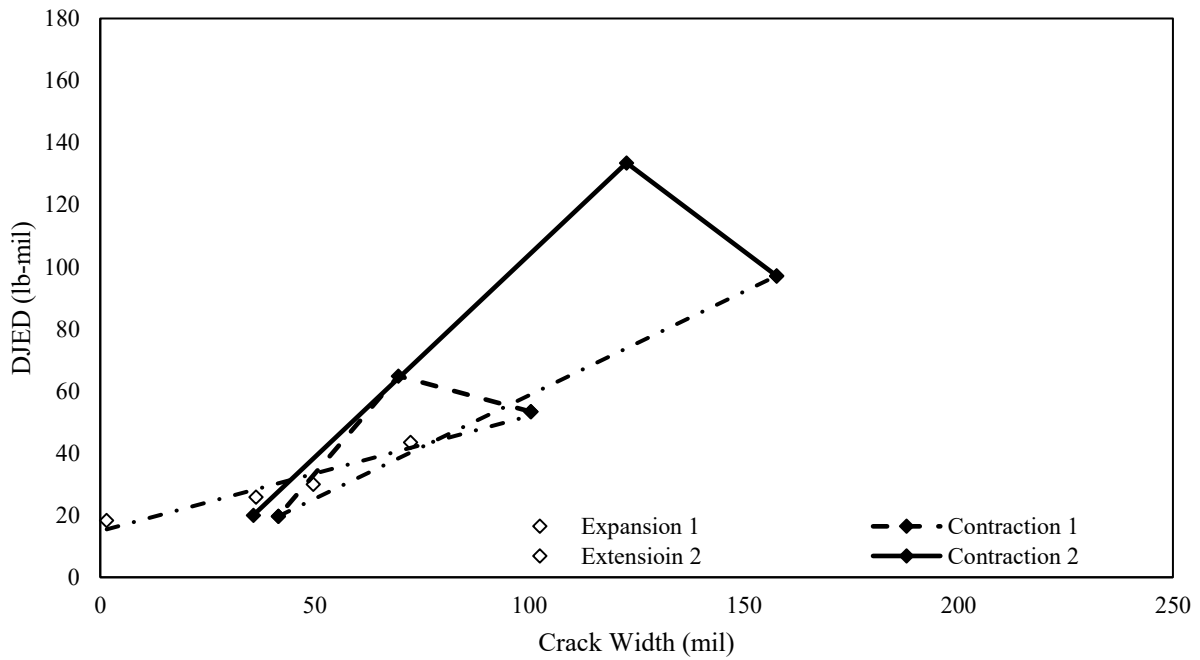
Figure F-59. The effect of joint expansion and contraction on DJED in terms of crack width (phase 2: specimen 1).

F-30
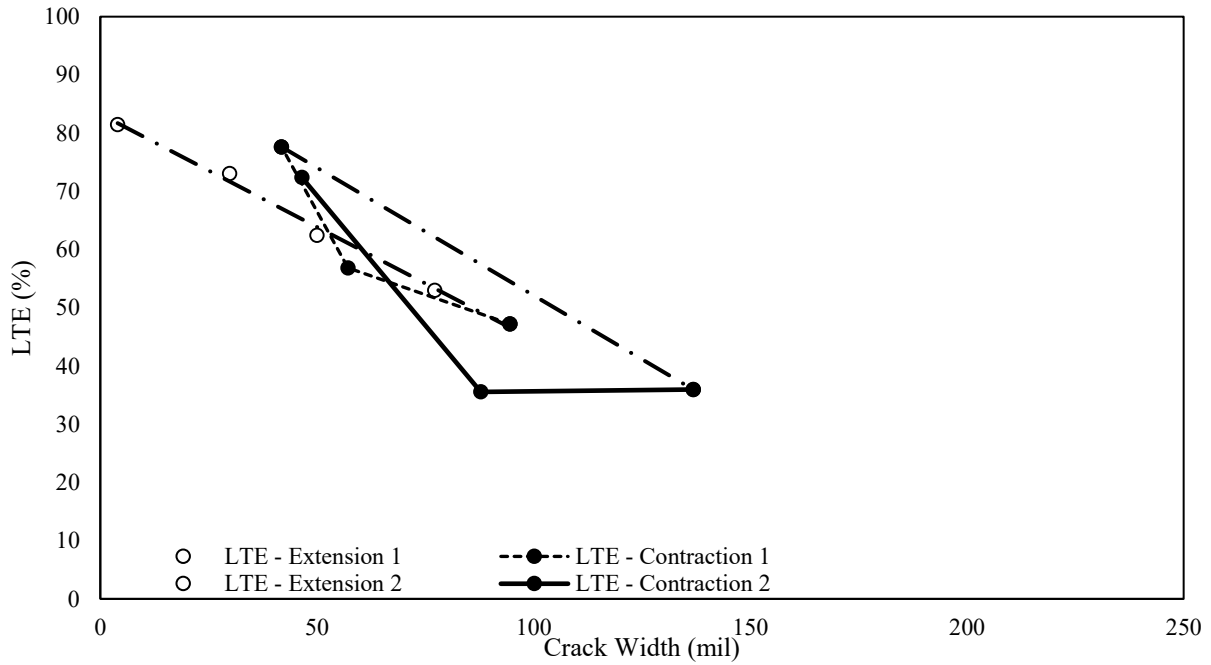
Figure F-60. The effect of joint expansion and contraction on LTE in terms of crack width (phase 2: specimen 2).
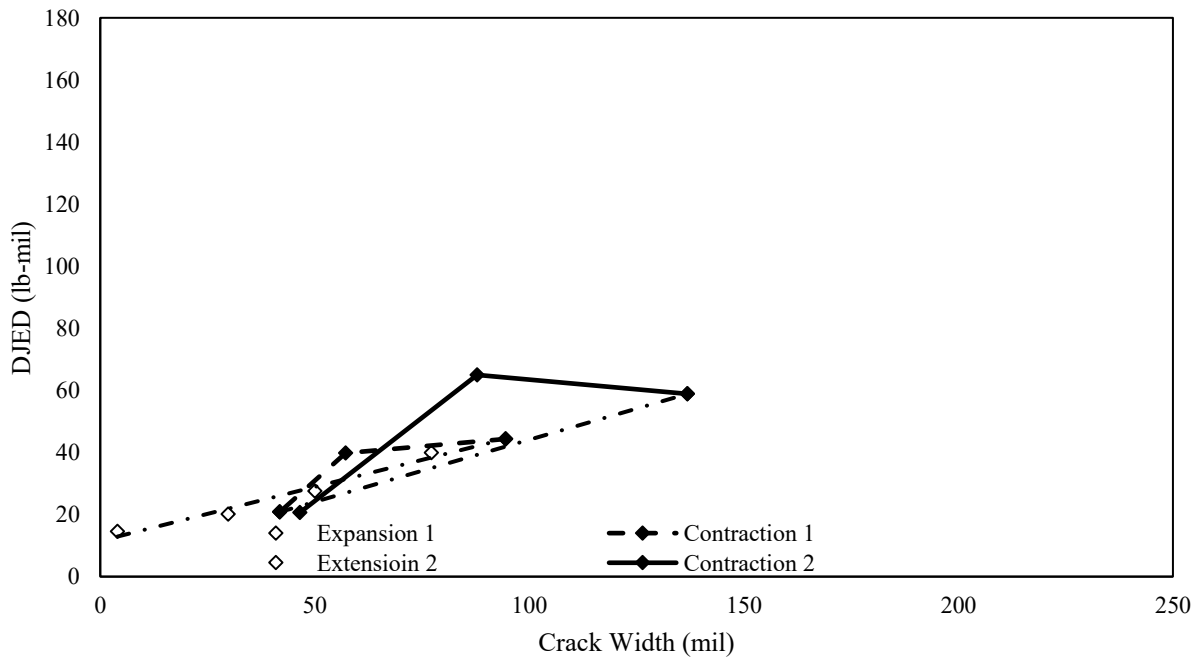
Figure F-61. The effect of joint expansion and contraction on DJED in terms of crack width (phase 2: specimen 2).
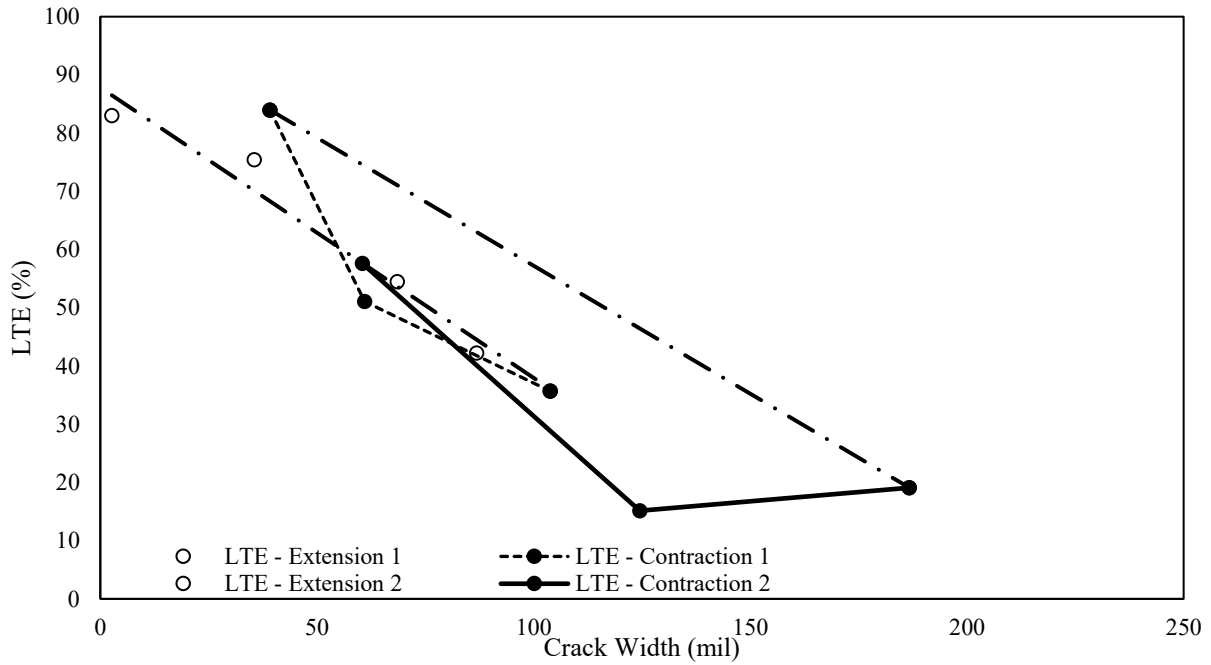
Figure F-62. The effect of joint expansion and contraction on LTE in terms of crack width (phase 2: specimen 3).
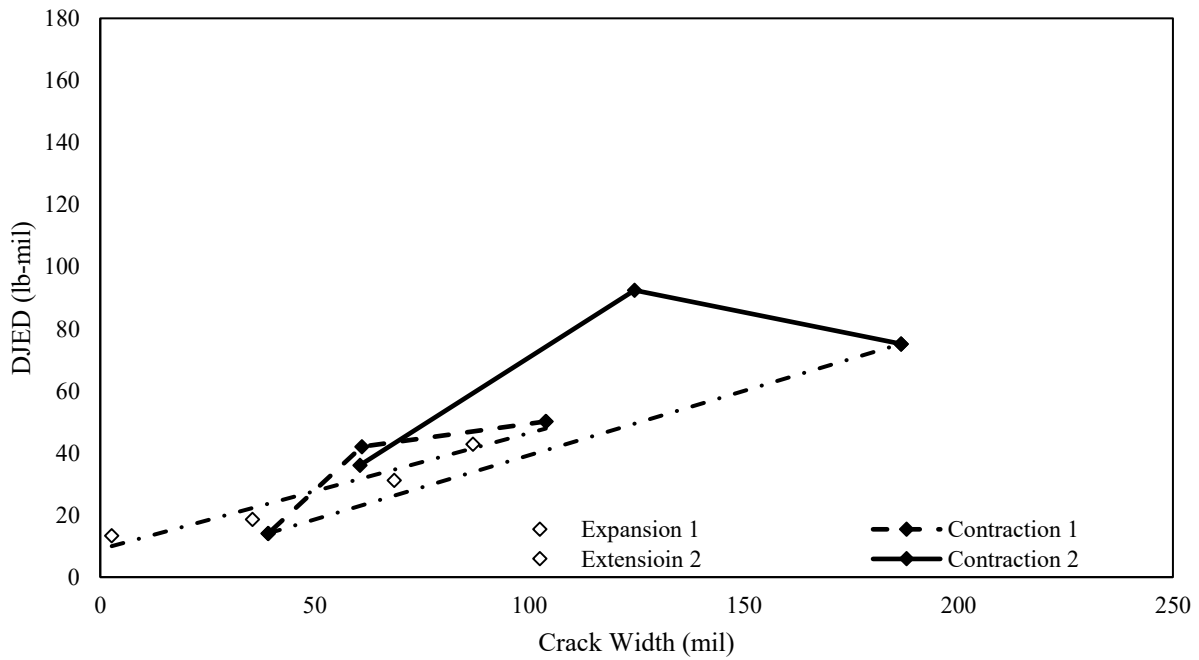
Figure F-63. The effect of joint expansion and contraction on DJED in terms of crack width (phase 2: specimen 3).
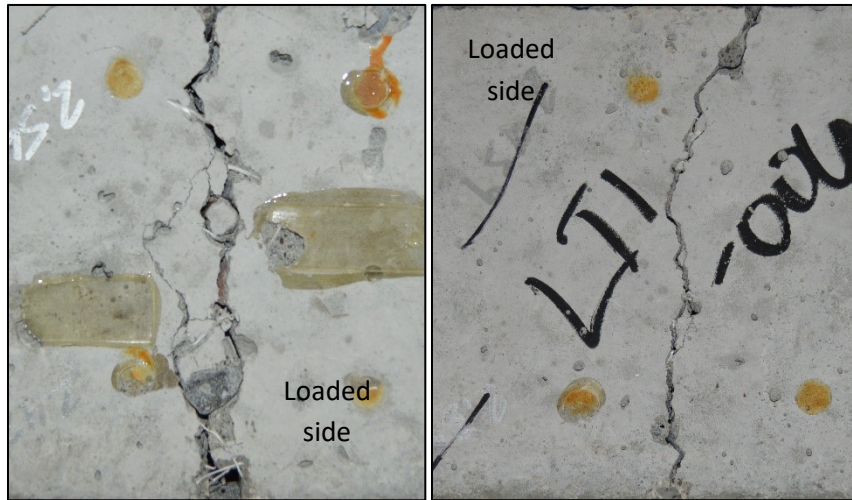
Phase 1: Specimen 1

Figure F-64. The front and back of the joint for specimen 1 in phase 1.
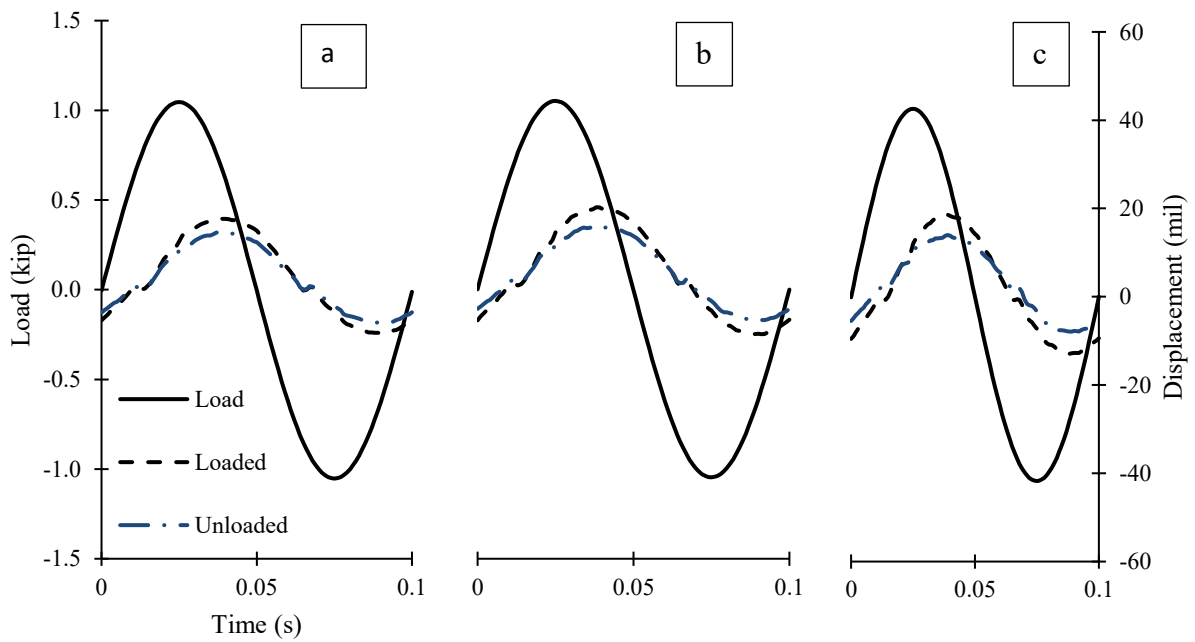
**Figure F-65. Cyclical plots at (a) 14 mils, (b) 45 mils, and (c) 90 mils crack widths.**
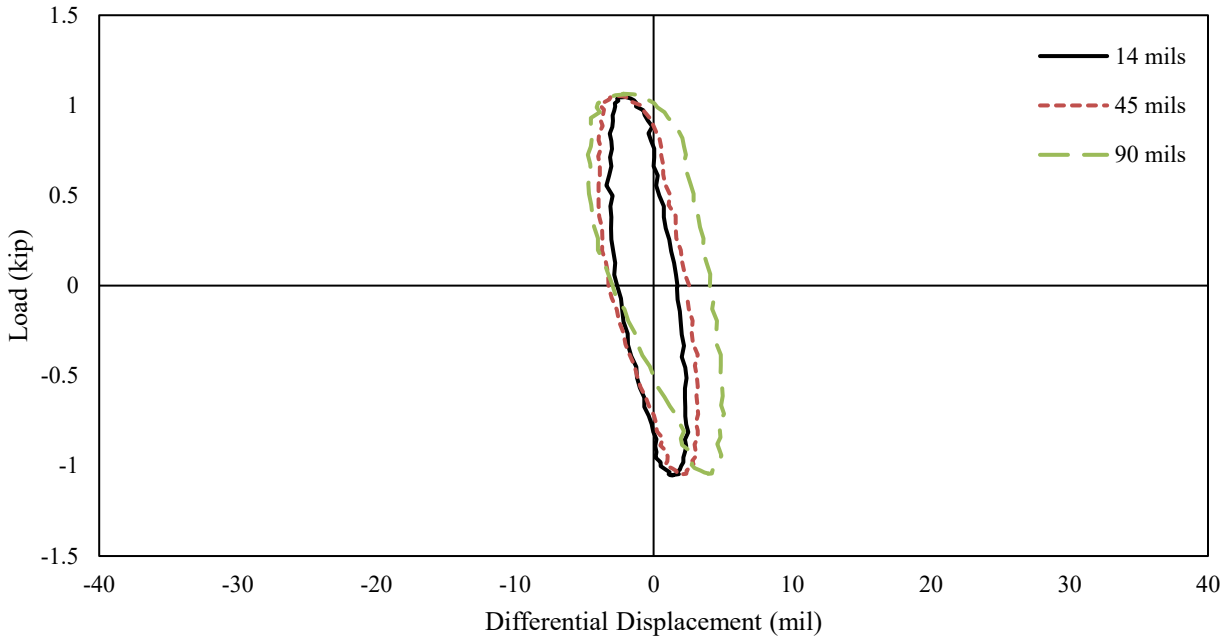
**Figure F-66. Hystereses at 14 mils, 45 mils, and 90 mils crack widths.**
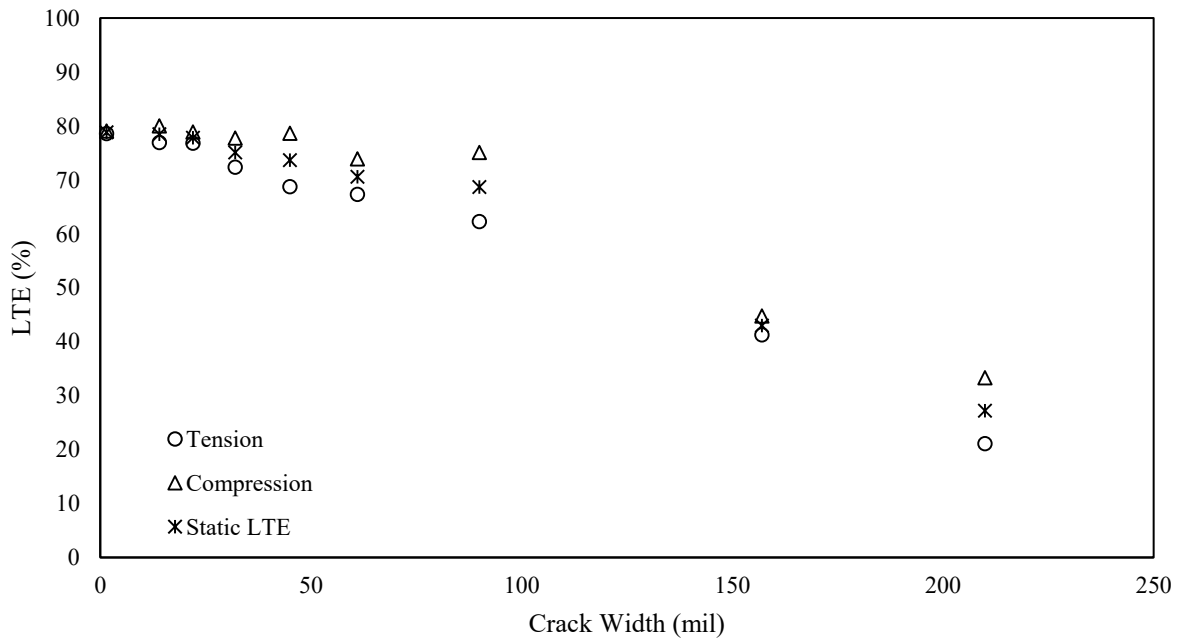
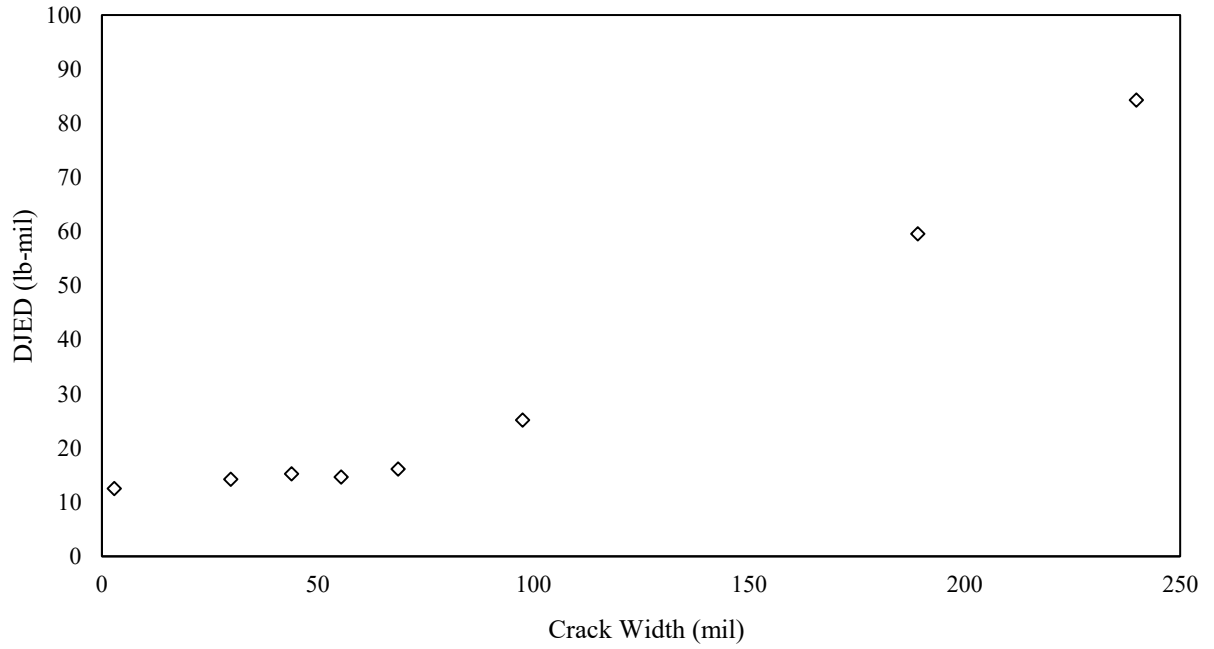

Figure F-67. LTE as a function of crack width.
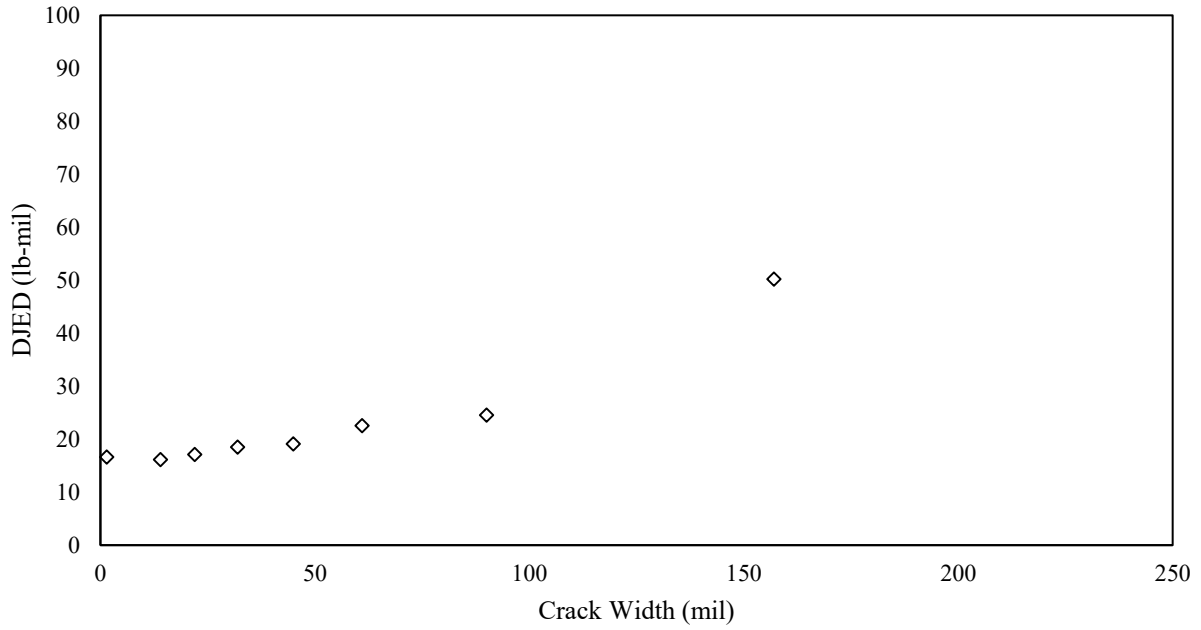
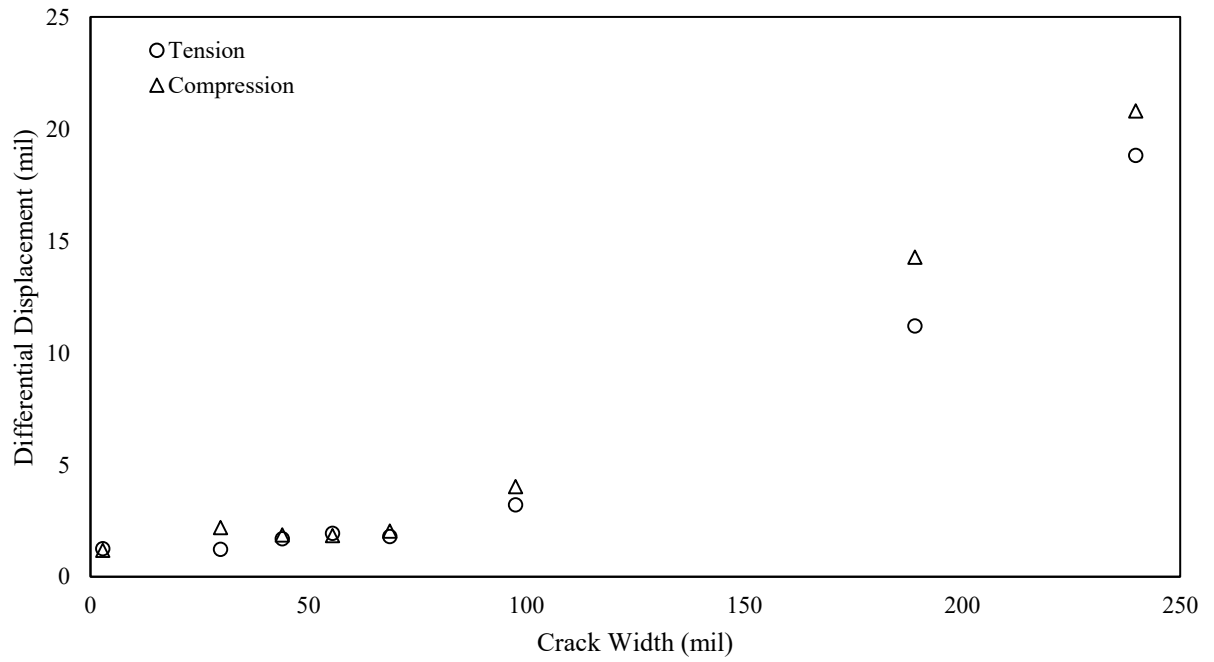**Figure F-68. DJED as a function of crack width.**
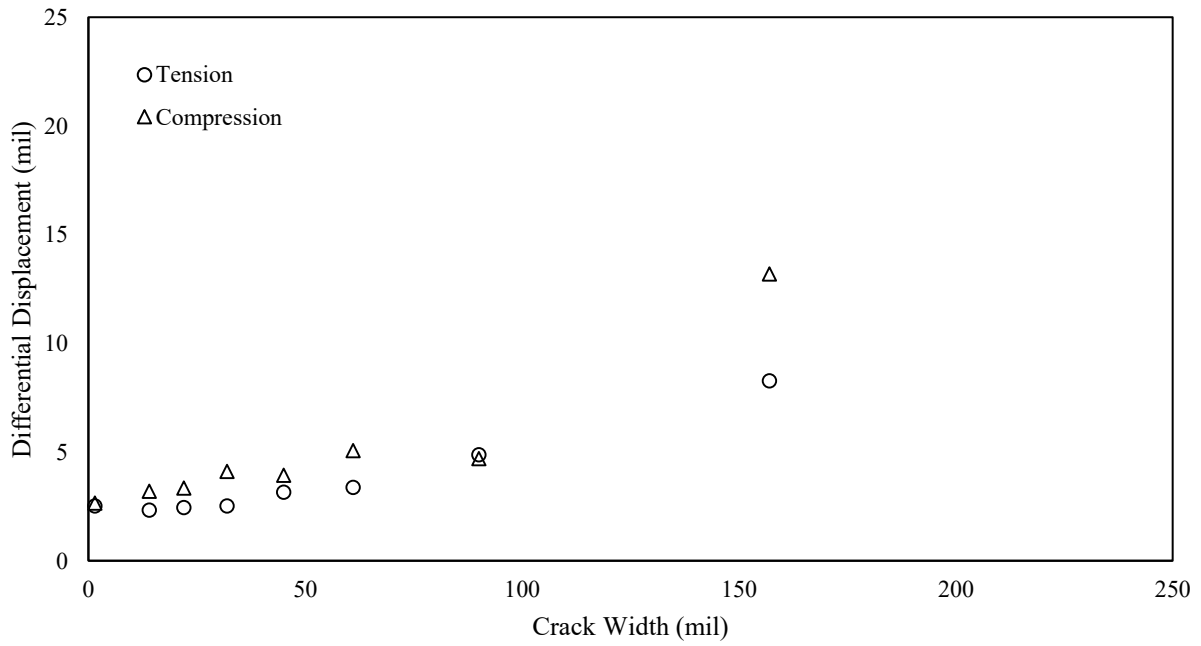
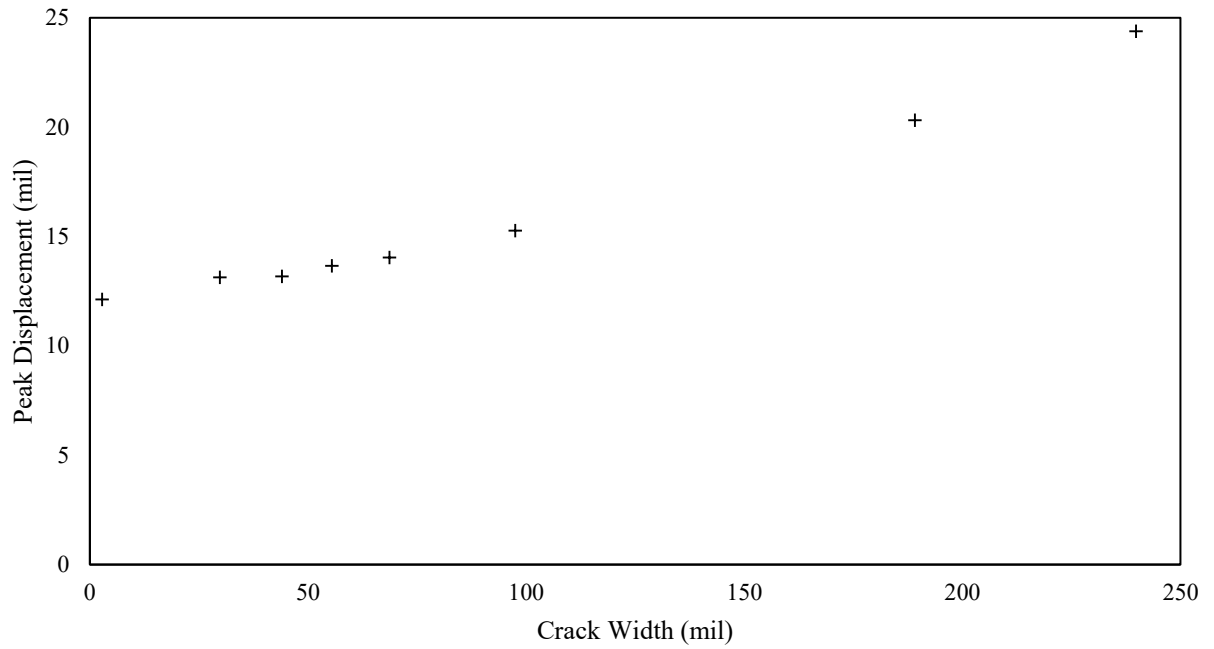**Figure F-69. Differential displacement as a function of crack width.**
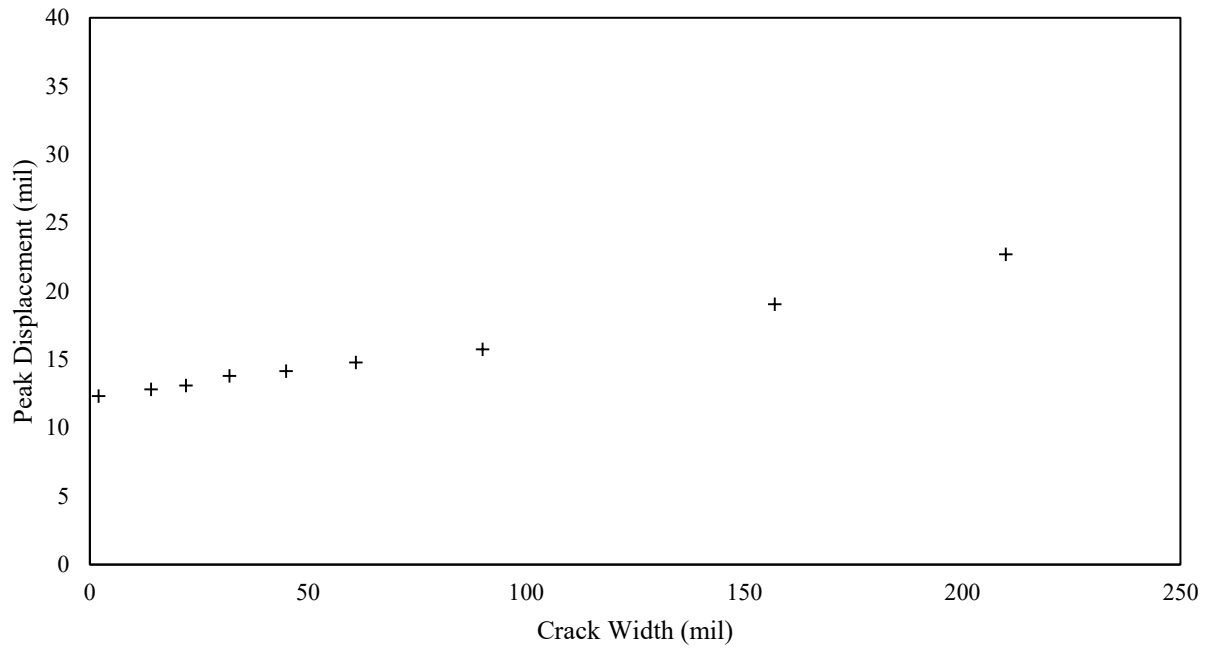
Figure F-70. Peak displacement as a function of crack width.
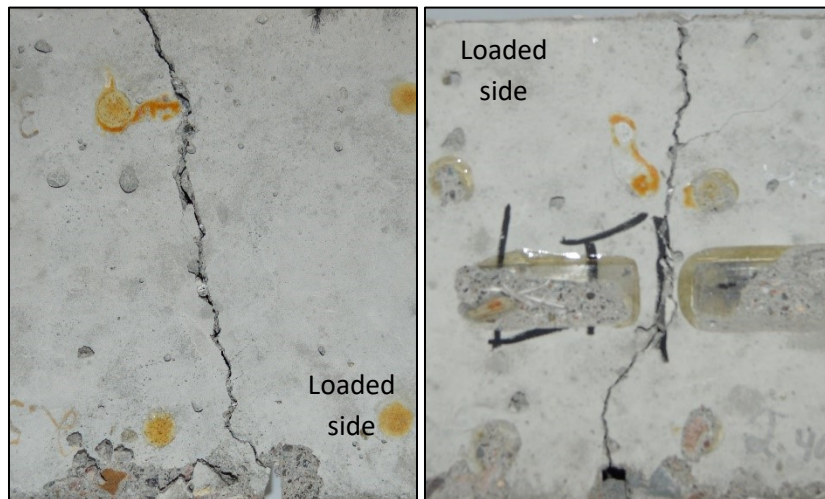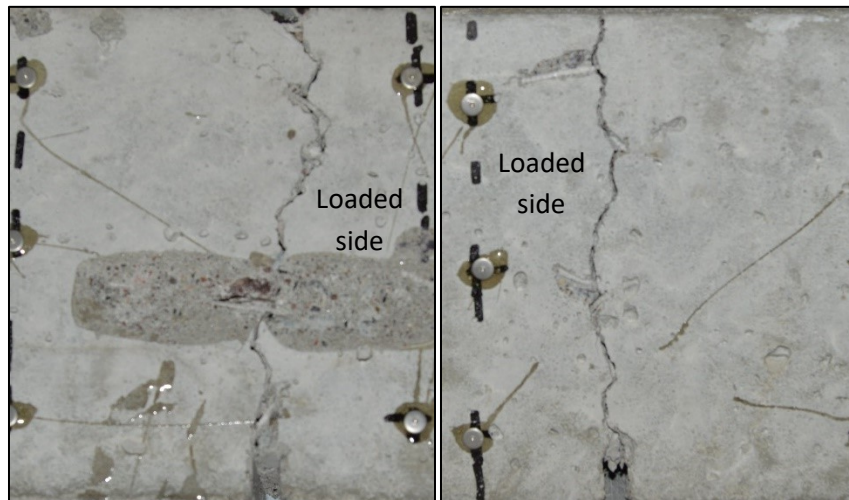
Phase 1: Specimen 2

Figure F-71. The front and back of the joint for specimen 2 in phase 1.
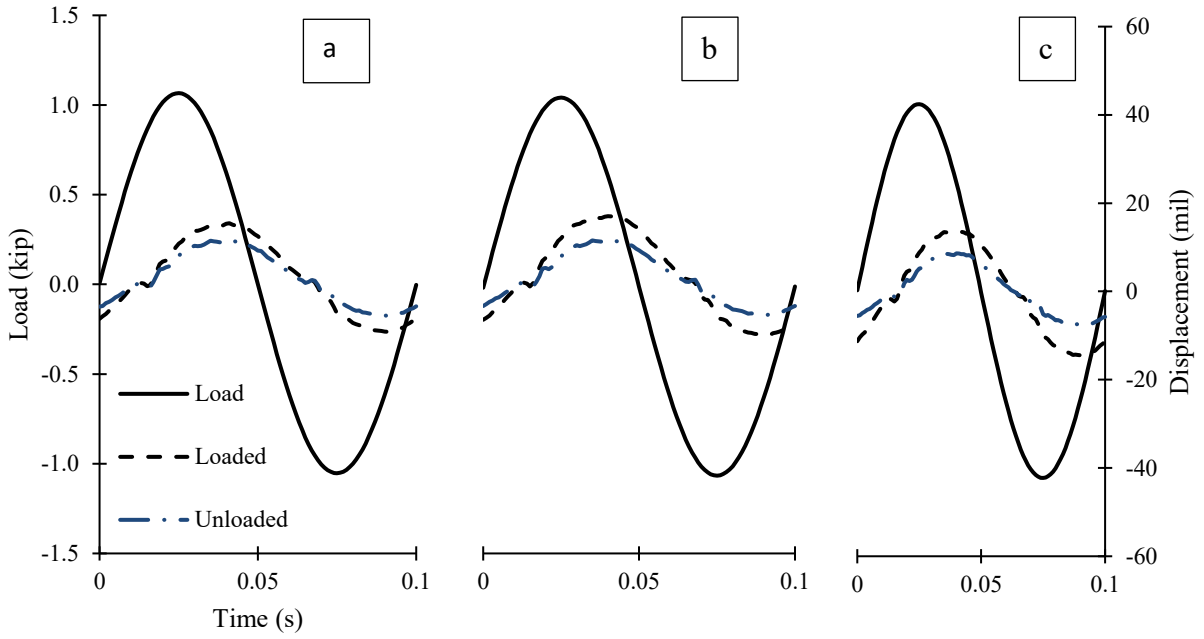
Figure F-72. Cyclical plots for (a) 32 mils, (b) 81 mils, and (c) 102 mils crack widths.
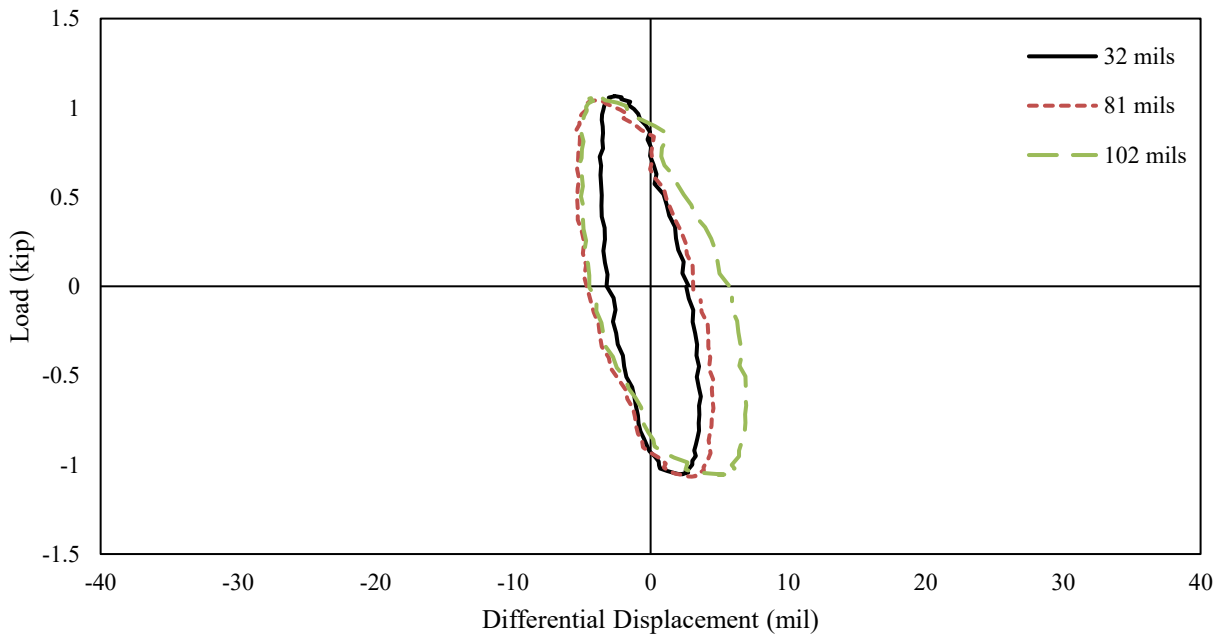
Figure F-73. Hystereses for 32 mils, 81 mils, and 102 mils crack widths.

F-37
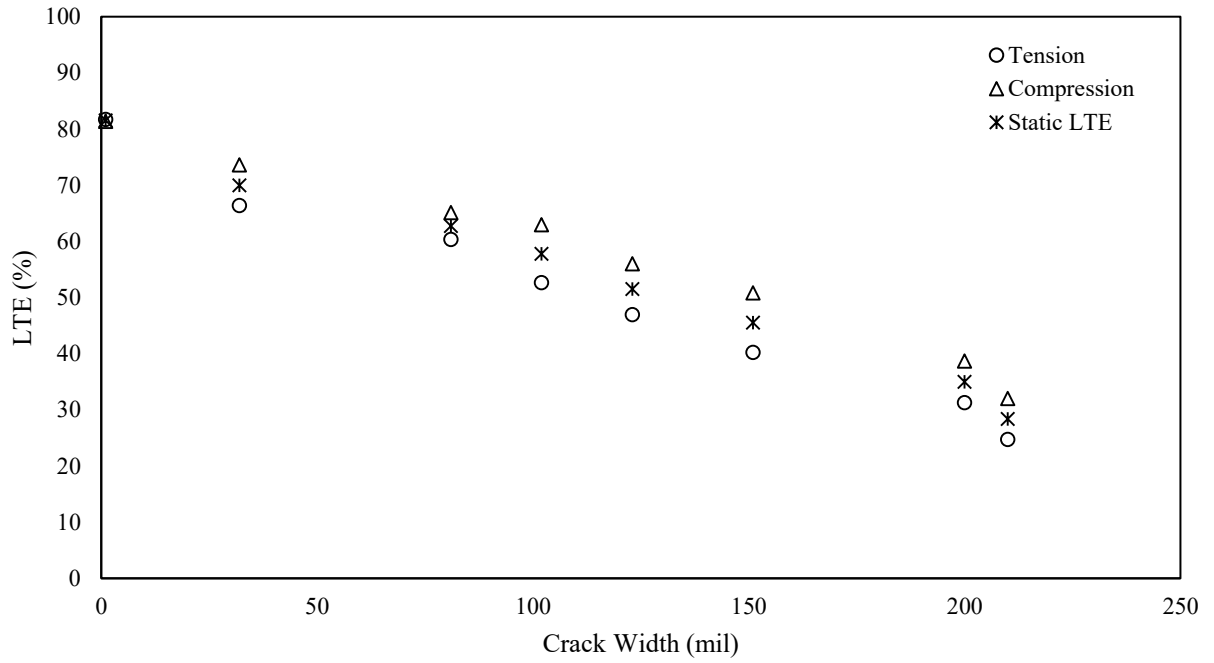
Figure F-74. LTE as a function of crack width.
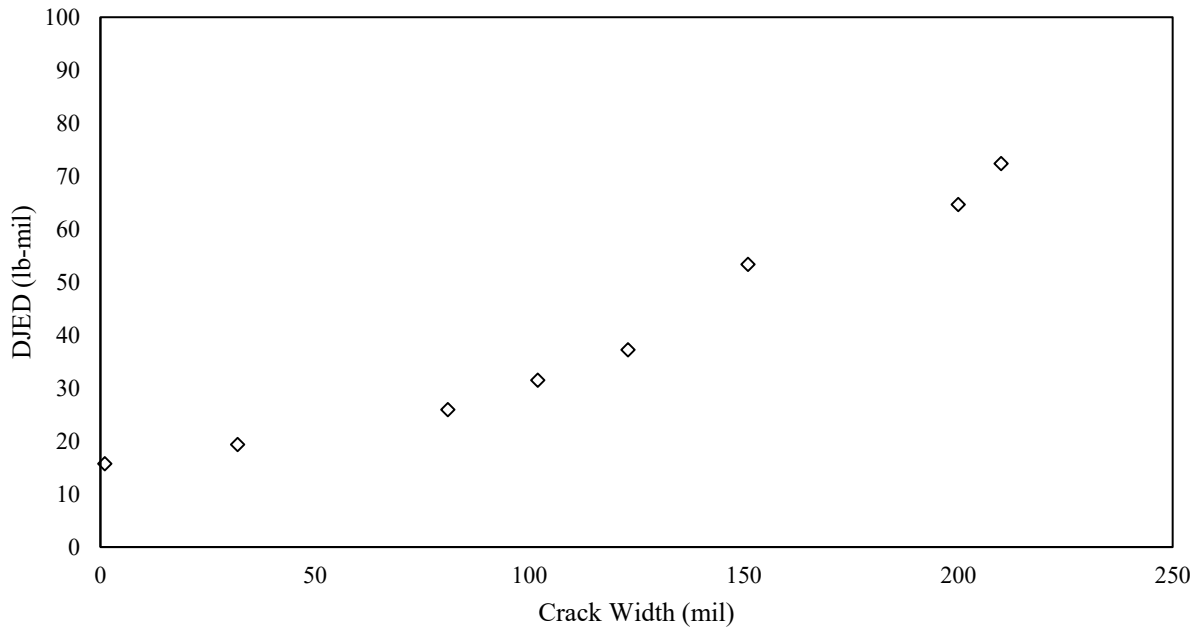
Figure F-75. DJED as a function of crack width.
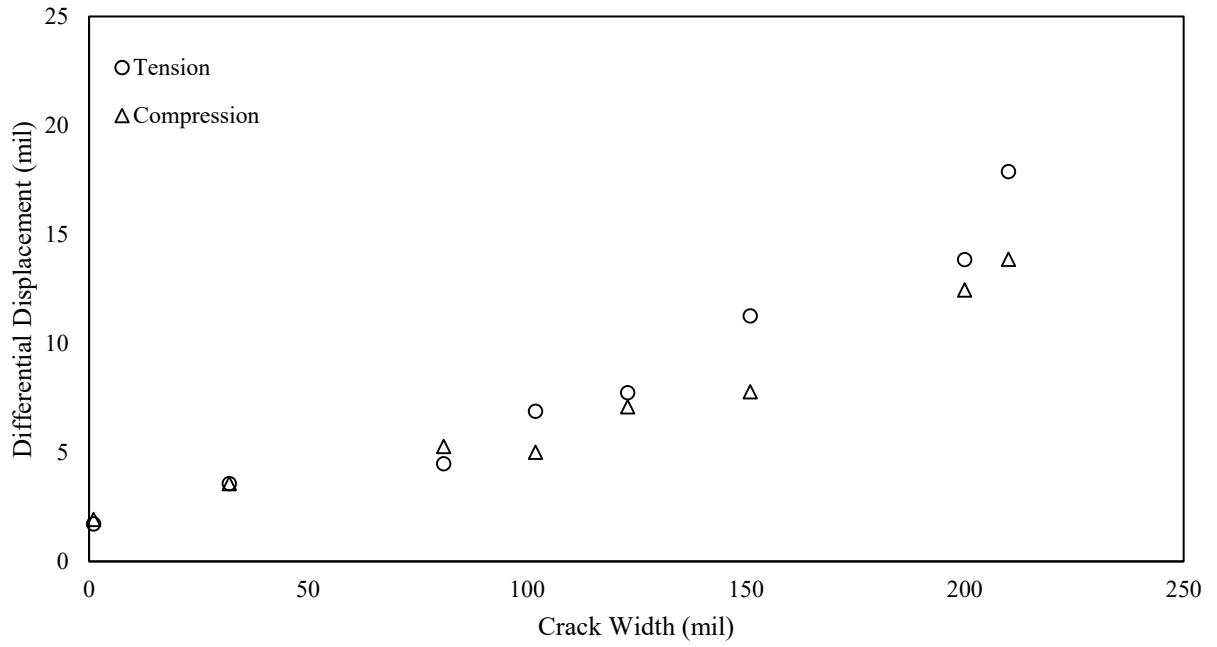
Figure F-76. Differential displacement as a function of crack width.
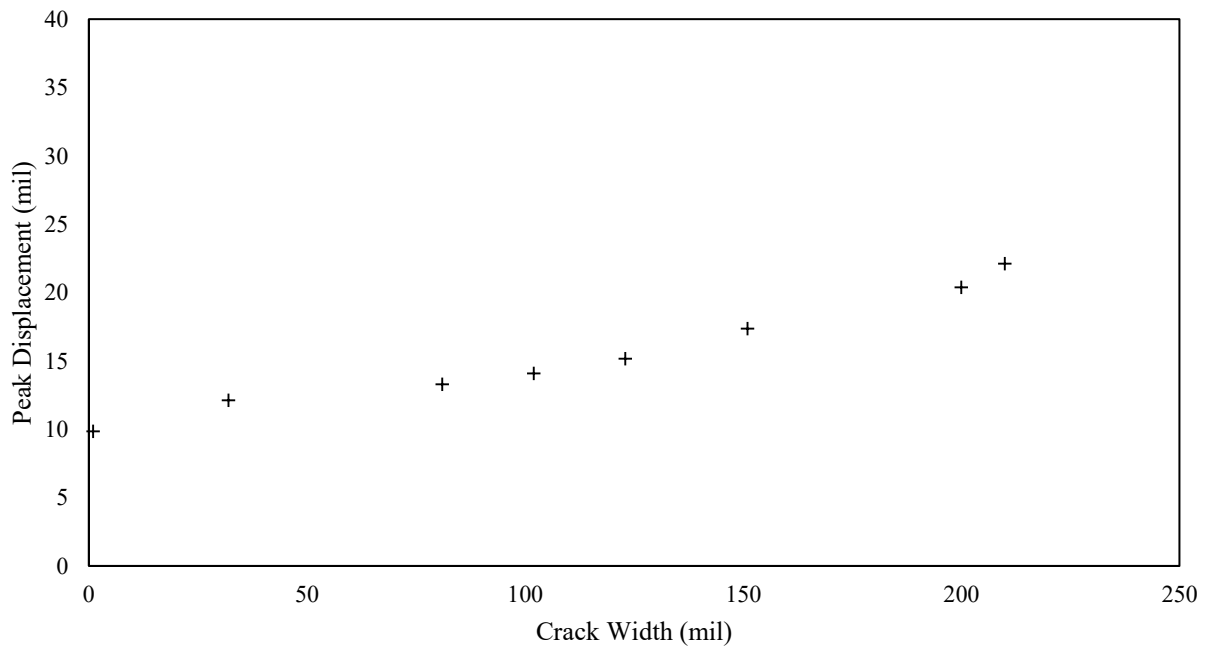
**Figure F-77. Peak displacement as a function of crack width.**

F-39
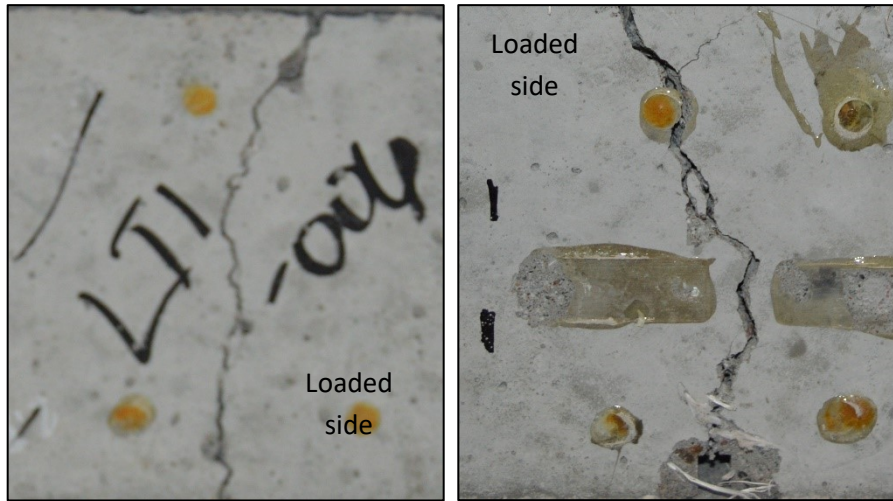
Figure F-78. The front and back of the joint for specimen 3 in phase 1.
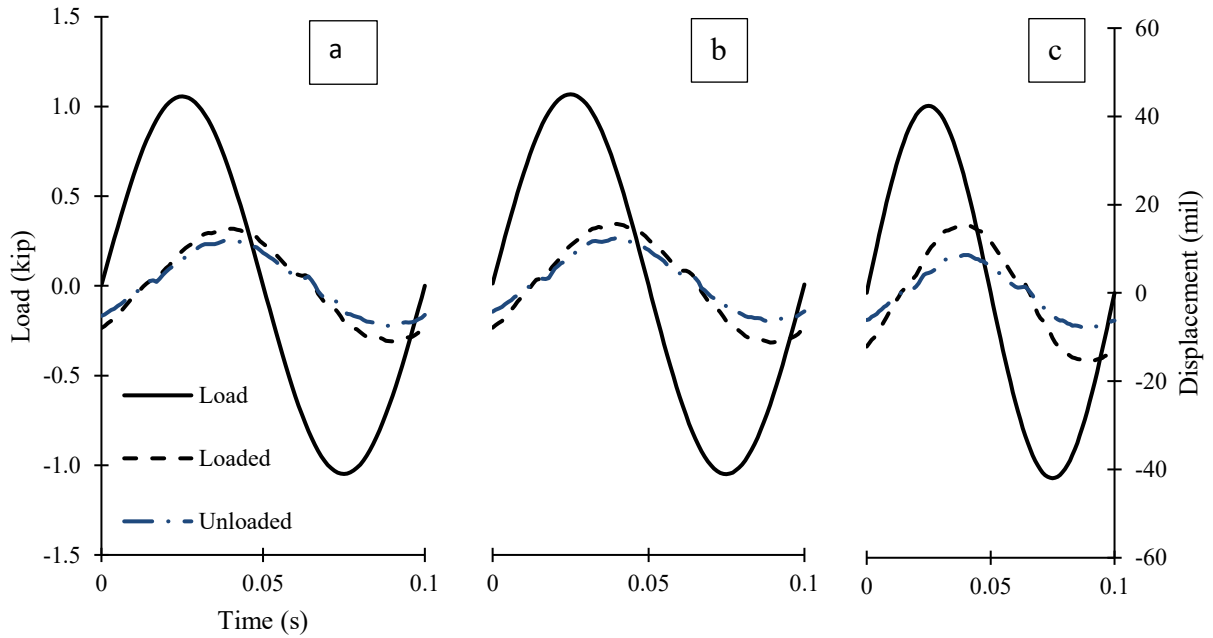
Figure F-79. Cyclical plots for (a) 30 mils, (b) 50 mils, and (c) 104 mils crack widths.
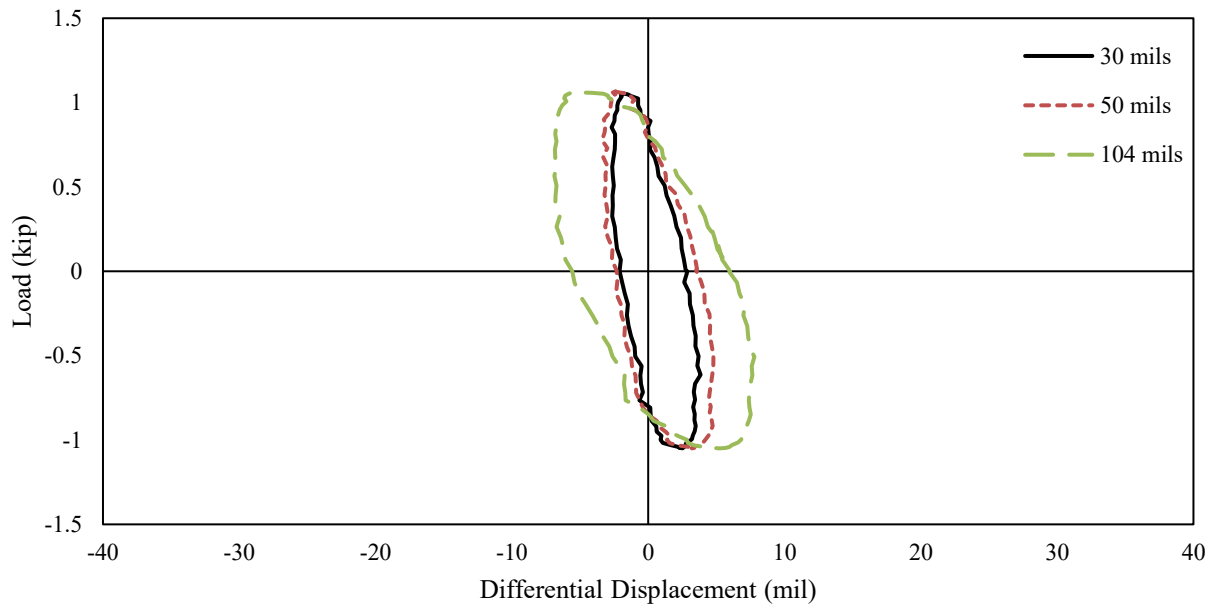
Figure F-80. Hystereses for 30 mils, 50 mils, and 104 mils crack widths.
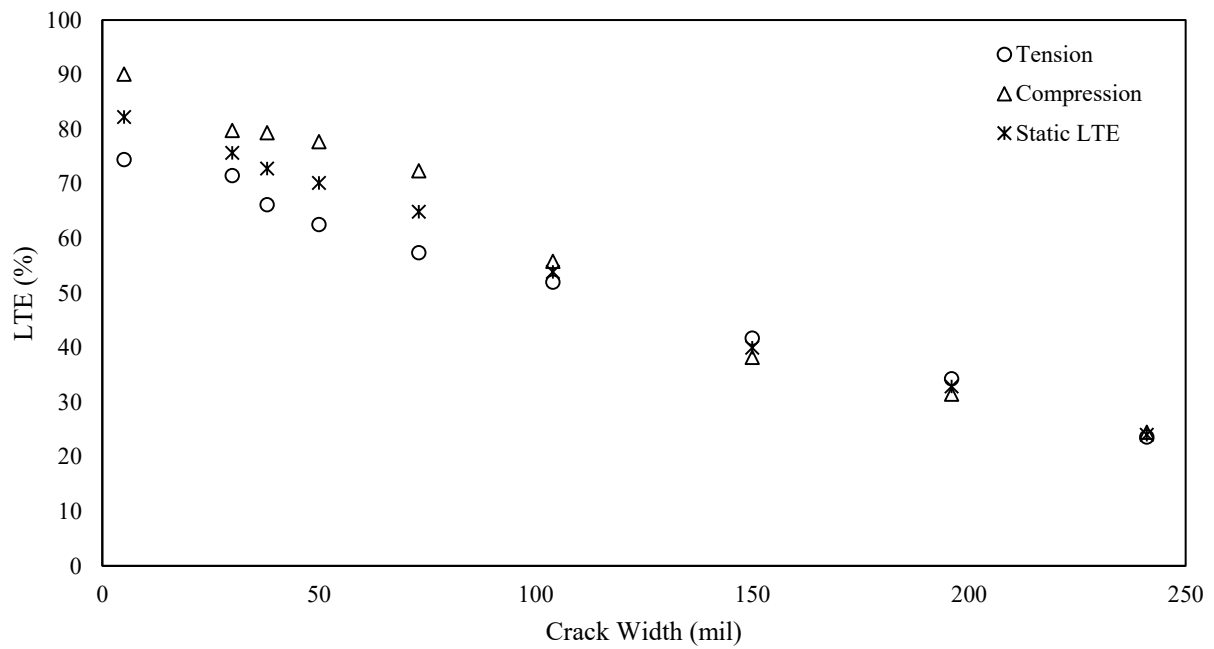
Figure F-81. LTE as a function of crack width.
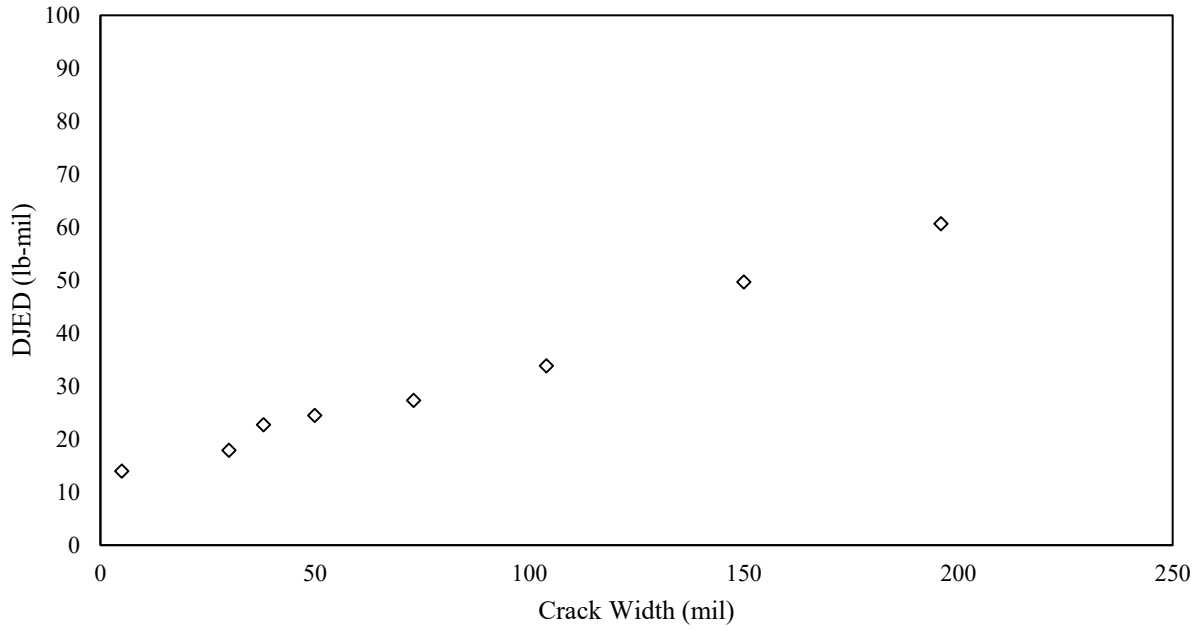
Figure F-82. DJED as a function of crack width.
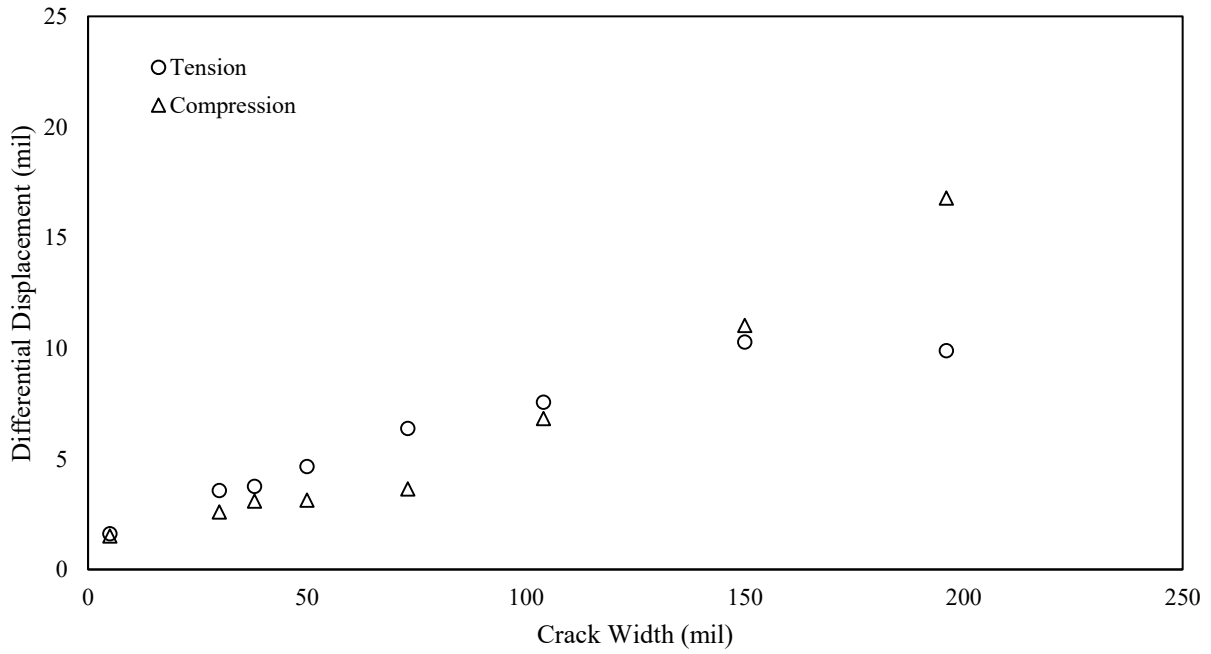
Figure F-83. Differential joint displacement as a function of crack width.
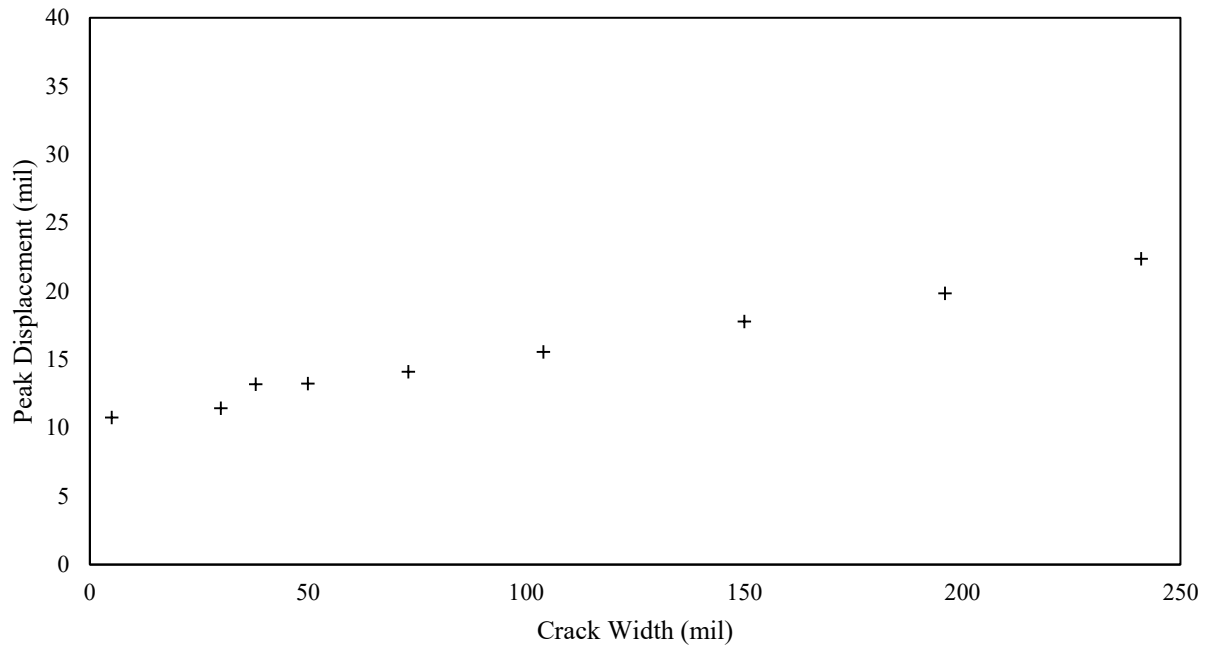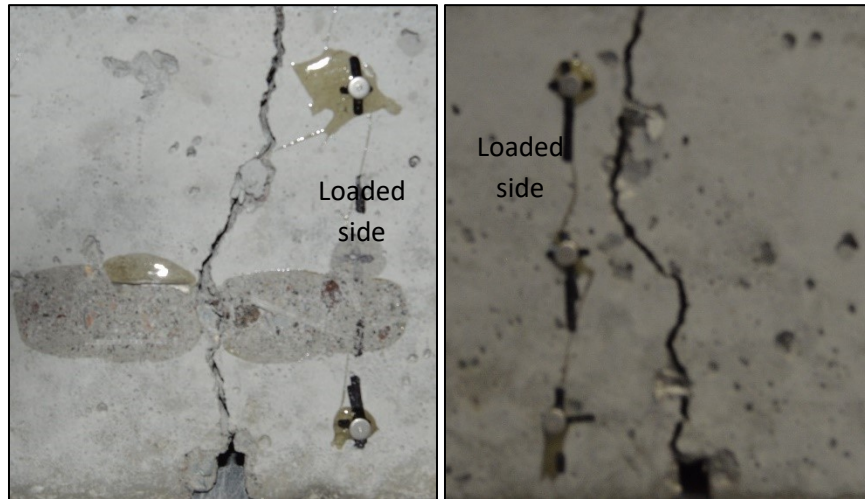
Figure F-84. Average loaded slab displacement as a function of crack width.
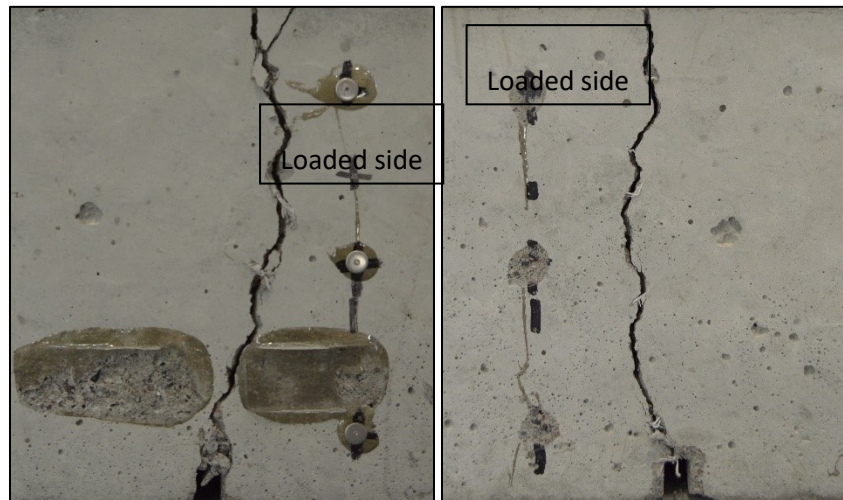
Phase 2: Specimen 1

*NO FATIGUE, ONLY CW VS. PERFORMANCE, SEE PHASE 3

Figure F-85. The front and back of the joint for specimen 1 in phase 2.

Phase 2: Specimen 2

Loaded side

Loaded side
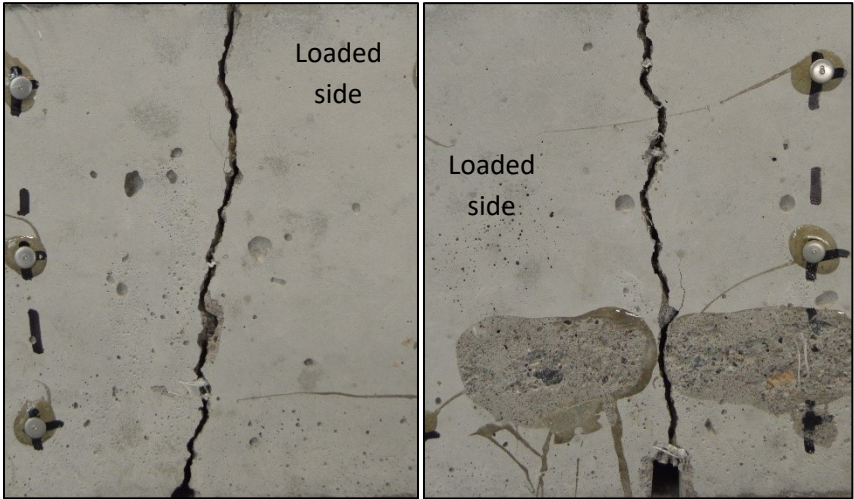
*NO FATIGUE, ONLY CW VS. PERFORMANCE, SEE PHASE 3

Figure F-86. The front and back of the joint for specimen 2 in phase 2.

Phase 2: Specimen 3

Loaded side

Loaded side
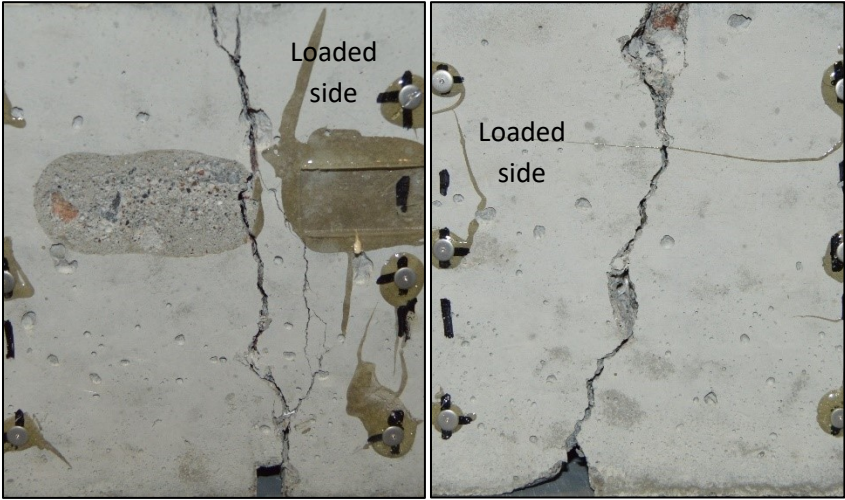
Figure F-87. The front and back of the joint for specimen 3 in phase 2.
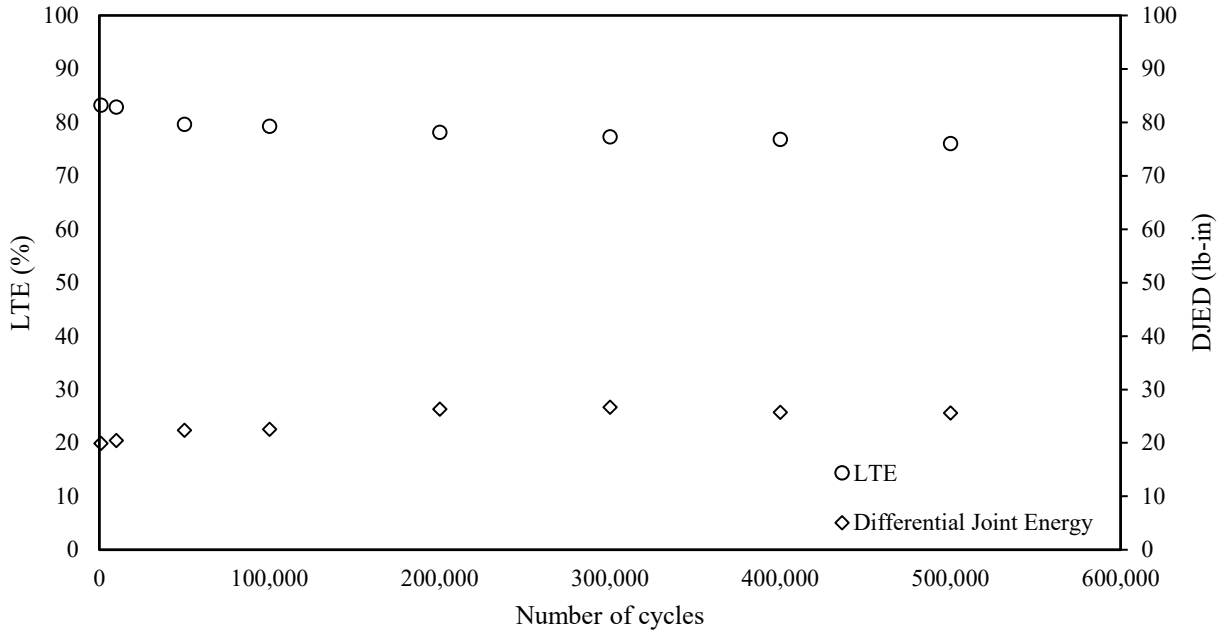
*Crack width ranged from 49 mils to 51 mils

Figure F-88. LTE and DJED as a function of repetitions (cycles).

Phase 3: Contraction and Rebound Performance
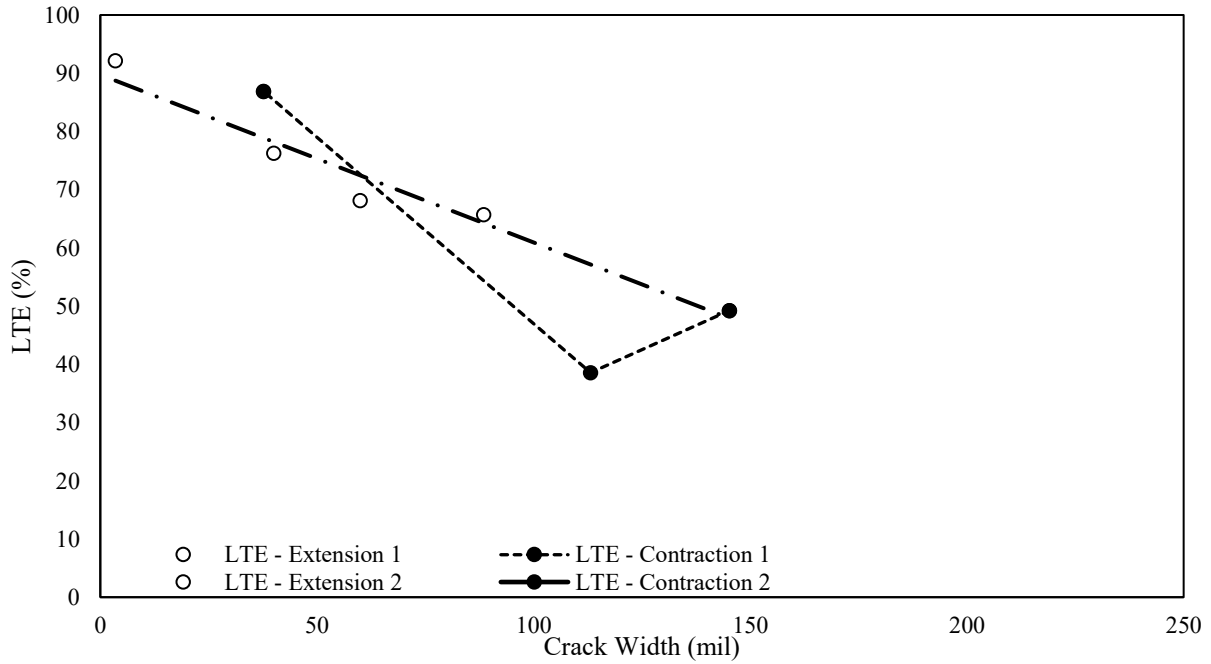
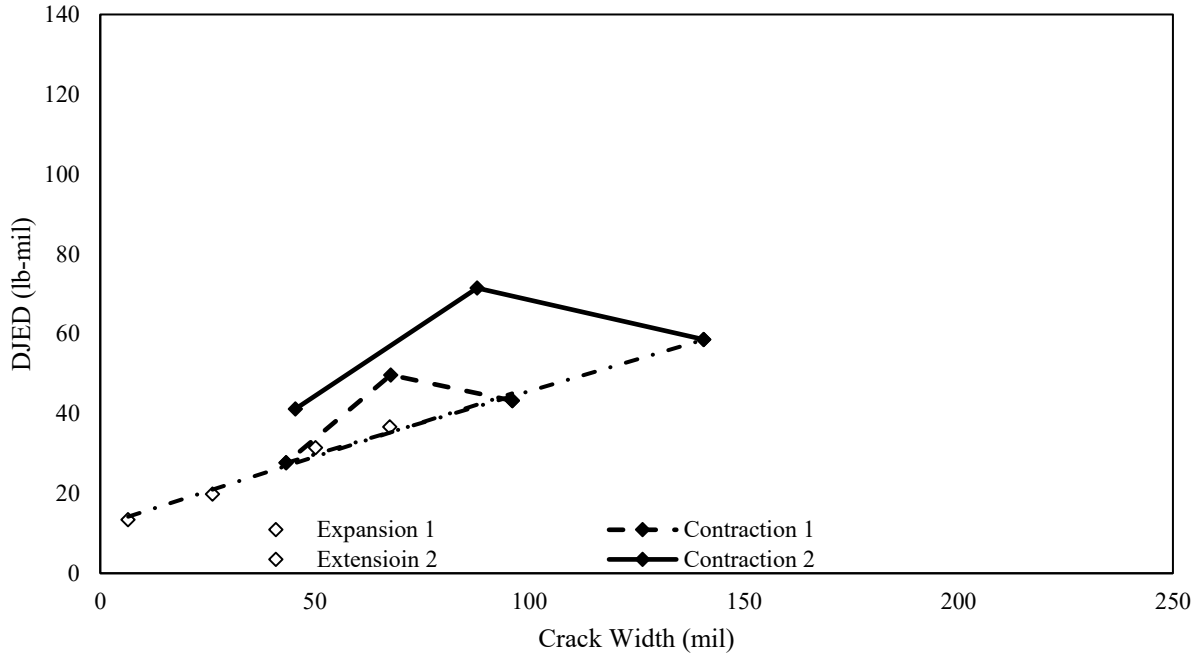**Figure F-89. The effect of joint expansion and contraction on LTE in terms of crack width (phase 2: specimen 1).**
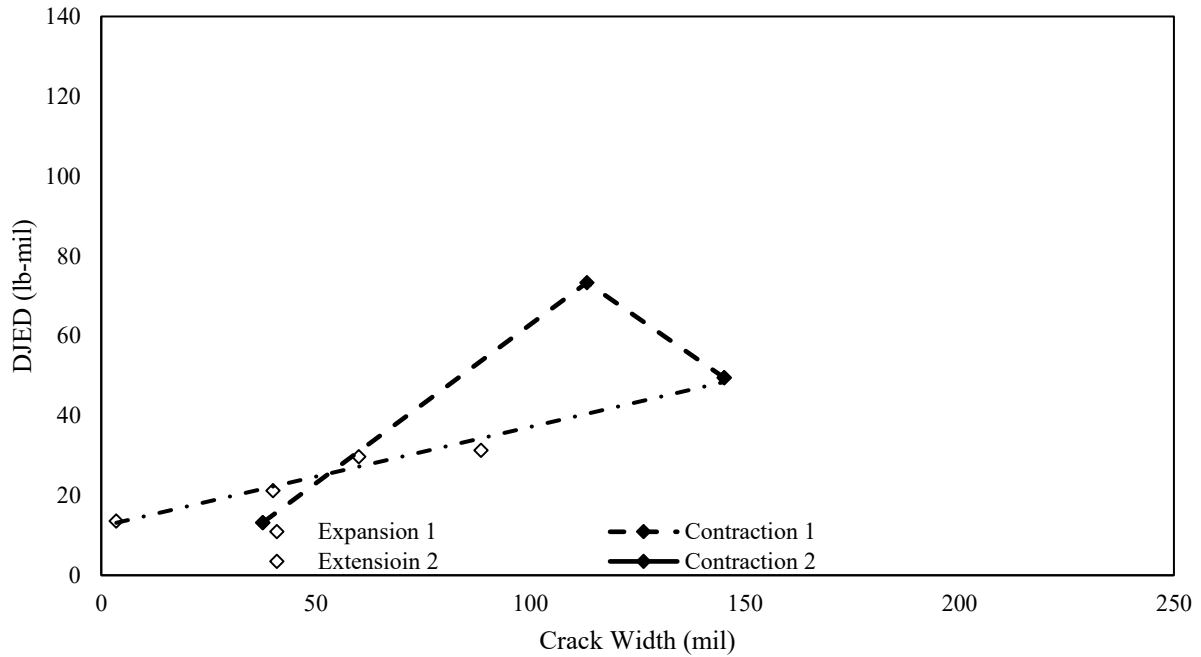
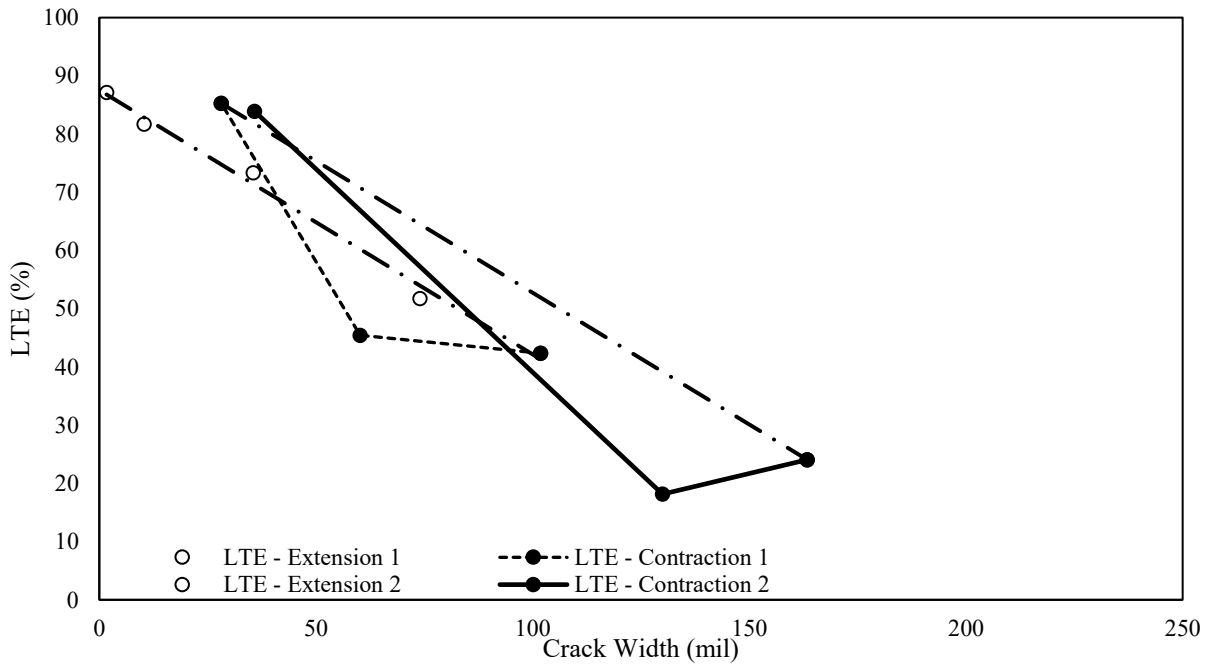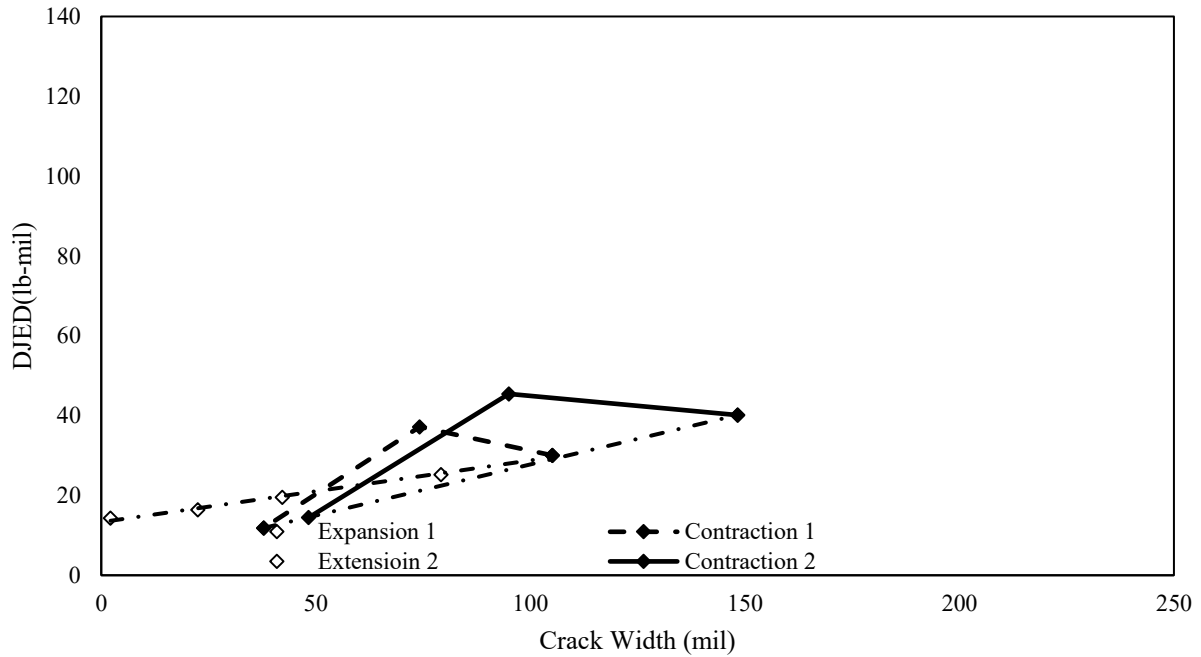**Figure F-90. The effect of joint expansion and contraction on DJED in terms of crack width (phase 2: specimen 1).**
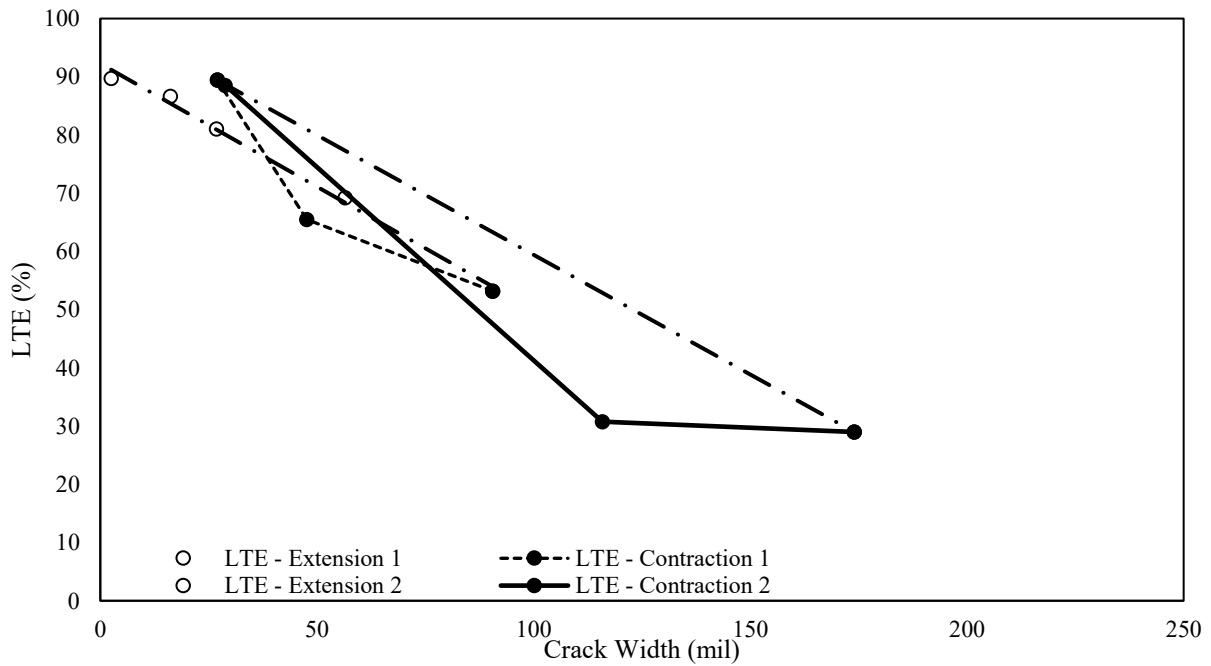
Figure F-91. The effect of joint expansion and contraction on LTE in terms of crack width (phase 2: specimen 2).
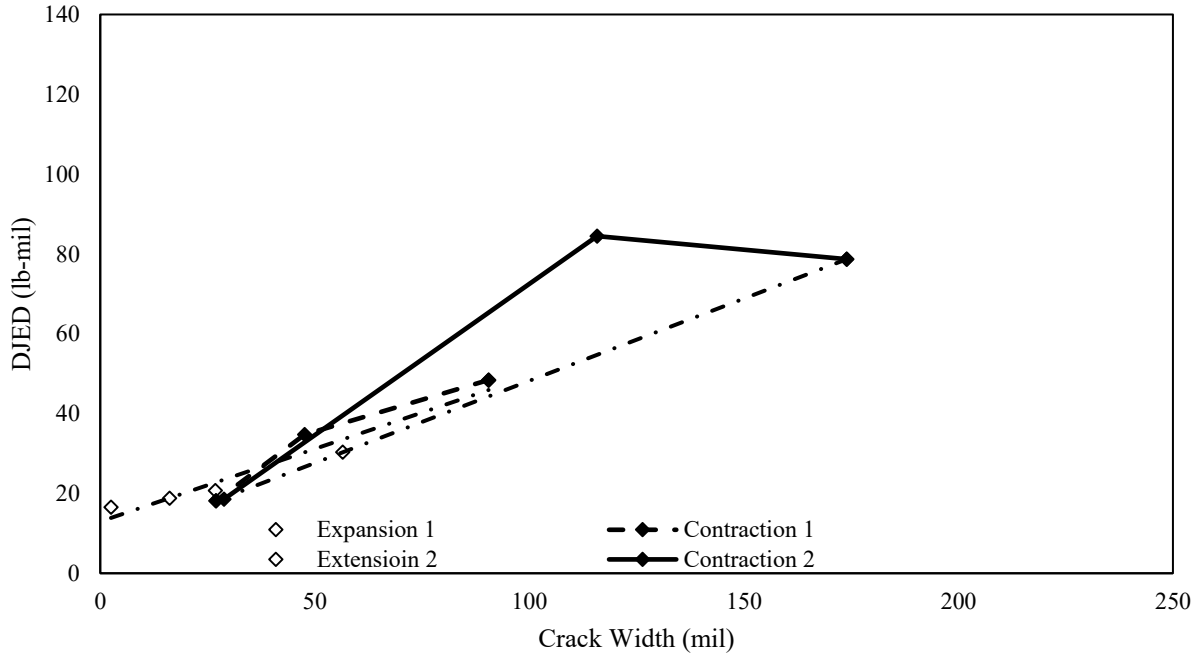
Figure F-92. The effect of joint expansion and contraction on DJED in terms of crack width (phase 2: specimen 2).
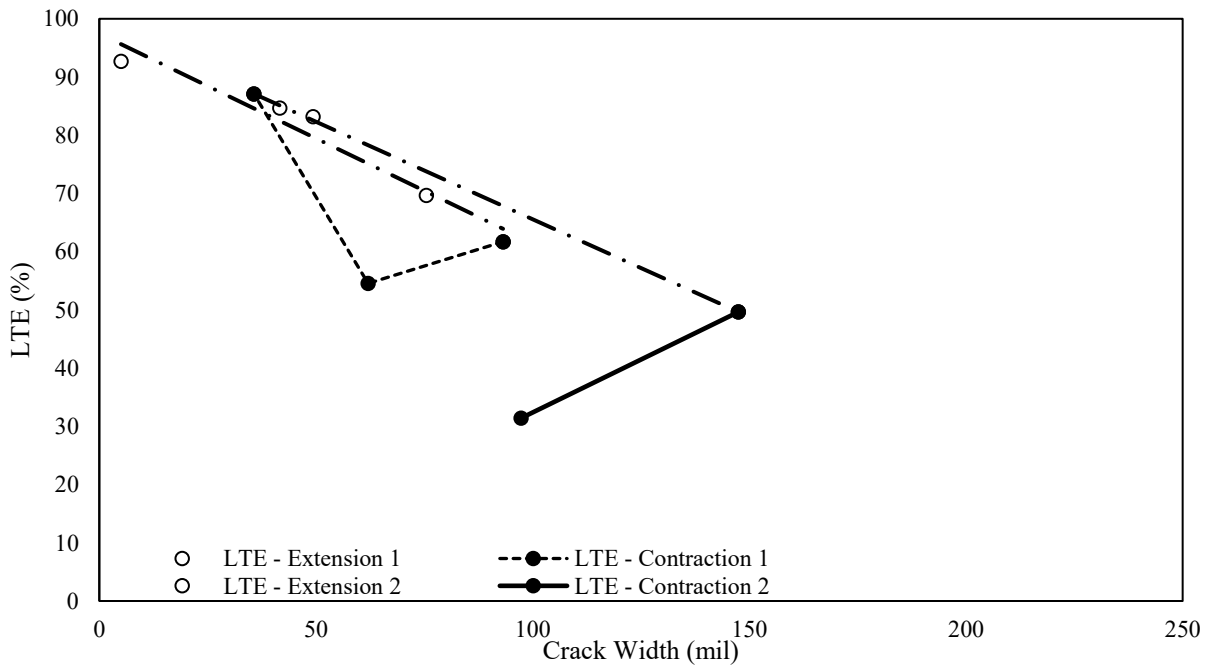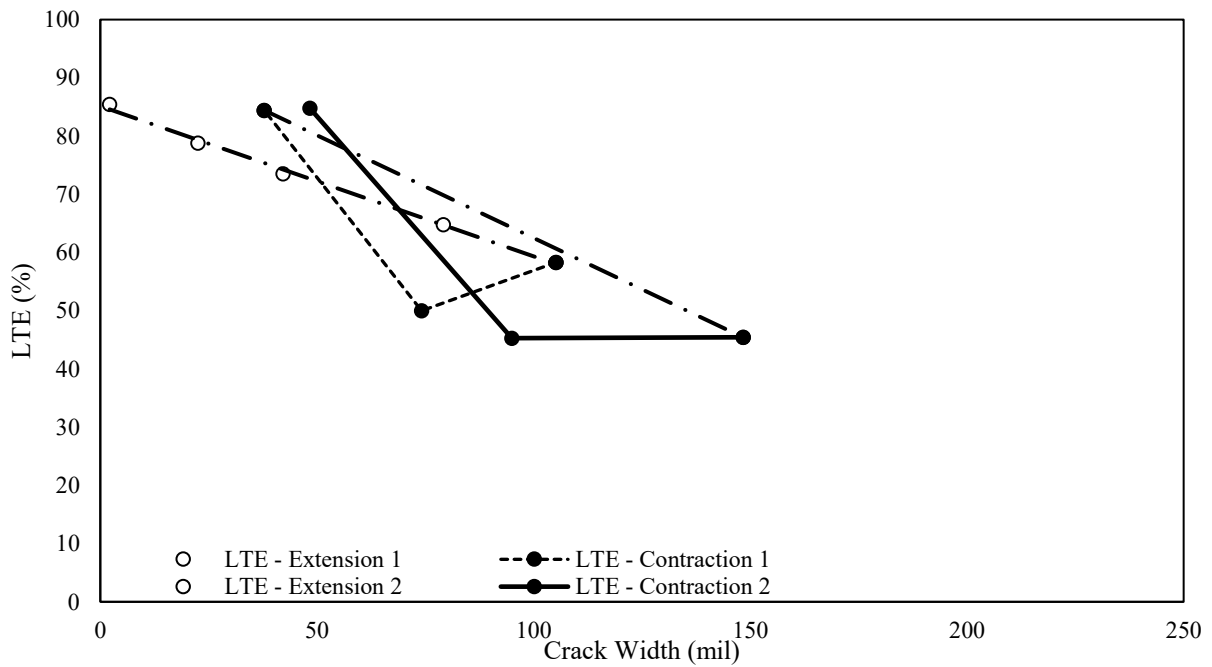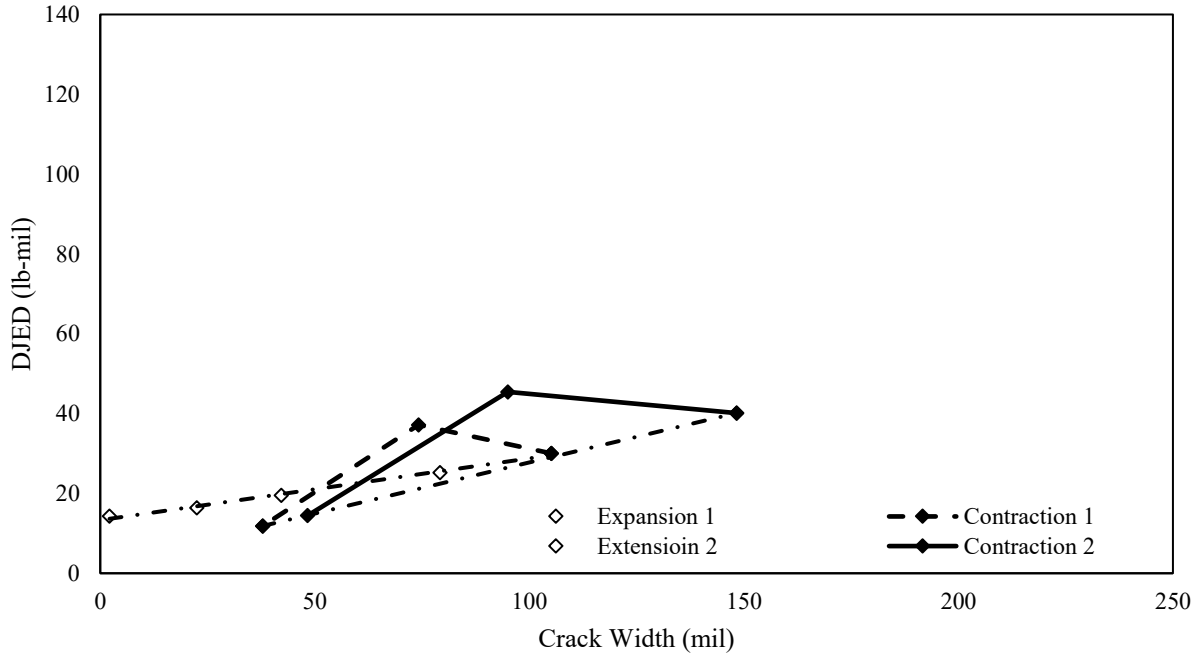

Figure F-93. The effect of joint expansion and contraction on LTE in terms of crack width (phase 2: specimen 3).
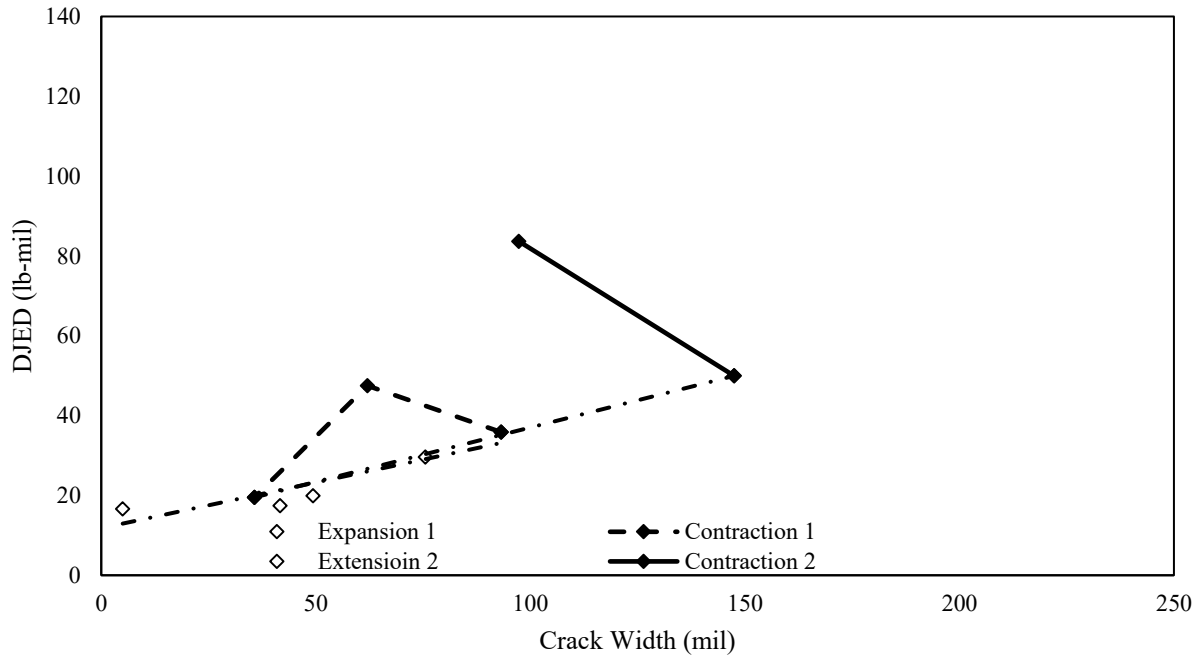
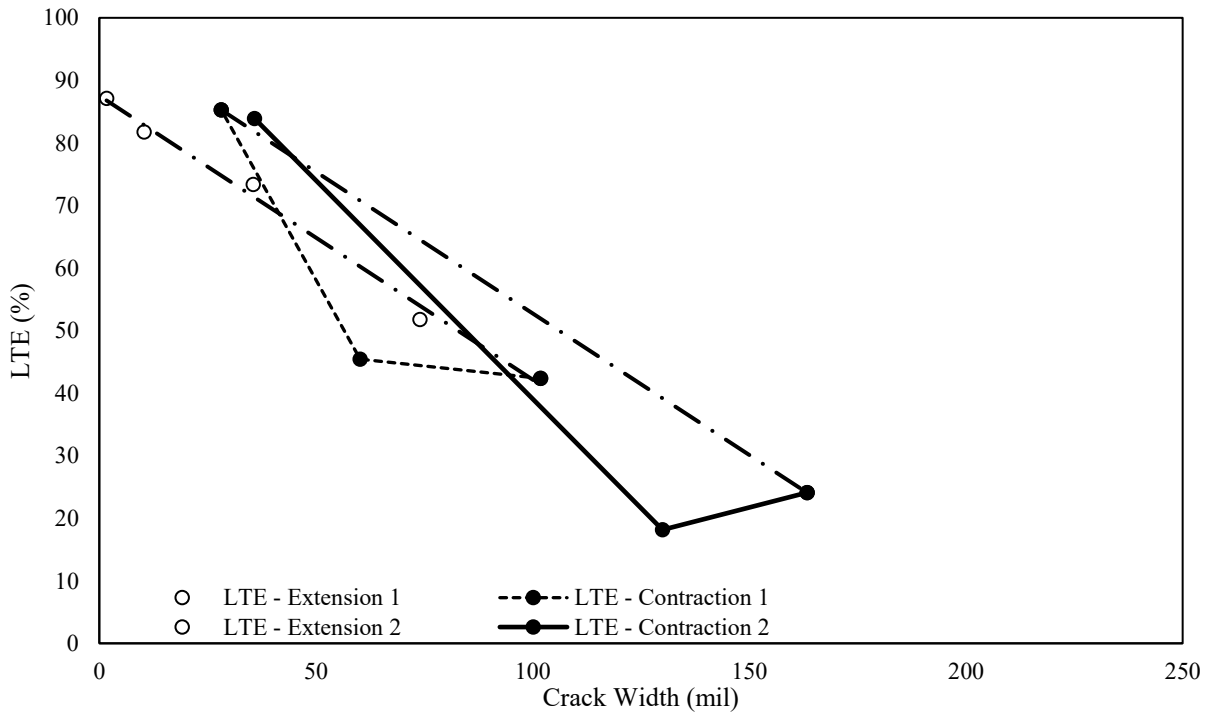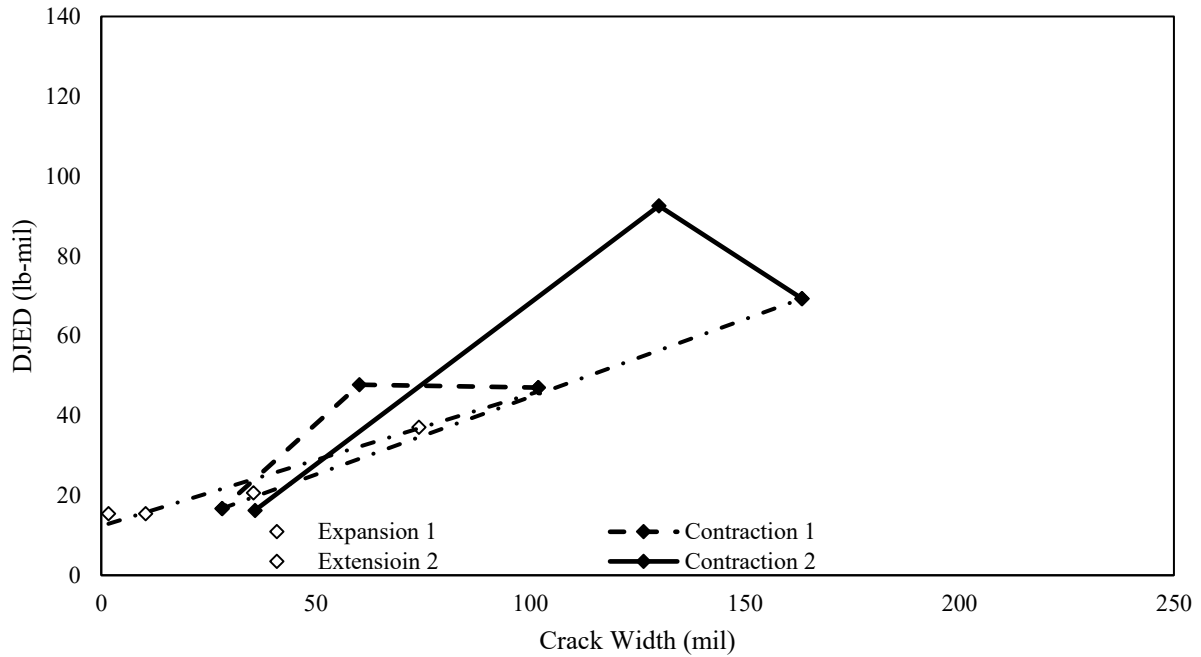**Figure F-94. The effect of joint expansion and contraction on DJED in terms of crack width (phase 2: specimen 3).**

S.C.6.5

Phase 1: Specimen 1
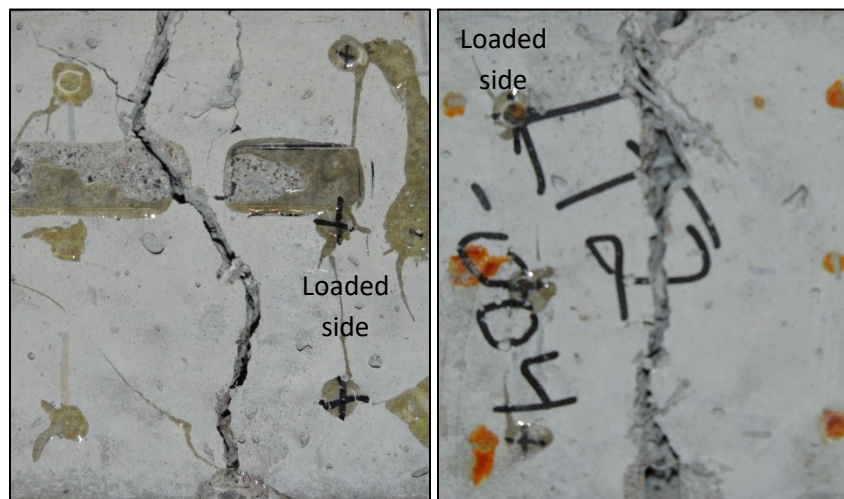
Figure F-95. The front and back of the joint for specimen 1 in phase 1.
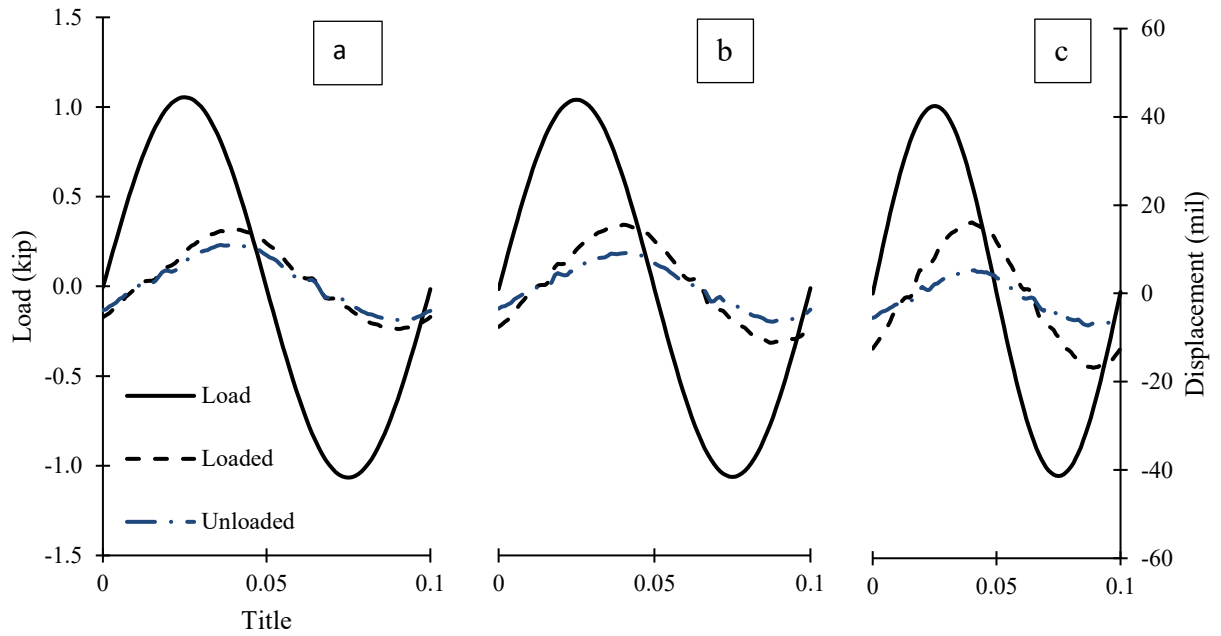
Figure F-96.Cyclical plots for (a) 10 mils, (b) 47 mils, and (c) 114 mils crack widths.
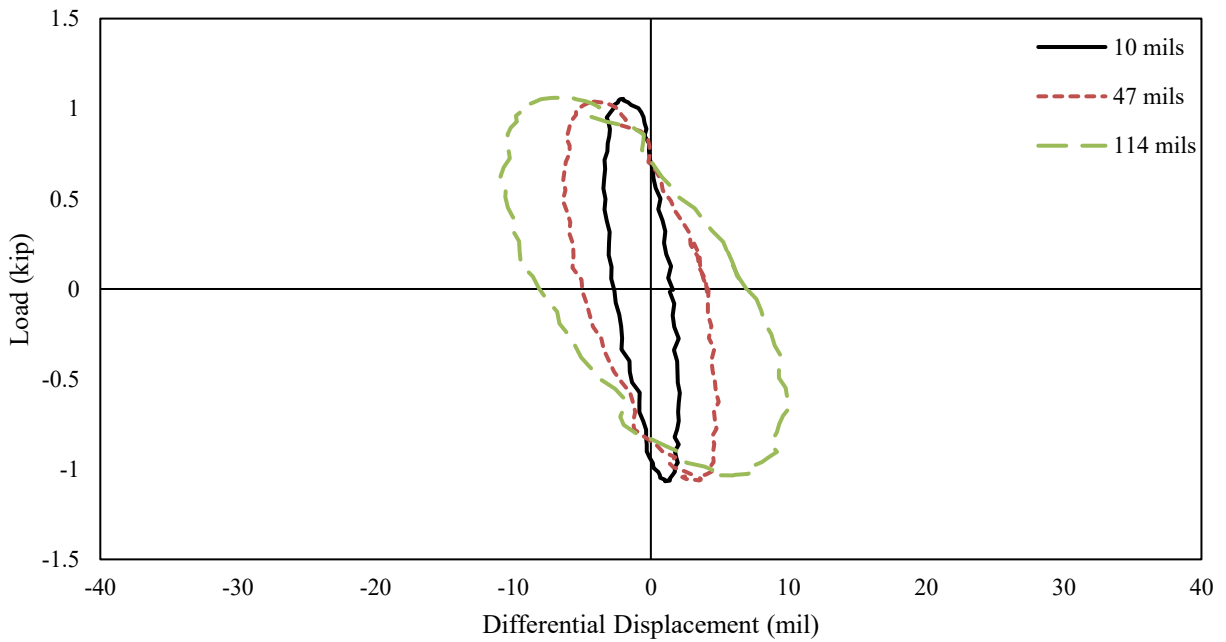
Figure F-97. Hystereses at 10 mils, 47 mils and, 114 mils crack width.
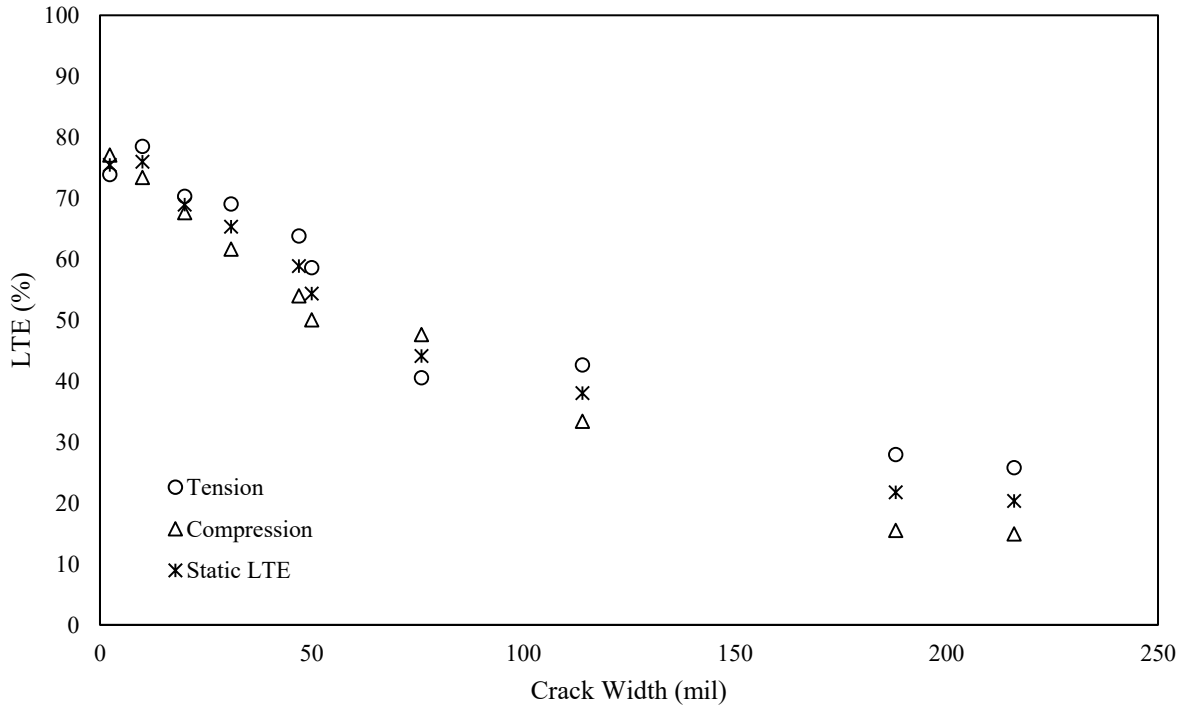
Figure F-98. LTE as a function of crack width.
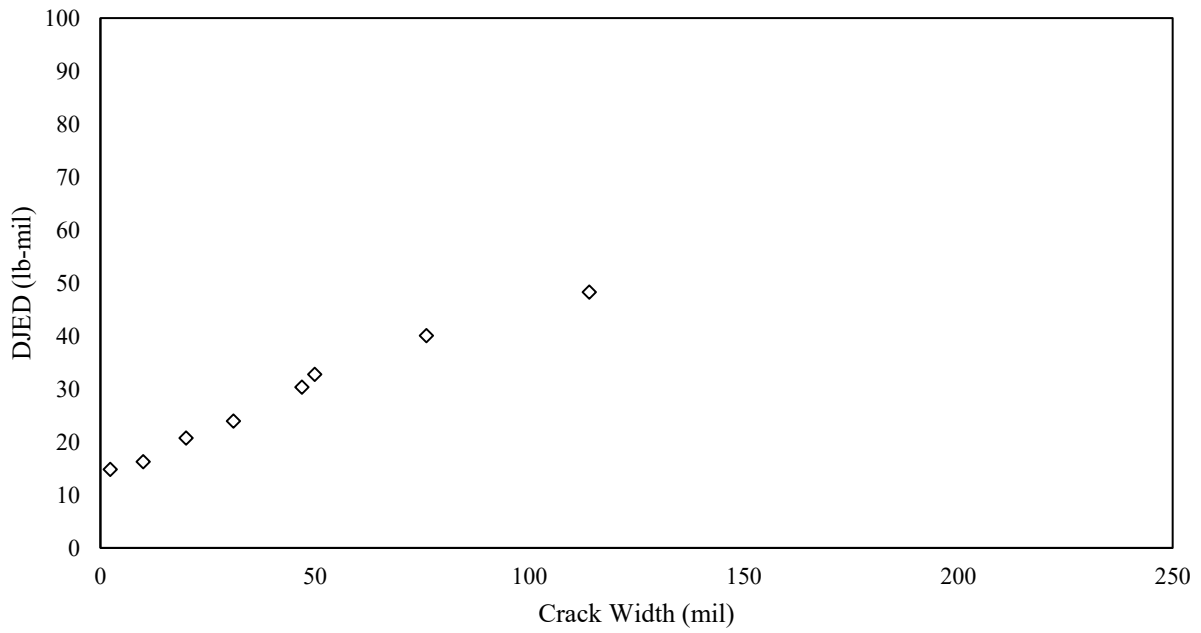
Figure F-99. DJED as a function of crack width.
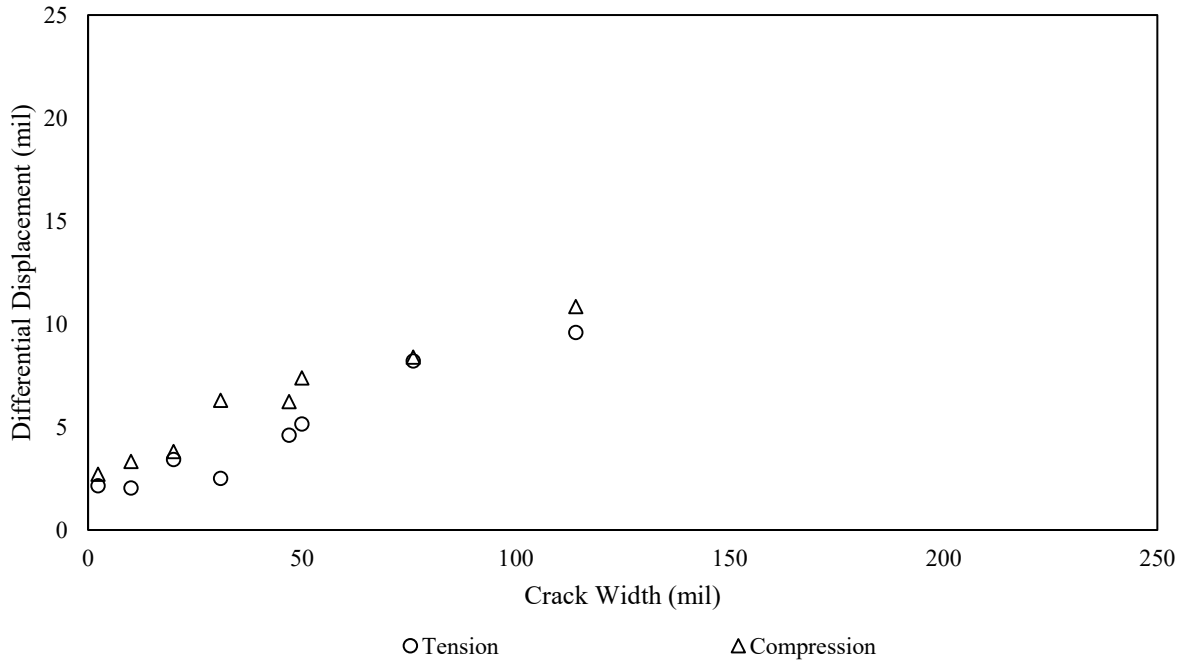
Figure F-100. Differential joint displacement as a function of crack width.
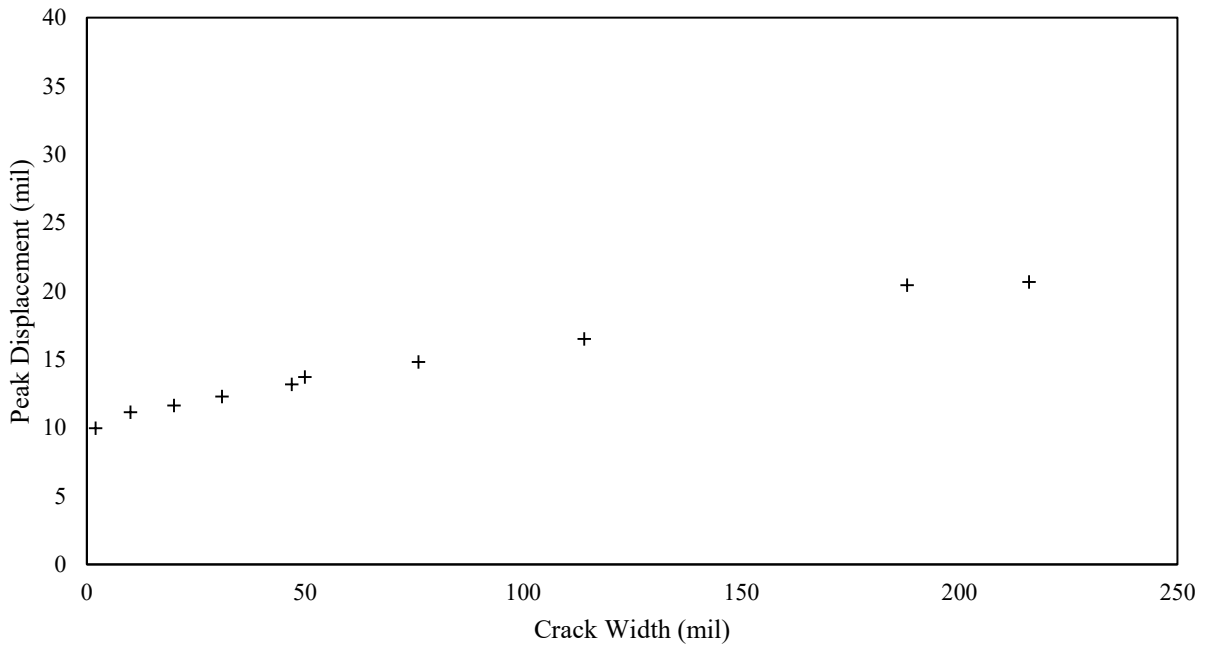
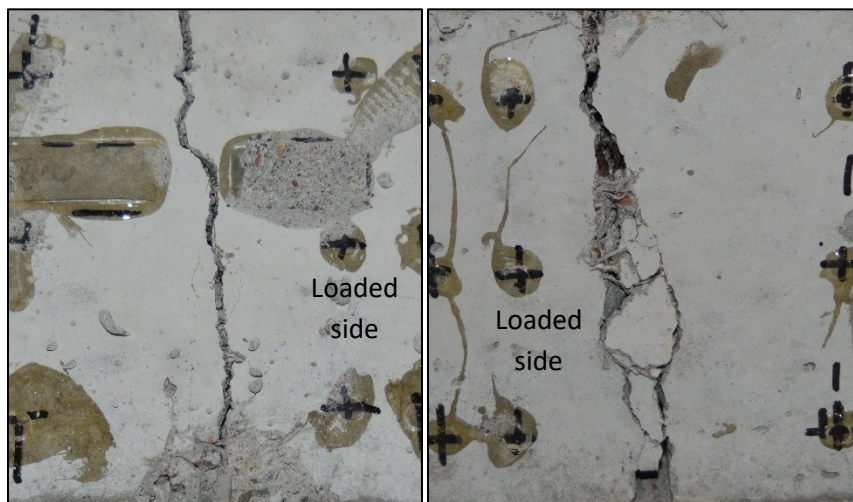**Figure F-101. Peak displacement as a function of crack width.**

F-51
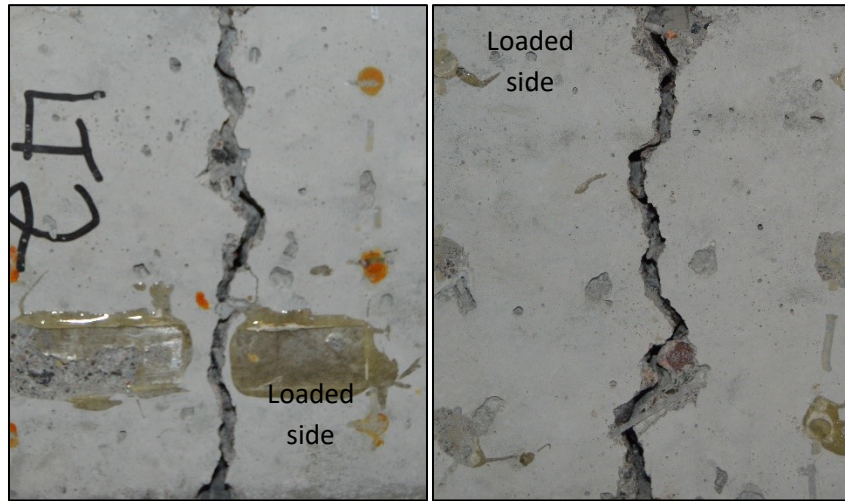
Figure F-102. The front and back of the joint for specimen 2 in phase 1.
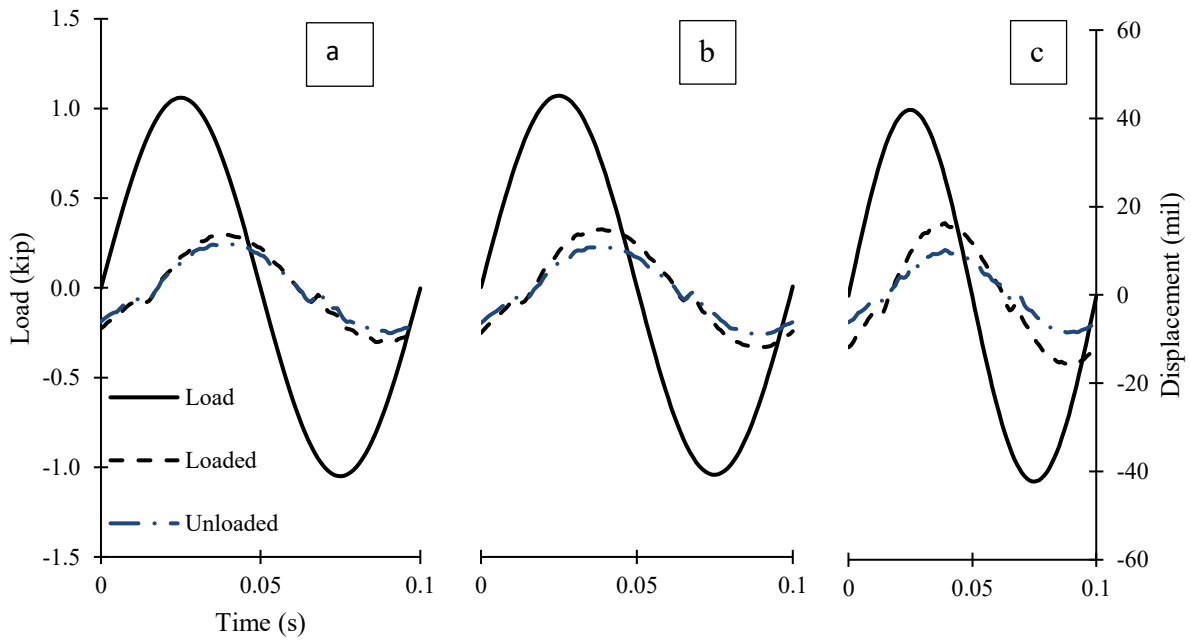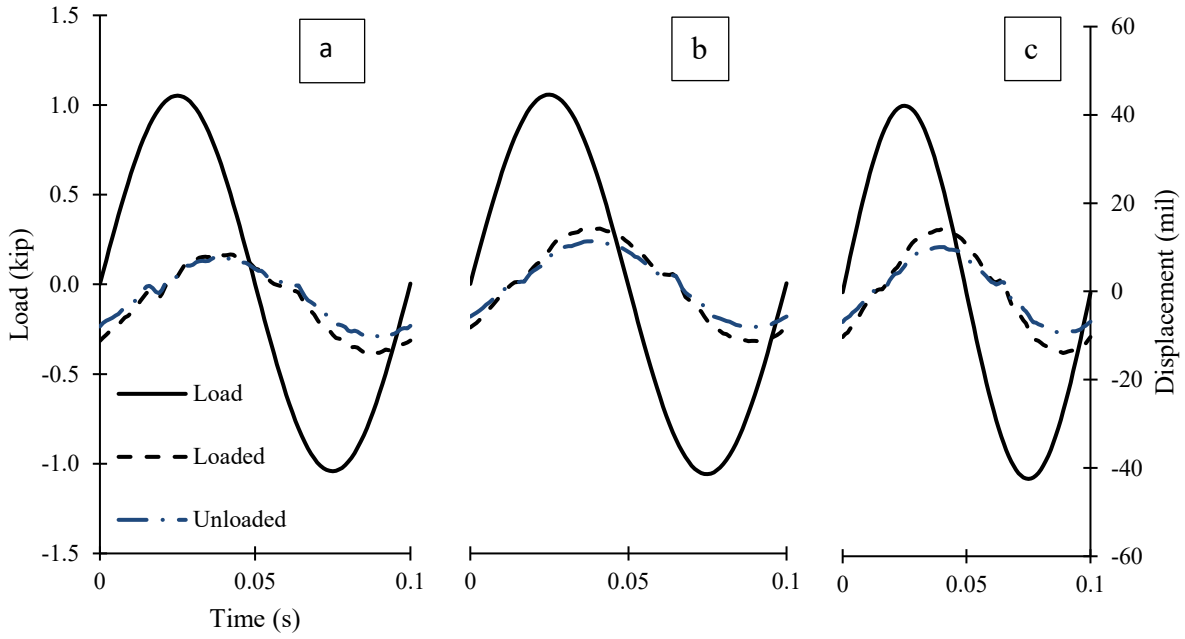

Figure F-103. Cyclical plots for (a) 13 mils, (b) 58 mils, and (c) 112 mils crack widths.
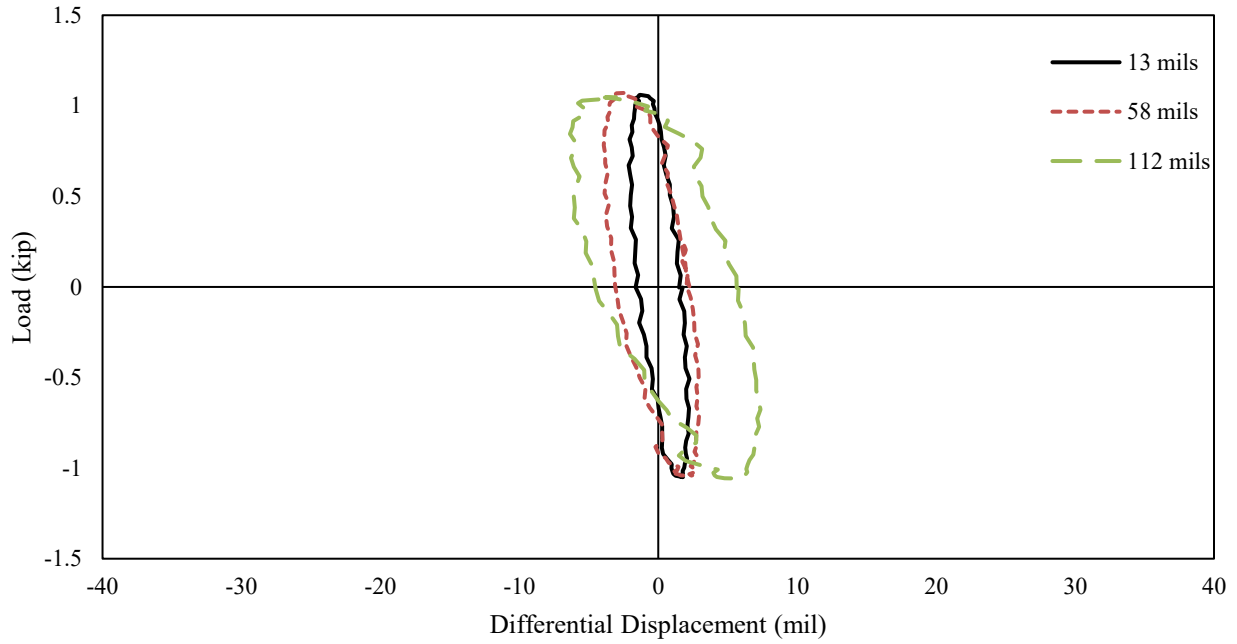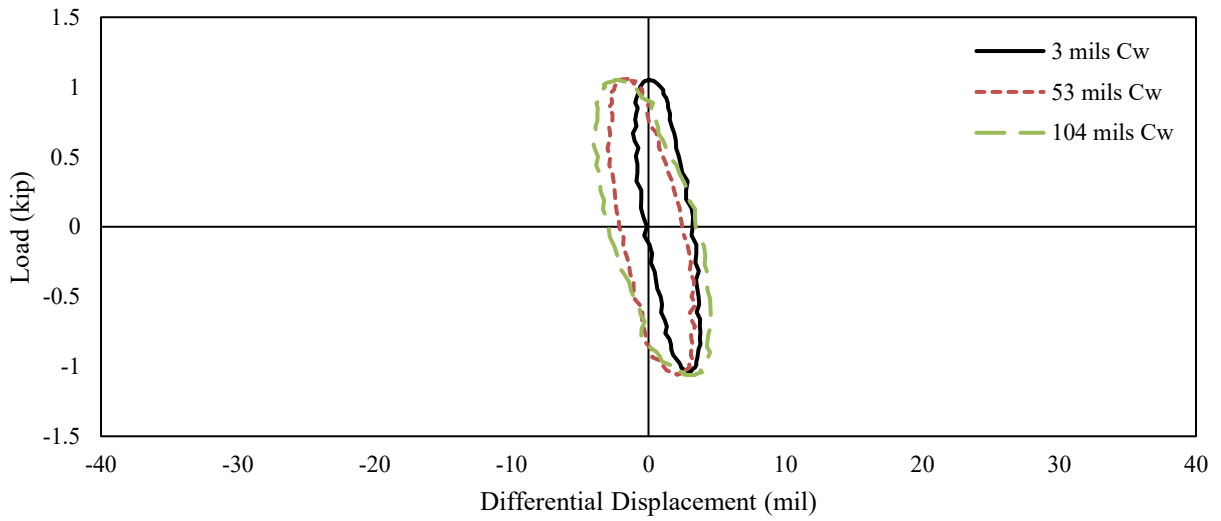
Figure F-104. Hystereses for 13 mils, 58 mils, and 112 mils crack widths.
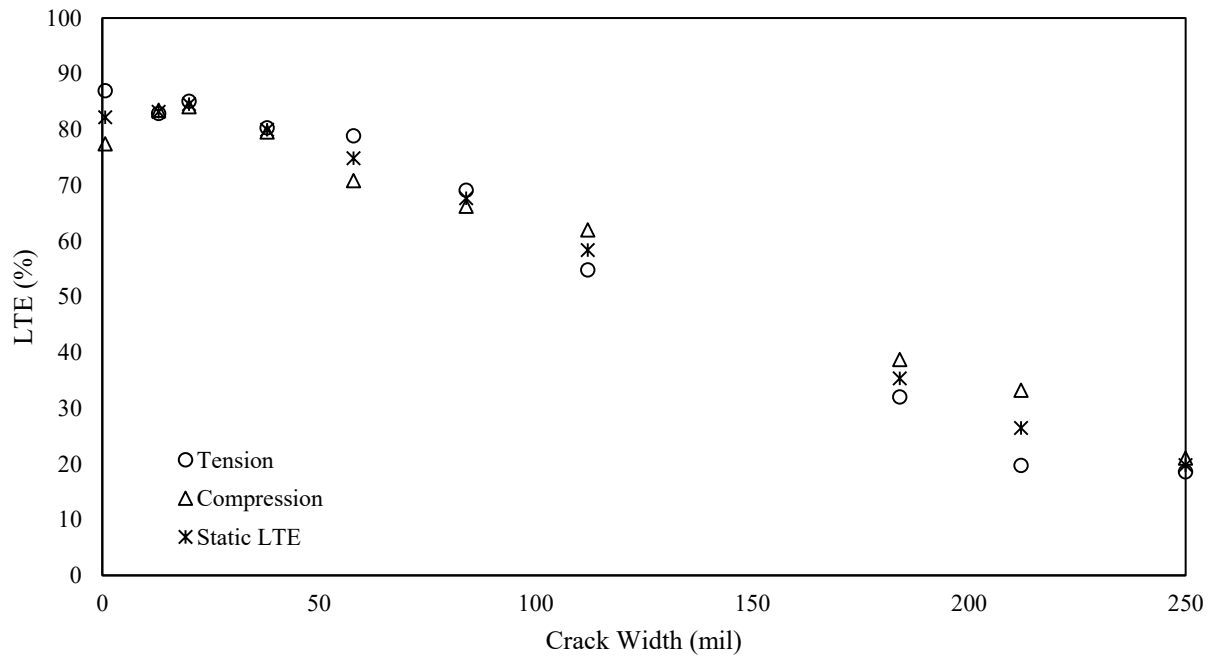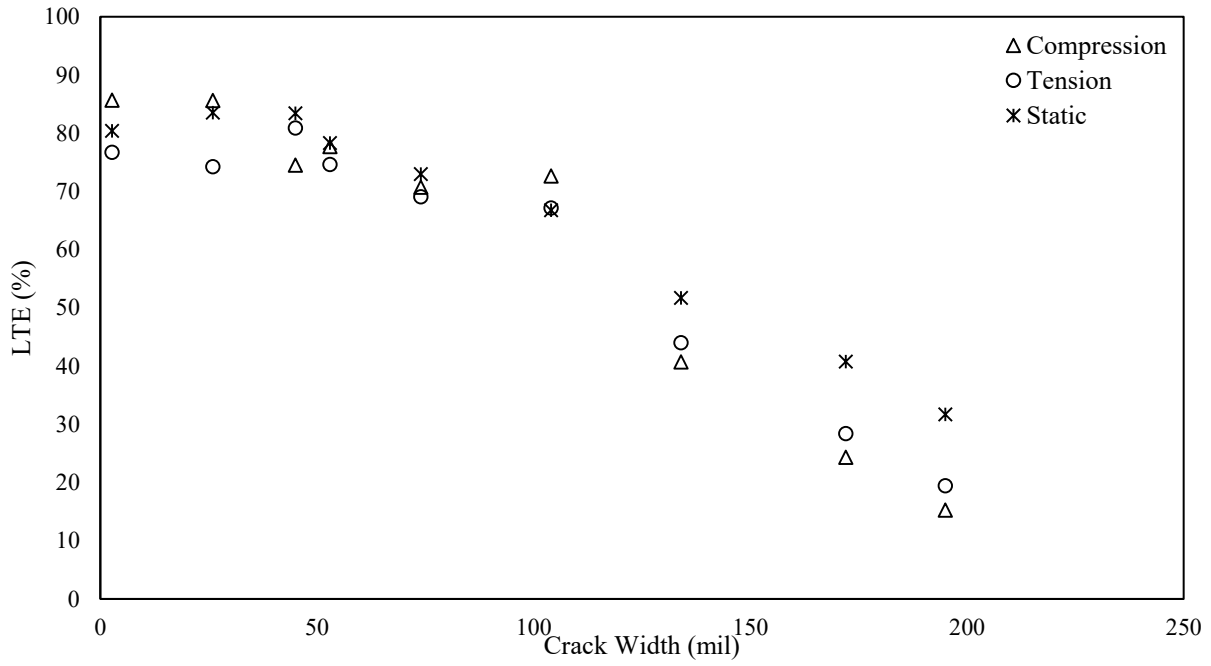

Figure F-105. LTE as a function of crack width.
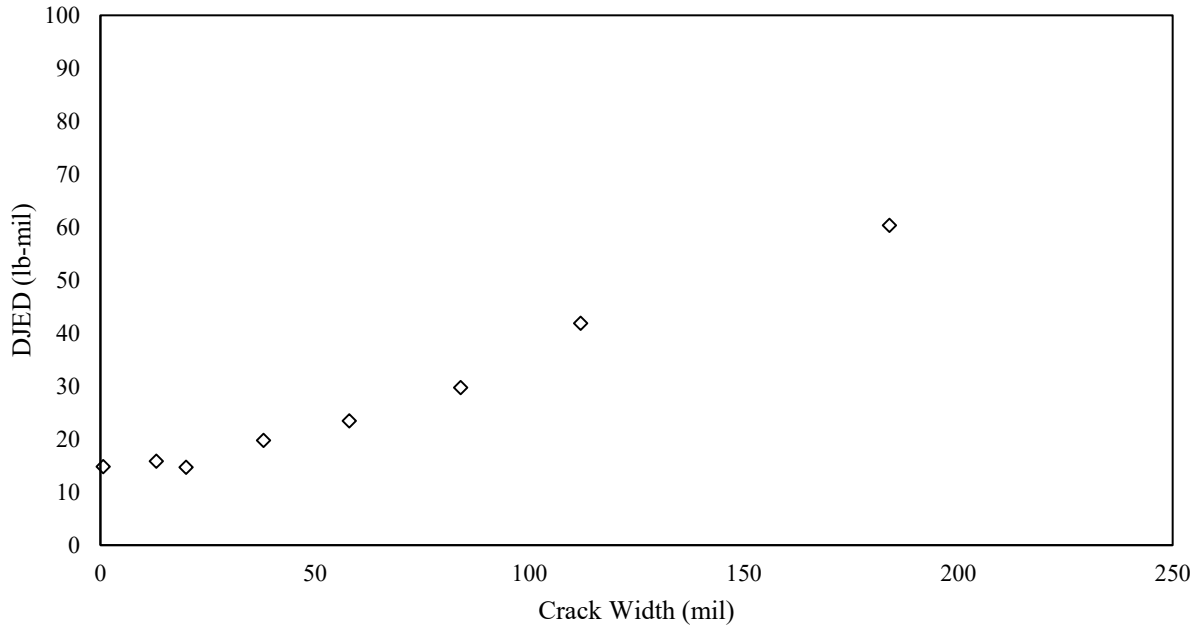
Figure F-106. DJED as a function of crack width.
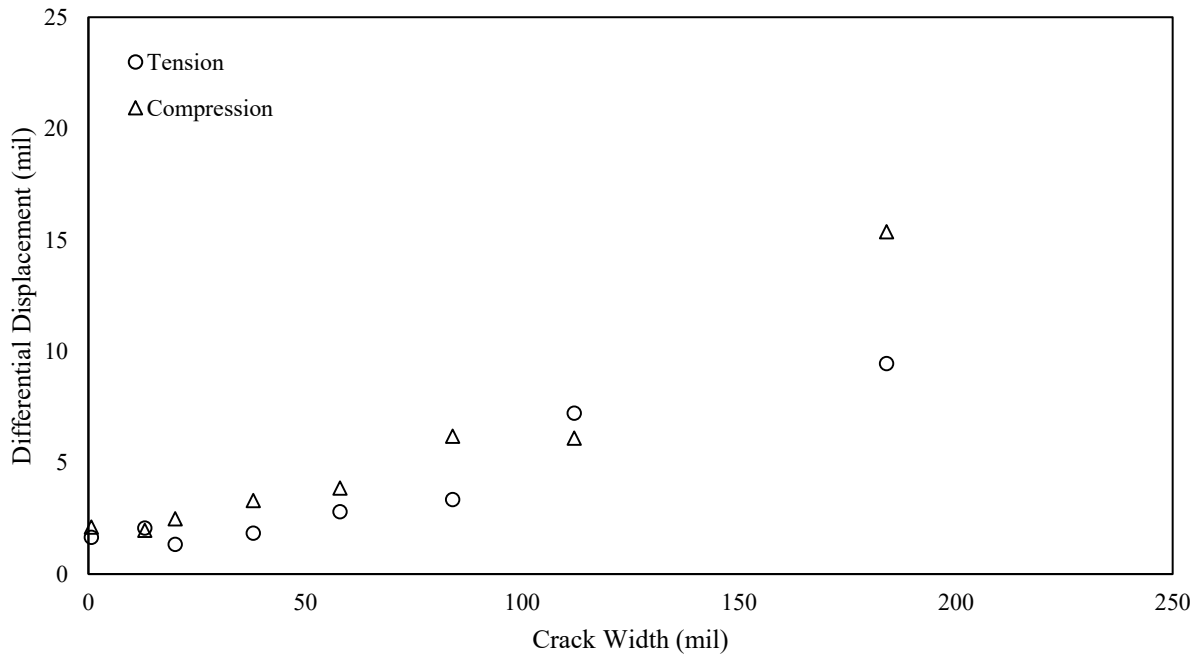
Figure F-107. Differential joint displacement as a function of crack width.
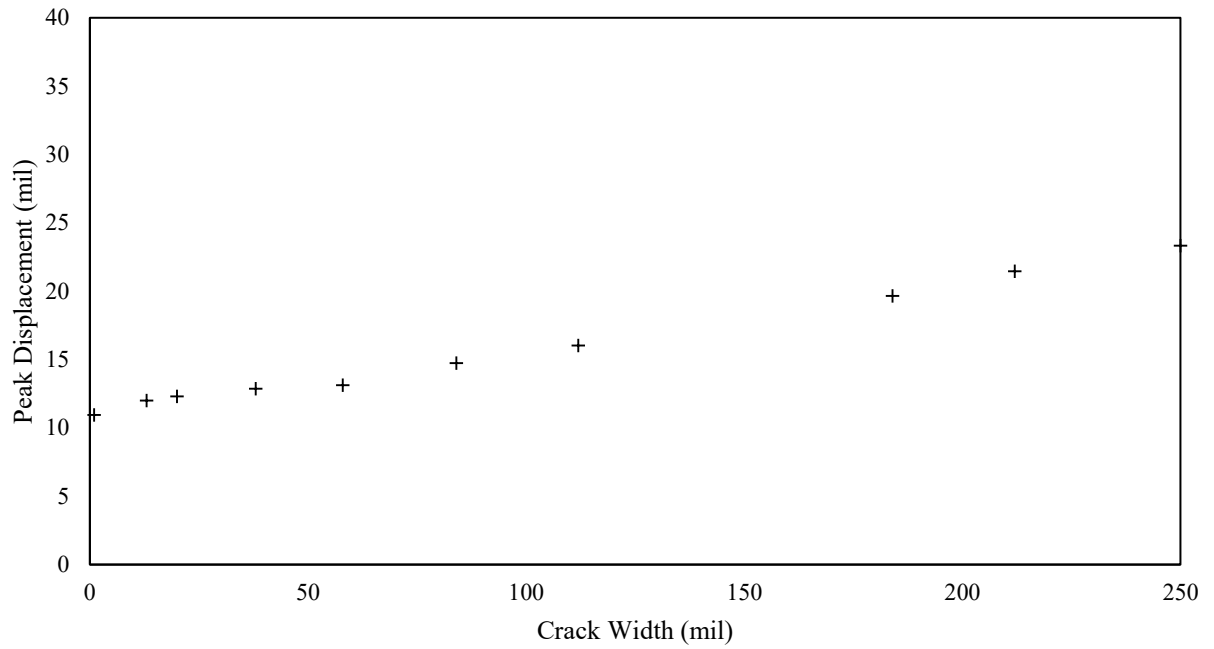
Figure F-108. Peak displacement as a function of crack width.

Phase 1: Specimen 3
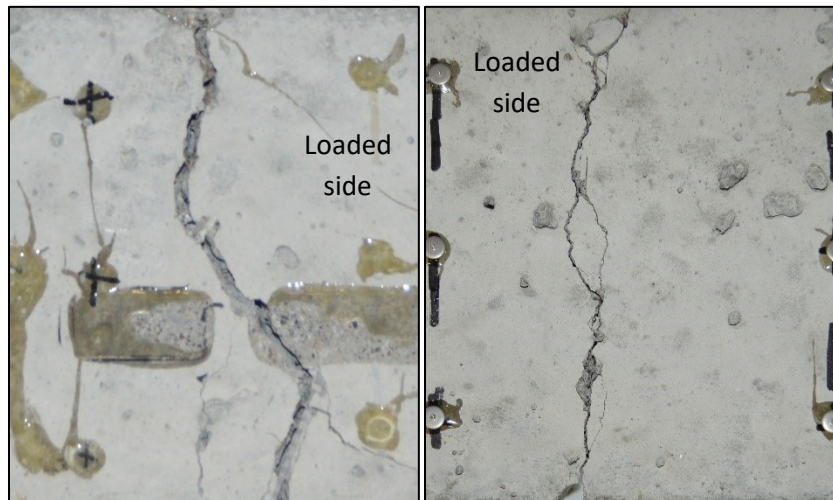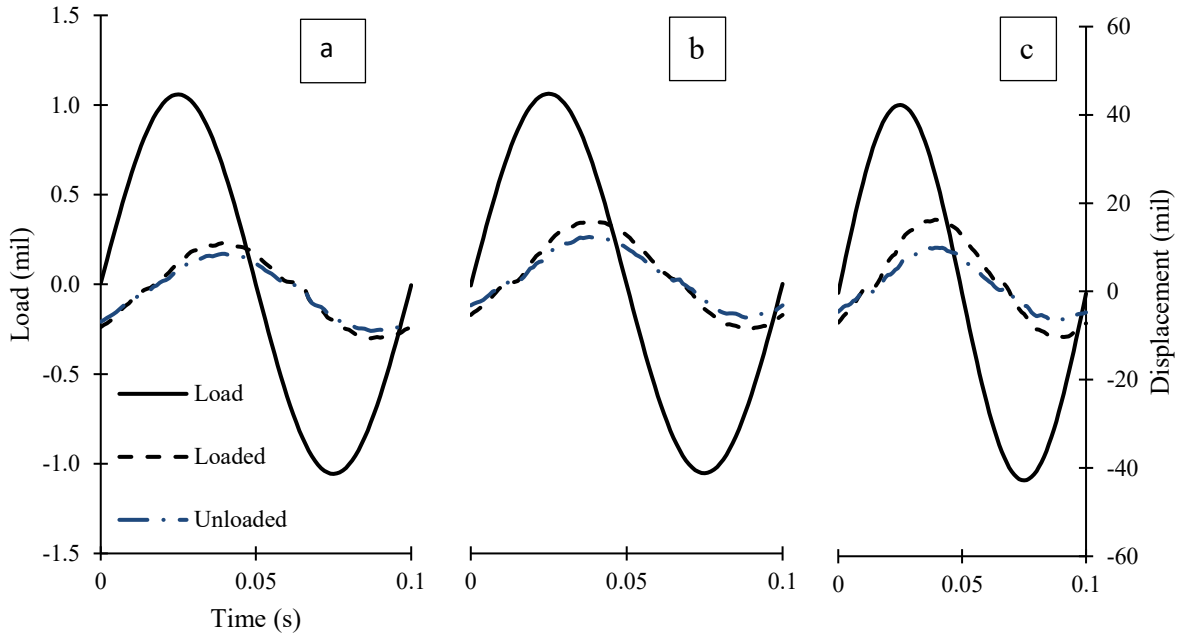
Figure F-109. Cyclical plots for (a) 3.2 mils, (b) 52 mils, and (c) 101 mils crack widths.
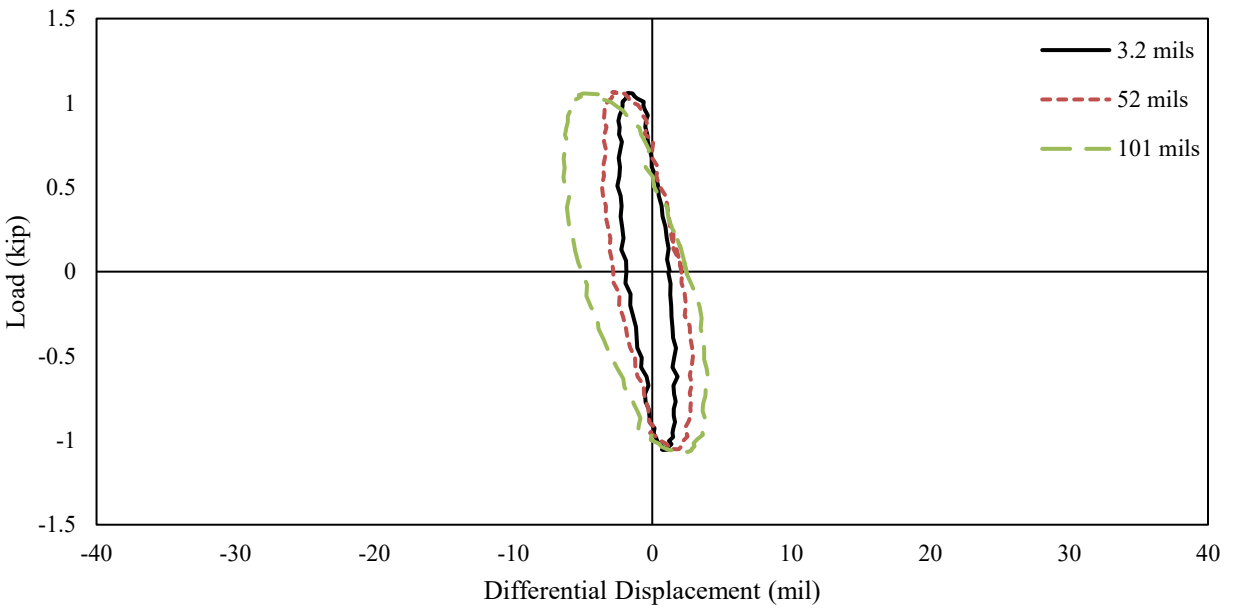
Figure F-110. Hystereses for 3.2 mils, 52 mils, and 101 mils crack widths.
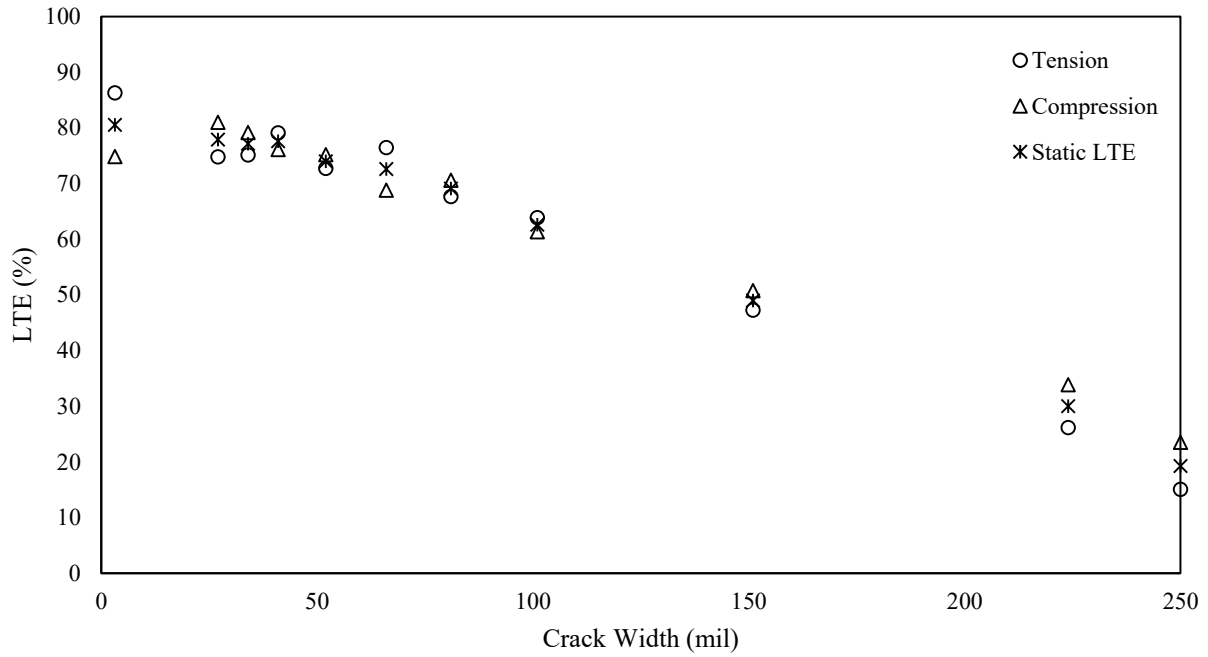
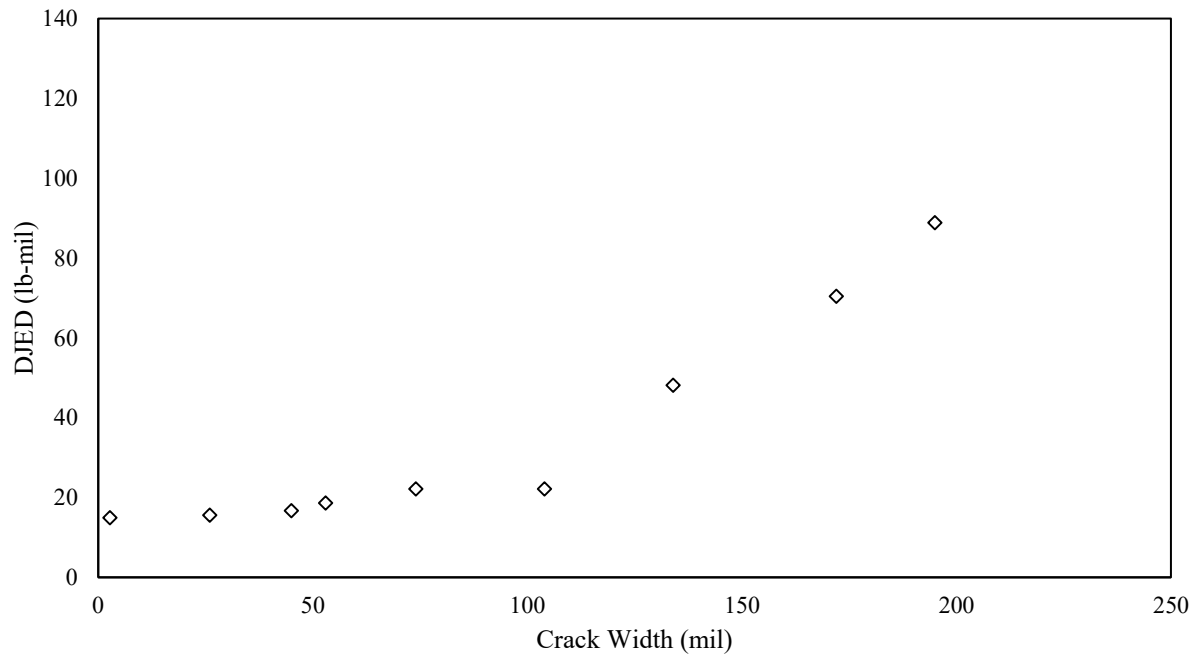**Figure F-111. LTE as a function of crack width.**
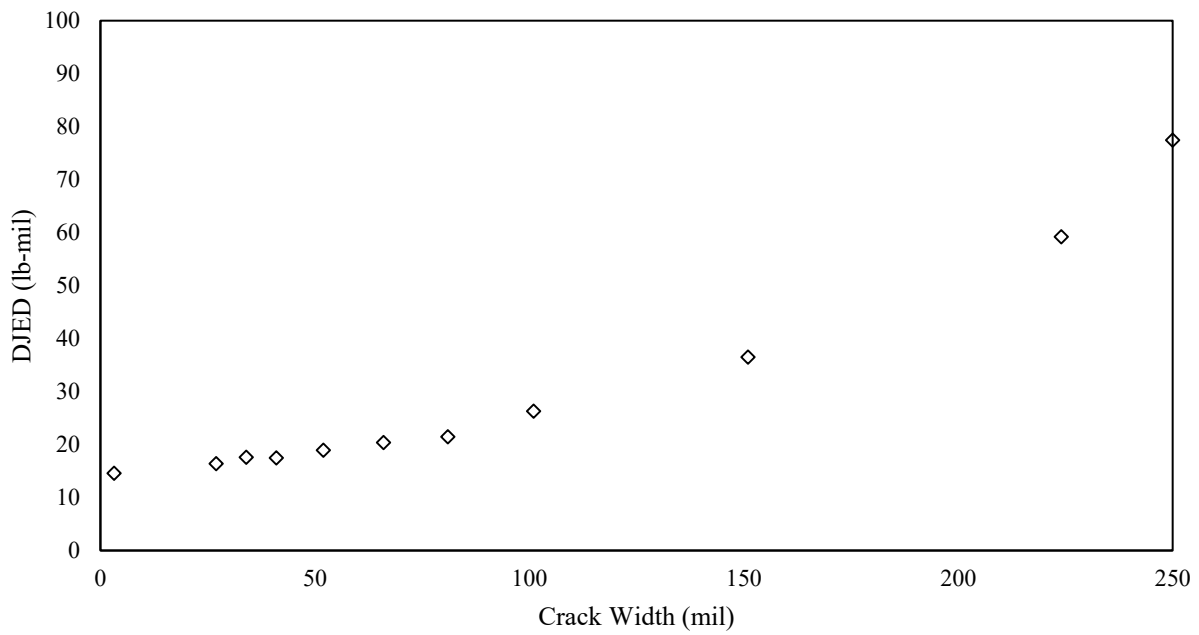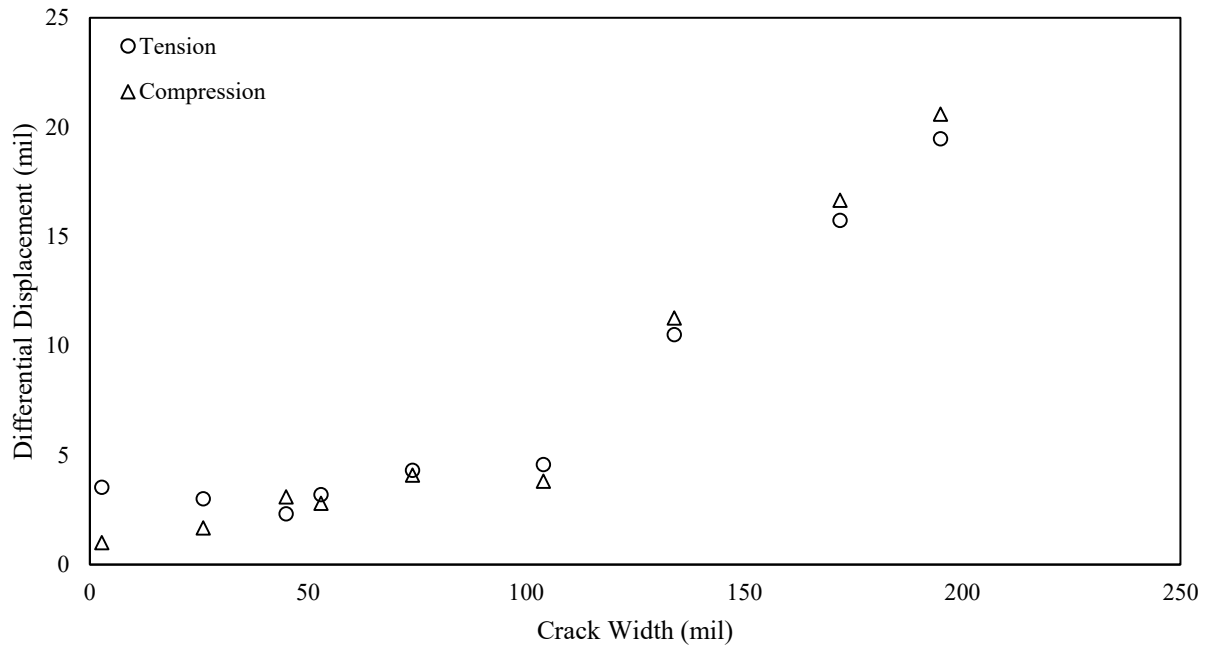

Figure F-112. DJED as a function of crack width.
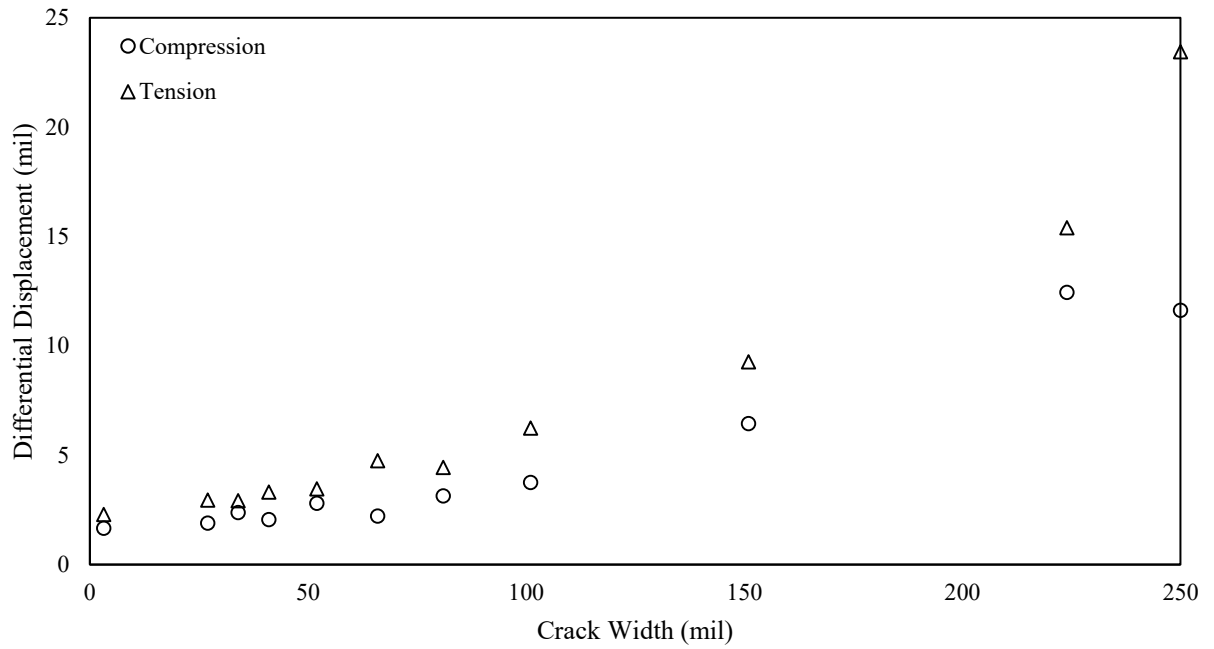
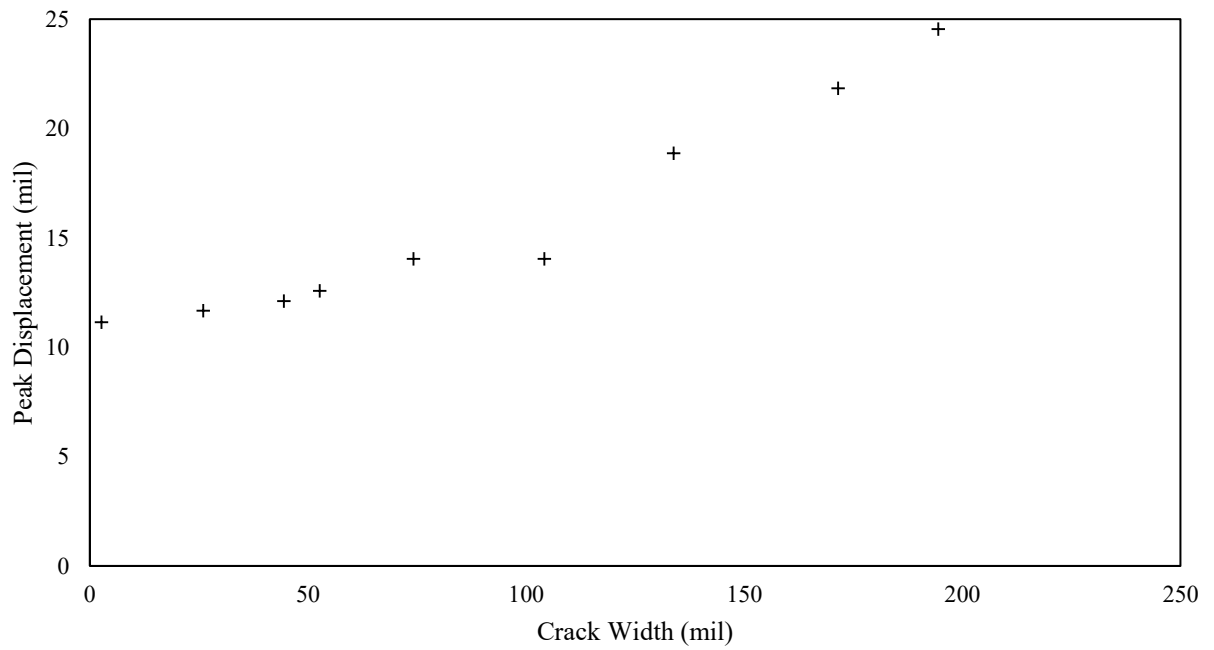**Figure F-113. Differential joint displacement as a function of crack width.**
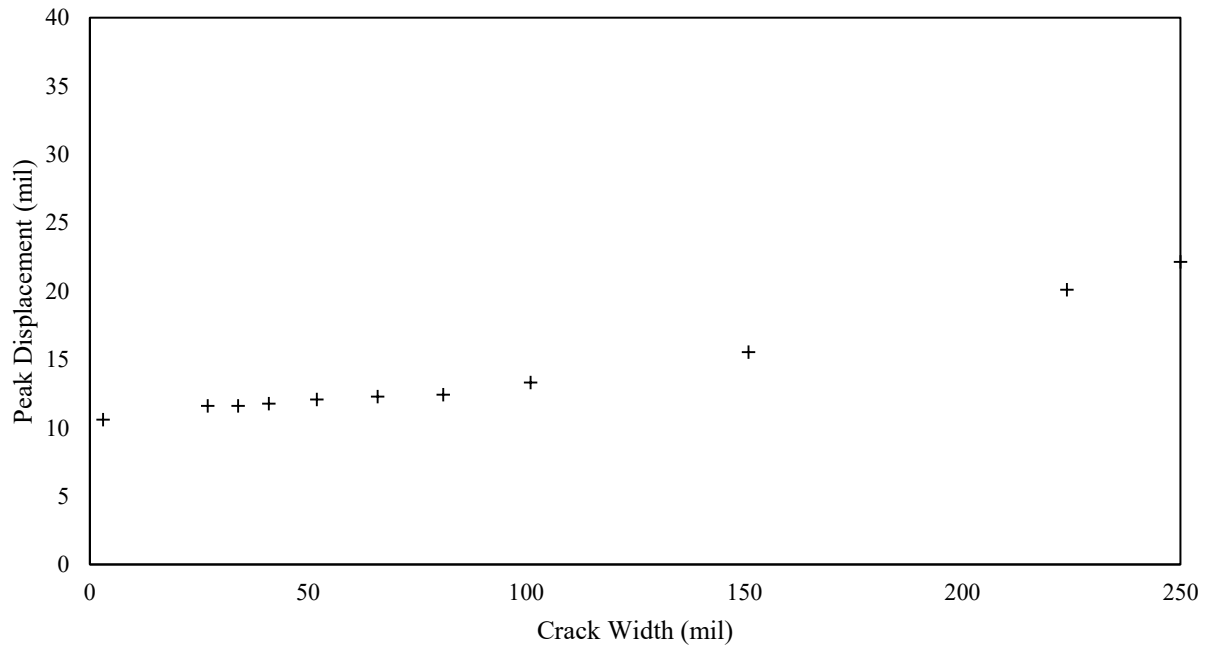
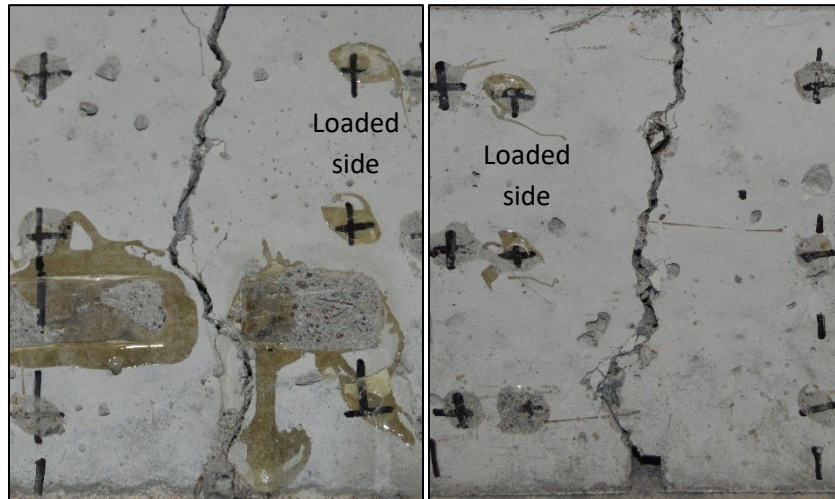

Figure F-114. Peak displacement as a function of crack width.
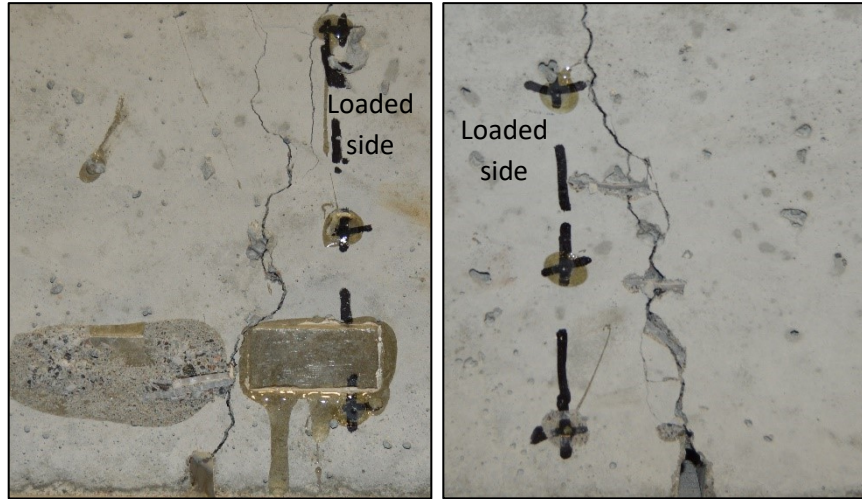
**Figure F-115. The front and back of the joint for specimen 1 in phase 2.**
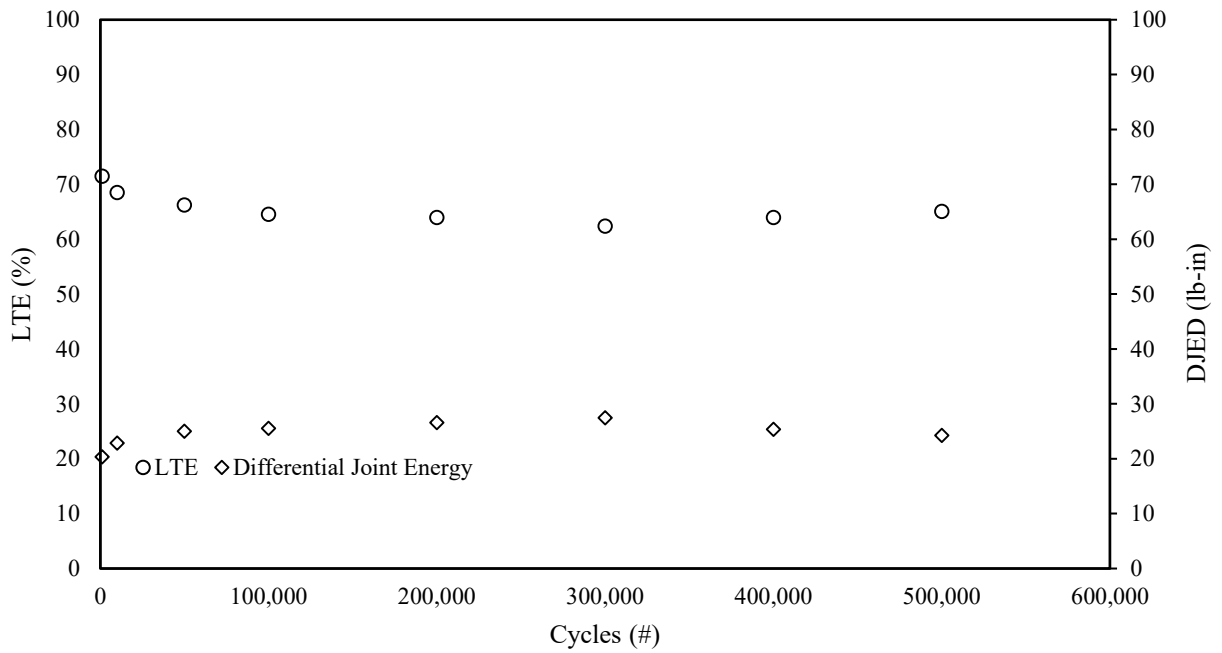
*Crack width ranged from 51 mils to 54 mils

Figure F-116. Average LTE and DJED as a function of cycles (repetitions).
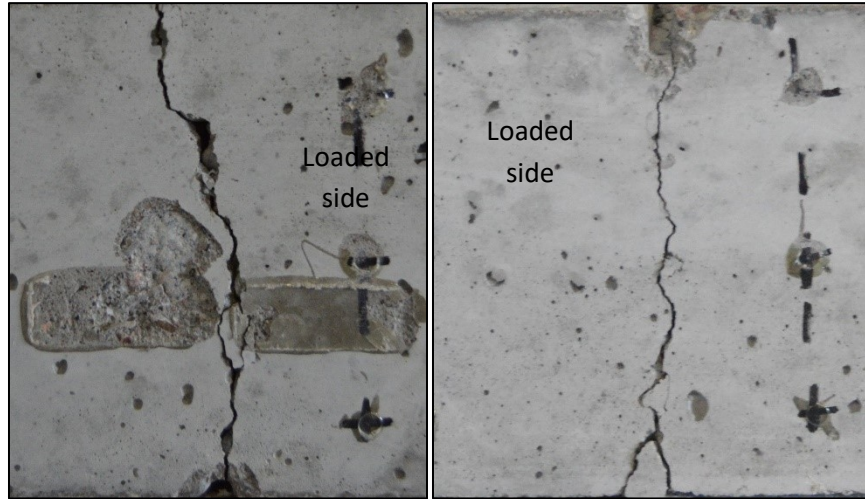
Figure F-117. The front and back of the joint for specimen 2 in phase 2.
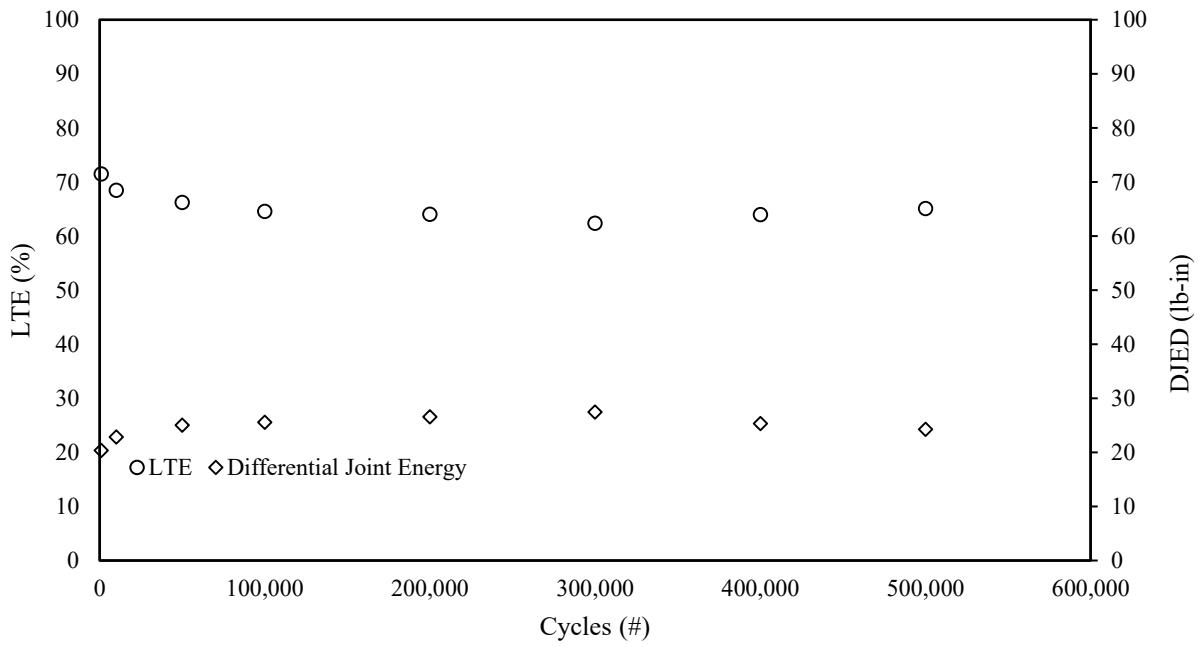
*Crack width 50 mils.

Figure F-118. DJED and Average LTE as a function of cycles (repetitions).
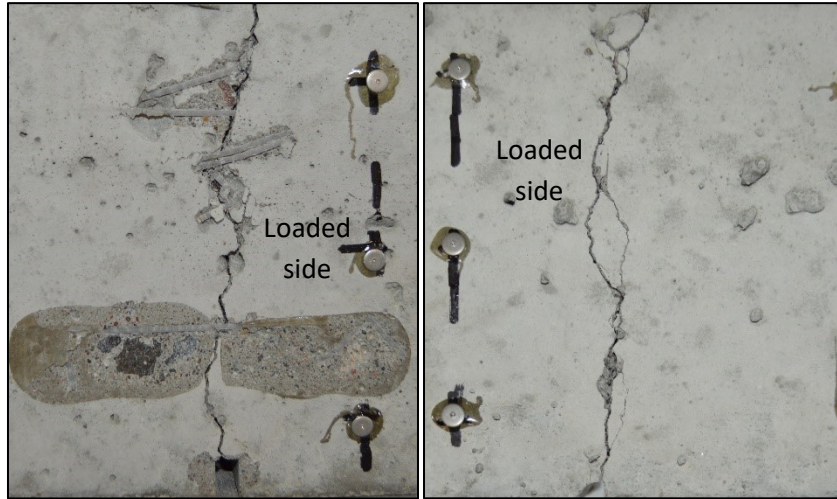
Figure F-119. The front and back of the joint for specimen 3 in phase 1.
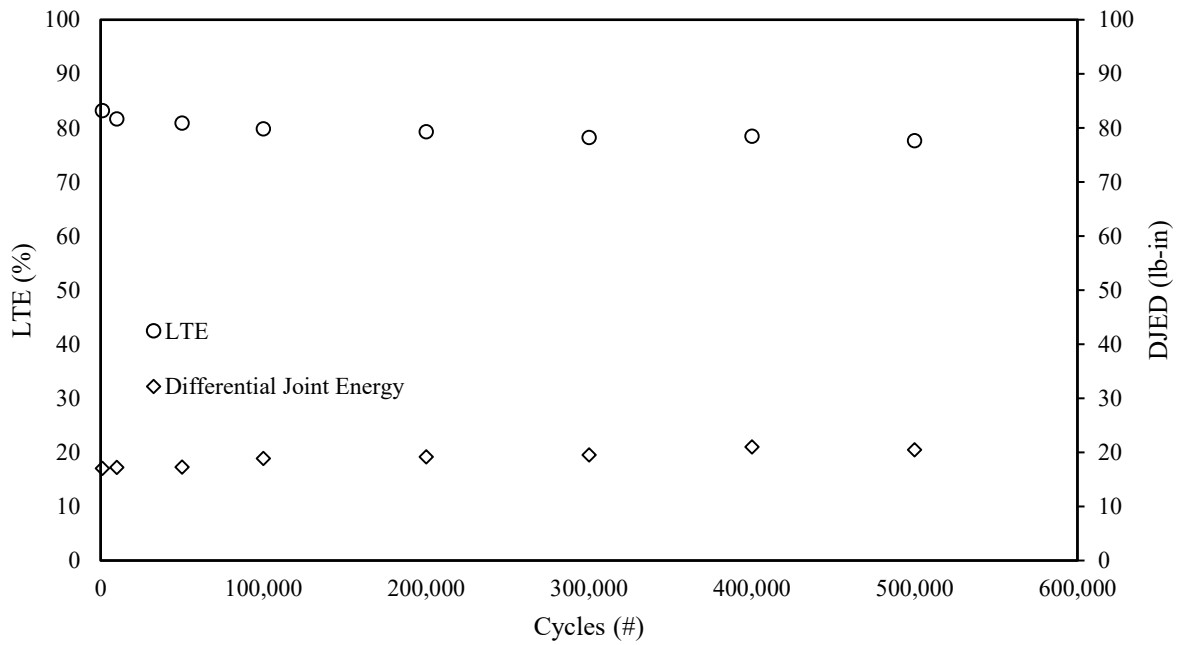
*Crack width ranged from 58 mils to 60 mils

Figure F-120. DJED and Average LTE as a function of cycles (repetitions).
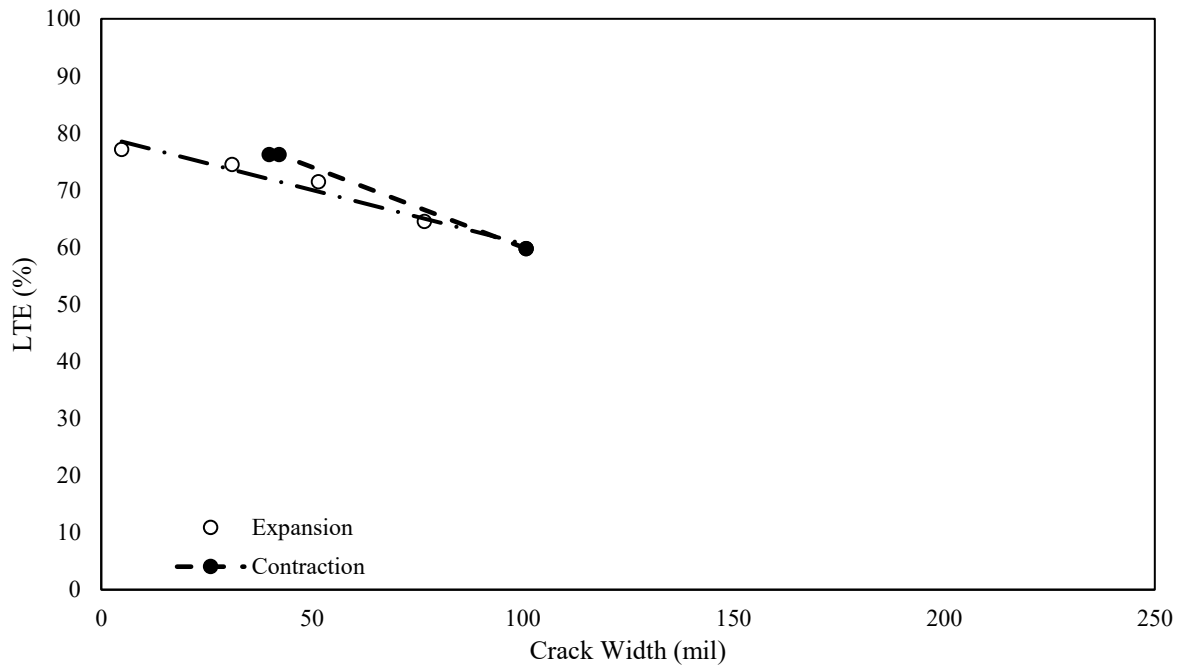
Figure F-121. The effect of joint expansion and contraction on average LTE in terms of crack width (phase 2: specimen 1).
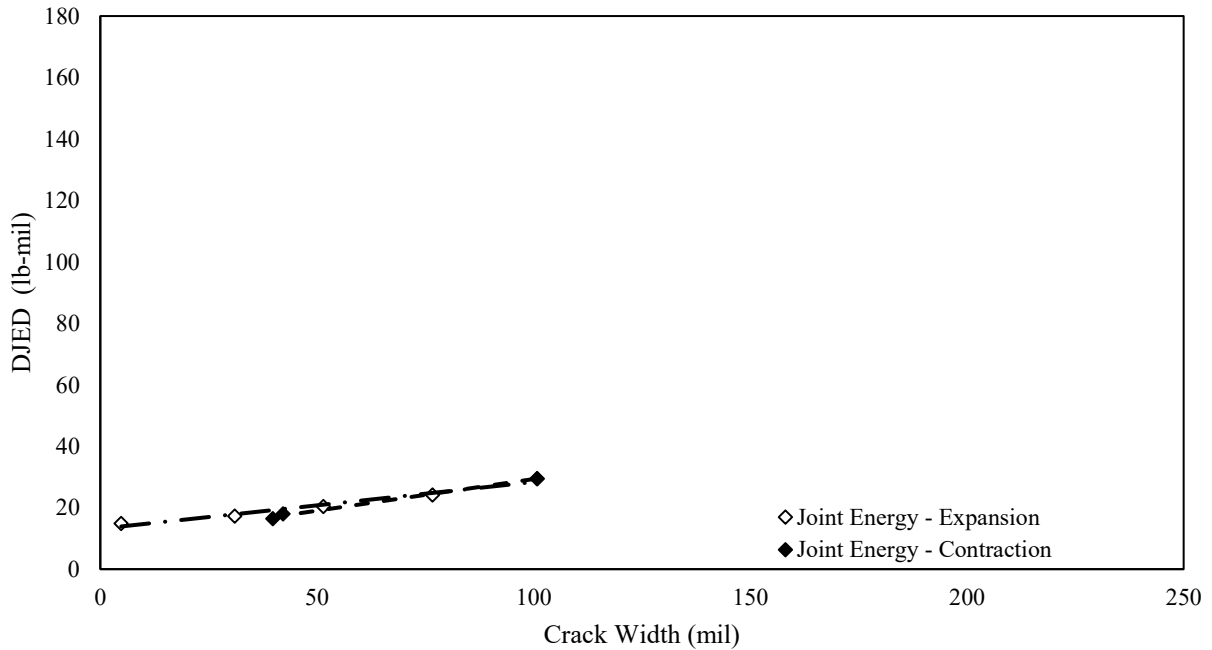
Figure F-122. The effect of joint expansion and contraction on DJED in terms of crack width (phase 2: specimen 1).

Figure F-123. The effect of joint expansion and contraction on average LTE in terms of crack width (phase 2: specimen 2).

Figure F-124. The effect of joint expansion and contraction on DJED in terms of crack width (phase 2: specimen 2).

Figure F-125. The effect of joint expansion and contraction on LTE in terms of crack width (phase 2: specimen 3).

Figure F-126. The effect of joint expansion and contraction on DJED in terms of crack width (phase 2: specimen 3).

Phase 1: Specimen 1

Figure F-127. The front and back of the joint for specimen 1 in phase 1.

Figure F-128. Cyclical plots for (a) 23 mils, (b) 51 mils, and (c) 103 mils crack widths.
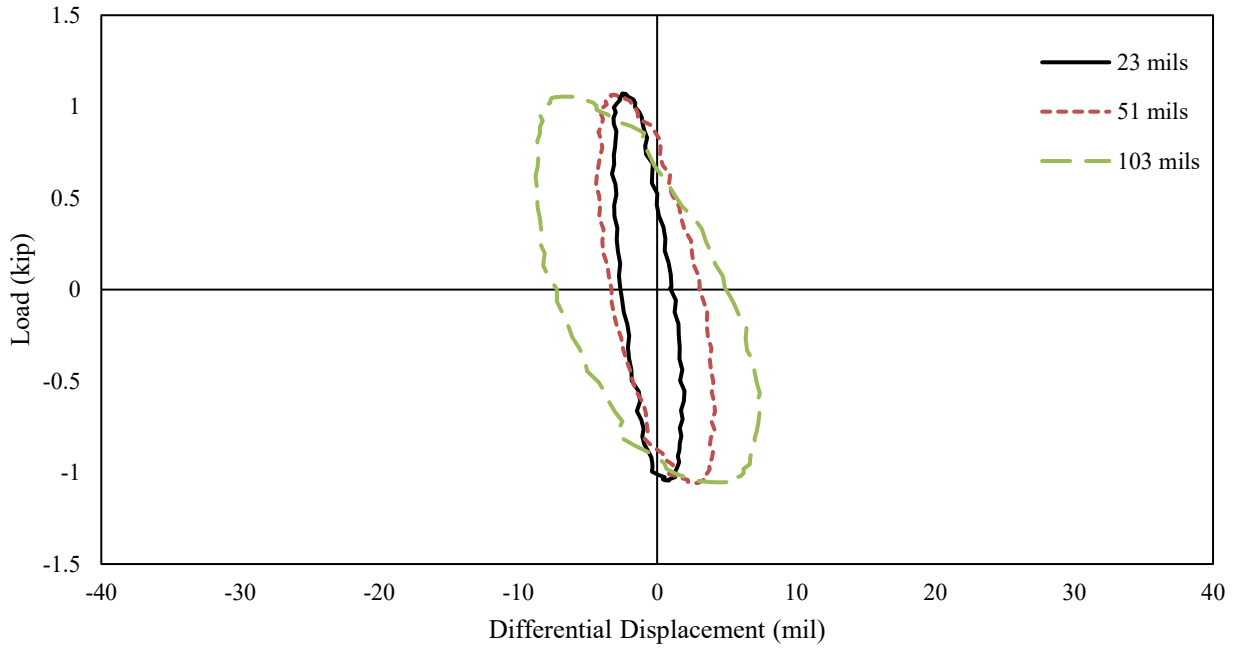
Figure F-129. Hystereses for 23 mils, 51 mils, and 103 mils crack widths.

Figure F-130. LTE as a function of crack width.

Figure F-131.DJED as a function of crack width.

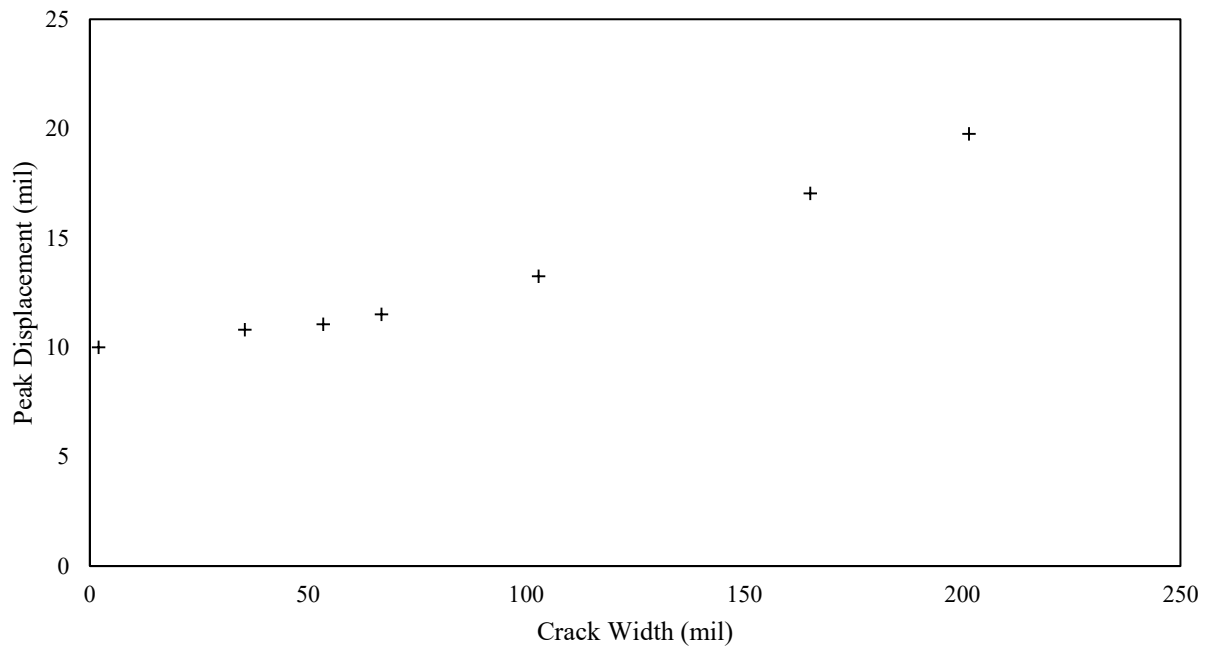**Figure F-132. Differential joint displacement as a function of crack with.**

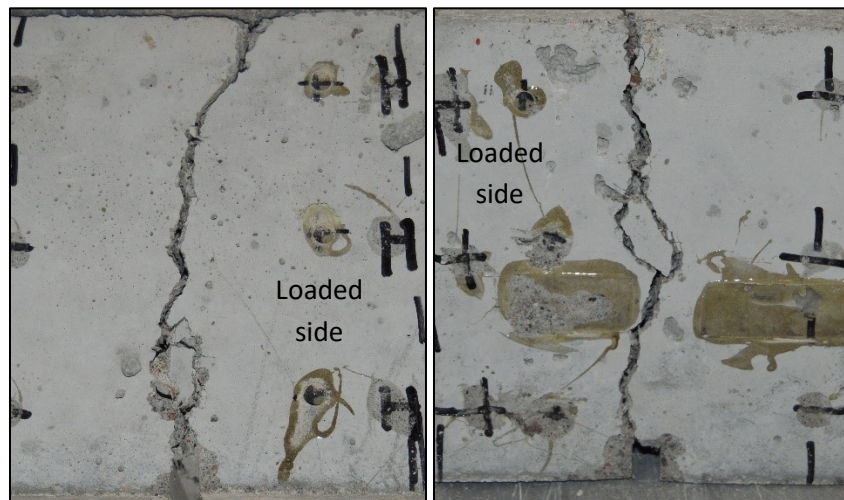**Figure F-133. Peak displacement as a function of crack width.**

Phase 1: Specimen 2

**Figure F-134. The front and back of the joint for specimen 2 in phase 1.**
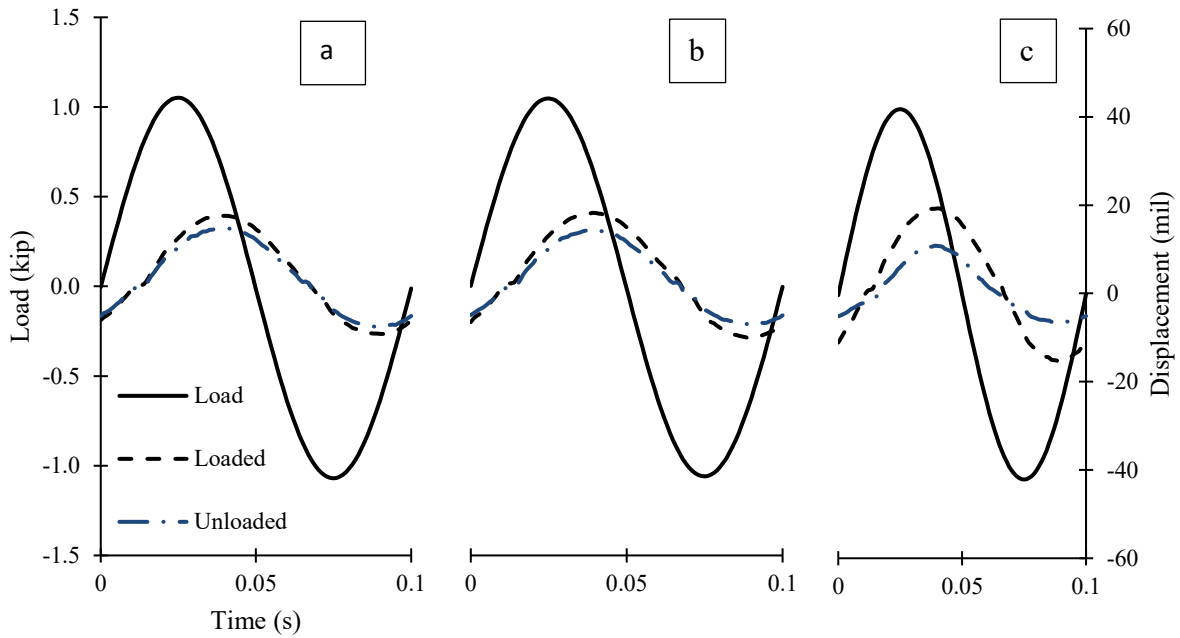
**Figure F-135. Cyclical plots for (a) 28.5 mils, (b) 57 mils, and (c) 124 mils crack widths.**
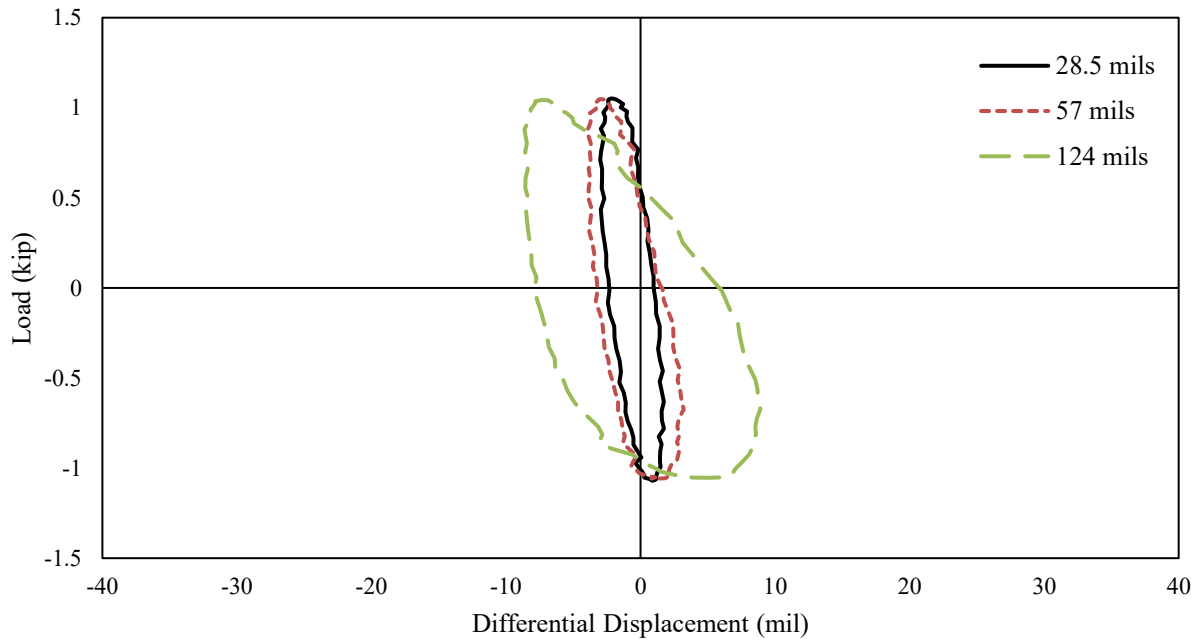
Figure F-136. Hystereses for 28.5 mils, 57 mils, and 124 mils crack widths.
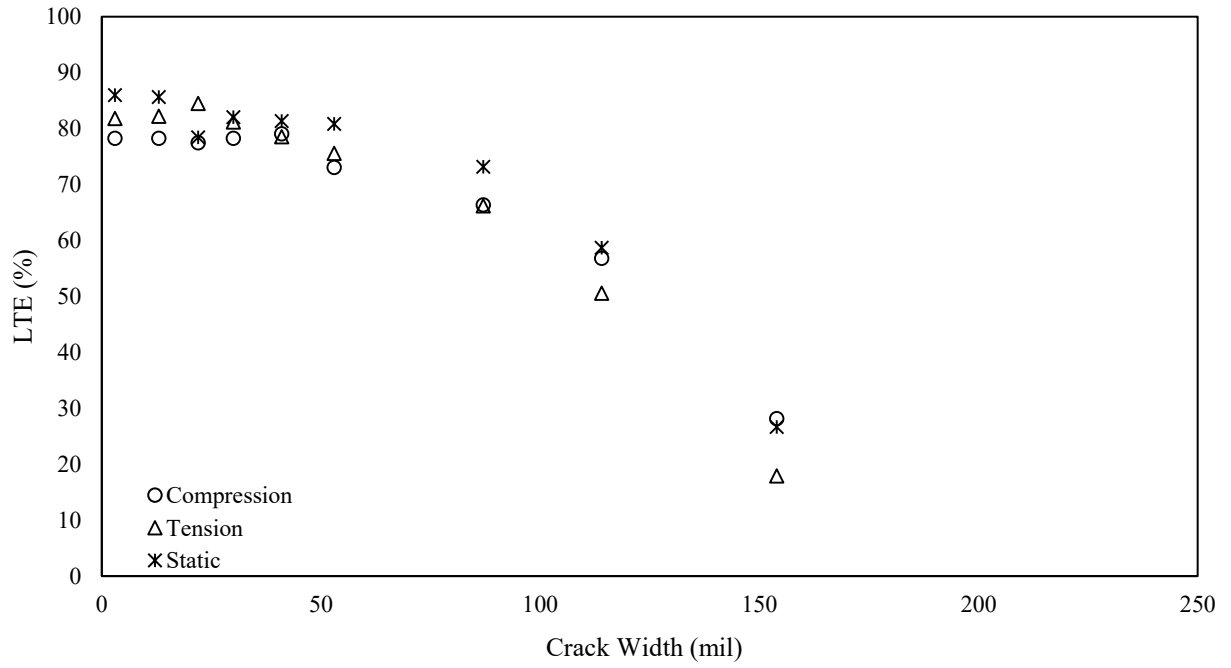
F-69
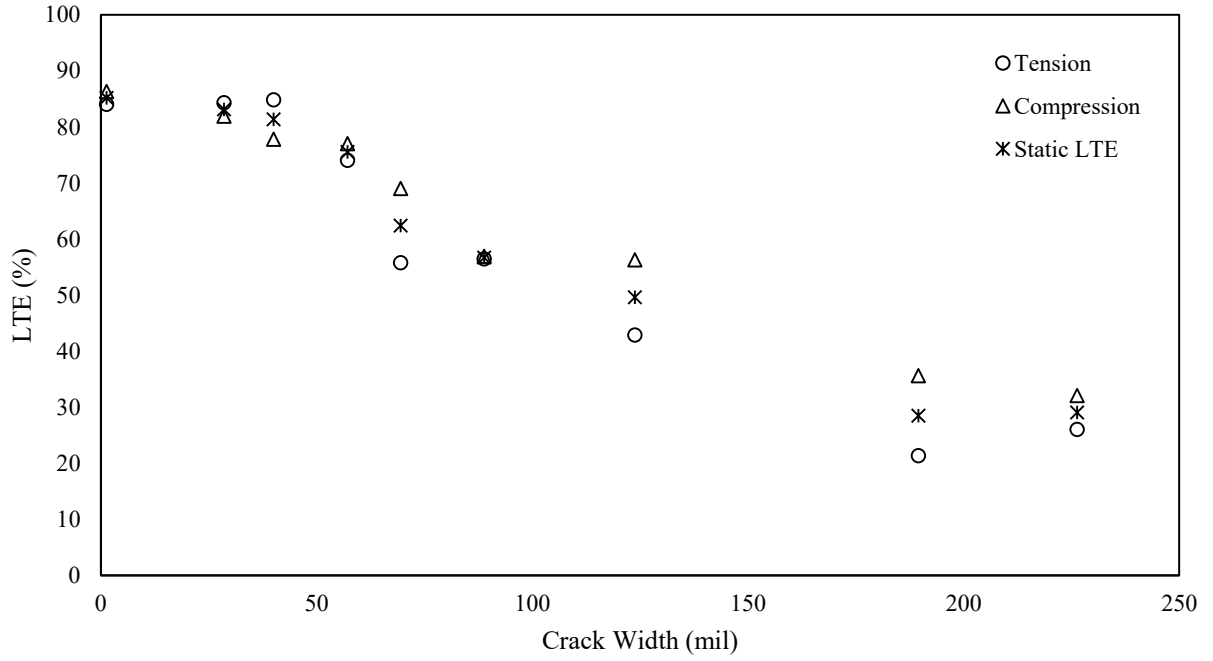
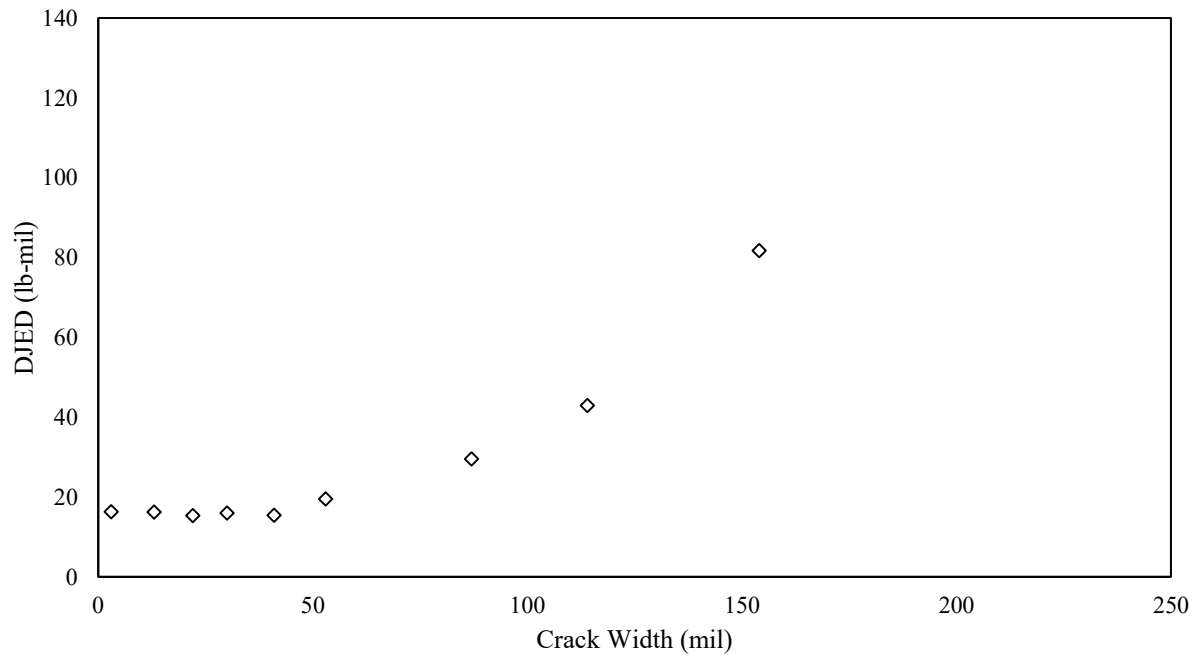**Figure F-137. LTE as a function of crack width.**
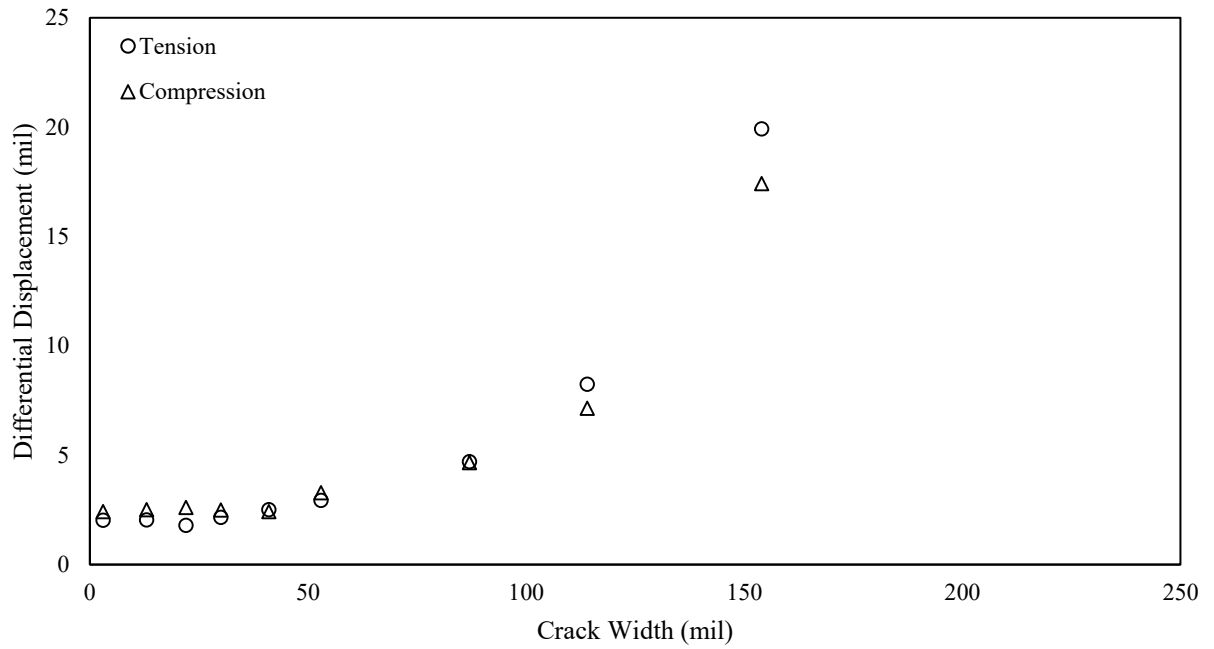

Figure F-138. DJED as a function of crack width.
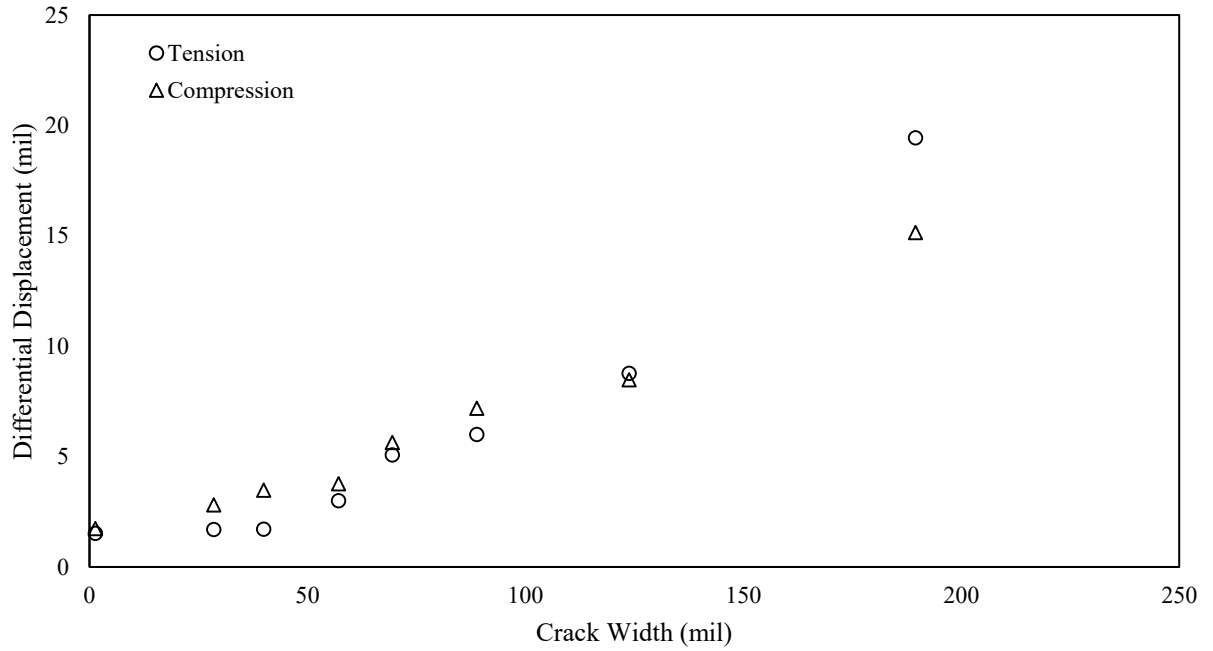
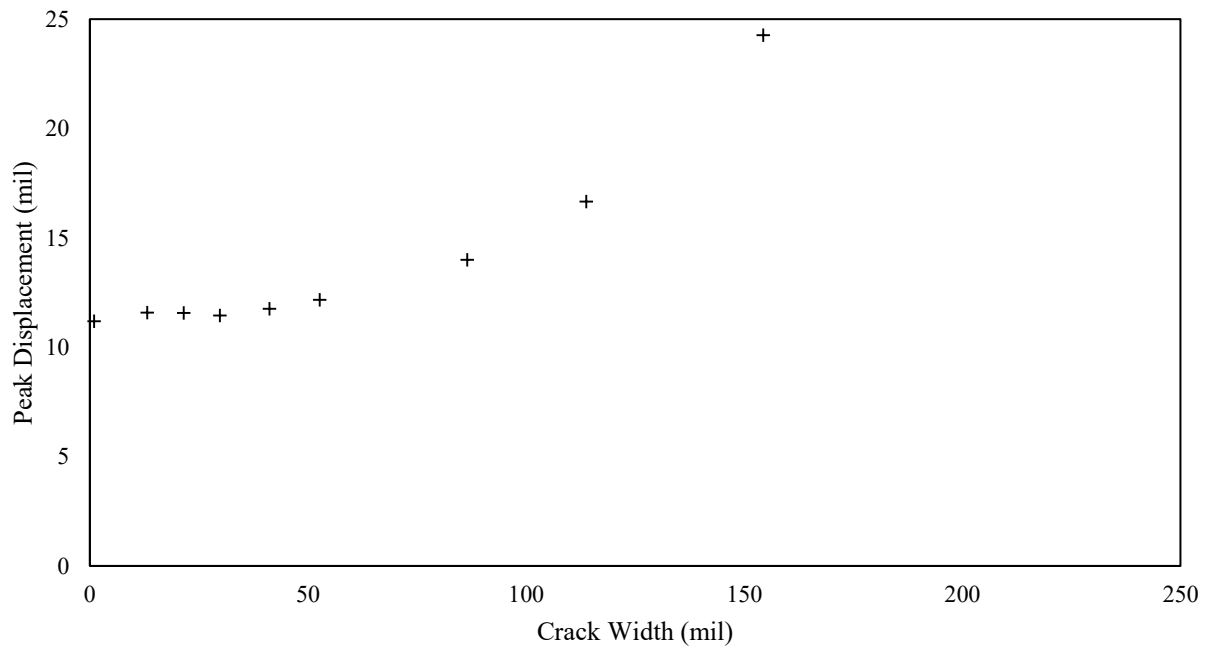**Figure F-139. Differential joint displacement as a function of crack width.**
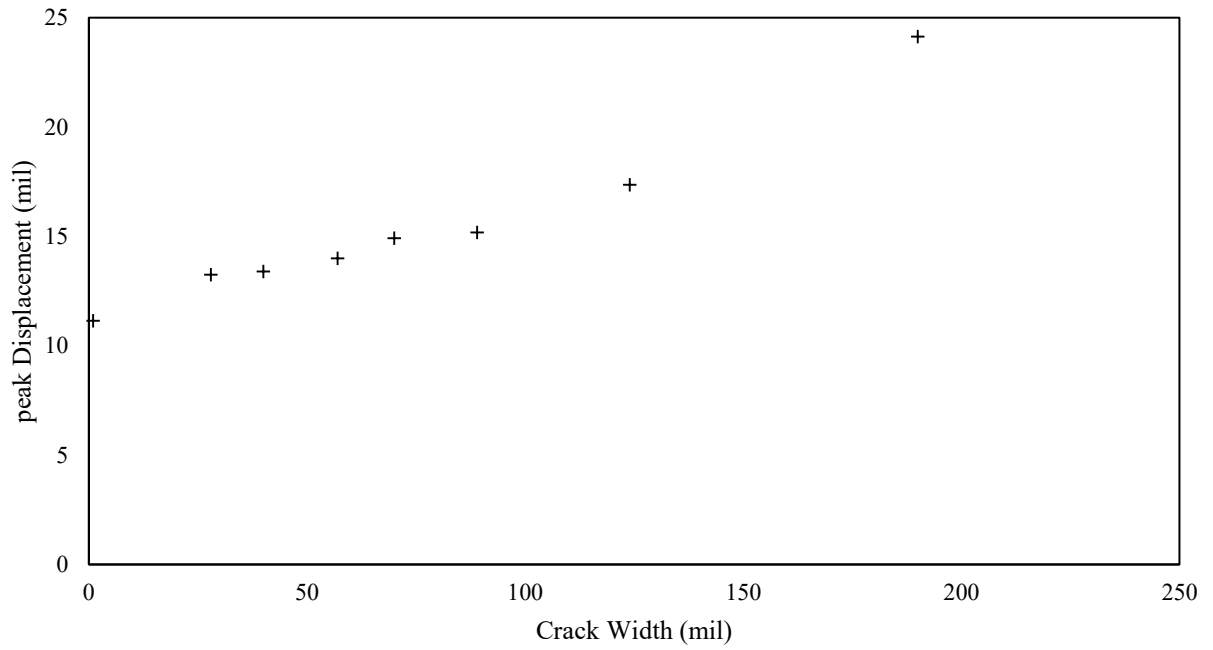
Figure F-140. Peak displacement as a function of crack width.
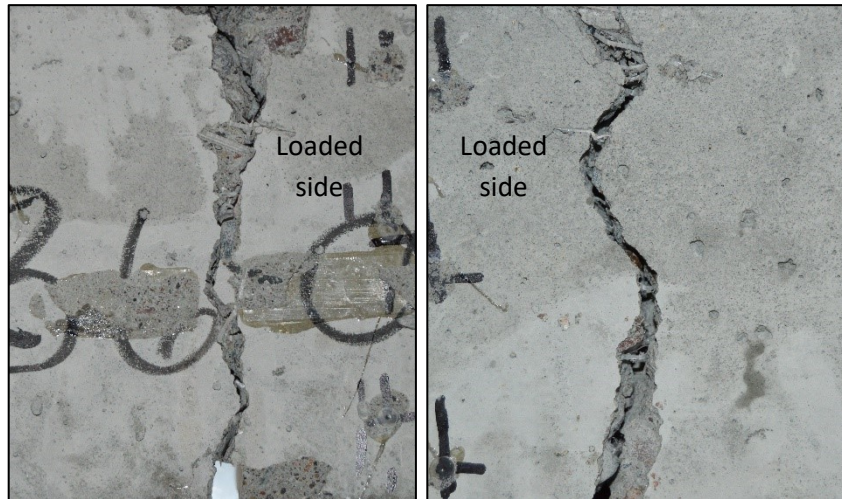
Figure F-141. The front and back of the joint for specimen 3 in phase 1.
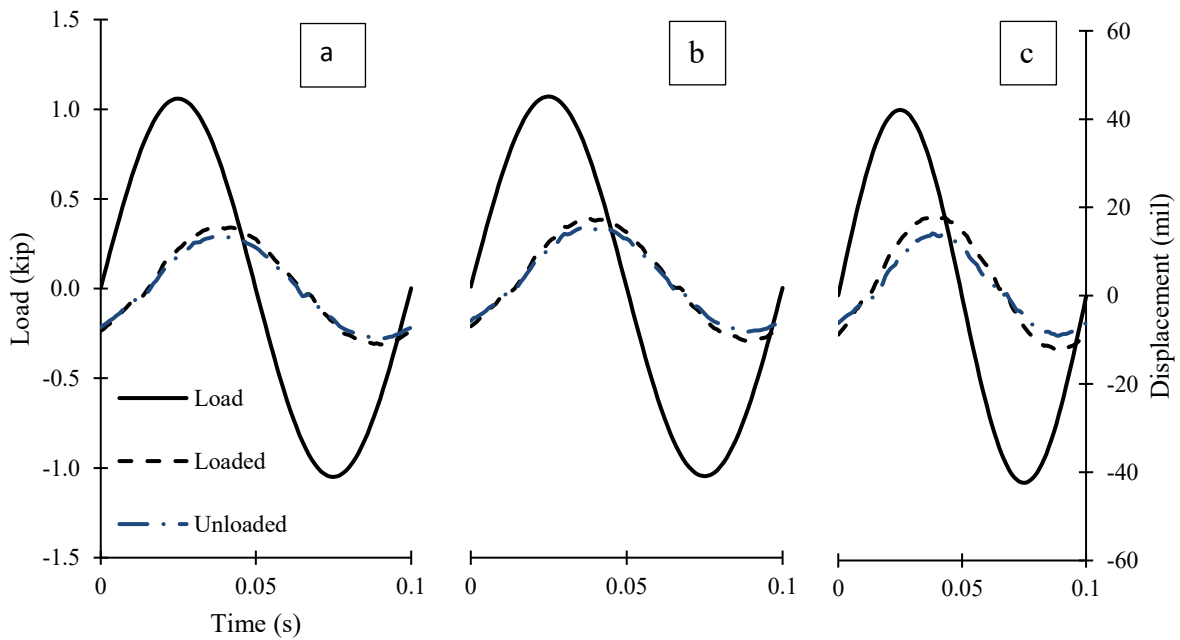
Figure F-142. Cyclical plots at (a) 29 mils, (b) 56 mils, and (c) 97.5 mils crack widths.
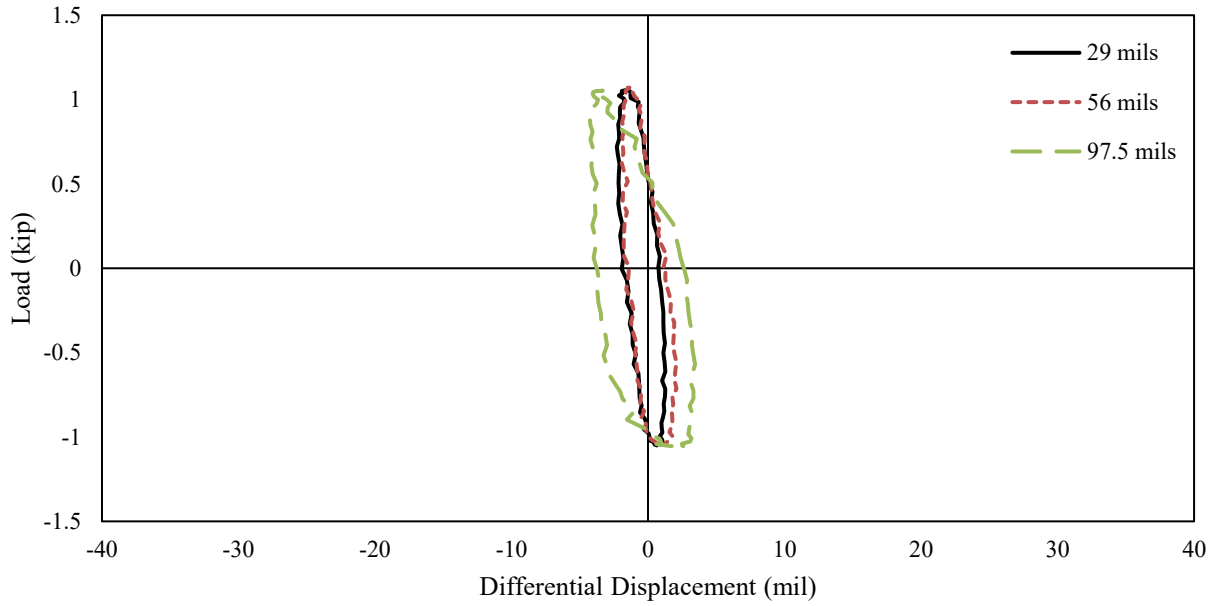
Figure F-143. Hystereses at 29 mils, 56 mils, and 97.5 mils crack widths.
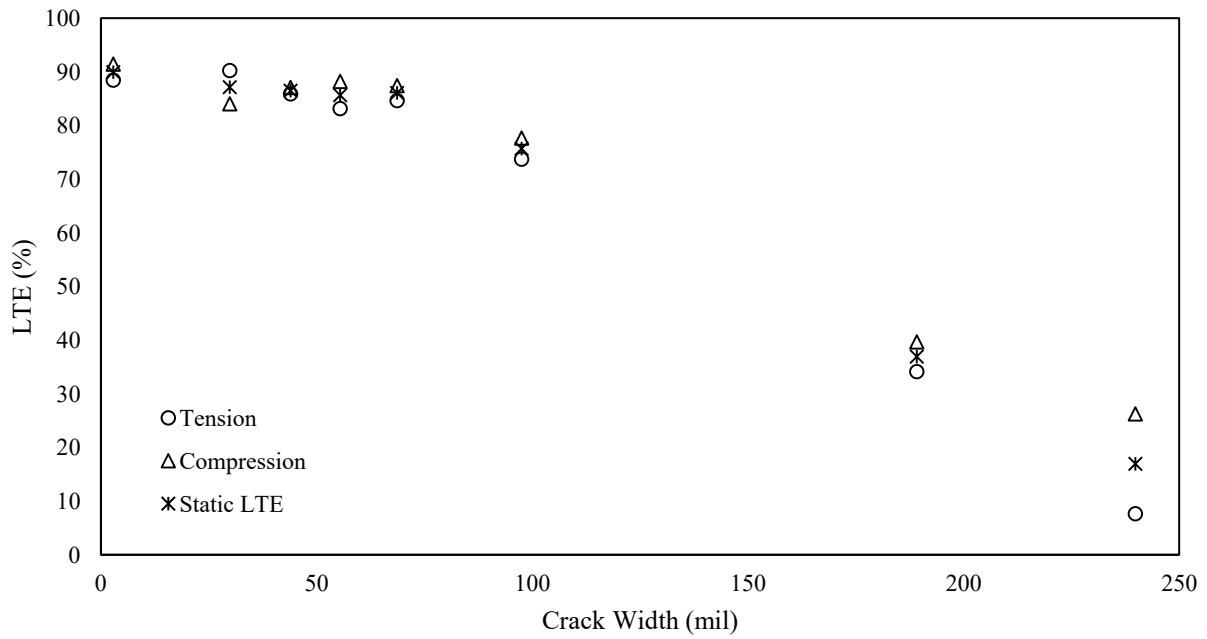
Figure F-144. LTE as a function of crack width.

F-73

Figure F-145. DJED as a function of crack width.

Figure F-146. Differential joint displacement as a function of crack width.

Figure F-147. Peak displacement as a function of crack width.

Phase 2: Specimen 1

Figure F-148. The front and back of the joint for specimen 1 in phase 2.
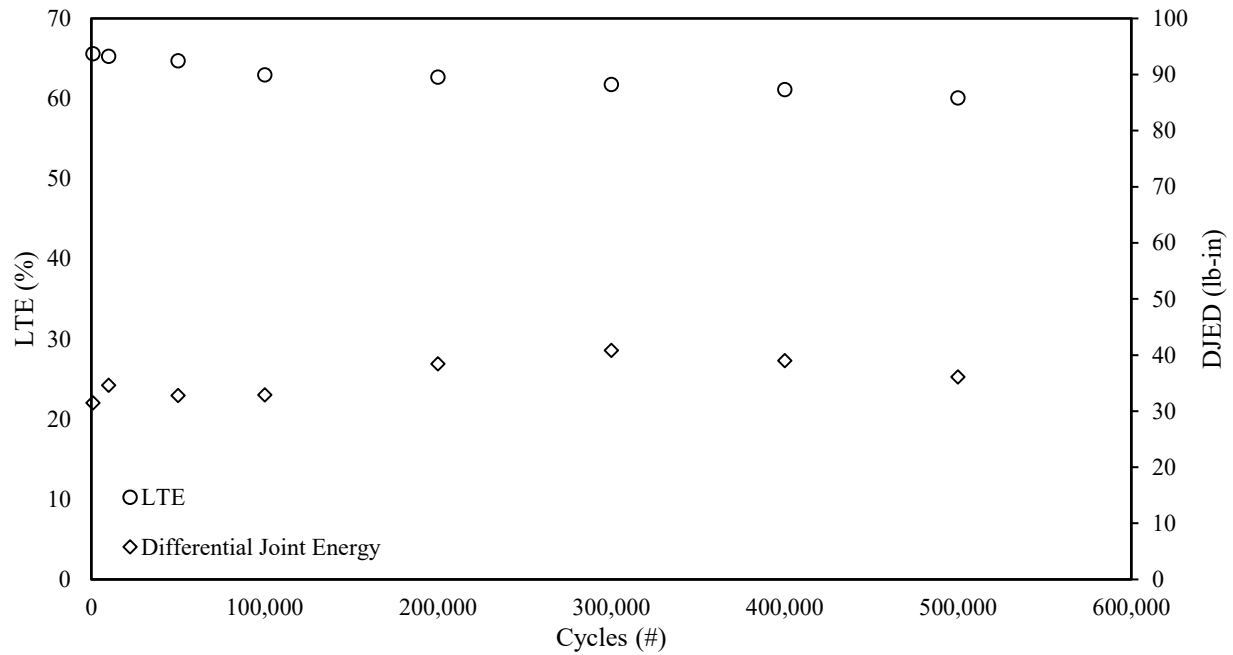
*Crack width ranged from 50 mils to 51 mils

Figure F-149. DJED and Average LTE as a function of cycles (repetitions).
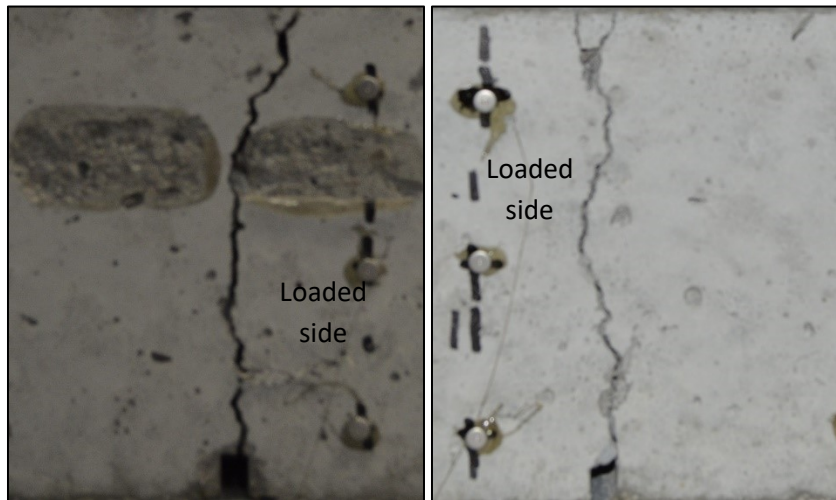
Phase 2: Specimen 2

*NO FATIGUE, ONLY CW VS. PERFORMANCE, SEE PHASE 3

Figure F-150. The front and back of the joint for specimen 2 in phase 2.

Phase 2: Specimen 3

*NO FATIGUE, ONLY CW VS. PERFORMANCE, SEE PHASE 3

Figure F-151. The front and back of the joint for specimen 3 in phase 2.

Phase 3: Contraction and Rebound Performance
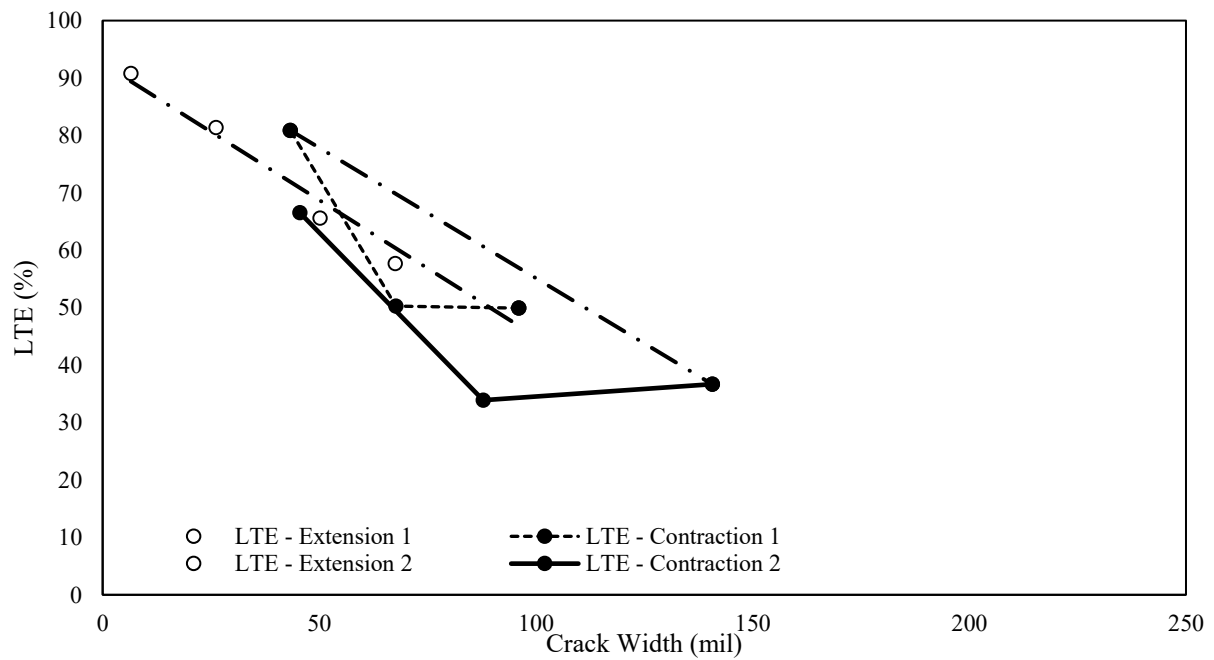
Figure F-152. The effect of joint expansion and contraction on average LTE in terms of crack width (phase 2: specimen 1).

Figure F-153. The effect of joint expansion and contraction on the DJE in terms of crack width (phase 2: specimen 1).

Figure F-154. The effect of joint expansion and contraction on average LTE in terms of crack width (phase 2: specimen 1).

Figure F-155. The effect of joint expansion and contraction on the DJE in terms of crack width (phase 2: specimen 1).

Figure F-156. The effect of joint expansion and contraction on average LTE in terms of crack width (phase 2: specimen 2).

Figure F-157. The effect of joint expansion and contraction on the DJED in terms of crack width (phase 2: specimen 2).

Figure F-158. The effect of joint expansion and contraction on average LTE in terms of crack width (phase 2: specimen 3).

Figure F-159. The effect of joint expansion and contraction on the DJED in terms of crack width (phase 2: specimen 3).

S.T.11.5

Phase 1: Specimen 1

Figure F-160. The front and back of the joint for specimen 1 in phase 1.

Figure F-161. Cyclical plots for (a) 3 mils, (b) 53 mils, and (c) 104 mils crack widths.

**Figure F-162. Hystereses at 3 mils, 53 mils and, 104 mils crack widths.**
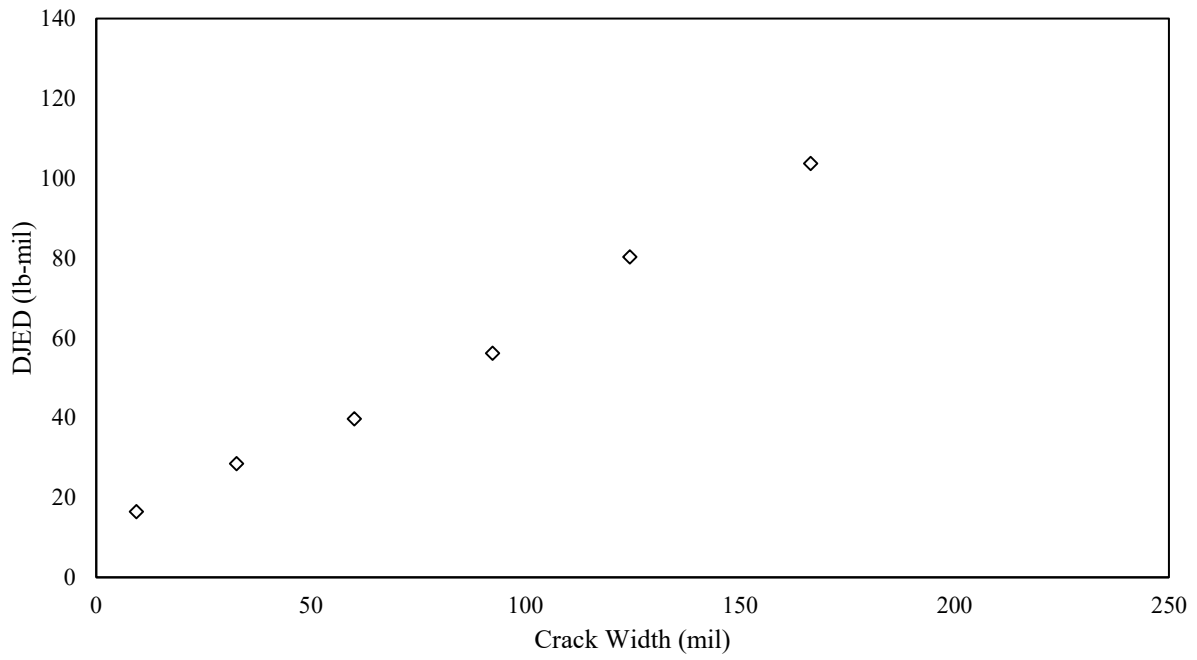
Figure F-163. LTE as a function of crack width.
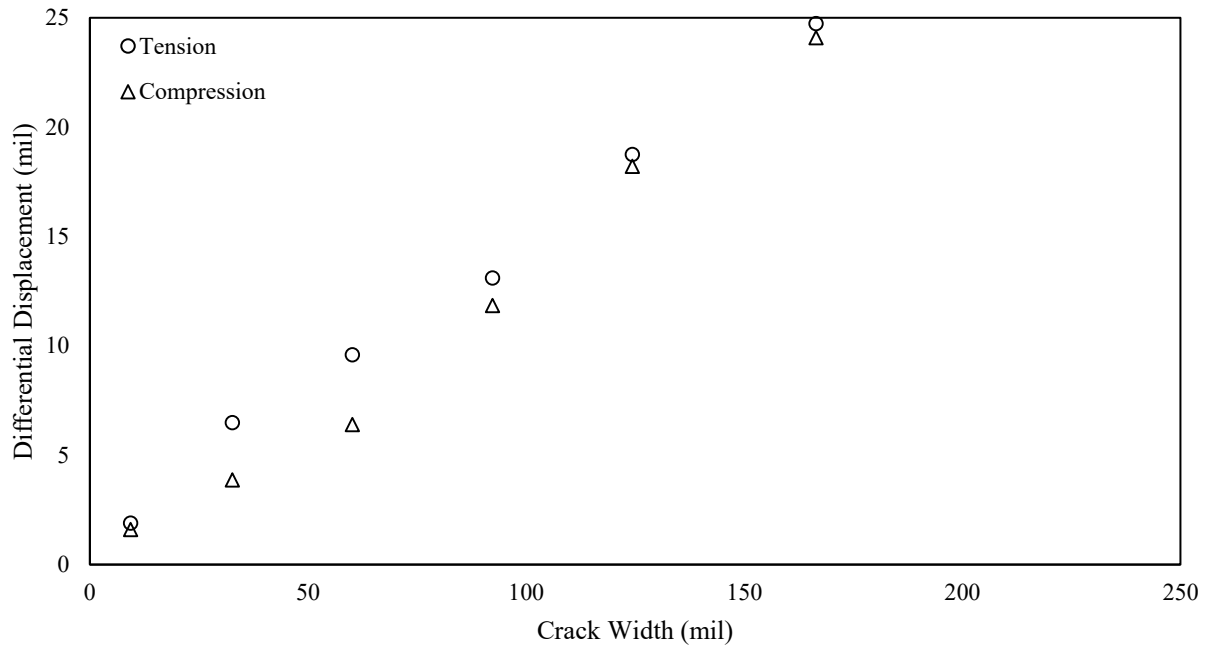

Figure F-164. DJED as a function of crack width.

F-83

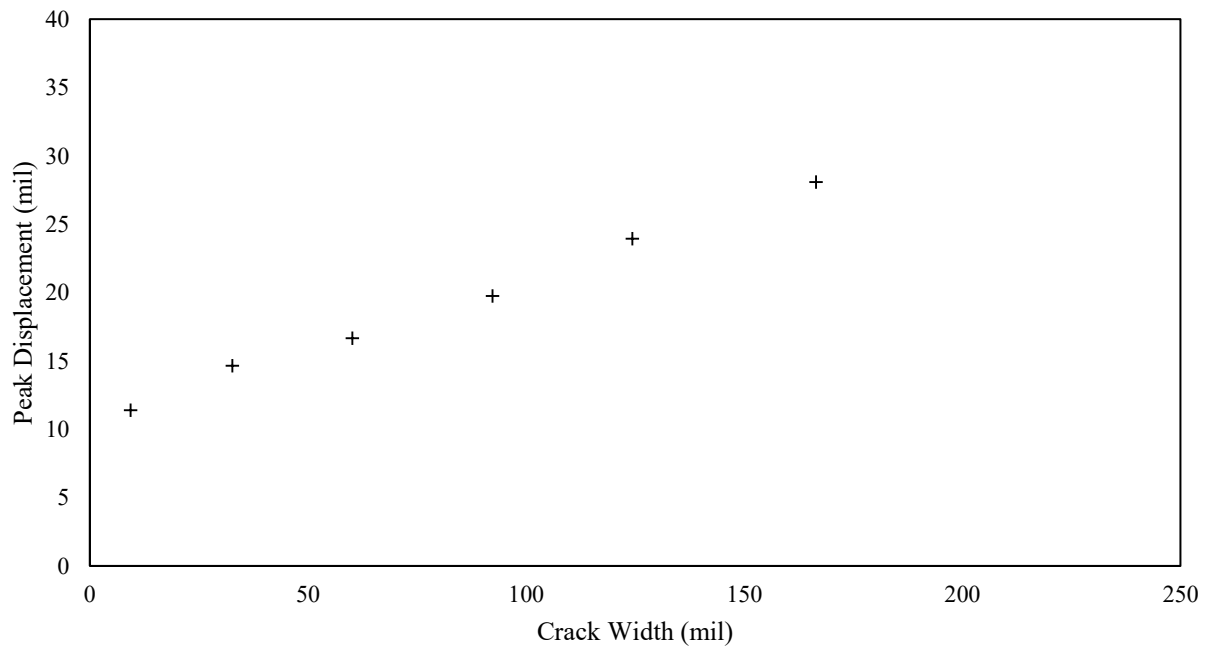**Figure F-165. Differential displacement as a function of crack width.**

Figure F-166. Peak displacement as a function of crack width.

Figure F-167. The front and back of the joint for specimen 2 in phase 1.
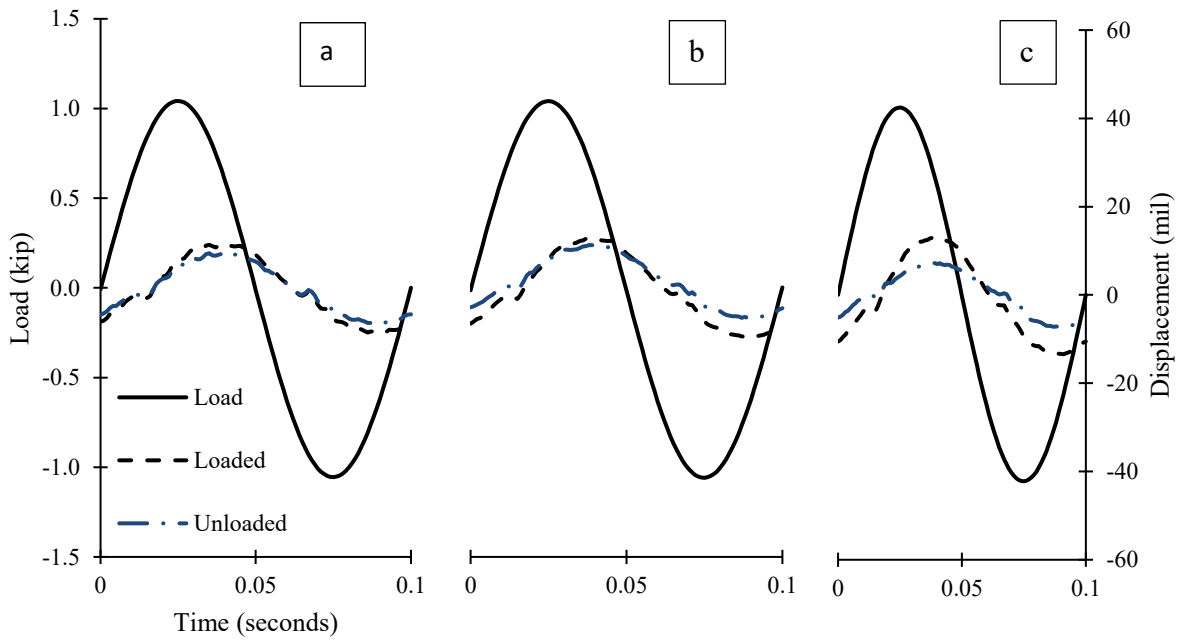
Figure F-168. Cyclical plots at (a) 2 mils, (b) 54 mils, and (c) 103 mils of crack widths.
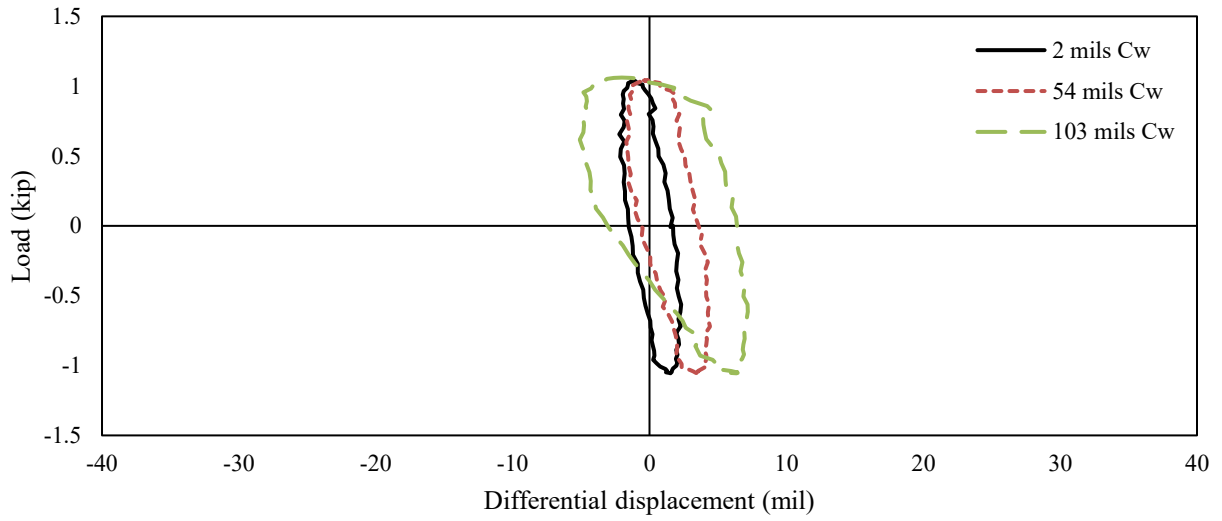
Figure F-169. Hystereses plot 2 mils, 54 mils, 103 mills of crack width.
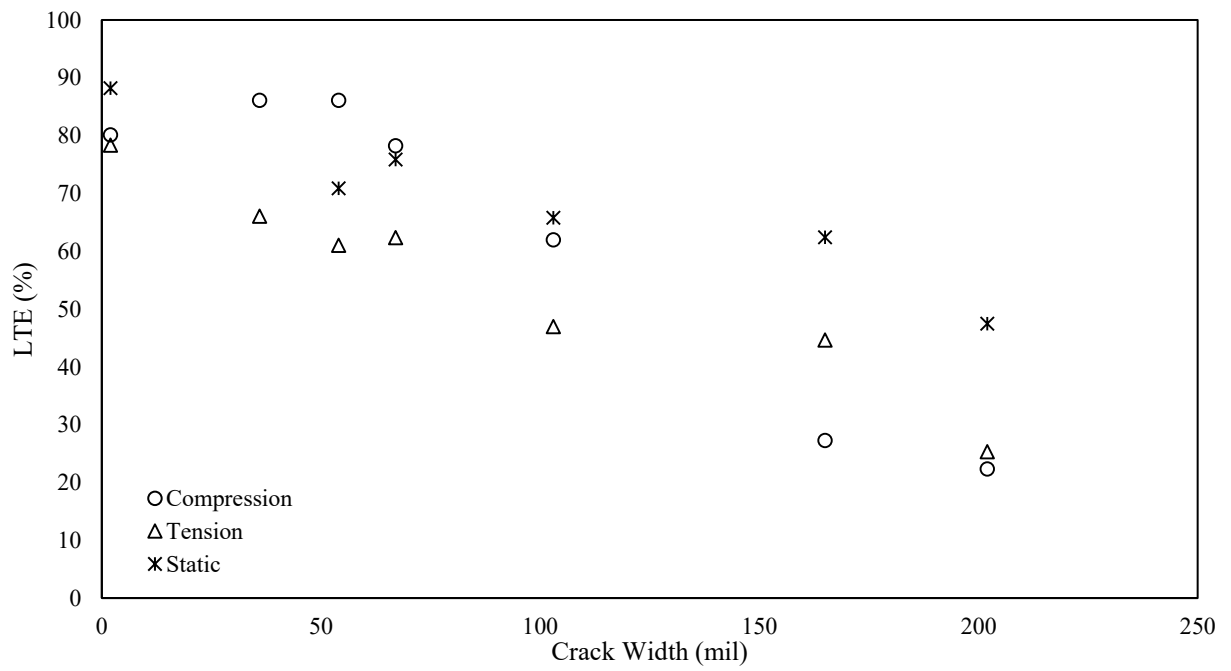
Figure F-170. LTE as a function of crack width.
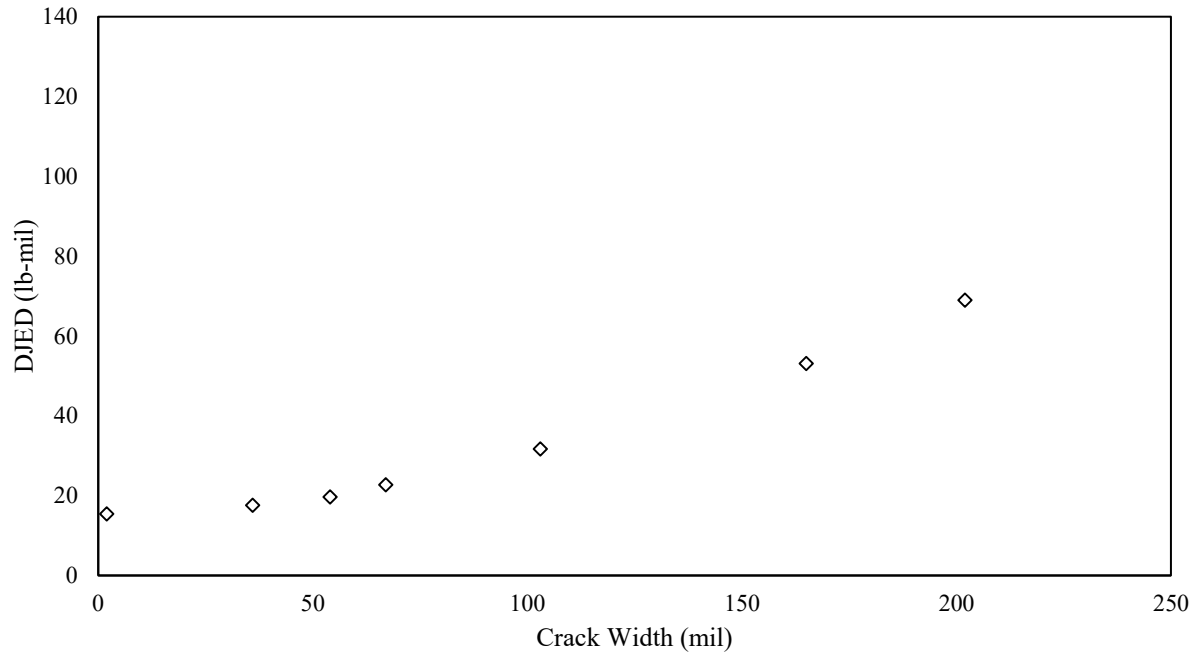
Figure F-171. DJED as a function of crack width.
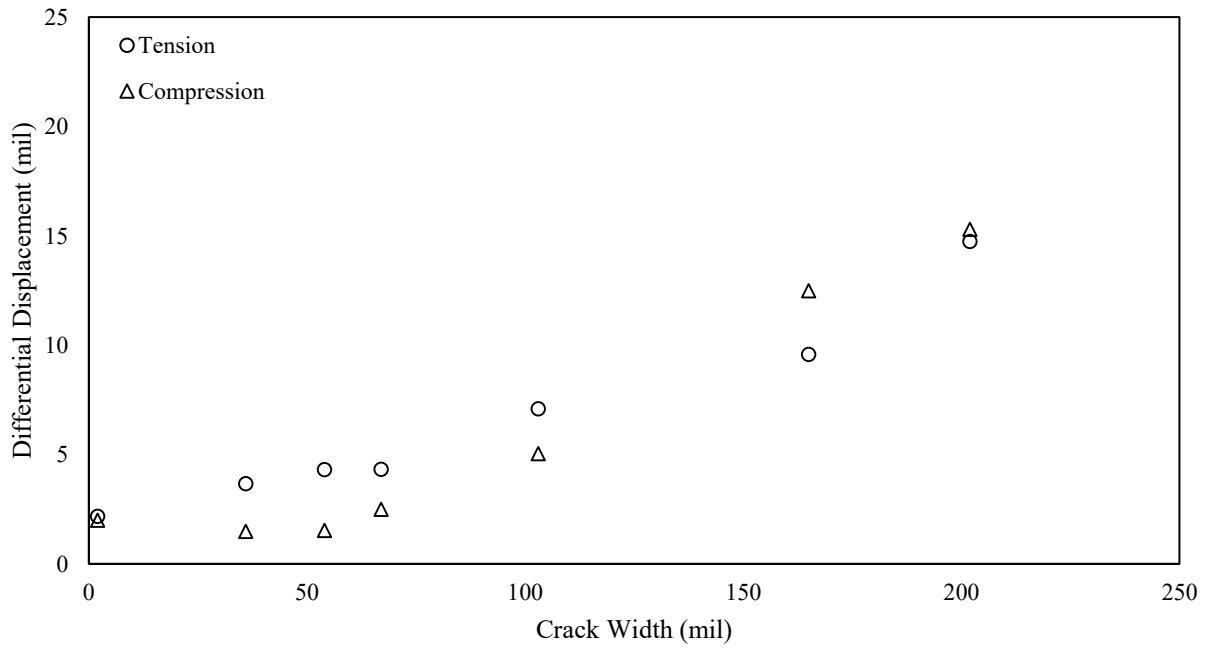
Figure F-172. Differential joint displacement as a function of crack width.

Figure F-173. Peak displacement as a function of crack width.

Phase 1: Specimen 3

Figure F-174. The front and back of the joint for specimen 3 in phase 1.
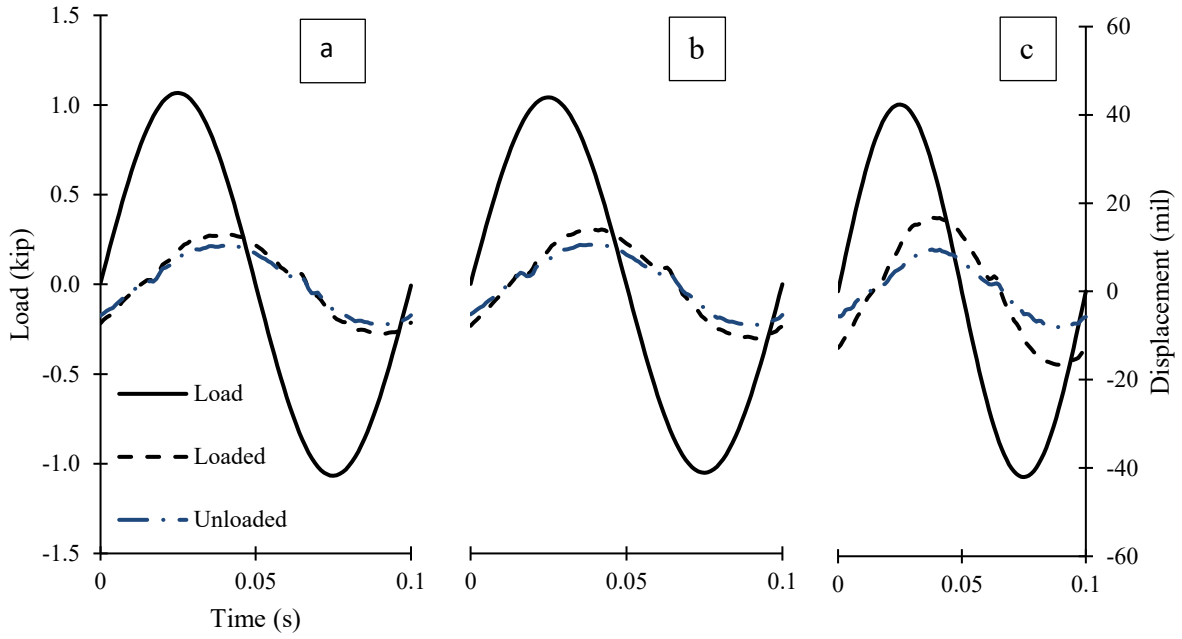
Figure F-175. Cyclical plots at (a) 3 mills, (b) 53 mils, and (c) 114 mils crack widths.
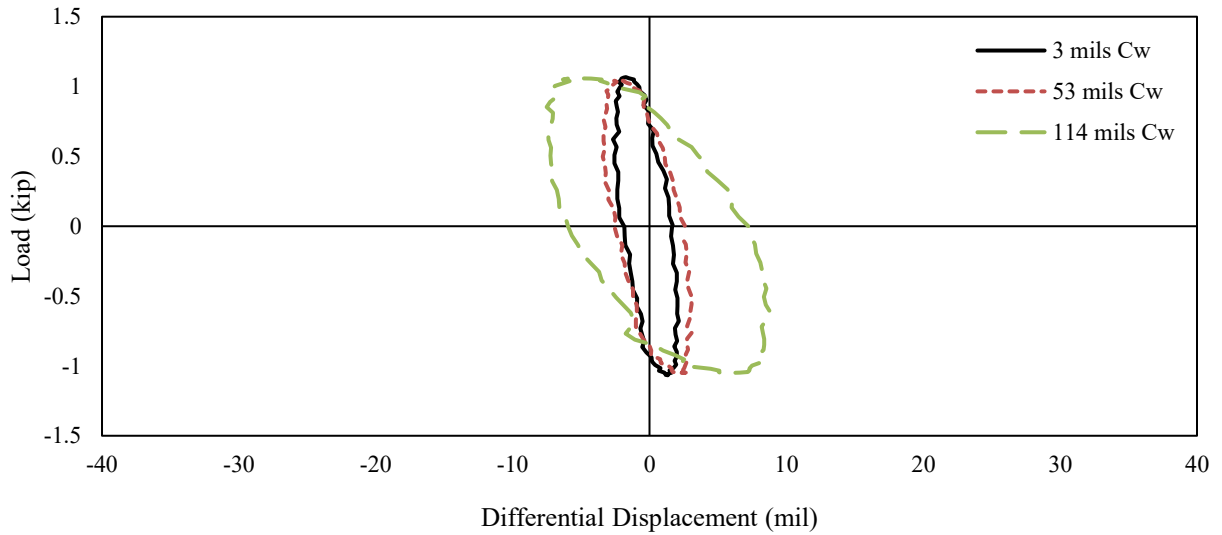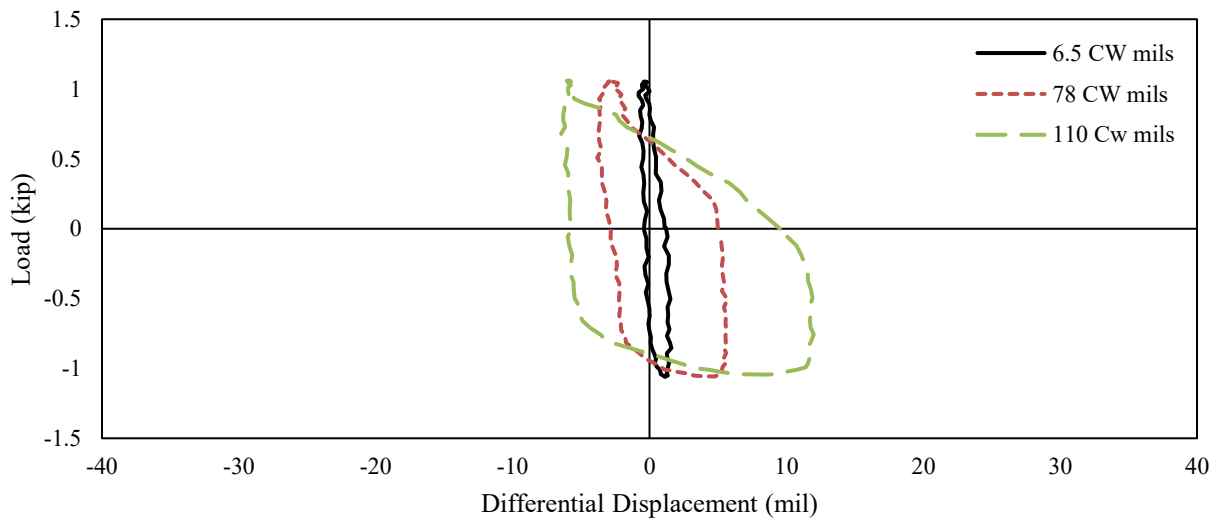

Figure F-176. Hystereses plots at 3 mills, 53 mils, and 114 mils crack widths.

F-89

Figure F-177. LTE as a function of crack width.

Figure F-178. DJED as a function of crack width.

Figure F-179. Differential displacement as a function of crack width.

Figure F-180. Peak displacement as a function of crack width

Phase 4: Specimen 1
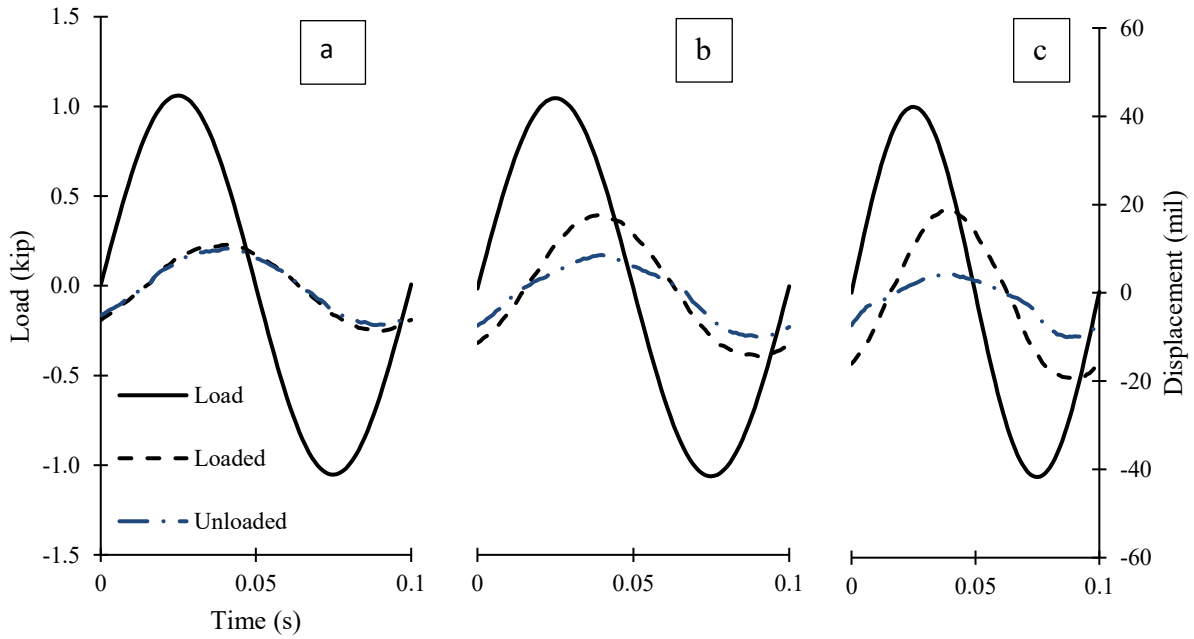
Figure F-181. Cyclical plots at (a) 5 mils, (b) 52 mils, and (c) 101 mils crack widths.
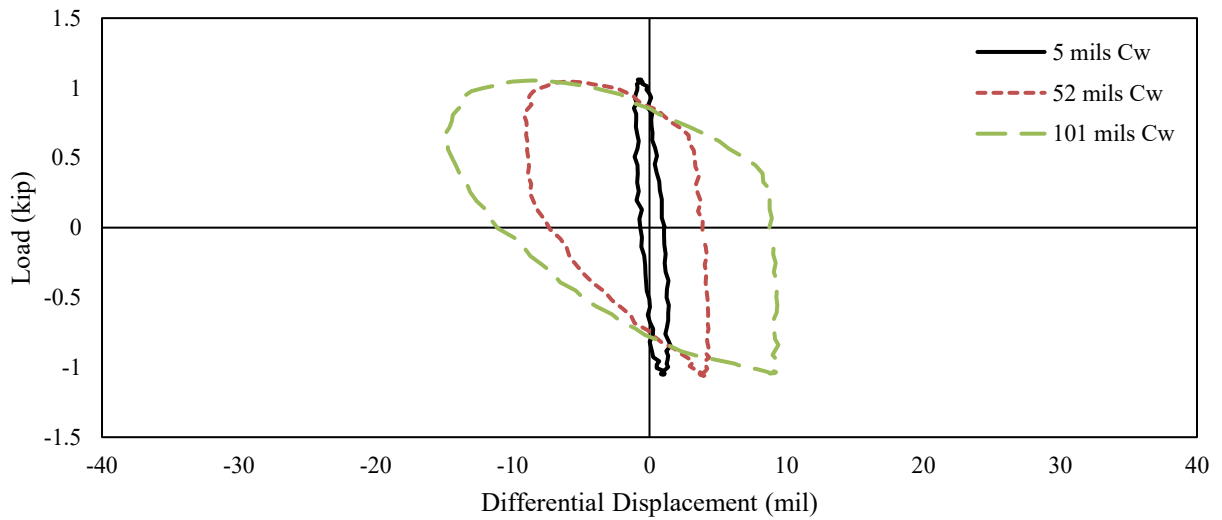
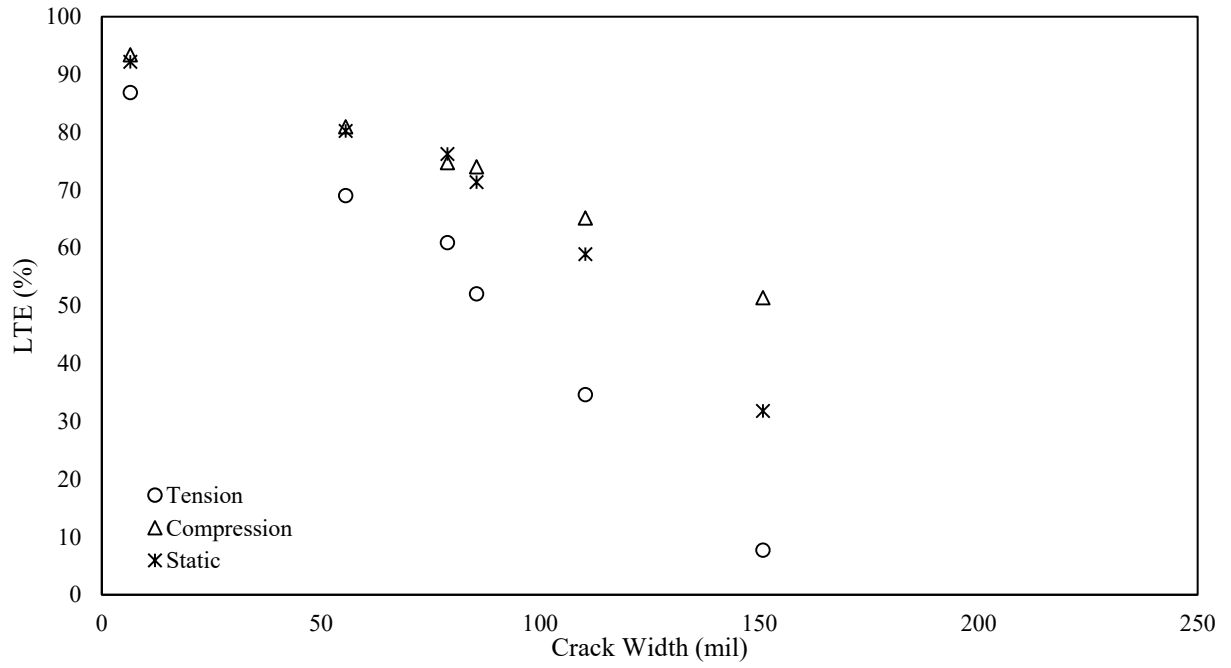**Figure F-182. Hystereses for 5 mils, 52 mils, and 101 mils crack widths.**
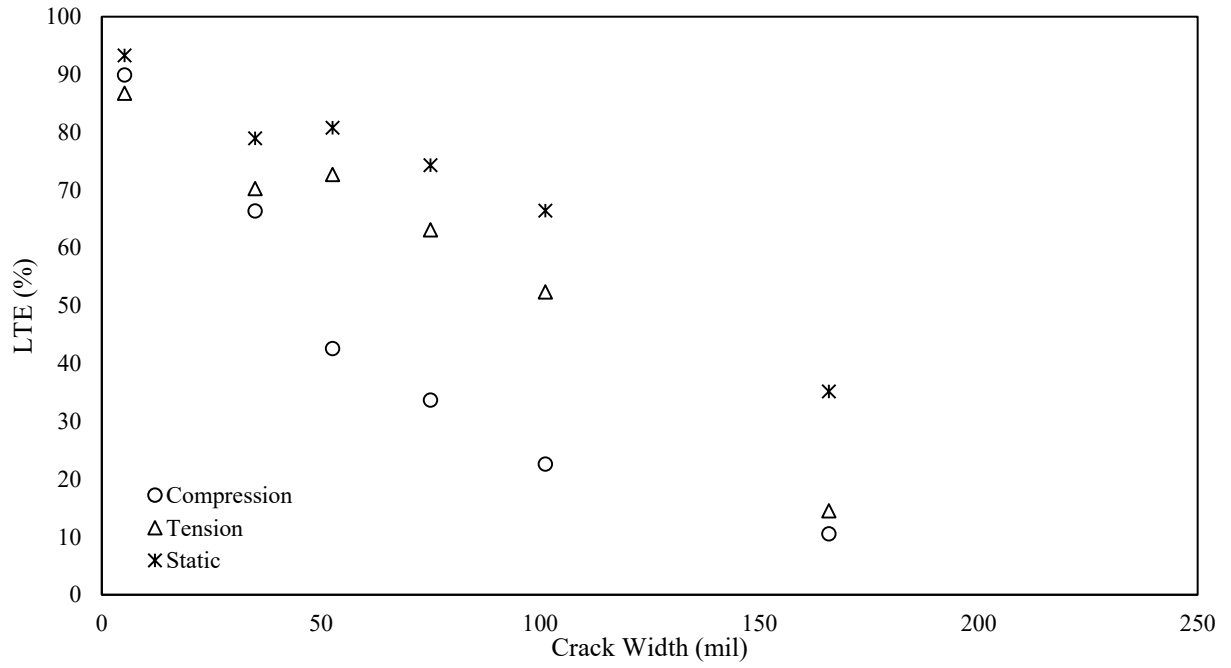
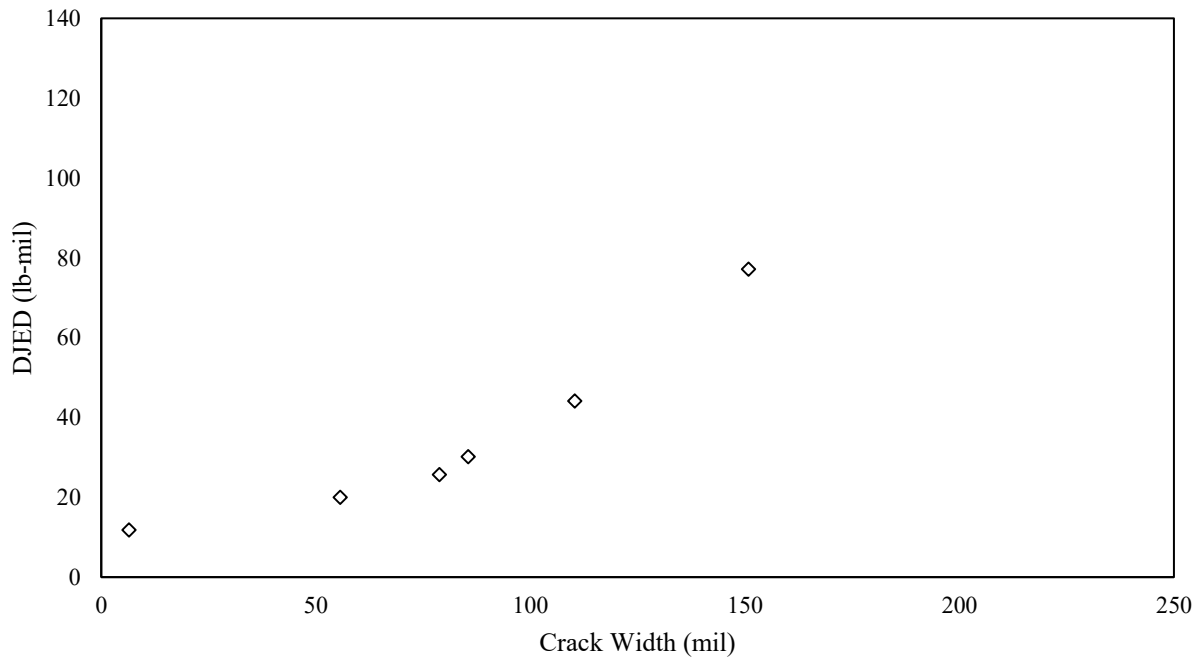**Figure F-183. LTE as a function of crack width.**
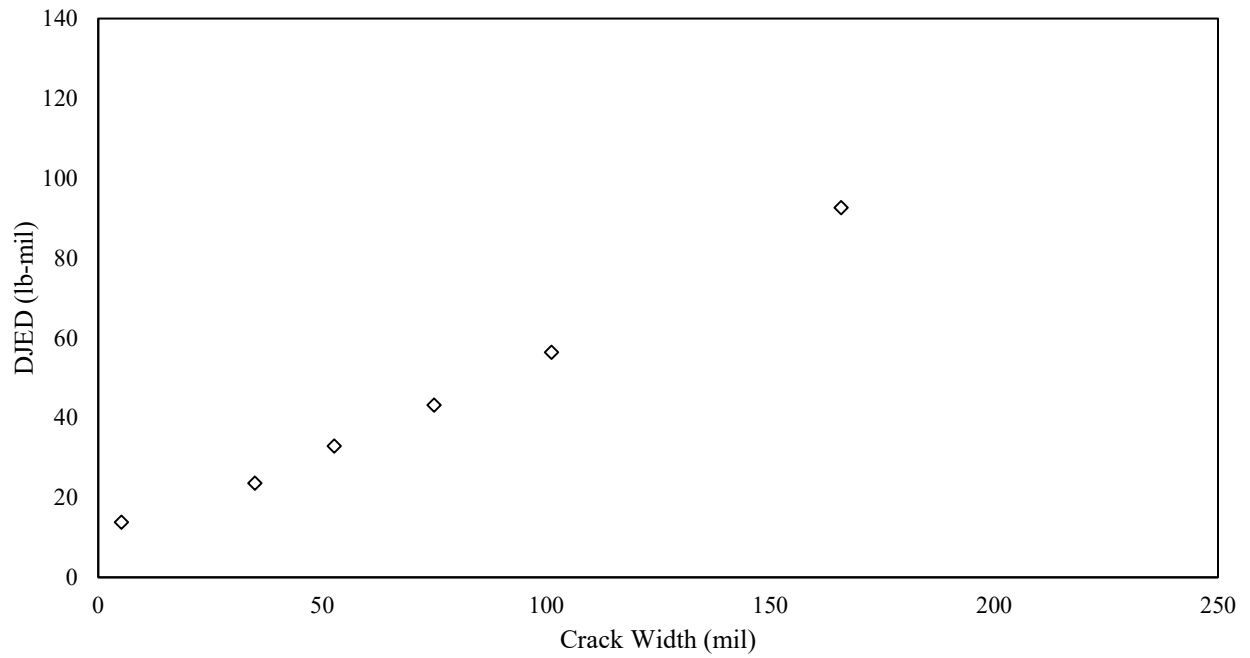
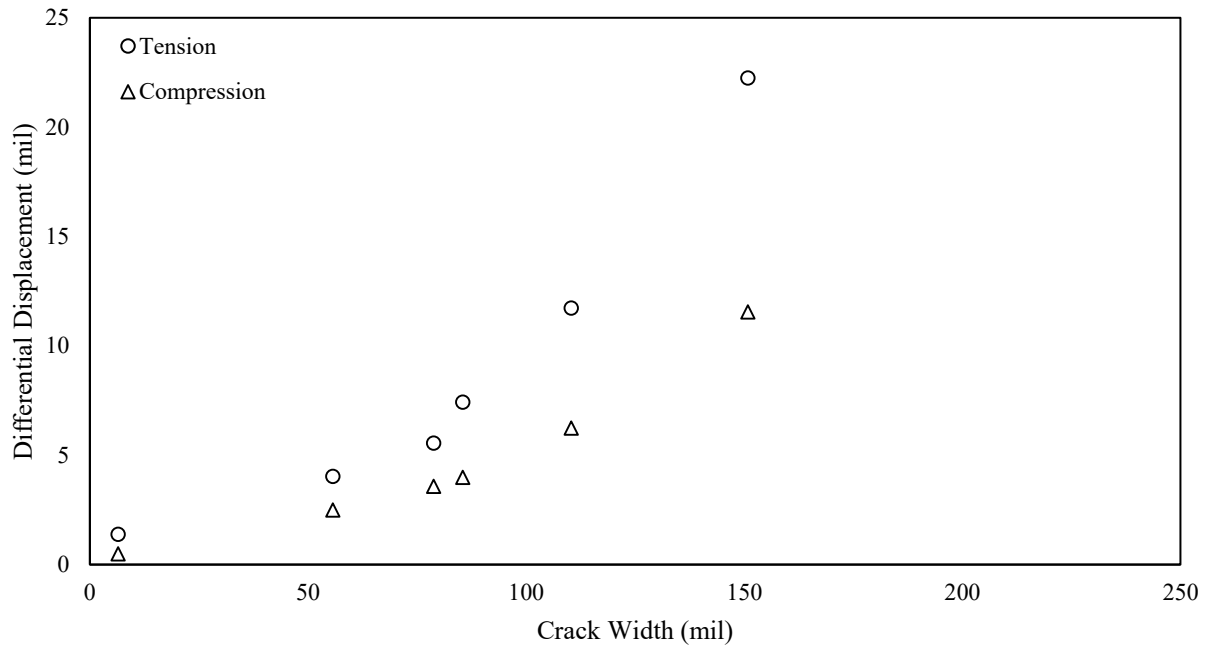**Figure F-184. DJED as a function of crack width.**

F-93
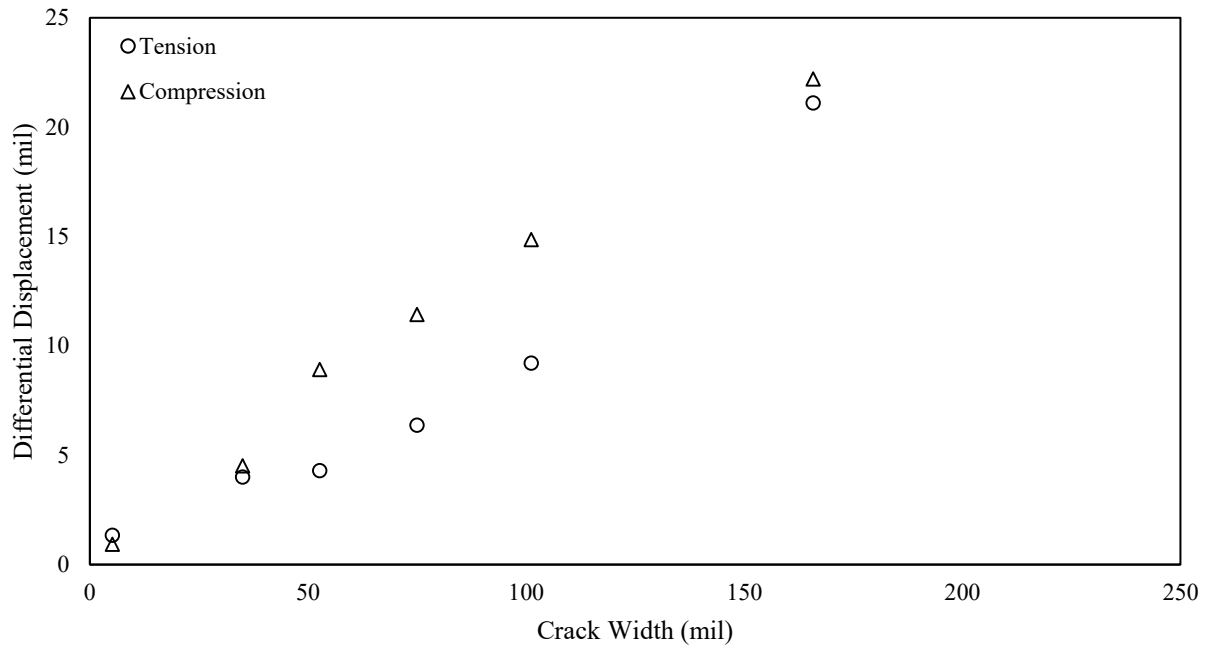
Figure F-185. Differential displacement as a function of crack width.
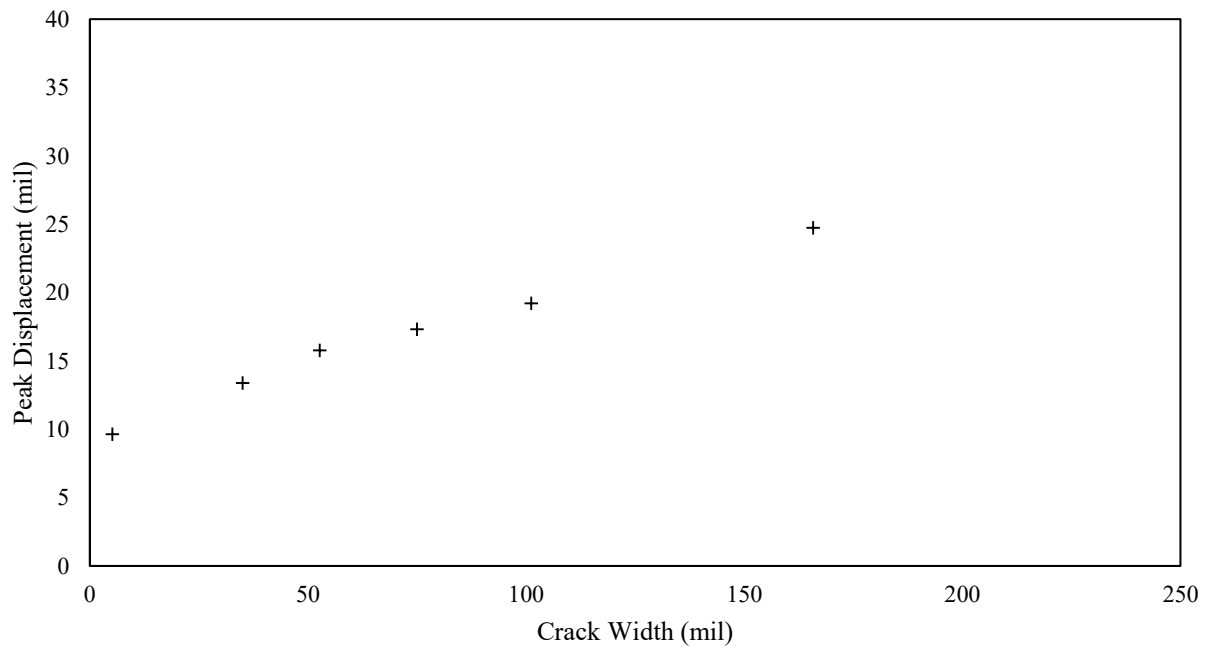
Figure F-186. Peak displacement as a function of crack width.
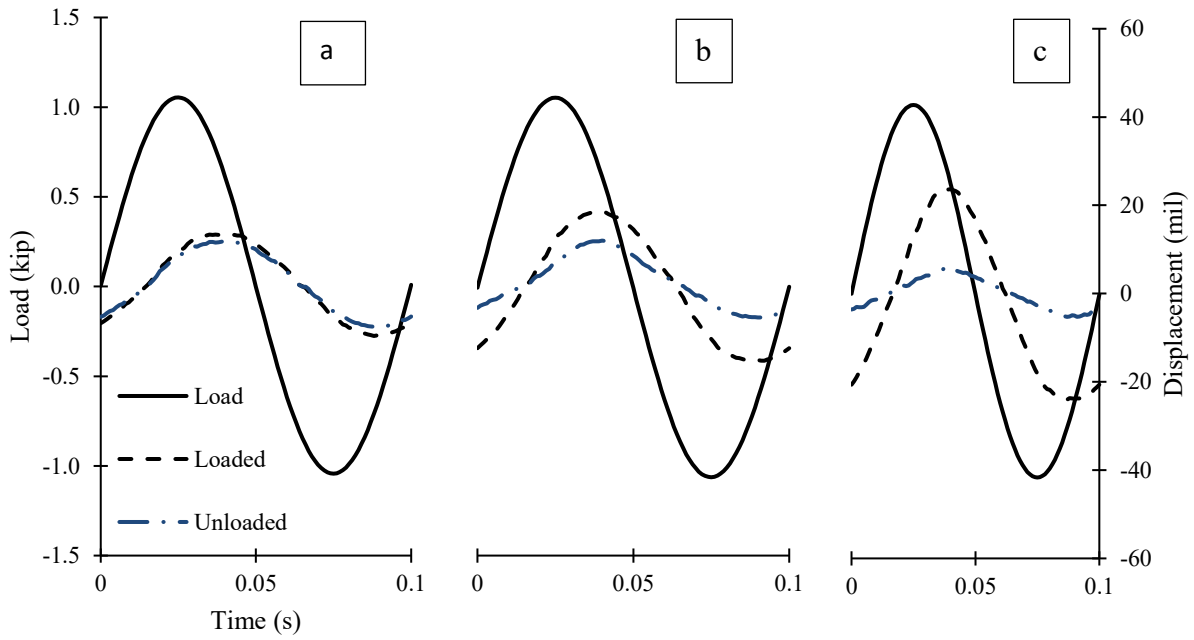
Figure F-187. Cyclical plots at (a) 9 mils, (b)60 mils, and (c)124 mils crack widths.
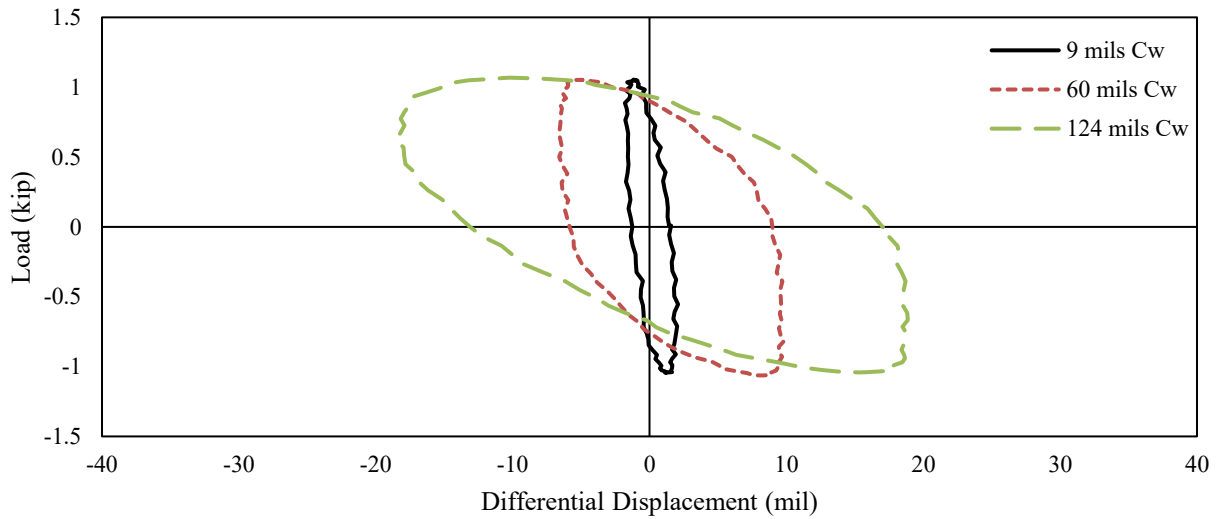
Figure F-188. Hystereses plots for 9 mils, 60 mils, and 124 mils crack widths.
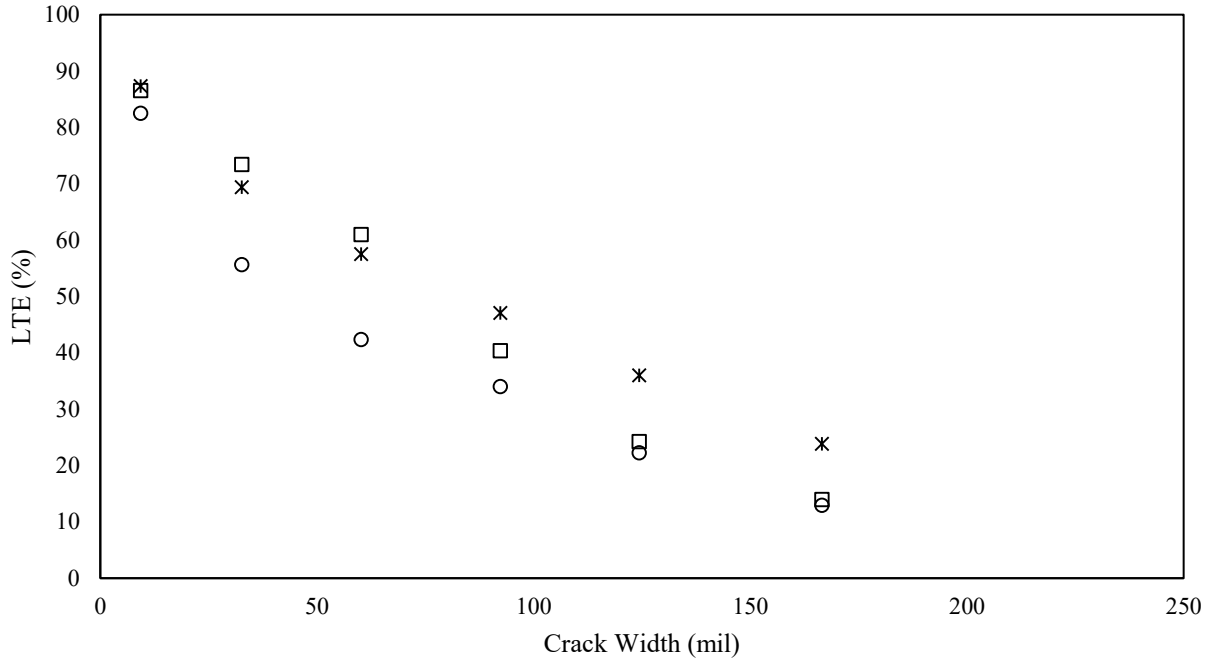
Figure F-189. LTE as a function of crack width.

Figure F-190. DJED as a function of crack width.

F-96

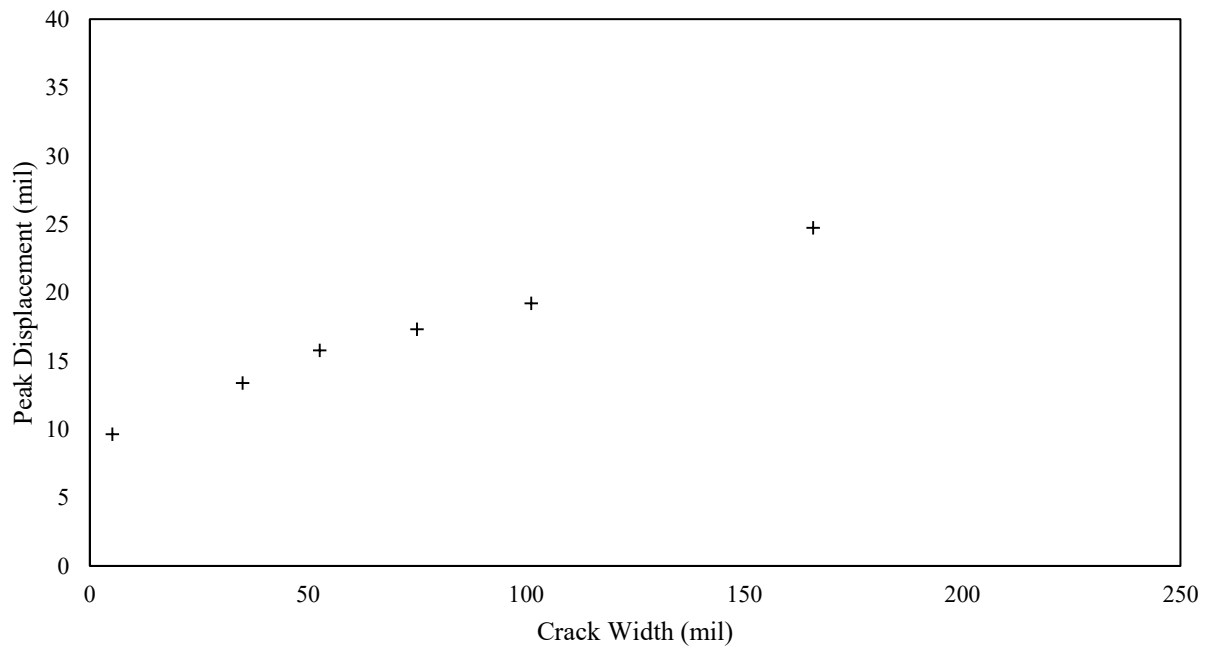**Figure F-191. Differential displacement as a function of crack width.**

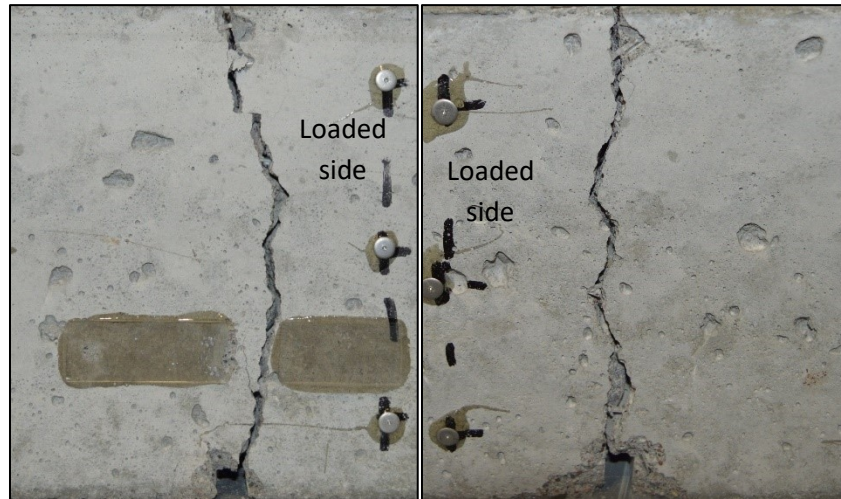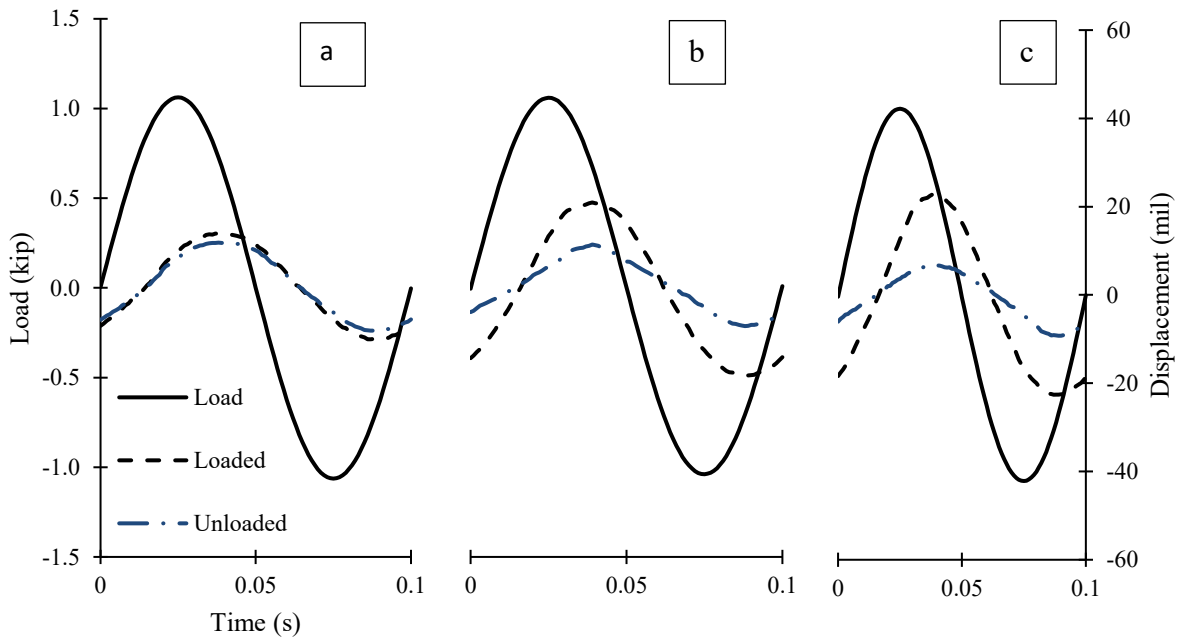**Figure F-192. Peak displacement as a function of crack width.**

F-97
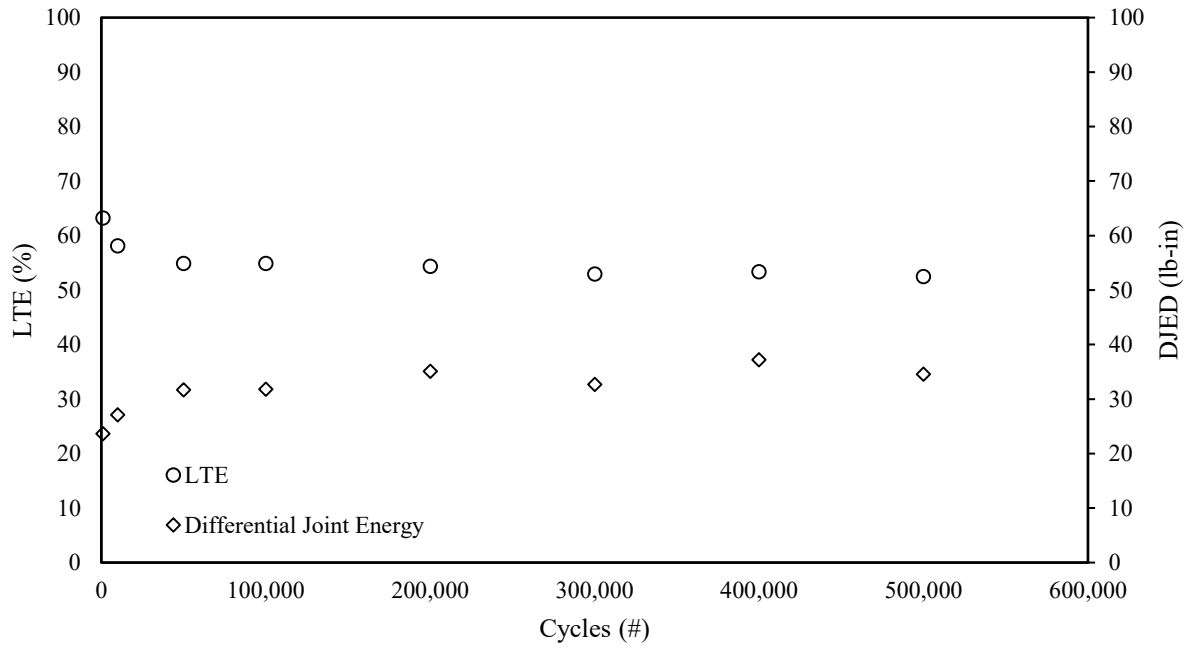
*Crack Width varied from 48 to 51 mils.

FigureF-193. DJED and Average LTE as a function of cycles (repetitions).
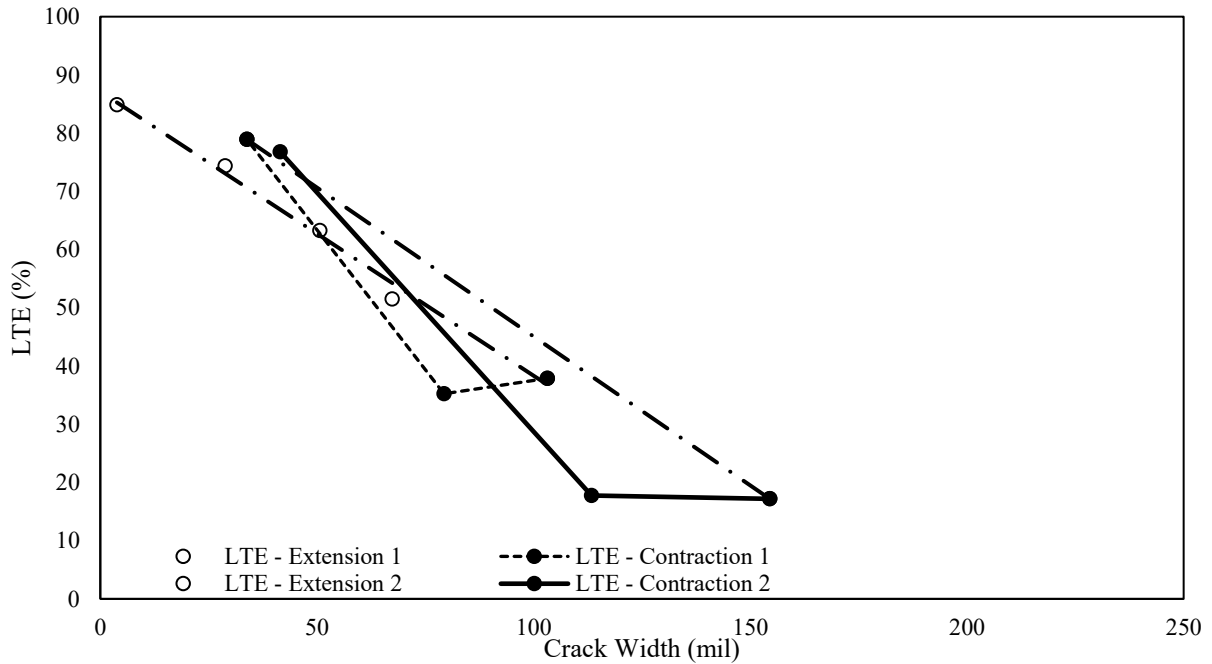
Figure F-194. The effect of joint expansion and contraction on average LTE in terms of crack.
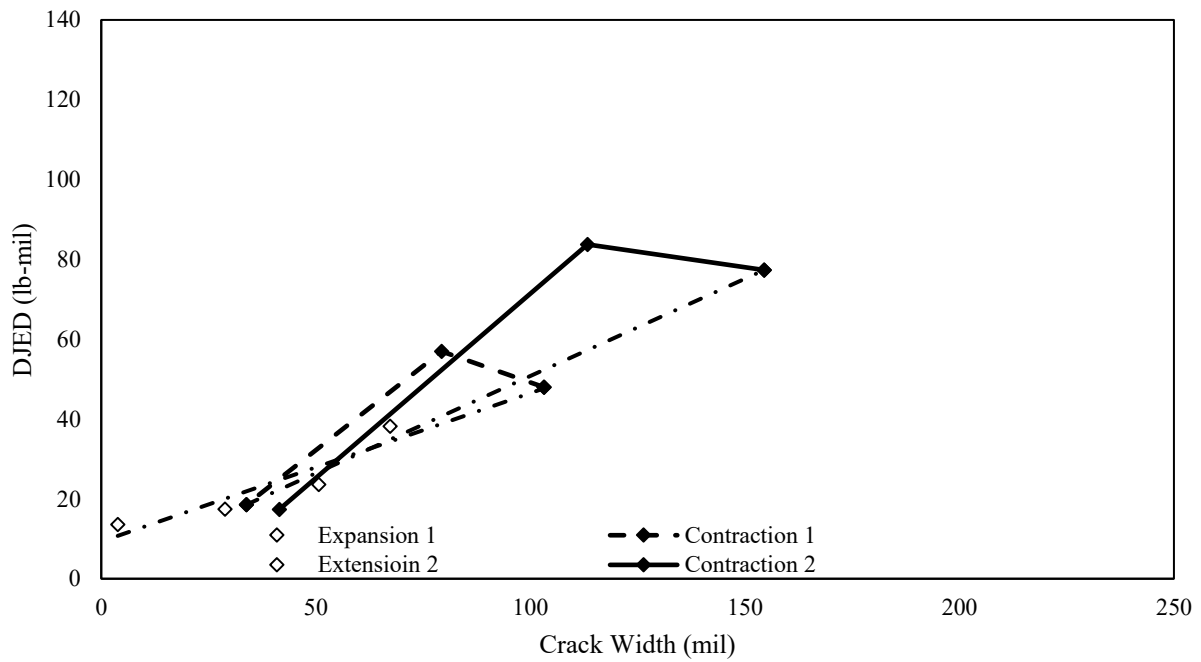
Figure F-195. The effect of joint expansion and contraction on average DJED in terms of crack.

S.E.9.25

Phase 4: Specimen 1
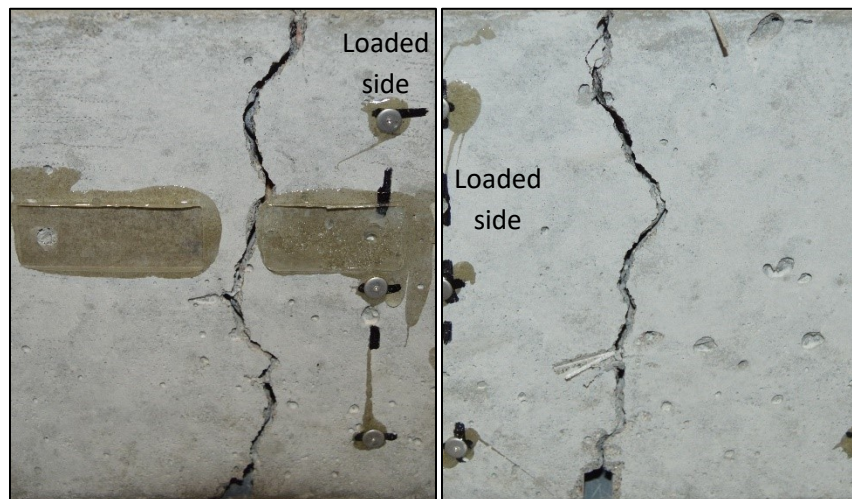
Figure F-196. The front and back of the joint for specimen 1 in phase 4.
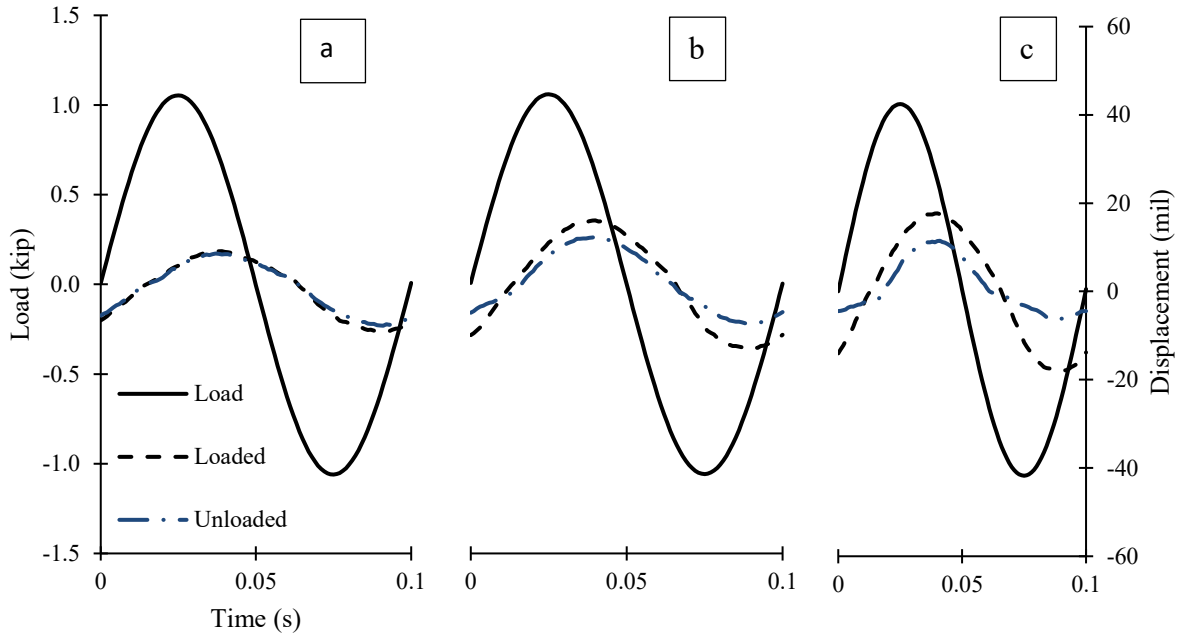
**Figure F-197. Cyclical plots at (a) 6.5 mils, (b)78 mils, and (c) 110 mils crack widths.**

Figure F-198. Hystereses for 6.5 mils, 78 mils, and 110 mils crack widths.
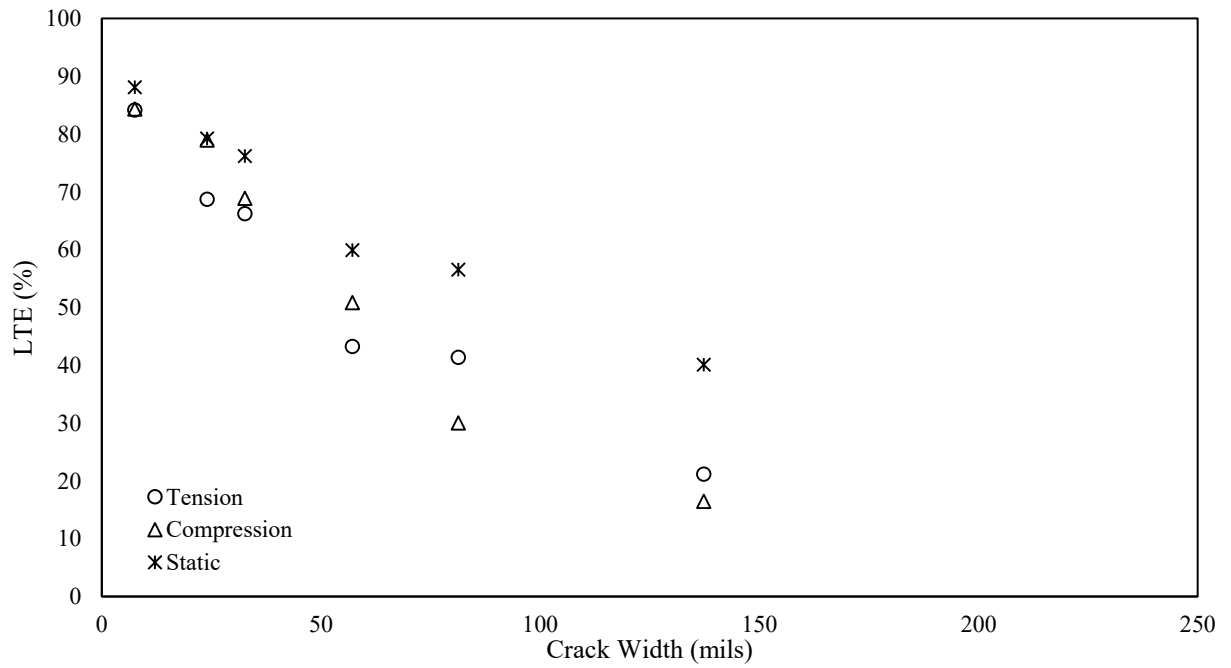
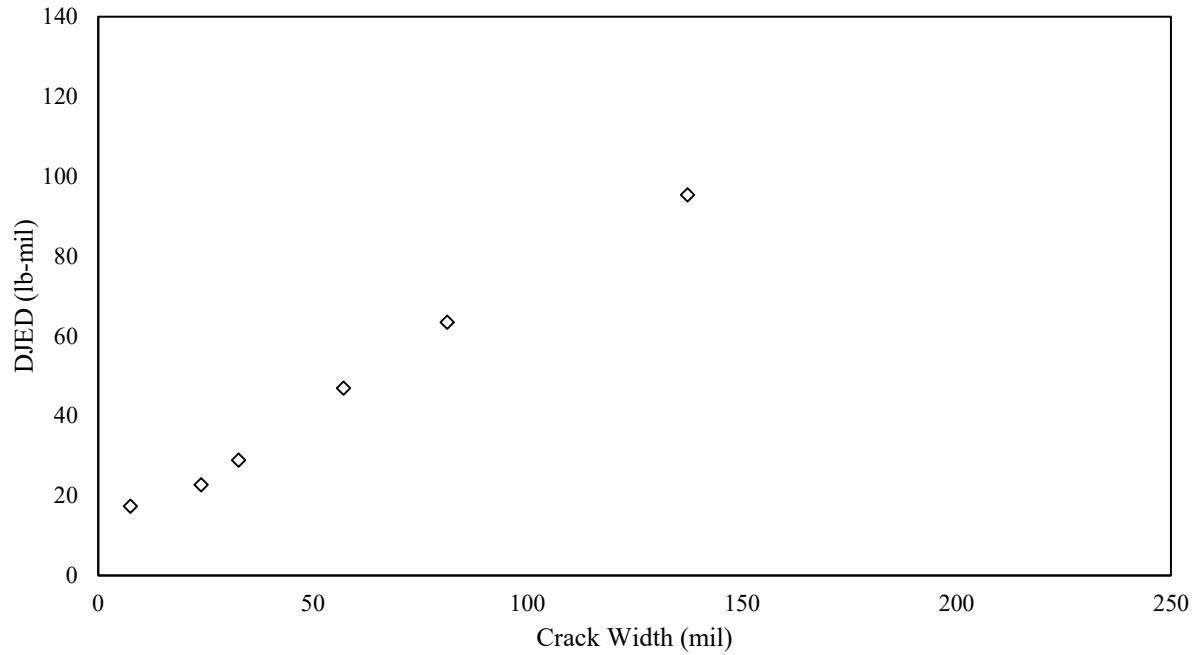**Figure F-199. LTE as a function of crack width.**
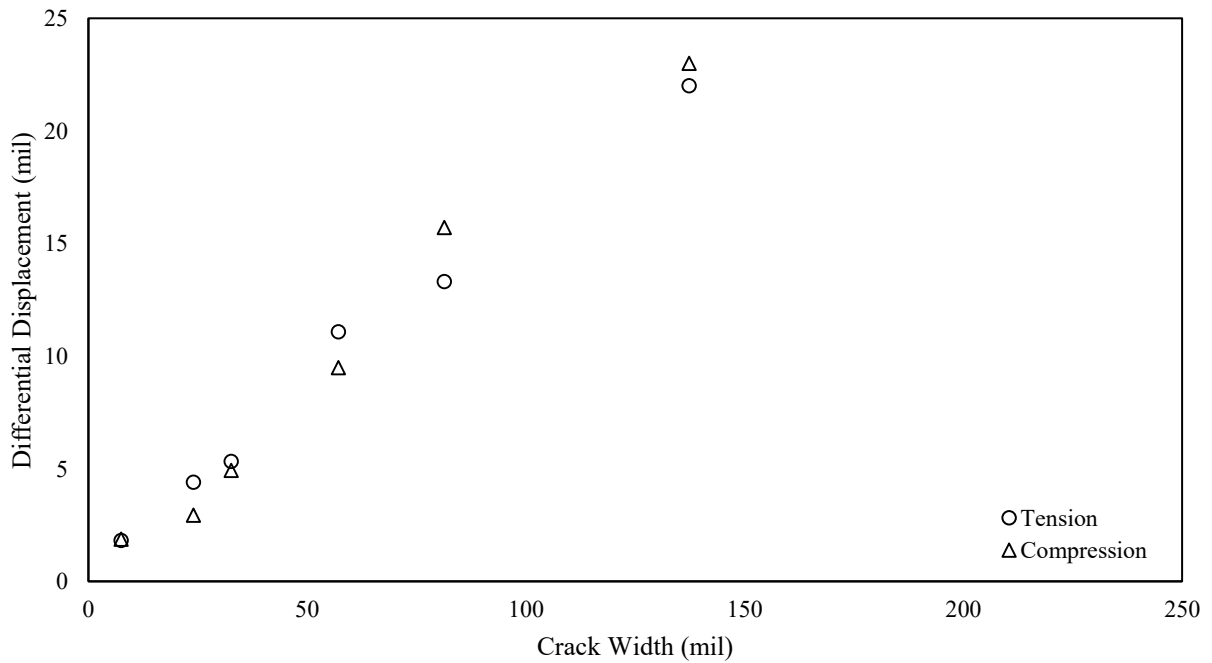

Figure F-200. DJED as a function of crack width.

F-101

Figure F-201. Differential displacement as a function of crack width.

Figure F-202. Peak displacement as a function of crack width.

Figure F-203. The front and back of the joint for specimen 2 in phase 4.

Figure F-204. Cyclical plots for (a) 7.5 mils, (b) 57 mils, and (c) 81 mils crack widths.
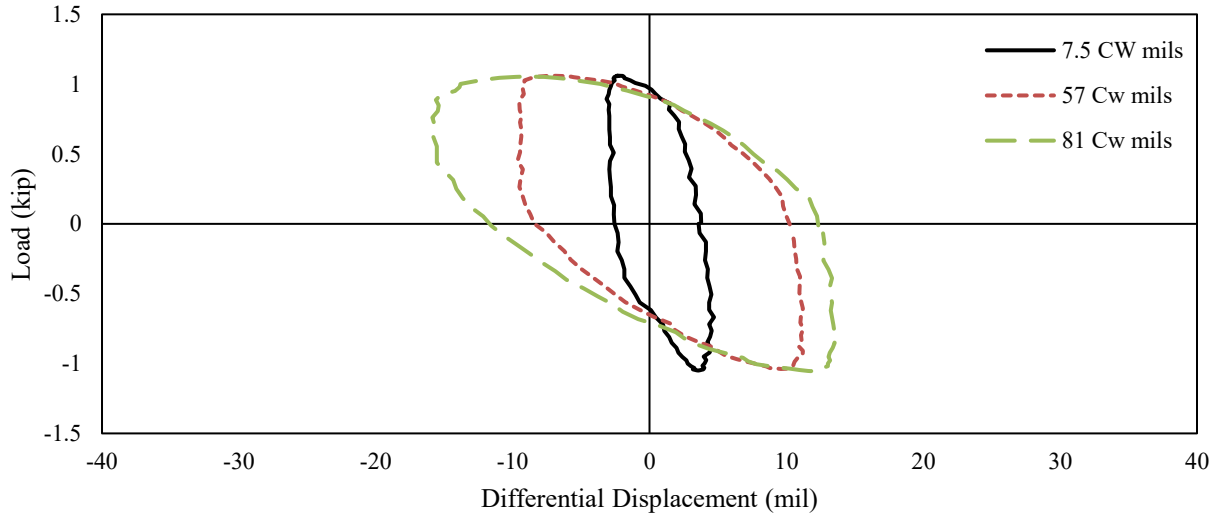
Figure F-205. Hystereses plots for 7.5 mils, 57 mils, and 81 mils crack widths.

Figure F-206. LTE as a function of crack width.

Figure F-207. DJED as a function of crack width.

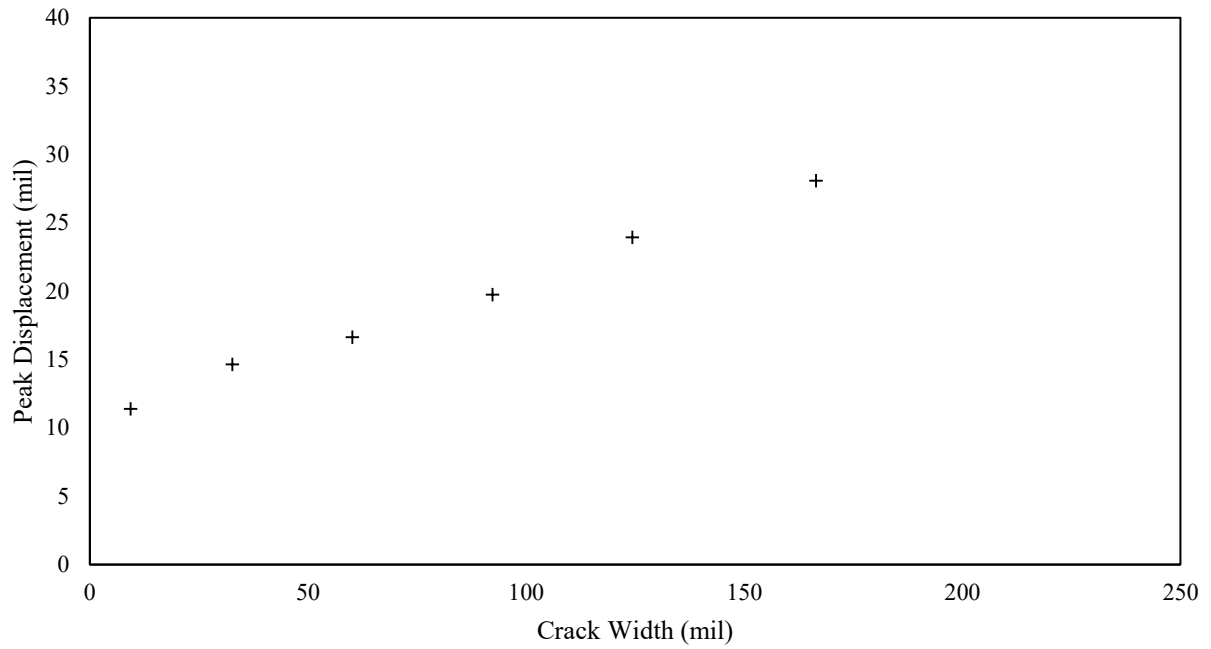**Figure F-208.Differential Displacement as a function of crack width.**

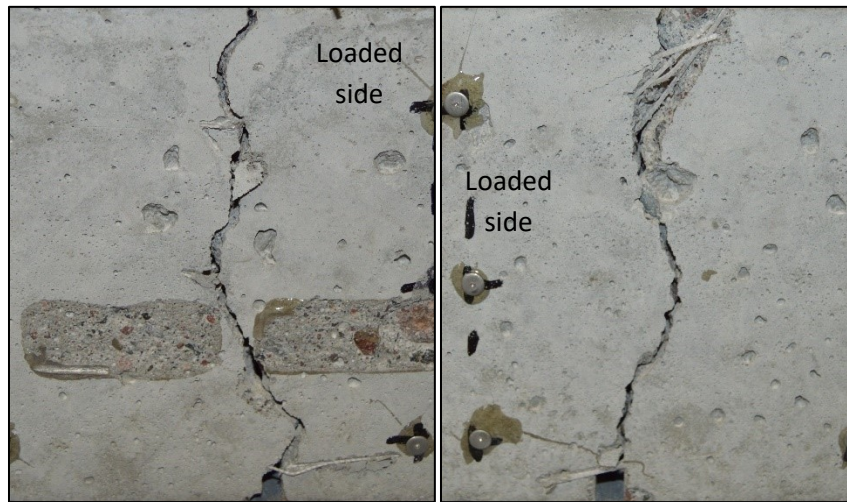**Figure F-209. Peak displacement as a function of crack width.**
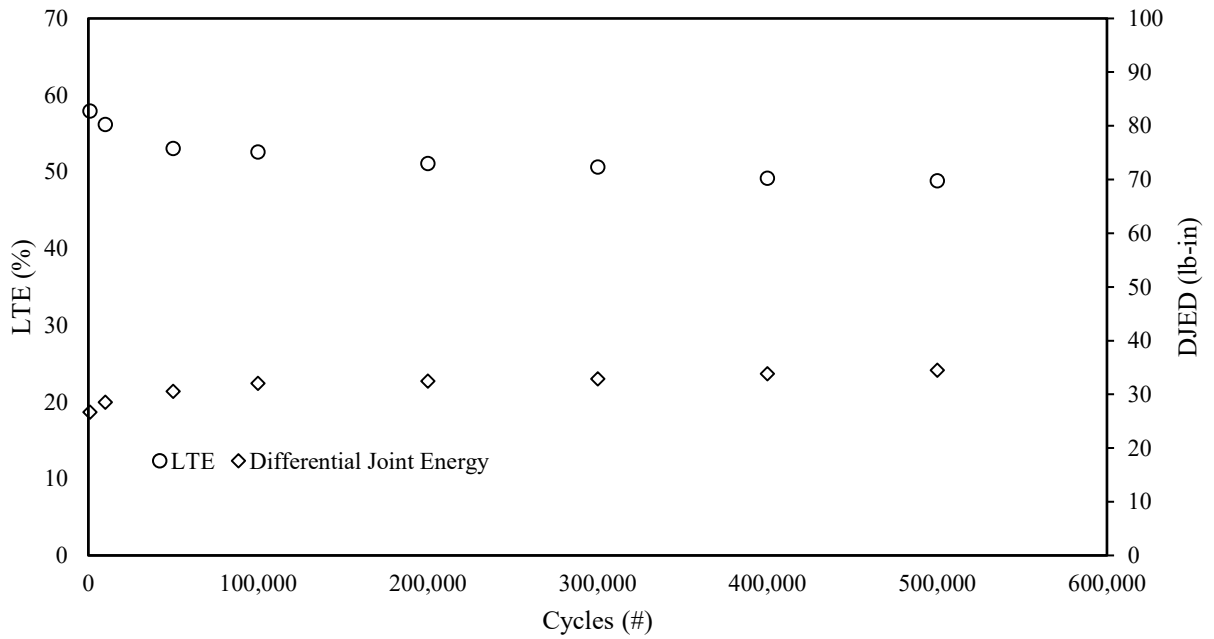
Phase 4: Specimen 3

Figure F-210. The front and back of the joint for specimen 3 in phase 4.

*Crack width ranged from 49 mils to 52 mils

Figure F-211. DJED and Average LTE as a function of cycles (repetitions).
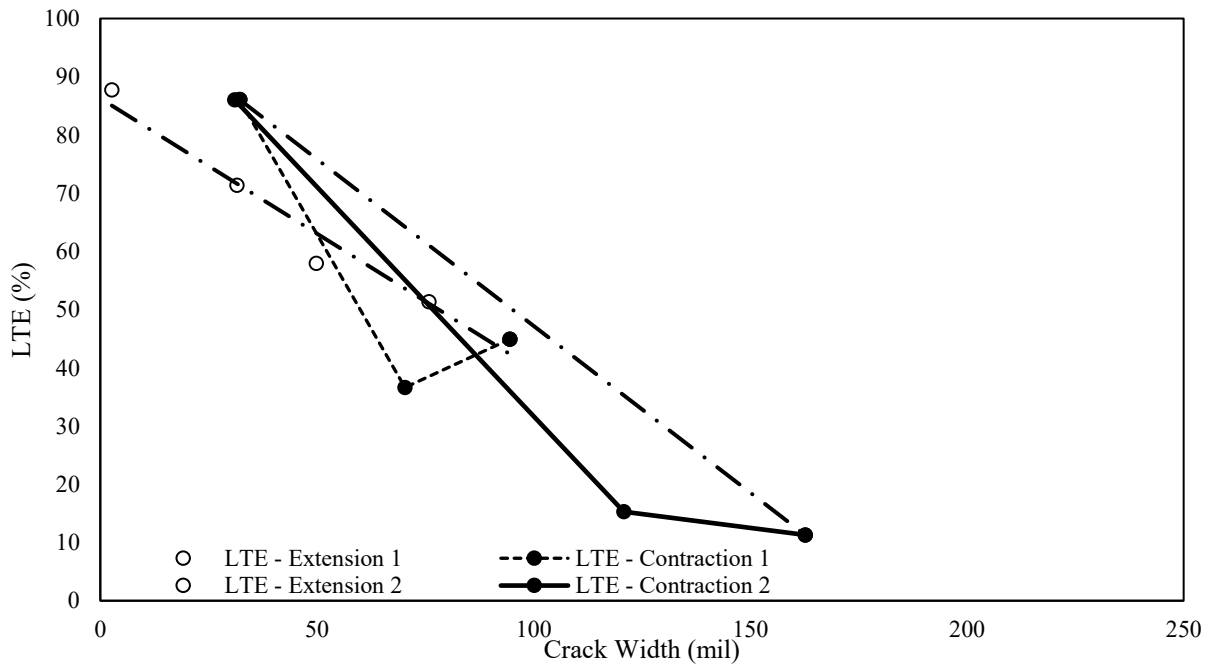

Figure F-212. The effect of joint expansion and contraction on average LTE in terms of crack width.
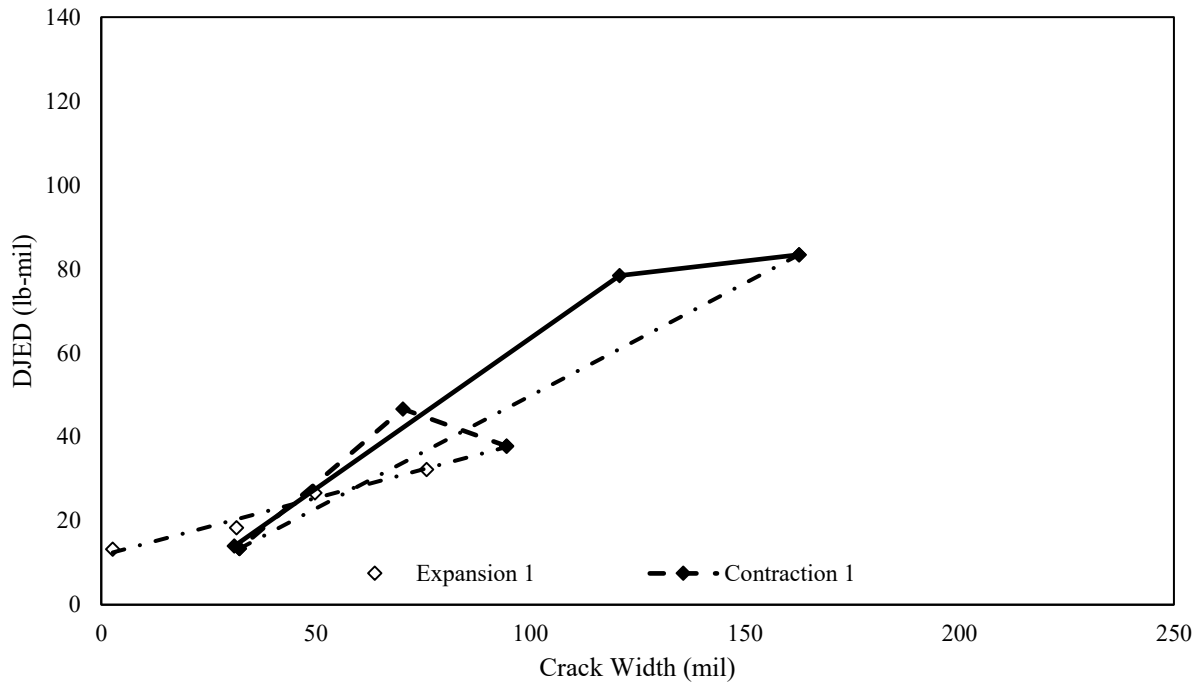
Figure F-213. The effect of joint expansion and contraction on average DJED in terms of crack width.